Roustem N. Miftahof

Biomechanics of the Human Stomach

Springer

Biomechanics of the Human Stomach

Roustem N. Miftahof

Biomechanics of the Human Stomach

Springer

Roustem N. Miftahof
Arabian Gulf University
Computational Biology and Medicine Centre
Manama, Bahrain

ISBN 978-3-319-59676-1 ISBN 978-3-319-59677-8 (eBook)
DOI 10.1007/978-3-319-59677-8

Library of Congress Control Number: 2017945381

Printed on acid-free paper

This Springer imprint is published by Springer Nature
The registered company is Springer International Publishing AG
The registered company address is: Gewerbestrasse 11, 6330 Cham, Switzerland

To my love

Preface

In questions of science, the authority of a thousand is not worth the humble reasoning of a single individual.
Galileo Galilei

Mathematical and computational methods have permeated nearly every filed of biological and medical science. This book is concerned with the mathematical modeling of complex biological systems and in particular the human stomach. The idea of writing the book has its roots in the 1980s when I first engaged myself in a research endeavor related to the biomechanics of the human stomach. Over the years, the subject has evolved and many new biological aspects have been added. The project follows the four modern P's approach (prevention, prediction, personalization, and precision in medicine) addressing the highly heterogeneous nature of processes underlying gastric motility disorders manifested as gastroparesis, functional dyspepsia, myenteric enteropathy, etc. This entails a deep and thorough understanding of driving pathophysiological mechanisms as well as the collaborative effort of specialists working in fundamental and biological science. Such a multidisciplinary partnership is vital because it upholds gnostic capabilities and provides the exchange of thoughts and ideas, thus offering broad perspectives into the evolution and management of diseases.

Prerequisites to the book are a knowledge of anatomy, morphology, and physiology of the human stomach along with familiarity of basic principles of biochemistry, pharmacology, numerical methods, and the mechanics of solids. I believe the book should serve as a text in computational systems biology classes at advanced undergraduate and/or first-year graduate levels and also as a companion to researchers and instructors of applied mathematics, biomedical engineering, physiology, and pharmacology and medical professionals.

Regarding the book structure conversant with my previous books on mathematical modeling with my previous books on the mathematical modeling and numerical simulation of the digestive tract, human urinary bladder and gravid human uterus may consider some materials to be repetitive. This is inevitable and has been done to collate all the required information so as not to distract the reader by

referring him/her to other sources. Besides, despite the fact that the urinary bladder and uterus lie in close proximity to each other in the lower abdomen, urologists rarely communicate with obstetricians, and it is highly unlikely that either of them would be concerned with problems of the stomach, located "distally" in the upper abdomen. Brief biological preliminaries and experimental facts given at the beginning of each chapter are sufficient to follow the arguments presented. However, the reader should not expect to find a complete biomedical survey on the subject and is advised to consult special literature for that.

Chapters 1 through 9 are dedicated to the foundations of the theory of soft shells, constitutive relations for the wall of the human stomach under uniaxial and biaxial loading, modeling of the tissue as a chemically reactive mechanical continuum, intrinsic regulatory and effector neuronal and interstitial cells of Cajal (ICC) networks, multiple neurotransmission and receptor polymodality in signal transduction, and the simulation of pharmacokinetics of major classes of drugs currently used to treat gastric motility disorders.

The novelty and the strength of the monograph are in the holistic modeling of the human stomach as a soft biological active shell. This has never been achieved before. Special attention is paid to the dynamic interplay of coupled electrical, chemoelectrical, mechanoelectrical events which occur in the myenteric nervous plexus, ICC, and smooth muscle syncytia at a cellular and tissue level.

A modern concept of SIP and the SIP/ganglion unit are introduced in Chap. 10. The effects of firing frequency of ICC, mechanical stimulation and neurotransmission by acetylcholine, nitric oxide, substance P, vasoactive intestinal polypeptide, serotonin, and motilin acting alone and/or conjointly on spiking activity and synchronization in SIPs in different regions of the stomach have indicated clearly the significance of multiple neurotransmission in gastric motility.

In Chap. 11, a model of the human stomach as a soft bioshell is formulated. Peculiarities in stress–strain distribution in the steer-horn, cascade, fish-hook, and J-shaped human stomachs in fasting and fed states are studied. The analysis of interaction between the myenteric nervous plexus and ICC/PDGFRα^{+}-MY (IM) suggests new mechanisms of production, stabilization, and propagation of slow waves in the stomach.

The focus of Chap. 12 is the myoelectrical and contractile activity after antrectomy, hemigastrectomy with Billroth I and II reconstructions and common bariatric procedures including sleeve gastrectomy, adjustable gastric banding and vagotomies. Results of numerical simulations provide quantitative and qualitative information about the effect of the extent of surgical damage sustained by the extrinsic and intrinsic innervation on the electromechanical activity in the postoperative organ.

The pathophysiology of gastric arrhythmias, myenteric neuropathy, gastroparesis, and functional dyspepsia is studied in Chap. 13. The importance of time, phase, and frequency dependences in firing by ICC and mechanical stimuli on the myoelectrical and propulsive activity of the stomach is analyzed.

Previously the not stated effects of metoclopramide, velusetrag, itopride, botulinum toxin, erythromycin, and sildenafil on gastric motility are investigated in Chap. 14. It is stressed that the choice of therapy and the efficacy of a drug should be evaluated against morphostructural pathological changes in the tissue and not only by its pharmacokinetic and pharmacodynamics characteristics.

Finally, what makes this book unique is that it guarantees the validity of given mathematical formulations and the reliability of numerical results. Strict mathematical proofs of the existence theorems for one- and two-dimensional nonlinear dynamics problems (courtesy of my colleague Prof. R. R. Shagidullin of Kazan Federal University, Tatarstan, Russia) are supported by dedicated and accurate numerical experiments. Until now, these issues have not been addressed in any research that employs mathematics as a tool.

The book was written at the Arabian Gulf University, Kingdom of Bahrain. I thank its president, Dr. Khalid A. N. Al-Ohaly, for his support. I am grateful to my colleague Ms. Wendy J. Pearson for reviewing the manuscript and providing corrections and valuable comments. My gratitude extends to my daughter Jasmine who ran many numerical simulations and assisted with artworks and my wife for her continuous support and understanding. I appreciate Markus Späth for recognition of the book's potential and the staff at Springer, Cham, Switzerland, for publishing this book. Finally,

> I am thankful to all those who said no to me. It's because of them, I did it myself.
>
> Albert Einstein

Roustem N. Miftahof

Contents

Notations

$\overset{0}{S}, S, \overset{*}{S}$	Cut, undeformed, and deformed (*) middle surface of a shell
S_z	Surface coplanar to S such that $S_z \parallel S$
S^r	Middle surface of a net
$\Sigma, \overset{*}{\Sigma}$	Boundary faces of an undeformed and deformed shell
$d\Sigma, d\overset{*}{\Sigma}$	Differential line elements on Σ, $\overset{*}{\Sigma}$
h	Thickness
x_1, x_2, x_3	Rectangular coordinates
$\{\bar{i}_1, \bar{i}_2, \bar{i}_3\}$	Orthonormal base of $\{x_1, x_2, x_3\}$
$\{\bar{k}_1, \bar{k}_2, \bar{k}_3\}$	Orthonormal base of $\{r, \varphi, z\}$
(α_1, α_2) $(\overset{*}{\alpha}_1, \overset{*}{\alpha}_2)$	Coordinates of the undeformed and deformed shell
$\bar{m}, \overset{*}{\bar{m}}$	Vectors normal to S and $\overset{*}{S}$
$\bar{\tau}, \bar{\tau}^z, \overset{*}{\bar{\tau}}$	Tangential vector to a line on S, S_z, $\overset{*}{S}$ or their boundaries
$\bar{n}, \bar{n}^z, \overset{*}{\bar{n}}$	Normal vector to a line on the boundary of S, S_z, and $\overset{*}{S}$
$\bar{r}, \overline{\rho}, \overset{*}{\overline{\rho}}$	Position vectors of points $M \in S$, $M_z \in S_z$, and $\overset{*}{M}_z \in \overset{*}{S}_z$, respectively
$\bar{r}_i, \overline{\rho}_i$	Tangential vectors to coordinate lines on S and S_z
$\{\bar{r}_1, \bar{r}_2, \bar{m}\}$ $\{\bar{r}^1, \bar{r}^2, \bar{m}\}$	Covariant and contravariant base at point $M \in S$
$\{\overline{\rho}_1, \overline{\rho}_2, \overline{\rho}_3\}$	Covariant base at point $M_z \in S_z$
$\{\bar{n}, \bar{\tau}, \bar{m}\}$ $\{\overset{*}{\bar{n}}, \overset{*}{\bar{\tau}}, \overset{*}{\bar{m}}\}$	Orthogonal bases on Σ and $\overset{*}{\Sigma}$, respectively

$\chi, \chi^z, \overset{*}{\chi}$	Angles between coordinate lines defined on S, S_z, $\overset{*}{S}$
γ	Shear angle
$A_i, \overset{*}{A}_i, H_i$	Lamé coefficients on S, $\overset{*}{S}$, and S_z
a_{ik}	Components of the metric tensor
$a, \overset{*}{a}$	Determinants of the metric tensor
b_{ik}	Components of the second fundamental form
$\bar{e}_i, \bar{e}_i^z, \overset{*}{\bar{e}}_i, \overset{*}{\bar{e}}_i^z$	Unit base vectors on S, S_z, and $\overset{*}{S}$
$ds, ds_z, \overset{*}{ds}$	Lengths of line elements on S, S_z, $\overset{*}{S}$
ds_Δ	Surface area of a differential element of S
$\Gamma_{ik,\,j}, \Gamma_{ik}^j$	Christoffel symbols of the first and second kind
A_{ik}^j	Deviator of the Christoffel symbols
$\overline{v}(\alpha_1, \alpha_2)$	Displacement vector
u_1, u_2, ω	Projections of the displacement vector on x_1, x_2, x_3 axes
$\varepsilon_{ik}, \varepsilon_{ik}^z$	Components of the tensor of planar deformation through points $M \in S$ and $M_z \in S_z$
$\tilde{\varepsilon}_{ik}, \overset{*}{\tilde{\varepsilon}}_{ik}$	Physical components of the tensor deformation in undeformed and deformed configurations of a shell
$\varepsilon_1, \varepsilon_2$	Principal physical components of the tensor of deformation
$\varsigma_{ij}, \Delta_{ij}$	Elastic and viscous parts of deformation
$\varepsilon_n, \varepsilon_\tau, \varepsilon_{n\tau}$	Components of deformation of the boundary of a shell in $\bar{n}$, $\overline{\tau}$ directions
$\underline{\varepsilon}_{ik}, \underline{\text{æ}}_{ik}$	Components of the tensor of tangent and bending fictitious deformations
λ_i, λ_c, l	Stretch ratios (subscripts c and l are referred to the circular and longitudinal directions of a bioshell)
$\mathbf{\Lambda}_1, \mathbf{\Lambda}_2$	Principal stretch ratios
$I_1^{(\mathbf{E})}, I_2^{(\mathbf{E})}$	Invariants of the tensor of deformation
$\text{æ}_n, \text{æ}_\tau, \text{æ}_{n\tau}$	Components of bending deformation and twist of the boundary of a shell in $\bar{n}$, $\overline{\tau}$ directions
$e_{nn}, e_{n\tau}, e_{\tau n}, \omega_n, \omega_\tau$	Rotation parameters
$e_{\alpha 1}, e_{\alpha 2}$	Elongations in direction α_1, α_2, respectively
$\underline{e}_i^k, \underline{e}_{ki}, \underline{\omega}_i$	Rotation parameters in fictitious deformation

k_{ii}, $\overset{*}{k}_{ii}$	Normal curvatures of S and $\overset{*}{S}$
k_{ik}, $\overset{*}{k}_{ik}$	Twist of S and $\overset{*}{S}$
k_n, k_τ, $\overset{*}{k}_n$, $\overset{*}{k}_\tau$	Normal curvatures in $\bar{n}, \overline{\tau}$, $\overset{*}{\bar{n}}$, $\overset{*}{\overline{\tau}}$ directions
$k_{n\tau}$, $\overset{*}{k}_{n\tau}$	Twist of the contour Σ and $\overset{*}{\Sigma}$
$1/R_{1,2}, 1/R_{1,2}{}^{*}$	Principal curvatures of S and $\overset{*}{S}$
K, K_0	The Gaussian curvature of S and $\overset{*}{S}$
$L_j^{'}(\varepsilon_{ik}), L_i(T_{ik})$	Differential operators
$\bar{p}_i$	Stress vectors
$\bar{R}_i$	Resultant of force vectors
$\bar{p}_{(+)}, \bar{p}_{(-)}$	External forces applied over the free surface area of a shell
$\overset{*}{\bar{p}}{}_n^z$	Normal stress vector on $\overset{*}{\Sigma}$
$\bar{F}$	Vector of mass forces per unit volume of the deformed element of a shell
$\bar{X}$	Resultant external force vector on $\overset{*}{S}$
$\bar{M}$	Resultant external moment of external forces on $\overset{*}{S}$
$\overset{*}{T}_{ii}$, $\overset{*}{T}_{ik}$, $\overset{*}{N}_i$	Normal, shear, and lateral forces per unit length
$T_{c,l}$	Total force per unit length
$T_{c,l}^p, T_{c,l}^a$	Passive and active components of the total forces per unit length
T_1^r, T_2^r	Forces per unit length of reinforced fibers
T_1, T_2	Principal stresses
$I_1^{(\mathbf{T})}, I_2^{(\mathbf{T})}$	Invariants of the stress tensor
$\overset{*}{M}_{ii}, \overset{*}{M}_{ik}$	Bending and twisting moments per unit length of a shell perpendicular to α_1, α_2 directions on $\overset{*}{S}$
$\overset{*}{M}_i$	Projections of the moment vector on $\overset{*}{\bar{e}}_1$, $\overset{*}{\bar{e}}_2$, $\overset{*}{\bar{m}}$
$\overset{*}{X}_i$	Projections of the external force vector on $\overset{*}{\bar{e}}_1$, $\overset{*}{\bar{e}}_2$, $\overset{*}{\bar{m}}$
$\bar{R}_n^*$	Resultant force vector per unit length acting on $d\overset{*}{\Sigma}_z$ in $\overset{*}{\bar{n}}$ direction

$\bar{M}_n^*$	Resultant moment vector per unit length acting on $d\overset{*}{\Sigma}_z$ in $\overset{*}{\bar{n}}$ direction
$\overset{*}{G}, \overset{*}{H}$	Bending and twisting moments in a boundary of a shell
$\bar{G}_i, \bar{M}_p, \bar{M}_q$	Resultant moment vectors per unit length of a soft shell
σ_{ij}	Stresses in a shell
σ_{ij}^{α}	Stresses in the α phase of a biomaterial
c_i	Material constants
d_m, d_f	Diameter of smooth muscle fiber and nerve terminal, respectively
$L, L^{\mathrm{s}}, L_0^{\mathrm{s}}$	Length of bioshell/muscle fiber, axon and nerve terminal, respectively
$\rho, \overset{*}{\rho}$	Density of undeformed and deformed material of a shell
ρ_{ζ}^{α}	Partial density of the ζth substrate in the α phase of a biomaterial
m_{ζ}^{α}	Mass of the ζth substrate in the α phase of a biomaterial
$\upsilon, \upsilon^{\alpha}$	Total and elementary volumes of a biomaterial
c_{ζ}^{α}	Mass concentration of the ζth substrate in the α phase of a biomaterial
η	Porosity of the phase α
Q_{ζ}^{e}, Q_{ζ}	Influxes of the ζth substrate into the phase α, external sources and exchange flux between phases
$\nu_{\zeta j}$	Stoichiometric coefficient in the jth chemical reaction
$U^{(\alpha)}$	Free energy
$s^{(\alpha)}, S_{\zeta}^{1}$	Entropy of the α phase and partial entropy of the entire biomaterial
μ_{ζ}^{α}	Chemical potential of the ζ th substrate in the α phase of a biomaterial
$\bar{q}$	Heat flux vector
$\boldsymbol{R}$	Dissipative function
Λ_j	Affinity constant of the jth chemical reaction
$\bar{J}_i, \bar{J}_o$	Intra- (i) and extracellular (o) ion currents
I_{m1}, I_{m2}	Transmembrane ion currents
I_{Appl}	Applied external membrane current
I_{ion}	Total ion current
$\tilde{I}_{Ca}^{s}, \tilde{I}_{Ca}^{f}, \tilde{I}_{Ca-K}, \tilde{I}_K$ $\tilde{I}_{Cl}, I_{Ca}, I_{Ca-K}, I_{Na}$ $I_K, I_{Cl}, \tilde{I}_{Na}, I_{Cl}$	Ion currents
Ψ_i, Ψ_o	Electrical potentials

V, V_n^s, V^e, V^d $V_l^s, V_c^s, V_i, \overset{0}{V}$	Transmembrane potentials
$V_{Ca}^{(\sim)}, V_{Ca-K}^{(\sim)}, V_{Na}^{(\sim)}$ $V_K^{(\sim)}, V_{Cl}^{(\sim)}$	Reversal membrane potentials for respective ion currents
$V_{syn}^{(+,-)}, V_{syn,0}$	Actual excitatory (+)/inhibitory (−) and resting synaptic membrane potentials
$C_m, C_n^s, C_p, C_a^f, C_d$	Membrane capacitances of smooth muscle, synapse, postsynaptic structures, axon and the free nerve endings, respectively
$R_{i(0)}^{ms}$	Membrane resistance
$\widehat{g}_{ij}, \widehat{g}_{oj}$	Intra- (i) and extracellular (o) conductivities
$\widehat{g}_{i(0)}^*$	Maximal intra- (i) and extracellular (o) conductivities
$g_{Ca(i)}, g_{Ca-K(i)}, g_{Na(i)}$ $g_{K(i)}, g_{Cl(i)}, \tilde{g}_{Ca}^f, \tilde{g}_{Ca}^s$ $\tilde{g}_K, \tilde{g}_{Ca-K}, \tilde{g}_{Cl}, \tilde{g}_{Na}$ $g_{Na}^f, g_K^f, g_{Cl}^f$	Maximal conductances of respective ion channels
$\tilde{m}, \tilde{h}, \tilde{n},$ $h_{Na}, n_K, z_{Ca},$ $\rho_\infty, \tilde{x}_{\mathrm{Ca}}$	Dynamic variables of respective ion currents
m_f, n_f, h_f	Dynamic variables of ion channels at the synapse
$\widetilde{\alpha}_y \widetilde{\beta}_y$	Activation and deactivation parameters of ion channels
$Z_{mn}^{(*)}$	"Biofactor"
$\left[\mathrm{Ca}_i^{2+}\right]$	Intracellular concentration of free Ca^{2+} ions
ϑ_{Ca}	Parameter of calcium inhibition
$\lambda, \hbar, \wp_{\mathrm{Ca}}$ $\tau_{\mathrm{Ca}}, \tau_{\mathrm{m}}$	Electrical numerical parameters and constants
$\breve{V}$	Volume of the bioshell
$p\left(\breve{V}\right)$	Intragastric pressure
$k_{(\pm)i}$	Rate constants of chemical reactions
$\chi_1, \ldots, \chi_n$	Physicochemical parameters
$\mathbf{A}, \mathbf{B}, \mathbf{C}, \mathbf{D}$	Matrices of rate coefficients
$\mathbf{X}(X_i)^{\mathrm{T}}, \mathbf{C_0}(C_i)^{\mathrm{T}}$	Vectors of reacting substrates

Abbreviations

5-HT	5-hydroxytryptamine, serotonin
AC	Adenylyl cyclase
ACh	Acetylcholine
AChE	Acetylcholinesterase
ACh-R	Acetylcholine-receptor complex
AGB	Adjustable gastric banding
ANNA-1	Antineuronal nuclear antibodies
AP(s)	Action potential(s)
ATP	Adenosine-5′-triphosphate
BK_{Ca}	Large conductance Ca^{2+} activated K^+ channel
BPD	Biliary pancreatic diversion
cAMP	Cyclic adenosine monophosphate
DAG	Diacylglycerol
DMV	Dorsal motor nucleus of the vagus
DP	Dominant pacemaker
ECM	Extracellular matrix
ENS	Enteric nervous system
EPSP	Excitatory postsynaptic potential
FD	Functional dyspepsia
GDP/DTP	Guanosine diphosphate/guanosine triphosphate
ICC(MY,IM)	Interstitial cells of Cajal (myenteric, intramuscular)
IGLE	Intraganglionic laminar ending
IMA	Intramuscular array
IP_3	Inositol-1,4,5-trisphosphate
IPSP	Inhibitory postsynaptic potential
K_{ATP}	ATP-sensitive K^+ channel
K_V	Voltage-gated K^+ channel
MAPK	Mitogen-activated protein kinase
MLCK	Myosin light chain kinase
MP	Myenteric nervous (Auerbach's) plexus

NA	Noradrenaline
NCSCs	Neural crest multipotent stem cells
NO	Nitric oxide
nNOS	Neuronal nitric oxide synthase
NTS	Nucleus tractus solitarius
PDE	Phosphodiesterase
PDGFRα^+	Platelet-derived growth factor receptor α
PGN	Preganglionic neuron
PIP_2	Inositide-4,5-bisphosphate
PKA	Protein kinase A
PKC	Protein kinase C
PLC	Phospholipase C
SG	Sleeve gastrectomy
SIP	Smooth muscle interstitial cells of Cajal-syncytium
SM(C)	Smooth muscle (cell)
SP	Substance P
SR	Sarcoplasmic reticulum
VIP	Vasoactive intestinal peptide

Chapter 1
Geometry of the Surface

Science is simply common sense at its best, that is, rigidly accurate on observation, and merciless to fallacy in logic.
Thomas Huxley

1.1 Anatomical and Morphological Considerations

The human stomach is the organ of the gastrointestinal tract located in the left upper quadrant of the abdomen. Its prime role is to accommodate and digest food. The shape of the stomach is greatly modified by changes within itself and in the surrounding viscera such that no one form can be described as typical. The existing classification of anatomical variants of the human stomach is based on radiological data. Four main types are proposed: J-shaped, hourglass (fish-hook), steer-horn and cascade (Fig. 1.1). The chief configurations under normal physiological conditions are determined by the amount of the contents, the stage of the digestive process, the degree of development of the gastric musculature, the condition of the adjacent organs, the loops of the small and large intestines, body habitus, sex and age.

The human stomach is more or less concave on its right side and convex on its left. The concave border is called the lesser curvature; the convex border, the greater curvature. The region that connects the lower esophagus with the upper part of the organ is called the cardia. The uppermost adjacent part to it is the fundus. The fundus adapts to the varying volume of ingested food and frequently contains a gas bubble, especially after a meal. The largest part of the stomach is known simply as the body (corpus). The antrum, the lowermost part, is usually funnel-shaped, with its narrow end connecting with the pyloric region. The latter empties into the duodenum, the upper division of the small intestine. The pyloric portion tends to curve to the right, slightly upward and backward.

The stomach functions as: (i) an expansile reservoir which allows the rapid consumption of large meals; the process is facilitated by relaxation of the stomach in response to food and is called gastric accommodation; (ii) a digestive and absorptive organ that breaks down large protein and carbohydrate molecules and thus facilitates their absorption, (iii) a part of the endocrine and immune system; it secretes multiple hormones and neurotransmitters, e.g. gastrin, histamine,

R.N. Miftahof, *Biomechanics of the Human Stomach*,
DOI 10.1007/978-3-319-59677-8_1

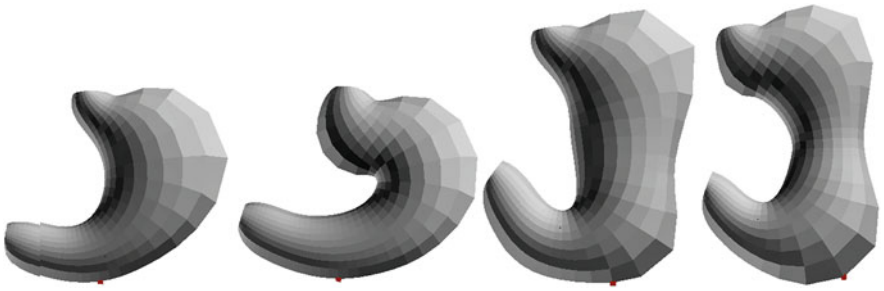

Fig. 1.1 Radiologically defined common anatomical shapes of the human stomach. *From left to right*: steer-horn, cascade, J-shape, hourglass (fish-hook)

endorphins, somatostatin, serotonin, intrinsic factor; (iv) a biomechanical system that grinds, mixes, forms and periodically discharges the preformed chyme into the duodenum as the physical and chemical condition of the mixture is rendered suitable for the next phase of digestion.

The effectiveness and diversity of physiological responses of the stomach to internal and external stimuli depend on the inherent activity of histomorphological elements: smooth muscle cells (SMCs), connective tissue matrix, neurons, interstitial cells and their topographical organization in gastric tissue (Suzuki 2000; Hirst and Suzuki 2006; Koh et al. 2003; Carniero et al. 1999). The mucosa is the innermost layer consisting of sheets of epithelial cells that line the outer surface of the gastrointestinal tract and have primarily secretory, digestive, absorptive and protective functions. The cells are tightly packed with little extracellular substance between them, and are supported on a basal membrane. One of the characteristics of the cells is a stable apico-basal polarity, which is expressed in morphological, electrophysiological and transport properties. The ionic channels are predominantly located within the apical membrane, while ion-pumps are situated in the basolateral domain. Such an arrangement is of morphomechanical importance as it guarantees the required amount of turgor pressure in the subepithelial cavities. The epithelial cells are bound together by tight junctions to form an integrated net that gives the cell sheet mechanical strength and makes it impermeable to passive diffusion of small molecules and solutes. Their role in the biodynamics of the organ, i.e. force-stretch ratio development, propulsion etc. is negligible.

The extracellular matrix (ECM) is comprised of three major types of macromolecules, i.e. fibers (elastin and collagen), proteoglycans and glycol-proteins. It provides the biochemically stable microenvironment for the tissue through soluble and insoluble mediators, and guarantees its strength and elasticity through structural and mechanical constraints. Elastin is composed of flexible cross-linked polypeptides and has a linear stress-strain relation of up to 200%. Collagen, on the other hand, has a more organized structure with both crystalline and amorphous phases (Hulmes et al. 1995). Its fibers have a diameter in the range of 25–50 nm, while fiber bundles are several hundred micrometers (Baer et al. 1991). The fibers are undulated in the undeformed state and become stiff when straightened under the action

of externally applied loads. Collagen exhibits a highly nonlinear stress-strain curve. The overall strength of soft tissues is strongly correlated with the elastin-collagen content and morphological characteristics: fibril length, diameter, distribution and orientation (Cowi 2000). The collagen and elastin fibers are loosely woven and densely packed in an ordered way to form a three dimensional supportive network for smooth muscle bundles and other multiple cellular elements. Such structural organization of the tissue provides the required stability of the wall, allowing organs to undergo reversible changes in length, while also offering remarkable properties of stiffness and elasticity.

The fibrillary network is bridged and linked by the anionic glycos-aminoglycans (GAGs), long unbranched carbohydrate chains attached to a protein core of the small proteoglycans. The proteioglycan aggregates resist compression and shear forces thus securing the shape of the biocomposite. This property is attributed to the GAGs, which contain negatively charged sulfate and carboxyl groups that can generate large electrostatic repulsive forces (Buschmann and Grodzinsky 1995).

The morphostructural contractile unit of the gastric wall is the smooth muscle cell (myocyte). It has a characteristic spindle-like shape measuring ~100–250 μm in length and ~5–6 μm in diameter. Its cytoplasm contains a centrally located nucleus, intracellular thin α and β-actin (~6 nm), intermediate, mainly desmin (~10 nm) (Malmqvist et al. 1991), and thick (~20–25 nm) filaments, mitochondria and fairly sparse elements of the sarcoplasmic reticulum. Thin α and β-actin filaments are arranged into a lattice attached to the cell membrane at the sites of dense bands (plaques). They guarantee the integrity, strength and high degree of deformability of the wall and provide binding sites for myosin thick filaments of the SM1B and SM2B types (Martin et al. 2007).

Regularly spaced dense bands are comprised of multifunctional proteins: integrins, desmin, vincullin, tensin, calponin, nonmuscle β- and γ-actins and filamin (Mabuchi et al. 1997; Small et al. 1986; Small and Gimona 1997). They establish direct structural and functional contacts between the intracellular cytoskeleton and the ECM. The anchoring plaques play an essential role in transmitting forces of contraction-relaxation in the tissue, and act as mechanosensors in gene expression signaling pathways, cell migration, growth, and adaptation (Geiger and Ginsberg 1991; Yamada and Geiger 1997; Zamir and Geiger 2001).

Myocytes are arranged into SM fasciculi, $\simeq 300 \pm 100$ μm, and further assembled into bundles, ≃1–2 mm in length. They are embedded into a network of collagenous and elastin fibers and are coupled, via gap junctions, into three distinct syncytia (muscle layers). The external longitudinal muscle layer continues from the esophagus into the duodenum. The middle uniform circular layer is the strongest and completely covers the stomach whilst the circular fibers are best developed in the antrum and pylorus. At the pyloric end, the circular muscle layer greatly thickens to form the pyloric sphincter. The innermost oblique muscular layer is limited chiefly to the cardiac region. Although syncytia within the tissue are morphologically distinct, there are intermediate muscle bundles that pass from one layer to the other. The thickness of the muscle layers can vary greatly between individuals and the anatomical part of the organ.

Electron microscopy and freeze fracture studies convincingly demonstrate that individual myocytes are interconnected by small and irregular gap junctions. Confocal immunofluorescence shows that they are formed mainly by the subunit proteins connexins–26, 32, 43 (Maes et al. 2015). They provide the structural basis for cytoplasmic continuity, mediate the movement of ions and small molecules, and support propagation, synchronization and long range integration of excitation as well as mechanical coupling in the gastric tissue. It is noteworthy that connexin–43 is present only in the circular muscle layer and not in the longitudinal muscle cells of the antrum and the corpus of the human stomach. Gap junctions are found in the antrum and in the outermost area of the greater curvature of the organ but are absent in the fundus, the innermost area of the corporal circular muscle layer, and at the pylorus.

The outermost tunica serosa is formed of densely packed collagen and elastin fibers that coat the entire organ and thus dictates its final shape.

The distinctive anatomical configuration of the human stomach correlates with its structural advantages. The organ contains optimal space both within and outside, exhibits a high degree of reserved strength and structural integrity along with efficient biomechanical functionality, has optimal strength-to-weight ratio, and is ideal for resisting (supporting) internal pressure and external loads. Results of contrast-enhanced CT scans of stomachs of average-normal subjects demonstrate smooth thickening of the distal antrum $h \sim 3.5$–6.6 mm compared to the anterior wall of the body of the organ, $h \sim 1.6$–2.4 mm. The mean thickness h varies greatly with the distension of the stomach (Miftakhov 1981; Pickhardt and Asher 2003). The longitudinal (subscript l) length, from the pole of the fundus towards the sinus of the organ, measures $L_l \sim 20$–30 cm and the circumferential (subscripts c) length, taken from the lesser curvature to the greater curvature, $L_c \sim 10$–15 cm (Schulze 2006). Regardless of the small thickness of the gastric wall and its characteristic dimensions, it is capable of holding 2–5 l of mixed content without increasing intraluminal pressure.

Consider the gastric wall as a body bounded by two closely spaced curved surfaces at a distance h, i.e. the serosa and mucosa. This body is called the shell of thickness h. Let the faces of the shell be smooth with no singularities. The shell is classified as thin or thick based on the value of $h/L_{c,l}$. Thus, the shell is considered to be thin if $\max(h/L_{c,l}) \sim 10^{-5} \div 10^{-2}$, and thick otherwise. The above estimate is very rough and in many practical applications, other geometric and mechanical characteristics could also be considered. For example, in most industrial engineering applications where structures experience small deformations, the conventional criteria, $\max(hk_i) < 1/20$, where k_i are the principal curvatures of the middle surface S of the shell, i.e. the surface at $z = 0$, is used. Real time three dimensional ultrasonography studies of the human stomach under constant intraluminal pressure, $p = 68.6$ Pa, reveal regional dependence and high variability of the principal curvatures: $k_l \sim 0.5$–1.3 (cm^{-1}) and $k_c \sim 1.2$–11.4 (cm^{-1}) (Liao et al. 2004). Applying the above criteria to an organ which undergoes large deformations and displacements along with significant changes in configurations depending on intragastric pressure, will erroneously put the stomach in the category of thick shells.

1.2 Intrinsic Geometry

Let the human stomach be represented as a smooth surface S in three dimensional Euclidean space. Assume that every point of the wall is associated with the curvilinear coordinates α_1, α_2 and the unit normal vector $\bar{m}$, such that the distance along $\bar{m}$ is given by z $(-0.5h(\alpha_1, \alpha_2) \leq z \leq 0.5h(\alpha_1, \alpha_2))$. It is referred to a right-handed global orthogonal Cartesian system x_1, x_2, x_3. Let S also be associated with a set of independent parameters α_1 and α_2, such that

$$x_1 = f_1(\alpha_1, \alpha_2), x_2 = f_2(\alpha_1, \alpha_2), x_3 = f_3(\alpha_1, \alpha_2), \tag{1.1}$$

where f_j $(j = 1, 2, 3)$ are single-valued functions that possess derivatives up to any required order. Putting $\alpha_1 =$ const and varying the parameter α_2 in f_j (c, α_2), we obtain a curve that lies entirely on S. Successively giving α_1 a series of constant values we obtain a family of curves along which only a parameter α_2 varies. These curves are called the α_2—coordinate lines. Similarly, setting $\alpha_2 =$ const we obtain the α_1-coordinate lines of S. We assume that only one curve of the family passes through a point of the given surface. Thus, any point M on S can be treated as a cross-intersection of the α_1- and α_2 curvilinear coordinate lines.

The position of a point M with respect to the origin O of the reference system is defined by the position vector $\bar{r}$ (Fig. 1.2)

$$\bar{r} = \bar{i}_1 x_1 + \bar{i}_2 x_2 + \bar{i}_3 x_3 = \sum_{i=1}^{3} \bar{i}_i x_i,$$

where $\{\bar{i}_1, \bar{i}_2, \bar{i}_3\}$ is the orthonormal triad of unit vectors associated with $\{x_1, x_2, x_3\}$. By the virtue of Eqs. (1.2) it can be written in the form

$$\bar{r} = \bar{i}_1 f_1(\alpha_1, \alpha_2) + \bar{i}_2 f_2(\alpha_1, \alpha_2) + \bar{i}_3 f_3(\alpha_1, \alpha_2). \tag{1.2}$$

Eq. (1.2) is the vector equation of a surface. Differentiating $\bar{r}$ with respect to α_i $(i = 1, 2)$ vectors tangent to the α_1- and α_2-coordinate lines are found to be

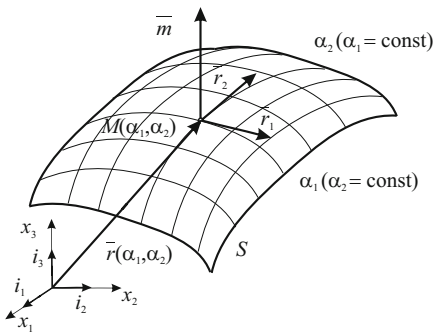

Fig. 1.2 Intrinsic parameterization of the surface

$$\bar{r}_1 = \frac{\partial \bar{r}}{\partial \alpha_1}, \quad \bar{r}_2 = \frac{\partial \bar{r}}{\partial \alpha_2}. \tag{1.3}$$

Modules and the scalar product of $\bar{r}_i$ $(i = 1, 2)$ are defined by

$$\begin{aligned} &|\bar{r}_1| = \bar{r}_1 \bar{r}_1 = A_1 = \sqrt{a_{11}}, \quad |\bar{r}_2| = \bar{r}_2 \bar{r}_2 = A_2 = \sqrt{a_{22}}, \\ &\bar{r}_1 \bar{r}_2 = A_1 A_2 \cos\chi = \sqrt{a_{12}}, \end{aligned} \tag{1.4}$$

where χ is the angle between coordinate lines, A_i are the Lamé parameters and a_{ik} are the coefficients of the metric tensor $\mathbf{A}$ on S. Using Eqs. (1.4) we introduce the unit vectors $\bar{e}_i$ in the direction of $\bar{r}_i$ which are described by

$$\bar{e}_1 = \frac{\bar{r}_1}{|\bar{r}_1|} = \frac{\bar{r}_1}{A_1}, \quad \bar{e}_2 = \frac{\bar{r}_2}{|\bar{r}_2|} = \frac{\bar{r}_2}{A_2}. \tag{1.5}$$

The vector $\bar{m}$ normal to $\bar{r}_1$ and $\bar{r}_2$ is found from

$$\bar{m} = \bar{r}_1 \times \bar{r}_2 \quad \text{and} \quad \bar{m}\bar{r}_1 = 0, \quad \bar{m}\bar{r}_2 = 0, \tag{1.6}$$

where $\bar{r}_1 \times \bar{r}_2$ is the vector product. The vectors $\bar{r}_1, \bar{r}_2$, and $\bar{m}$ are linearly independent and comprise a covariant base $\{\bar{r}_1, \bar{r}_2, \bar{m}\}$ on S. The reciprocal base $\{\bar{r}^1, \bar{r}^2, \bar{m}\}$ is defined by

$$\bar{r}^1 = \frac{\bar{r}_2 \times \bar{m}}{\bar{r}_1(\bar{r}_2 \times \bar{m})}, \quad \bar{r}^2 = \frac{\bar{m} \times \bar{r}_1}{\bar{r}_2(\bar{m} \times \bar{r}_1)}, \tag{1.7}$$

where $\bar{r}_i(\bar{m} \times \bar{r}_j)$ is the scalar triple product. Evidently, the vectors $\bar{r}^k$ and $\bar{r}_i$ are mutually orthogonal, i.e.

$$\bar{r}^k \bar{r}_i = \delta_i^k, \quad \bar{r}^k \bar{m} = 0.$$

Here δ_i^k is the Kronecker delta such that $\delta_i^k = 1$ if $i = k$ and $\delta_i^k = 0$ if $i \neq k$. Let $\bar{m}(\bar{r}_i \times \bar{r}_k) = c_{ik}$ and $\bar{m}(\bar{r}^i \times \bar{r}^k) = c^{ik}$. Hence,

$$\begin{aligned} &c_{ik}\bar{m} = \bar{r}_i \times \bar{r}_k, \quad c^{ik}\bar{m} = \bar{r}^i \times \bar{r}^k, \\ &c_{ik}\bar{r}^k = \bar{m} \times \bar{r}_i, \quad c^{ik}\bar{r}_i = \bar{m} \times \bar{r}^i. \end{aligned} \tag{1.8}$$

It follows that

$$\begin{aligned} &c^{ii} = 0, \quad c^{12} = -c^{12} = 1/\sqrt{a}, \quad a = (A_1 A_2 \sin\chi)^2 \\ &c_{ii} = 0, \quad c_{12} = -c_{12} = \sqrt{a}, \end{aligned} \tag{1.9}$$

$$c_{ik}c^{km} = \delta^m{}_i, \quad c_{ik}c^{ki} = \delta^i{}_i = 2, \quad (i, k = 1, 2) \tag{1.10}$$

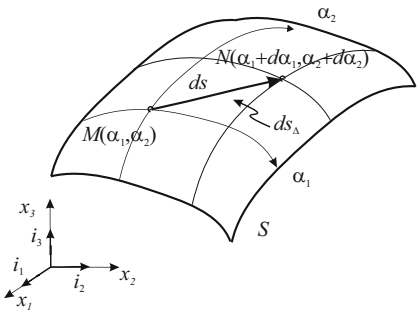

Fig. 1.3 First fundamental form of the surface

The length of a line element between two infinitely close points $M\,(x_1, x_2, x_3)$ and $N\,(x_1 + dx_1,\, x_2 + dx_2\,, x_3 + dx_3)$ (Fig. 1.3) is given by

$$ds^2 = {dx_1}^2 + {dx_2}^2 + {dx_3}^2 = |d\bar{r}|^2 = |\bar{r}_i d\alpha_i|^2.$$

Using Eqs. (1.4) in the above we have

$$ds^2 = A_1^2 d\alpha_1^2 + 2A_1 A_2 \cos\chi d\alpha_1 d\alpha_2 + A_2^2 d\alpha_2^2 = a_{ik} d\alpha_i d\alpha_k. \tag{1.11}$$

The quadratic form (Eq. 1.11) is called the first fundamental form of the surface. It allows us to calculate the length of line elements, the angle between coordinate curves and the surface area

$$ds_\Delta = |\bar{r}_1 \times \bar{r}_2| d\alpha_1 d\alpha_2 = \sqrt{a}\, d\alpha_1 d\alpha_2, \tag{1.12}$$

and therefore, it fully describes the intrinsic geometry of S.

1.3 Extrinsic Geometry

Let Γ be a non-singular curve on S parameterized by arc length s (Fig. 1.4)

$$\bar{r} = \bar{r}(s) = \bar{r}(\alpha_1(s), \alpha_2(s)).$$

Differentiating $\bar{r}(s)$ with respect to s the unit vector $\overline{\tau}$ tangent to Γ is found to be

$$\overline{\tau} = \frac{d\bar{r}}{ds} = \bar{r}_1 \frac{d\alpha_1}{ds} + \bar{r}_2 \frac{d\alpha_2}{ds}. \tag{1.13}$$

Applying the Frenet-Serret formula, for the derivative of $\overline{\tau}$ with respect to s we get

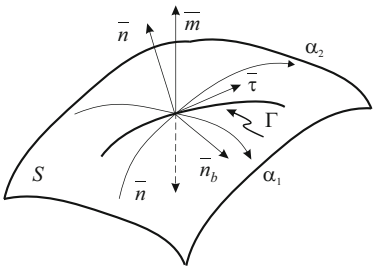

Fig. 1.4 Extrinsic geometry of the surface and a local base $\{\bar{n}, \bar{n}_b, \bar{\tau}\}$ associated with a curve Γ

$$\frac{d\bar{\tau}}{ds} = \frac{\bar{n}}{R_c}, \tag{1.14}$$

where $1/R_c$ is the curvature and $\bar{n}$ is the vector normal to Γ. Substituting Eq. (1.7) into (1.8) we obtain

$$\bar{n} = \sum_{i=1}^{2} \sum_{k=1}^{2} \bar{r}_{ik} \frac{d\alpha_i}{ds} \frac{d\alpha_k}{ds} + \bar{r}_1 \frac{d\alpha_1^2}{ds} + \bar{r}_2 \frac{d\alpha_2^2}{ds} \tag{1.15}$$

where

$$\bar{r}_{ik} = \frac{\partial^2 \bar{r}}{\partial \alpha_i \partial \alpha_k} = \frac{\partial^2 \bar{r}}{\partial \alpha_k \partial \alpha_i}, \quad \bar{r}_{ik} = \bar{r}_{ki}.$$

Let φ be the angle between the vectors $\bar{m}$ and $\bar{n}$ such that $\bar{m}\bar{n} = \cos\varphi$. Then the scalar product of Eq. (1.15) by $\bar{m}$ yields

$$\frac{\cos\varphi}{R_c} = \frac{b_{11} d\alpha_1^2 + 2b_{12} d\alpha_1 d\alpha_2 + b_{22} d\alpha_2^2}{ds^2}, \tag{1.16}$$

where

$$b_{11} = \bar{m}\bar{r}_{11}, \quad b_{12} = \bar{m}\bar{r}_{12} = \bar{m}\bar{r}_{21}, \quad b_{22} = \bar{m}\bar{r}_{22}. \tag{1.17}$$

The quadratic form

$$b_{11} d\alpha_1^2 + 2b_{12} d\alpha_1 d\alpha_2 + b_{22} d\alpha_2^2$$

is called the second fundamental form of the surface. Differentiating Eq. (1.6) with respect to α_i we find

$$b_{ik} = -\bar{m}_i \bar{r}_k = -\bar{m}_i \bar{r}_i, \tag{1.18}$$

here

$$\bar{m}_i = \frac{\partial \bar{m}}{\partial \alpha_i}. \tag{1.19}$$

A normal section at $\forall M(\alpha_1, \alpha_2) \in S$ is the section by some plane that contains the vector $\bar{m} \perp S$. Assuming $\varphi = \pi$, which implies that $\bar{m}$ and $\bar{n}$ are oriented in opposite directions, from Eq. (1.10) for the curvature of the normal section $1/R_n$, we obtain

$$-\frac{1}{R_n} = \frac{b_{11}d\alpha_1^2 + 2b_{12}d\alpha_1 d\alpha_2 + b_{22}d\alpha_2^2}{A_1^2 d\alpha_1^2 + 2A_1A_2 d\alpha_1 d\alpha_2 + A_2^2 d\alpha_2^2}. \tag{1.20}$$

Henceforth, we assume that the coordinate lines are arranged in such a way that $\bar{m}$ is positive when pointing from the concave to the convex side of the surface. Putting $\alpha_2 = \text{const}$ and $\alpha_1 = \text{const}$ in Eq. (1.20), for the curvatures k_{11}, k_{22} of the normal sections in the direction of α_1, α_2 we find

$$\frac{1}{R_{\alpha_1}} := k_{11} = -\frac{b_{11}}{A_1^2}, \quad \frac{1}{R\alpha_2} := k_{22} = -\frac{b_{22}}{A_2^2}, \tag{1.21a}$$

and the twist k_{12} of the surface

$$\frac{1}{R_{\alpha_1\alpha_2}} := k_{12} = -\frac{b_{12}}{A_1 A_2}. \tag{1.21b}$$

It becomes evident from the above considerations that the second fundamental form describes the intrinsic geometry of the surface.

At any point $M(\alpha_1, \alpha_2) \in S$ there exist two normal sections where $1/R_n$ assumes extreme values. They are called principal sections. Two perpendicular directions at M belonging to the corresponding tangent plane are called the principal directions and the principal curvatures $(1/R)_{\max} = 1/R_1$, and $(1/R)_{\min} = 1/R_2$ (Fig. 1.5). Thus, there is at least one set of principal directions at any point on S. A curve on the surface such that the tangent at any point to it is collinear with the principal direction is called the line of curvature. Thus, two lines of curvature intersect at right-angles and pass through each point of S. We assume that the coordinate lines

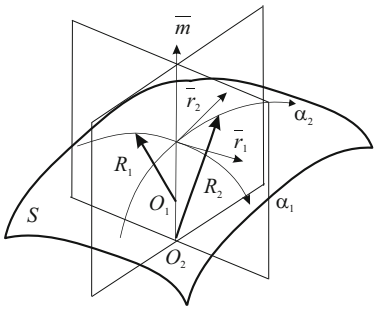

Fig. 1.5 Normal curvatures R_1, R_2 of the surface

α_1, α_2 are the lines of curvature ($\chi = \pi/2$, $b_{12} = 0$). Such coordinates have an advantage over other coordinate systems since the governing equations in them have a relatively simple form.

Let $\bar{r}_{ik}$ be second derivatives of the position vector with respect to $\alpha_{i(k)}$ ($i, k = 1, 2$). Decomposing $\bar{r}_{ik}$ with respect to the covariant base $\{\bar{r}_1, \bar{r}_2, \bar{m}\}$ we get

$$\bar{r}_{ik} = \Gamma^1_{ik}\bar{r}_1 + \Gamma^2_{ik}\bar{r}_2 + \bar{m}b_{ik}. \tag{1.22a}$$

Here Γ^j_{ik} ($\Gamma^j_{ik} = \bar{r}^j\bar{r}_{ik}$) are the Christoffel symbols of the second kind. Multiplying subsequently both sides of Eq. (1.22a) by $\bar{r}_1$ and $\bar{r}_2$, and making use of Eqs. (1.4), (1.6) we find

$$\begin{aligned}\bar{r}_1\bar{r}_{ik} &= \Gamma^1{}_{ik}A_1^2 + \Gamma^2{}_{ik}A_1A_2\cos\chi\\ \bar{r}_2\bar{r}_{ik} &= \Gamma^1{}_{ik}A_1A_2\cos\chi + \Gamma^2{}_{ik}A_2^2.\end{aligned}$$

Solving the system with respect to Γ^j_{ik} we obtain

$$\begin{aligned}a\Gamma^1_{ik} &= A_2^2(\bar{r}_1\bar{r}_{ik}) - A_1A_2\cos\chi(\bar{r}_2\bar{r}_{ik})\\ a\Gamma^2_{ik} &= A_1^2(\bar{r}_2\bar{r}_{ik}) - A_1A_2\cos\chi(\bar{r}_1\bar{r}_{ik})\end{aligned} \tag{1.22b}$$

Differentiating $\bar{r}_1^2 = A_1^2, \bar{r}_2^2 = A_2^2$ and $\bar{r}_1\bar{r}_2 = A_1A_2\cos\chi$ with respect to α_1 and α_2, we find

$$\bar{r}_i\bar{r}_{ii} = A_i\frac{\partial A_i}{\partial\alpha_1}, \quad \bar{r}_1\bar{r}_{12} = A_1\frac{\partial A_1}{\partial\alpha_2}, \quad \bar{r}_2\bar{r}_{12} = A_2\frac{\partial A_2}{\partial\alpha_1} \tag{1.22c}$$

$$\bar{r}_2\bar{r}_{11} + \bar{r}_1\bar{r}_{12} = \frac{\partial a_{12}}{\partial\alpha_1} = a_{12,1} \tag{1.22d}$$

$$\bar{r}_2\bar{r}_{12} + \bar{r}_1\bar{r}_{22} = \frac{\partial a_{12}}{\partial\alpha_2} = a_{12,2}, \tag{1.22e}$$

here $a_{12} = a_{21} = A_1A_2\cos\chi$, $a_{12,i} = \frac{\partial a_{12}}{\partial\alpha_1}$. From (1.22c) and (1.22d, 1.22e) we have

$$\begin{aligned}\bar{r}_2\bar{r}_{11} &= \frac{\partial a_{12}}{\partial\alpha_1} - A_1\frac{\partial A_1}{\partial\alpha_2},\\ \bar{r}_1\bar{r}_{12} &= \frac{\partial a_{12}}{\partial\alpha_2} - A_2\frac{\partial A_2}{\partial\alpha_1}.\end{aligned} \tag{1.22f}$$

Substituting expressions (1.22c) and (1.22f) into (1.22b) we obtain

$$
\begin{aligned}
a\Gamma_{11}^{1} &= A_1 A_2^2 \frac{\partial A_1}{\partial \alpha_1} - a_{12}\left(\frac{\partial a_{12}}{\partial \alpha_1} - A_1 \frac{\partial A_1}{\partial \alpha_2}\right) \\
a\Gamma_{12}^{1} &= A_1 A_2^2 \frac{\partial A1}{\partial \alpha_2} - A_2 a_{12} \frac{\partial A_2}{\partial \alpha_1} \\
a\Gamma_{22}^{1} &= A_2^2 \frac{\partial a_{12}}{\partial \alpha_2} - A_2^3 \frac{\partial A_2}{\partial \alpha_1} - A_2 a_{12} \frac{\partial A_2}{\partial \alpha_2} \\
a\Gamma_{22}^{2} &= A_2 A_1^2 \frac{\partial A_2}{\partial \alpha_2} - a_{12}\left(\frac{\partial a_{12}}{\partial \alpha 2} - A_2 \frac{\partial A_2}{\partial \alpha_1}\right) \\
a\Gamma_{12}^{2} &= A_2 A_1^2 \frac{\partial A_2}{\partial \alpha_1} - A_1 a_{12} \frac{\partial A_1}{\partial \alpha_2} \\
a\Gamma_{11}^{2} &= A_1^2 \frac{\partial a_{12}}{\partial \alpha 1} - A_1^3 \frac{\partial A_1}{\partial \alpha_2} - A_1 a_{12} \frac{\partial A_1}{\partial \alpha_1}
\end{aligned}
\tag{1.23}
$$

Derivatives of the normal vector $\bar{m}$ with respect to α_i, lay in the tangent plane $(\bar{r}_1, \bar{r}_2)$ of S. Decomposing $\bar{m}_i (i = 1, 2)$ along $\bar{r}_i$ we get

$$
\bar{m}_i = -b_i^1 \bar{r}_1 - b_i^2 \bar{r}_2, \tag{1.24}
$$

where b_i^1, b_i^2 are the mixed coefficients of the second fundamental form. The scalar product of Eq. (1.24) by $\bar{r}_1$ and $\bar{r}_2$, respectively, yields

$$
\begin{aligned}
\bar{m}_i \bar{r}_1 &= -b_i^1 \bar{r}_1^2 - b_i^2 \bar{r}_2 \bar{r}_1, \\
\bar{m}_i \bar{r}_2 &= -b_i^1 \bar{r}_1 \bar{r}_2 - b_i^2 \bar{r}_2^2.
\end{aligned}
$$

Using Eqs. (1.4), (1.18), b_{1i}, b_{2i} are found to be

$$
\begin{aligned}
b_{1i} &= A_1^2 b_i^1 + a_{12} b_i^2, \\
b_{2i} &= A_2^2 b_i^2 + a_{12} b_i^1.
\end{aligned}
\tag{1.25}
$$

It is easy to show that

$$
\begin{aligned}
b_i^1 &= \frac{1}{A_1 \sin^2 \chi}\left(\frac{b_{i1}}{A_1} - \frac{b_{i2}}{A_2}\cos\chi\right) \\
b_i^2 &= \frac{1}{A_2 \sin^2 \chi}\left(\frac{b_{i2}}{A_2} - \frac{b_{i1}}{A_1}\cos\chi\right)
\end{aligned}
\tag{1.26}
$$

Assuming that the surface is referred to orthogonal coordinates $\chi = \pi/2$, $a_{12} = a_{12} = 0$, $a = (A_1 A_2)^2$, Eqs. (1.23) take the form

$$\begin{aligned}
\Gamma_{11}^1 &= \frac{1}{A_1}\frac{\partial A_1}{\partial \alpha_1}, \quad \Gamma_{12}^1 = \frac{1}{A_1}\frac{\partial A_1}{\partial \alpha_2} \quad \Gamma_{22}^1 = -\frac{A_2}{A_1^2}\frac{\partial A_2}{\partial \alpha_1}, \\
\Gamma_{22}^2 &= \frac{1}{A_2}\frac{\partial A_2}{\partial \alpha_2}, \quad \Gamma_{12}^2 = \frac{1}{A_2}\frac{\partial A_2}{\partial \alpha_1}, \quad \Gamma_{11}^2 = -\frac{A_1}{A_2^2}\frac{\partial A_1}{\partial \alpha_2}
\end{aligned} \tag{1.27}$$

Substituting Eqs. (1.27) into Eq. (1.22a) and making use of Eqs. (1.5), (1.22b, 1.22c), the formulas for derivatives of unit vectors $\bar{e}_1$ and $\bar{e}_2$ are found to be

$$\begin{aligned}
\frac{\partial \bar{e}_1}{\partial \alpha_1} &= -\frac{\bar{e}_2}{A_2}\frac{\partial A_1}{\partial \alpha_2} - A_1 k_{11}\bar{m}, \quad \frac{\partial \bar{e}_1}{\partial \alpha_2} = -\frac{\bar{e}_2}{A_1}\frac{\partial A_2}{\partial \alpha_1} - A_2 k_{12}\bar{m} \\
\frac{\partial \bar{e}_2}{\partial \alpha_1} &= -\frac{\bar{e}_1}{A_2}\frac{\partial A_1}{\partial \alpha_2} - A_1 k_{12}\bar{m}, \quad \frac{\partial \bar{e}_2}{\partial \alpha_2} = -\frac{\bar{e}_1}{A_1}\frac{\partial A_2}{\partial \alpha_1} - A_2 k_{22}\bar{m}.
\end{aligned} \tag{1.28}$$

From Eqs. (1.24) we have

$$A_1^2 b_i^1 = b_{1i}, \quad A_2^2 b_i^1 = b_{i2},$$

from where, using Eqs. (1.18), we get

$$A_1 b_i^1 = -A_i k_{1i}, \quad A_2 b_i^1 = -A_i k_{2i}.$$

Substituting the above into Eq. (1.24), and using Eq. (1.5), we obtain

$$\bar{m}_i = A_i(k_{1i}\bar{e}_i + k_{2i}\bar{e}_i) \tag{1.29}$$

If the coordinate lines are the lines of principal curvature ($k_{12} = 0, k_{ii} = 1/R_i$), Eqs. (1.28) and (1.29) can be simplified to take the form

$$\frac{\partial \bar{e}_1}{\partial \alpha_1} = -\frac{\bar{e}_2}{A_2}\frac{\partial A_1}{\partial \alpha_2} - \bar{m}\frac{A_1}{R_1}, \quad \frac{\partial \bar{e}_1}{\partial \alpha_2} = \frac{\bar{e}_2}{A_1}\frac{\partial A_2}{\partial \alpha_1},$$

$$\frac{\partial \bar{e}_2}{\partial \alpha_1} = \frac{\bar{e}_1}{A_1}\frac{\partial A_1}{\partial \alpha_2}, \quad \frac{\partial \bar{e}_2}{\partial \alpha_2} = -\frac{\bar{e}}{A_1}\frac{\partial A_2}{\partial \alpha_1} - \bar{m}\frac{A_2}{R_2}.$$

$$R_i \bar{m}_i = A_i \bar{e}_i \tag{1.30}$$

1.4 Equations of Gauss and Codazzi

Coefficients of the first and second fundamental forms are interdependent and satisfy the three differential Gauss-Codazzi equations. The Gauss formula defines the Gaussian curvature K of the surface

$$K = \frac{1}{R_1 R_2} = \frac{b_{11} - b_{12}^2}{a} = \frac{A_1 A_2 \left(k_{11} k_{22} - k_{12}^2\right)}{a}. \tag{1.31}$$

With the help of Eqs. (1.21a, 1.21b), (1.26) it can be written in the form

$$\frac{b_{11} - b_{12}^2}{A_1 A_2 \sin\chi} = \frac{\partial^2 \chi}{\partial\alpha_1 \partial\alpha_2} + \frac{\partial}{\partial\alpha_1} \frac{\frac{\partial A_2}{\partial\alpha_1} - \cos\chi \frac{\partial A_1}{\partial\alpha_2}}{A_1 \sin\chi} + \frac{\partial}{\partial\alpha_2} \frac{\frac{\partial A_1}{\partial\alpha_2} - \cos\chi \frac{\partial A_2}{\partial\alpha_1}}{A_2 \sin\chi} \tag{1.32}$$

To derive the Codazzi equations we proceed from

$$\frac{\partial b_{11}}{\partial\alpha_2} - \frac{\partial b_{12}}{\partial\alpha_1} = -\frac{\partial \bar{r}_1 \bar{m}_1}{\partial\alpha_2} + \frac{\partial \bar{r}_2 \bar{m}_2}{\partial\alpha_1} = -\bar{m}_1 \bar{r}_{12} + \bar{m}_2 \bar{r}_{22}.$$

Substituting $\bar{r}_{ik}$ given by Eqs. (1.22a) the first Codazzi equation is found to be

$$\frac{\partial b_{11}}{\partial\alpha_2} - \frac{\partial b_{12}}{\partial\alpha_1} = -\bar{m}_1 \left(\Gamma_{12}^1 \bar{r}_1 + \Gamma_{12}^2 \bar{r}_2\right) + \bar{m}_2 \left(\Gamma_{11}^1 \bar{r}_1 + \Gamma_{11}^2 \bar{r}_2\right) =$$

$$= \Gamma_{12}^1 b_{11} + \left(\Gamma_{12}^2 - \Gamma_{11}^2\right) b_{12} - \Gamma_{11}^2 b_{22}. \tag{1.33}$$

Here use is made of Eq. (1.18) and the fact that $\bar{m}_i \bar{m} = 0$.

Similarly, proceeding from the difference $\frac{\partial b_{22}}{\partial\alpha_1} - \frac{\partial b_{12}}{\partial\alpha_2}$ and repeating the steps as above, we obtain the second Codazzi equation

$$\frac{\partial b_{22}}{\partial\alpha_1} - \frac{\partial b_{12}}{\partial\alpha_2} = \Gamma_{12}^1 b_{22} + \left(\Gamma_{12}^1 - \Gamma_{22}^2\right) b_{12} - \Gamma_{22}^1 b_{11}. \tag{1.34}$$

The Chrystoffel symbols Γ_{ik}^j in (1.26a,b) satisfy (1.17).

Substituting Eqs. (1.21a, 1.21b) into the left-hand side of Eq. (1.34), we get

$$\frac{\partial b_{11}}{\partial\alpha_2} - \frac{\partial b_{12}}{\partial\alpha_1} = A_1 \left(\frac{\partial A_1 k_{12}}{\partial\alpha_1} - \frac{\partial A_1 k_{11}}{\partial\alpha_2}\right) + A_2 k_{12} \frac{\partial A_1}{\partial\alpha_1} - A_1 k_{11} \frac{\partial A_1}{\partial\alpha_2}. \tag{1.35}$$

On using Eq. (1.35) in (1.33) and dividing the resultant equation by $-A_1$and $-A_2$, respectively, we obtain

$$\begin{aligned}
&\frac{\partial A_1 k_{11}}{\partial \alpha_2} - \frac{\partial A_2 k_{12}}{\partial \alpha_1} + k_{11}\left(\frac{\partial A_1}{\partial \alpha_2} - A_1\Gamma_{12}^1\right) - \\
&-A_2 k_{12}\left(\frac{1}{A_1}\frac{\partial A_1}{\partial \alpha_1} - \Gamma_{11}^1 + \Gamma_{12}^2\right) - \frac{A_2^2 k_{22}\Gamma_{11}^1}{A_1} = 0, \quad A_2^2 = (A_2)^2. \\
&\frac{\partial A_2 k_{22}}{\partial \alpha_1} - \frac{\partial A_1 k_{12}}{\partial \alpha_2} + k_{22}\left(\frac{\partial A_2}{\partial \alpha_1} - A_2\Gamma_{12}^2\right) - \\
&-A_1 k_{12}\left(\frac{1}{A_2}\frac{\partial A_2}{\partial \alpha_2} - \Gamma_{22}^2 + \Gamma_{12}^1\right) - \frac{A_1^2 k_{11}\Gamma_{22}^2}{A_2} = 0.
\end{aligned} \tag{1.36}$$

In the case of orthogonal coordinates Eqs. (1.32), (1.36) can be written in the form

$$\begin{aligned}
&\frac{\partial}{\partial \alpha_1}\left(\frac{1}{A_1}\frac{\partial A_2}{\partial \alpha_1}\right) + \frac{\partial}{\partial \alpha_2}\left(\frac{1}{A_2}\frac{\partial A_1}{\partial \alpha_2}\right) = A_1 A_2\left(k_{12}^2 - k_{11}k_{22}\right) = -\frac{A_1 A_2}{R_1 R_2}, \\
&\frac{\partial A_1 k_{11}}{\partial \alpha_2} - \frac{\partial A_2 k_{12}}{\partial \alpha_1} - k_{12}\frac{\partial A_2}{\partial \alpha_1} - k_{22}\frac{\partial A_1}{\partial \alpha_2} = 0, \\
&\frac{\partial A_2 k_{22}}{\partial \alpha_1} - \frac{\partial A_1 k_{12}}{\partial \alpha_2} - k_{12}\frac{\partial A_1}{\partial \alpha_2} - k_{11}\frac{\partial A_2}{\partial \alpha_1} = 0.
\end{aligned} \tag{1.37}$$

Here use is made of Eq. (1.27) for the Christoffel symbols Γ_{ik}^j.

If the coordinate lines are the lines of curvature ($k_{12} = 0, k_{ii} = 1/R_i$), then Eqs. (1.37) take the simpliest form

$$\begin{aligned}
&\frac{\partial}{\partial \alpha_1}\left(\frac{1}{A_1}\frac{\partial A_2}{\partial \alpha_1}\right) + \frac{\partial}{\partial \alpha_2}\left(\frac{1}{A_2}\frac{\partial A_1}{\partial \alpha_2}\right) = -\frac{A_1 A_2}{R_1 R_2} \\
&\frac{\partial}{\partial \alpha_2}\left(\frac{A_1}{R_1}\right) = \frac{1}{R_2}\left(\frac{\partial A_1}{\partial \alpha_1}\right), \quad \frac{\partial}{\partial \alpha_1}\left(\frac{A_2}{R_2}\right) = \frac{1}{R_1}\left(\frac{\partial A_2}{\partial \alpha_1}\right).
\end{aligned} \tag{1.38}$$

1.5 General Curvilinear Coordinates

Consider a non-singular surface S_z that is located at a distance z to S and $S_z \| S$. Let $\overline{\rho}$ be the position vector of a point $M_z \in S_z$ (Fig. 1.6)

$$\overline{\rho}(\alpha_1, \alpha_2) = \bar{r}(\alpha_1, \alpha_2) + z\bar{m}(\alpha_1, \alpha_2). \tag{1.39}$$

Here z is the normal distance measured from the point $M \in S$ and to M_z. Differentiating Eq. (1.39) with respect to α_i and z, we find

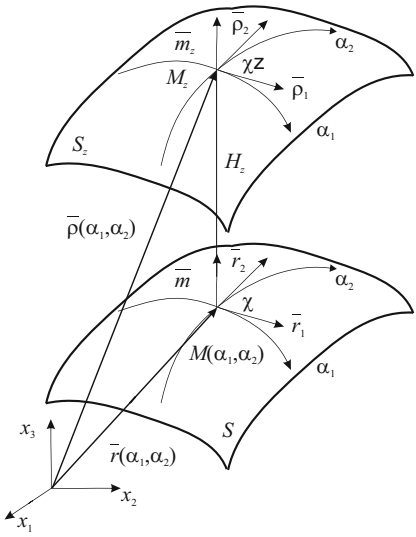

Fig. 1.6 Parameterization of the equidistant surface S_z

$$\overline{\rho}_i = \frac{\partial \overline{\rho}}{\partial \alpha_i} = \bar{r}_i + \bar{m}_i z, \quad \overline{\rho}_3 = \frac{\partial \overline{\rho}}{\partial z} = \bar{m}_i. \tag{1.40}$$

The vectors $\overline{\rho}_1, \overline{\rho}_2$ are tangent to the α_1, α_2-coordinate lines and are linearly independent. Thus, together with $\overline{\rho}_3$, they comprise a local base $\{\overline{\rho}_1, \overline{\rho}_2, \overline{\rho}_3\}$ at M_z.

Substituting $\bar{m}_i$ given by Eq. (1.24) into (1.40), we get

$$\overline{\rho}_1 = \bar{r}_1\left(1 - zb_1^1\right) - \bar{r}_1 z b_1^2, \quad \overline{\rho}_2 = \bar{r}_2\left(1 - zb_2^2\right) - \bar{r}_1 z b_1^1, \quad \overline{\rho}_3 = \bar{m}. \tag{1.41}$$

If the coordinate system is orthogonal then using Eq. (1.29) for $\bar{m}_i$ we obtain

$$\overline{\rho}_i = A_i \bar{e}_i + (A_i k_{1i} \bar{e}_1 + k_{2i} \bar{e}_2) z, \quad \overline{\rho}_3 = \bar{m}. \tag{1.42}$$

Further, if the coordinate lines are the lines of curvature, Eqs. (1.42) become

$$\overline{\rho}_i = A_i \bar{e}_i + (1 + z/R_i), \quad \overline{\rho}_3 = \bar{m}. \tag{1.43}$$

The scalar product of Eqs. (1.41) and (1.42) by $\bar{m}$, yields

$$\overline{\rho}_i \bar{m} = 0. \tag{1.44}$$

Let g_{ik} and H_i be the scalar product of $\overline{\rho}_i$ and $\overline{\rho}_k$ in general and orthogonal curvilinear coordinates, respectively,

$$g_{ik} = \overline{\rho}_i \overline{\rho}_k \quad (i, k = 1, 2) \tag{1.45}$$

$$H_i = |\overline{\rho}_i|, \tag{1.46}$$

H_i are the Lamé coefficients of S_z. The unit vectors $\bar{e}_i^z \in S_z$ are given by

$$\bar{e}_i^z = \frac{\overline{\rho}_i}{H_i}, \tag{1.47}$$

Making use of Eqs. (1.42) in (1.47), for $\bar{e}_1^z$, $\bar{e}_2^z$ we find

$$\begin{aligned} \bar{e}_1^z &= \frac{A_1}{H_1}(\bar{e}_1 + \bar{e}_1 k_{11} z + \bar{e}_2 k_{12} z), \\ \bar{e}_2^z &= \frac{A_2}{H_2}(\bar{e}_2 + \bar{e}_2 k_{22} z + \bar{e}_1 k_{12} z). \end{aligned} \tag{1.48}$$

One use of Eqs. (1.42) and (1.47) in (1.48), after simple algebra, we obtain

$$\begin{aligned} H_1 &= A_1\sqrt{(1+k_{11}z)^2 + k_{12}z^2} = A_1(1 + k_{11}z + \ldots) \\ H_2 &= A_2\sqrt{(1+k_{22}z)^2 + k_{12}z^2} = A_2(1 + k_{22}z + \ldots). \end{aligned} \tag{1.49}$$

In Eqs. (1.49) we neglected terms $O(z^2)$. Such approximation is proven to be satisfactory for z sufficiently small compared to the degree of accuracy required in practical applications. If the coordinate lines are the lines of curvature, $k_{12} = 0$, the formulas (1.49) become accurate

$$H_i = A_i(1 + k_{ii}z) = A_i(1 + k_{11}z/R_{ii}) \tag{1.50}$$

Also the unit vectors $\bar{e}_i^z \in S_z$ and $\bar{e}_i \in S$ become identical if the chosen coordinate lines are the lines of curvature. Indeed, by setting $k_{12} = 0$ in Eq. (1.48) and using formula (1.50), we obtain

$$\bar{e}_1^z = \bar{e}_1, \quad \bar{e}_2^z = \bar{e}_2. \tag{1.51}$$

The length of a line element on S_z is given by

$$\begin{aligned} (ds^z)^2 = |d\overline{\rho}|^2 = |\overline{\rho}_1 d\alpha_1 + \overline{\rho}_2 d\alpha_2 + \bar{m}dz|^2 = \\ = g_{11}d\alpha_1^2 + 2g_{12}d\alpha_1 d\alpha_2 + dz^2, \end{aligned} \tag{1.52}$$

Substituting Eqs. (1.39) into Eq. (1.45), we get

$$g_{ik} = \bar{r}_i \bar{r}_k + 2\bar{m}_i \bar{r}_k z + \bar{m}_i \bar{m}_k z^2.$$

Further, with the help of Eqs. (1.4), (1.24), we obtain

$$\begin{aligned} g_{ik} &= A_i(1 + 2k_{ii}z) + (\bar{m}_i z)^2, \\ g_{12} &= A_1A_2(\cos\chi + 2k_{12}z) + \bar{m}_1\bar{m}_2z^2 \end{aligned} \tag{1.53}$$

Neglecting higher-order terms $O(z^2)$, we find

$$g_{ik} = A_i(1 + 2k_{ii}z), \quad g_{12} = A_1A_2(\cos\chi + 2k_{12}z) \tag{1.54}$$

Assume the coordinate system is orthogonal $g_{12} = \overline{\rho}_1\overline{\rho}_2 = 0$. Hence from Eq. (1.54) we have $k_{12}z \approx 0$. Note, that the condition (1.51) remains valid in orthogonal coordinates even if the coordinate lines are not the lines of curvature.

Let χ^z be the angle between coordinate lines on S_z. Since

$$g_{12} = \overline{\rho}_1\overline{\rho}_2 = |\overline{\rho}_1| \cdot |\overline{\rho}_2| \cos\chi^z,$$

then

$$\cos\chi^z = \frac{g_{12}}{|\overline{\rho}_1| \cdot |\overline{\rho}_2|} = \frac{g_{12}}{\sqrt{g_{11}g_{12}}}$$

Using Eqs. (1.54), we get

$$\cos\chi^z = \frac{\cos\chi + 2k_{12}z}{\sqrt{(1 + 2k_{11}z)(1 + 2k_{22}z)}}. \tag{1.55}$$

We conclude this section with some useful formulas for the cross product of vectors

$$\begin{aligned} &H_2(\overline{\rho}_1 \times \bar{m}) = -\overline{\rho}_2H_1, \quad H_1(\overline{\rho}_2 \times \bar{m}) = \overline{\rho}_1H_2, \quad H_1H_2(\overline{\rho}_1 \times \overline{\rho}_2) = \bar{m}, \\ &A_2(\bar{r}_1 \times \bar{m}) = -A_1\bar{r}_2, \quad A_1(\bar{r}_2 \times \bar{m}) = A_2\bar{r}_1, \quad A_1A_2(\bar{r}_1 \times \bar{r}_2) = \bar{m}, \end{aligned} \tag{1.56}$$

$$(\bar{e}_1 \times \bar{m}) = \bar{e}_2, \quad (\bar{e}_2 \times \bar{m}) = \bar{e}_1, \quad (\bar{e}_1 \times \bar{e}_2) = \bar{m}. \tag{1.57}$$

1.6 Deformation of the Surface

As a result of deformation the surface S changes into a new surface $\overset{*}{S}$ with a point $M \in S$ sent into the point $\overset{*}{M} \in \overset{*}{S}$. Henceforth, all quantities that refer to the deformed configuration we shall designate by an asterisk (*) unless otherwise specified. Let $\overline{\nu}$ (α_1, α_2) be the vector of displacement of point M. Then the position of $\overset{*}{M}$ after deformation (Fig. 1.7) is described by

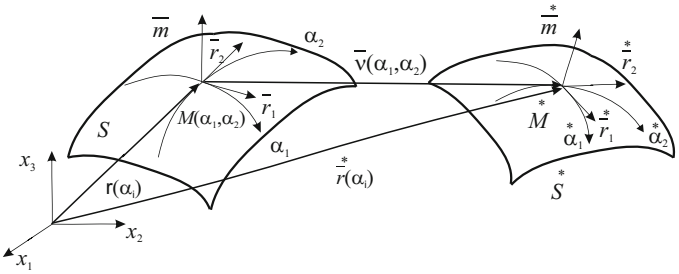

Fig. 1.7 Deformation of the surface

$$\overset{*}{\bar{r}}(\alpha_1,\alpha_2) = \bar{r}(\alpha_1,\alpha_2) + \bar{\nu}(\alpha_1,\alpha_2). \tag{1.58}$$

Projections of $\bar{\nu}$ onto the base $\{\bar{e}_1, \bar{e}_2, \bar{m}\}$ are given by

$$u_1 = \bar{\nu}\bar{e}_1 = \bar{\nu}\bar{r}_1/A_1, \quad u_2 = \bar{\nu}\bar{e}_2 = \bar{\nu}\bar{r}_2/A_2 \quad \omega = \bar{\nu}\bar{m}. \tag{1.59}$$

Hence

$$\bar{\nu} = u_1\bar{e}_1 + u_2\bar{e}_2 + \omega\bar{m}, \tag{1.60}$$

where u_1, u_2 are the tangent, and ω is the normal displacement (deflection), respectively.

Differentiating Eq. (1.58) with respect to α_i and using Eqs. (1.28), (1.29), we find

$$\begin{aligned} \overset{*}{\bar{r}}_1 &= A_1\{(1+e_{11})\bar{e}_1 + e_{12}\bar{e}_2 + \bar{m}\varpi_1\}, \\ \overset{*}{\bar{r}}_2 &= A_2\{e_{21}\bar{e}_1 + (1+e_{22})\bar{e}_2 + \bar{m}\varpi_2\}, \end{aligned} \tag{1.61}$$

where

$$\begin{aligned} e_{11} &= \frac{1}{A_1}\frac{\partial u_1}{\partial\alpha_1} + \frac{u_2}{A_1A_2}\frac{\partial A_1}{\partial\alpha_2} + k_{11}\omega, \quad & e_{22} &= \frac{1}{A_2}\frac{\partial u_2}{\partial\alpha_2} + \frac{u_1}{A_1A_2}\frac{\partial A_2}{\partial\alpha_1} + k_{22}\omega \\ e_{12} &= \frac{1}{A_1}\frac{\partial u_2}{\partial\alpha_1} - \frac{u_1}{A_1A_2}\frac{\partial A_1}{\partial\alpha_2} + k_{12}\omega, \quad & e_{21} &= \frac{1}{A_2}\frac{\partial u_1}{\partial\alpha_2} - \frac{u_1}{A_1A_2}\frac{\partial A_2}{\partial\alpha_2} + k_{21}\omega, \\ \varpi_1 &= \frac{1}{A_1}\frac{\partial\omega}{\partial\alpha_1} - k_{11}u_1 - k_{12}u_2, & \varpi_2 &= \frac{1}{A_2}\frac{\partial\omega}{\partial\alpha_2} - k_{22}u_1 - k_{21}u_1. \end{aligned} \tag{1.62}$$

The length of a line element on the deformed surface $\overset{*}{S}$ is defined by

$$\left(d\overset{*}{s}\right)^2 = \left(\overset{*}{A}_1\right)^2 d\alpha_1^2 + 2\overset{*}{A}_1\overset{*}{A}_2\, d\alpha_1 d\alpha_2 + \left(\overset{*}{A}_2\right)^2 d\alpha_2^2 = \overset{*}{a}_{ij}\, d\alpha_i d\alpha_j, \tag{1.63}$$

here

$$\overset{*}{A}_1 = \left|\overset{*}{\bar{r}}_1\right|, \quad \overset{*}{A}_2 = \left|\overset{*}{\bar{r}}_2\right|, \quad \overset{*}{a}_{12} = \overset{*}{\bar{r}}_1 \overset{*}{\bar{r}}_2 = \overset{*}{A}_1 \overset{*}{A}_2 \cos \overset{*}{\chi}, \tag{1.64}$$

$\overset{*}{\chi}$ is the angle between coordinate lines on $\overset{*}{S}$. Substituting Eqs. (1.61) into (1.64) we find

$$\left(\overset{*}{A}_1\right)^2 = A_1^2(1 + 2\varepsilon_{11}), \quad \left(\overset{*}{A}_2\right)^2 = A_2^2(1 + 2\varepsilon_{22}), \tag{1.65}$$

$$\cos \overset{*}{\chi} = \frac{2\varepsilon_{12}}{\sqrt{(1 + 2\varepsilon_{11})(1 + 2\varepsilon_{22})}}, \tag{1.66}$$

where

$$\begin{aligned} 2\varepsilon_{11} &= 2e_{11} + e_{11}^2 + e_{12}^2 + \varpi_1^2, \\ 2\varepsilon_{22} &= 2e_{22} + e_{22}^2 + e_{21}^2 + \varpi_2^2, \\ 2\varepsilon_{12} &= (1 + e_{11})e_{21} + (1 + e_{22})e12 + \varpi_1\varpi_2. \end{aligned} \tag{1.67}$$

To provide a physically appealing explanation for ε_{ik} $(i, k = 1, 2)$, consider the lengths of the same line element before $(ds)_i$ and after deformation $\left(d\overset{*}{s}\right)_i$

$$(ds)_1 = A_1 \partial\alpha_1, \quad (ds)_2 = A_2 \partial\alpha_2,$$

$$\left(d\overset{*}{s}\right)_1 = \overset{*}{A}_1 \partial\alpha_1, \quad \left(d\overset{*}{s}\right)_2 = \overset{*}{A}_2 \partial\alpha_2.$$

Relative elongations $e_{\alpha 1}, e_{\alpha 2}$, along the α_1, α_2-lines and the shear angle γ between them, are found to be

$$e_{\alpha i} = \frac{ds_i^* - ds_i}{ds_i} = \sqrt{1 + 2\varepsilon_{ii}} - 1, \quad (i = 1, 2) \tag{1.68}$$

$$\cos \overset{*}{\chi} = \cos\left(\frac{\pi}{2} - \gamma\right) = \sin\gamma = \frac{2\varepsilon_{12}}{\sqrt{(1 + 2\varepsilon_{11})(1 + 2\varepsilon_{22})}}. \tag{1.69}$$

It follows from Eqs. (1.68), (1.69) that ε_{11}, ε_{22} describe tangent deformations along the coordinate lines and ε_{12} is the shear deformation that characterizes the change in γ.

Changes in curvatures, $æ_{ii}$, and the twist, $æ_{12,}$ of the surface are described by

$$æ_{11} = \frac{1}{\overset{*}{R}_1} - \frac{1}{R_1} = \overset{*}{k}_{11} - k_{11} \quad æ_{22} = \frac{1}{\overset{*}{R}_2} - \frac{1}{R_2} = \overset{*}{k}_{22} - k_{22}$$

$$æ_{12} = æ_{21} = \overset{*}{k}_{12} - k_{12} = \overset{*}{k}_{21} - k_{21}. \tag{1.70}$$

Here $\frac{1}{R_i}$ and $\frac{1}{R_i^*}$ are curvatures of coordinate lines before and after deformation,

and $\overset{*}{k}_{ij} = -\overset{*}{b}_{ij}/\overset{*}{A}_i\,\overset{*}{A}_j$ $(i,j=1,2)$.

To express $\overset{*}{\bar{m}}$ in terms of the middle surface displacements we proceed from the formula

$$\overset{*}{\bar{m}} = \left(\overset{*}{\bar{r}}_1 \times \overset{*}{\bar{r}}_2\right) / \overset{*}{A}_1\,\overset{*}{A}_2\,\sin\overset{*}{\chi}.$$

Substituting $\overset{*}{A}_i$ and $\sin\overset{*}{\chi}$ given by Eqs. (1.65), (1.66) into the above, we find

$$\overset{*}{\bar{m}} = \left(\overset{*}{\bar{r}}_1 \times \overset{*}{\bar{r}}_2\right) / \overset{*}{A}_1\,\overset{*}{A}_2\sqrt{\mathfrak{A}}, \quad \overset{*}{A}_1\,\overset{*}{A}_2\,\sin\overset{*}{\chi} = A_1A_2\sqrt{\mathfrak{A}}. \tag{1.71}$$

Here

$$\mathfrak{A} = 1 + 2(\varepsilon_{11}+\varepsilon_{22}) + \left(\varepsilon_{11}\varepsilon_{22} - \varepsilon_{12}^2\right) \tag{1.72}$$

Substituting $\overset{*}{\bar{r}}_1$ given by Eqs. (1.61), (1.57) into (1.71), we find

$$\overset{*}{\bar{m}} = (\bar{e}_1\mathbb{S}_1 + \bar{e}_2\mathbb{S}_2 + \bar{m}\mathbb{S}_3)/\sqrt{\mathfrak{A}}, \tag{1.73}$$

where

$$\begin{aligned} &\mathbb{S}_1 = e_{12}\varpi_2 - (1+e_{22})\varpi_1, \quad \mathbb{S}_2 = e_{21}\varpi_1 - (1+e_{11})\varpi_2, \\ &\mathbb{S}_3 = (1+e_{11})(1+e_{22}) - e_{12}e_{21}. \end{aligned} \tag{1.74}$$

The scalar product of Eqs. (1.61) and (1.73) by $\bar{e}_i$ and $\bar{m}$, yields

$$\cos\left(\overset{*}{\bar{r}}_1, \bar{e}_k\right) = (\delta_{ik}+e_{ik})/\sqrt{1+2\varepsilon_{ii}}, \quad \cos\left(\overset{*}{\bar{r}}_1, \bar{m}\right) = \varpi_i/\sqrt{1+2\varepsilon_{ii}},$$

$$\cos(\bar{m}, \bar{e}_k) = \mathbb{S}_k/\sqrt{\mathfrak{A}}, \quad \cos\left(\overset{*}{\bar{m}}, \bar{m}\right) = \mathbb{S}_3/\sqrt{\mathfrak{A}}.$$

The quantities e_{ik}, ϖ_i, $\mathbb{S}_i$, $\mathbb{S}_3$ describe the rotations of tangent and normal vectors during deformation.

Differentiating Eq. (1.73) with respect to α_i and making use of Eqs. (1.28), (1.29), we find

$$\sqrt{\mathfrak{A}}\,\overset{*}{\bar{m}}_i = A_i(\bar{e}_1\mathfrak{M}_{i1} + \bar{e}_2\mathfrak{M}_{i2} + \bar{m}\mathfrak{M}_{i3}) - \overset{*}{\bar{m}}\,\frac{\partial\sqrt{\mathfrak{A}}}{\partial\alpha_i}, \tag{1.75}$$

where

$$
\begin{aligned}
\mathfrak{M}_{11} &= \frac{1}{A_1}\frac{\partial \mathbb{S}_1}{\partial \alpha_1} + \frac{\mathbb{S}_2}{A_1 A_2}\frac{\partial A_1}{\partial \alpha_2} + k_{11}\mathbb{S}_3, \\
\mathfrak{M}_{21} &= \frac{1}{A_2}\frac{\partial \mathbb{S}2}{\partial \alpha_2} + \frac{\mathbb{S}_1}{A_2 A_1}\frac{\partial A_2}{\partial \alpha_1} + k_{22}\mathbb{S}_3, \\
\mathfrak{M}_{12} &= \frac{1}{A_1}\frac{\partial \mathbb{S}_2}{\partial \alpha_1} - \frac{\mathbb{S}_1}{A_1 A_2}\frac{\partial A_1}{\partial \alpha_2} + k_{12}\mathbb{S}_3, \\
\mathfrak{M}_{22} &= \frac{1}{A_2}\frac{\partial \mathbb{S}_1}{\partial \alpha_2} - \frac{\mathbb{S}_2}{A_1 A_2}\frac{\partial A_2}{\partial \alpha_1} + k_{12}\mathbb{S}_3, \\
\mathfrak{M}_{13} &= \frac{1}{A_1}\frac{\partial \mathbb{S}_3}{\partial \alpha_1} - k_{11}\mathbb{S}_1 - k_{12}\mathbb{S}_2, \\
\mathfrak{M}_{23} &= \frac{1}{A_2}\frac{\partial \mathbb{S}_3}{\partial \alpha_2} - k_{22}\mathbb{S}_2 - k_{12}\mathbb{S}_1.
\end{aligned}
\tag{1.76}
$$

Substituting Eqs. (1.60) into (1.75), and using the fact that $\overset{*}{\bar{m}}\,\overset{*}{\bar{r}}_j = 0$, $A_i A_1 \overset{*}{k}_{i1} = \overset{*}{\bar{m}}_i\,\overset{*}{\bar{r}}_1$, $A_i A_2 \overset{*}{k}_{i2} = \overset{*}{\bar{m}}_i\,\overset{*}{\bar{r}}_2$, we obtain

$$
\begin{aligned}
\sqrt{\mathfrak{A}}\,\overset{*}{k}_{i1} &= (1+e_{11})\mathfrak{M}_{i1} + e_{12}\mathfrak{M}_{i2} + \overline{\omega}_1\mathfrak{M}_{i3}, \\
\sqrt{\mathfrak{A}}\,\overset{*}{k}_{i2} &= e_{21}\mathfrak{M}_{i1} + (1+e_{22})\mathfrak{M}_{i2} + \overline{\omega}_2\mathfrak{M}_{i3}
\end{aligned}
\tag{1.77}
$$

e_{ik}, ϖ_i, $\mathbb{S}_i$, $\mathbb{S}_3$ satisfy the following algebraic equalities

$$
\begin{aligned}
\mathbb{S}_1(1+e_{11}) + e_{12}\mathbb{S}_2 + \mathbb{S}_3\varpi_1 = 0, \\
\mathbb{S}_2(1+e_{22}) + e_{21}\mathbb{S}_1 + \mathbb{S}_3\varpi_2 = 0.
\end{aligned}
\tag{1.78}
$$

Eqs. (1.78) can be verified by substituting $\overset{*}{\bar{r}}_j$ and $\overset{*}{\bar{m}}$ given by Eqs. (1.61), (1.73) into equality $\overset{*}{\bar{m}}\,\overset{*}{\bar{r}}_j = 0$. The following is also true

$$
\begin{aligned}
&\mathbb{S}_1 e_{12} - \mathbb{S}_2(1+e_{11}) = (1+2\varepsilon_{11}) - 2\varepsilon_{12}\varpi_1 = f_{12} \\
&\mathbb{S}_3(1+e_{11}) - \mathbb{S}_1\varpi_1 = (1+e_{22})(1+2\varepsilon_{11}) - 2\varepsilon_{12}e_{12} = g_{12} \qquad \overset{\longleftrightarrow}{1,2} \\
&\mathbb{S}_3 e_{12} - \mathbb{S}_2\varpi_1 = (1+e_{22})\ \ 2\varepsilon_{11} - (1+2\varepsilon_{11})e_{12} = h_{12}
\end{aligned}
\tag{1.79}
$$

The result can be confirmed by substituting $\mathbb{S}_i$, $\mathbb{S}_3$ given by Eqs. (1.74) and making use of Eqs. (1.67).

Substituting Eqs. (1.76) into Eqs. (1.78), we find

$$\begin{aligned}
&\sqrt{\mathfrak{A}}\overset{*}{k}_{11} = \frac{1}{A_1}\left[(1+e_{11})\frac{\partial \mathbb{S}_1}{\partial \alpha_1} + e_{12}\frac{\partial \mathbb{S}_2}{\partial \alpha_1} + \overline{\omega}_1\frac{\partial \mathbb{S}_3}{\partial \alpha_1}\right] - \\
&-\frac{f_{12}}{A_1A_2}\frac{\partial A_1}{\partial \alpha_2} + k_{11}g_{12} + k_{12}h_{12} \\
&\sqrt{\mathfrak{A}}\overset{*}{k}_{22} = \frac{1}{A_1}\left[e_{21}\frac{\partial \mathbb{S}_1}{\partial \alpha_1} + (1+e_{22})\frac{\partial \mathbb{S}_2}{\partial \alpha_1} + \overline{\omega}_2\frac{\partial \mathbb{S}_3}{\partial \alpha_1}\right] + \\
&+\frac{f_{12}}{A_1A_2}\frac{\partial A_1}{\partial \alpha_2} - k_{11}h_{12} - k_{12}g_{12}
\end{aligned} \tag{1.80}$$

Differentiating Eqs. (1.80) with respect to α_1, we get

$$\begin{aligned}
&(1+e_{11})\frac{\partial \mathbb{S}_1}{\partial \alpha_1} + e_{12}\frac{\partial \mathbb{S}_2}{\partial \alpha_1} + \overline{\omega}_1\frac{\partial \mathbb{S}_3}{\partial \alpha_1} = -\mathbb{S}_1\frac{\partial e_{11}}{\partial \alpha_1} - \mathbb{S}_2\frac{\partial e_{12}}{\partial \alpha_1} - \mathbb{S}_3\frac{\partial \overline{\omega}_1}{\partial \alpha_1}, \\
&(1+e_{22})\frac{\partial \mathbb{S}_2}{\partial \alpha_1} + e_{21}\frac{\partial \mathbb{S}_1}{\partial \alpha_1} + \overline{\omega}_2\frac{\partial \mathbb{S}_3}{\partial \alpha_1} = -\mathbb{S}_2\frac{\partial e_{22}}{\partial \alpha_1} - \mathbb{S}_1\frac{\partial e_{21}}{\partial \alpha_1} - \mathbb{S}_3\frac{\partial \overline{\omega}_2}{\partial \alpha_1}
\end{aligned} \tag{1.81}$$

Substituting the right-hand sides of Eqs. (1.81) into (3.22), the final formulas for the curvatures $\overset{*}{k}_{11}$, $\overset{*}{k}_{22}$ are found to be

$$\begin{aligned}
&\sqrt{\mathfrak{A}}\overset{*}{k}_{11} = -\frac{1}{A_1}\left(\mathbb{S}_1\frac{\partial e_{11}}{\partial \alpha_1} + \mathbb{S}_2\frac{\partial e_{12}}{\partial \alpha_1} + \mathbb{S}_3\frac{\partial \overline{\omega}_1}{\partial \alpha_1}\right) - \frac{f_{12}}{A_1A_2}\frac{\partial A_1}{\partial \alpha_2} + k_{11}g_{12} + k_{12}h_{12}, \\
&\sqrt{\mathfrak{A}}\overset{*}{k}_{22} = -\frac{1}{A_1}\left(\mathbb{S}_2\frac{\partial e_{22}}{\partial \alpha_1} + \mathbb{S}_1\frac{\partial e_{21}}{\partial \alpha_1} + \mathbb{S}_3\frac{\partial \overline{\omega}_2}{\partial \alpha_1}\right) + \frac{f_{12}}{A_1A_2}\frac{\partial A_1}{\partial \alpha_2} - k_{11}h_{12} - k_{12}g_{12}.
\end{aligned} \tag{1.82}$$

Formulas (1.82) are obtained under the first Kirchhoff-Love hypothesis. The essence of the hypothesis is that normals to the undeformed middle surface S remain straight and normal to the deformed middle surface and undergo no extension, i.e. $\overset{*}{m}\,\overset{*}{r}_j = \overset{*}{m}\,\overset{*}{\rho}_j = g_{j3} = 0$ and $\varepsilon^z_{j3} = 0$. The hypotheses were first formulated by Kirchhoff for thin plates and later applied by Love for thin shells. They are known as the Kirchhoff-Love hypotheses and are fundamental in the theory of thin shells. Additional hypotheses will be introduced in the text as needed.

1.7 Equations of Compatibility

For the surface to retain continuity during deformation, the parameters ε_{ik} and $\varkappa_{ik}$ $(i, k = 1, 2)$ must satisfy the three differential called the equations of continuity of deformations. They can be obtained by subtracting the Gauss-Codazzi equations formulated for the undeformed state from the corresponding equations for the

deformed configuration. The Gauss formula for the deformed surface $\overset{*}{S}$ is given by (see Eq. 1.32)

$$\frac{\partial^2 \overset{*}{\chi}}{\partial\alpha_1\partial\alpha_2}+\frac{\partial}{\partial\alpha_1}\frac{\frac{\partial \overset{*}{A}_2}{\partial\alpha_1}-\cos\overset{*}{\chi}\frac{\partial \overset{*}{A}_1}{\partial\alpha_2}}{\overset{*}{A}_1\sin\overset{*}{\chi}}+\frac{\partial}{\partial\alpha_2}\frac{\frac{\partial \overset{*}{A}_1}{\partial\alpha_2}-\cos\overset{*}{\chi}\frac{\partial \overset{*}{A}_2}{\partial\alpha_1}}{\overset{*}{A}_2\sin\overset{*}{\chi}}=$$

$$=\frac{\overset{*}{b}{}^2_{12}-\overset{*}{b}_{11}\overset{*}{b}_{22}}{\overset{*}{A}_1\overset{*}{A}_2\sin\overset{*}{\chi}}. \tag{1.83}$$

Substituting

$$\overset{*}{A}_1\overset{*}{A}_2\sin\overset{*}{\chi}=A_1A_2\sqrt{\mathfrak{A}},$$
$$\cos\overset{*}{\chi}=2\varepsilon_{12}/\sqrt{\mathbb{S}_{11}\mathbb{S}_{22}},$$
$$\sin\overset{*}{\chi}=\sqrt{\mathfrak{A}}/\sqrt{\mathbb{S}_{11}\mathbb{S}_{22}},$$

$$\frac{\partial\overset{*}{\chi}}{\partial\alpha_i}=-\frac{1}{\sin\overset{*}{\chi}}\frac{\partial\cos\overset{*}{\chi}}{\partial\alpha_i}=\frac{1}{\sqrt{\mathfrak{A}}}\left[-2\frac{\partial\varepsilon_{12}}{\partial\alpha_i}+\varepsilon_{12}\frac{\partial}{\partial\alpha_i}\ln\left(\mathbb{S}_{11}\mathbb{S}_{22}\right)\right]$$

into Eq. (1.83) we get

$$\frac{\partial}{\partial\alpha_1}\frac{1}{\sqrt{\mathfrak{A}}}\left[-\frac{\partial\varepsilon_{12}}{\partial\alpha_2}+\frac{\varepsilon_{12}}{2}\frac{\partial}{\partial\alpha_2}\ln\left(\mathbb{S}_{11}\mathbb{S}_{22}\right)+\frac{\overset{*}{A}_2}{A_1A_2}\left(\frac{\partial \overset{*}{A}_2}{\partial\alpha_1}-\cos\overset{*}{\chi}\frac{\partial \overset{*}{A}_1}{\partial\alpha_2}\right)\right]+$$

$$+\frac{\partial}{\partial\alpha_2}\frac{1}{\sqrt{\mathfrak{A}}}\left[-\frac{\partial\varepsilon_{12}}{\partial\alpha_1}+\frac{\varepsilon_{12}}{2}\frac{\partial}{\partial\alpha_1}\ln\left(\mathbb{S}_{11}\mathbb{S}_{22}\right)+\frac{\overset{*}{A}_2}{A_1A_2}\left(\frac{\partial \overset{*}{A}_1}{\partial\alpha_2}-\cos\overset{*}{\chi}\frac{\partial \overset{*}{A}_2}{\partial\alpha_1}\right)\right]=$$

$$=\frac{1}{\sqrt{\mathfrak{A}}}\frac{\overset{*}{b}{}^2_{12}-\overset{*}{b}_{11}\overset{*}{b}_{22}}{A_1A_2}. \tag{1.84}$$

Further, using Eqs. (1.65), (1.66) in (1.84), the first Gauss formula is found to be

$$\frac{\partial}{\partial\alpha_1}\frac{1}{A_1\sqrt{\mathfrak{A}}}\left[\frac{A_1\varepsilon_{12}}{2}\frac{\partial}{\partial\alpha_1}\ln\frac{\mathbb{S}_{22}}{\mathbb{S}_{11}}+\frac{\partial A_2\varepsilon_{22}}{\partial\alpha_1}-\frac{\partial A_1\varepsilon_{12}}{\partial\alpha_2}-\varepsilon_{12}\frac{\partial A_1}{\partial\alpha_2}++\varepsilon_{22}\frac{\partial A_2}{\partial\alpha_1}+\frac{\partial A_2}{\partial\alpha_1}\right]$$
$$+\frac{\partial}{\partial\alpha_2}\frac{1}{A_2\sqrt{\mathfrak{A}}}\left[\frac{A_2\varepsilon_{21}}{2}\frac{\partial}{\partial\alpha_2}\ln\frac{\mathbb{S}_{11}}{\mathbb{S}_{22}}+\frac{\partial A_1\varepsilon_{11}}{\partial\alpha_2}--\frac{\partial A_2\varepsilon_{21}}{\partial\alpha_1}-\varepsilon_{21}\frac{\partial A_2}{\partial\alpha_1}+\varepsilon_{11}\frac{\partial A_1}{\partial\alpha_2}+\frac{\partial A_1}{\partial\alpha_2}\right]$$
$$=\frac{1}{\sqrt{\mathfrak{A}}}\frac{\overset{*}{b}{}^2_{12}-\overset{*}{b}_{11}\overset{*}{b}_{22}}{A_1A_2}.$$

It can be written in more concise form as

$$\frac{\partial}{\partial\alpha_1}\frac{1}{A_1\sqrt{\mathfrak{A}}}\left[\frac{A_1\varepsilon_{12}}{2}\frac{\partial}{\partial\alpha_2}\ln\frac{\mathbb{S}_{22}}{\mathbb{S}_{11}}+L'_2(\varepsilon_{ik})+(1+\varepsilon_{11}+\varepsilon_{22})\frac{\partial A_2}{\partial\alpha_1}\right]+$$
$$+\frac{\partial}{\partial\alpha_2}\frac{1}{A_2\sqrt{\mathfrak{A}}}\left[\frac{A_2\varepsilon_{21}}{2}\frac{\partial}{\partial\alpha_2}\ln\frac{\mathbb{S}_{11}}{\mathbb{S}_{22}}+L'_1(\varepsilon_{ik})+(1+\varepsilon_{11}+\varepsilon_{22})\frac{\partial A_1}{\partial\alpha_2}\right]=$$
$$=A_1A_2\frac{1}{\sqrt{\mathfrak{A}}}\left(\overset{*}{k}{}^2_{12}-\overset{*}{k}_{11}\overset{*}{k}_{22}\right),\tag{1.85}$$

where the differential operators $L'_j(\varepsilon_{ik})$ are defined by

$$L'_1(\varepsilon_{ik})=\frac{\partial A_1\varepsilon_{11}}{\partial\alpha_2}-\frac{\partial A_2\varepsilon_{12}}{\partial\alpha_1}-\varepsilon_{22}\frac{\partial A_1}{\partial\alpha_1}-\varepsilon_{12}\frac{\partial A_2}{\partial\alpha_1},$$
$$L'_2(\varepsilon_{ik})=\frac{\partial A_2\varepsilon_{22}}{\partial\alpha_1}-\frac{\partial A_1\varepsilon_{12}}{\partial\alpha_2}-\varepsilon_{11}\frac{\partial A_2}{\partial\alpha_1}-\varepsilon_{12}\frac{\partial A_1}{\partial\alpha_2},$$

Let $\overset{*}{K}$ be the Gaussian curvature of the deformed surface $\overset{*}{S}$

$$\overset{*}{K}=k^2_{12}-k_{11}k_{22}=\frac{1}{A_1A_2}\left[\frac{\partial}{\partial\alpha_1}\left(\frac{1}{A_1}\frac{\partial A_2}{\partial\alpha_1}\right)+\frac{\partial}{\partial\alpha_2}\left(\frac{1}{A_2}\frac{\partial A_1}{\partial\alpha_2}\right)\right].\tag{1.86}$$

With the help of Eq. (1.86), the first equation in (1.85) can be written as

$$\frac{\partial}{\partial\alpha_1}\frac{1}{A_1\sqrt{\mathfrak{A}}}\left[\frac{A_1\varepsilon_{12}}{2}\frac{\partial}{\partial\alpha_2}\ln\frac{\mathbb{S}_{22}}{\mathbb{S}_{11}}+L'_2(\varepsilon_{ik})+(1+\varepsilon_{11}+\varepsilon_{22})\frac{\partial A_2}{\partial\alpha_1}\right]+$$
$$+\frac{\partial}{\partial\alpha_2}\frac{1}{A_2\sqrt{\mathfrak{A}}}\left[\frac{A_2\varepsilon_{21}}{2}\frac{\partial}{\partial\alpha_2}\ln\frac{\mathbb{S}_{11}}{\mathbb{S}_{22}}+L'_1(\varepsilon_{ik})+(1+\varepsilon_{11}+\varepsilon_{22})\frac{\partial A_1}{\partial\alpha_2}\right]=$$
$$=A_1A_2\frac{1}{\sqrt{\mathfrak{A}}}(K-K_0).\tag{1.87}$$

The increment to the Gaussian curvature is defined by

$$K - \overset{*}{K} = \varpi_{12}^2 - \varpi_{11}\varpi_{22} + 2k\varpi_{12} - k_{11}\varpi_{11} - k_{22}\varpi_{11}. \tag{1.88}$$

To obtain other two equations, recall the Codazzi formulas

$$\frac{\partial \overset{*}{b}_{11}}{\partial \alpha_2} - \frac{\partial \overset{*}{b}_{12}}{\partial \alpha_1} - \overset{*}{\Gamma}{}_{12}^{1}\ \overset{*}{b}_{11} - \left(\overset{*}{\Gamma}{}_{12}^{2} - \overset{*}{\Gamma}{}_{11}^{1}\right) \overset{*}{b}_{12} + \overset{*}{\Gamma}{}_{11}^{2}\ \overset{*}{b}_{22} = 0.$$

Here $\overset{*}{\Gamma}{}_{ik}^{j}$ are the Christoffel symbols of $\overset{*}{S}$. Substituting $\overset{*}{b}_{ij} = -A_i A_j \overset{*}{k}_{ij} = A_i A_j (k_{ij} + \varpi_{ij})$, we get

$$\begin{aligned} &\frac{\partial A_1 A_2 (k_{12} + \varpi_{12})}{\partial \alpha_1} - \frac{\partial A_1^2 (k_{11} + \varpi_{11})}{\partial \alpha_2} + A_1^2\, \overset{*}{k}_{11}\ \ \overset{*}{\Gamma}{}_{12}^{1} + \\ &+ A_1 A_2\, \overset{*}{k}_{12} \left(\overset{*}{\Gamma}{}_{12}^{2} - \overset{*}{\Gamma}{}_{11}^{1}\right) - A_2^2\, \overset{*}{k}_{22}\, \overset{*}{\Gamma}{}_{11}^{2} = 0. \end{aligned} \tag{1.89}$$

Subtracting Eqs. (1.37) and dividing the resultant by $-A_1$, the compatibility are found to be

$$\begin{aligned} &\frac{\partial A_1 \varpi_{11}}{\partial \alpha_2} - \frac{\partial A_2 \varpi_{12}}{\partial \alpha_1} - \varpi_{12} \frac{\partial A_1}{\partial \alpha_2} + A_2\, \overset{*}{k}_{12} \left(A_{11}^1 - A_{12}^2\right) - \\ &- A_1\, \overset{*}{k}_{11}\, A_{12}^1 + \frac{A_2^2}{A_1} \overset{*}{k}_{22}\, A_{11}^2 = 0, \\ &\frac{\partial A_2 \varpi_{22}}{\partial \alpha_1} - \frac{\partial A_1 \varpi_{12}}{\partial \alpha_2} - \varpi_{12} \frac{\partial A_2}{\partial \alpha_1} + A_1\, \overset{*}{k}_{12} \left(A_{22}^2 - A_{12}^1\right) - \\ &- A_2\, \overset{*}{k}_{22}\, A_{12}^2 + \frac{A_1^1}{A_2} \overset{*}{k}_{11}\, A_{22}^1 = 0. \end{aligned} \tag{1.90}$$

In the above we made use of the following formulas for derivatives

$$\begin{aligned} \frac{\partial A_1 A_2 (k_{12} + \varpi_{12})}{\partial \alpha_1} &= A_1 \frac{\partial A_2 (k_{12} + \varpi_{12})}{\partial \alpha_1} + A_2 (k_{12} + \varpi_{12}) \frac{\partial A_1}{\partial \alpha_1}, \\ \frac{\partial A_1^2 (k_{11} + \varpi_{11})}{\partial \alpha_2} &= A_1 \frac{\partial A_1 (k_{11} + \varpi_{11})}{\partial \alpha_2} + A_1 (k_{11} + \varpi_{11}) \frac{\partial A_1}{\partial \alpha_2}, \end{aligned}$$

Let A_{ik}^j be the components of the Christoffel deviator given by

$$A_{ik}^j = \overset{*}{\Gamma}{}_{ik}^{j} - \Gamma_{ik}^j \tag{1.91}$$

Defining differential operators $L_j'(\varpi_{ik})$ by

$$
\begin{aligned}
L'_1(\varkappa_{ik}) &= \frac{\partial A_1 \varkappa_{11}}{\partial \alpha_2} - \frac{\partial A_2 \varkappa_{12}}{\partial \alpha_1} - \varkappa_{12}\frac{\partial A_2}{\partial \alpha_1} - \varkappa_{22}\frac{\partial A_1}{\partial \alpha_2},\\
L'_2(\varkappa_{ik}) &= \frac{\partial A_2 \varkappa_{22}}{\partial \alpha_1} - \frac{\partial A_1 \varkappa_{12}}{\partial \alpha_2} - \varkappa_{12}\frac{\partial A_1}{\partial \alpha_2} - \varkappa_{11}\frac{\partial A_2}{\partial \alpha_1},
\end{aligned}
\tag{1.92}
$$

Eqs. (1.89) can be written in the form

$$
\begin{aligned}
L'_1(\varkappa_{ik}) + A_2 \overset{*}{k}_{12}\left(A^1_{11} - A^2_{12}\right) - A_1 \overset{*}{k}_{11} A^1_{12} + \frac{A^2_2}{A_1}\overset{*}{k}_{22} A^2_{11} = 0,\\
L'_2(\varkappa_{ik}) + A_1 \overset{*}{k}_{12}\left(A^2_{22} - A^1_{12}\right) - A_2 \overset{*}{k}_{22} A^2_{12} + \frac{A^2_1}{A_2}\overset{*}{k}_{22} A^1_{22} = 0,
\end{aligned}
\tag{1.93}
$$

Substituting $\overset{*}{A}_i, \overset{*}{a}, \overset{*}{\chi}$ into Eqs. (1.23), for $\overset{*}{\Gamma}{}^j_{ik}$ we obtain

$$
\begin{aligned}
&\overset{*}{a}\overset{*}{\Gamma}{}^1_{11} = \overset{*}{A}_1 \overset{*}{A}{}^2_2 \frac{\partial \overset{*}{A}_1}{\partial \alpha_1} - \overset{*}{a}_{12}\left(\frac{\partial \overset{*}{a}_{12}}{\partial \alpha_1} - \overset{*}{A}_1 \frac{\partial \overset{*}{A}_1}{\partial \alpha_2}\right),\\
&\overset{*}{a}\overset{*}{\Gamma}{}^1_{12} = \overset{*}{A}_1 \overset{*}{A}{}^2_2 \frac{\partial \overset{*}{A}_1}{\partial \alpha_2} - \overset{*}{A}_2 \overset{*}{a}_{12}\frac{\partial \overset{*}{A}_1}{\partial \alpha 1},\\
&\overset{*}{a}\overset{*}{\Gamma}{}^2_{11} = \overset{*}{A}{}^2_1 \frac{\partial \overset{*}{a}_{12}}{\partial \alpha_1} - \overset{*}{A}_1 \overset{*}{a}_{12}\frac{\partial \overset{*}{A}_1}{\partial \alpha_1} - \overset{*}{A}{}^3_1 \frac{\partial \overset{*}{A}_1}{\partial \alpha_2},\\
&\overset{*}{a} = a\mathfrak{A}, \qquad \overset{*}{a}_{12} = \overset{*}{A}_1 \overset{*}{A}_2 \cos \overset{*}{\chi}.
\end{aligned}
\tag{1.94}
$$

Making use of Eqs. (1.23) and (1.94) in (1.91), the final formulas for the Chrystoffel deviators become

$$
\begin{aligned}
\mathfrak{A}A^1_{11} &= \frac{\varepsilon_{12}}{A_1 A_2}\frac{\partial A^2_1 \mathbb{S}_{11}}{\partial \alpha_2} - \frac{4\varepsilon_{12}}{A_2}\frac{\partial A_2 \varepsilon_{12}}{\partial \alpha_1} + \mathbb{S}_{22}\frac{\partial \varepsilon_{11}}{\partial \alpha_1},\\
\mathfrak{A}A^2_{11} &= \frac{A_1 I}{A^2_2}\frac{\partial A_1}{\partial \alpha_2} + -\frac{\mathbb{S}_{11}}{A^2_2}\left(2A_1\frac{\partial A_2 \varepsilon_{12}}{\partial \alpha_1} - \frac{1}{2}\frac{\partial A^2_1 \mathbb{S}_{11}}{\partial \alpha_2}\right) - \frac{2A_2\varepsilon_{12}}{A_2}\frac{\partial \varepsilon_{11}}{\partial \alpha_1},\\
\mathfrak{A}A^2_{12} &= \mathbb{S}_{11}\frac{\partial \varepsilon_{22}}{\partial \alpha_1} - \frac{\varepsilon_{12}}{A_1 A_2}\frac{\partial A^2_1 \mathbb{S}_{11}}{\partial \alpha_2} + \frac{4\varepsilon^2_{12}}{A_2}\frac{\partial A_2}{\partial \alpha_1},\\
\mathfrak{A}A^2_{22} &= \frac{\varepsilon_{12}}{A_1 A_2}\frac{\partial A^1_2 \mathbb{S}_{22}}{\partial \alpha_1} - \frac{4\varepsilon_{12}}{A_1}\frac{\partial A_1 \varepsilon_{12}}{\partial \alpha_2} + \mathbb{S}_{11}\frac{\partial \varepsilon_{11}}{\partial \alpha_1},\\
\mathfrak{A}A^1_{22} &= \frac{A_2 I}{A^1_1}\frac{\partial A_2}{\partial \alpha_1} - \frac{\mathbb{S}_{22}}{A^1_1}\left(2A_2\frac{\partial A_1 \varepsilon_{12}}{\partial \alpha_2} - \frac{1}{2}\frac{\partial A^1_2 \mathbb{S}_{22}}{\partial \alpha_1}\right) - \frac{2A_1\varepsilon_{12}}{A_1}\frac{\partial \varepsilon_{22}}{\partial \alpha_2},\\
\mathfrak{A}A^1_{12} &= \mathbb{S}_{22}\frac{\partial \varepsilon_{11}}{\partial \alpha_2} - \frac{\varepsilon_{12}}{A_1 A_2}\frac{\partial A^1_2 \mathbb{S}_{22}}{\partial \alpha_1} + \frac{4\varepsilon^2_{12}}{A_1}\frac{\partial A_1}{\partial \alpha_2}.
\end{aligned}
\tag{1.95}
$$

References

Baer E, Cassidy JJ, Hiltner A (1991) Hierarchical structure of collagen composite systems. Pure Appl Chem 63:961–973

Buschmann MD, Grodzinsky AJ (1995) A molecular model of proteoglycan-associated electrostatic forces in cartilage mechanics. J Biomech Eng 117:179–192

Carniero AA, Baffa O, Oliveira RB (1999) Study of stomach motility using relaxation of magnetic tracers. Phys Med Biol 44:1691–1697

Cowi SC (2000) How is a tissue built? Trans ASME J Biomech Eng 122:553–559

Geiger B, Ginsberg D (1991) The cytoplasmic domain of adherenstype junctions. Cell Mot Cytoskel 20:1–6

Hirst DGS, Suzuki H (2006) Involvement of interstitial cells of Cajal in the control of smooth muscle excitability. J Physiol 576:651–652

Hulmes DJS, Wess TJ, Prockop DJ, Fratzl P (1995) Radial packing, order and disorder in collagen fibrils. Biophys J 68:1661–1670

Koh SD, Ward SM, Tamas O, Sanders KM, Horowitz B (2003) Conductances responsible for slow wave generation and propagation in interstitial cells of Cajal. Curr Opin Pharm 3:579–582

Liao D, Gregersen H, Hausken T, Gilja OH, Mundt M, Kassab G (2004) Analysis of surface geometry of the human stomach using real-time 3-D ultrasonography in vivo. Neurogastroent Mot 16(3):315–324

Mabuchi K, Li B, Ip W, Tao T (1997) Association of calponin with desmin inter-mediate filaments. J Biol Chem 272:22662–22666

Maes M, Cogliati B, Yanguas SC, Willebrords J, Vinken M (2015) Roles of connexins and pannexins in digestive homeostasis. Cell Mol Life Sci 72(15):2809–2821

Malmqvist U, Arner A, Uvelius B (1991) Contractile and cytoskeletal proteins in smooth muscle during hypertrophy and its reversal. Am J Physiol Cell Physiol 260:C1085–C1093

Martin AF, Bhatti S, Pyne-Geithman GJ, Farjah M, Manaves V, Walker L, Franks R, Strauch AR, Paul RJ (2007) Expression and function of COOH terminal myosin heavy chain isoforms in mouse smooth muscle. Am J Physiol Cell Physiol 293:C238–C245

Miftakhov RN (1981) Micromechanics of tissue fracture in uniaxial elongation. Shell Inter Fluids Acad Sci USSR:205–214

Pickhardt PJ, Asher DB (2003) Wall thickening of the gastric antrum as a normal finding: miltidetector CT with cadaveric comparison. Am J Radiol 181(4):973–979

Schulze K (2006) Imaging and modeling of digestion in the stomach and the duodenum. Neurogastroent Mot 18(3):172–183

Small JV, Gimona M (1997) The cytoskeleton of the vertebrate smooth muscle cell. Acta Physiol Scand 164:341–348

Small JV, Furst DO, De Mey J (1986) Localization of filamin in smooth muscle. J Cell Biol 102:210–220

Suzuki H (2000) Cellular mechanisms of myogenic activity in gastric smooth muscle. Jpn J Physiol 50:289–301

Yamada KM, Geiger B (1997) Molecular interactions in cell adhesion complexes. Curr Opin Cell Biol 9:76–85

Zamir E, Geiger B (2001) Molecular complexity and dynamics of cell-matrix adhesions. J Cell Sci 114:3583–3590

Chapter 2
Parameterization of Shells of Complex Geometry

Simplicity is the ultimate sophistication.
Leonardo da Vinci

2.1 Fictitious Deformations

Most biological shells are of complex geometry. Convenient parameterization of such shells is a difficult analytical task and sometimes is even unfeasible. Almost all numerical methods, on the other hand, are based on discretization of the computational domain and as such may appear to be secluded from the problem. However, computational algorithms are most efficient and accurate only when they operate in regular, canonical domains and become computationally demanding and suffer the loss of accuracy in complex domains. Therefore, the question of parameterization of shells of complex geometry becomes of utmost importance (Galimov and Paimushin 1985).

Let an arbitrary point $M(\alpha_1, \alpha_2) \in S$ and its ε_M- domain be in one-to-one correspondence with a point $\overset{*}{M}\left(\overset{*}{\alpha}_1, \overset{*}{\alpha}_2\right)$ and its $\overset{*}{\varepsilon}_{*M}$ - domain on the deformed middle surface $\overset{*}{S}$ (Fig. 2.1). The transformation is defined analytically by

$$\overset{*}{\alpha}_i = \overset{*}{\alpha}_i(\alpha_1, \alpha_2), \tag{2.1}$$

where (α_1, α_2) and $\left(\overset{*}{\alpha}_1, \overset{*}{\alpha}_2\right)$ are the coordinates on S and $\overset{*}{S}$, respectively.

Assuming that Eq. (2.1) is continuously differentiable and $\det(\partial \overset{*}{\alpha}_i / \partial \alpha_k) \neq 0$ $(i, k = 1, 2)$, the inverse transformation is found to be

$$a_i = a_i\left(\overset{*}{\alpha}_1, \overset{*}{\alpha}_2\right). \tag{2.2}$$

The coefficients of the direct and inverse transformations are given by

R.N. Miftahof, *Biomechanics of the Human Stomach*,
DOI 10.1007/978-3-319-59677-8_2

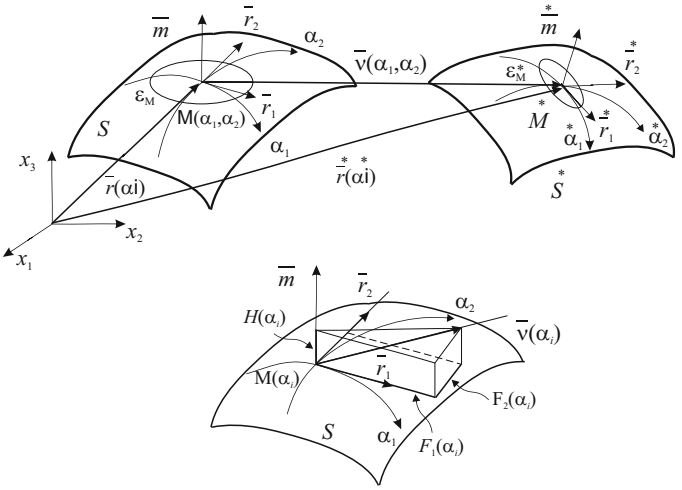

Fig. 2.1 Continuous transformation of an ε_M- domain of the surface S. Decomposition of the displacement vector $\nu(\alpha_1, \alpha_2)$ in the undeformed base $\{\bar{r}_1, \bar{r}_2, \bar{m}\}$

$$C_i^k = \frac{\partial \overset{*}{\alpha}_k}{\partial \alpha_i}, \quad C = \det\left(C_i^k\right), \tag{2.3}$$

$$\overset{*}{C}{}_i^k = \frac{\partial \alpha_k}{\partial \overset{*}{\alpha}_i}, \quad \overset{*}{C} = \det\left(\overset{*}{C}{}_i^k\right), \tag{2.4}$$

Assuming that $C \neq 0$, $C^* \neq 0$, we have

$$\begin{aligned} &\sum_{i=1}^{2} C_i^k \overset{*}{C}{}_k^i = 1, \quad \sum_{i=1}^{2} C_i^k \overset{*}{C}{}_j^k = 0 \qquad (i \neq j), \\ &C \overset{*}{C} = 1, \quad \overset{*}{C}{}_i^k = \left[C_k^i\right]/C. \end{aligned} \tag{2.5}$$

Here $\left[C_k^i\right]$ is the cofactor to the element C_k^i of the matrix (C_i^k).

It follows from the above considerations that the surface $\overset{*}{S}$ can also be referred to the coordinates α_i. Then, the vector equations of S and $\overset{*}{S}$ are given by

$$\begin{aligned} &\bar{r} = \bar{r}(\alpha_1, \alpha_2), \\ &\overset{*}{\bar{r}} = \overset{*}{\bar{r}}\left(\overset{*}{\alpha}_1, \overset{*}{\alpha}_2\right) = \overset{*}{\bar{r}}\left[f_1(\alpha_1, \alpha_2), f_2(\alpha_1, \alpha_2)\right] = \bar{r}(\alpha_1, \alpha_2) + \bar{\nu}(\alpha_1, \alpha_2). \end{aligned} \tag{2.6}$$

Here use is made of Eq. (1.58), $\bar{\nu}(\alpha_1, \alpha_2)$ is the displacement vector.

Lengths of a linear element $ds, d\overset{*}{s}$ before and after transformation are given by Eqs. (1.11), (1.63). Let the stretch ratio be defined by

$$\lambda_i = \frac{d\overset{*}{s}}{ds} = \sqrt{\frac{\overset{*}{\alpha}_{ik}}{a_{ik}}} \quad (i,k=1,2). \tag{2.7}$$

If $\lambda_i > 1$ then the element experiences elongation, and if $\lambda_i < 1$ - contraction during transformation.

Similarly, the change of the area of a surface element is defined by

$$\delta s_\Delta = ds_\Delta / \overset{*}{ds}_\Delta = \sqrt{a/\overset{*}{a}}, \tag{2.8}$$

where areas ds_Δ, $\overset{*}{ds}_\Delta$ are calculated using Eq. (1.12). If $\delta s_\Delta > 1$ then the surface undergoes expansion and if $\delta s_\Delta < 1$ - compression.

Expanding $\bar{\nu}(\alpha_1,\alpha_2)$ in the bases $\{\bar{r}_1,\bar{r}_2,\bar{m}\}$ and $\{\bar{r}^1,\bar{r}^2,\bar{m}\}$, we get (Fig. 2.1)

$$\begin{aligned}\bar{\nu}(\alpha_1,\alpha_2) &= \sum_{i=1}^{2} \mathrm{F}_i(\alpha_1,\alpha_2)\bar{r}^i + \mathrm{H}(\alpha_1,\alpha_2)\bar{m} = \\ &= \sum_{i=1}^{2} \mathrm{F}^i(\alpha_1,\alpha_2)\bar{r}_i + \mathrm{H}(\alpha_1,\alpha_2)\bar{m}.\end{aligned} \tag{2.9}$$

Substituting Eq. (2.9) into (2.6) we obtain

$$\begin{aligned}\overset{*}{\bar{r}} &= \bar{r}(\alpha_1,\alpha_2) + \sum_{i=1}^{2} \mathrm{F}_i(\alpha_1,\alpha_2)\bar{r}^i + \mathrm{H}(\alpha_1,\alpha_2)\bar{m} = \\ &= \bar{r}(\alpha_1,\alpha_2) + \sum_{i=1}^{2} \mathrm{F}^i(\alpha_1,\alpha_2)\bar{r}_i + \mathrm{H}(\alpha_1,\alpha_2)\bar{m}.\end{aligned} \tag{2.10}$$

Evidently, the transformation (2.10) can be achieved by deformation of the middle surface S. For the purpose of parameterization of the surface $\overset{*}{S}$ the transformation could be performed fictitiously. Therefore, such transformation is called the fictitious deformation. The problem is to construct the three functions $\mathrm{F}_i(\alpha_i)$ and $\mathrm{H}(\alpha_i)$ $(i = 1, 2)$.

Differentiating Eq. (2.10) with respect to α_i and using Eqs. (1.22), (1.24), vectors $\overset{*}{\bar{r}}_i$ tangent to coordinate lines $\overset{*}{\alpha}_i$ on $\overset{*}{S}$ are found to

$$\overset{*}{\bar{r}}_i = \sum_{k=1}^{2} \left(\delta_{ik} + \underline{e}_i^k\right)\bar{r}_k + \omega_i\bar{m} = \sum_{k=1}^{2} \left(a_{ik} + \underline{e}_{ik}\right)\bar{r}^k + \underline{\omega}_i\bar{m}. \tag{2.11}$$

Here

$$\underline{e}_i^k = \frac{\partial \mathrm{F}^k}{\partial \alpha_i} + \sum_{s=1}^{2} \Gamma_{is}^k \mathrm{F}^s(\alpha_i) - \mathrm{H}(\alpha_i) b_i^k := \nabla_i \mathrm{F}^k(\alpha_i) - \mathrm{H}(\alpha_i) b_i^k,$$

$$\underline{e}_{ki} = \frac{\partial \mathrm{F}_k}{\partial \alpha_i} - \sum_{s=1}^{2} \Gamma_{ik}^s \mathrm{F}_s(\alpha_i) - \mathrm{H}(\alpha_i) b_{ik} := \nabla_i \mathrm{F}_k(\alpha_i) - \mathrm{H}(\alpha_i) b_{ik}, \tag{2.12}$$

$$\underline{\omega}_i = \frac{\partial \mathrm{H}(\alpha_i)}{\partial \alpha_i} + b_i^k \mathrm{F}_k(\alpha_i),$$

and $\nabla_i(\ldots)$ is the covariant derivative in metric a_{jk}, δ_{ik} is the Kronecker delta, b_{ik}, b_i^k are the components of the second fundamental form of S. Substituting Eq. (2.11) into (1.4) the components of the metric tensor $\overset{*}{\mathbf{A}}$ on $\overset{*}{S}$ are found to be

$$\overset{*}{\alpha}_{ik} = a_{ik} + 2\underline{\varepsilon}_{ik}, \tag{2.13}$$

where $\underline{\varepsilon}_{ik}$ are the components of the tensor of tangent fictitious deformations given by [compare to Eqs. (1.67), Chap. 1]

$$2\underline{\varepsilon}_{ik} = \overset{*}{\bar{r}}_i \overset{*}{\bar{r}}_k - \bar{r}_i \bar{r}_k = \underline{e}_{ik} + \underline{e}_{ki} + a_{js} \underline{e}_{ij} \underline{e}_{ks} + \varpi_i \varpi_k. \tag{2.14}$$

In just the same way as we introduced bending deformations $\varkappa_{ik}$, we introduce bending fictitious deformations of the surface S

$$\underline{\varkappa}_{ik} = b_{ik} - \overset{*}{b}_{ik}. \tag{2.15}$$

The components $\underline{\varepsilon}_{ik}$ and $\underline{\varkappa}_{ik}$ are interdependent and satisfy the conditions of continuity similar to those given by Eqs. (1.85), (1.90). Expressing $\underline{\varepsilon}_{ik}$ and $\underline{\varkappa}_{ik}$ in terms of $\mathrm{F}_i(\alpha_i)$ and $\mathrm{H}(\alpha_i)$ we find that the continuity conditions require existence of continuous derivatives of the functions up to order three at all regular points of the undeformed surface S.

2.2 Parameterization of the Equidistant Surface

Let a point $M(\alpha_1, \alpha_2) \in S$ be in one-to-one correspondence with point $M_z(\alpha_1, \alpha_2)$ on an equidistant surface S_z ($S_z \parallel S$). The position vector $\overline{\rho}$ of M_z is given by

$$\overline{\rho}(\alpha_1, \alpha_2) = \bar{r}(\alpha_1, \alpha_2) + \mathrm{H}^z \bar{m}, \tag{2.16}$$

where $\mathrm{H}^z = \text{const}$. Comparison of Eqs. (2.16) and (2.10) shows that the surface S_z can be obtained from S by fictitious deformation, i.e. by continuous displacement of

all points on S by H^z in the direction of the normal vector $\bar{m}(\bar{m}\perp S)$ (Fig. 1.5). Since $\mathrm{F}_i(\alpha_1,\alpha_2)=0$ and $\partial\mathrm{H}^z/\partial\alpha_i=0$ in (2.16), $\underline{e}_i^k$, $\underline{e}_{ki}$, $\underline{\omega}_i$ take the form

$$\underline{e}_i^k=-\mathrm{H}^z b_i^k,\quad \underline{e}_{ki}=-\mathrm{H}^z b_{ik},\quad \underline{\omega}_i=0. \tag{2.17}$$

Bases vectors $\overline{\rho}_i$ on S_z are defined by

$$\overline{\rho}_i:=\frac{\partial\overline{\rho}}{\partial\alpha_i}=\sum_{k=1}^{2}\left(\delta^k{}_i-\mathrm{H}^z b_i^k\right)\bar{r}_k=\sum_{k=1}^{2}\theta_i^k\bar{r}_k. \tag{2.18}$$

Hence, the components a_{ik}^z of the metric tensor on S_z are

$$a_{ik}^z=\overline{\rho}_i\overline{\rho}_k=\sum_{s=1}^{2}\sum_{n=1}^{2}\theta_i^s\theta_k^n a_{sn}=a_{ik}-2\mathrm{H}^z b_{ik}+(\mathrm{H}^z)^2\xi_{ik}, \tag{2.19}$$

where ξ_{ik} are the components of the third metric tensor of S are given by

$$\xi_{ik}=\sum_{n=1}^{2}b^n{}_i b_{nk}=2\Gamma b_{ik}-Ka_{ik}. \tag{2.20}$$

Here Γ, K are the mean and the Gaussian curvature of S, respectively.
Since $\bar{m}=\bar{m}_z$ $(\bar{m}_z\perp S_z)$,

$$b_{ik}^z=-\overline{\rho}_i\bar{m}_z=-\overline{\rho}_i\bar{m}=-\bar{r}_n\bar{m}_k\left(\delta_i^n-\mathrm{H}^z b_i^n\right)=$$

$$=b_{nk}\left(\delta_i^n-\mathrm{H}^z b_i^n\right)=b_{ik}-\mathrm{H}^z\xi_{ik}.$$

From the above with the help of Eq. (2.16), we find

$$b_{ik}^z=\sum_{n=1}^{2}b_{nk}\xi_i^n=b_{ik}(1-2\Gamma\mathrm{H}^z)+a_{ik}K\mathrm{H}^z. \tag{2.21}$$

Making use of Eq. (2.18) in the vector product $(\overline{\rho}_1\times\overline{\rho}_2)$, we obtain

$$\begin{aligned}&\overline{\rho}_1\times\overline{\rho}_2=\sum_{k=1}^{2}\sum_{j=1}^{2}(\bar{r}_k\times\bar{r}_j)\theta^k{}_1\theta^j{}_2=(\bar{r}_1\times\bar{r}_2)\left(\theta_1^1\theta_2^2-\theta_1^2\theta_2^1\right)=\\&=(\bar{r}_1\times\bar{r}_2)\left(1-2\Gamma\mathrm{H}^z+K(\mathrm{H}^z)^2\right).\end{aligned} \tag{2.22}$$

Recalling that $(\overline{\rho}_1\times\overline{\rho}_2)^2=a^z$ and $(\bar{r}_1\times\bar{r}_2)^2=a$, we get, finally

$$a^z = a\Big(1 - 2\Gamma \mathrm{H}^z + K(\mathrm{H}^z)^2\Big)^2. \tag{2.23}$$

Thus, the change of a given surface element on S during transformation is found to be

$$\delta s_\Delta = \sqrt{a/a^z} = \Big(1 - 2\Gamma \mathrm{H}^z + K(\mathrm{H}^z)^2\Big) = \big(\theta_1^1\theta_2^2 - \theta_1^2\theta_2^1\big). \tag{2.24}$$

The Gaussian curvature of S_z is determined by

$$a^z K^z := b_{11}^z b_{22}^z - b_{12}^z b_{21}^z = \big(\theta_1^1\theta_2^2 - \theta_1^2\theta_2^1\big)\big(b_1^1 b_2^2 - b_2^1 b_1^2\big).$$

Using Eq. (2.24) in the above, for the Gaussian curvature of S_z we find

$$a^z K^z = a d_s^2 K. \tag{2.25}$$

The coefficients of the first and second fundamental forms of S_z satisfy the Gauss-Codazzi equations

$$a^z K^z = \frac{\partial \Gamma_{h,ij}^z}{\partial \alpha_k} - \frac{\partial \Gamma_{h,ik}^z}{\partial \alpha_j} + \sum_{s=1}^{2}\Big(\Gamma_{ik}^{(z)s}\Gamma_{s,hj}^z - \Gamma_{ij}^{(z)s}\Gamma_{s,hk}^z\Big), \tag{2.26}$$

$$\frac{\partial b_{ij}^z}{\partial \alpha_k} - \frac{\partial b_{ik}^z}{\partial \alpha_j} + \sum_{s=1}^{2}\Big(\Gamma^{(z)s}{}_{ij} b_{sk}^z - \Gamma^{(z)s}{}_{ik} b_{sj}^z\Big) = 0. \tag{2.27}$$

Here $\Gamma^z{}_{h,ij}$, $\Gamma^{(z)s}{}_{ij}$ are the Christoffel symbols of the first and second kind, respectively, given by

$$\begin{aligned} \Gamma_{h,ij}^z &= \frac{1}{2}\Big(\frac{\partial a_{jh}^z}{\partial \alpha_i} + \frac{\partial a_{ih}^z}{\partial \alpha_j} - \frac{\partial a_{ij}^z}{\partial \alpha_h}\Big), \\ \Gamma_{ij}^{(z)s} &= a^{sh}\Gamma_{h,ij}^z. \end{aligned} \tag{2.28}$$

2.3 A Single Function Variant of the Method of Fictitious Deformation

Complex biological shells may resemble classical canonical surfaces. For example, the large intestine—the goffered cylinder bears a resemblance to a circular cylinder, the urinary bladder—the prolate spheroid could be viewed as a sphere, the antropyloric region of the stomach and the ureteropelvic junction of the kidney—the distorted funnel is similar to a cone, etc. Let S be a reference canonical surface

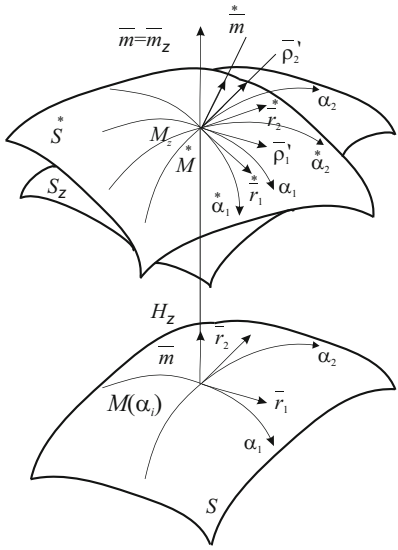

Fig. 2.2 Fictitious deformation of the surface

for $\overset{*}{S}$. Assume that the vector $\bar{m}(\bar{m}\perp S)$ drawn at any point M on S intersects the surface $\overset{*}{S}$ only once (Fig. 2.2). Setting $\mathrm{F}_i(\alpha_1,\alpha_2)=0$ from Eq. (2.9) for the displacement vector we have

$$\overline{v}(\alpha_1,\alpha_2)=\mathrm{H}(\alpha_1,\alpha_2)\bar{m}. \tag{2.29}$$

Here $\mathrm{H}(\alpha_i)$ is the distance measured along $\bar{m}$ from the surface S to $\overset{*}{S}$. Evidently, the vector equation of $\overset{*}{S}$ can be written as

$$\overset{*}{\bar{r}}=\bar{r}(\alpha_1,\alpha_2)+\mathrm{H}(\alpha_1,\alpha_2)\bar{m}. \tag{2.30}$$

Let

$$\mathrm{H}(\alpha_1,\alpha_2)=\mathrm{H}^z+\overset{*}{\mathrm{H}}(\alpha_1,\alpha_2). \tag{2.31}$$

Then substituting Eq. (2.31) in (2.30) we get

$$\overset{*}{\bar{r}}=\bar{r}(\alpha_1,\alpha_2)+\left(\mathrm{H}^z+\overset{*}{\mathrm{H}}(\alpha_1,\alpha_2)\right)\bar{m}. \tag{2.32}$$

Eq. (2.32) describes the superposition of two consecutive transformations: first, the transformation of the canonical surface S onto an equidistant surface S_z followed by the second transformation of S_z to $\overset{*}{S}$.

Differentiating Eq. (2.30) with respect to α_i and using $\bar{m}_i = -b_i^k \bar{r}_k$, bases vectors $\overset{*}{\bar{r}}_i$ on to $\overset{*}{S}$ are found to be

$$\overset{*}{\bar{r}}_i = \sum_{k=1}^{2} \bar{r}_k \left(\delta_i^k - \mathrm{H}(\alpha_i) b_i^k\right) + \frac{\partial \mathrm{H}(\alpha_i)}{\partial \alpha_i} \bar{m}. \tag{2.33}$$

Making use of Eqs. (2.18), (2.31) in (2.33) we get

$$\overset{*}{\bar{r}}_i = \overline{\rho}_i' + \frac{\partial \overset{*}{\mathrm{H}}(\alpha_i)}{\partial \alpha_i} \bar{m}, \tag{2.34}$$

here

$$\overline{\rho}_i' = \overline{\rho}_i + \overset{*}{\mathrm{H}}(\alpha_i) \sum_{k=1}^{2} b_i^k \bar{r}_k.$$

Vectors $\overline{\rho}_i'$ lay in the tangent plane of the equidistant surface S_z and are collinear to vectors $\bar{r}_i \in S$. Therefore, at any point $\overset{*}{M}\left(\overset{*}{\alpha}_1, \overset{*}{\alpha}_2\right) \in \overset{*}{S}$ we can introduce two interrelated orthogonal bases, i.e. the main basis $\left\{\overset{*}{\bar{r}}_1, \overset{*}{\bar{r}}_2, \bar{m}\right\}$ with vectors $\overset{*}{\bar{r}}_i$ tangent to the coordinate lines $\overset{*}{\alpha}_i$ and the vector $\bar{m}$ normal to $\overset{*}{S}$, and an auxiliary basis $\left\{\overline{\rho}_1', \overline{\rho}_2', \bar{m}'\right\}$. The latter also serves as the main basis for the surface S_z that runs through $\overset{*}{M}$ parallel to S and $\bar{m}' = \bar{m}$.

Substituting Eq. (2.34) in (1.4) and using the fact that $\overline{\rho}_i' \bar{m} = 0$, for the components of the metric tensor $\overset{*}{\mathbf{A}}$ we find

$$\overset{*}{\alpha}_{ik} = a_{ik}^z + \frac{\partial \overset{*}{\mathrm{H}}(\alpha_i)}{\partial \alpha_i} \frac{\partial \overset{*}{\mathrm{H}}(\alpha_i)}{\partial \alpha_k}. \tag{2.35}$$

Here

$$\begin{aligned} a_{ik}^z &= \sum_{s=1}^{2} \sum_{n=1}^{2} \left(\delta_i^s - \mathrm{H}(\alpha_i) b_i^s\right) \left(\delta_k^n - \mathrm{H}(\alpha_i) b_k^n\right) a_{sn} = \\ &= a_{ik} - 2\mathrm{H}(\alpha_i) b_{ik} + \mathrm{H}(\alpha_i)^2 \xi_{ik} = \\ &= a_{ik} \left(1 + \overset{*}{\mathrm{H}}(\alpha_i)^2 K\right) + 2\left(\Gamma \overset{*}{\mathrm{H}}(\alpha_i) - 1\right) \overset{*}{\mathrm{H}}(\alpha_i) b_k^i. \end{aligned} \tag{2.36}$$

where use is made of Eqs. (2.19), (2.20). On use of Eq. (2.35), (2.36) in (2.13) for the tensor of tangent fictitious deformations $2\underline{\varepsilon}_{ik}$ we obtain

$$2\underset{ik}{\varepsilon} = 2\underset{ik}{\varepsilon^z} + \frac{\partial \overset{*}{\mathrm{H}}(\alpha_i)}{\partial \alpha_i}\frac{\partial \overset{*}{\mathrm{H}}(\alpha_i)}{\partial \alpha_k},$$
$$2\underset{ik}{\varepsilon^z} = 2\mathrm{H}(\alpha_i)b_{ik} + \mathrm{H}(\alpha_i)^2\xi_{ik}. \tag{2.37}$$

From Eq. (2.25) the determinant $\overset{*}{a}$ is found to be

$$\overset{*}{a} = a^z + a^z_{11}\left(\frac{\partial \overset{*}{\mathrm{H}}(\alpha_i)}{\partial \alpha_2}\right)^2 + a^z_{22}\left(\frac{\partial \overset{*}{\mathrm{H}}(\alpha_i)}{\partial \alpha_1}\right)^2 - 2a^z_{12}\frac{\partial \overset{*}{\mathrm{H}}(\alpha_i)}{\partial \alpha_1}\frac{\partial \overset{*}{\mathrm{H}}(\alpha_i)}{\partial \alpha_2}, \tag{2.38}$$

where the determinant a^z is given by Eq. (2.23).

Substituting Eq. (2.34) into formula $\overset{*}{\bar{m}} = (1/2)\,\overset{*}{c}{}^{ik}\left(\overset{*}{\bar{r}}_i, \overset{*}{\bar{r}}_k\right)$ and using Eqs. (1.8)–(1.10) for the normal vector $\overset{*}{\bar{m}}\left(\overset{*}{\bar{m}} \perp \overset{*}{S}\right)$ we have

$$\overset{*}{\bar{m}} = \frac{1}{2}\sqrt{\frac{a_z}{a}}c^{ik}_z\left[\left(\overline{\rho}'_i, \overline{\rho}'_k\right) + \frac{\partial \overset{*}{\mathrm{H}}(\alpha_i)}{\partial \alpha_k}\left(\overline{\rho}'_i, \bar{m}\right) + \frac{\partial \overset{*}{\mathrm{H}}(\alpha_i)}{\partial \alpha_i}\left(\bar{m}, \overline{\rho}'_k\right)\right] =$$

$$= \frac{\mathrm{H}_0}{2}\sum_{i=1}^{2}\sum_{k=1}^{2}c^{ik}_z\left(\bar{m}c^z_{ik} + \sum_{j=1}^{2}\left(c^z_{ij}\overline{\rho}'^j\frac{\partial \overset{*}{\mathrm{H}}(\alpha_i)}{\partial \alpha_k} - c^z_{jk}\overline{\rho}'^j\frac{\partial \overset{*}{\mathrm{H}}(\alpha_i)}{\partial \alpha_i}\right)\right) =$$

$$= \mathrm{H}_0\left(\bar{m} - \sum_{i=1}^{2}\overline{\rho}'^i\frac{\partial \overset{*}{\mathrm{H}}(\alpha_i)}{\partial \alpha_i}\right) = \mathrm{H}_0\left(\bar{m} - \sum_{k=1}^{2}\overline{\rho}'_i a^{ik}_z\frac{\partial \overset{*}{\mathrm{H}}(\alpha_i)}{\partial \alpha_k}\right), \tag{2.39}$$

where

$$a_z = a\mathrm{H}_0^2, \quad \mathrm{H}_0 = \left(1 + \sum_{i=1}^{2}\sum_{k=1}^{2}a^{ik}_z\frac{\partial \overset{*}{\mathrm{H}}(\alpha_i)}{\partial \alpha_i}\frac{\partial \overset{*}{\mathrm{H}}(\alpha_i)}{\partial \alpha_k}\right).$$

Further, substituting $\overline{\rho}'_i = \overline{\rho}_i + \overset{*}{\mathrm{H}}(\alpha_i)b^k_i\bar{r}_k$ into (2.39) for $\overset{*}{\bar{m}}$ in terms of bases vectors $\bar{r}_k \in S$ we obtain

$$\overset{*}{\bar{m}} = \mathrm{H}_0\left(\bar{m} - \bar{r}_k a^{ik}_z\frac{\partial \overset{*}{\mathrm{H}}(\alpha_i)}{\partial \alpha_k}\left(\delta^k_i - \mathrm{H}(\alpha_i)\mathrm{b}^k_i\right)\right). \tag{2.40}$$

Differentiating Eq. (2.39) with respect to α_i we get

$$\overset{*}{\bar{m}}_i = \mathrm{H}_0 \left(\bar{m} - \sum_{k=1}^{2} \overline{\rho}'^k \frac{\partial \overset{*}{\mathrm{H}}(\alpha_i)}{\partial \alpha_k} \right) \frac{\partial \mathrm{H}_0}{\partial \alpha_i} + \mathrm{H}_0 \frac{\partial}{\partial \alpha_i} \left(\bar{m} - \sum_{k=1}^{2} \overline{\rho}'^k \frac{\partial \overset{*}{\mathrm{H}}(\alpha_i)}{\partial \alpha_k} \right). \quad (2.41)$$

Using Eq. (2.39) the first term in the above can be written in the form

$$\bar{m} - \bar{r}^k \frac{\partial \overset{*}{\mathrm{H}}(\alpha_i)}{\partial \alpha_k} = \frac{\overset{*}{\bar{m}}_i}{\mathrm{H}_0} \frac{\partial \mathrm{H}_0}{\partial \alpha_i}. \quad (2.42)$$

In the second term we introduce the covariant derivative with respect to a^z_{ik} as (see Eq. (2.12))

$$\frac{\partial}{\partial \alpha_i} \left(\bar{m} - \sum_{k=1}^{2} \overline{\rho}'^k \frac{\partial \overset{*}{\mathrm{H}}(\alpha_i)}{\partial \alpha_k} \right) := \nabla^z_i \left(\bar{m} - \sum_{k=1}^{2} \overline{\rho}'^k \frac{\partial \overset{*}{\mathrm{H}}(\alpha_i)}{\partial \alpha_k} \right) =$$

$$= \bar{m} - \sum_{k=1}^{2} \frac{\partial \overset{*}{\mathrm{H}}(\alpha_i)}{\partial \alpha_k} \nabla^z_i \overline{\rho}'^k - \sum_{k=1}^{2} \overline{\rho}'^k \nabla^z_i \left(\frac{\partial \overset{*}{\mathrm{H}}(\alpha_i)}{\partial \alpha_k} \right), \quad (2.43)$$

Derivatives of vectors $\overline{\rho}'_i$ and $\bar{m}$ can be found from Eqs. (1.18) and (1.22) by substituting $\overline{\rho}'_i$ for $\bar{r}_i$. Since the components of the second fundamental form of S_z in terms of b_{ik} are given by

$$b^z_{ik} = \sum_{n=1}^{2} b_{nk} \theta^n_i = b_{ik}(1 - 2\Gamma \mathrm{H}(\alpha_i)) + a_{ik} K \mathrm{H}(\alpha_i),$$
$$b^{(z)k}_i = \sum_{s=1}^{2} a^{ks}_z b^z_{is}. \quad (2.44)$$

Thus, Eq. (2.43) can be written in the form

$$\frac{\partial}{\partial \alpha_i} \left(\bar{m} - \overline{\rho}'^k \frac{\partial \overset{*}{\mathrm{H}}(\alpha_i)}{\partial \alpha_k} \right) = \bar{m} - \sum_{k=1}^{2} \frac{\partial \overset{*}{\mathrm{H}}(\alpha_i)}{\partial \alpha_k} b^{(z)k}_i \bar{m} - \sum_{k=1}^{2} \overline{\rho}'^k \nabla^z_i \frac{\partial \overset{*}{\mathrm{H}}(\alpha_i)}{\partial \alpha_k}. \quad (2.45)$$

Substituting Eqs. (2.42), (2.45) into (2.41) for $\overset{*}{\bar{m}}_i$ we get, finally,

$$\overset{*}{\bar{m}}_i = \frac{\overset{*}{\bar{m}}_i}{\mathrm{H}_0}\frac{\partial \mathrm{H}_0}{\partial \alpha_i} + \mathrm{H}_0\left(\bar{m} - \frac{\partial \overset{*}{\mathrm{H}}(\alpha_i)}{\partial \alpha_k} b_i^{(z)k}\bar{m} - \overline{\rho}'^k \nabla_i^z \frac{\partial \overset{*}{\mathrm{H}}(\alpha_i)}{\partial \alpha_k}\right). \tag{2.46}$$

The coefficients b_{ik} are found from Eq. (1.18) by substituting Eqs. (2.34), (2.46)

$$\begin{aligned} b_{ik} &= \mathrm{H}_0 \sum_{j=1}^{2}\left(b_{ij}^{(z)}\left(\delta_k^j + a_z^{ji}\frac{\partial \overset{*}{\mathrm{H}}(\alpha_i)}{\partial \alpha_i}\frac{\partial \overset{*}{\mathrm{H}}(\alpha_i)}{\partial \alpha_k}\right) + \nabla_i^z\left(\frac{\partial \overset{*}{\mathrm{H}}(\alpha_i)}{\partial \alpha_k}\right)\right) = \\ &= \mathrm{H}_0 \sum_{j=1}^{2}\left(b_i^{(z)j}\left(a_{kj}^z - \frac{\partial \overset{*}{\mathrm{H}}(\alpha_i)}{\partial \alpha_k}\frac{\partial \overset{*}{\mathrm{H}}(\alpha_i)}{\partial \alpha_j}\right) + \nabla_i^z\left(\frac{\partial \overset{*}{\mathrm{H}}(\alpha_i)}{\partial \alpha_k}\right)\right) = \\ &= \mathrm{H}_0 \sum_{j=1}^{2}\left(b_i^{(z)j}a_{kj} + \nabla_i^z\left(\frac{\partial \overset{*}{\mathrm{H}}(\alpha_i)}{\partial \alpha_k}\right)\right). \end{aligned} \tag{2.47}$$

The Christoffel symbols $\overset{*}{\Gamma}_{ij,k}$ of the first kind are calculated from $\overset{*}{\Gamma}_{ij,k} = \overset{*}{\bar{r}}_{ij}\overset{*}{\bar{r}}_k$. Thus differentiating Eq. (2.33) with respect to α_j and multiplying the resultant equation by $\overset{*}{\bar{r}}_i$, we find

$$\overset{*}{\Gamma}_{ij,k} = \Gamma_{ij,k}^{(z)} + \frac{\partial^2 \overset{*}{\mathrm{H}}(\alpha_i)}{\partial \alpha_i \partial \alpha_j}\frac{\partial \overset{*}{\mathrm{H}}(\alpha_i)}{\partial \alpha_k}, \tag{2.48}$$

where $\Gamma_{ij,k}^{(z)}$ are calculated using (2.28). The Christoffel symbols of the second kind $\overset{*}{\Gamma}_{ij}^k$ are found to be

$$\begin{aligned} \overset{*}{\Gamma}_{ij}^{\ k} &= \overset{*}{a}^{\alpha k}\overset{*}{\Gamma}_{ij,\alpha} = \\ &= \left(\Gamma_{ij,\alpha}^{(z)} + \frac{\partial^2 \overset{*}{\mathrm{H}}(\alpha_i)}{\partial \alpha_i \partial \alpha_j}\right)\left(a_z^{\alpha k} - \mathrm{H}_0^2 \sum_{m=1}^{2}\sum_{j=1}^{2} a_z^{\alpha m}a_z^{jk}\frac{\partial \overset{*}{\mathrm{H}}(\alpha_i)}{\partial \alpha_m}\frac{\partial \overset{*}{\mathrm{H}}(\alpha_i)}{\partial \alpha_j}\right), \end{aligned} \tag{2.49}$$

where

$$\overset{*}{a}^{\alpha k} = a_z^{\alpha k} - \mathrm{H}_0^2 \sum_{j=1}^{2}\sum_{m=1}^{2} a_z^{\alpha m}a_z^{jk}\frac{\partial \overset{*}{\mathrm{H}}(\alpha_i)}{\partial \alpha_m}\frac{\partial \overset{*}{\mathrm{H}}(\alpha_i)}{\partial \alpha_j}.$$

2.4 Parameterization of a Complex Surface in Preferred Coordinates

The problem of parameterization of a complex surface simplifies significantly if the surface S is referred to coordinate lines (α_1, α_2) that are the lines of curvature. Differentiating Eq. (2.30) with respect to α_i with the help of Eq. (1.30) the base vectors $\overset{*}{\bar{r}}_i \in \overset{*}{S}$ are found to be

$$\overset{*}{\bar{r}}_i = A_i^z(\bar{e}_i + y_i\bar{m}). \tag{2.50}$$

Here $A_i^z = A_i\theta_i = A_i[1 + \mathrm{H}(\alpha_i)/R_i]$, A_i are the Lamé parameters, R_i are the radii of the principal curvature, $\bar{e}_i$ are the unit vectors on S. The coefficients y_i are given by

$$y_i = \frac{1}{A_i^z}\frac{\partial \mathrm{H}(\alpha_j)}{\partial \alpha_i} \equiv \frac{1}{A_i\left[1 + \mathrm{H}(\alpha_j)/R_i\right]}\frac{\partial \mathrm{H}(\alpha_j)}{\partial \alpha_i}. \tag{2.51}$$

The first term in Eq. (2.50) defines the bases vectors $\overline{\rho}_i'$ on the equidistant surface S_z. Hence, at any point $\overset{*}{M} \in \overset{*}{S}$ the unit vector $\bar{e}_i^z = \overline{\rho}_i/A_i^z(\bar{e}_i^z \in S_z)$ equals unit vector $\bar{e}_i$ defined on the canonical surface S: $\bar{e}_i^z = \bar{e}_i$.

Analogously to Eq. (2.40), for decomposition of the normal vector $\overset{*}{\bar{m}}$ we have

$$\overset{*}{\bar{m}} = \varsigma(\bar{m} - \varsigma_i\bar{e}_i). \tag{2.52}$$

On use of Eqs. (2.50) (2.52) the scalar product of Eq. (2.52) by $\overset{*}{\bar{m}}$ and $\overset{*}{\bar{r}}_i$ yields

$$\varsigma_i = y_i, \quad \varsigma = 1/\sqrt{1 + y^2{}_1 + y^2{}_2}.$$

Hence,

$$\overset{*}{\bar{m}} = \varsigma(\bar{m} - y_i\bar{e}_i) = \frac{1}{\sqrt{1 + y^2{}_1 + y^2{}_2}}(\bar{m} - y_1\bar{e}_1 - y_2\bar{e}_2). \tag{2.53}$$

Substituting Eq. (2.50) in $\overset{*}{a}_{ik} = \overset{*}{\bar{r}}_i\, \overset{*}{rk}_i$ we obtain

$$\overset{*}{a}_{ik} = A_i^z A_k^z(\delta_{ik} + y_i y_k). \tag{2.54}$$

The determinant of the metric tensor $\overset{*}{\mathbf{A}}$ on $\overset{*}{S}$ is found to be

$$\overset{*}{a} = \overset{*}{a}_{11}\overset{*}{a}_{22} - \overset{*}{a}{}^{2}_{12} = a^z_{11}a^z_{22}\left(1 + y_1^2 + y_2^2 + y_1^2y_2^2\right)$$
$$- a^z_{11}a^z_{22}y_1^2y_2^2 = a^z_{11}a^z_{22}\left(1 + y_1^2 + y_2^2\right) = \frac{a^z_{11}a^z_{22}}{\varsigma^2}. \qquad (2.55)$$

The contravariant components $\overset{*}{a}{}^{ik}$ of $\overset{*}{\mathbf{A}}$ are calculated as

$$\overset{*}{a}{}^{11} = \frac{\overset{*}{a}_{22}}{\overset{*}{a}} = \frac{\left(1 + y_2^2\right)\varsigma^2}{a^z_{11}}, \quad \overset{*}{a}{}^{22} = \frac{\left(1 + y_1^2\right)\varsigma^2}{a^z_{22}}, \quad \overset{*}{a}{}^{12} = -\frac{a^z_{22}}{\overset{*}{a}} = -\frac{y_1y_2\varsigma^2}{A_1^zA_2^z}. \qquad (2.56)$$

Differentiating Eq. (2.53) with respect to α_i we get

$$\begin{aligned}
\overset{*}{\bar{m}}_1 &= \frac{\partial\varsigma}{\partial\alpha_1}(\bar{m} - y_i\bar{e}_i) + \varsigma\left[\frac{A_1}{R_1}\bar{e}_1 - \frac{\partial y_i}{\partial\alpha_1}\bar{e}_i + \right.\\
&\left. + \frac{\partial\varsigma}{\partial\alpha_1}\left(\frac{A_1}{R_1}\bar{m} + \frac{\bar{e}_2}{A_2}\frac{\partial A_1}{\partial\alpha_2}\right) - \frac{\partial\varsigma}{\partial\alpha_2}\frac{\bar{e}_1}{A_2}\frac{\partial A_1}{\partial\alpha_2}\right],\\
\overset{*}{\bar{m}}_2 &= \frac{\partial\varsigma}{\partial\alpha_2}(\bar{m} - y_i\bar{e}_i) + \varsigma\left[\frac{A_2}{R_2}\bar{e}_2 - \frac{\partial y_i}{\partial\alpha_2}\bar{e}_i + \right.\\
&\left. + \frac{\partial\varsigma}{\partial\alpha_2}\left(\frac{A_2}{R_2}\bar{m} + \frac{\bar{e}_1}{A_1}\frac{\partial A_2}{\partial\alpha_1}\right) - \frac{\partial\varsigma}{\partial\alpha_1}\frac{\bar{e}_2}{A_1}\frac{\partial A_2}{\partial\alpha_1}\right]
\end{aligned} \qquad (2.57)$$

where use is made of Eqs. (1.30). Substituting Eqs. (2.49), (2.57) into $\overset{*}{b}_{ik} = -\overset{*}{\bar{m}}_i\overset{*}{\bar{r}}_k$ we obtain

$$\begin{aligned}
\overset{*}{b}_{11} &= -A_1^z\varsigma\left(\frac{A_1}{R_1}\sqrt{1 + y_1^2} - \frac{\partial y_1}{\partial\alpha_1} - \frac{y_2}{A_2}\frac{\partial A_1}{\partial\alpha_2}\right),\\
\overset{*}{b}_{22} &= -A_2^z\varsigma\left(\frac{A_2}{R_2}\sqrt{1 + y_2^2} - \frac{\partial y_2}{\partial\alpha_2} - \frac{y_1}{A_1}\frac{\partial A_2}{\partial\alpha_1}\right),\\
\overset{*}{b}_{12} &= -A_2^z\varsigma\left(y_1y_2\frac{A_1}{R_1} - \frac{\partial y_2}{\partial\alpha_1} - \frac{y_1}{A_2}\frac{\partial A_1}{\partial\alpha_2}\right) = \overset{*}{b}_{21}.
\end{aligned} \qquad (2.58)$$

Formulas (2.48), (2.49) and (2.28) are used to calculate the Christoffel symbols $\overset{*}{\Gamma}{}^{k}_{ij}$ on $\overset{*}{S}$. $\Gamma^{(z)k}_{ij}$ are calculated from Eqs. (1.27) by replacing A_i^z and their derivatives for A_i and $\partial A_i/\partial\alpha_{1,2}$, respectively.

For example, consider a shell of complex geometry $\overset{*}{S}$ as shown in Fig. 2.3.

Let a cylinder of a constant radius R_0 be the reference surface for $\overset{*}{S}$. Its orientation with respect to $\overset{*}{S}$ is such that the function $\mathrm{H}(\alpha_i)$ and its derivatives satisfy the uniqueness of transformation (2.30).

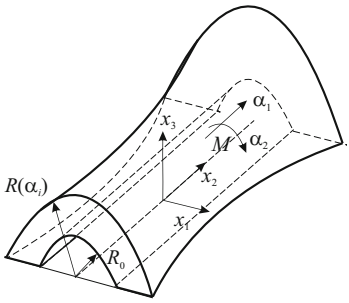

Fig. 2.3 A shell of complex geometry in relation to the canonical cylindrical surface

Introduce polar coordinates α_1, α_2 on S, such that α_1 is the axial and α_2 is the polar angular coordinate. They are related to the global Cartesian coordinates by

$$\bar{r}(\alpha_i) = x\bar{i} + y\bar{j} + z\bar{k} = R_0(\bar{i}\sin\alpha_2 + \bar{k}\cos\alpha_2) + \alpha_1\bar{j}. \tag{2.59}$$

The Lamé parameters A_i and curvatures k_{ij} are given by

$$\begin{aligned} &A_1 = 1, \quad A_2 = R_0, \\ &k_{11} = 1/R_1 = 0, \quad k_{12} = 0, \quad k_{22} = 1/R_2 = 1/R_0. \end{aligned} \tag{2.60}$$

For the coefficients $\theta_i = 1 + \mathrm{H}(\alpha_i)/R_i$ we have

$$\theta_1 = 1, \quad \theta_2 = 1 + \mathrm{H}(\alpha_i)/R_0. \tag{2.61}$$

Hence, from Eq. (2.51) for y_i we obtain

$$y_1 = \frac{\partial \mathrm{H}(\alpha_i)}{\partial \alpha_1}, \quad y_2 = \frac{1}{R_0 + \mathrm{H}(\alpha_j)}. \tag{2.62}$$

Substituting Eqs. (2.60)–(2.62) in (2.54) we find

$$\begin{aligned} &\overset{*}{a}_{11} = 1 + y_1^2 = 1 + \left(\tfrac{\partial \mathrm{H}(\alpha_i)}{\partial \alpha_1}\right)^2, \\ &\overset{*}{a}_{22} = (R_0 + \mathrm{H}(\alpha_i))^2\left(1 + y_2^2\right) = (R_0 + \mathrm{H}(\alpha_i))^2 + \left(\tfrac{\partial \mathrm{H}(\alpha_i)}{\partial \alpha_2}\right)^2, \\ &\overset{*}{a}_{12} = \overset{*}{a}_{21} = (R_0 + \mathrm{H}(\alpha_i))^2 y_1 y_2 = \frac{\partial \mathrm{H}(\alpha_i)}{\partial \alpha_1}\frac{\partial \mathrm{H}(\alpha_i)}{\partial \alpha_2}. \end{aligned} \tag{2.63}$$

The coefficients of the second fundamental form are found to be

$$
\begin{aligned}
&\overset{*}{b}_{11} = \varsigma \frac{\partial y_1}{\partial \alpha_1} = \varsigma \frac{\partial^2 \mathrm{H}(\alpha_i)}{\partial \alpha_1^2}, \\
&\overset{*}{b}_{12} = \overset{*}{b}_{21} = \varsigma \left(\frac{\partial y_1}{\partial \alpha 2} - y_1 y_2 \right) = \\
&\quad = \varsigma \left(\frac{\partial^2 \mathrm{H}(\alpha_i)}{\partial \alpha_1 \partial \alpha_2} - \frac{1}{R_0 + \mathrm{H}(\alpha_i)} \frac{\partial \mathrm{H}(\alpha_i)}{\partial \alpha_1} \frac{\partial \mathrm{H}(\alpha_i)}{\partial \alpha_2} \right), \\
&\overset{*}{b}_{22} = -\frac{1}{R_0 + \mathrm{H}(\alpha_i)} \varsigma \left(1 - \frac{1}{R_0 + \mathrm{H}(\alpha_i)} \frac{\partial^2 \mathrm{H}(\alpha_i)}{\partial \alpha_1 \partial \alpha_2} + \left(\frac{\partial \mathrm{H}(\alpha_i)/\partial \alpha_2}{R_0 + \mathrm{H}(\alpha_i)} \right)^2 \right).
\end{aligned}
\tag{2.64}
$$

Here

$$
\varsigma = \sqrt{1 + \frac{\partial^2 \mathrm{H}(\alpha_i)}{\partial \alpha_1^2} + \left(\frac{\partial \mathrm{H}(\alpha_i)/\partial \alpha_2}{R_0 + \mathrm{H}(\alpha_i)} \right)^2}.
$$

Substituting Eq. (2.63) into (2.47) after some algebra for $\overset{*}{\Gamma}{}_{ij}^{k}$ we have

$$
\begin{aligned}
&\overset{*}{a}\,\Gamma_{11}^1 = \frac{\partial \mathrm{H}(\alpha_i)}{\partial \alpha_1} \left[(R_0 + \mathrm{H}(\alpha_i))^2 \frac{\partial^2 \mathrm{H}(\alpha_i)}{\partial \alpha_1^2} - 2 \frac{\partial \mathrm{H}(\alpha_i)}{\partial \alpha_1} \frac{\partial \mathrm{H}(\alpha_i)}{\partial \alpha_2} \frac{\partial^2 \mathrm{H}(\alpha_i)}{\partial \alpha_1 \partial \alpha_2} \right], \\
&\overset{*}{a}\,\Gamma_{11}^2 = \frac{\partial \mathrm{H}(\alpha_i)}{\partial \alpha_2} \frac{\partial^2 \mathrm{H}(\alpha_i)}{\partial \alpha_1^2}, \\
&\overset{*}{a}\,\Gamma_{12}^1 = (R_0 + \mathrm{H}(\alpha_i)) \frac{\partial \mathrm{H}(\alpha_i)}{\partial \alpha_1} \left[(R_0 + \mathrm{H}(\alpha_i)) \frac{\partial^2 \mathrm{H}(\alpha_i)}{\partial \alpha_1 \partial \alpha_2} - \frac{\partial \mathrm{H}(\alpha_i)}{\partial \alpha_1} \frac{\partial \mathrm{H}(\alpha_i)}{\partial \alpha_2} \right], \\
&\overset{*}{a}\,\Gamma_{22}^1 = (R_0 + \mathrm{H}(\alpha_i))^3 \frac{\partial \mathrm{H}(\alpha_i)}{\partial \alpha_1} \left[\frac{1}{(R_0 + \mathrm{H}(\alpha_i))} \frac{\partial^2 \mathrm{H}(\alpha_i)}{\partial \alpha_2^2} - \right. \\
&\qquad \left. -2 \left(\frac{1}{(R_0 + \mathrm{H}(\alpha_i))} \frac{\partial \mathrm{H}(\alpha_i)}{\partial \alpha_2} \right)^2 - 1 \right], \\
&\overset{*}{a}\,\Gamma_{12}^2 = \frac{\partial^2 \mathrm{H}(\alpha_i)}{\partial \alpha_1 \partial \alpha_2} \frac{\partial \mathrm{H}(\alpha_i)}{\partial \alpha_2} + (R_0 + \mathrm{H}(\alpha_i)) \frac{\partial \mathrm{H}(\alpha_i)}{\partial \alpha_1} \left(1 + \left(\frac{\partial \mathrm{H}(\alpha_i)}{\partial \alpha_1} \right)^2 \right), \\
&\overset{*}{a}\,\Gamma_{22}^2 = \frac{\partial \mathrm{H}(\alpha_i)}{\partial \alpha_2} \left[R_0 + \mathrm{H}(\alpha_i) + \frac{\partial^2 \mathrm{H}(\alpha_i)}{\partial \alpha_2^2} - 2 \frac{\partial \mathrm{H}(\alpha_i)}{\partial \alpha_1} \frac{\partial \mathrm{H}(\alpha_i)}{\partial \alpha_2} \frac{\partial^2 \mathrm{H}(\alpha_i)}{\partial \alpha_1 \partial \alpha_2} \right],
\end{aligned}
\tag{2.65}
$$

where $\overset{*}{a} = (R_0 + \mathrm{H}(\alpha_i))^2/\varsigma^2$, and use is made of Eq. (2.63).

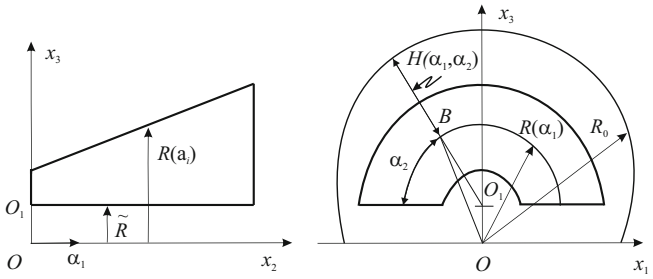

Fig. 2.4 Parameterization of a shell of complex geometry and construction of $H(\alpha_1, \alpha_2)$ function

To construct the unknown function $H(\alpha_i)$ let the surface of revolution $\overset{*}{S}$ (Fig. 2.4) be defined by

$$\overset{*}{R} = \overset{*}{R}(x) = \overset{*}{R}(\alpha_i).$$

From geometric analysis of ΔOO_1B we have

$$R_0 = H(\alpha_i) + \overline{O_1B}, \tag{2.66}$$
$$\left(\overline{OB}\right)^2 = \left(\overline{O_1B}\right)^2 + \left(\overline{O_1O}\right)^2 + 2\overline{O_1B} \cdot \overline{OB_1} \sin\alpha_2.$$

Since $\overline{OB} = \overset{*}{R}(\alpha_1), \overline{OO_1} = \tilde{R}$ the last equation can be written as

$$\left(\overline{O_1B}\right)^2 + 2\overline{O_1B} \cdot \tilde{R} \sin\alpha_2 + \tilde{R}^2 - \overset{*}{R}^2(\alpha_1) = 0.$$

On use of Eqs. (2.66) in the above, we obtain

$$H(\alpha_1, \alpha_2) = R_0 + \tilde{R} \sin\alpha_2 \pm \sqrt{\overset{*}{R}^2(\alpha_1) - \tilde{R}^2 \cos^2\alpha_2}. \tag{2.67a}$$

For $\tilde{R} = 0$ Eq. (2.67a) should satisfy the equality $\overline{O_1B} = \overset{*}{R}(\alpha_1)$. Therefore the final form for $H(\alpha_i)$ is found to be

$$H(\alpha_1, \alpha_2) = R_0 + \tilde{R} \sin\alpha_2 - \sqrt{\overset{*}{R}^2(\alpha_1) - \tilde{R}^2 \cos^2\alpha_2}. \tag{2.67b}$$

Knowing $H(\alpha_i)$ from Eqs. (2.55)–(2.65) we find coefficients and parameters that characterize geometry of the surface $\overset{*}{S}$. It is noteworthy that Eq. (2.30) can also be used to parameterize composite shells of complex geometry with variable thickness of layers.

2.5 Parameterization of Complex Surfaces on Plane

Consider a complex planar surface $\overset{*}{S}$ that is referred to coordinates $\overset{*}{\alpha}_1, \overset{*}{\alpha}_2$. Let S be the reference canonical surface to $\overset{*}{S}$ parameterized by orthogonal coordinates α_1, α_2 (Fig. 2.5). Assume that the coordinate lines are oriented along the contour C of S. Setting $\mathrm{H}(\alpha_1, \alpha_2) = 0$ in Eq. (2.10) and using Eq. (2.9) the position of a point $\overset{*}{M}$ $(\alpha_1, \alpha_2) \in \overset{*}{S}$ is given by

$$\overset{*}{\bar{r}} = \bar{r}(\alpha_1, \alpha_2) + \bar{v}(\alpha_1, \alpha_2) = \bar{r}(\alpha_1, \alpha_2) + \sum_{i=1}^{2} \mathrm{F}_i(\alpha_1, \alpha_2)\bar{e}_i. \tag{2.68}$$

Here the meaning of parameters is as described by Eqs. (1.4), (1.5), (2.9) and (2.10). Evidently, Eq. (2.68) describes the fictitious tangent deformation of the surface S onto $\overset{*}{S}$.

Differentiating Eq. (2.68) with respect to α_i, for tangent vectors $\overset{*}{\bar{r}}_i$ we get

$$\overset{*}{\bar{r}}_i = A_i \sum_{k=1}^{2} \left(\delta_{ik} + \underline{e}_{ik}\right)\bar{e}_k, \tag{2.69}$$

where the rotation parameters are given by

$$\underline{e}_{11} = \frac{1}{A_1}\frac{\partial \mathrm{F}_1(\alpha_i)}{\partial \alpha_1} + \frac{\partial A_1}{\partial \alpha_2}\frac{\mathrm{F}_2(\alpha_i)}{A_1 A_2}, \quad \underline{e}_{22} = \frac{1}{A_2}\frac{\partial \mathrm{F}_2(\alpha_i)}{\partial \alpha_2} + \frac{\partial A_2}{\partial \alpha_1}\frac{\mathrm{F}_1(\alpha_i)}{A_1 A_2},$$
$$\underline{e}_{12} = \frac{1}{A_1}\frac{\partial \mathrm{F}_2(\alpha_i)}{\partial \alpha_1} - \frac{\partial A_1}{\partial \alpha_1}\frac{\mathrm{F}_1(\alpha_i)}{A_1 A_2}, \quad \underline{e}_{21} = \frac{1}{A_2}\frac{\partial \mathrm{F}_1(\alpha_i)}{\partial \alpha_2} - \frac{\partial A_2}{\partial \alpha_1}\frac{\mathrm{F}_2(\alpha_i)}{A_1 A_2}.$$

Using Eq. (2.69) the components of the tensor $\overset{*}{\mathrm{A}}$ at $\overset{*}{M}(\alpha_i) \in \overset{*}{S}$ are found to be

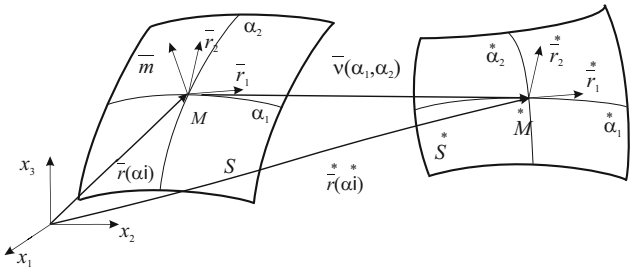

Fig. 2.5 Parameterization of a planar surface of complex geometry

$$\overset{*}{a}_{ik} = A_i A_k \left(\delta_{ik} + 2\underline{\varepsilon}_{ik}\right), \tag{2.70}$$

here $\underline{\varepsilon}_{ik}$ are the physical components of the tensor of fictitious tangent deformation of S given by

$$2\underline{\varepsilon}_{ik} = \underline{e}_{ik} + \underline{e}_{ki} + \underline{e}_{is}\underline{e}_{ks}. \tag{2.71}$$

From Eq. (2.70) the determinant of $\overset{*}{\mathrm{A}}$ is calculated as

$$\overset{*}{a} = (A_1 A_2)^2 \left[\left(1 + \underline{e}_{11}\right)\left(1 + \underline{e}_{22}\right) - \underline{e}_{12}\underline{e}_{21}\right]. \tag{2.72}$$

Making use of Eqs. (2.70), (2.72) in the formulas $\overset{*}{a}^{ii} = \overset{*}{a}_{ii}/\overset{*}{a}$, $\overset{*}{a}^{12} = \overset{*}{a}^{21} = -\overset{*}{a}_{12}/\overset{*}{a}$, one can find the contravariant components of $\overset{*}{\mathrm{A}}$. On use of $\overset{*}{a}^{ik}$ and Eqs. (2.69), (2.70) for vectors of the reciprocal basis $\overset{*}{\bar{r}}^{i}$ we obtain

$$\overset{*}{\bar{r}}^{i} = \sum_{k=1}^{2} \overset{*}{a}^{ik}\, \overset{*}{\bar{r}}_{k} = \frac{1}{\overset{*}{a}} \sum_{s=1}^{2} \sum_{k=1}^{2} \mathrm{sgn} A_i A_k \left(\delta_{ik} + 2\underline{\varepsilon}_{ik}\right)\left(\delta_{is} + \underline{e}_{is}\right)\bar{e}_s. \tag{2.73}$$

Finally, with the help of Eqs. (2.69) and (2.73) we calculate the Chrystoffel symbols of the first and second kind.

In the above derivations we assumed that coordinates α_1, α_2 are linearly independent. To remain such after transformation the tangent vectors $\overset{*}{\bar{r}}_i$ should remain non-collinear $\forall \overset{*}{M}(\alpha_1, \alpha_2) \in \overset{*}{S}$. If at any point $\overset{*}{\bar{r}}_1 \times \overset{*}{\bar{r}}_2 = 0$ then transformation (2.68) at this point experiences singularity. Substituting Eq. (2.65) and using the fact that $\bar{e}_1 \times \bar{e}_2 = 0$, after some algebra, we obtain

$$A_i A_k \left[\left(1 + \underline{e}_{11}\right)\left(1 + \underline{e}_{22}\right) - \underline{e}_{12}\underline{e}_{21}\right](e_1 \times e_2) = 0. \tag{2.74}$$

The condition of singularity is then becomes

$$A_i A_k \left[\left(1 + \underline{e}_{11}\right)\left(1 + \underline{e}_{22}\right) - \underline{e}_{12}\underline{e}_{21}\right] = \sqrt{\overset{*}{a}} = 0, \tag{2.75}$$

where use is made of Eq. (2.72).

As a final point of our discussion consider a problem of parameterization of a complex surface bounded by four smooth continuous lines (Fig. 2.6). Let the straight lines connecting corner points A, B and C, D intersect at point O.

Assume that the contour lines in polar coordinates (r, φ) $(r = \alpha_1, \varphi = \alpha_2)$ are given analytically by

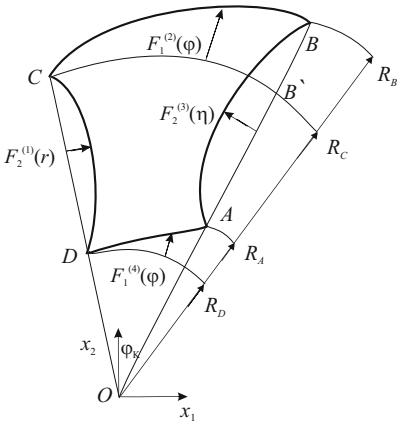

Fig. 2.6 A complex surface bounded by four continuous lines and its parameterization

$$C_1 : \mathrm{F}_2^{(1)}(r), \quad C_2 : R_c + \mathrm{F}_1^{(2)}(\varphi), \qquad C_3 : \mathrm{F}_2^{(3)}(\eta), \quad C_4 : R_D + \mathrm{F}_1^{(4)}(\varphi), \quad (2.76)$$
$$(R_D \le r \le R_C, 0 \le \varphi \le \varphi_k, 0 \le \eta \le R_B - R_C)$$

where $R_{A,B,C,D}$ are the radii and φ_k is the angle between the rays $\overline{OB}$ and $\overline{OC}$, $\mathrm{F}_2^{(1)}(r)$, $\mathrm{F}_2^{(3)}(\eta)$ are the normal distances measured from $\overline{OC}$ and $\overline{OB}$ to the contour lines C_1, C_3, respectively.

Affine transformation of the line segment $\overline{AB}$ with coordinates $u = 0$, $u = R_B - R_A$, on to the line segment $\overline{A'B'}$ is given by

$$u = \xi_1 + \xi_2 r. \quad (2.77)$$

Making use of boundary conditions

$$r = R_D : u = 0; \quad r = R_C : u = R_B - R_A, \quad (2.78)$$

the coefficients ξ_1, ξ_2 are found to be

$$\xi_1 = -R_D \xi_2, \quad \xi_2 = (R_B - R_A)/(R_C - R_D).$$

Therefore, $u = \xi_2(r - R_D)$. This allows to write the equation for C_3 in the form

$$\mathrm{F}_2^{(3)}(u) = \mathrm{F}_2^{(3)}[\xi_2(r - R_D)].$$

Expanding functions $\mathrm{F}_i(r, \varphi)$ $(i = 1, 2)$ in the form

$$\begin{aligned} \mathrm{F}_1(r, \varphi) &= \varsigma_1(\varphi) + r\varsigma_2(r), \\ \mathrm{F}_2(r, \varphi) &= \varsigma_3(r) + \varphi\varsigma_4(r), \end{aligned} \quad (2.79)$$

and using boundary conditions given by Eqs. (2.76), the coefficients of expansion ς_j are found to be

$$\begin{aligned} &r = R_D : \mathrm{F}_1(R_D, \varphi) = \mathrm{F}_1^{(4)}(\varphi), \\ &r = R_C : \mathrm{F}_1(R_C, \varphi) = F_1^{(2)}(\varphi), \\ &\varphi = 0 : \mathrm{F}_2(r, 0) = \mathrm{F}_2^{(1)}(r), \\ &\varphi = \varphi_k : \mathrm{F}_2(r, \varphi_k) = \mathrm{F}_2^{(3)}[\xi_2(r - R_D)]. \end{aligned} \tag{2.80}$$

Here $\varphi_k = \angle COB$. From Eqs. (2.79), (2.80) we obtain

$$\begin{aligned} \varsigma_1(\varphi) &= \mathrm{F}_1^{(4)}(\varphi) - \frac{R_D}{R_D - R_C}\Big(\mathrm{F}_1^{(4)}(\varphi) - \mathrm{F}_1^{(2)}(\varphi)\Big). \\ \varsigma_2(\varphi) &= \frac{1}{R_D - R_C}\Big(\mathrm{F}_1^{(4)}(\varphi) - \mathrm{F}_1^{(2)}(\varphi)\Big), \\ \varsigma_3(r) &= \mathrm{F}_2^{(1)}(r) \\ \varsigma_4(r) &= \frac{1}{\varphi_k}\Big(\mathrm{F}_2^{(3)}[\xi_2(r - R_D)] - \mathrm{F}_2^{(1)}(r)\Big). \end{aligned}$$

Substituting the above into (2.79) we get

$$\begin{aligned} \mathrm{F}_1(r, \varphi) &= \mathrm{F}_1^{(4)}(\varphi) + \frac{r - R_D}{R_D - R_C}\Big(\mathrm{F}_1^{(4)}(\varphi) - \mathrm{F}_1^{(2)}(\varphi)\Big), \\ \mathrm{F}_2(r, \varphi) &= \mathrm{F}_2^{(1)}(r) + \frac{\varphi}{\varphi_k}\Big(\mathrm{F}_2^{(3)}[\xi_2(r - R_D)] - \mathrm{F}_2^{(1)}(r)\Big). \end{aligned} \tag{2.81}$$

The unit base vectors $\bar{e}_{ik}$ are given by

$$\begin{aligned} \bar{e}_{11} &= \frac{R_D}{R_D - R_C}\Big(\mathrm{F}_1^{(4)}(\varphi) - \mathrm{F}_1^{(2)}(\varphi)\Big), \\ \bar{e}_{12} &= \frac{\varphi}{\varphi_k}\frac{d}{dr}\Big(\mathrm{F}_2^{(3)}[\xi_2(r - R_D)] - \mathrm{F}_2^{(1)}(r)\Big), \\ \bar{e}_{21} &= \frac{1}{r}\left(\frac{d\mathrm{F}_1^{(4)}(\varphi)}{d\varphi} + \frac{r - R_D}{R_D - R_C}\frac{d}{d\varphi}\Big(\mathrm{F}_1^{(4)}(\varphi) - \mathrm{F}_1^{(2)}(\varphi)\Big) - \right. \\ &\quad \left. - \mathrm{F}_2^{(1)}(r) - \frac{\varphi}{\varphi_k}\Big(\mathrm{F}_2^{(3)}[\xi_2(r - R_D)] - \mathrm{F}_2^{(1)}(r)\Big)\right), \\ \bar{e}_{22} &= \frac{1}{r}\left(\frac{\mathrm{F}_2^{(3)}[\xi_2(r - R_D)] - \mathrm{F}_2^{(1)}(r)}{\varphi_k} + \mathrm{F}_1^{(4)}(\varphi) + \frac{r - R_D}{R_D - R_C}\Big(\mathrm{F}_1^{(4)}(\varphi) - \mathrm{F}_1^{(2)}(\varphi)\Big)\right). \end{aligned} \tag{2.82}$$

Making use of Eqs. (2.82) in (2.71) we find the components of fictitious deformation $2\underset{*}{\varepsilon}_{ik}$ and the Christoffel symbols $\overset{*}{\Gamma}{}_{ij}^{k}$ on $\overset{*}{S}$.

If the complex surface $\overset{*}{S}$ had three corner points, such that $R_D \to 0, R_A \to 0, \left(\mathrm{F}_1^{(4)}(\varphi) \equiv 0\right)$, then the corner points A and D would merge to a single point O. In this case the transformation would have had singularity at O, as discussed above.

Reference

Galimov KZ, Paimushin VN (1985) Theory of shells of complex geometry (Geometrical problems of the theory of shells). Kazan University Press, Kazan

Chapter 3
Nonlinear Theory of Thin Shells

Mathematics is a game played according to certain simple rules with meaningless marks on paper.

David Hilbert

3.1 Deformation of the Shell

We shall base all our discussion of the deformation of thin shells upon the first Kirchhoff hypothesis. Let the middle surface S of the undeformed thin shell be associated with the orthogonal curvilinear coordinates α_1, α_2. The position vector $\overline{\rho}$ of an arbitrary point M_z on the equidistant surface S_z ($S_z \| S$) is given by Eq. (1.39), where $z \in [-h/2, +h/2]$ and h is the thickness of the shell. The coordinate vectors and the Lamé coefficients satisfy Eqs. (1.42, 1.49).

The length of a line element on S_z is given by

$$(ds_z)^2 = H_1^2 d{\alpha_1}^2 + H_2^2 d\alpha_2^2 + dz^2, \tag{3.1}$$

where

$$(ds_z)_1 = H_1 d\alpha_1 \quad (ds_z)_2 = H_2 d\alpha_2, \tag{3.2}$$

are the lengths of line elements in the direction of α_1, α_2-coordinates.

In the deformed configuration the position vector $\overset{*}{\overline{\rho}}$ of point $\overset{*}{M}_z \in \overset{*}{S}_z$ is given by

$$\overset{*}{\overline{\rho}} = \overline{\rho}(\alpha_1, \alpha_2) + \overline{\nu}_z(\alpha_1, \alpha_2, z), \tag{3.3}$$

where $\overline{\nu}_z$ is the displacement vector. Since for thin shells $z \ll 1$ we assume $\overset{*}{z} \approx z$. The first fundamental form of $\overset{*}{S}_z$ is

R.N. Miftahof, *Biomechanics of the Human Stomach*,
DOI 10.1007/978-3-319-59677-8_3

$$\left(\overset{*}{ds_z}\right)^2 = \overset{*}{g}_{11}\, d\alpha_1^2 + 2\,\overset{*}{g}_{12}\, d\alpha_1 d\alpha_2 + \overset{*}{g}_{22}\, d\alpha_2^2 + dz^2, \tag{3.4}$$

$$\left(\overset{*}{ds_z}\right)_1 = \sqrt{\overset{*}{g}_{11}}\, d\alpha_1, \quad \left(\overset{*}{ds_z}\right)_2 = \sqrt{\overset{*}{g}_{22}}\, d\alpha_2. \tag{3.5}$$

Here $\overset{*}{g}_{ik} = \overset{*}{\overline{\rho}}_i \overset{*}{\overline{\rho}}_k$ $(i, k = 1, 2)$ and vectors $\overset{*}{\overline{\rho}}_1$, $\overset{*}{\overline{\rho}}_2$, tangent to coordinate lines are obtained by differentiating Eq. (3.3) with respect to α_1, α_2

$$\begin{aligned}
\overset{*}{\overline{\rho}}_1 &= \overset{*}{\overline{r}}_1 \left(1 - z\, \overset{*}{b}_1^1\right) - \overset{*}{\overline{r}}_2 z\, \overset{*}{b}_1^2 \\
\overset{*}{\overline{\rho}}_2 &= \overset{*}{\overline{r}}_2 \left(1 - z\, \overset{*}{b}_2^2\right) - \overset{*}{\overline{r}}_1 z\, \overset{*}{b}_2^1 \\
\overset{*}{\overline{\rho}}_3 &= \overset{*}{\overline{m}}
\end{aligned} \tag{3.6}$$

Let ε_{11}^z, ε_{22}^z be deformations through point $M_z \in S_z$ in the direction of α_1, α_2 coordinates defined by

$$\varepsilon_{11}^z = \frac{\left(\overset{*}{ds_z}\right)_1 - (ds_z)_1}{(ds_z)_1}, \quad \varepsilon_{22}^z = \frac{\left(\overset{*}{ds_z}\right)_2 - (ds_z)_2}{(ds_z)_2}. \tag{3.7}$$

Substituting Eqs. (3.1, 3.4) into (3.7), we obtain

$$\varepsilon_{11}^z = \left(\sqrt{\overset{*}{g}_{11}} - H_1\right)/H_1, \quad \varepsilon_{22}^z = \left(\sqrt{\overset{*}{g}_{22}} - H_2\right)/H_2. \tag{3.8}$$

Using Eqs. (1.45, 1.53), the angle $\overset{*}{\chi}_z$ between the vectors $\overset{*}{\overline{\rho}}_1$and $\overset{*}{\overline{\rho}}_2$is found to be

$$\cos \overset{*}{\chi}_z = \frac{\overset{*}{\overline{\rho}}_1 \overset{*}{\overline{\rho}}_2}{\left|\overset{*}{\overline{\rho}}_1\right| \left|\overset{*}{\overline{\rho}}_2\right|} = \frac{\overset{*}{g}_{12}}{\sqrt{\overset{*}{g}_{11}\overset{*}{g}_{22}}}, \tag{3.9}$$

where

$$\begin{aligned}
\overset{*}{g}_{ii} &= \overset{*}{A}_1^2 \left(1 + 2\,\overset{*}{k}_{ii}\, z\right) + \left(\overset{*}{\bar{m}}_i\, z\right)^2, \\
\overset{*}{g}_{12} &= \overset{*}{A}_1\, \overset{*}{A}_2 \left(\cos \overset{*}{\chi} + 2\,\overset{*}{k}_{12}\, z\right) + \overset{*}{\bar{m}}_1 \overset{*}{\bar{m}}_2 z^2.
\end{aligned} \tag{3.10}$$

Let $\varepsilon^z{}_{12}$ be the shear deformation i.e. the change in the angle between initially orthogonal coordinate lines $2\varepsilon_{12}^z = \pi/2 - \overset{*}{\chi}_z$ Evidently,

$$\cos \overset{*}{\chi}_z \coloneqq \sin 2\varepsilon_{12}^z = \frac{\overset{*}{g}_{12}}{\sqrt{\overset{*}{g}_{22}\overset{*}{g}_{11}}}. \tag{3.11}$$

Making use of Eq. (3.6) and the fact $\overset{*}{\bar{r}}_1\overset{*}{\bar{m}} = 0$, we find

$$\overset{*}{g}_{13} = \overset{*}{\bar{\rho}}_1\,\overset{*}{\bar{m}} = 0, \quad \overset{*}{g}_{23} = \overset{*}{\bar{\rho}}_2\,\overset{*}{\bar{m}} = 0, \quad \overset{*}{g}_{33} = \overset{*}{\bar{m}}\,\overset{*}{\bar{m}} = 1.$$

It follows from the above that the deformation over the thickness of the shell equals zero

$$2\varepsilon_{i3}^z = \frac{\overset{*}{g}_{i3}}{\sqrt{\overset{*}{g}_{ii}\;\overset{*}{g}_{33}}} = 0, \quad \varepsilon_{33}^z = \left(\sqrt{\overset{*}{g}_{33}} - H_3\right)/H_3 = 0, \quad \left(\overset{*}{g}_{i3} = 0, H_3 = 1\right).$$

In applications it is more convenient to use deformations ε_{ik}^z expressed in terms of the undeformed middle surface S. Thus, neglecting terms $O(z^2)$ in Eq. (2.10), we have

$$\overset{*}{g}_{ii} = \overset{*}{A}_i^2\left(1 + 2\overset{*}{k}_{ii}z\right), \quad \overset{*}{g}_{12} = \overset{*}{A}_1\,\overset{*}{A}_2\left(\cos\overset{*}{\chi} + 2\overset{*}{k}_{12}\,z\right). \tag{3.12}$$

Taking the square root of both sides

$$\sqrt{\overset{*}{g}_{ii}} \approx \overset{*}{A}_i\left(1 + \overset{*}{k}_{ii}\,z\right) + \ldots, \tag{3.13a}$$

and substituting Eqs. (3.13a, 1.49) into (3.8), $\varepsilon^z{}_{ii}$ are found to be

$$\varepsilon_{ii}^z = \left[\overset{*}{A}_i - A_i + \left(\overset{*}{A}_i\;\overset{*}{k}_{ii} - A_i k_{ii}\right)z\right]/A_i(1 + k_{ii}z), \quad (i = 1, 2) \tag{3.13b}$$

Applying Eqs. (1.65, 1.69), the term in parenthesis can be written as

$$\begin{aligned}
&\overset{*}{A}_i\;\overset{*}{k}_{ii} - A_i k_{ii} = A_i\sqrt{(1 + 2\varepsilon_{ii})}\,\overset{*}{k}_{ii} - A_i k_{ii} = \\
&= A_i\left(\sqrt{(1 + 2\varepsilon_{ii})}\,\overset{*}{k}_{ii} - k_{ii}\right) = A_i\varpi_{ii}\sqrt{1 + 2\varepsilon_{ii}} + A_i k_{ii}\sqrt{1 + 2\varepsilon_{ii}}.
\end{aligned}$$

Reverse substitution yields

$$\begin{aligned}
\varepsilon_{ii}^z = \big[&A_i\left(\sqrt{1 + 2\varepsilon_{ii}} - 1\right) + A_i\varpi_{ii}z\sqrt{1 + 2\varepsilon_{ii}} + \\
&+ A_i k_{ii}z\sqrt{1 + 2\varepsilon_{ii}}\big]/A_i(1 + k_{ii}z).
\end{aligned} \tag{3.13c}$$

Hence, deformation of the equidistant surface S_z of the shell is fully determined in terms of tangent deformations and curvatures of the middle surface S. Similarly, introducing $\overset{*}{g}_{12}$ and $\sqrt{\overset{*}{g}_{ii}}$ given by Eqs. (3.12, 3.13a) into (3.11), we obtain

$$\sin 2\varepsilon_{12}^{z} = \frac{\left(\cos \overset{*}{\chi} + 2\overset{*}{k}_{12} z\right)}{\left(1 + \overset{*}{k}_{11} z\right)\left(1 + \overset{*}{k}_{22} z\right)}.$$

Since $\overset{*}{k}_{12} z \approx æ_{12} z$, we have

$$\sin 2\varepsilon_{12}^{z} = \frac{\cos \overset{*}{\chi} + 2æ_{12} z}{\left(1 + \overset{*}{k}_{11} z\right)\left(1 + \overset{*}{k}_{22} z\right)}.$$

Because for thin shells $1 + k_{ii} z \approx 1$, $1 + \overset{*}{k}_{ii} z \approx 1$, the final formulas for tangent and shear deformations of S_z, take the form

$$\varepsilon_{ii}^{z} = \sqrt{1 + 2\varepsilon_{ii}}\left(1 + z\overset{*}{k}_{ii}\right) - 1, \quad \sin 2\varepsilon_{12}^{z} = \frac{1}{2}\left(\cos \overset{*}{\chi} + 2æ_{12} z\right). \tag{3.14}$$

3.2 Forces and Moments

Consider a differential element in the deformed shell bounded by the surfaces $\alpha_i = \text{const}$, $\alpha_i + d\alpha_i = \text{const}$, and $\overset{*}{z} \pm 0.5h$ (Fig. 3.1). Internal forces acting upon the element are given by $\bar{p}_1 \overset{*}{H}_2 d\alpha_2 dz$ and $\bar{p}_2 \overset{*}{H}_1 d\alpha_1 dz$. Here $\bar{p}_i$ are stress vectors, $\overset{*}{H}_2 d\alpha_2 dz$, $\overset{*}{H}_1 d\alpha_1 dz$ are the surface areas of differential boundary elements at

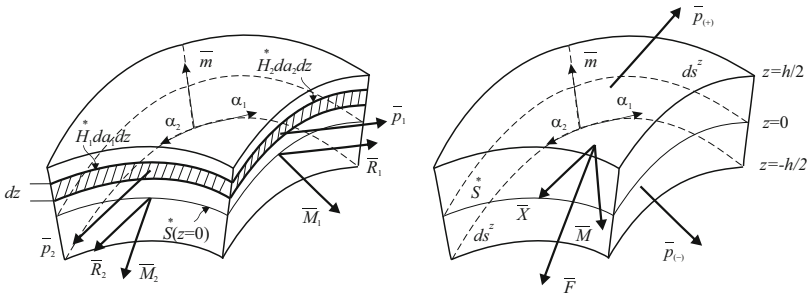

Fig. 3.1 Forces and moments acting upon a three dimensional solid

$z = \text{const}$. Integrating the internal forces over the thickness of the shell, we obtain the resultant of force vectors, $\bar{R}_1, \bar{R}_2$ in the form

$$\bar{R}_1 = \int_{z_1}^{z_2} \bar{p}_1 \overset{*}{H}_2 \, d\alpha_2 dz, \quad \bar{R}_2 = \int_{z_1}^{z_2} \bar{p}_2 \overset{*}{H}_1 \, d\alpha_1 dz, \quad (z_1 = -h/2, z_2 = +h/2).$$

Dividing $\bar{R}_i$ by the length of linear elements, $\overset{*}{A}_i \, d\alpha_i = A_i \sqrt{1 + 2\varepsilon_{ii}} d\alpha_i$ $(i = 1, 2)$, we find

$$\bar{R}_1 = \frac{\displaystyle\int_{z_1}^{z_2} \bar{p}_1 \overset{*}{H}_2 \, dz}{A_2 \sqrt{1 + 2\varepsilon_{22}}}, \quad \bar{R}_2 = \frac{\displaystyle\int_{z_1}^{z_2} \bar{p}_2 \overset{*}{H}_1 \, dz}{A_1 \sqrt{1 + 2\varepsilon_{11}}}. \tag{3.15}$$

Similar reasoning leads to the definition of the resultant internal moment vectors. The moment of the force $\bar{p}_1$, acting on the face $\alpha_1 = \text{const}$, about the centre of the middle surface $\overset{*}{S}$ is $\left(\overset{*}{\bar{m}} z \times \bar{p}_1 \overset{*}{H}_2 \, d\alpha_2 dz \right)$. Here $\overset{*}{\bar{m}} z$ is the radius vector of $\bar{p}_1$. Hence, the resultant moment vector of internal forces $\bar{M}_1$ is given by

$$\bar{M}_1 = \int_{z_1}^{z_2} \overset{*}{\bar{m}} z \times \bar{p}_1 \overset{*}{H}_2 d\alpha_2 dz.$$

Dividing the above by the length of a line segment in the direction of α_2-coordinate, $\overset{*}{A}_2 \, d\alpha_2 = A_2 \sqrt{(1 + 2\varepsilon_{22})} d\alpha_2$, we obtain

$$\bar{M}_1 = \frac{1}{A_2 \sqrt{(1 + 2\varepsilon_{22})}} \int_{z_1}^{z_2} \left(\overset{*}{\bar{m}} z \times \bar{p}_1 \right) \overset{*}{H}_2 \, dz. \tag{3.16a}$$

Similarly, we define the resultant moment vector $\bar{M}_2$ as

$$\bar{M}_2 = \frac{1}{A_1 \sqrt{1 + 2\varepsilon_{11}}} \int_{z_1}^{z_2} \left(\overset{*}{\bar{m}} z \times \bar{p}_2 \right) \overset{*}{H}_1 \, dz. \tag{3.16b}$$

The above discussion implies that the internal forces acting on the differential element are statically equivalent to the resultant force and moment vectors, $\bar{R}_i, \bar{M}_i$.

Consider external forces acting on the free surfaces $z = \pm 0.5h$ of the shell. Let:

(i) $\bar{p}_{(+)}$ and $\bar{p}_{(-)}$ be the external forces applied on the surface of area $d\sigma^z$

$$d\sigma^z = \overset{*}{H}_1 \overset{*}{H}_2 d\alpha_1 d\alpha_2 \approx$$
$$\approx A_1 A_2 (1 + (k_{11} + \varkappa_{11})z)(1 + (k_{22} + \varkappa_{22})z)\sqrt{1 + 2\varepsilon_{11}}\sqrt{1 + 2\varepsilon_{22}} d\alpha_1 d\alpha_2,$$

(ii) $\bar{F}$ be the vector of mass forces per unit volume $d\Omega$ of the deformed element

$$d\Omega = \overset{*}{H}_1 \overset{*}{H}_2 d\alpha_1 d\alpha_2 d\overset{*}{z} \approx$$
$$\approx A_1 A_2 (1 + (k_{11} + \varkappa_{11})z)(1 + (k_{22} + \varkappa_{22})z)\sqrt{1 + 2\varepsilon_{11}}\sqrt{1 + 2\varepsilon_{22}} d\alpha_1 d\alpha_2 d\overset{*}{z},$$

here $H^{(+)}{}_1$, $H^{(-)}{}_2$ are the values of H_i^* at $z = \pm 0.5h$, respectively.

Then, the resultant external force vectors are defined by

$$\bar{p}_{(+)} H^{(+)}{}_1 H^{(+)}{}_2 d\alpha_1 d\alpha_2 \quad \text{and} \quad \bar{p}_{(-)} H^{(-)}{}_1 H^{(-)}{}_2 d\alpha_1 d\alpha_2.$$

Their sum divided by the surface area of a deformed element, $\overset{*}{A}_1 \overset{*}{A}_2 d\alpha_1 d\alpha_2$, yields

$$\frac{\bar{p}_{(+)} H^{(+)}{}_1 H^{(+)}{}_2 d\alpha_1 d\alpha_2 + \bar{p}_{(-)} H^{(-)}{}_1 H^{(-)}{}_2 d\alpha_1 d\alpha_2}{A_1 A_2 \sqrt{(1 + 2\varepsilon_{11})(1 + 2\varepsilon_{22})} d\alpha_1 d\alpha_2} =$$
$$= \frac{\bar{p}_z \overset{*}{H}_1 \overset{*}{H}_2}{A_1 A_2 \sqrt{(1 + 2\varepsilon_{11})(1 + 2\varepsilon_{22})}}. \tag{3.17}$$

Here $(\bar{p}_z)_{z=0.5h} = \bar{p}_{(+)}$, $(\bar{p}_z)_{z=-0.5h} = -\bar{p}_{(-)}$, $\bar{p}_{-z} = -\bar{p}_z$.

Similarly, dividing the resultant of the mass force $\bar{F}$ given by

$$\int_{z_1}^{z_2} \bar{F} d\sigma^{z^*} dz = \int_{z_1}^{z_2} \bar{F} \overset{*}{H}_1 \overset{*}{H}_2 d\alpha_1 d\alpha_2 dz,$$

by $\overset{*}{A}_1 \overset{*}{A}_2 d\alpha_1 d\alpha_2$ and taking the sum of the resultant with Eq. (3.17), we obtain

$$\bar{X} A_1 A_2 = \frac{\bar{p}_z \overset{*}{H}_1 \overset{*}{H}_2}{\sqrt{(1 + 2\varepsilon_{11})(1 + 2\varepsilon_{22})}} + \int_{z_1}^{z_2} \frac{\bar{F} \overset{*}{H}_1 \overset{*}{H}_2 dz}{\sqrt{(1 + 2\varepsilon_{11})(1 + 2\varepsilon_{22})}}. \tag{3.18}$$

$\bar{X}$ is the resultant external force vector referred to the deformed middle surface $\overset{*}{S}$ of the shell.

Moments of external forces about an arbitrary point on $\overset{*}{S}$ are given by

$$\left(\frac{\overset{*}{\bar{m}} h}{2} \times \bar{p}_{(+)} H^{(+)}{}_1 H^{(+)}{}_2 d\alpha_1 d\alpha_2 \right) \quad \text{and} \quad \left(\frac{\overset{*}{\bar{m}} h}{2} \times \bar{p}_{(-)} H^{(-)}{}_1 H^{(-)}{}_2 d\alpha_1 d\alpha_2 \right).$$

Their sum divided by the surface area $\overset{*}{A}_1 \overset{*}{A}_2 d\alpha_1 d\alpha_2$ yields

$$\left(\overset{*}{\bar{m}}\, z \times \bar{p}_{(z)} \frac{\overset{*}{H}_1 \overset{*}{H}_2}{A_1 A_2 \sqrt{(1+2\varepsilon_{11})(1+2\varepsilon_{22})}} \right)_{z_1}^{z_2}.$$

Analogously, the moment of $\bar{F}$ per unit area of the element $\overset{*}{S}$ is given by

$$\int_{z_1}^{z_2} \left(\overset{*}{\bar{m}}\, z \times \bar{F} \right) \frac{\overset{*}{H}_1 \overset{*}{H}_2 \, d\alpha_1 d\alpha_2 dz}{A_1 A_2 \sqrt{(1+2\varepsilon_{11})(1+2\varepsilon_{22})} d\alpha_1 d\alpha_2} =$$

$$= \int_{z_1}^{z_2} \left(\overset{*}{\bar{m}}\, z \times \bar{F} \right) \frac{\overset{*}{H}_1 \overset{*}{H}_2 \, dz}{A_1 A_2 \sqrt{(1+2\varepsilon_{11})(1+2\varepsilon_{22})}}.$$

Hence, the resultant external moment vector $\bar{M}$ of external forces is found to be

$$\begin{aligned} \bar{M} A_1 A_2 = & \left(\overset{*}{\bar{m}}\, z \times \bar{p}_{(z)} \frac{\overset{*}{H}_1 \overset{*}{H}_2}{\sqrt{(1+2\varepsilon_{11})(1+2\varepsilon_{22})}} \right)_{z_1}^{z_2} + \\ & + \int_{z_1}^{z_2} \left(\overset{*}{\bar{m}}\, z \times \bar{F} \right) \frac{\overset{*}{H}_1 \overset{*}{H}_2 \, dz}{\sqrt{(1+2\varepsilon_{11})(1+2\varepsilon_{22})}}, \end{aligned} \tag{3.19}$$

Again, we have arrived at the conclusion that the external forces acting upon the differential element are statically equivalent to the resultants of external force and moment vectors, $\bar{X}$ and $\bar{M}$.

Decomposing $\bar{p}_i$, $\bar{p}_z$ and $\bar{F}$ in the direction of unit vectors $\overset{*}{\bar{e}}{}_1^z = \overline{\rho}_1^* / \overset{*}{H}_1$, $\overset{*}{\bar{e}}{}_2^z = \overline{\rho}_2^* / \overset{*}{H}_2$ and $\overset{*}{\bar{e}}{}_3^z = \overset{*}{\bar{m}}$, we have

$$\begin{aligned} \bar{p}_1 &= \sigma_{11} \overset{*}{\bar{e}}{}_1^z + \sigma_{12} \overset{*}{\bar{e}}{}_2^z + \sigma_{13} \overset{*}{\bar{m}}, \\ \bar{p}_2 &= \sigma_{21} \overset{*}{\bar{e}}{}_1^z + \sigma_{22} \overset{*}{\bar{e}}{}_2^z + \sigma_{23} \overset{*}{\bar{m}}, \\ \bar{p}_z &= \sigma_{31} \overset{*}{\bar{e}}{}_1^z + \sigma_{32} \overset{*}{\bar{e}}{}_2^z + \sigma_{33} \overset{*}{\bar{m}}, \\ \bar{F} &= \overset{*}{F}_1 \overset{*}{\bar{e}}{}_1^z + \overset{*}{F}_2 \overset{*}{\bar{e}}{}_2^z + \overset{*}{F}_3 \overset{*}{\bar{m}}, \end{aligned} \tag{3.20}$$

where σ_{ij} $(i, j = 1, 2)$ are the internal stresses $(\sigma_{ij} = \sigma_{ji})$ and F_j^* are the projections of $\bar{F}$ on the base $\{\overset{*}{\bar{e}}{}_1^z, \overset{*}{\bar{e}}{}_2^z, \overset{*}{\bar{m}}\}$ (Fig. 3.2). Substituting Eq. (2.20) into (3.15, 3.16a), for $\bar{R}_i$ and $\bar{M}_i$, we find

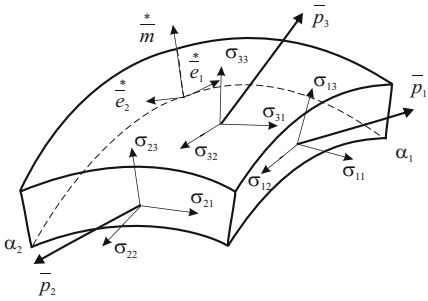

Fig. 3.2 Internal stresses in a shell

$$A_2\sqrt{(1+2\varepsilon_{22})}\bar{R}_1 = \int_{z_1}^{z_2}\left(\sigma_{11}\overset{*}{\bar{e}}{}_1^z + \sigma_{12}\overset{*}{\bar{e}}{}_2^z + \sigma_{13}\overset{*}{\bar{m}}\right)\overset{*}{H}_2 dz,$$

$$A_1\sqrt{(1+2\varepsilon_{11})}\bar{R}_2 = \int_{z_1}^{z_2}\left(\sigma_{21}\overset{*}{\bar{e}}{}_1^z + \sigma_{22}\overset{*}{\bar{e}}{}_2^z + \sigma_{23}\overset{*}{\bar{m}}\right)\overset{*}{H}_1 dz,$$

$$A_2\sqrt{(1+2\varepsilon_{22})}\bar{M}_1 = \int_{z_1}^{z_2}\left(\overset{*}{\bar{m}}z \times \left(\sigma_{11}\overset{*}{\bar{e}}{}_1^z + \sigma_{12}\overset{*}{\bar{e}}{}_2^z\right)\right)\overset{*}{H}_2 dz,$$

$$A_1\sqrt{(1+2\varepsilon_{11})}\bar{M}_2 = \int_{z_1}^{z_2}\left(\overset{*}{\bar{m}}z \times \left(\sigma_{21}\overset{*}{\bar{e}}{}_1^z + \sigma_{22}\overset{*}{\bar{e}}{}_2^z\right)\right)\overset{*}{H}_1 dz.$$

Since $\overset{*}{\bar{e}}{}_1^z = \overset{*}{\bar{e}}_1$, $\overset{*}{\bar{e}}{}_2^z = \overset{*}{\bar{e}}_2$, (Eq. 1.51) we have

$$A_2\sqrt{(1+2\varepsilon_{22})}\bar{R}_1 = \int_{z_1}^{z_2}\left(\sigma_{11}\overset{*}{\bar{e}}_1 + \sigma_{12}\overset{*}{\bar{e}}_2 + \sigma_{13}\overset{*}{\bar{m}}\right)\overset{*}{H}_2 dz,$$

$$A_1\sqrt{(1+2\varepsilon_{11})}\bar{R}_2 = \int_{z_1}^{z_2}\left(\sigma_{21}\overset{*}{\bar{e}}_1 + \sigma_{22}\overset{*}{\bar{e}}_2 + \sigma_{23}\overset{*}{\bar{m}}\right)\overset{*}{H}_1 dz,$$

$$A_2\sqrt{(1+2\varepsilon_{22})}\bar{M}_1 = \int_{z_1}^{z_2}\left(\overset{*}{\bar{m}}z \times \left(\sigma_{11}\overset{*}{\bar{e}}_1 + \sigma_{12}\overset{*}{\bar{e}}_2\right)\right)\overset{*}{H}_2 dz$$

$$A_1\sqrt{(1+2\varepsilon_{11})}\bar{M}_2=\int\limits_{z_1}^{z_2}\left(\overset{*}{\bar{m}}z\times\left(\sigma_{21}\overset{*}{\bar{e}}_1+\sigma_{22}\overset{*}{\bar{e}}_2\right)\right)\overset{*}{H}_1dz$$

where (see Eqs. (1.61, 1.72))

$$\begin{aligned}\overset{*}{\bar{e}}_1&=[\bar{e}_1(1+e_{11})+\bar{e}_2e_{22}+\bar{m}\varpi_1]/(1+2\varepsilon_{11}),\\ \overset{*}{\bar{e}}_2&=[\bar{e}_1e_{11}+\bar{e}_2(1+e_{22})+\bar{m}\varpi_2]/(1+2\varepsilon_{22}),\\ \overset{*}{\bar{m}}&=(\bar{e}_1E_1+\bar{e}_2E_2+mE_3)/\sqrt{\mathfrak{A}}.\end{aligned}\tag{3.21}$$

On use of Eq. (1.57), $\bar{R}_i$ and $\bar{M}_i$ can be written in the form

$$\bar{R}_1=\overset{*}{T}_{11}\overset{*}{\bar{e}}_1+\overset{*}{T}_{12}\overset{*}{\bar{e}}_2+\overset{*}{N}_1\overset{*}{\bar{m}},\quad \bar{R}_2=\overset{*}{T}_{21}\overset{*}{\bar{e}}_1+\overset{*}{T}_{22}\overset{*}{\bar{e}}_2+\overset{*}{N}_2\overset{*}{\bar{m}},\tag{3.22}$$

$$\bar{M}_1=\overset{*}{M}_{11}\overset{*}{\bar{e}}_2-\overset{*}{M}_{12}\overset{*}{\bar{e}}_1,\qquad \bar{M}_2=\overset{*}{M}_{21}\overset{*}{\bar{e}}_2-\overset{*}{M}_{22}\overset{*}{\bar{e}}_1,\tag{3.23}$$

here

$$\begin{aligned}&A_2\sqrt{(1+2\varepsilon_{22})}\overset{*}{T}_{11}=\int\limits_{z_1}^{z_2}\sigma_{11}\overset{*}{H}_2dz,\quad A_2\sqrt{(1+2\varepsilon_{22})}\overset{*}{T}_{12}=\int\limits_{z_1}^{z_2}\sigma_{12}\overset{*}{H}_2dz,\\ &A_2\sqrt{(1+2\varepsilon_{22})}\overset{*}{N}_1=\int\limits_{z_1}^{z_2}\sigma_{13}\overset{*}{H}_2dz,\quad A_1\sqrt{(1+2\varepsilon_{11})}\overset{*}{T}_{21}=\int\limits_{z_1}^{z_2}\sigma_{21}\overset{*}{H}_1dz,\\ &A_1\sqrt{(1+2\varepsilon_{11})}\overset{*}{T}_{22}=\int\limits_{z_1}^{z_2}\sigma_{22}\overset{*}{H}_1dz,\quad A_1\sqrt{(1+2\varepsilon_{11})}\overset{*}{N}_2=\int\limits_{z_1}^{z_2}\sigma_{23}\overset{*}{H}_1dz,\\ &A_2\sqrt{(1+2\varepsilon_{22})}\overset{*}{M}_{11}=\int\limits_{z_1}^{z_2}\sigma_{11}\overset{*}{H}_2zdz,\quad A_2\sqrt{(1+2\varepsilon_{22})}\overset{*}{M}_{12}=\int\limits_{z_1}^{z_2}\sigma_{12}\overset{*}{H}_2zdz,\\ &A_1\sqrt{(1+2\varepsilon_{11})}\overset{*}{M}_{21}=\int\limits_{z_1}^{z_2}\sigma_{21}\overset{*}{H}_1zdz,\quad A_1\sqrt{(1+2\varepsilon_{11})}\overset{*}{M}_{22}=\int\limits_{z_1}^{z_2}\sigma_{22}\overset{*}{H}_1zdz.\end{aligned}\tag{3.24}$$

Vectors $\overset{*}{T}_{i1}\overset{*}{\bar{e}}_1+\overset{*}{T}_{i2}\overset{*}{\bar{e}}_2$ lay in the tangent plane of the deformed middle surface $\overset{*}{S}$. They are called the in-plane forces, namely: $\overset{*}{T}_{11}$, $\overset{*}{T}_{22}$ are normal forces, $\overset{*}{T}_{12}$, $\overset{*}{T}_{21}$—shear forces, $\overset{*}{N}_i$—lateral (cut) forces. The moments $\overset{*}{M}_{11}$, $\overset{*}{M}_{22}$ are bending, and $\overset{*}{M}_{12}$, $\overset{*}{M}_{21}$ are twisting moments (Fig. 3.3). Since for thin shells, terms of order $O(h/R)$ can be neglected without the loss of accuracy required, from Eq. (3.24) we get

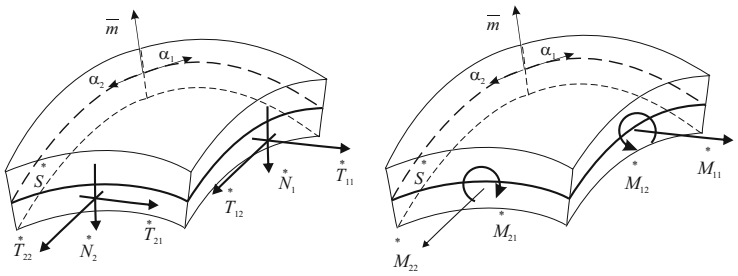

Fig. 3.3 Forces and moments in a thin shell

$$\begin{aligned}
\sqrt{(1+2\varepsilon_{ik})}\,\overset{*}{T}_{ik} &= \int_{z_1}^{z_2}\sigma_{ik}dz,\\
\sqrt{(1+2\varepsilon_{ik})}\,\overset{*}{N}_{i} &= \int_{z_1}^{z_2}\sigma_{i3}dz,\\
\sqrt{(1+2\varepsilon_{ik})}\,\overset{*}{M}_{ik} &= \int_{z_1}^{z_2}\sigma_{ik}z dz.
\end{aligned} \tag{3.25}$$

On use of Eqs. (3.20) in (3.18, 3.19) and neglecting terms $\overset{*}{k}_{ii}\, z \ll 1$, we find

$$\begin{aligned}
\bar{X}A_1A_2 &= \overset{*}{X}_1\overset{*}{\bar{e}}_1 + \overset{*}{X}_2\overset{*}{\bar{e}}_2 + \overset{*}{X}_3\overset{*}{\bar{m}},\\
\bar{M} &= \overset{*}{M}_1\overset{*}{\bar{e}}_2 - \overset{*}{M}_2\overset{*}{\bar{e}}_1,
\end{aligned} \tag{3.26}$$

where

$$\begin{aligned}
\overset{*}{X}_i &= \frac{\sigma_{i3}}{\sqrt{(1+2\varepsilon_{11})(1+2\varepsilon_{22})}} + \int_{z_1}^{z_2}\frac{\overset{*}{F}_i dz}{\sqrt{(1+2\varepsilon_{11})(1+2\varepsilon_{22})}},\\
\overset{*}{X}_3 &= \frac{\sigma_{33}}{\sqrt{(1+2\varepsilon_{11})(1+2\varepsilon_{22})}} + \int_{z_1}^{z_2}\frac{\overset{*}{F}_3 dz}{\sqrt{(1+2\varepsilon_{11})(1+2\varepsilon_{22})}},\\
\overset{*}{M}_i &= \frac{\sigma_{i3}z}{\sqrt{(1+2\varepsilon_{11})(1+2\varepsilon_{22})}} + \int_{z_1}^{z_2}\frac{\overset{*}{F}_i z dz}{\sqrt{(1+2\varepsilon_{11})(1+2\varepsilon_{22})}}.
\end{aligned}$$

Here $\overset{*}{X}_i$ and $\overset{*}{M}_i$ are the projections of the external force and moment vectors on the base $\{\overset{*}{\bar{e}}_1,\overset{*}{\bar{e}}_2,\overset{*}{\bar{m}}\}\in\overset{*}{S}$.

3.3 Equations of Equilibrium

From the modeling perspective, a thin shell can be treated as a three-dimensional solid. However, the complexity of the problem would be reduced significantly if its dimensionality could be reduced from three to two. To achieve this reduction, we introduce the second Kirchhoff-Love hypothesis. It states that "the transverse normal stress is significantly smaller compared to other stresses in the shell, $\sigma_{33} \ll \sigma_{ik}$, $(i, k = 1, 2)$ and thus may be neglected". In addition, recalling that the deformed state of the shell is completely defined in terms of deformations and curvatures of its middle surface, the shell can be regarded as a two-dimensional solid. Thus the equilibrium conditions analysis can be based on the study of the resultant forces and moments taken over the thickness of the shell (Galimov 1975; Galimov et al. 1996).

Assume that the initial undeformed state of the shell is stress-free. We shall derive the differential equations of equilibrium of a shell in terms of the deformed configuration. We proceed from the vector equations of equilibrium for a three dimensional solid given by

$$\frac{\partial \bar{p}_1 \overset{*}{H}_2}{\partial \alpha_1} + \frac{\partial \bar{p}_2 \overset{*}{H}_1}{\partial \alpha_2} + \frac{\partial \bar{p}_z \overset{*}{H}_1 \overset{*}{H}_2}{\partial z} + \bar{F} \overset{*}{H}_1 \overset{*}{H}_1 = 0, \tag{3.27}$$

$$\left(\overline{p}_1^* \times \bar{p}_1\right) \overset{*}{H}_2 + \left(\overline{p}_1^* \times \bar{p}_2\right) \overset{*}{H}_1 + \left(\overset{*}{\bar{m}} \times \bar{p}_z\right) \overset{*}{H}_1 \overset{*}{H}_2 = 0. \tag{3.28}$$

Multiplying Eq. (3.27) by dz and integrating over the thickness of the shell, $z\in[z_1,z_2]$, we obtain

$$\frac{\partial A_2 \bar{R}_1}{\partial \alpha_1} + \frac{\partial A_1 \bar{R}_2}{\partial \alpha_2} + A_1 A_2 \bar{X} = 0. \tag{3.29}$$

Here $\bar{R}_i$ and $\bar{X}$ satisfy Eqs. (3.15) and (3.18).

Integrating the vector product of Eq. (3.27) and $\overset{*}{\bar{m}}\, z$ over z, we find

$$\int_{z_1}^{z_2} \left(\overset{*}{\bar{m}}\, z \times \left(\frac{\partial \bar{p}_1 \overset{*}{H}_2}{\partial \alpha_1} + \frac{\partial \bar{p}_2 \overset{*}{H}_1}{\partial \alpha_2} + \frac{\partial \bar{p}_z \overset{*}{H}_1 \overset{*}{H}_2}{\partial z} + \bar{F} \overset{*}{H}_1 \overset{*}{H}_2 \right) \right) dz = 0. \tag{3.30}$$

Since

$$\int_{z_1}^{z_2}\left(\overset{*}{\bar{m}}z\times\frac{\partial\bar{p}_1\overset{*}{H}_2}{\partial\alpha_1}\right)dz=\int_{z_1}^{z_2}\frac{\partial}{\partial\alpha_1}\left(\overset{*}{\bar{m}}z\times\bar{p}_1\overset{*}{H}_2\right)dz-\int_{z_1}^{z_2}\frac{\partial}{\partial\alpha_1}\left(\overset{*}{\bar{m}}_1z\times\bar{p}_1\overset{*}{H}_2\right)dz=$$

$$=\frac{\partial A_2\bar{M}_1}{\partial\alpha_1}-\int_{z_1}^{z_2}\left(\left(\overset{*}{\bar{\rho}}_1-\overset{*}{\bar{r}}_1\right)\times\frac{\partial\bar{p}_1\overset{*}{H}_2}{\partial\alpha_1}\right)dz=$$

$$=\frac{\partial A_2\bar{M}_1}{\partial\alpha_1}+\left(\overset{*}{\bar{r}}_1\times\bar{R}_1\right)A_2-\int_{z_1}^{z_2}\left(\overset{*}{\bar{\rho}}_1\times\bar{p}_1\right)\overset{*}{H}_2\,dz, \tag{3.31}$$

$$\int_{z_1}^{z_2}\left(\overset{*}{\bar{m}}z\times\frac{\partial\bar{p}_2\overset{*}{H}_1}{\partial\alpha_2}\right)dz=\frac{\partial A_1\bar{M}_2}{\partial\alpha_2}+\left(\overset{*}{\bar{r}}_2\times\bar{R}_2\right)A_1-\int_{z_1}^{z_2}\left(\overset{*}{\bar{\rho}}_2\times\bar{p}_2\right)\overset{*}{H}_1\,dz,$$

$$\overset{*}{\bar{m}}_1z=\overset{*}{\bar{\rho}}_1-\overset{*}{\bar{r}}_1,\qquad\overset{*}{\bar{m}}_2z=\overset{*}{\bar{\rho}}_2-\overset{*}{\bar{r}}_2,$$

substituting the left-hand sides of Eq. (3.31) into (3.30), with the help of Eq. (3.28), we get

$$\frac{\partial A_2\bar{M}_1}{\partial\alpha_1}+\frac{\partial A_1\bar{M}_2}{\partial\alpha_2}+A_1\left(\overset{*}{\bar{r}}_1\times\bar{R}_2\right)+A_2\left(\overset{*}{\bar{r}}_2\times\bar{R}_1\right)+A_1A_2\bar{M}=0. \tag{3.32}$$

Here $\bar{M}_i$ and $\bar{M}$ satisfy Eqs. (3.16a, 3.19). Although Eqs. (3.29, 3.32) are derived under the assumption $h=\text{const}$, they are also valid for shells of variable thickness $h=h\,(\alpha_1,\alpha_2)$.

Substituting $\bar{R}_i$, $\bar{X}$ given by Eqs. (3.22, 3.27) into (3.29), for the equilibrium equations we have

$$\begin{aligned}
&\frac{\partial A_2\overset{*}{T}_{11}}{\partial\alpha_1}+\frac{\partial A_1\overset{*}{T}_{21}}{\partial\alpha_2}+\overset{*}{T}_{12}\frac{A_2}{\overset{*}{A}_2}\frac{\partial\overset{*}{A}_1}{\partial\alpha_2}-\overset{*}{T}_{22}\frac{A_1}{\overset{*}{A}_1}\frac{\partial\overset{*}{A}_2}{\partial\alpha_1}+\\
&\qquad+\overset{*}{A}_1A_2\overset{*}{N}_1\overset{*}{k}_{11}+A_1\overset{*}{A}_2\overset{*}{N}_2\overset{*}{k}_{12}+A_1A_2\overset{*}{X}_1=0,\\
&\frac{\partial A_1\overset{*}{T}_{22}}{\partial\alpha_2}+\frac{\partial A_2\overset{*}{T}_{12}}{\partial\alpha_1}+\overset{*}{T}_{21}\frac{A_1}{\overset{*}{A}_1}\frac{\partial\overset{*}{A}_2}{\partial\alpha_1}-\overset{*}{T}_{11}\frac{A_2}{\overset{*}{A}_2}\frac{\partial\overset{*}{A}_1}{\partial\alpha_2}+\\
&\qquad+A_2\overset{*}{A}_1\overset{*}{N}_1\overset{*}{k}_{21}+\overset{*}{A}_2A_1\overset{*}{N}_2\overset{*}{k}_{22}+A_1A_2\overset{*}{X}_2=0,
\end{aligned} \tag{3.33}$$

$$\frac{\partial A_2 \overset{*}{N}_1}{\partial \alpha_1} + \frac{\partial A_1 \overset{*}{N}_2}{\partial \alpha_2} - \overset{*}{A}_1 A_2 \overset{*}{T}_{11} \overset{*}{k}_{11} - A_1 \overset{*}{A}_2 \overset{*}{T}_{22} \overset{*}{k}_{22} - \\ - A_1 \overset{*}{A}_2 \overset{*}{T}_{12} \overset{*}{k}_{12} - A_1 \overset{*}{A}_2 \overset{*}{T}_{21} \overset{*}{k}_{12} + A_1 A_2 \overset{*}{X}_3 = 0. \tag{3.34a}$$

In deriving Eqs. (3.33), (3.34a) use is made of formulas for $\frac{\partial \overset{*}{\bar{e}}_i}{\partial \alpha_k}$ and $\overset{*}{\bar{m}}_i$

$$\frac{\partial \overset{*}{\bar{e}}_1}{\partial \alpha_1} = -\frac{\overset{*}{\bar{e}}_2}{\overset{*}{A}_2} \frac{\partial \overset{*}{A}_1}{\partial \alpha_2} - \overset{*}{A}_1 \overset{*}{k}_{11} \overset{*}{\bar{m}}, \quad \frac{\partial \overset{*}{\bar{e}}_1}{\partial \alpha_2} = \frac{\overset{*}{\bar{e}}_2}{\overset{*}{A}_1} \frac{\partial \overset{*}{A}_2}{\partial \alpha_1} - \overset{*}{A}_2 \overset{*}{k}_{12} \overset{*}{\bar{m}},$$

$$\frac{\partial \overset{*}{\bar{e}}_2}{\partial \alpha_1} = \frac{\overset{*}{\bar{e}}_1}{\overset{*}{A}_2} \frac{\partial \overset{*}{A}_1}{\partial \alpha_2} - \overset{*}{A}_1 \overset{*}{A}_{12} \overset{*}{\bar{m}}, \quad \frac{\partial \overset{*}{\bar{e}}_2}{\partial \alpha_2} = -\frac{\overset{*}{\bar{e}}_1}{\overset{*}{A}_1} \frac{\partial \overset{*}{A}_2}{\partial \alpha_1} - \overset{*}{A}_2 \overset{*}{k}_{22} \overset{*}{\bar{m}}, \tag{3.34b}$$

$$\overset{*}{\bar{m}}_i = \overset{*}{A}_i \left(\overset{*}{k}_{1i} \overset{*}{\bar{e}}_1 + \overset{*}{k}_{2i} \overset{*}{\bar{e}}_2 \right), \tag{3.34c}$$

Analogously, substituting $\bar{M}_i$, $\bar{M}$ given by Eqs. (3.23, 3.27) into (3.32) with the help of Eqs. (3.22, 3.34b, 3.34c), the equilibrium equations of moments take the form

$$\frac{\partial A_2 \overset{*}{M}_{11}}{\partial \alpha_1} + \frac{\partial A_1 \overset{*}{M}_{21}}{\partial \alpha_2} + \overset{*}{M}_{12} \frac{A_2}{\overset{*}{A}_2} \frac{\partial \overset{*}{A}_1}{\partial \alpha_2} - \overset{*}{M}_{22} \frac{A_1}{\overset{*}{A}_1} \frac{\partial \overset{*}{A}_2}{\partial \alpha_1} + \\ + \overset{*}{A}_1 A_2 \overset{*}{M}_1 - A_1 \overset{*}{A}_2 \overset{*}{N}_1 = 0, \\ \frac{\partial A_2 \overset{*}{M}_{12}}{\partial \alpha_1} + \frac{\partial A_1 \overset{*}{M}_{22}}{\partial \alpha_2} + \overset{*}{M}_{21} \frac{A_1}{\overset{*}{A}_1} \frac{\partial \overset{*}{A}_2}{\partial \alpha_1} - \overset{*}{M}_{11} \frac{A_2}{\overset{*}{A}_2} \frac{\partial \overset{*}{A}_1}{\partial \alpha_2} + \\ + \overset{*}{A}_2 A_1 \overset{*}{M}_2 - A_2 \overset{*}{A}_1 \overset{*}{N}_2 = 0, \tag{3.35}$$

$$A_1 \overset{*}{A}_2 \overset{*}{T}_{12} - \overset{*}{A}_1 A_2 \overset{*}{T}_{21} + A_1 \overset{*}{A}_2 \overset{*}{M}_{12} \overset{*}{k}_{11} - \overset{*}{A}_1 A_2 \overset{*}{M}_{21} \overset{*}{k}_{22} + \\ + \overset{*}{A}_1 A_2 \overset{*}{M}_{22} \overset{*}{k}_{12} - A_1 \overset{*}{A}_2 \overset{*}{M}_{11} \overset{*}{k}_{12} = 0. \tag{3.36}$$

The system of Eqs. (3.33–3.36) contains six unknowns: $\overset{*}{T}_{ik}, \overset{*}{N}_i$ and $\overset{*}{M}_{ik} (i, k = 1, 2)$. Introducing differential operators defined by

$$
\begin{aligned}
L_1\left(\overset{*}{T}_{ik}\right) &= \frac{\partial A_2 \overset{*}{T}_{11}}{\partial \alpha_1} + \frac{\partial A_1 \overset{*}{T}_{21}}{\partial \alpha_2} + \overset{*}{T}_{12} \frac{A_2}{\overset{*}{A}_2} \frac{\partial \overset{*}{A}_1}{\partial \alpha_2} - \overset{*}{T}_{22} \frac{A_1}{\overset{*}{A}_1} \frac{\partial \overset{*}{A}_2}{\partial \alpha_1}, \\
L_2\left(\overset{*}{T}_{ik}\right) &= \frac{\partial A_2 \overset{*}{T}_{12}}{\partial \alpha_1} + \frac{\partial A_1 \overset{*}{T}_{22}}{\partial \alpha_2} + \overset{*}{T}_{21} \frac{A_1}{\overset{*}{A}_1} \frac{\partial \overset{*}{A}_2}{\partial \alpha_1} - \overset{*}{T}_{11} \frac{A_2}{\overset{*}{A}_2} \frac{\partial \overset{*}{A}_1}{\partial \alpha_2},
\end{aligned}
\tag{3.37}
$$

$$
\begin{aligned}
L_1\left(\overset{*}{M}_{ik}\right) &= \frac{\partial A_2 \overset{*}{M}_{11}}{\partial \alpha_1} + \frac{\partial A_1 \overset{*}{M}_{21}}{\partial \alpha_2} + \overset{*}{M}_{12} \frac{A_2}{\overset{*}{A}_2} \frac{\partial \overset{*}{A}_1}{\partial \alpha_2} - \overset{*}{M}_{22} \frac{A_1}{\overset{*}{A}_1} \frac{\partial \overset{*}{A}_2}{\partial \alpha_1}, \\
L_2\left(\overset{*}{M}_{ik}\right) &= \frac{\partial A_2 \overset{*}{M}_{12}}{\partial \alpha_1} + \frac{\partial A_1 \overset{*}{M}_{22}}{\partial \alpha_2} + \overset{*}{M}_{21} \frac{A_1}{\overset{*}{A}_1} \frac{\partial \overset{*}{A}_2}{\partial \alpha_1} - \overset{*}{M}_{11} \frac{A_2}{\overset{*}{A}_2} \frac{\partial \overset{*}{A}_1}{\partial \alpha_2},
\end{aligned}
\tag{3.38}
$$

the first two equations in (3.33) and (3.35), can be written in the form

$$
\begin{aligned}
L_1\left(\overset{*}{T}_{ik}\right) + \overset{*}{A}_1 A_2 \overset{*}{N}_1 \overset{*}{k}_{11} + A_1 \overset{*}{A}_2 \overset{*}{N}_2 \overset{*}{k}_{12} + A_1 A_2 \overset{*}{X}_1 = 0, \\
L_2\left(\overset{*}{T}_{ik}\right) + \overset{*}{A}_2 A_1 \overset{*}{N}_2 \overset{*}{k}_{22} + A_2 \overset{*}{A}_1 \overset{*}{N}_1 \overset{*}{k}_{21} + A_1 A_2 \overset{*}{X}_2 = 0,
\end{aligned}
\tag{3.39}
$$

$$
\begin{aligned}
\frac{\partial A_2 \overset{*}{N}_1}{\partial \alpha_1} + \frac{\partial A_1 \overset{*}{N}_2}{\partial \alpha_2} - \overset{*}{A}_1 A_2 \overset{*}{T}_{11} \overset{*}{k}_{11} - A_1 \overset{*}{A}_2 \overset{*}{T}_{22} \overset{*}{k}_{22} - \\
- A_1 \overset{*}{A}_2 \overset{*}{T}_{12} \overset{*}{k}_{12} - A_1 \overset{*}{A}_2 \overset{*}{T}_{21} \overset{*}{k}_{12} + A_1 A_2 \overset{*}{X}_3 = 0,
\end{aligned}
\tag{3.40}
$$

$$
\begin{aligned}
L_1\left(\overset{*}{M}_{ik}\right) + \overset{*}{A}_1 A_2 \overset{*}{M}_1 - A_1 \overset{*}{A}_2 \overset{*}{N}_1 = 0, \\
L_2\left(\overset{*}{M}_{ik}\right) + \overset{*}{A}_2 A_1 \overset{*}{M}_1 - A_2 \overset{*}{A}_1 \overset{*}{N}_1 = 0,
\end{aligned}
\tag{3.41}
$$

$$
\begin{aligned}
A_1 \overset{*}{A}_2 \overset{*}{T}_{12} - \overset{*}{A}_1 A_2 \overset{*}{T}_{21} + A_1 \overset{*}{A}_2 \overset{*}{M}_{12} \overset{*}{k}_{11} - \overset{*}{A}_1 A_2 \overset{*}{M}_{21} \overset{*}{k}_{22} + \\
+ \overset{*}{A}_1 A_2 \overset{*}{M}_{22} \overset{*}{k}_{12} - A_1 \overset{*}{A}_2 \overset{*}{M}_{11} \overset{*}{k}_{12} = 0.
\end{aligned}
\tag{3.42}
$$

Equations (3.39)–(3.42) are nonlinear. The nonlinearity is introduced by the curvatures of the surface, $\overset{*}{k}_{ij} = k_{ij} + \varkappa_{ij}$, projections of the forces and moments $\overset{*}{X}_i, \overset{*}{X}_3, \overset{*}{M}_i, \overset{*}{T}_{ik}, \overset{*}{N}_i, \overset{*}{M}_{ik}$ on the deformed axes, and, additionally, may be brought in by constitutive relations for the constructive material of a shell.

Proceeding from the second equation of equilibrium (3.29) and projecting it onto the orthogonal base $\{\bar{e}_1, \bar{e}_2, \bar{m}\}$, for the tangent T_{ik} and lateral forces N_i, we find

$$T_{11} = \bar{R}_1 \bar{e}_1, \quad T_{12} = \bar{R}_1 \bar{e}_2, \quad T_{21} = \bar{R}_2 \bar{e}_1, \quad T_{22} = \bar{R}_2 \bar{e}_2,$$
$$N_i = \bar{R}_i \bar{m}, \quad X_i = \bar{X} \bar{e}_i, \quad X_3 = \bar{X} \bar{m}.$$

Substituting expressions for $\bar{R}_i$, $\bar{X}$ and $\overset{*}{\bar{e}}_1$, $\overset{*}{\bar{e}}_2$, $\overset{*}{\bar{m}}$ given by Eqs. (3.21, 3.23, 3.27), we obtain

$$\begin{aligned}
T_{11} &= \left(\overset{*}{T}_{11} \overset{*}{\bar{e}}_1 + \overset{*}{T}_{12} \overset{*}{\bar{e}}_2 + \overset{*}{N}_1 \overset{*}{\bar{m}} \right) \bar{e}_1 = \overset{*}{T}_{11} (1 + e_{11})/(1 + 2\varepsilon_{11}) + \\
&\qquad + \overset{*}{T}_{12} e_{12}/(1 + 2\varepsilon_{22}) + \overset{*}{N}_1 \mathbb{S}_1/\sqrt{\mathfrak{A}}, \\
T_{12} &= \overset{*}{T}_{11} e_{12}/(1 + 2\varepsilon_{11}) + \overset{*}{T}_{12} (1 + e_{22})/(1 + 2\varepsilon_{22}) + \overset{*}{N}_1 \mathbb{S}_2/\sqrt{\mathfrak{A}}, \\
T_{22} &= \overset{*}{T}_{21} e_{12}/(1 + 2\varepsilon_{11}) + \overset{*}{T}_{22} (1 + e_{22})/(1 + 2\varepsilon_{22}) + \overset{*}{N}_2 \mathbb{S}_2/\sqrt{\mathfrak{A}}, \\
T_{21} &= \overset{*}{T}_{21} (1 + e_{11})/(1 + 2\varepsilon_{11}) + \overset{*}{T}_{22} e_{21}/(1 + 2\varepsilon_{22}) + \overset{*}{N}_2 \mathbb{S}_1/\sqrt{\mathfrak{A}},
\end{aligned} \tag{3.43}$$

$$\begin{aligned}
N_1 &= \overset{*}{T}_{11} \varpi_1/(1 + 2\varepsilon_{11}) + \overset{*}{T}_{12} \varpi_2/(1 + 2\varepsilon_{22}) + \overset{*}{N}_1 \mathbb{S}_3/\sqrt{\mathfrak{A}}, \\
N_2 &= \overset{*}{T}_{22} \varpi_2/(1 + 2\varepsilon_{22}) + \overset{*}{T}_{21} \varpi_1/(1 + 2\varepsilon_{11}) + \overset{*}{N}_2 \mathbb{S}_3/\sqrt{\mathfrak{A}}, \\
X_1 &= \overset{*}{X}_1 (1 + e_{11})/(1 + 2\varepsilon_{11}) + \overset{*}{X}_2 e_{12}/(1 + 2\varepsilon_{22}) + \overset{*}{X}_3 \varpi_1/\sqrt{\mathfrak{A}}, \\
X_2 &= \overset{*}{X}_1 e_{21}/(1 + 2\varepsilon_{11}) + \overset{*}{X}_2 (1 + e_{22})/(1 + 2\varepsilon_{22}) + \overset{*}{X}_3 \varpi_2/\sqrt{\mathfrak{A}}, \\
X_3 &= \left(\overset{*}{X}_1 \mathbb{S}_1 + \overset{*}{X}_2 \mathbb{S}_2 + \overset{*}{X}_3 \mathbb{S}_3 \right)/\sqrt{\mathfrak{A}}.
\end{aligned} \tag{3.44}$$

Analogously, substituting Eqs. (1.19, 1.23), into (3.29) we obtain the equilibrium equations for the thin shell in terms of the undeformed configuration

$$\begin{aligned}
&L1(T_{ik}) + A_1 A_2 N_1 k_{11} + A_1 A_2 N_2 k_{12} + A_1 A_2 X_1 = 0, \\
&L2(T_{ik}) + A_1 A_2 N_2 k_{22} + A_1 A_2 N_1 k_{21} + A_1 A_2 X_2 = 0,
\end{aligned} \tag{3.45}$$

$$\begin{aligned}
&\frac{\partial A_2 N_1}{\partial \alpha_1} + \frac{\partial A_1 N_2}{\partial \alpha_2} - A_1 A_2 T_{11} k_{11} - A_1 A_2 T_{22} k_{22} - \\
&\qquad - A_1 A_2 T_{12} k_{12} - A_1 A_2 T_{21} k_{12} + A_1 A_2 X_2 = 0.
\end{aligned} \tag{3.46}$$

The resultant internal and external force vectors $\bar{R}_i$ and $\bar{X}$ are given by

$$\begin{aligned}\bar{R}_1 &= T_{11}\bar{e}_1 + T_{12}\bar{e}_2 + N_1\bar{m},\\ \bar{R}_2 &= T_{21}\bar{e}_1 + T_{22}\bar{e}_2 + N_2\bar{m},\\ \bar{X} &= X_1\bar{e}_1 + X_2\bar{e}_2 + X_3\bar{m}.\end{aligned} \tag{3.47}$$

The equilibrium equations for moments Eqs. (3.41, 3.42) can be recast in similar way. The resultant equations are very bulky and are not given here.

References

Galimov KZ (1975) Foundations of the nonlinear theory of thin shells. Kazan University Publisher, Kazan

Galimov KZ, Paimushin VN, Teregulov IG (1996) Foundations of the nonlinear theory of shells. Kazan University Publisher, Kazan

Chapter 4
Soft Shells

The secret of getting ahead is getting started.
Mark Twain

4.1 Deformation of Soft Shell

A class of thin shells that:

(i) possess low resistance to stretching and zero-order flexural rigidity;
(ii) undergo finite deformations;
(iii) withstand only stretch but not compression forces;
(iv) its actual configuration is defined by internal/external loads per unit surface area only;
(v) its stress-strain states are fully described by in-plane membrane forces per unit length,

is called soft shells. Because soft shells acquire multiple forms in the absence of loads, it is instructive to introduce into consideration the cut configuration $\overset{0}{S}$ of the shell, in addition to the undeformed S and deformed $\overset{*}{S}$ configurations (Fig. 4.1). It defines the configuration with accuracy of bending in absence of loads.

Assume that the middle surface S of an undeformed soft shell coincides with its cut surface $\overset{0}{S}$ ($\overset{0}{S} \equiv S$). Let S be parameterized by curvilinear coordinates α_1, α_2. A point $M(\alpha_1, \alpha_2) \in S$ is described by the position vector $\bar{r}(\alpha_1, \alpha_2)$. As a result of action of external and or internal loads the shell will deform to attain a new configuration $\overset{*}{S}$. Assume that deformation is such that $\forall M(\alpha_1, \alpha_2) \rightarrow \overset{*}{M}\left(\overset{*}{\alpha}_1, \overset{*}{\alpha}_2\right)$ and is a homeomorphism. Thus, the inverse transformation exists.

Deformation of linear elements along the α_1, α_2-coordinate lines is described by stretch ratios λ_i ($i = 1, 2$) and elongations $e_{\alpha i}$ given by Eqs. (1.68, 2.3), respectively,

R.N. Miftahof, *Biomechanics of the Human Stomach*,
DOI 10.1007/978-3-319-59677-8_4

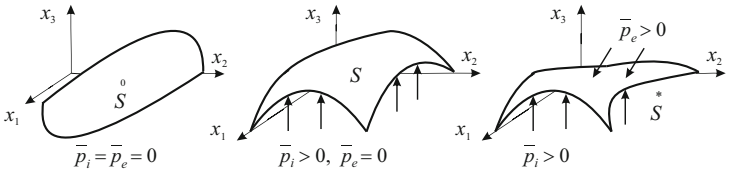

Fig. 4.1 The cut (ironed out), initial (undeformed) and actual (deformed) configurations of a soft shell

$$e_{\alpha i} = \frac{\overset{*}{ds}_i - ds_i}{ds_i} = \lambda_i - 1 = \frac{\sqrt{\overset{*}{a}_{ii}}}{\sqrt{a_{ii}}} - 1. \tag{4.1}$$

Changes in the angle between coordinate lines and the surface area are described by Eqs. (1.69, 2.4) or in equivalent from

$$\gamma = \overset{(0)}{\chi} - \overset{*}{\chi} = \overset{(0)}{\chi} - \cos^{-1}\frac{a_{12}}{\sqrt{a_{11}a_{22}}}. \tag{4.2}$$

$$\delta s_\Delta = \frac{\overset{*}{ds}_\Delta}{ds_\Delta} = \frac{\sqrt{\overset{*}{a}}}{\sqrt{a}} = \frac{\sqrt{\overset{*}{a}_{11}\ \overset{*}{a}_{22}}\sin\overset{*}{\chi}}{\sqrt{a_{11}a_{22}}\sin\overset{(0)}{\chi}} = \lambda_1\lambda_2\frac{\sin\overset{*}{\chi}}{\sin\overset{(0)}{\chi}}. \tag{4.3}$$

In the above use is made of Eqs. (1.4, (1.12, 2.3).

Vectors $\bar{r}_i, \bar{r}_k$ tangent to coordinate lines on S and $\overset{*}{S}$ are defined by Eqs. (1.3, 1.4). Making use of Eqs. (2.3, 2.4), we have

$$\bar{r}_i = \sum_{k=1}^{2} C_i^k \overset{*}{\bar{r}}_k, \quad \overset{*}{\bar{r}}_i = \sum_{k=1}^{2} \overset{*}{C}_i^k \bar{r}_k. \tag{4.4}$$

Hence, the unit vectors $\bar{e}_i \in S$, $\overset{*}{\bar{e}}_i \in \overset{*}{S}$ are found to be

$$\bar{e}_i = \frac{\bar{r}_i}{|\bar{r}_i|} = \frac{\bar{r}_i}{\sqrt{a_{ii}}} = \sum_{k=1}^{2} C_i^k \left(\overset{*}{\bar{r}}_k \sqrt{\frac{a_{ii}}{\overset{*}{a}_{kk}}}\right) = \sum_{k=1}^{2} \hat{C}_i^k \overset{*}{\bar{e}}_k, \quad \overset{*}{\bar{e}}_i = \sum_{k=1}^{2} \hat{C}_i^k \bar{e}_k, \tag{4.5}$$

where the following notations are introduced

$$\hat{C}_i^k = C_i^k \sqrt{\frac{\overset{*}{a}_{kk}}{a_{ii}}}, \quad \overset{*}{\hat{C}}_i^k = \overset{*}{C}_i^k \sqrt{\frac{a_{kk}}{\overset{*}{a}_{ii}}}. \tag{4.6}$$

With the help of Eq. (4.6), the scalar and vector products of unit vectors $\overset{*}{\bar{e}}_i$ and $\bar{e}_k{}^*$ are found to be

$$\begin{aligned}
\overset{*}{\bar{e}}_i \cdot \overset{*}{\bar{e}}_k &:= \cos\chi^*_{ik} = \sum_{j=1}^{2}\sum_{n=1}^{2} \bar{e}_j \cdot \bar{e}_n \overset{*}{\hat{C}}{}_i^j \overset{*}{\hat{C}}{}_k^n = \sum_{j=1}^{2}\sum_{n=1}^{2} \overset{*}{\hat{C}}{}_i^j \overset{*}{\hat{C}}{}_k^n \overset{(0)}{\chi}_{jn}, \\
\overset{*}{\bar{e}}_i \times \overset{*}{\bar{e}}_k &:= \overset{*}{\bar{m}} \sin\chi^*_{ik} = \sum_{j=1}^{2}\sum_{n=1}^{2} \bar{e}_j \times \bar{e}_n \overset{*}{\hat{C}}{}_i^j \overset{*}{\hat{C}}{}_k^n = \sum_{j=1}^{2}\sum_{n=1}^{2} \overset{*}{\hat{C}}{}_i^j \overset{*}{\hat{C}}{}_k^n \overset{*}{\bar{m}} \sin\overset{(0)}{\chi}_{jn}.
\end{aligned} \tag{4.7}$$

In just the same way, proceeding from the scalar and vector multiplication of $\bar{e}_i$ by $\bar{e}_k$, it can be shown that

$$\begin{aligned}
\cos\overset{(0)}{\chi}_{ik} &= \sum_{j=1}^{2}\sum_{n=1}^{2} \hat{C}_i^j \hat{C}_k^n \cos\chi^*_{jn}, \\
\sin\overset{(0)}{\chi}_{ik} &= \sum_{j=1}^{2}\sum_{n=1}^{2} \hat{C}_i^j \hat{C}_k^n \sin\chi^*_{jn}.
\end{aligned} \tag{4.8}$$

To calculate the coefficients C_i^k, $\overset{*}{\hat{C}}{}_i^k$, we proceed from geometric considerations. Let vectors $\bar{e}_i$, $\overset{*}{\bar{e}}_i$ at point $\overset{*}{M}\left(\overset{*}{\alpha}_1, \overset{*}{\alpha}_2\right) \in \overset{*}{S}$ be oriented as shown (Fig. 4.2). Decomposing $\overset{*}{\bar{e}}_i$ in the directions of $\bar{e}_k$, we have

$$\overset{*}{\hat{C}}{}_1^1 = \overline{MC}, \quad \overset{*}{\hat{C}}{}_1^2 = \overline{CD}, \quad \overset{*}{\hat{C}}{}_2^1 = -\overline{AB}, \quad \overset{*}{\hat{C}}{}_2^2 = \overline{MB}. \tag{4.9}$$

Solving ΔMCD and ΔMBA, we find

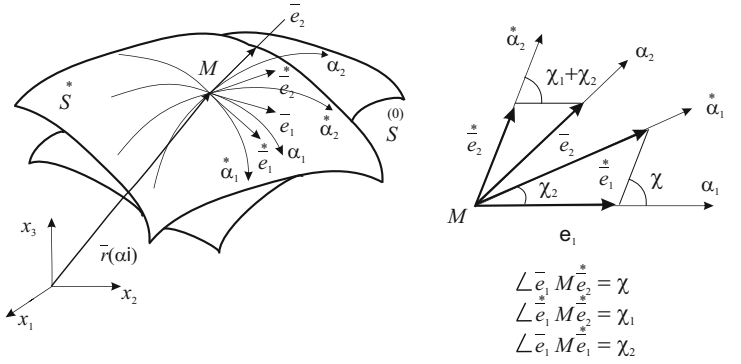

Fig. 4.2 Deformation of an element of a soft shell

$$\begin{aligned}
&\overset{*}{\hat{C}}{}_1^1 = \sin\left(\overset{*}{\chi} - \overset{*}{\chi}_2\right)/\sin\overset{*}{\chi}, \quad \overset{*}{\hat{C}}{}_1^2 = \sin\overset{*}{\chi}_2/\sin\overset{*}{\chi},\\
&\overset{*}{\hat{C}}{}_2^1 = -\sin\left(\overset{*}{\chi}_1 + \overset{*}{\chi}_2 - \overset{*}{\chi}\right)/\sin\overset{*}{\chi}, \quad \overset{*}{\hat{C}}{}_2^2 = \sin\left(\overset{*}{\chi}_1 + \overset{*}{\chi}_2\right)/\sin\overset{*}{\chi},\\
&\overset{*}{\hat{C}} = \det\overset{*}{\hat{C}}{}_i^k = \sin\overset{*}{\chi}_1/\sin\overset{*}{\chi}.
\end{aligned} \tag{4.10}$$

Similarly, expanding unit vectors $\bar{e}_i$ along $\overset{*}{\bar{e}}_k$, we obtain

$$\begin{aligned}
&\hat{C}_1^1 = \sin\left(\overset{0}{\chi}_1 + \overset{0}{\chi}_2\right)/\sin\overset{0}{\chi}_1, \quad \hat{C}_1^2 = -\sin\overset{0}{\chi}_2/\sin\overset{0}{\chi}_1,\\
&\hat{C}_2^1 = \sin\left(\overset{0}{\chi}_1 + \overset{0}{\chi}_2 - \overset{0}{\chi}\right)/\sin\overset{0}{\chi}_1, \quad \hat{C}_2^2 = \sin\left(\overset{0}{\chi} - \overset{0}{\chi}_2\right)/\sin\overset{0}{\chi}_1,\\
&\hat{C} = \det\hat{C}_i^k = \sin\overset{0}{\chi}/\sin\overset{0}{\chi}_1.
\end{aligned} \tag{4.11}$$

Note, that the coefficients C_i^k, $\overset{*}{\hat{C}}{}_i^k$ are the functions of $\overset{0}{\chi}_i$ and $\overset{*}{\chi}_i$, while $\hat{C}_i^k$, $\overset{*}{\hat{C}}{}_i^k$ depend on $\bar{r}_i$ and $\overset{*}{\bar{r}}_i$ and the actual configuration of a shell.

Let the cut configuration of a soft shell $\overset{0}{S}$ be different from the undeformed configuration S. We introduce the coefficients of transformation $\bar{r}_i \in \overset{0}{S} \to \overset{*}{S}$ by

$$\hat{\overset{*}{C}}{}_i^k = C_i^k\sqrt{\frac{\overset{*}{a}_{kk}}{\overset{0}{a}_{ii}}}, \quad \overset{*}{\hat{C}}{}_i^k = \overset{*}{C}{}_i^k\sqrt{\frac{\overset{0}{a}_{kk}}{\overset{*}{a}_{ii}}}, \tag{4.12}$$

where $\overset{0}{a}_{ii}$, $\overset{*}{a}_{ii}$ are the components of the metric tensor $\mathbf{A}$ on $\overset{0}{S}$ and $\overset{*}{S}$, respectively. Eliminating C_i^k, $\overset{*}{C}{}_i^k$ from Eq. (4.6), for the coefficients of the cut and deformed surfaces we obtain

$$\hat{C}_i^k = \hat{\overset{*}{C}}{}_i^k\frac{\overset{*}{\lambda}_k}{\lambda_i}, \quad \overset{*}{\hat{C}}{}_i^k = \overset{*}{\hat{C}}{}_i^k\frac{\lambda_k}{\overset{*}{\lambda}_i}. \tag{4.13}$$

Similarly to Eq. (4.14), we introduce the coefficients

$$\overset{*}{\hat{C}}{}_i^k = \left[\hat{C}_k^i\right]/\hat{C}, \quad \overset{*}{\hat{C}}{}_i^k = \left[\hat{\overset{*}{C}}{}_k^i\right]/\hat{\overset{*}{C}}, \tag{4.14}$$

where

$$\hat{C} = C\sqrt{\frac{\overset{*}{a}_{11}\,\overset{*}{a}_{22}}{\overset{0}{a}_{11}\,\overset{0}{a}_{22}}}, \quad \hat{\overset{*}{C}} = C\sqrt{\frac{\overset{*}{a}_{11}\,\overset{*}{a}_{22}}{\overset{0}{a}_{11}\,\overset{0}{a}_{22}}}. \tag{4.15}$$

Finally, from Eqs. (4.12)–(4.15), we get

$$\hat{C} = \hat{\overset{*}{C}} \frac{\overset{*}{\lambda}_1 \overset{*}{\lambda}_2}{\lambda_1 \lambda_2}. \tag{4.16}$$

Let $\mathbf{E}$ be the tensor of deformation of $S\left(S = \overset{0}{S}\right)$ given by

$$\mathbf{E} = \sum_{i=1}^{2} \sum_{k=1}^{2} \varepsilon_{ik} \vec{r}^{\,i} \vec{r}^{\,k}, \tag{4.17}$$

where

$$\varepsilon_{ik} = \frac{\overset{*}{a}_{ik} - a_{ik}}{2}. \tag{4.18}$$

Substituting Eqs. (1.4, 2.3) into (4.18) for ε_{ik}, we find

$$\varepsilon_{ik} = \frac{\left(\lambda_i \lambda_k \cos \overset{*}{\chi} - \cos \chi\right) \sqrt{a_{ii} a_{kk}}}{2}. \tag{4.19}$$

It is easy to show that the following relations hold

$$\begin{aligned} \varepsilon_{ik} &= \sum_{j=1}^{2} \sum_{n=1}^{2} \varepsilon^*_{jn} C_i^j C_k^n, \quad \varepsilon^{ik} = \sum_{j=1}^{2} \sum_{n=1}^{2} \overset{*}{\varepsilon}{}^{jn} C_j^i C_n^k, \\ \overset{*}{\varepsilon}_{ik} &= \sum_{j=1}^{2} \sum_{n=1}^{2} \varepsilon_{jn} \overset{*}{C}{}_i^j \overset{*}{C}{}_k^n, \quad \overset{*}{\varepsilon}{}^{ik} = \sum_{j=1}^{2} \sum_{n=1}^{2} \varepsilon^{jn} C_j^i C_n^k. \end{aligned} \tag{4.20}$$

In the theory of soft thin shells stretch ratios and membrane forces per unit length of a differential element are preferred to traditional deformations and stresses per unit cross-sectional area of the shell. Thus, dividing Eq. (4.19) by the surface area $\sqrt{a_{ii} a_{kk}}$ of an element, we get

$$\widetilde{\varepsilon}_{ik} := \frac{\varepsilon_{ik}}{\sqrt{a_{ii} a_{kk}}} = \frac{\left(\lambda_i \lambda_k \cos \overset{*}{\chi} - \cos \chi\right)}{2}, \tag{4.21}$$

$\widetilde{\varepsilon}_{ik}$ are called the physical components of $\mathbf{E}$. Using Eqs. (4.20), for $\overset{*}{\widetilde{\varepsilon}}_{ik}$ in terms of the deformed configuration, we obtain

$$\overset{*}{\widetilde{\varepsilon}}_{ik} = \sum_{j=1}^{2} \sum_{n=1}^{2} \widetilde{\varepsilon}_{jn} \overset{*}{C}{}_i^j \overset{*}{C}{}_k^n \frac{\sqrt{a_{jj} a_{nn}}}{\sqrt{\overset{*}{a}_{jj} \overset{*}{a}_{nn}}}, \tag{4.22}$$

where the coefficients $\overset{*}{C}{}_i^j$ satisfy Eqs. (2.3, 2.4).

Making use of Eq. (4.21) in (2.3, 4.2) for λ_i and γ, we find

$$\begin{aligned}\lambda_i &= 1+\varepsilon_i = \sqrt{1+2\widetilde{\varepsilon}_{ii}},\\ \gamma &= \overset{(0)}{\chi} - \cos^{-1}\frac{2\widetilde{\varepsilon}_{12}+\cos\overset{(0)}{\chi}}{\sqrt{(1+2\widetilde{\varepsilon}_{11})}\sqrt{(1+2\widetilde{\varepsilon}_{22})}}.\end{aligned} \tag{4.23}$$

Substituting $\hat{\overset{0}{C}}{}_i^k$, $\hat{\overset{*}{C}}{}_i^k$ given by Eqs. (4.12) in (4.22), we have

$$\overset{*}{\widetilde{\varepsilon}}_{ik} = \sum_{j=1}^{2}\sum_{n=1}^{2}\widetilde{\varepsilon}_{jn}\,\hat{\overset{*}{C}}{}_i^j\,\hat{\overset{*}{C}}{}_k^n \quad \widetilde{\varepsilon}_{ik} = \sum_{j=1}^{2}\sum_{n=1}^{2}\overset{*}{\widetilde{\varepsilon}}{}^m{}_{jn}\hat{\overset{0}{C}}{}_i^j\,\hat{\overset{0}{C}}{}_k^n. \tag{4.24}$$

Finally, formulas for $\overset{*}{\widetilde{\varepsilon}}_{ik}$ in terms of $\overset{0}{S}$-configuration of the soft shell takes the form

$$\begin{aligned}\overset{*}{\widetilde{\varepsilon}}_{11} &= \left[\widetilde{\varepsilon}_{11}\sin^2\left(\overset{0}{\chi}-\overset{0}{\chi}_2\right)+\widetilde{\varepsilon}_{22}\sin^2\overset{0}{\chi}_2+2\widetilde{\varepsilon}_{12}\sin\left(\overset{0}{\chi}-\overset{0}{\chi}_2\right)\sin\overset{0}{\chi}_2\right]/\sin^2\overset{0}{\chi}\\ \overset{*}{\widetilde{\varepsilon}}_{12} &= \left[-\widetilde{\varepsilon}_{11}\sin\left(\overset{0}{\chi}-\overset{0}{\chi}_2\right)\sin\left(\overset{0}{\chi}_1+\overset{0}{\chi}_2-\overset{0}{\chi}\right)+\widetilde{\varepsilon}_{22}\sin\overset{0}{\chi}_2\sin\left(\overset{0}{\chi}_1+\overset{0}{\chi}_2\right)-\right.\\ &\quad\left.+\widetilde{\varepsilon}_{12}\left(\cos\left(\overset{0}{\chi}_1+2\overset{0}{\chi}_2-\overset{0}{\chi}\right)-\cos\overset{0}{\chi}\cos\overset{0}{\chi}_1\right)\right]/\sin^2\overset{0}{\chi}\\ \overset{*}{\widetilde{\varepsilon}}_{22} &= \left[\widetilde{\varepsilon}_{11}\sin^2\left(\overset{0}{\chi}_1+\overset{0}{\chi}_2-\overset{0}{\chi}\right)++\widetilde{\varepsilon}_{22}\sin^2\left(\overset{0}{\chi}_1+\overset{0}{\chi}_2\right)-\right.\\ &\quad\left.-2\widetilde{\varepsilon}_{12}\sin\left(\overset{0}{\chi}_1+\overset{0}{\chi}_2-\overset{0}{\chi}\right)\sin\left(\overset{0}{\chi}_1+\overset{0}{\chi}_2\right)\right]/\sin^2\overset{0}{\chi}.\end{aligned} \tag{4.25}$$

With the help of Eq. (4.21) in (4.24) the physical components can also be expressed in terms of stretch ratios and shear angles as

$$\overset{*}{\lambda}_i\,\overset{*}{\lambda}_k\cos\overset{*}{\chi}_{ik} - \cos\overset{0}{\chi}_{ik} = \sum_{j=1}^{2}\sum_{n=1}^{2}\left(\lambda_j\lambda_n\cos\chi_{jn} - \cos\overset{0}{\chi}_{jn}\right)\hat{\overset{*}{C}}{}_i^j\,\hat{\overset{*}{C}}{}_k^n. \tag{4.26}$$

Further, on use of Eqs. (4.7, 4.10, 4.26) in terms of $\overset{0}{S}$-configuration takes the form

$$\overset{*}{\lambda}_i\,\overset{*}{\lambda}_k\cos\overset{*}{\chi}_{ik} = \sum_{j=1}^{2}\sum_{n=1}^{2}\lambda_j\lambda_n\,\hat{\overset{*}{C}}{}_i^j\,\hat{\overset{*}{C}}{}_k^n\cos\overset{0}{\chi}_{jn}, \tag{4.27}$$

or in expanded form

$$
\begin{aligned}
\overset{*}{\lambda}_1 &= \Big[\lambda_1^2 \sin^2\Big(\overset{0}{\chi} - \overset{0}{\chi}_2\Big) + \lambda_2^2 \sin^2 \overset{0}{\chi}_2 + \\
&\quad + 2\lambda_1\lambda_2 \sin\Big(\overset{0}{\chi} - \gamma\Big) \sin\Big(\overset{0}{\chi} - \overset{0}{\chi}_2\Big) \sin \overset{0}{\chi}_2\Big]^{1/2} / \sin^2 \overset{0}{\chi}, \\
\overset{*}{\gamma} &= \overset{0}{\chi}_1 - \cos^{-1}\Big[\Big(-\lambda_1^2 \sin\Big(\overset{0}{\chi} - \overset{0}{\chi}_2\Big) \sin\Big(\overset{0}{\chi}_1 + \overset{0}{\chi}_2 - \overset{0}{\chi}\Big) + \\
&\quad + \lambda_2^2 \sin \overset{0}{\chi}_2 \sin\Big(\overset{0}{\chi}_1 + \overset{0}{\chi}_2\Big) + \lambda_1\lambda_2\big(\cos\Big(\hat{\delta} + 2\overset{0}{\chi}_2 - \overset{0}{\chi}\Big) - \\
&\quad - \cos \overset{0}{\chi} \cos \overset{0}{\chi}_1\big) \cos\Big(\overset{0}{\chi} - \gamma\Big)\Big)\Big(\overset{*}{\lambda}_1 \overset{*}{\lambda}_2 \sin^2 \overset{0}{\chi}\Big)^{-1}\Big] \\
\overset{*}{\lambda}_2 &= \Big[\lambda_1^2 \sin^2\Big(\overset{0}{\chi}_1 + \overset{0}{\chi}_2 - \overset{0}{\chi}\Big) + \lambda_2^2 \sin^2\Big(\overset{0}{\chi}_1 + \overset{0}{\chi}_2\Big) - \\
&\quad - 2\lambda_1\lambda_2 \cos\Big(\overset{0}{\chi} - \Delta\overset{*}{\chi}\Big) \sin\Big(\overset{0}{\chi}_1 + \overset{0}{\chi}_2 - \overset{0}{\chi}\Big) \sin\Big(\overset{0}{\chi}_1 + \overset{0}{\chi}_2\Big)\Big]^{1/2} / \sin^2 \overset{0}{\chi}
\end{aligned}
\tag{4.28}
$$

Formulas (4.27, 4.28) are preferred in practical applications particularly when dealing with finite deformations of shells.

4.2 Principal Deformations

At any point $\overset{*}{M} \in \overset{*}{S}$, there exist two mutually orthogonal directions that remain orthogonal during deformation and along which the components of **E,** attain the maximum and minimum value. They are called the principal directions.

To find the orientation of the principal axes, we proceed as follows. Let $\overset{(0)}{\varphi}$, $\overset{*}{\varphi}$ be the angles of the direction away from the base vectors $\bar{e}_1 \in \overset{(0)}{S}$, $\overset{*}{\bar{e}}_1 \in \overset{*}{S}$, respectively. We assume that the cut and undeformed configurations are indistinguishable $\overset{0}{S} = S$. Then, setting $\overset{0}{\chi}_2 = \overset{0}{\varphi}$ in the first equation of (4.25), we have

$$
\overset{*}{\tilde{\varepsilon}}_{11} \sin^2 \overset{0}{\chi} = \tilde{\varepsilon}_{11} \sin^2\Big(\overset{0}{\chi} - \overset{0}{\varphi}\Big) + 2\tilde{\varepsilon}_{12} \sin\Big(\overset{0}{\chi} - \overset{0}{\varphi}\Big) \sin \overset{0}{\varphi} + \tilde{\varepsilon}_{22} \sin^2 \overset{0}{\varphi}. \tag{4.29}
$$

After simple rearrangements it can be written in the form

$$
\varepsilon = a_0 + b_0 \cos 2\overset{0}{\varphi} + c_0 \sin 2\overset{0}{\varphi}, \tag{4.30}
$$

where

$$
\begin{aligned}
a_0 &= \left[\frac{1}{2}(\widetilde{\varepsilon}_{11}+\widetilde{\varepsilon}_{22})-\widetilde{\varepsilon}_{12}\cos\overset{0}{\chi}\right]/\sin^2\overset{0}{\chi}, \\
b_0 &= \left[\frac{1}{2}(\widetilde{\varepsilon}_{11}-\widetilde{\varepsilon}_{22})+\left(\widetilde{\varepsilon}_{12}-\widetilde{\varepsilon}_{11}\cos\overset{0}{\chi}\right)/\cos\overset{0}{\chi}\right]/\sin^2\overset{0}{\chi}, \\
c_0 &= \left(\widetilde{\varepsilon}_{12}-\widetilde{\varepsilon}_{11}\cos\overset{0}{\chi}\right)/\sin\overset{0}{\chi}.
\end{aligned}
\tag{4.31}
$$

Differentiating Eq. (4.30) with respect to $\overset{0}{\varphi}$ and equating the resultant equation to zero, for the principal axes on the surface $\overset{(0)}{S}$, we find ($b_0 \neq 0$)

$$
\tan 2\overset{0}{\varphi} = \frac{c_0}{b_0} = \frac{2\left(\widetilde{\varepsilon}_{11}\cos\overset{0}{\chi}-\widetilde{\varepsilon}_{12}\right)\sin\overset{0}{\chi}}{\widetilde{\varepsilon}_{11}\cos 2\overset{0}{\chi}-2\widetilde{\varepsilon}_{12}\cos\overset{0}{\chi}+\widetilde{\varepsilon}_{22}}. \tag{4.32}
$$

Substituting Eq. (4.32) into (4.30), we obtain the principal physical components ε_1, ε_2 of $\mathbf{E}$

$$
\begin{aligned}
\varepsilon_{1,2} = a_0^2 \pm \sqrt{b_0^2+c_0^2} = \frac{\widetilde{\varepsilon}_{11}+\widetilde{\varepsilon}_{22}-2\widetilde{\varepsilon}_{12}\cos\overset{0}{\chi}}{2\sin^2\overset{0}{\chi}} \pm \\
\pm\frac{1}{\sin^2\overset{0}{\chi}}\sqrt{\frac{(\widetilde{\varepsilon}_{11}-\widetilde{\varepsilon}_{22})^2}{4}+\widetilde{\varepsilon}_{12}^2+\widetilde{\varepsilon}_{11}\widetilde{\varepsilon}_{22}\cos^2\overset{0}{\chi}-\widetilde{\varepsilon}_{12}(\widetilde{\varepsilon}_{11}+\widetilde{\varepsilon}_{22})\cos\overset{0}{\chi}}.
\end{aligned}
\tag{4.33}
$$

Henceforth, we assume that max ε_1 is achieved in the direction of the principal axis defined by the angle $\overset{0}{\varphi}_1 = \overset{0}{\varphi}$, and min ε_2-along the axis, defined by the angle $\overset{0}{\varphi}_2 = \overset{0}{\varphi}+\pi/2$. Since for the principal directions $\overset{0}{\chi}_1 \equiv \pi/2$, from the second Eq. (4.25), we find

$$
\overset{*}{\widetilde{\varepsilon}}_{12} = -b_0\sin 2\overset{0}{\varphi}+c_0\cos 2\overset{0}{\varphi}. \tag{4.34}
$$

Dividing both sides of Eq. (4.34) by $c_0\cos 2\overset{0}{\varphi}$ and using Eq. (4.32), we find $\overset{*}{\widetilde{\varepsilon}}_{12} = 0$. Thus, there exist indeed two mutually orthogonal directions at $\forall M(\alpha_i) \in \overset{(0)}{S}$ that remain orthogonal throughout deformation. Similar result, i.e. $\overset{*}{\gamma} = 0$, can be obtained from Eq. (6.9) by setting $\overset{0}{\chi} = \pi/2$.

Substituting Eq. (4.21) in (4.32, 4.33) for the orientation of the principal axes on $\overset{0}{S}$ and the principal stretch ratios, we obtain

$$\tan 2\overset{0}{\varphi}_1 = \frac{2\left[\lambda_1\lambda_2 \cos\left(\overset{0}{\chi} - \overset{*}{\gamma}\right) - \lambda_1^2 \cos \overset{0}{\chi}\right] \sin \overset{0}{\chi}}{\lambda_1^2 - \lambda_2^2 + 2\left[\lambda_1\lambda_2 \cos\left(\overset{0}{\chi} - \overset{*}{\gamma}\right) - \lambda_1^2 \cos \overset{0}{\chi}\right] \cos \overset{0}{\chi}}, \tag{4.35}$$

$$\overset{0}{\varphi}_2 = \overset{0}{\varphi}_1 + \pi/2,$$

$$\begin{aligned}\Lambda^2_{1,2} = \Big[&\left(\lambda_1^2 + \lambda_2^2\right)/2 - \lambda_1\lambda_2 \cos\left(\overset{0}{\chi} - \overset{*}{\gamma}\right) \cos \overset{0}{\chi} \pm \\ &\pm\Big(\left(\lambda_1^2 + \lambda_2^2\right)^2/4 + \lambda^2{}_1\lambda^2{}_2 \cos\left(2\overset{0}{\chi} - \overset{*}{\gamma}\right) \cos \overset{*}{\gamma} - \\ &-\lambda_1\lambda_2\left(\lambda_1^2 + \lambda_2^2\right) \cos\left(\overset{0}{\chi} - \overset{*}{\gamma}\right) \cos \overset{0}{\chi}\Big)^{1/2}\Big]^{1/2} / \sin \overset{0}{\chi}.\end{aligned} \tag{4.36}$$

To find the orientation of the principal axes on the deformed surface $\overset{*}{S}$, consider a triangular element on S bounded by the two principal axes and the α_1-coordinate line (Fig. 4.3). Geometric analysis leads to the following obvious equalities

$$\begin{aligned}&\cos \overset{*}{\varphi}_1 = \frac{d\overset{*}{s}_1}{ds_1} = \frac{\mathbf{\Lambda}_1}{\lambda_1}\cos \overset{(0)}{\varphi}_1, \quad \sin \overset{*}{\varphi}_1 = \frac{d\overset{*}{s}_2}{ds_1} = \frac{\mathbf{\Lambda}_2}{\lambda_1}\sin \overset{(0)}{\varphi}_1. \\ &\tan \overset{*}{\varphi}_1 = \frac{d\overset{*}{s}_2}{d\overset{*}{s}_1} = \frac{\mathbf{\Lambda}_2}{\mathbf{\Lambda}_1}\tan \overset{(0)}{\varphi}_1.\end{aligned} \tag{4.37}$$

On use of Eqs. (4.35, 4.36) from the above, we find the angles for the principal axes $\overset{*}{\varphi}_1$ and $\overset{*}{\varphi}_2 = \overset{*}{\varphi}_1 + \pi/2$.

Finally, substituting Eqs. (4.3, 4.21) into expressions for the first and second invariants of the tensor of deformation **E** defined by

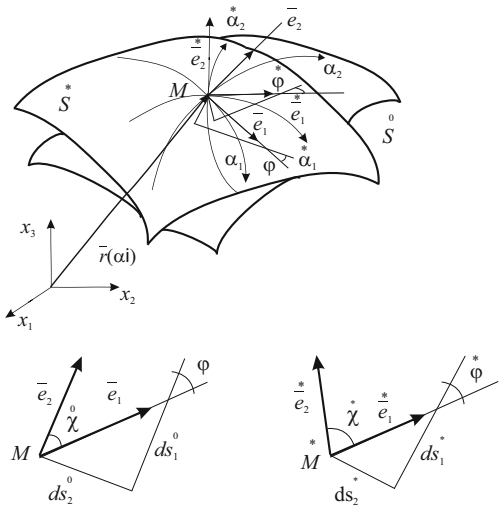

Fig. 4.3 Principal deformations

$$
\begin{aligned}
I^{(\mathbf{E})}{}_1 &= \varepsilon_1 + \varepsilon_2 = \overset{*}{\widetilde{\varepsilon}}_{11} + \overset{*}{\widetilde{\varepsilon}}_{22} = \left(\widetilde{\varepsilon}_{11} - 2\widetilde{\varepsilon}_{12}\cos\overset{0}{\chi} + \widetilde{\varepsilon}_{22}\right)/\sin^2\overset{0}{\chi}, \\
I^{(\mathbf{E})}{}_2 &= \varepsilon_1\varepsilon_2 = \overset{*}{\widetilde{\varepsilon}}_{11}\,\overset{*}{\widetilde{\varepsilon}}_{22} - \left(\overset{*}{\widetilde{\varepsilon}}_{12}\right)^2 = \left[\widetilde{\varepsilon}_{11}\widetilde{\varepsilon}_{22} - (\widetilde{\varepsilon}_{12})^2\right]/\sin^2\overset{0}{\chi}.
\end{aligned}
\tag{4.38}
$$

for the principal stretch ratios and the shear angle, we get

$$
\begin{aligned}
\mathbf{\Lambda}^2{}_1 + \mathbf{\Lambda}^2{}_2 &= \left(\overset{*}{\lambda}_1\right)^2 + \left(\overset{*}{\lambda}_2\right)^2 = \\
&= \left(\lambda_1^2 + \lambda_2^2 - 2\lambda_1\lambda_2\cos\left(\overset{0}{\chi} - \gamma\right)\cos\overset{0}{\chi}\right)/\sin^2\overset{0}{\chi}, \\
\mathbf{\Lambda}_1\mathbf{\Lambda}_2 &= \sqrt{1 + 2I^{(\mathbf{E})}{}_1 + 4I^{(\mathbf{E})}{}_2} = \overset{*}{\lambda}_1\,\overset{*}{\lambda}_2\cos\gamma = \lambda_1\lambda_2\sin\left(\overset{0}{\chi} - \gamma\right)/\sin\overset{0}{\chi}.
\end{aligned}
\tag{4.39}
$$

The last equation is also used to calculate the change of the surface area of S.

4.3 Membrane Forces

The stress state of a differential element of the soft shell is described entirely by in-plane tangent $T_{ii}(T^{ii})$ and shear $T_{ik}(T^{ik})(i \neq k)$ forces per unit length of the element. To study the equilibrium of the shell, we proceed from consideration of triangular elements ΔMAB and ΔMCD on $\overset{*}{S}$ (Fig. 4.4). Analysis of force distribution in the elements yields

$$
\begin{aligned}
-\overline{MA}\sum_{k=}^{2}\overset{*}{T}{}^{1k}\,\overset{*}{\bar{e}}_k + \overline{MB}\sum_{i=1}^{2}T^{1i}\bar{e}_i + \overline{AB}\sum_{i=1}^{2}T^{2i}\bar{e}_i = 0, \\
\overline{MD}\sum_{k=1}^{2}\overset{*}{T}{}^{2k}\,\overset{*}{\bar{e}}_k + \overline{CD}\sum_{i=1}^{2}T^{1i}\bar{e}_i - \overline{MC}\sum_{i=1}^{2}T^{2i}\bar{e}_i = 0,
\end{aligned}
\tag{4.40}
$$

where $\overset{*}{\hat{C}}{}_1^1 = \overline{MC}$, $\overset{*}{\hat{C}}{}_1^2 = \overline{CD}$, $\overset{*}{\hat{C}}{}_2^1 = -\overline{AB}$, $\overset{*}{\hat{C}}{}_2^2 = \overline{MB}$ (Eq. 6.9). The scalar product of Eqs. (4.40) and $\overset{*}{\bar{e}}{}^k$ yields

$$
\begin{aligned}
\overset{*}{T}{}^{1k} &= \sum_{i=1}^{2}\left(T^{1i}\hat{C}_i^k\,\overset{*}{\hat{C}}{}_2^2 - T^{2i}\hat{C}_i^k\,\overset{*}{\hat{C}}{}_2^1\right), \\
\overset{*}{T}{}^{2k} &= \sum_{i=1}^{2}\left(-T^{1i}\hat{C}_i^k\,\overset{*}{\hat{C}}{}_1^2 + T^{2i}\hat{C}_i^k\,\overset{*}{\hat{C}}{}_1^1\right).
\end{aligned}
$$

where use is made of Eqs. (4.5). Substituting $\overset{*}{\hat{C}}{}_i^k$ given by Eq. (4.14) for $\hat{C}_i^k$, we find

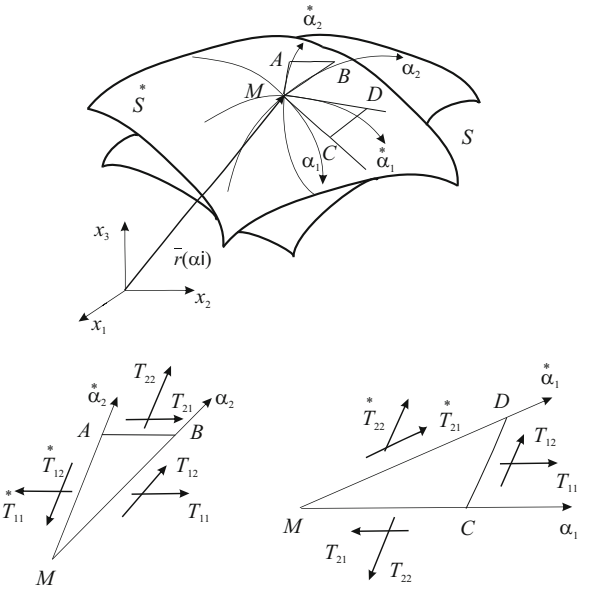

Fig. 4.4 Membrane forces in a soft shell

$$\overset{*}{T}{}^{ik} = \frac{1}{C}\sum_{j=1}^{2}\sum_{n=1}^{2} T^{jn}\hat{C}_j^i\hat{C}_n^k. \tag{4.41}$$

On use of Eqs. (4.11), the components of the membrane forces are found to be

$$\begin{aligned}
\overset{*}{T}{}^{11} &= \left\{T^{11}\sin^2\left(\overset{0}{\chi}_1+\overset{0}{\chi}_2\right) + T^{22}\sin^2\left(\overset{0}{\chi}_1+\overset{0}{\chi}_2-\overset{0}{\chi}\right)+\right.\\
&\quad \left.+2T^{12}\sin\left(\overset{0}{\chi}_1+\overset{0}{\chi}_2-\overset{0}{\chi}\right)\sin\left(\overset{0}{\chi}_1+\overset{0}{\chi}_2\right)\right\}/\sin\overset{0}{\chi}\sin\overset{0}{\chi}_1\\
\overset{*}{T}{}^{12} &= \left\{-T^{11}\sin\overset{0}{\chi}_2\sin\left(\overset{0}{\chi}_1+\overset{0}{\chi}_2\right) + T^{22}\sin\left(\overset{0}{\chi}_1+\overset{0}{\chi}_2-\overset{0}{\chi}\right)\sin\left(\overset{0}{\chi}-\overset{0}{\chi}_2\right)+\right.\\
&\quad \left.+T^{12}\left[\cos\left(\overset{0}{\chi}_1+2\overset{0}{\chi}_2-\overset{0}{\chi}\right) - \cos\overset{0}{\chi}\cos\overset{0}{\chi}_1\right]\right\}/\sin\overset{0}{\chi}\sin\overset{0}{\chi}_1,\\
\overset{*}{T}{}^{22} &= \left\{T^{11}\sin^2\overset{0}{\chi}_2 - 2T^{12}\sin\left(\overset{0}{\chi}-\overset{0}{\chi}_2\right)\sin\overset{0}{\chi}_2 + T^{22}\sin^2\left(\overset{0}{\chi}-\overset{0}{\chi}_2\right)\right\}/\sin\overset{0}{\chi}\sin\overset{0}{\chi}_1
\end{aligned} \tag{4.42}$$

Introducing the tensor of membrane forces **T**

$$\mathbf{T} = \sum_{j=1}^{2}\sum_{n=1}^{2} T^{ik}\bar{r}_i\bar{r}_k = \frac{1}{\sin\overset{*}{\chi}}\sum_{j=1}^{2}\sum_{n=1}^{2}\tilde{T}^{ik}\bar{e}_i\bar{e}_k, \tag{4.43}$$

where $\tilde{T}^{ik}$ are the physical components of **T**, and using Eq. (4.5), $\tilde{T}^{ik}$ can be expressed in terms of $\overset{*}{\tilde{T}}{}^{ik}$ as

$$\mathbf{T} = \frac{1}{\sin \overset{*}{\chi}} \sum_{j=1}^{2} \sum_{n=1}^{2} \tilde{T}^{ik} \bar{e}_i \bar{e}_k = \frac{1}{\sin \overset{*}{\chi}_1} \sum_{j=1}^{2} \sum_{n=1}^{2} \overset{*}{\tilde{T}}^{jn} \overset{*}{\bar{e}}_i \overset{*}{\bar{e}}_k$$
$$= \frac{1}{\sin \overset{*}{\chi}_1} \sum_{j=1}^{2} \sum_{n=1}^{2} \overset{*}{\tilde{T}}^{jn} \bar{e}_i \bar{e}_k \overset{*}{\hat{C}}{}_j^i \overset{*}{\hat{C}}{}_n^k .$$

Further, making use of Eq. (4.11), we obtain

$$\mathbf{T} = \frac{1}{\overset{*}{C}} \sum_{j=1}^{2} \sum_{n=1}^{2} \overset{*}{\tilde{T}}^{jn} \overset{*}{\hat{C}}{}_j^i \overset{*}{\hat{C}}{}_n^k . \tag{4.44}$$

Substituting $\overset{*}{\hat{C}}{}_j^i$ given by Eqs. (4.10), we get

$$\begin{aligned}
\tilde{T}^{11} &= \left\{ \overset{*}{\tilde{T}}^{11} \sin^2\left(\overset{*}{\chi} - \overset{*}{\chi}_2\right) + \overset{*}{\tilde{T}}^{22} \sin^2\left(\overset{*}{\chi}_1 + \overset{*}{\chi}_2 - \overset{*}{\chi}\right) - \right. \\
&\qquad \left. - 2\overset{*}{\tilde{T}}^{12} \sin\left(\overset{*}{\chi}_1 + \overset{*}{\chi}_2 - \overset{*}{\chi}\right) \sin\left(\overset{*}{\chi} - \overset{*}{\chi}_2\right) \right\} / \sin \overset{*}{\chi} \sin \overset{*}{\chi}_1 , \\
\tilde{T}^{12} &= \left\{ \overset{*}{\tilde{T}}^{11} \sin \overset{*}{\chi}_2 \sin\left(\overset{*}{\chi} - \overset{*}{\chi}_2\right) + \overset{*}{\tilde{T}}^{22} \sin\left(\overset{*}{\chi}_1 + \overset{*}{\chi}_2 - \overset{*}{\chi}\right) \sin\left(\overset{*}{\chi}_1 + \overset{*}{\chi}_2\right) + \right. \\
&\qquad \left. + \overset{*}{\tilde{T}}^{12} \left[\cos\left(\overset{*}{\chi}_1 + 2\overset{*}{\chi}_2 - \chi\right) - \cos \overset{*}{\chi} \cos \overset{*}{\chi}_1 \right] \right\} / \sin \overset{*}{\chi} \sin \overset{*}{\chi}_1 , \\
\tilde{T}^{22} &= \left\{ \overset{*}{\tilde{T}}^{11} \sin \overset{*}{\chi}_2 - 2\overset{*}{\tilde{T}}^{12} \sin\left(\overset{*}{\chi}_1 + \overset{*}{\chi}_2\right) \sin \overset{*}{\chi}_2 + \tilde{T}^{*22} \sin^2\left(\overset{*}{\chi}_1 + \overset{*}{\chi}_2\right) \right\} / \sin \overset{*}{\chi} \sin \overset{*}{\chi}_1 .
\end{aligned} \tag{4.45}$$

Using Eqs. (4.13) after simple rearrangements, Eq. (4.44) takes the form

$$\frac{\lambda_1 \lambda_2}{\lambda_i \lambda_k} \tilde{T}^{ik} = \frac{1}{\overset{*}{\hat{C}}} \sum_{j=1}^{2} \sum_{n=1}^{2} \frac{\overset{*}{\lambda}_1}{\overset{*}{\lambda}_j} \frac{\overset{*}{\lambda}_2}{\overset{*}{\lambda}_n} \overset{*}{\tilde{T}}^{jn} \overset{*}{\hat{C}}{}_j^j \overset{*}{\hat{C}}{}_n^k . \tag{4.46}$$

Formulas (4.46) are preferred to Eq. (4.44) in applications. First, the coefficients $\overset{*}{\hat{C}}{}_n^k$ are used in calculations of both deformations and membrane forces. Second, $\overset{*}{\hat{C}}{}_n^k$ depend only on parameterization of the initial configuration of the shell. Therefore, once calculated they can be used throughout.

4.4 Principal Membrane Forces

As in the case of principal deformations at any point $\overset{*}{M} \in \overset{*}{S}$, there exist two mutually orthogonal directions that remain orthogonal throughout deformation and along which $\mathbf{T}$ attains the extreme values. They are called the principal directions and the principal membrane forces, respectively.

Assuming that the coordinates $\overset{*}{\alpha}_i \in \overset{*}{S}$ and $\alpha_i \in S$ are related by the angle $\overset{*}{\psi}$, then, setting $\overset{*}{\chi}_1 = \pi/2$ and $\overset{*}{\chi}_2 = \psi$ in Eqs. (4.42), we find

$$\begin{aligned}
\overset{*}{T}^{11} &= \left\{T^{11}\cos^2\overset{*}{\psi} + T^{22}\cos^2\left(\overset{*}{\chi} - \overset{*}{\psi}\right) + 2T^{12}\cos\overset{*}{\psi}\cos\left(\overset{*}{\chi} - \overset{*}{\psi}\right)\right\}/\sin\overset{*}{\chi} \\
\overset{*}{T}^{12} &= \left\{-T^{11}\cos\overset{*}{\psi}\sin\overset{*}{\psi} + T^{12}\sin\left(\overset{*}{\chi} - 2\overset{*}{\psi}\right) + T^{22}\cos\left(\overset{*}{\chi} - \overset{*}{\psi}\right)\sin\left(\overset{*}{\chi} - \overset{*}{\psi}\right)\right\}/\sin\overset{*}{\chi} \\
\overset{*}{T}^{22} &= \left\{T^{11}\sin^2\overset{*}{\psi} - 2T^{12}\sin\left(\overset{*}{\chi} - \overset{*}{\psi}\right)\sin\overset{*}{\psi} + T^{22}\sin^2\left(\overset{*}{\chi} - \overset{*}{\psi}\right)\right\}/\sin\overset{*}{\chi}.
\end{aligned} \tag{4.47}$$

Equations (4.47) can be written in the form

$$\begin{aligned}
\overset{*}{T}^{11} &= a_1 + b_1\cos 2\overset{*}{\psi} + c_1\sin 2\overset{*}{\psi}, \\
\overset{*}{T}^{12} &= -b_1\sin 2\overset{*}{\psi} + c_1\cos 2\overset{*}{\psi}, \\
\overset{*}{T}^{22} &= a_1 - b_1\cos 2\overset{*}{\psi} - c_1\sin 2\overset{*}{\psi},
\end{aligned} \tag{4.48}$$

where the following notations are introduced

$$\begin{aligned}
a_1 &= \left[\frac{1}{2}\left(T^{11} + T^{22}\right) - T^{12}\cos\overset{*}{\chi}\right]/\sin\overset{*}{\chi}, \\
b_1 &= \left[\frac{1}{2}\left(T^{11} + T^{22}\right) + \left(T^{12} + T^{22}\cos\overset{*}{\chi}\right)\cos\overset{*}{\chi}\right]/\sin\overset{*}{\chi}, \\
c_1 &= T^{12} + T^{22}\cos\overset{*}{\chi}.
\end{aligned}$$

Differentiating T^{ii^*} with respect to $\overset{*}{\psi}$ and equating the result to zero, we obtain

$$\tan 2\overset{*}{\psi} = \frac{c_1}{b_1} = \frac{2\left(T^{12} + T^{22}\cos\overset{*}{\chi}\right)\sin\overset{*}{\chi}}{T^{11} + 2T^{12}\cos\overset{*}{\chi} + T^{22}\cos 2\overset{*}{\chi}}. \tag{4.49}$$

Solving the above for $\overset{*}{\psi}$ for the directional angles of the principal axes, we get

$$\tan 2\overset{*}{\psi}_1 = \frac{2\left(T^{12} + T^{22}\cos\overset{*}{\chi}\right)\sin\overset{*}{\chi}}{T^{11} + 2T^{12}\cos\overset{*}{\chi} + T^{22}\cos 2\overset{*}{\chi}},$$
$$\overset{*}{\psi}_2 = \overset{*}{\psi}_1 + \pi/2. \tag{4.50}$$

Substituting Eq. (4.49) into (4.48), we have

$$\overset{*}{T}^{11} = a_1 + \sqrt{b_1^2 + c_1^2}, \quad \overset{*}{T}^{12} = 0, \quad \overset{*}{T}^{22} = a_1 - \sqrt{{b_1}^2 + {c_1}^2}.$$

From Eq. (4.48) the principal membrane forces T_1, T_2 are found to be

$$T_{1,2} = a_1{}^2 \pm \sqrt{{b_1}^2 + {c_1}^2} = \frac{1}{\sin\overset{*}{\chi}}\left\{\frac{T^{11} + T^{22}}{2} + T^{12}\cos\overset{*}{\chi} \pm \right.$$
$$\left. \pm\sqrt{\tfrac{1}{4}\left(T^{11} - T^{22}\right)^2 + \left(T^{12}\right)^2 + T^{12}\left(T^{11} + T^{22}\right)\cos\overset{*}{\chi} + T^{11}T^{22}\cos^2\overset{*}{\chi}}\right\}. \tag{4.51}$$

Thus, at each point of the surface of the soft shell there are two mutually orthogonal directions that remain orthogonal throughout deformation. Henceforth, we assume that $T_1 \geq T_2$, i.e. the maximum stress is in the direction of the principal axis defined by the angle $\overset{*}{\psi}_1$, and the minimum—by the angle $\overset{*}{\psi}_2$.

Analogously to the invariants of the tensor of deformation described by Eqs. (4.38), we introduce the first and second invariants of **T**

$$I^{(\mathbf{T})}{}_1 = T_1 + T_2 = \overset{*}{T}^{11} + \overset{*}{T}^{22} = \left(T^{11} + T^{22} + 2T^{12}\cos\overset{*}{\chi}\right)/\sin\overset{*}{\chi},$$
$$I^{(\mathbf{T})}{}_2 = T_1T_2 = \overset{*}{T}^{11}\,\overset{*}{T}^{22} - \left(\overset{*}{T}^{12}\right)^2 = T^{11}T^{22} - \left(T^{12}\right)^2. \tag{4.52}$$

4.5 Corollaries of the Fundamental Assumptions

The fundamental assumptions stated in the beginning of the chapter have several corollaries specific to thin soft shells.

1. The zero-flexural rigidity state is natural and unique to thin soft shells in contrast to thin elastic shells with finite bending rigidity.
2. Soft shells do not resist compression forces and thus $T_1 > 0, T_2 > 0$ and $I^{(\mathbf{T})}{}_1 \geq 0$, $I^{(\mathbf{T})}{}_2 \geq 0$.
3. Shear membrane forces are significantly smaller compared to stretch forces, $T_{12} \approx 10^{-3}\max T_{ii}$.
4. Areas of the soft shell, where $\mathbf{\Lambda}_1 < 1$ and $\mathbf{\Lambda}_2 < 1$, attain multiple configurations and are treated as the zero-stressed areas.

5. Stress states of the soft shell are classified as: (i) biaxial, if $T_1 > 0, T_2 > 0$, ($I^{(\mathbf{T})}{}_1 > 0$, $I^{(\mathbf{T})}{}_2 > 0$), (ii) uniaxial, if either $T_1 = 0$, $T_2 > 0$ or $T_1 > 0$, $T_2 = 0$, ($I^{(\mathbf{T})}{}_1 > 0$, $I^{(\mathbf{T})}{}_2 = 0$), and (iii) unstressed, if $T_1 = 0$ and $T_2 = 0$, ($I^{(\mathbf{T})}{}_1 = I^{(\mathbf{T})}{}_2 = 0$).
6. Constitutive relations for the uniaxial stress-strain state (Fig. 4.5) are functions of either $\mathbf{\Lambda}_1$ or $\mathbf{\Lambda}_2$ and empirical mechanical constants c_m given by

$$\begin{aligned} T_1 &= f_1\left(\mathbf{\Lambda}_1, c_1, \ldots c_m, Z_{ij}\right) \quad \text{for} \quad \mathbf{\Lambda}_1 > 1, \ \mathbf{\Lambda}_2 < 1, \\ T_2 &= f_2\left(\mathbf{\Lambda}_2, c_1, \ldots c_m, Z_{ij}\right) \quad \text{for} \quad \mathbf{\Lambda}_1 < 1, \mathbf{\Lambda}_2 \geq 1. \end{aligned} \tag{4.53}$$

7. Constitutive relations for the in-plane biaxial state (Fig. 4.5), $\mathbf{\Lambda}_1 > 1$, $\mathbf{\Lambda}_2 > 1$ ($T_1 > 0, T_2 > 0$) have the form

$$\begin{aligned} T_1 &= F_1\left(\mathbf{\Lambda}_1, \mathbf{\Lambda}_2, \varphi, c_1, \ldots c_m, Z_{ij}\right), \\ T_2 &= F_2\left(\mathbf{\Lambda}_1, \mathbf{\Lambda}_2, \varphi, c_1, \ldots c_m, Z_{ij}\right), \\ \psi &= \psi\left(\mathbf{\Lambda}_1, \mathbf{\Lambda}_2, \varphi, c_1, \ldots c_m, Z_{ij}\right). \end{aligned} \tag{4.54}$$

In general $f_n(\ldots) \neq F_n(\ldots)$, however, $f_n(\ldots)$ can be defined uniquely if $F_n(\ldots)$ is known.

Constitutive relations for biological tissues are derived either analytically or obtained experimentally. Continuum models typically allow greater computational efficiency and are easily integrated into multicomponent mathematical models. However, the identification of homogenized parameters and constants of the models can be a formidable challenge. Therefore, it is common practice to use approximations of experimental results from uniaxial, biaxial and shear tests conducted on isolated tissue samples. Constitutive relations for soft biological tissues, e.g. the skin, the stomach, the gallbladder, are usually obtained along structurally preferred directions that are defined by the orientation of reinforced smooth muscle, collagen and elastin fibers, and thus, make them easy to use in calculations.

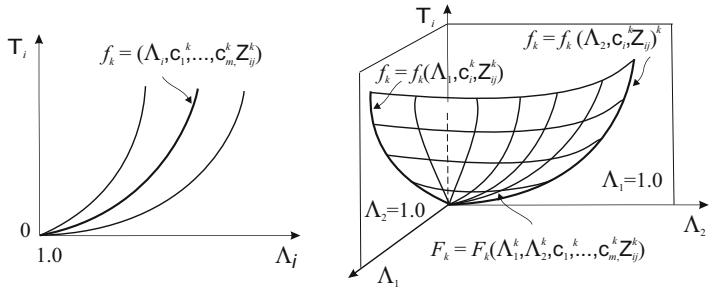

Fig. 4.5 Uniaxial (**a**) and biaxial (**b**) constitutive relations for soft biological tissues

If constitutive relations are obtained in the directions different from the actual parameterization of the shell, the task then is to learn to calculate membrane forces in the principal directions. Consider two typical situations:

Case 1. Constitutive relations are given by Eq. (4.54). Then,

(i) from Eqs. (4.35, 4.36), we calculate the principal deformations $\mathbf{\Lambda}_1, \mathbf{\Lambda}_2$ and the angle $\overset{*}{\varphi}_1$,

(ii) using Eqs. (4.54), we compute the principal membrane forces T_1 and T_2 and the angle ψ,

(iii) finally, setting $\overset{*}{\chi}_1 = \pi/2, \overset{*}{\chi}_2 = \psi, \overset{*}{T}{}^{11} = T_1, \overset{*}{T}{}^{22} = T_2, \overset{*}{T}{}^{12} = 0$ in Eqs. (4.45), we find

$$\begin{aligned}
\tilde{T}^{11} &= \left\{T_1 \sin^2(\chi-\psi) + T_2 \cos^2(\chi-\psi)\right\}/\sin\chi, \\
\tilde{T}^{12} &= \left\{T_1 \sin\psi \sin(\chi-\psi) - T_2 \cos\psi \cos(\chi-\psi)\right\}/\sin\chi, \\
\tilde{T}^{22} &= \left\{T_1 \sin^2\psi + T_2 \cos^2\psi\right\}/\sin\chi.
\end{aligned} \tag{4.55}$$

Case 2. Constitutive relations are formulated for the orientation of reinforced fibers, superscript (r),

$$\begin{aligned}
T^r{}_1 &= F^r{}_1\left(\lambda^r{}_1, \lambda^r{}_2, \gamma^r, c_1, \ldots c_m, Z_{ij}\right), \\
T^r{}_2 &= F^r{}_2\left(\lambda^r{}_1, \lambda^r{}_2, \gamma^r, c_1, \ldots c_m, Z_{ij}\right), \\
S^r &= S^r\left(\lambda^r{}_1, \lambda^r{}_2, \gamma^r, c_1, \ldots c_m, Z_{ij}\right).
\end{aligned} \tag{4.56}$$

Let $\overset{*}{\alpha}_i \in \overset{*}{S}$ be an auxillary orthogonal coordinate system oriented with respect to a set of reinforced fibers by $\overset{*}{\psi}$. Then,

(i) setting $\chi_1 = \pi/2, \chi_2 = \psi, \overset{*}{\chi}_1 = \pi/2 - \gamma^r$ in Eq. (4.28), where $\lambda^r_1 := \overset{*}{\lambda}_1$, $\lambda^r_2 := \overset{*}{\lambda}_2$, for the stretch ratios and the shear angle γ^r, we have

$$\begin{aligned}
\lambda^r_1 &= \left(\lambda_1^2 \sin^2\left(\overset{0}{\chi} - \overset{0}{\psi}\right) + \lambda_2^2 \sin^2\overset{0}{\psi} + 2\lambda_1\lambda_2 \cos\overset{0}{\chi} \sin\left(\overset{0}{\chi} - \overset{0}{\psi}\right) \sin\overset{0}{\psi}\right)^{1/2} / \sin\overset{0}{\chi}, \\
\gamma^r &= \sin^{-1}\left(\frac{1}{\lambda_1\lambda_2 \sin^2\overset{0}{\chi}}\left(-\frac{1}{2}\lambda^2{}_1 \sin 2\left(\overset{0}{\chi} - \overset{0}{\psi}\right) + \frac{1}{2}\lambda_2^2 \sin 2\overset{0}{\psi} + \lambda_1\lambda_2 \cos\overset{0}{\chi} \sin\left(\overset{0}{\chi} - \overset{0}{\psi}\right)\right)\right) \\
\lambda^r_2 &= \left(\lambda_1^2 \cos^2\left(\overset{0}{\chi} - \overset{0}{\psi}\right) + \lambda_2^2 \cos^2\overset{0}{\psi} - 2\lambda_1\lambda_2 \cos\left(\overset{0}{\chi} - \overset{0}{\psi}\right) \cos\overset{0}{\chi} \cos\overset{0}{\psi}\right)^{1/2} / \sin\overset{0}{\chi},
\end{aligned} \tag{4.57}$$

(ii) using Eqs. (4.56) we find $T^r{}_1$, $T^r{}_2$ and S^r,

(iii) the angle $\overset{*}{\psi}$ is found from Eq. (6.34) by putting $\overset{*}{\chi}_1 = \overset{*}{\psi}$, $\overset{*}{\chi}_2 = 0$, $\overset{*}{\lambda}_1 = \lambda_1$, $\overset{*}{\lambda}_2 = \lambda^r_1$,

$$\overset{*}{\psi} = \cos^{-1}\left(\frac{1}{\lambda_1^r \sin \overset{0}{\chi}}\left(\lambda_1 \sin\left(\overset{0}{\chi} - \overset{0}{\psi}\right) + \lambda_2 \cos \overset{0}{\chi} \sin \overset{0}{\psi}\right)\right), \tag{4.58}$$

(iv) finally, setting $\overset{*}{\chi}_1 = \pi/2 - \gamma^r$, $\overset{*}{\chi}_2 = \overset{*}{\psi}$, $T_1^r := \overset{*}{\tilde{T}}^{11}$, $T_2^r := \overset{*}{\tilde{T}}^{22}$, $S^r := \overset{*}{\tilde{T}}^{12}$ in Eqs. (4.45), we obtain

$$\begin{aligned}
\tilde{T}^{11} &= \left\{T^r{}_1 \sin^2\left(\overset{*}{\chi} - \overset{*}{\psi}\right) + T^r{}_2 \cos^2\left(\overset{*}{\chi} - \overset{*}{\psi} + \gamma^r\right) - \right. \\
&\left. -2S^r \cos\left(\overset{*}{\chi} - \overset{*}{\psi} + \gamma^r\right) \sin\left(\overset{*}{\chi} - \overset{*}{\psi}\right)\right\} / \sin \overset{*}{\chi} \cos \gamma^r, \\
\tilde{T}^{12} &= \left\{T^r{}_1 \sin\mu \sin\left(\overset{*}{\chi} - \overset{*}{\psi}\right) - T^r{}_2 \cos\left(\overset{*}{\psi} + \gamma^r\right) \cos\left(\overset{*}{\chi} - \overset{*}{\psi} + \gamma^r\right) + \right. \\
&\left. + S^r\left[\sin\left(\overset{*}{\chi} - 2\overset{*}{\psi} + \gamma^r\right) - \cos \overset{*}{\chi} \sin \gamma^r\right]\right\} / \sin \overset{*}{\chi} \cos \gamma^r, \\
\tilde{T}^{22} &= \left\{T^r{}_1 \sin^2 \overset{*}{\psi} - 2S^r \sin\left(\overset{*}{\psi} - \gamma^r\right) \sin \overset{*}{\psi} + T^r{}_2 \cos^2\left(\overset{*}{\psi} - \gamma^r\right)\right\} / \sin \overset{*}{\chi} \cos \gamma^r.
\end{aligned} \tag{4.59}$$

Formulas (4.59) can be written in more concise form if we introduce generalized forces defined by $N^{ik} = T^{ik}(\lambda_k/\lambda_i)$,

$$\overset{*}{N}{}^{11} = T_1^r \frac{\lambda_2^r}{\lambda_1^r}, \quad \overset{*}{N}{}^{22} = T_2^r \frac{\lambda_1^r}{\lambda_2^r}, \quad \overset{*}{N}{}^{12} = S^r.$$

Then, Eq. (4.46) take the form

$$N^{ik} = \frac{1}{\hat{\hat{C}}} \overset{*}{\sum_{j=1}^{2}} \sum_{n=1}^{2} \overset{*}{N}{}^{jn} \hat{\hat{C}}_j^{*i} \hat{\hat{C}}_n^{*k}. \tag{4.60}$$

Substituting $\hat{\hat{C}}_j^{*i}$ given by Eqs. (4.12, 4.14), we find

$$\begin{aligned}
N^{11} &= \left\{\overset{*}{N}{}^{11} \sin^2\left(\overset{0}{\chi} - \overset{0}{\chi}_2\right) + \overset{*}{N}{}^{22} \sin^2\left(\overset{0}{\chi}_1 + \overset{0}{\chi}_2 - \overset{0}{\chi}\right) - \right. \\
&\left. -2\overset{*}{N}{}^{12} \sin\left(\overset{0}{\chi}_1 + \overset{0}{\chi}_2 - \overset{0}{\chi}\right) \sin\left(\overset{0}{\chi} - \overset{0}{\chi}_2\right)\right\} / \sin \overset{0}{\chi} \sin \overset{0}{\chi}_1 \\
N^{12} &= \left\{\overset{*}{N}{}^{11} \sin \overset{0}{\chi}_2 \sin\left(\overset{0}{\chi} - \overset{0}{\chi}_2\right) + \overset{*}{N}{}^{22} \sin\left(\overset{0}{\chi}_1 + \overset{0}{\chi}_2 - \overset{0}{\chi}\right) \sin\left(\overset{0}{\chi}_1 + \overset{0}{\chi}_2\right) + \right. \\
&\left. + \overset{*}{N}{}^{12}\left[\cos\left(\overset{0}{\chi}_1 + 2\overset{0}{\chi}_2 - \overset{0}{\chi}\right) - \cos \overset{0}{\chi} \cos \overset{0}{\chi}_1\right]\right\} / \sin \overset{0}{\chi} \sin \overset{0}{\chi}_1, \\
N^{22} &= \left\{\overset{*}{N}{}^{11} \sin^2 \overset{0}{\chi}_2 - 2\overset{*}{N}{}^{12} \sin\left(\overset{0}{\chi}_1 + \overset{0}{\chi}_2\right) \sin \overset{0}{\chi}_2 + \right. \\
&\left. + \overset{*}{N}{}^{22} \sin^2\left(\overset{0}{\chi}_1 + \overset{0}{\chi}_2\right)\right\} / \sin \overset{0}{\chi} \sin \overset{0}{\chi}_1
\end{aligned} \tag{4.61}$$

Putting $\overset{0}{\chi}_1 = \pi/2, \overset{0}{\chi}_2 = \overset{0}{\psi}$ in Eqs. (4.61), for the membrane forces in terms of the undeformed surface S ($\overset{0}{S} = S$), we have

$$\tilde{T}^{11} = \frac{\lambda_1}{\lambda_2}\left(T_1^r\frac{\lambda_2^r}{\lambda_1^r}\sin^2\left(\overset{0}{\chi}-\overset{0}{\psi}\right) + T_2^r\frac{\lambda_1^r}{\lambda_2^r}\cos^2\left(\overset{0}{\chi}-\overset{0}{\psi}\right) - 2S^r\sin 2\left(\overset{0}{\chi}-\overset{0}{\psi}\right)\right)/\sin\overset{0}{\chi},$$

$$\tilde{T}^{12} = \left(T_1^r\frac{\lambda_2^r}{\lambda_1^r}\sin^2\left(\overset{0}{\chi}-\overset{0}{\psi}\right)\sin\overset{0}{\psi} - T_2^r\frac{\lambda_1^r}{\lambda_2^r}\cos^2\left(\overset{0}{\chi}-\overset{0}{\psi}\right)\cos\overset{0}{\psi} + S^r\sin\left(\overset{0}{\chi}-2\overset{0}{\psi}\right)\right) \times/\sin\overset{0}{\chi},$$

$$\tilde{T}^{22} = \frac{\lambda_2}{\lambda_1}\left(T_1^r\frac{\lambda_2^r}{\lambda_1^r}\sin^2\overset{0}{\psi} + T_2^r\frac{\lambda_1^r}{\lambda_2^r}\cos^2\overset{0}{\psi} + S^r\sin 2\overset{0}{\psi}\right)/\sin\overset{0}{\chi}. \tag{4.62}$$

Formulas (4.62) depend only on parameterization of S and the axes of anisotropy. Thus, they are less computationally demanding compared to Eqs. (4.58, 4.59).

4.6 Nets

A special class of soft shell, where discrete reinforced fibers are the main structural and weight bearing elements, is called the nets. Depending on engineering design and practical needs, the fibers may remain discrete or embedded in the connective matrix. Although the nets have distinct discrete structure, they are modeled as a solid continuum. Since the nets have very low resistance to shear forces, then $T_{12} = 0$ ($S^r \equiv 0$) and the resultant formulas obtained in the previous paragraphs are valid in modeling nets.

Consider a net with the cell structure of a parallelogram. Let the sides of the cell be formed by two distinct families of reinforced fibers (Fig. 4.6). Their mechanical properties are described by

$$\begin{aligned} T_1^r &= F_1^r\left(\lambda_1^r, \lambda_2^r, \gamma^r, c_1, \ldots c_m, Z_{ij}\right), \\ T_2^r &= F_2^r\left(\lambda_1^r, \lambda_2^r, \gamma^r, c_1, \ldots c_m, Z_{ij}\right), \end{aligned} \tag{4.63}$$

where the meaning of parameters and constants are as discussed above.

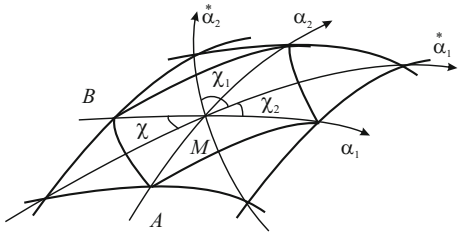

Fig. 4.6 A structural element of the net formed by two distinct types of reinforced fibers

Let the undeformed ($S \equiv \overset{0}{S}$) configuration of the net be parameterized by α_1^*, α_2^* coordinates oriented along the reinforced fibers. For force distribution in the net we have to

(i) find the stretch ratios $\lambda_1^r = \overset{*}{\lambda}_1, \lambda_2^r = \overset{*}{\lambda}_2$, using Eqs. (4.28)
(ii) substituting $\lambda_1^r = \overset{*}{\lambda}_1, \lambda_2^r = \overset{*}{\lambda}_2$ in Eq. (4.63) calculate T_1^r, T_2^r,
(iii) making use of Eqs. (4.59) or (4.62) find for the membrane forces in terms of S-configuration

$$\begin{aligned}
\tilde{T}^{11} &= \frac{\lambda_1}{\lambda_2}\left(T_1^r\frac{\lambda_2^r}{\lambda_1^r}\sin^2\left(\overset{0}{\chi}-\overset{0}{\psi}\right)+T_2^r\frac{\lambda_1^r}{\lambda_2^r}\cos^2\left(\overset{0}{\chi}-\overset{0}{\psi}\right)\right)/\sin\overset{0}{\chi},\\
\tilde{T}^{12} &= \left(T_1^r\frac{\lambda_2^r}{\lambda_1^r}\sin^2\left(\overset{0}{\chi}-\overset{0}{\psi}\right)\sin\overset{0}{\psi}-T_2^r\frac{\lambda_1^r}{\lambda_2^r}\cos^2\left(\overset{0}{\chi}-\overset{0}{\psi}\right)\cos\overset{0}{\psi}\right)/\sin\overset{0}{\chi},\\
\tilde{T}^{22} &= \frac{\lambda_2}{\lambda_1}\left(T_1^r\frac{\lambda_2^r}{\lambda_1^r}\sin^2\overset{0}{\psi}+T_2^r\frac{\lambda_1^r}{\lambda_2^r}\cos^2\overset{0}{\psi}\right)/\sin\overset{0}{\chi}.
\end{aligned} \tag{4.64}$$

The principal membrane forces and their directions are found from Eqs. (4.50, 4.51) by putting $T^{12} = S^r = 0$, $T^{11} = T_1^r$, $T^{22} = T_2^r$

$$\begin{aligned}
T_{1,2} &= \frac{\left(T_1^r+T_2^r\right)\pm\sqrt{\left(T_1^r-T_2^r\right)^2+4T_1^rT_2^r\cos^2\overset{*}{\chi}}}{2\sin\overset{*}{\chi}},\\
\tan 2\overset{*}{\psi}_1 &= \frac{T_2^r\sin 2\overset{*}{\chi}}{T_1^r+T_2^r\cos 2\overset{*}{\chi}},\\
\overset{*}{\psi}_2 &= \overset{*}{\psi}_1+\pi/2.
\end{aligned} \tag{4.65}$$

In particular,

(i) if $\overset{*}{\chi} = \pi/2$ then $\psi_1{}^* = 0$, $T_1 = T_1^r$, $T_2 = T_2^r$;
(ii) if $T_1^r = 0$ then $\psi_1{}^* = 0$, $T_1 = T_1^r/\sin\overset{*}{\chi}$, $T_2 = 0$;
(iii) if $T_2^r = 0$ then $\psi_1{}^* = \overset{*}{\chi}$, $T_1 = T_2^r/\sin\overset{*}{\chi}$, $T_2 = 0$.

Corollary 5 of the fundamental assumptions for the nets is given by

$$\begin{aligned}
I^{(\mathbf{T})}{}_1 &= T_1+T_2 = \frac{1}{\sin\overset{*}{\chi}}\left(T_1^r+T_2^r\right)\geq 0,\\
I^{(\mathbf{T})}{}_2 &= T_1T_2 = T_1{}^rT_2^r \geq 0.
\end{aligned} \tag{4.66}$$

4.7 Equations of Motion in General Curvilinear Coordinates

Let $\Delta \overset{(*)}{\sigma}$ and $\Delta \overset{(*)}{m}$ be the surface area and mass of a differential element of the soft shell in undeformed and deformed configurations. Position of a point $\overset{*}{M} \in \overset{*}{S}$ at any moment of time t is given by vector $\bar{r}(\alpha_1, \alpha_2, t)$. Densities of the material in undeformed, ρ, and deformed, $\overset{*}{\rho}$, states are defined by

$$\rho = \lim_{\Delta\sigma \to 0} \frac{\Delta m}{\Delta \sigma} = \frac{dm}{d\sigma} \quad \text{and} \quad \overset{*}{\rho} = \lim_{\Delta \overset{*}{\sigma} \to 0} \frac{\Delta \overset{*}{m}}{\Delta \overset{*}{\sigma}} = \frac{d \overset{*}{m}}{d \overset{*}{\sigma}}, \tag{4.67}$$

where

$$d\sigma = \sqrt{a} d\alpha_1 d\alpha_2, \quad d \overset{*}{\sigma} = \sqrt{\overset{*}{a}} d\alpha_1 d\alpha_2,$$

Applying the law of conservation of the mass to Eq. (4.67) we find

$$dm = d \overset{*}{m} = \overset{*}{\rho}\, d \overset{*}{\sigma} = \overset{*}{\rho} \sqrt{\overset{*}{a}} d\alpha_1 d\alpha_2 = \rho \sqrt{\overset{*}{a}} d\alpha_1 d\alpha_2.$$

It follows that

$$\overset{*}{\rho} = \rho \sqrt{a / \overset{*}{a}}. \tag{4.68}$$

Let $\bar{p}_s(\alpha_1, \alpha_2, t)$ be the resultant of the external, $\bar{p}_{(+)}(\alpha_1, \alpha_2, t)$, and internal, $\bar{p}_{(-)}(\alpha_1, \alpha_2, t)$, forces distributed over the outer and inner surfaces of the shell

$$\bar{p}_s(\alpha_1, \alpha_2, t) = \bar{p}_{(+)}(\alpha_1, \alpha_2, t) + \bar{p}_{(-)}(\alpha_1, \alpha_2, t).$$

The density of the resultant force per unit area of a deformed element $\bar{p}_s$ is defined by

$$\bar{p}(\alpha_1, \alpha_2, t) = \lim_{\Delta \overset{*}{\sigma} \to 0} \frac{\bar{p}_s}{\Delta \overset{*}{\sigma}}. \tag{4.69}$$

Similarly, we introduce the density of the mass force $\bar{F}(\alpha_1, \alpha_2, t)$ by

$$\bar{f}(\alpha_1, \alpha_2, t) = \lim_{\Delta m \to 0} \frac{\bar{F}}{\Delta m} = \frac{d\bar{F}}{dm} = \frac{1}{\rho} \frac{d\bar{F}}{d\sigma}. \tag{4.70}$$

The resultant stress vectors $\bar{R}_i$ acting upon the differential element are found to be

$$\bar{R}_1 = -\left(T^{11}\bar{e}_1 + T^{12}\bar{e}_2\right)\sqrt{\overset{*}{a}_{22}}d\alpha_2, \quad \bar{R}_2 = -\left(T^{21}\bar{e}_1 + T^{22}\bar{e}_2\right)\sqrt{\overset{*}{a}_{11}}d\alpha_1,$$

$$-\left(\bar{R}_1 + \frac{\partial \bar{R}_1}{\partial \alpha_1}d\alpha_1\right) = -\left(T^{11}\bar{e}_1 + T^{12}\bar{e}_2\right)\sqrt{\overset{*}{a}_{22}}d\alpha_2 -$$

$$-\frac{\partial}{\partial \alpha_1}\left(T^{11}\bar{e}_1 + T^{12}\bar{e}_2\right)\sqrt{\overset{*}{a}_{22}}d\alpha_1 d\alpha_2,$$

$$-\left(\bar{R}_2 + \frac{\partial \bar{R}_2}{\partial \alpha_2}d\alpha_2\right) = -\left(T^{21}\bar{e}_1 + T^{22}\bar{e}_2\right)\sqrt{\overset{*}{a}_{11}}d\alpha_1 -$$

$$-\frac{\partial}{\partial \alpha_2}\left(T^{21}\bar{e}_1 + T^{22}\bar{e}_2\right)\sqrt{\overset{*}{a}_{11}}d\alpha_1 d\alpha_2. \tag{4.71}$$

Applying the law of conservation of momentum to Eqs. (4.69)–(4.71), for the equation of motion of the soft shell we get

$$\overset{*}{\rho}\frac{d^2\bar{r}(\alpha_1, \alpha_2, t)}{dt^2} = -\frac{\partial \bar{R}_1}{\partial \alpha_1}d\alpha_1 - \frac{\partial \bar{R}_2}{\partial \alpha_2}d\alpha_2 + \bar{p} + \bar{f}\overset{*}{\rho}, \tag{4.72}$$

where $\frac{d^2\bar{r}}{dt^2}$ is acceleration. Substituting $\bar{R}_i$ and $\overset{*}{\rho}$ given by Eqs. (4.68, 4.71) into (4.72), we get

$$\rho\sqrt{a}\frac{d^2\bar{r}}{dt^2} = \frac{\partial}{\partial \alpha_1}\left[\left(T^{11}\bar{e}_1 + T^{12}\bar{e}_2\right)\sqrt{\overset{*}{a}_{22}}\right] +$$

$$+\frac{\partial}{\partial \alpha_2}\left[\left(T^{21}\bar{e}_1 + T^{22}\bar{e}_2\right)\sqrt{\overset{*}{a}_{11}}\right] + \bar{p}\sqrt{\overset{*}{a}} + \bar{f}\rho\sqrt{a}. \tag{4.73}$$

Let $\bar{G}_i$, $\bar{M}_p$ and $\bar{M}_f$ be the resultant moment vectors acting on the element of the shell defined by

$$\bar{G}_1 = \bar{r} \times \bar{R}_1, \quad \bar{G}_2 = \bar{r} \times \bar{R}_2$$

$$-\left(\bar{G}_1 + \frac{\partial \bar{G}_1}{\partial \alpha_1}d\alpha_1\right), \quad -\left(\bar{G}_2 + \frac{\partial \bar{G}_2}{\partial \alpha_2}d\alpha_2\right) \quad (a_i + da_i = \text{const}) \tag{4.74}$$

$$\bar{M}_p = (\bar{r} \times \bar{p})\sqrt{\overset{*}{a}}d\alpha_1 d\alpha_2, \quad \bar{M}_f = (\bar{r} \times \bar{f})\rho\sqrt{\overset{*}{a}}d\alpha_1 d\alpha_2.$$

Assuming the shell is in equilibrium, the sum of the moments vanishes. Hence

$$-\frac{\partial \bar{G}_1}{\partial \alpha_1}d\alpha_1 - \frac{\partial \bar{G}_2}{\partial \alpha_2}d\alpha_2 + \bar{M}_p + \bar{M}_q = 0. \tag{4.75}$$

Substituting $\bar{G}_i$, $\bar{M}_p$ and $\bar{M}_f$ in (4.75), we obtain

$$\left[-\left(\bar{r}\times\frac{\partial\bar{R}_1}{\partial\alpha_1}d\alpha_1\right)-\left(\bar{r}\times\frac{\partial\bar{R}_2}{\partial\alpha_2}d\alpha_2\right)+(\bar{r}\times\bar{p})+(\bar{r}\times\bar{f})\right]-$$
$$-(\bar{r}\times\bar{R}_1)d\alpha_1-(\bar{r}\times\bar{R}_2)d\alpha_2=0.$$

Further, on use of Eq. (4.71), we find

$$\left[\bar{e}_1\times\left(T^{11}\bar{e}_1+T^{12}\bar{e}_2\right)+\bar{e}_2\times\left(T^{21}\bar{e}_1+T^{22}\bar{e}_2\right)\right]\sqrt{\overset{*}{a}_{11}}\sqrt{\overset{*}{a}_{22}}d\alpha_1d\alpha_2-$$
$$-\bar{r}\times\left[\underline{-\frac{\partial\bar{R}_1}{\partial\alpha_1}d\alpha_1-\frac{\partial\bar{R}_2}{\partial\alpha_2}d\alpha_2+\bar{p}+\bar{f}}\right]=0. \tag{4.76}$$

Since the underlined term equals zero, we have

$$(\bar{e}_1\times\bar{e}_2)T^{12}+(\bar{e}_2\times\bar{e}_1)T^{21}=0. \tag{4.77}$$

It follows immediately from the above $T^{12}=T^{21}$.

Remarks

1. If a soft shell is parameterized along the principal axes then $T^{11}=T_1$, $T^{22}=T_2$, $T^{12}=0$, $a_{12}{}^{*}=a_{12}=0$ and the equation of motion (4.73) takes the simplest form

$$\rho\sqrt{a}\frac{d^2\bar{r}}{dt^2}=\frac{\partial}{\partial\alpha_1}\left[T_1\sqrt{\overset{*}{a}_{22}}\bar{e}_1\right]+\frac{\partial}{\partial\alpha_2}\left[T_2\sqrt{\overset{*}{a}_{11}}\bar{e}_2\right]+\bar{p}\sqrt{\overset{*}{a}}+\bar{f}\rho\sqrt{a} \tag{4.78}$$

2. During the dynamic process of deformation different parts of the soft shell may undergo different stress-strain states. The biaxial stress-state occurs when $I^{(\mathbf{T})}{}_1=T_1+T_2>0$, $I^{(\mathbf{T})}{}_2=T_1T_2>0$, the uniaxial state develops in areas where $I^{(\mathbf{T})}{}_1>0$, $I^{(\mathbf{T})}{}_2=0$, and the zero stress-state takes place anywhere in the shell where $I^{(\mathbf{T})}{}_1=I^{(\mathbf{T})}{}_2=0$. The uniaxially stressed area ($T_2=0$) will develop wrinkles oriented along the action of the positive principal membrane force T_1. The equation of motion for the wrinkled area becomes

$$\rho\sqrt{a}\frac{d^2\bar{r}}{dt^2}=\frac{\partial}{\partial\alpha_1}\left[T_1\sqrt{\overset{*}{a}_{22}}\bar{e}_1\right]+\bar{p}\sqrt{\overset{*}{a}}+\bar{f}\rho\sqrt{a}. \tag{4.79}$$

To preserve smoothness and continuity of the surface $\overset{*}{S}$, the uniaxially stressed area is substituted by an ironed surface made out of an array of closely packed reinforced fibers. Such approach allows one to use the equations of motion (4.72) throughout the deformed surface $\overset{*}{S}$.

The governing system of equations of dynamics of the soft shell includes the equations of motion (4.73, 4.78), constitutive relations (4.53), (4.54) or (4.63), initial and boundary conditions, and the conditions given by Corollary 5.

4.8 Governing Equations in Orthogonal Cartesian Coordinates

Let a soft shell be associated with an orthogonal Cartesian coordinate system x_1, x_2, x_3

$$\begin{aligned} x_1 &= x_1(\alpha_1, \alpha_2, t), \\ x_2 &= x_2(\alpha_1, \alpha_2, t), \\ x_3 &= x_3(\alpha_1, \alpha_2, t). \end{aligned} \tag{4.80}$$

The position vector of point $M(\alpha_1,\alpha_2)\in S$ and its derivatives are given by

$$\bar{r} = \bar{i}_1 x_1 + \bar{i}_2 x_2 + \bar{i}_3 x_3 = \sum_{k=1}^{3} x_k \bar{i}_k, \tag{4.81}$$

$$\bar{r}_i = \frac{\partial \bar{r}}{\partial \alpha_i} = \sum_{k=1}^{3} \frac{\partial x_k}{\partial \alpha_i} \bar{i}_k = \sum_{k=1}^{3} \bar{r}_{ik} \bar{i}_k, \quad (i = 1, 2) \tag{4.82}$$

where $\bar{r}_{ik} = \frac{\partial x_k}{\partial \alpha_i}$ is the projection of the i^{th} basis vector on the x_1, x_2, x_3 axes.

Decomposing the unit vectors $\bar{e}_i = \bar{r}_i/|\bar{r}_i|$ along the base $\{\bar{i}_1, \bar{i}_2, \bar{i}_3\}$, we get

$$\bar{e}_i = \sum_{k=1}^{3} l_{ik} \bar{i}_k = \frac{\bar{r}_i}{\sqrt{\overset{*}{a}_{ii}}} = \frac{\bar{r}_{ik}}{\sqrt{\overset{*}{a}_{ii}}} \bar{i}_k = l_{ik} \bar{i}_k, \tag{4.83}$$

where l_{ik} are the direction cosines defined by

$$l_{ik} \coloneqq \cos(\bar{e}_i, \bar{i}_k) = \bar{r}_{ik}/\sqrt{\overset{*}{a}_{ii}}. \tag{4.84}$$

The vector $\bar{m}$ normal to $\bar{e}_i$ ($\bar{m} \perp \bar{e}_i$) is given by

$$\bar{m} = (\bar{e}_1 \times \bar{e}_2) \frac{\sqrt{\overset{*}{a}_{11} \overset{*}{a}_{22}}}{\sqrt{\overset{*}{a}}} \tag{4.85}$$

With the help of Eqs. (4.83, 4.85), the direction cosines $l_{3k} = \cos(\bar{m}, \bar{i}_k)$ are found to be

$$
\begin{aligned}
l_{31} &= (l_{12}l_{23} - l_{13}l_{22})\sqrt{\overset{*}{a}_{11}\ \overset{*}{a}_{22}}/\sqrt{\overset{*}{a}}, \\
l_{32} &= (l_{13}l_{21} - l_{11}l_{23})\sqrt{\overset{*}{a}_{11}\ \overset{*}{a}_{22}}/\sqrt{\overset{*}{a}}, \\
l_{33} &= (l_{11}l_{22} - l_{12}l_{21})\sqrt{\overset{*}{a}_{11}\ \overset{*}{a}_{22}}/\sqrt{\overset{*}{a}}.
\end{aligned} \tag{4.86}
$$

Scalar products $\bar{e}_i\bar{e}_k$ yield

$$
\begin{aligned}
&\bar{e}_1\bar{e}_2 = l_{11}l_{21} + l_{12}l_{22} + l_{13}l_{23} = \cos\overset{*}{\chi} = a^*_{12}/\sqrt{\overset{*}{a}_{11}\ \overset{*}{a}_{22}} \\
&\bar{e}_i\bar{e}_2 = l_{i1}l_{31} + l_{i2}l_{32} + l_{i3}l_{33} = 0, \\
&\bar{e}_k\bar{e}_k = l^2_{k1} + l^2_{k2} + l^2_{k3} = 1.
\end{aligned} \tag{4.87}
$$

Expanding $\bar{p}, \bar{f}$ in the direction of $\bar{e}_i$ and $\bar{i}_i$, respectively, we obtain

$$
\bar{p} = \bar{e}_1 p_1 + \bar{e}_2 p_2 + \bar{m} p_3, \tag{4.88}
$$

$$
\bar{f} = \bar{i}_1 f_1 + \bar{i}_2 f_2 + \bar{i}_3 f_3. \tag{4.89}
$$

Substituting Eqs. (4.84, 4.86, 4.88, 4.89) in (4.77), the equation of motion of the soft shell takes the form

$$
\begin{aligned}
\rho\sqrt{a}\frac{d^2x_1}{dt^2} &= \frac{\partial}{\partial\alpha_1}\left[\left(T^{11}l_{11} + T^{12}l_{21}\right)\sqrt{\overset{*}{a}_{22}}\right] + \frac{\partial}{\partial\alpha_2}\left[\left(T^{12}l_{11} + T^{22}l_{21}\right)\sqrt{\overset{*}{a}_{11}}\right] + \\
&+ (p_1l_{11} + p_2l_{21})\sqrt{\overset{*}{a}} + p_3(l_{21}l_{23} - l_{13}l_{22})\sqrt{\overset{*}{a}_{11}\ \overset{*}{a}_{22}} + \rho f_1\sqrt{a}, \\
\rho\sqrt{a}\frac{d^2x_2}{dt^2} &= \frac{\partial}{\partial\alpha_1}\left[\left(T^{11}l_{12} + T^{12}l_{22}\right)\sqrt{\overset{*}{a}_{22}}\right] + \frac{\partial}{\partial\alpha_2}\left[\left(T^{12}l_{12} + T^{22}l_{22}\right)\sqrt{\overset{*}{a}_{11}}\right] + \\
&+ (p_1l_{12} + p_2l_{22})\sqrt{\overset{*}{a}} + p_3(l_{13}l_{21} - l_{11}l_{23})\sqrt{\overset{*}{a}_{11}\ \overset{*}{a}_{22}} + \rho f_2\sqrt{a}, \\
\rho\sqrt{a}\frac{d^2x_3}{dt^2} &= \frac{\partial}{\partial\alpha_1}\left[\left(T^{11}l_{13} + T^{12}l_{23}\right)\sqrt{\overset{*}{a}_{22}}\right] + \frac{\partial}{\partial\alpha_2}\left[\left(T^{12}l_{13} + T^{22}l_{23}\right)\sqrt{\overset{*}{a}_{11}}\right] + \\
&+ (p_1l_{13} + p_2l_{23})\sqrt{\overset{*}{a}} + p_3(l_{11}l_{22} - l_{12}l_{21})\sqrt{\overset{*}{a}_{11}\ \overset{*}{a}_{22}} + \rho f_3\sqrt{a}.
\end{aligned} \tag{4.90}
$$

Here d^2x_i/dt^2 $(i = 1, 2, 3)$ are the components of the vector of acceleration. Eqs. (4.90) should be complemented by constitutive relations (4.53), (4.54) or (4.63), initial and boundary conditions, and the conditions given by Corollary 5.

$$
\bar{e}_n\bar{e}_n = l^2_{n1} + l^2_{n2} + l^2_{n3} = 1, \ (n = 1, 2, 3)
$$

Expanding the resultant of external, $\bar{p}$, and mass, $\bar{f}$, forces in the direction of unit vectors $\bar{e}_i$, we get

$$\bar{p} = \bar{e}_1 p_1 + \bar{e}_2 p_2 + \bar{e}_3 p_3, \tag{4.91}$$

$$\bar{f} = \bar{k}_1 f_r + \bar{k}_2 f_\varphi + \bar{k}_3 f_z. \tag{4.92}$$

Finally, to close a mathematical problem should be complemented by constitutive relations (4.53), (4.54) or (4.63), initial and boundary conditions, and the conditions given by Corollary 5.

Reference

Ridel VV, Gulin BV (1990) Dynamics of soft shells. Nauka, Moscow

Chapter 5
Boundary Conditions

To improve is to change; to be perfect is to change often.
Winston Churchill

5.1 Geometry of the Boundary

Consider the contour curve C on the boundary of the undeformed shell parameterized by arc length s

$$\bar{r} = \bar{r}(s) = \bar{r}(\alpha_1(s), \alpha_2(s)), \tag{5.1}$$

Let $\{\bar{n},\bar{\tau},\bar{m}\}$ be the orthogonal base of C (Fig. 5.1). Here $\bar{n}$, $\bar{\tau}$ are unit vectors normal and tangent to C, respectively, and $\bar{m}$ is the vector normal to the middle surface S. The three unit vectors are linearly independent

$$\bar{n} = \bar{\tau} \times \bar{m}, \quad \bar{\tau} = \bar{m} \times \bar{n}, \quad \bar{m} = \bar{n} \times \bar{\tau}. \tag{5.2}$$

Differentiating Eq. (5.1) with respect to s and using Eq. (1.13), the tangent vector $\bar{\tau}$ is found to be

$$\bar{\tau} = \frac{d\bar{r}}{ds} = \bar{r}_1 \frac{d\alpha_1}{ds} + \bar{r}_2 \frac{d\alpha_2}{ds} = \bar{e}_1 \tau_1 + \bar{e}_2 \tau_2. \tag{5.3}$$

Projections of $\bar{\tau}$ on unit vectors $\bar{e}_i \in S$ $(i = 1, 2)$ are given by

$$\tau_1 = A_1 \frac{d\alpha_1}{ds}, \quad \tau_2 = A_2 \frac{d\alpha_2}{ds}. \tag{5.4}$$

Decomposing the normal vector $\bar{n}$ in the direction of $\bar{e}_i$ yields

R.N. Miftahof, *Biomechanics of the Human Stomach*,
DOI 10.1007/978-3-319-59677-8_5

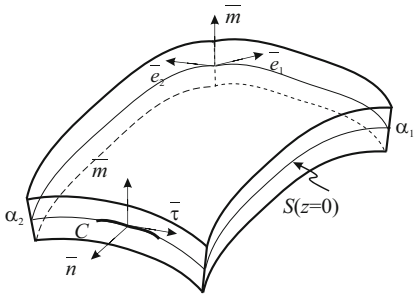

Fig. 5.1 An orthonormal base $\{\bar{n}, \bar{\tau}, \bar{m}\}$ associated with the boundary

$$\bar{n} = (\bar{e}_1\tau_1 + \bar{e}_2\tau_2) \times \bar{m} = \bar{e}_1\tau_2 - \bar{e}_2\tau_1, \quad \bar{n} = \bar{e}_1 n_1 + \bar{e}_2 n_2. \tag{5.5}$$

From Eqs. (5.4, 5.5), projections of $\bar{n}$, are found to be

$$n_1 = \tau_2 = A_2 \frac{d\alpha_2}{ds}, \quad n_2 = -\tau_1 = -A_1 \frac{d\alpha_1}{ds}, \tag{5.6}$$

Since $\bar{n} \perp \bar{\tau}$, it follows that $\tau_1 n_1 + \tau_2 n_2 = 0$.

Let k_n, k_τ be normal curvatures in the direction of $\bar{n}$ and $\bar{\tau}$, and $k_{n\tau}$ be the twist of the contour line C

$$k_n = \sum_{i=1}^{2}\sum_{j=1}^{2} k_{ij} n_i n_j, \quad k_\tau = \sum_{i=1}^{2}\sum_{j=1}^{2} k_{ij} \tau_i \tau_j, \quad k_{n\tau} = \sum_{i=1}^{2}\sum_{j=1}^{2} k_{ij} \tau_i n_j, \tag{5.7}$$

k_{ij} satisfy Eqs. (1.21a, b).

Let ds_z be the length of a line element on a contour curve C_z of the equidistant surface S_z ($S_z \parallel S$), and $\bar{\tau}^z$, $\bar{n}^z$ be unit tangent vectors to C_z. Then

$$\bar{\tau}^z = \bar{e}^z{}_1 \tau_1^z + \bar{e}^z{}_2 \tau_2^z, \quad \tau_1^z = H_1 \frac{d\alpha_1}{ds_z}, \quad \tau_2^z = H_2 \frac{d\alpha_2}{ds_z}, \tag{5.8}$$

$$n_1^z = H_2 \frac{d\alpha_2}{ds_z}, \quad n_2^z = H_1 \frac{d\alpha_1}{ds_z}, \tag{5.9}$$

where τ_i^z, n_i^z ($i = 1, 2$) are the projections of $\bar{\tau}^z, \bar{n}^z$ on vectors $\bar{e}^z{}_i \in S_z$. From Eqs. (5.6, 5.9) for projections of $\bar{n}$ on tangents to the coordinate lines on S_z, we have

$$n_1^z = \frac{H_2}{A_2}\frac{ds}{ds_z} n_1, n_2^z = \frac{H_1}{A_1}\frac{ds}{ds_z} n_2. \tag{5.10}$$

Although Eqs. (5.2)–(5.10) are obtained in terms of the undeformed shell, they are also valid for the deformed configuration. Thus,

$$\overset{*}{\tau}_i = \overset{*}{A}_i \frac{d\alpha_i}{d\overset{*}{s}}, \quad \overset{*}{n}_i = (-1)^{i+1} \overset{*}{A}_i \frac{d\alpha_i}{d\overset{*}{s}}, \quad (i = 1, 2) \tag{5.11}$$

where $\overset{*}{\tau}_i$, $\overset{*}{n}_i$, $\overset{*}{ds}$ are expressed in terms of the contour line $\overset{*}{C}$ and have the meaning as described above. Assuming that deformations on the boundary are small, we have $\overset{*}{A}_i \approx A_i$, $d\overset{*}{s} \approx ds$, from Eq. (5.1) we have

$$\overset{*}{\tau}_i \approx \tau_i, \quad \overset{*}{n}_i \approx n_i. \tag{5.12}$$

It implies that projections of $\overset{*}{\bar{\tau}}$ and $\overset{*}{\bar{n}}$ on the coordinate axes of the deformed middle surface $\overset{*}{S}$ equal projections of the same vectors on the undeformed middle surface S.

For curvatures k_n^*, k_τ^* in the direction of $\overset{*}{\bar{n}}$ and $\overset{*}{\bar{\tau}}$, and twist $k_{n\tau}^*$ of $\overset{*}{C}$ we have

$$\begin{aligned} k_n^* &= \sum_{i=1}^{2}\sum_{j=1}^{2} k_{ij}^* n_i^* n_j^* \approx \sum_{i=1}^{2}\sum_{j=1}^{2} k_{ij}^* n_i n_j, \\ k_\tau^* &= \sum_{i=1}^{2}\sum_{j=1}^{2} k_{ij}^* \tau_i^* \tau_j^* \approx \sum_{i=1}^{2}\sum_{j=1}^{2} k_{ij}^* \tau_i \tau_j, \\ k_{n\tau}^* &= \sum_{i=1}^{2}\sum_{j=1}^{2} k_{ij}^* \tau_i^* n_j^* \approx \sum_{i=1}^{2}\sum_{j=1}^{2} k_{ij}^* \tau_i n_j, \end{aligned} \tag{5.13}$$

where Eqs. (5.7, 5.12) are used. Formulas for the deformed contour are similar to those given by Eq. (5.10) and have the form

$$\overset{*}{n}_1^z = \frac{\overset{*}{H}_2}{\overset{*}{A}_2} \frac{\overset{*}{ds}}{\overset{*}{ds}_z} \overset{*}{n}_1, \quad \overset{*}{n}_2^z = \frac{\overset{*}{H}_1}{\overset{*}{A}_1} \frac{\overset{*}{ds}}{\overset{*}{ds}_z} \overset{*}{n}_2. \tag{5.14}$$

5.2 Stresses on the Boundary

Let $\overset{*}{\bar{p}}_n^z$ be the normal stress vector acting upon a differential element of the boundary $\overset{*}{\Sigma}^z$ of the deformed shell located at a distance $\overset{*}{z} \approx z$ from the middle surface $\overset{*}{S}$ (Fig. 5.2)

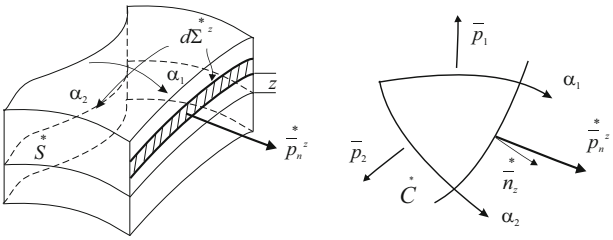

Fig. 5.2 Stresses on the boundary of a shell

$$\overset{*}{\bar{p}}_n^{z} = \bar{p}_1 \overset{*}{n}_1^{z} + \bar{p}_2 \overset{*}{n}_2^{z} + \bar{p}_3 \overset{*}{\bar{m}}. \tag{5.15}$$

Here $\overset{*}{n}_1^{z}$ are the projections of $\overset{*}{n}^{z}$ on $\overset{*}{\bar{e}}_i^{z} \in \overset{*}{S}$, and $\bar{p}_i$ are the stress vectors acting upon the faces $\alpha_1 = \text{const}$, $\alpha_2 = \text{const}$. Since $\overset{*}{n}^{z} \perp \overset{*}{\bar{m}}$, the third component in Eq. (5.15) vanishes, $\bar{p}_3 \overset{*}{\bar{m}} = 0$.

The surface area $d\overset{*}{\Sigma}_z$ of a differential element on the edge is given by

$$d\overset{*}{\Sigma}_z = d\overset{*}{s}_z \, d\overset{*}{z}. \tag{5.16}$$

The resultant force $\bar{R}_n^*$ and moment $\bar{M}_n^*$ vectors per unit length of $\overset{*}{C}$ acting upon $d\overset{*}{\Sigma}_z$ are given by

$$\bar{R}_n^* = \int_{z_1}^{z_2} \overset{*}{\bar{p}}_n^{z} \frac{d\overset{*}{\Sigma}_z}{d\overset{*}{s}}, \quad \bar{M}_n^* = \int_{z_1}^{z_2} \left(\overset{*}{\bar{m}} \overset{*}{z} \times \overset{*}{\bar{p}}_n^{z} \right) \frac{d\overset{*}{\Sigma}_z}{d\overset{*}{s}}. \tag{5.17}$$

Using Eqs. (5.15, 5.16) they can be written as

$$\bar{R}_{n^*} = \int_{z_1}^{z_2} \left(\bar{p}_1 \overset{*}{n}_1^{z} + \bar{p}_2 \overset{*}{n}_2^{z} \right) \frac{d\overset{*}{s}_z \, d\overset{*}{z}}{d\overset{*}{s}},$$

$$\bar{M}_n^* = \int_{z_1}^{z_2} \left(\overset{*}{\bar{m}} \overset{*}{z} \times \left(\bar{p}_1 \overset{*}{n}_1^{z} + \bar{p}_2 \overset{*}{n}_2^{z} \right) \right) \frac{d\overset{*}{s}_z \, d\overset{*}{z}}{d\overset{*}{s}}.$$

Substituting $\overset{*}{n}_i^{z}$ given by Eq. (5.14), and using approximations (5.12), $\bar{R}_n^*$, $\bar{M}_n^*$ on the skewed faces of the boundary are found to be

$$\begin{aligned}\bar{R}_n^* &= \bar{R}_1 \overset{*}{n}_1 + \bar{R}_2 \overset{*}{n}_2 \approx \bar{R}_1 n_1 + \bar{R}_2 n_2,\\ \bar{M}_n^* &= \bar{M}_1 \overset{*}{n}_1 + \bar{M}_2 \overset{*}{n}_2 \approx \bar{M}_1 n_1 + \bar{M}_2 n_2.\end{aligned} \tag{5.18}$$

Decomposing $\bar{R}_n^*, \bar{M}_n^*$ along the base $\{\overset{*}{n}, \overset{*}{\tau}, \overset{*}{m}\}$and substituting $\bar{R}_i$ and $\bar{M}_i$ given by Eqs. (3.22, 3.23), we get

$$\begin{aligned}\bar{R}_n^* &= \sum_{i=1}^{2}\sum_{k=1}^{2} \overset{*}{e}_1 \overset{*}{T}_{ik} \overset{*}{n}_i + \overset{*}{m}\left(\overset{*}{N}_1 \overset{*}{n}_1 + \overset{*}{N}_2 \overset{*}{n}_2\right),\\ \bar{M}_n^* &= \overset{*}{e}_2\left(\overset{*}{M}_{11} n_1 + \overset{*}{M}_{21} n_2\right) - \overset{*}{e}_1\left(\overset{*}{M}_{12} n_1 + \overset{*}{M}_{22} n_2\right),\end{aligned} \tag{5.19}$$

where $\overset{*}{T}_{ik}$, $\overset{*}{N}_i$ and $\overset{*}{M}_{ik}$ are the in-plane forces and moments.

Let $T_{n}^{*}, T_{n\tau}^{**}$ and $\overset{*}{N}$ be the normal, tangent and lateral forces acting on $\overset{*}{\Sigma}$

$$T_{n}^{*} = \bar{R}_{n}^{*} \overset{*}{n}, \quad T_{n\tau}^{**} = \bar{R}_{n}^{*} \overset{*}{\tau}, \quad \overset{*}{N} = \bar{R}_{n}^{*} \overset{*}{m}.$$

On use of $\bar{R}_{n}^{*}$ (Eq. 5.19) and approximations (5.12), we find

$$\begin{aligned}T_{n}^{*} &= \sum_{i=1}^{2}\sum_{k=1}^{2} \overset{*}{T}_{ik} \overset{*}{n}_i \overset{*}{n}_k \approx \sum_{i=1}^{2}\sum_{k=1}^{2} \overset{*}{T}_{ik} n_i n_k\\ T_{n\tau}^{**} &= \sum_{i=1}^{2}\sum_{k=1}^{2} \overset{*}{T}_{ik} \overset{*}{n}_i \overset{*}{\tau}_k \approx \sum_{i=1}^{2}\sum_{k=1}^{2} \overset{*}{T}_{ik} n_i \tau_k\\ \overset{*}{N} &= \overset{*}{N}_1 \overset{*}{n}_1 + \overset{*}{N}_2 \overset{*}{n}_2 \approx \overset{*}{N}_1 n_1 + \overset{*}{N}_2 n_2.\end{aligned} \tag{5.20}$$

Projecting $\bar{M}_{n}^{*}$ on the tangent and normal planes to the boundary we get

$$\overset{*}{G} = \bar{M}_{n}^{*} \overset{*}{\tau}, \quad \overset{*}{H} = \bar{M}_{n}^{*} \overset{*}{n},$$

where $\overset{*}{G}, \overset{*}{H}$ are is the bending and twisting moments. Substituting $\bar{M}_{n}^{*}$ (Eq. 5.19), we obtain

$$\overset{*}{G} = \overset{*}{\overline{\tau}}_2 \left(\overset{*}{M}_{11} \overset{*}{n}_1 + \overset{*}{M}_{21} \overset{*}{n}_2 \right) - \overset{*}{\overline{\tau}}_1 \left(\overset{*}{M}_{21} \overset{*}{n}_1 + \overset{*}{M}_{22} \overset{*}{n}_2 \right),$$
$$\overset{*}{H} = \overset{*}{\bar{n}}_2 \left(\overset{*}{M}_{11} \overset{*}{n}_1 + \overset{*}{M}_{21} \overset{*}{n}_2 \right) - \overset{*}{\bar{n}}_1 \left(\overset{*}{M}_{21} \overset{*}{n}_1 + \overset{*}{M}_{22} \overset{*}{n}_2 \right).$$

Making use of Eq. (5.6), after simple algebra, we find

$$\begin{aligned} \overset{*}{G} &= \sum_{i=1}^{2} \sum_{k=1}^{2} \overset{*}{M}_{ik} \, \overset{*}{n}_i \, \overset{*}{n}_k \approx \sum_{i=1}^{2} \sum_{k=1}^{2} \overset{*}{M}_{ik} \, n_i n_k \\ \overset{*}{H} &= -\sum_{i=1}^{2} \sum_{k=1}^{2} \overset{*}{M}_{ik} \, \overset{*}{n}_i \, \overset{*}{\tau}_k \approx -\sum_{i=1}^{2} \sum_{k=1}^{2} \overset{*}{M}_{ik} \, n_i \tau_k . \end{aligned} \tag{5.21}$$

Decomposing the resultant force and moment vectors in the directions of $\{\overset{*}{\bar{n}}, \overset{*}{\overline{\tau}}, \overset{*}{\bar{m}}\}$, we get

$$\bar{R}_{\underset{n}{*}} = T_{\underset{n}{*}} \overset{*}{\bar{n}} + T_{\underset{n\tau}{**}} \overset{*}{\overline{\tau}} + \overset{*}{N} \, \overset{*}{\bar{m}}, \quad \bar{M}_{\underset{n}{*}} = H_{\underset{n}{*}} \bar{n}_* + \overset{*}{G} \, \overset{*}{\overline{\tau}}. \tag{5.22}$$

The result of the above considerations is that the stressed state on the edge of the thin shell is determined in terms of five variables, namely, $T_{\underset{n}{*}}, T_{\underset{n\tau}{**}}, \overset{*}{N}, \overset{*}{G}$ and $\overset{*}{H}$. However, as we shall show soon, the twisting moment $\overset{*}{H}$ can be replaced by a statically equivalent force $\frac{-\partial \overset{*}{H} \bar{m}^*}{\partial \overset{*}{s}}$ per unit arc length of $\overset{\frown}{c_0 c_1}$ of the contour $\overset{*}{C}$. The substitution, according to the Saint-Venant principle, will have no effect on the stress state in the thin shell at distances sufficiently far away from the boundary.

Let $\overset{*}{H}$ be the twisting moment vector acting at point $c_0 \in \overset{*}{C}$ (Fig. 5.3). Consider a vicinity of the point c_0. Approximating the arc $\overset{\frown}{c_0 c_1}$ by a straight line $\overline{c_0 c_1}$ of a length $d\overset{*}{s}$ the resultant vector of twisting moment $\overset{*}{H} \, \overset{*}{\bar{n}} \, d\overset{*}{s}$ acting upon $\overline{c_0 c_1}$ can be substituted by a statically equivalent couple given by $\left(-\overset{*}{H} \, \overset{*}{\bar{m}}, + \overset{*}{H} \, \overset{*}{\bar{m}} \right)$

$$\overset{*}{H} \, \overset{*}{\bar{n}} \, d\overset{*}{s} \propto \left(-\overset{*}{H} \, \overset{*}{\bar{m}}, + \overset{*}{H} \, \overset{*}{\bar{m}} \right).$$

The vector $\overset{*}{\bar{m}}$ is orthogonal to $\overset{*}{S}$ and vector $\overset{*}{\bar{n}}$ is orthogonal to $\overset{*}{\bar{m}}$ at c_0 and points towards the reader. The forces $\pm \overset{*}{H} \, \overset{*}{\bar{m}}$ are collinear with the vector $\overset{*}{\bar{m}}$ at c_{01}—the middle point of $\overline{c_0 c_1}$. Then the moment of the couple about point c_{01} is indeed equals

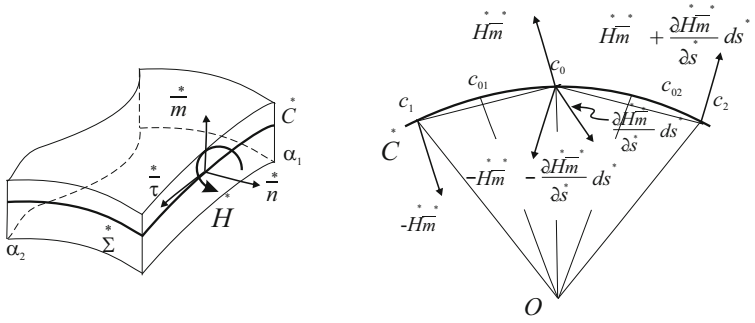

Fig. 5.3 Substitution of the twist moment H by a statically equivalent distributed force $\partial \overset{*}{H}\, \overset{*}{\bar{m}} / \partial \overset{*}{s}$ acting on the boundary of a shell

$$\overset{*}{\bar{\tau}}\, d\overset{*}{s} \times \overset{*}{H}\, \overset{*}{\bar{m}} = \left(\overset{*}{\bar{\tau}} \times \overset{*}{\bar{m}}\right) \overset{*}{H}\, d\overset{*}{s} = \overset{*}{H}\, \overset{*}{\bar{n}}\, d\overset{*}{s},$$

where $\overset{*}{\bar{\tau}}\, d\overset{*}{s} \approx \overline{c_0 c_1}$.

In just the same way, it can be shown that the torque exerted on the segment $\overline{c_0 c_2}$ is statically equivalent to the couple applied at points c_0 and c_2, respectively. They are oriented along $\overset{*}{\bar{m}}$ at c_{02}—the middle point of $\overline{c_0 c_2}$, and equal

$$-\left(\overset{*}{H}\, \overset{*}{\bar{m}} + \frac{\partial \overset{*}{H}\, \overset{*}{\bar{m}}}{\partial \overset{*}{s}} d\overset{*}{s}\right), \left(\overset{*}{H}\, \overset{*}{\bar{m}} + \frac{\partial \overset{*}{H}\, \overset{*}{\bar{m}}}{\partial \overset{*}{s}} d\overset{*}{s}\right).$$

The geometric sum of forces applied at point c_0 is $-\frac{\partial \overset{*}{H}\, \overset{*}{\bar{m}}}{\partial \overset{*}{s}} d\overset{*}{s}$. It follows that the twisting moment $\overset{*}{H}$ per unit length of the countour $\overset{*}{C}$ is statically equivalent indeed to the distributed force of density $-\frac{\partial \overset{*}{H}\, \overset{*}{\bar{m}}}{\partial \overset{*}{s}} d\overset{*}{s}$.

The resultant force and moment vectors $\bar{R}^*_n$ and $\bar{M}^*_n$ acting upon $\overset{*}{\Sigma}$ are statically equivalent to the generalized force vector

$$\overline{\Phi} = \bar{R}^*_n - \frac{\partial \overset{*}{H}\, \overset{*}{\bar{m}}}{\partial \overset{*}{s}} d\overset{*}{s}, \tag{5.23}$$

and the bending moment

$$\overset{*}{G} = \sum_{i=1}^{2}\sum_{k=1}^{2} \overset{*}{M}_{ik}\, \overset{*}{n}_i\, \overset{*}{n}_k \approx \sum_{i=1}^{2}\sum_{k=1}^{2} \overset{*}{M}_{ik}\, n_i n_k. \tag{5.24}$$

Here $\overset{*}{H}$ and $\bar{R}_{\overset{*}{n}}$ satisfy Eqs. (5.21, 5.22), respectively.

In the above derivations we assumed that the boundary is non-singular and closed. If there are singularities, e.g. corner points along the edge of the boundary, then the force $-\partial \overset{*}{H}\, \overset{*}{\bar{m}} / \partial \overset{*}{s}$ should be supplemented by forces $\left(\pm \overset{*}{H}\, \overset{*}{\bar{m}}\right)$ acting at the corners.

5.3 Static Boundary Conditions

Since stresses on the boundary $\overset{*}{\Sigma}$ of the shell are statically equivalent to three forces $T_{\overset{*}{n}}, T_{\overset{**}{n\tau}}, \overset{*}{N}$ and two moments $\overset{*}{G}, \overset{*}{H}$, then five static conditions should be prescribed on the boundary. However, it was first shown by Kirchhoff for thin shells, that the number of boundary conditions could be reduced to four. Kirchhoff based his proof on the assumption that stresses that produce the twisting moment $\overset{*}{H}$ are negligible and therefore, can be substituted by the distributed force of density $-\partial \overset{*}{H}\, \overset{*}{\bar{m}} / \partial \overset{*}{s}$.

Let the deformed middle surface $\overset{*}{S}$ be parameterized by rectangular curvilinear coordinates. Assume that $\overline{\Phi}^s$, $\overset{*}{G}^s$ are applied external load and bending moment vectors per unit length of the deformed contour $\overset{*}{C}$. Then, the static boundary conditions take the form

$$\overline{\Phi}^s = \bar{R}_{\overset{*}{n}} - \frac{\partial \overset{*}{H}\, \overset{*}{\bar{m}}}{\partial \overset{*}{s}}, \quad \overset{*}{G}^s = \sum_{i=1}^{2}\sum_{k=1}^{2} \overset{*}{M}_{ik}\, \overset{*}{n}_i\, \overset{*}{n}_k \approx \sum_{i=1}^{2}\sum_{k=1}^{2} \overset{*}{M}_{ik}\, n_i n_k \tag{5.25}$$

where $\bar{R}_{\overset{*}{n}}, \overset{*}{H}$ satisfy Eqs. (5.21, 5.22), respectively. Projections of $\overline{\Phi}^s$ on $\{\overset{*}{\bar{n}}, \overset{*}{\bar{\tau}}, \overset{*}{\bar{m}}\}$ are given by

$$\overset{*}{\bar{n}}\, \Phi^s_{\overset{*}{n}} + \overset{*}{\bar{\tau}}\, \Phi^s_{\overset{*}{\tau}} + \overset{*}{\bar{m}}\, \Phi^s_{\overset{*}{m}} = \bar{R}_{\overset{*}{n}} - \frac{\partial \overset{*}{H}\, \overset{*}{\bar{m}}}{\partial \overset{*}{s}}.$$

The scalar product of the above by $\overset{*}{\bar{n}}$, $\overset{*}{\bar{\tau}}$ and $\overset{*}{\bar{m}}$ yields

$$\Phi^{s}_{\ n} = T_{n} - \bar{n}\, H \frac{\partial \bar{m}}{\partial s}, \quad \Phi^{s}_{\ \tau} = T_{n\tau} - \bar{\tau}\, H \frac{\partial \bar{m}}{\partial s}, \quad \Phi^{s}_{\ m} = N_{n} - \frac{\partial H}{\partial s}$$

Here use is made of $\bar{n}\,\bar{m} = \bar{\tau}\,\bar{m} = \bar{m}\,\partial\,\bar{m}/\partial s = 0$. Since

$$\bar{m}_{i} = A_{i}\left(\bar{e}_{1} k_{1i} + \bar{e}_{2} k_{2i}\right), \quad A_{i} \frac{\partial \alpha_{i}}{\partial s_{*}} = \tau_{i}, \tag{5.26}$$

for derivative $\partial\,\bar{m}/\partial s$ we have

$$\frac{\partial \bar{m}}{\partial s} = \bar{m}_{1} \frac{\partial \alpha_{1}}{\partial s} + \bar{m}_{2} \frac{\partial \alpha_{2}}{\partial s} = \sum_{i=1}^{2}\sum_{j=1}^{2} A_{i}\, \bar{e}_{j}\, k_{ij} \frac{\partial \alpha_{i}}{\partial s_{*}} = \sum_{i=1}^{2}\sum_{j=1}^{2} \bar{e}_{j}\, k_{ij}\, \tau_{i}\,.$$

The scalar products of $\partial\,\bar{m}/\partial s$ by $\bar{n}$ and $\bar{\tau}$ are found to be

$$\begin{aligned} \bar{n} \frac{\partial \bar{m}}{\partial s} &= \sum_{i=1}^{2}\sum_{j=1}^{2} \left(\bar{n}\, \bar{e}_{j}\right) k_{ij}\, \tau_{i} = k_{n\tau} \\ \bar{\tau} \frac{\partial \bar{m}}{\partial s} &= \sum_{i=1}^{2}\sum_{j=1}^{2} \left(\bar{\tau}\, \bar{e}_{j}\right) k_{ij}\, \tau_{i} = k_{\tau}\,, \end{aligned} \tag{5.27}$$

where use is made of approximations given by Eqs. (5.12). Applying Eqs. (5.27) in (5.23), boundary conditions are found to be

$$\begin{aligned} \Phi^{s}_{\ n} &= T_{n} - H k_{n\tau}, \quad \Phi^{s}_{\ \tau} = T_{n\tau} - H k_{\tau}\,, \\ \Phi^{s}_{\ m} &= N_{n} - \frac{\partial H}{\partial s} \approx N_{n} - \frac{\partial H}{\partial s}, \quad G^{s} \approx \sum_{i=1}^{2}\sum_{k=1}^{2} M_{ik}\, n_{i} n_{k}, \end{aligned} \tag{5.28}$$

In the above we assumed that $d s \approx ds$. Eqs. (5.28) contain nonlinearities that are introduced by $k_{n\tau}$, k_{τ} and projections of the external load vector $\overline{\Phi}^{s}$. For example, if φ is the angle between the positive orientation of the α_1 axis and the vector $\bar{n}$, then the projections of $\bar{n}$ and $\bar{\tau}$ on the undeformed contour of the shell are given by

$$\tau_{1} = -n_{2} = -\sin\varphi, \quad \tau_{2} = n_{1} = \cos\varphi. \tag{5.29}$$

Given below are some commonly used boundary conditions.

(1) Clamped edge:

$$u_n = u\tau = \omega = 0, \quad \frac{\partial \omega}{\partial n} = 0, \tag{5.30}$$

where u_n is the projection of the displacement vector $\overline{\nu}$ on the vector $\bar{n}$ perpendicular to the contour $C \in \Sigma$, $u\tau$ is the projection of $\overline{\nu}$ on the vector $\overline{\tau}$, and ω is the normal displacement (deflection)

$$u_n = \overline{\nu}\bar{n} = u_1 n_1 + u_2 n_2, \quad u_n = \overline{\nu\tau} = u_1\tau_1 + u_2\tau_2.$$

The last condition in (Eq. 5.30) implies that the rotation about the vector $\overline{\tau}$ equals zero: $\overset{*}{\bar{n}}\bar{m} = 0$.

(2) Simply supported edge:

$$u_n = u\tau = \omega = 0, \quad \overset{*}{G}{}^s = \sum_{i=1}^{2}\sum_{k=1}^{2} \overset{*}{M}_{ik}\, \overset{*}{n}_i\, \overset{*}{n}_k \approx \sum_{i=1}^{2}\sum_{k=1}^{2} \overset{*}{M}_{ik}\, n_i n_k = 0, \tag{5.31}$$

where $\overset{*}{G}{}^s$ is the bending moment.

(3) Freely supported edge with a single degree of freedom in the normal direction:

$$u_n = u\tau = 0, \quad \overset{*}{G}{}^s = 0, \quad N_{\overset{*}{n}} - \frac{\partial \overset{*}{H}}{\partial \overset{*}{s}} \approx N_{\overset{*}{n}} - \frac{\partial \overset{*}{H}}{\partial s} = 0. \tag{5.32}$$

(4) Free edge:

$$T_{\overset{*}{n}} - \overset{*}{H}\, \overset{*}{k}_{n\tau} = 0, \quad T_{\overset{**}{n\tau}} - \overset{*}{H}\, \overset{*}{k}_{\tau} = 0, N_{\overset{*}{n}} - \frac{\partial \overset{*}{H}}{\partial \overset{*}{s}} \approx N_{\overset{*}{n}} - \frac{\partial \overset{*}{H}}{\partial s}$$
$$= 0, \sum_{i=1}^{2}\sum_{k=1}^{2} \overset{*}{M}_{ik}\, \overset{*}{n}_i\, \overset{*}{n}_k \approx \sum_{i=1}^{2}\sum_{k=1}^{2} \overset{*}{M}_{ik}\, n_i n_k = 0. \tag{5.33}$$

where the meaning of parameters is as above.

5.4 Deformations of the Edge

Consider deformations of a line element on $d\Sigma$. Assume that it is orthogonal to the undeformed middle surface S of the shell. Tangent ε_n, ε_τ, bending ϖ_n, ϖ_τ shear $\varepsilon_{n\tau}$, deformations and twist $\varpi_{n\tau}$ of the edge of the shell are defined by

$$\varepsilon_n = \sum_{i=1}^{2}\sum_{k=1}^{2}\varepsilon_{ik}n_i n_k, \quad \varepsilon_\tau = \sum_{i=1}^{2}\sum_{k=1}^{2}\varepsilon_{ik}\tau_i\tau_k, \quad \varepsilon_{n\tau} = \sum_{i=1}^{2}\sum_{k=1}^{2}\varepsilon_{ik}\tau_i n_k, \tag{5.34}$$

$$æ_n = \sum_{i=1}^{2}\sum_{k=1}^{2}æ_{ik}n_i n_k, \quad æ_\tau = \sum_{i=1}^{2}\sum_{k=1}^{2}æ_{ik}\tau_i\tau_k, \quad æ_{n\tau} = \sum_{i=1}^{2}\sum_{k=1}^{2}æ_{ik}\tau_i n_k \tag{5.35}$$

where n_1, n_2 satisfy Eqs. (5.29).

Applying Eqs. (5.34) and expressions for the Lamé parameters

$$\overset{*}{A}{}_i^2 = A_i^2(1+2\varepsilon_{ii}), \quad \overset{*}{A}_1\,\overset{*}{A}_2\cos\overset{*}{\chi} = 2\varepsilon_{12}A_1A_2, \quad \tau_i ds = A_i d\alpha_i,$$

the length of a line element $\overset{*}{ds}$ on $\overset{*}{C}$ is given by

$$\left(d\overset{*}{s}\right)^2 = \overset{*}{A}{}_1^2\, d\alpha_1{}^2 + 2\overset{*}{A}_1\,\overset{*}{A}_2\cos\overset{*}{\chi}\, d\alpha_1 d\alpha_2 + \overset{*}{A}{}_2^2\, d\alpha_2{}^2 = (1+2\varepsilon_\tau)ds^2. \tag{5.36}$$

Unit vectors $\overset{*}{\overline{\tau}}$ and $\overline{\tau}$ are given by

$$\overset{*}{\overline{\tau}} = \frac{d\,\overset{*}{\bar{r}}}{d\,\overset{*}{s}} = \frac{d\,\overset{*}{\bar{r}}}{ds}\frac{ds}{d\,\overset{*}{s}} = \left(\overline{\tau} + \frac{d\bar{\nu}}{ds}\right)\Big/\sqrt{1+2\varepsilon_\tau}, \quad \overline{\tau} = \frac{d\bar{r}}{ds}, \tag{5.37}$$

where use is made of Eqs. (5.35).

The vector $\overset{*}{\bar{m}}$ normal to the surface $\overset{*}{S}$ is found from

$$\overset{*}{\bar{m}} = \left(\overset{*}{\bar{r}}_1 \times \overset{*}{\bar{r}}_2\right)\Big/\sqrt{\overset{*}{a}}, \tag{5.38}$$

where $\overset{*}{a}$ is the invariant of the first fundamental form given by

$$\overset{*}{a} = (A_1A_2)^2\mathfrak{A}, \quad \mathfrak{A} = 1 + 2(\varepsilon_n + \varepsilon_\tau) + 4\left(\varepsilon_n\varepsilon_\tau - \varepsilon^2{}_{n\tau}\right). \tag{5.39}$$

Derivatives of the displacement vector in the direction of $\bar{n}$ and $\overline{\tau}$ are

$$\frac{d\bar{\nu}}{ds} = \frac{\overline{\tau}_1}{A_1}\frac{d\bar{\nu}}{d\alpha_1} + \frac{\overline{\tau}_2}{A_2}\frac{d\bar{\nu}}{d\alpha_2}, \quad \frac{d\bar{\nu}}{ds_n} = \frac{n_1}{A_1}\frac{d\bar{\nu}}{d\alpha_1} + \frac{n_2}{A_2}\frac{d\bar{\nu}}{d\alpha_2}. \tag{5.40}$$

Here s, s_n are the lengths of line elements on C and C_n, such that $C_n \perp C$, and $\overline{\tau} = \frac{d\bar{r}}{ds}$, $\bar{n} = \frac{d\bar{r}}{ds_n}$. Solving Eqs. (5.40) for $d\bar{\nu}/d\alpha_i$ we find

$$\frac{1}{A_i}\frac{d\overline{\nu}}{d\alpha_i} = \tau_i \frac{d\overline{\nu}}{ds} + n_i \frac{d\overline{\nu}}{ds_n}. \tag{5.41}$$

Since $\bar{e}_i = \overline{\tau}\tau_i + \bar{n}n_i$, from Eq. (3.41) for vectors $\overset{*}{\bar{r}}_i$, we obtain

$$\bar{r}_i^* = \overset{*}{\bar{r}} + \frac{d\overline{\nu}}{d\alpha_i} = A_i\left(\bar{e}_i + \frac{1}{A_i}\frac{d\overline{\nu}}{ds}\right) = A_i\left(\underline{a}\tau_i + \underline{b}n_i\right). \tag{5.42}$$

Here we have introduced the following notations

$$\underline{a} = \frac{d\overset{*}{\bar{r}}}{ds} = \overline{\tau} + \frac{d\overline{\nu}}{ds}, \quad \underline{b} = \frac{d\overset{*}{\bar{r}}}{ds_n} = \bar{n} + \frac{d\overline{\nu}}{ds_n}. \tag{5.43}$$

Substituting Eq. (5.42) into (5.38), we get

$$\begin{aligned}\overset{*}{\bar{m}} &= (b \times a)/\sqrt{\mathfrak{A}} \\ &= \left\{\bar{m} + \left(\bar{n} \times \frac{d\overline{\nu}}{ds}\right) + \left(\frac{d\overline{\nu}}{ds_n} \times \overline{\tau}\right) + \left(\frac{d\overline{\nu}}{ds_n} \times \frac{d\overline{\nu}}{ds}\right)\right\}/\sqrt{\mathfrak{A}}.\end{aligned} \tag{5.44}$$

On use of Eq. (5.42) and equality $\bar{r}_i = A_i(\overline{\tau}\tau_i + \bar{n}n_i)$, from $2A_iA_k\varepsilon_{ik} = \overset{*}{\bar{r}}_i\,\overset{*}{\bar{r}}_k - \bar{r}_i\bar{r}_k$ (see Eqs.(1.67)) for deformation on the edge of the shell we have

$$2\varepsilon_{ik} = \left(\underline{a}\tau_i + \underline{b}n_i\right)\left(\underline{a}\tau_k + \underline{b}n_k\right) - (\overline{\tau}\tau_i + \bar{n}n_i)(\overline{\tau}\tau_k + \bar{n}n_k). \tag{5.45}$$

Further, with the help of Eq. (5.45) from Eqs. (5.34), we obtain

$$\begin{aligned}\varepsilon_n &= \bar{n}\frac{d\overline{\nu}}{ds_n} + \frac{1}{2}\left(\frac{d\overline{\nu}}{ds_n}\right)^2, \quad \varepsilon_\tau = \overline{\tau}\frac{d\overline{\nu}}{ds_n} + \frac{1}{2}\left(\frac{d\overline{\nu}}{ds_n}\right)^2, \\ 2\varepsilon_{n\tau} &= \bar{n}\frac{d\overline{\nu}}{ds_n} + \overline{\tau}\frac{d\overline{\nu}}{ds_n} + \frac{d\overline{\nu}}{ds}\frac{d\overline{\nu}}{ds_n},\end{aligned} \tag{5.46}$$

where use is made of the facts $\bar{n} \perp \overline{\tau}$, $n^2{}_1 + n^2{}_2 = \tau^2{}_1 + \tau^2{}_2 = 1$.

To express the vector $\overset{*}{\bar{n}}$ in terms of the displacements, we substitute $\overset{*}{\overline{\tau}}, \overset{*}{\bar{m}}$ given by Eqs. (5.37, 5.44) into equality $\overset{*}{\bar{n}} = \overset{*}{\overline{\tau}} \times \overset{*}{\bar{m}}$. After simple algebra we find

$$\overset{*}{\bar{n}}\sqrt{\mathfrak{A}(1 + 2\varepsilon_\tau)} = (1 + 2\varepsilon_\tau)\underline{b} - 2\varepsilon_{n\tau} \cdot \underline{a} \tag{5.47}$$

To decompose the right-hand sides of Eqs. (5.46) in the base $\{\bar{n},\ \overline{\tau},\ \bar{m}\}$, we proceed from formulas for derivatives of $\bar{n}$, $\overline{\tau}$, $\bar{m}$ with respect to s and s_n, given by

$$\frac{d\bar{n}}{ds} = \text{æ}\bar{\tau} - \bar{m}k_{n\tau}, \quad \frac{d\bar{\tau}}{ds} = -\bar{m}k_{\tau} - \text{æ}\bar{n}, \quad \frac{d\bar{m}}{ds} = \bar{n}k_{n\tau} + \bar{\tau}k_{\tau}, \tag{5.48}$$

$$\frac{d\bar{n}}{ds_n} = -\bar{m}k_{\tau} - \text{æ}'\bar{\tau}, \quad \frac{d\bar{\tau}}{ds_n} = \text{æ}'\bar{n} - \bar{m}k_{n\tau}, \quad \frac{d\bar{m}}{ds_n} = \bar{\tau}k_{n\tau} + \bar{n}k_n. \tag{5.49}$$

Here k_n, k_τ, $k_{n\tau}$ satisfy Eqs. (5.7) and

$$\begin{aligned} k_n &= \bar{n}\frac{d\bar{\tau}}{ds_n} = -\bar{\tau}\frac{d\bar{n}}{ds_n}, \quad k_\tau = \bar{\tau}\frac{d\bar{m}}{ds_n} = -\bar{m}\frac{d\bar{\tau}}{ds_n}, \\ k_{n\tau} &= \bar{n}\frac{d\bar{m}}{ds_n} = -\bar{m}\frac{d\bar{n}}{ds_n}. \end{aligned} \tag{5.50}$$

$\text{æ}, \text{æ}'$ are the geodesic curvatures of the contour lines C, C_n ($C_n \perp C$) are described by

$$\text{æ} = \bar{\tau}\frac{d\bar{n}}{ds} = -\bar{n}\frac{d\bar{\tau}}{ds}, \quad \text{æ}' = \bar{\tau}\frac{d\bar{n}}{ds_n} = -\bar{n}\frac{d\bar{\tau}}{ds_n}, \tag{5.51}$$

or in the expanded form

$$\begin{aligned} \text{æ} &= \frac{d\varphi}{ds} + \frac{\cos\varphi}{A_1A_2}\frac{\partial A_2}{\partial \alpha_1} + \frac{\sin\varphi}{A_1A_2}\frac{\partial A_1}{\partial \alpha_2}, \\ \text{æ}' &= -\frac{d\varphi}{ds_n} - \frac{\sin\varphi}{A_1A_2}\frac{\partial A_2}{\partial \alpha_1} + \frac{\cos\varphi}{A_1A_2}\frac{\partial A_1}{\partial \alpha_2}. \end{aligned} \tag{5.52}$$

Expanding the displacement vector $\bar{\nu}$ along the base $\{\bar{n}, \bar{\tau}, \bar{m}\}$

$$\bar{\nu} = \bar{n}u_n + \bar{\tau}u_\tau + \bar{m}\omega, \tag{5.53}$$

and differentiating Eq. (5.53) with respect to s and s_n, we find

$$\frac{d\bar{\nu}}{ds} = \bar{n}e_{\tau n} + \bar{\tau}e_{\tau\tau} + \bar{m}\omega_\tau, \quad \frac{d\bar{\nu}}{ds_n} = \bar{n}e_{nn} + \bar{\tau}e_{n\tau} + \bar{m}\omega_n. \tag{5.54}$$

Here $e_{nn}, e_{n\tau}, e_{\tau n}, \omega_n, \omega_\tau$ are the rotation angles given by

$$e_{\tau n} = \frac{du_n}{ds} - \text{æ}u_\tau + \varpi k_{n\tau}, \quad e_{\tau\tau} = \frac{du_\tau}{ds} + \text{æ}u_n + \varpi k_\tau, \tag{5.55}$$

$$e_{nn} = \frac{du_n}{ds_n} + \text{æ}'u_\tau + \varpi k_n, \quad e_{n\tau} = \frac{du_\tau}{ds_n} - \text{æ}'u_n + \varpi k_{n\tau},$$

$$\omega_\tau = \frac{d\varpi}{ds} - k_{n\tau}u_n - k_\tau u_\tau, \quad \omega_n = \frac{d\varpi}{ds_n} - k_n u_n - k_{n\tau}u_\tau. \tag{5.56}$$

In the above, use is made of Eqs. (5.48, 5.49). Substituting Eqs. (5.54) into Eq. (5.44), we have

$$\overset{*}{\bar{m}}\sqrt{\mathfrak{A}} = \bar{n}\mathbb{S}_n + \overline{\tau}\mathbb{S}_\tau + \bar{m}\mathbb{S}_3, \tag{5.57}$$

where

$$\begin{aligned}
\mathbb{S}_n &= \omega_\tau e_{n\tau} - \omega_n(1 + e_{\tau\tau}),\\
\mathbb{S}_\tau &= \omega_n e_{\tau n} - \omega_\tau(1 + e_{nn}),\\
\mathbb{S}_3 &= (1 + e_{\tau\tau})(1 + e_{nn}) - e_{\tau n}e_{n\tau}.
\end{aligned} \tag{5.58}$$

Let $\overset{*}{k}_n$, $\overset{*}{k}_\tau$, $\overset{*}{k}_{n\tau}$ be the curvature and twist of the contour $\overset{*}{C}$ (see Eq. (5.13))

$$\begin{aligned}
\overset{*}{k}_n &= \sum_{i=1}^{2}\sum_{j=1}^{2} \overset{*}{k}_{ij} n_i n_j = \underline{b}\frac{d\,\overset{*}{\bar{m}}}{ds_n} = -\overset{*}{\bar{m}}\frac{d\underline{b}}{ds_n},\\
\overset{*}{k}_\tau &= \sum_{i=1}^{2}\sum_{j=1}^{2} \overset{*}{k}_{ij} \tau_i \tau_j = \underline{a}\frac{d\,\overset{*}{\bar{m}}}{ds} = -\overset{*}{\bar{m}}\frac{d\underline{a}}{ds},\\
\overset{*}{k}_{n\tau} &= \sum_{i=1}^{2}\sum_{j=1}^{2} \overset{*}{k}_{ij} \tau_i n_j = \underline{b}\frac{d\,\overset{*}{\bar{m}}}{ds} = -\bar{m}_i^{*}\frac{d\underline{b}}{ds}.
\end{aligned} \tag{5.59}$$

Using Eq. (5.59), the bending deformation of the boundary of the shell is found to be

$$\begin{aligned}
&\text{æ}_n = \overset{*}{k}_n - k_n = \bar{m}\frac{d\bar{n}}{ds_n} - \overset{*}{\bar{m}}\frac{d\underline{b}}{ds_n}, \quad \text{æ}_\tau = \bar{m}\frac{d\overline{\tau}}{ds} - \overset{*}{\bar{m}}\frac{d\underline{a}}{ds},\\
&\text{æ}_{n\tau} = \bar{m}\frac{d\bar{n}}{ds} - \overset{*}{\bar{m}}\frac{d\underline{b}}{ds}.
\end{aligned} \tag{5.60}$$

Curvatures of $\overset{*}{C}$ are calculated as

$$\begin{aligned}
\overset{*}{k}_{\overset{*}{\tau}} &= -\overset{*}{\bar{m}}\frac{d\,\overset{*}{\overline{\tau}}}{d\,\overset{*}{s}} = -\frac{\overset{*}{\bar{m}}}{\sqrt{(1 + 2\varepsilon_\tau)}}\frac{d\,\overset{*}{\overline{\tau}}}{d\,\overset{*}{s}},\\
\overset{*}{k}_{\overset{**}{m\tau}} &= -\overset{*}{\bar{m}}\frac{d\,\overset{*}{\bar{n}}}{d\,\overset{*}{s}} = -\frac{\overset{*}{\bar{m}}}{\sqrt{(1 + 2\varepsilon_\tau)}}\frac{d\,\overset{*}{\bar{n}}}{d\,\overset{*}{s}}.
\end{aligned} \tag{5.61}$$

Substituting $\overset{*}{\overline{\tau}}$ and $\overset{*}{\bar{n}}$ given by Eqs. (5.37, 5.47) into (5.61) and on use of the fact that $\overset{*}{\bar{m}}\,\underline{a} = \overset{*}{\bar{m}}\,\underline{b} = 0$, we obtain

$$\overset{*}{k}_{\tau} = -\frac{\overset{*}{k}_{\tau}}{\sqrt{(1+2\varepsilon_{\tau})}}, \quad \overset{*}{k}_{n\tau} = -\frac{\left(\overset{*}{k}_{n\tau} + 2\overset{*}{k}_{n\tau}\varepsilon_{\tau} - 2\overset{*}{k}_{\tau}\varepsilon_{n\tau}\right)}{\sqrt{\mathfrak{A}(1+2\varepsilon_{\tau})}}. \tag{5.62}$$

Here $\overset{*}{k}_{\tau} = k_{\tau} + æ_{\tau}$, $\overset{*}{k}_{n\tau} = k_{n\tau} + æ_{n\tau}$ and satisfy Eqs. (5.59).

5.5 Equations of Gauss-Codazzi for the Boundary

As a final point of our discussion, we derive the Gauss-Codazzi equations for the undeformed boundary of the thin shell. For the integral of a vector (scalar) function $f(\alpha_1,\alpha_2)$ to exist, the following should hold

$$\frac{\partial}{\partial s_n}\left(\frac{\partial f}{\partial s}\right) - \frac{\partial}{\partial s}\left(\frac{\partial f}{\partial s_n}\right) = æ'\frac{\partial f}{\partial s_n} - æ\frac{\partial f}{\partial s}. \tag{5.63}$$

Substituting vector $\bar{m}$ $(\bar{m}\perp S)$ for f and using Eqs. (5.48, 5.49), we obtain

$$\frac{\partial}{\partial s_n}(\bar{n}k_{n\tau} + \overline{\tau}k_{\tau}) - \frac{\partial}{\partial s}(\overline{\tau}k_{n\tau} + \bar{n}k_n) = æ'(\overline{\tau}k_{n\tau} + \bar{n}k_n) - æ(\bar{n}k_{n\tau} + \overline{\tau}k_{\tau}). \tag{5.64}$$

Carrying differentiation (5.64) and equating the coefficients of $\bar{n}, \overline{\tau}$ and $\bar{m}$ to zero, the Codazzi formulas are found to be

$$\begin{aligned} &\frac{\partial k_{n\tau}}{\partial s_n} - \frac{\partial k_n}{\partial s} + æ'(k_{\tau} - k_n) + 2æk_{n\tau} = 0, \\ &\frac{\partial k_{\tau}}{\partial s_n} - \frac{\partial k_{n\tau}}{\partial s} + æ(k_{\tau} - k_n) - 2æ'k_{n\tau} = 0. \end{aligned} \tag{5.65}$$

Similarly, substituting $\overline{\tau}$ for f, we find

$$-\frac{\partial}{\partial s_n}(\bar{m}k_{\tau} + æ\bar{n}) - \frac{\partial}{\partial s}(æ'\bar{n} - \bar{m}k_{n\tau}) = æ'(\bar{n}æ' - \bar{m}k_{n\tau}) + æ(\bar{m}k_{\tau} + \bar{n}æ),$$

from where after differentiation and setting to zero the coefficients of $\bar{n}$, we obtain the Gauss formula

$$\frac{\partial æ}{\partial s_n} - \frac{\partial æ'}{\partial s} + æ'^2 + æ^2 = k_{n\tau}^2 + k_n k_{\tau}. \tag{5.66}$$

Equating the coefficients of $\bar{m}$ to zero, we again obtain the Codazzi formulas. Formulas (5.63)–(5.66) can also be expressed in terms of the deformed boundary of the shell.

Chapter 6
Continuum Model of the Biological Tissue

Everything is theoretically impossible, until it is done.
Robert A. Heinlein

6.1 The Gastric Wall as a Mechanochemical Continuum

The connection between the geometrical and statical quantities studied in the previous chapters must be complemented by equations establishing relationships among the stresses and deformations, their rates, temperature and structural changes of constructive materials, e.g. the tissue that forms the wall of a biological shell. The complete theoretical formulation is best achieved with application of the principles of thermodynamics supported by extensive experimentation, including in-plane and complex loading testing. The advantage of such approach is that it employs generalized quantities like entropy, free energy, Gibb's potential, as fundamental descriptors. Specific problems are encountered due to discrete morphological structure of the biological tissue and the continuum scale, which is typically ~1 μm. For example, because of existing anisotropy, multidimensional strain data from the uniaxial experiments are not enough to extrapolate to the fully three-dimensional constitutive equations. Further, small specimen sizes, tethering effects, heterogeneity of deformation, difficulty in maintaining constant force distribution along specimen edges, make experiments on soft tissues very difficult. Also being heterogeneous, anisotropic, non-linear, viscoelastic, incompressible composites, soft biomaterials defy simple material models. Accounting for these particulars in constitutive models and both experimental evaluations remains a great challenge.

There is no strict method of deciding on a specific choice of form of the model. The process of formulation is somewhat arbitrary and depends on the investigators needs and preferences. In the book we shall adopt the phenomenological approach (Nikitin 1980) to model a soft biocomposite—the wall of gastrointestinal organs. Our derivations will be based on the following histological assumptions:

(i) the biomaterial is a three-phase, multicomponent, mechanochemically active, anisotropic medium; phase 1 comprises the connective tissue net,

R.N. Miftahof, *Biomechanics of the Human Stomach*,
DOI 10.1007/978-3-319-59677-8_6

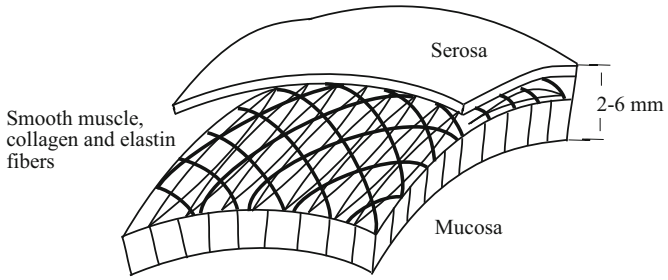

Fig. 6.1 The wall of the human stomach as a biological composite

phase 2—mechanochemically active smooth muscle fibers, and phase 3—inert myofibrils (Fig. 6.1);

(ii) the phase interfaces are semipermeable to certain substrates;

(iii) smooth muscle, collagen and elastin fibers are the main weight bearing and active force generating elements;

(iv) the biocomposite endows properties of general curvilinear anisotropy and viscoelasticity; the viscous properties are due to smooth muscle fiber mechanics and the elastic properties depend mainly on the collagen and elastin fibers;

(v) active forces of contraction-relaxation produced by smooth muscle are the result of multicascade intracellular mechanochemical reactions; the reactions run in a large number of small loci that are evenly distributed throughout the whole volume of the tissue; the sources of chemical reagents are uniformly dispersed within volume of the composite and are ample;

(vi) there are no temperature and/or deformation gradients within the tissue;

(vii) the biocomposite is incompressible and statistically homogeneous.

All equations to follow are written for the averaged parameters. Here we adopt the following notation: the quantities obtained by averaging over the volume of a particular phase are contained in the angle brackets, and those free of brackets are attained by averaging over the entire volume.

Let ρ be the mean density of the tissue. The partial density of the ζ^{th} substrate $\left(\zeta = \overline{1,n}\right)$ in the β phase ($\beta = 1, 2, 3$) is defined as

$$\rho_\zeta^\beta = m_\zeta^\beta / \upsilon,$$

where m_ζ^β is the mass of the ζ^{th} substrate, υ is the total elementary volume of the tissue $\upsilon = \sum_{\beta=1}^{3} \upsilon^\beta$. The mass and the effective concentrations of substrates are

$$c_\zeta^\beta = \rho_\zeta^\beta / \rho, \quad \left\langle c^\beta \right\rangle = m_\zeta^\beta / \upsilon^\beta \rho^\beta. \tag{6.1}$$

Assuming $\rho = \langle \rho^\beta \rangle = \text{const}$, we have

$$\left\langle \rho^{\beta} \right\rangle = \sum_{\zeta=1}^{n} \frac{m_{\zeta}^{\beta}}{v^{\beta}}. \tag{6.2}$$

Setting $\beta = 1$ we find

$$\left\langle \rho^{1} \right\rangle = \sum_{\zeta=1}^{n} \frac{m_{\zeta}^{1}}{v^{1}} = \sum_{\zeta=1}^{n} \frac{\rho_{\zeta}^{1} v}{v^{1}} = \sum_{\zeta=1}^{n} \frac{c_{\zeta}^{1} \rho v}{v^{1}} = \rho \sum_{\zeta=1}^{n} \frac{c_{\zeta}^{1}}{\eta},$$

where η is the porosity of phase β ($\eta = v/v^{\beta}$). It is easy to show that

$$\eta = \sum_{\zeta=1}^{n} c_{\zeta}^{1} \equiv c^{1}. \tag{6.3}$$

Hence the mass c_{ζ}^{β} and the effective $\left\langle c_{\zeta}^{\beta} \right\rangle$ concentrations are interrelated by $c_{\zeta}^{\beta} = \eta \left\langle c_{\zeta}^{\beta} \right\rangle$. The sum of all concentrations c_{ζ}^{β} in the medium equals one ($\sum_{\zeta=1}^{n} c_{\zeta}^{\beta} = 1$).

Change in the concentration of constituents in different phases is due to the exchange of the matter among phases, external fluxes, chemical reactions and diffusion. Since chemical reactions run only in phase 2 and the substrates move at the same velocity, there is no diffusion within phases. Hence, the equations of the conservation of mass of the ζth substrate in the medium is given by

$$\rho \frac{dc_{\zeta}^{1}}{dt} = Q_{\zeta}^{1}, \quad \rho \frac{dc_{\zeta}^{2}}{dt} = Q_{\zeta}^{2} + \sum_{j=1}^{r} \nu_{\zeta j} J_{j}, \quad \rho \frac{dc_{\zeta}^{3}}{dt} = Q_{\zeta}^{3}. \tag{6.4}$$

Here Q_{ς}^{β} is the velocity of influx of the ς^{th} substrate into the phase α, $\nu_{\zeta j} J_{j}$ is the rate of ζ^{th} formation in the j^{th} chemical reaction ($j = \overline{1, r}$). The quantity $\nu_{\zeta j}$ is related to the molecular mass M_{ς} of the substrate ζ and is analogous to the stoichiometric coefficient in the jth reaction. $\nu_{\zeta j}$ takes positive values if the substrate is formed and becomes negative if the substrate disassociates. Since the mass of reacting components is conserved in each chemical reaction, we have

$$\sum_{\zeta=1}^{n} \nu_{\zeta j} = 0.$$

Assume that there is a flux Q_{ς}^{β} of the matter into: (i) phase 1 from external sources and phase 3, (ii) phase 2 from phases 1 and 3 only, and (iii) phase 3 from phase 2. Hence, we have

$$Q_{\zeta}^{1} = -Q_{\zeta} + Q_{\zeta}^{e}, \quad Q_{\zeta}^{2} = Q_{\zeta} + Q_{\zeta}^{m}, \quad Q_{\zeta}^{3} = -Q_{\zeta}^{m}, \tag{6.5}$$

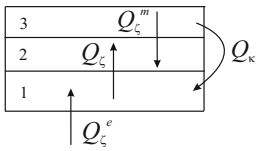

Fig. 6.2 Flux exchanges in a three-phase biocomposite

where Q_ζ^e is the flux of externally distributed sources, Q_ζ is the exchange flux between phases, Q_ζ^m is the flux of the matter from phase 3 into phase 2 (Fig. 6.2). Applying the incompressibility condition to Eq. (4.5), we have

$$\sum_{\zeta=1}^{n} Q_\zeta^e = 0.$$

Let also $\sum_{\zeta=1}^{n} Q_\zeta = 0$. Assuming that the effective concentration of substrates in phase 3 remains constant throughout, $\left\langle c_\zeta^3 \right\rangle = \text{const}$ and using Eqs. (6.5) in (6.4), we obtain

$$\rho \frac{dc_\zeta^1}{dt} = -Q_\zeta + Q_\zeta^e, \quad \rho \frac{\partial c_\zeta^2}{\partial t} = Q_\zeta - Q_\zeta^3 + \sum_{j=1}^{r} \nu_{\zeta j} J_j, \quad \rho \frac{\partial c_\zeta^3}{\partial t} = -Q_\zeta. \tag{6.6}$$

In the above, we neglected the convective transport of the matter within phases.

The equations of continuity and the conservation of momentum for the tissue treated as a three-dimensional solid in a fixed Cartesian coordinate system (x_1, x_2, x_3) is given by

$$\frac{\partial u}{\partial x_1} + \frac{\partial v}{\partial x_2} + \frac{\partial w}{\partial x_3} = 0, \tag{6.7}$$

$$\rho \frac{\partial^2 u_i}{\partial t^2} = \frac{\partial \sigma_{ij}}{\partial x_j} + \rho f_i. \tag{6.8}$$

Here u, v, w are the components of the displacement vector, f_i is the mass force, and σ_{ij} $(i, j = x_1, x_2, x_3)$ are stresses (see Chap. 2).

Let $U^{(\beta)}$, $s^{(\beta)}$, σ_{ij}^α be the free energy, entropy and stresses of each phase. Hence the Gibbs relations for each phase are defined by

$$c^1 \left\langle U^1 \right\rangle = U^1{}_0 \left(c_\zeta^1, T \right) + \frac{1}{2\rho} E_{ijlm} \varepsilon_{ij} \varepsilon_{lm} \tag{6.9}$$

$$c^\beta \left\langle U^\beta \right\rangle = U_0^\beta \left(c_\zeta^\beta, T \right) + \frac{1}{2\rho} Y_{ijlm} \varsigma_{ij}^\beta \varsigma_{lm}^\beta \tag{6.10}$$

$$d\left(c^1\left\langle U^1\right\rangle\right) = dU^1 = \frac{1}{\rho}c^1\left\langle\sigma^1\right\rangle_{ij}d\varepsilon^1_{ij} - \\ -c^1\left\langle s^1\right\rangle dT + \sum_{\varsigma=1}^{n}\left\langle\mu^1_\zeta\right\rangle d\left\langle c^1_\zeta\right\rangle \tag{6.11}$$

$$d\left(c^\beta\left\langle U^\beta\right\rangle\right) = dU^\beta = \frac{1}{\rho}c^\beta\left\langle\sigma^\beta\right\rangle_{ij}d\varsigma^\beta_{ij} - \\ -c^\beta\left\langle s^\beta\right\rangle dT + \sum_{\varsigma=1}^{n}\left\langle\mu^\beta_\zeta\right\rangle d\left\langle c^\beta_\zeta\right\rangle \tag{6.12}$$

$$\left\langle\mu^\beta_\zeta\right\rangle = \partial\left\langle U^\beta\right\rangle/\partial\left\langle c^\beta_\zeta\right\rangle, \quad \left\langle s^\beta\right\rangle = \partial\left\langle U^\beta\right\rangle/\partial T, \quad (\beta = 2,3)$$

where T is temperature, μ^β_ζ is the chemical potential of the ζ^{th} substrate in the β phase, $\mu^\beta_\zeta = \partial c^\beta\left\langle U^\beta\right\rangle/\partial c^\beta_\zeta$, ς_{ij} is the elastic and Δ_{ij} is the viscous part of deformation ($\varepsilon^\beta_{ij} = \varsigma^\beta_{ij} + \Delta^\beta_{ij}$, $\beta = 2, 3$). Making use of equality

$$\partial\left(c^\beta\left\langle U^\beta\right\rangle\right)/\partial c^\beta_\zeta = \left\langle\mu^\beta_\zeta\right\rangle + \left\langle U^\beta\right\rangle - \sum_{\varsigma=1}^{n}\left\langle\mu^\beta_\zeta\right\rangle\left\langle c^\beta_\zeta\right\rangle,$$

Equations (6.11, 6.12) can be written as

$$d\left(c^1\left\langle U^1\right\rangle\right) = \frac{1}{\rho}c^1\left\langle\sigma^1\right\rangle_{ij}d\varepsilon^1_{ij} - c^1\left\langle s^1\right\rangle dT + \sum_{\varsigma=1}^{n}\mu^1_\zeta dc^1_\zeta \tag{6.13}$$

$$d\left(c^\beta\left\langle U^\beta\right\rangle\right) = \frac{1}{\rho}c^\beta\left\langle\sigma^\beta\right\rangle_{ij}d\varsigma^\beta_{ij} - c^\beta\left\langle s^\beta\right\rangle dT + \sum_{\varsigma=1}^{n}\mu^\beta_\zeta dc^\beta_\zeta \quad (\beta = 2,3).$$

Assuming that the mass sources are present only in phases 1 and 2, the general heat flux and the second law of thermodynamics for the tissue are described by

$$dU = \frac{1}{\rho}\sigma_{ij}d\varepsilon_{ij} - sdT - dq' + \frac{1}{\rho}\sum_{\varsigma=1}^{n}\frac{\partial F}{\partial c^1{}_\varsigma}Q^e_\zeta dt, \tag{6.14}$$

$$Tds = dq^e + dq' + \sum_{\varsigma=1}^{n}TS^1{}_\varsigma\frac{Q^e_\zeta}{\rho}dt, \tag{6.15}$$

$$S^1_\zeta = \left(\frac{\partial s}{\partial c^1_\zeta}\right)_{T,c^i{}_\vartheta(\vartheta\neq\zeta),\varsigma_{ij},\varepsilon_{ij}} = \frac{\partial^2 F}{\partial T\partial c^1_\zeta}.$$

Here $U = \sum_{\beta=1}^{3}c^\beta\left\langle U^\beta\right\rangle$, $s = \sum_{\beta=1}^{3}c^\beta\left\langle s^\beta\right\rangle$, $\sigma_{ij} = \sum_{\alpha=1}^{3}c^\beta\left\langle\sigma^\beta\right\rangle_{ij}$, and S^1_ζ is the partial entropy of the biocomposite.

To complete the formulation of the model we need to specify thermodynamic fluxes Q_ζ^e, Q_ζ, J_j and stresses $\sigma_{ij}^{(\beta)}$.

Let the heart flux $\bar{q}$ be given by

$$\rho dq^{(e)} = -\left(\frac{\partial q_x}{\partial x} + \frac{\partial q_y}{\partial y} + \frac{\partial q_z}{\partial z}\right)dt \equiv -\mathrm{div}\bar{q}dt.$$

On use of Eq. (6.13) in (6.14, 6.15), the equation of the balance of entropy of the composite takes the form

$$\rho\frac{ds}{dt} - \sum_{\zeta=1}^{n}\frac{\partial s}{\partial c_\zeta^1}Q_\zeta^e = -\mathrm{div}\frac{\bar{q}}{T} + \frac{\boldsymbol{R}}{T}, \tag{6.16}$$

$$\boldsymbol{R} = -\frac{\bar{q}}{T}\left(\frac{\partial T}{\partial x} + \frac{\partial T}{\partial y} + \frac{\partial T}{\partial z}\right) + \sigma_{ij}^2\frac{d\Delta_{ij}^2}{dt} + \sigma^3{}_{ij}\frac{d\Delta_{ij}^3}{dt} + \\ + \sum_{\varsigma=1}^{n}\left(\mu_\zeta^1 - \mu_\zeta^2\right)Q_\zeta^e + \sum_{\varsigma=1}^{n}\left(\mu_\zeta^3 - \mu_\zeta^2\right)Q_\zeta^e - \sum_{j=1}^{r}J_j\Lambda_j, \tag{6.17}$$

$$\Lambda_j = \sum_{\zeta=1}^{n}\nu_{\varsigma j}\mu_\zeta^2. \tag{6.18}$$

Here $\boldsymbol{R}$ is the dissipative function, Λ_j is the affinity constant of the jth chemical reaction.

Let thermodynamic forces acting in the system be

$$-\frac{1}{T^2}\left(\frac{\partial T}{\partial x} + \frac{\partial T}{\partial y} + \frac{\partial T}{\partial z}\right), \quad \frac{1}{T}\frac{d\Delta_{ij}^2}{dt}, \quad \frac{1}{T}\frac{d\Delta_{ij}^3}{dt}, \\ \frac{\left(\mu_\varsigma^1 - \mu_\varsigma^2\right)}{T}, \quad \frac{\left(\mu_\varsigma^3 - \mu_\varsigma^2\right)}{T}, \quad -\frac{\Lambda_j}{T}. \tag{6.19}$$

Assuming linear relationship among thermodynamics fluxes $\bar{q}$, $\sigma_{ij}^{(\alpha)}$, Q_ζ^e, Q_ζ, J_j and thermodynamic forces, we have

$$q_i = -W_{ij}\frac{\partial T}{\partial x_j}, \tag{6.20}$$

$$\sigma_{kl}^1 = E_{ijkl}\varepsilon_{ij}, \tag{6.21}$$

$$\sigma_{kl}^2 = B_{ijkl}\frac{d\Delta_{ij}^2}{dt} + B_{klij}^*\frac{d\Delta_{ij}^3}{dt} + \sum_{\beta=1}^{r} D_{\beta kl}^*\Lambda_\beta - \\ -\sum_{\alpha=1}^{n} O_{\alpha kl}^*\left(\mu_\alpha^1 - \mu_\alpha^2\right) - \sum_{\alpha=1}^{n} Y_{\alpha kl}^*\left(\mu_\alpha^3 - \mu_\alpha^2\right), \tag{6.22}$$

$$\sigma_{ij}^3 = B_{ijkl}^*\frac{d\Delta_{ij}^2}{dt} + B_{ijkl}\frac{d\Delta_{ij}^3}{dt} + \sum_{\beta=1}^{r} D_{\beta ij}^*\Lambda_\beta - \\ -\sum_{\alpha=1}^{n} O_{\alpha kl}^*\left(\mu_\alpha^1 - \mu_\alpha^2\right) - \sum_{\alpha=1}^{n} V_{\alpha kl}^*\left(\mu_\alpha^3 - \mu_\alpha^2\right), \tag{6.23}$$

$$J_\beta = D_{\beta ij}\frac{d\Delta_{ij}^2}{dt} + D_{\beta kl}^*\frac{d\Delta_{ij}^2}{dt} - \sum_{\gamma=1}^{r} {}^1 l_{\beta\gamma}\Lambda_\beta + \\ +\sum_{\alpha=1}^{n} {}^2 l_{\alpha\beta}\left(\mu_\alpha^1 - \mu_\alpha^2\right) + \sum_{\alpha=1}^{n} {}^3 l_{\alpha\beta}\left(\mu_\alpha^3 - \mu_\alpha^2\right), \tag{6.24}$$

$$Q_\alpha = O_{\alpha ij}\frac{d\Delta_{ij}^2}{dt} + O_{\alpha kl}^*\frac{d\Delta_{ij}^3}{dt} - \sum_{\beta=1}^{r} {}^2 l_{\alpha\beta}\Lambda_\beta + \\ +\sum_{\beta=1}^{n} {}^4 l_{\alpha\beta}\left(\mu_\beta^1 - \mu_\beta^2\right) + \sum_{\gamma=1}^{n} {}^5 l_{\beta\gamma}\left(\mu_\gamma^3 - \mu_\gamma^2\right), \tag{6.25}$$

$$Q_n{}^e = Y_{nij}\frac{d\Delta_{ij}^2}{dt} + Y_{nkl}^*\frac{d\Delta_{ij}^3}{dt} - \sum_{\beta=1}^{r} {}^3 l_{n\beta}\Lambda_\beta + \\ +\sum_{\alpha=1}^{n} {}^5 l_{n\alpha}\left(\mu_\alpha^1 - \mu_\alpha^2\right) - \sum_{\alpha=1}^{n} {}^6 l_{n\alpha}\left(\mu_\alpha^3 - \mu_\alpha^2\right). \tag{6.26}$$

Here ${}^m l_{n\alpha,n\beta,\alpha\beta,\beta\gamma}$ ($m = \overline{1,6}$) are scalars, $B_{ijkl}^{(*)}, E_{ijkl}$, $D_{nij}^{(*)}$, $Y_{\alpha ij}^{(*)}$, $O_{\alpha ij}^{(*)}$, W_{ij} are the parameters of tensorial nature. They satisfy the Onsager reciprocal relations

$$B_{ijkl}^{(*)} = B_{klij}^{(*)}, \quad D_{nij}^* = -D_{nij}, \quad W_{ji} = W_{ij},$$
$$V_{\alpha ij}^* = -V_{\alpha ij}, \quad O_{\alpha ij}^* = -O_{\alpha ij}, \quad {}^m l_{n\alpha,n\beta,\alpha\beta,\beta\gamma} = {}^m l_{\alpha n,\beta n,\beta\alpha,\gamma\beta}.$$

For example, assuming that the tissue is transversely anisotropic, then B_{ijkl}, D_{nij} are defined by

$$B_{ikjl} = \lambda_1\left(\delta_{ik}\delta_{jl} + \delta_{il}\delta_{jk} - \tfrac{2}{3}\delta_{ij}\delta_{kl}\right) + \lambda_2\left(\delta_{ij}b_{kl} + \delta_{kl}b_{ij} - \tfrac{1}{3}\delta_{ij}\delta_{kl} - 3b_{ij}b_{kl}\right) + \\ +\lambda_3\left(\delta_{ik}b_{jl} + \delta_{jk}b_{il} + \delta_{il}b_{jk} + \delta_{jl}b_{ik} - 4b_{ij}b_{kl}\right)$$
$$D_{nij} = D_n\left(\delta_{ij} - 3b_{ij}\right) \quad (n = 1, 2, \ldots, r).$$

Multiple experimental data on uniaxial and biaxial loading show that collagen and elastin fibers possess nonlinear elastic and muscle tissue—viscoelastic characteristics. Hence, for stresses we have

$$\sigma_{ij} = \sum_{\alpha=1}^{3} \sigma_{ij}^{\alpha} = c^1 E_{ijkl}\varepsilon_{kl} + c^2 E_{ijkl}^{\nu e}\left(\varepsilon_{kl} - \Delta_{kl}^2\right) + c^3 E_{ijkl}^{\nu e}\left(\varepsilon_{kl} - \Delta_{kl}^3\right), \tag{6.27}$$

where $E_{ijkl}^{\nu e}$ is the tensor of viscous characteristics ($E_{ijkl}^{\nu e} = E_{klij}^{\nu e}$). Differentiating Eq. (6.27) with respect to time, the constitutive relations of the mechanochemically active biological tissue are found to be

$$\begin{aligned}
&B_{klij}^{*}\underline{E}_{ijmn}^{\nu e}\frac{d\sigma_{kl}}{dt} + \left(\mathbf{I} - \frac{1}{c^3}B_{klij}^{*}\underline{E}_{ijmn}^{\nu e}\frac{dc^3}{dt}\right)\sigma_{kl} = c^1 E_{ijmn}\varepsilon_{ij} - \\
&\quad - \left(\frac{c^1}{c^3}B_{klij}^{*}\underline{E}_{ijmn}^{\nu e}E_{mnkl}\frac{dc^3}{dt} + B_{klij}^{*}\underline{E}_{ijmn}^{\nu e}E_{mnkl}\frac{dc^1}{dt}\right)\varepsilon_{mn} - \\
&\quad - \frac{c^2}{c^3}B_{klij}^{*}\frac{dc^3}{dt}\varepsilon_{mn} + B_{ijmn}^{*}\left(c^1\underline{E}_{ijkl}^{\nu e}E_{klmn} + c^2 + c^3\right)\frac{d\varepsilon_{ij}}{dt} - \\
&\quad - B_{ijmn}^{*}\left(\frac{dc^2}{dt} - \frac{c^2 dc^3}{c^3\, dt}\right)\frac{d\Delta_{ij}^2}{dt} + c^2 Z_{mn} + c^3 Z_{mn}^{*},
\end{aligned}$$

$$B_{ijmn}^{*}\underline{E}_{ijkl}^{ve}\frac{d\Delta^2{}_{kl}}{dt} - \varsigma_{mn}^2 + \underline{E}^{ve}{}_{ijmn}Z_{ij} = 0,$$

$$B_{ijmn}^{*}\underline{E}_{ijkl}^{ve}\frac{d\Delta_{kl}^3}{dt} - \varsigma_{mn}^3 + \underline{E}^{ve}{}_{ijmn}Z_{ij}^{*} = 0,$$

$$\begin{aligned}
c^2\frac{dZ_{mn}}{dt} &= B_{mnij}^{\mathrm{T}}\frac{d\Delta^3{}_{ij}}{dt} + \sum_{\beta=1}^{r} D_{\beta mn}^{*}\Lambda_{\beta} - \sum_{\alpha=1}^{n} O_{\alpha mn}^{*}\left(\mu_{\alpha}^1 - \mu_{\alpha}^2\right) - \\
&\quad - \sum_{\alpha=1}^{n} Y_{\alpha mn}^{*}\left(\mu_{\alpha}^3 - \mu_{\alpha}^2\right), \\
c^3\frac{dZ_{mn}^{*}}{dt} &= B_{mnij}\frac{d\Delta_{ij}^2}{dt} + \sum_{\beta=1}^{r} D_{\beta mn}\Lambda_{\beta} - \sum_{\alpha=1}^{n} O_{\alpha mn}\left(\mu_{\alpha}^1 - \mu_{\alpha}^2\right) - \\
&\quad - \sum_{\alpha=1}^{n} Y_{\alpha mn}\left(\mu_{\alpha}^3 - \mu_{\alpha}^2\right), \\
&\left(\mathbf{B}^{\mathrm{T}} = \mathbf{B}\right).
\end{aligned} \tag{6.28}$$

Here $\underline{\mathbf{E}}$ is the tensor inverse to $\mathbf{E}$ ($\underline{\mathbf{E}}\mathbf{E} = \mathbf{I}$), $\mathbf{I}$ is the identity tensor, Z_{ij}^{*} is the "biofactor" that accounts for various biological phenomena including electromechanical, chemical, remodeling, aging, etc in the tissue.

Although the system of Eqs. (6.28) describes the mechanics of biocomposites, it does not provide required relationships between in-plane forces, moments and deformations in the thin shell. To establish the missing link, consider the distribution of ε_{ik}^{z} and stresses σ_{ik} $(i, k = 1, 2, 3)$ in the shell. Recalling the first Kirchhoff-Love geometric hypothesis, $\varepsilon_{13}^{z} = \varepsilon_{23}^{z} = 0$, it would be appealing to exclude the shear stresses and lateral forces from the equilibrium equations by neglecting the terms $\sigma_{13} = \sigma_{23} = 0$, $N_1^{*} = N_2 = 0^{*}$. However, it would strongly violate the equilibrium conditions. Accepting the second Kirchhoff-Love hypothesis, which states that the normal stress σ_{33} is significantly smaller compared to σ_{ij} $(i, k = 1, 2)$, we can eliminate only the terms containing σ_{33}. Then, Eqs. (6.28) take the form

$$
\begin{aligned}
B_{klij}^{*}\underline{E}_{ijmn}^{ve}\frac{d\sigma_{kl}}{dt}+\left(\mathbf{I}-\frac{1}{c^3}B_{klij}^{*}\underline{E}_{ijmn}^{ve}\frac{dc^3}{dt}\right)\sigma_{kl} &= c^1\underline{E}_{ijmn}^{ve}\varepsilon_{ij}^{z}- \\
-B_{klij}^{*}\underline{E}^{ve}{}_{ijmn}E_{mnkl}\left(\frac{c^1dc^3}{c^3\,dt}+\frac{dc^1}{dt}\right)\varepsilon_{mn}^{z}- & \\
-\frac{c^2}{c^3}B_{klij}^{*}\frac{dc^3}{dt}\varepsilon^{z}{}_{mn}+B_{ijmn}^{*}\left(c^1\underline{E}^{ve}{}_{ijkl}E_{klmn}+c^2+c^3\right)\frac{d\varepsilon^{z}{}_{ij}}{dt}- & \\
-B_{ijmn}^{*}\left(\frac{dc^2}{dt}-\frac{c^2dc^3}{c^3\,dt}\right)\frac{d\Delta_{ij}^{z2}}{dt}+c^2Z_{mn}+c^3Z_{mn}^{*}, &
\end{aligned}
$$

$$
B_{ijmn}^{*}\underline{E}^{ve}{}_{ijkl}\frac{d\Delta_{kl}^{z2}}{dt}-\varsigma_{mn}^{z2}+\underline{E}^{ve}{}_{ijmn}Z_{ij}=0,
$$

$$
B_{ijmn}^{*}\underline{E}^{ve}{}_{ijkl}\frac{d\Delta_{kl}^{z3}}{dt}-\varsigma_{mn}^{z3}+\underline{E}^{ve}{}_{ijmn}Z_{ij}^{*}=0,
$$

$$
\begin{aligned}
c^2\frac{dZ_{mn}}{dt} &= B_{ijmn}^{\mathrm{T}}\frac{d\Delta_{ij}^{z3}}{dt}+\sum_{\beta=1}^{r}D_{\beta mn}^{*}\Lambda_{\beta}-\sum_{\alpha=1}^{n}O_{\alpha mn}^{*}\left(\mu_{\alpha}^{1}-\mu_{\alpha}^{2}\right)- \\
&\quad -\sum_{\alpha=1}^{n}Y_{\alpha mn}^{*}\left(\mu_{\alpha}^{3}-\mu_{\alpha}^{2}\right), \\
c^3\frac{dZ_{mn}^{*}}{dt} &= B_{mnij}\frac{d\Delta_{ij}^{z2}}{dt}+\sum_{\beta=1}^{r}D_{\beta mn}\Lambda_{\beta}-\sum_{\alpha=1}^{n}O_{\alpha mn}\left(\mu_{\alpha}^{1}-\mu_{\alpha}^{2}\right)- \\
&\quad -\sum_{\alpha=1}^{n}Y_{\alpha mn}\left(\mu_{\alpha}^{3}-\mu_{\alpha}^{2}\right).
\end{aligned}
\tag{6.29}
$$

Finally, substituting ε_{ik}^{z} given by Eq. (6.14) and solving the resultant equations for σ_{11}, σ_{22}, and σ_{12}, we obtain constitutive relations for the mechanochemically active biocomposite in terms of deformations, curvature and twist of the middle

surface of the shell. Applying σ_{ik} in Eqs. (3.25) and integrating it over the thickness of the shell, we find explicit relations for the in-plane forces T^*_{ij} and moments M^*_{ij}. In general, the end formulas are very bulky and are not given here. In applications though, depending on a specific tissue, the formulas can be simplified to a certain degree and even take an elegant form.

6.2 Biological Factor

Consider smooth muscle syncytia to be electrically excitable biological medium (Plonsey and Barr 1984). Applying Ohm's law we have

$$\bar{J}_i = -\left(\hat{g}_{i1}\frac{\partial \Psi_i}{\partial x_1}\bar{e}_1 + \hat{g}_{i2}\frac{\partial \Psi_i}{\partial x_2}\bar{e}_2\right), \tag{6.30}$$

$$\bar{J}_o = -\left(\hat{g}_{o1}\frac{\partial \Psi_o}{\partial x_1}\bar{e}_1 + \hat{g}_{o2}\frac{\partial \Psi_o}{\partial x_2}\bar{e}_2\right), \tag{6.31}$$

where $\bar{J}_i, \bar{J}_o$ are the intra- (i) and extracellular (o) currents, Ψ_i, Ψ_o are the scalar electrical potentials, $\hat{g}_{ij}, \hat{g}_{oj}$ ($j = 1, 2$) are the conductivities, and $\bar{e}_1, \bar{e}_2$ are the unit vectors in the directions of α_1, α_2 coordinate lines. Both cellular spaces are coupled through the transmembrane current I_{m1} and potential V_m as

$$I_{m1} = -\mathrm{div}\bar{J}_i = \mathrm{div}\bar{J}_o, \tag{6.32}$$

$$V_m = \Psi_i - \Psi_o. \tag{6.33}$$

Substituting Eqs. (6.30, 6.31) into (6.32), we get

$$I_{m1} = \hat{g}_{i1}\frac{\partial^2 \Psi_i}{\partial \alpha_1^2}\bar{e}_1 + \hat{g}_{i2}\frac{\partial^2 \Psi_i}{\partial \alpha_2^2}\bar{e}_2, \tag{6.34}$$

$$I_{m1} = -\hat{g}_{o1}\frac{\partial^2 \Psi_o}{\partial \alpha_1^2}\bar{e}_1 + \hat{g}_{o2}\frac{\partial^2 \Psi_o}{\partial \alpha_2^2}\bar{e}_2. \tag{6.35}$$

Equating Eqs. (6.34) and (6.35), we find

$$(\hat{g}_{i1} + \hat{g}_{o1})\frac{\partial^2 \Psi_i}{\partial \alpha_1^2} + (\hat{g}_{i2} + \hat{g}_{o2})\frac{\partial^2 \Psi_i}{\partial \alpha_2^2} = \hat{g}_{o1}\frac{\partial^2 V_m}{\partial \alpha_1^2} + \hat{g}_{o2}\frac{\partial^2 V_m}{\partial \alpha_2^2}. \tag{6.36}$$

Solving Eq. (6.36) for Ψ_i, we obtain

$$\Psi_i = \frac{1}{4\pi}\iint\left(\frac{\hat{g}_{o1}}{\hat{g}_{i1}+\hat{g}_{o1}}\frac{\partial^2 V_m}{\partial X'^2}+\frac{\hat{g}_{o2}}{\hat{g}_{i2}+\hat{g}_{o2}}\frac{\partial^2 V_m}{\partial Y'^2}\right)+ \\ +\left[\log\left((X-X')^2+(Y-Y')^2\right)\right]dX'dY',$$

where the following substitutions are used: $X=\alpha_1/\sqrt{g_{i1}+g_{o1}}$, $Y=\alpha_2/\sqrt{\hat{g}_{i2}+\hat{g}_{o2}}$. Here the integration variables are primed, and the unprimed variables indicate the space point (α_1', α_2') at which Ψ_i is evaluated. The reverse substitutions of X and Y gives

$$\Psi_i = \frac{1}{4\pi}\iint\left(\hat{g}_{o1}\frac{\partial^2 V_m}{\partial X'^2}+\hat{g}_{o2}\frac{\partial^2 V_m}{\partial Y'^2}\right)+ \\ +\left[\log\left(\frac{\left(\alpha_1-\alpha_1'\right)^2}{\hat{g}_{i1}+\hat{g}_{o1}}+\frac{\left(\alpha_2-\alpha_2'\right)^2}{\hat{g}_{i2}+\hat{g}_{o2}}\right)\right]\frac{d\alpha_1' d\alpha_2'}{\sqrt{(\hat{g}_{i1}+\hat{g}_{o1})(\hat{g}_{i2}+\hat{g}_{o2})}} \tag{6.37}$$

Introducing Eq. (6.37) into (6.34), after some algebra we obtain

$$I_{m1} = \frac{\widetilde{\mu}_1-\widetilde{\mu}_2}{2\pi G(1+\widetilde{\mu}_1)(1+\widetilde{\mu}_2)}\iint\left(\hat{g}_{o1}\frac{\partial^2 V_m}{\partial X'^2}+\hat{g}_{o2}\frac{\partial^2 V_m}{\partial Y'^2}\right)\times \\ \times\left[\left(\frac{\left(\alpha_1-\alpha_1'\right)^2}{G_1}-\frac{\left(\alpha_2-\alpha_2'\right)^2}{G_2}\right)\Big/\left(\frac{\left(\alpha_1-\alpha_1'\right)^2}{G_1}+\frac{\left(\alpha_2-\alpha_2'\right)^2}{G_2}\right)^2\right]d\alpha_1' d\alpha_2', \tag{6.38}$$

here

$$G_1=\hat{g}_{i1}+\hat{g}_{o1},\quad G_2=\hat{g}_{i2}+\hat{g}_{o2},$$
$$G=\sqrt{G_1G_2},\quad \widetilde{\mu}_1=\hat{g}_{o1}/\hat{g}_{i1},\quad \widetilde{\mu}_2=\hat{g}_{o2}/\hat{g}_{i2}.$$

Substituting Eq. (6.37) into (6.34), we find the contribution of an ε-neighborhood of $(\alpha_1'=0, \alpha_2'=0)$ to I_{m1}. Using the transformations given by $X=\alpha_1/\sqrt{\hat{g}_{i1}}$, $Y=\alpha_2/\sqrt{\hat{g}_{i2}}$, we find

$$I_{m2} = \frac{\sqrt{\hat{g}_{i1}\hat{g}_{i2}}}{4\pi G}\left(\hat{g}_{o1}\frac{\partial^2 V_m}{\partial X'^2}+\hat{g}_{o2}\frac{\partial^2 V_m}{\partial Y'^2}\right)_{\alpha_1'=\alpha_2'=0}\times \\ \times\int \text{divgrad}\left[\log\left(\frac{X'^2}{G_1/\hat{g}_{i1}}+\frac{Y'^2}{G_2/\hat{g}_{i2}}\right)\right]d\alpha_1' d\alpha_2'. \tag{6.39}$$

Applying the divergence theorem and performing the gradient operation, the integral in Eq. (6.39) is converted to a line integral

$$\int \frac{\left(2X^{'}\hat{g}_{i1}/G_1\right)\bar{e}_1 + \left(2Y^{'}\hat{g}_{i2}/G_2\right)\bar{e}_2}{\left(X^{'2}\hat{g}_{i1}/G_1\right) + \left(Y^{'2}\hat{g}_{i2}/G_2\right)} \cdot \bar{n}dC^{'}, \tag{6.40}$$

where $dC^{'}$ is an element of the ε-contour. The result of integration yields

$$I_{m2} = \left(\hat{g}_{o1}\frac{\partial^2 V_m}{\partial \alpha_1^{'2}} + \hat{g}_{o2}\frac{\partial^2 V_m}{\partial \alpha_2^{'2}}\right)\left(\frac{\hat{g}_{i2}}{G_2} + \frac{2(\widetilde{\mu}_1 - \widetilde{\mu}_2)}{\pi(1+\widetilde{\mu}_1)(1+\widetilde{\mu}_2)}\tan^{-1}\sqrt{\frac{G_1}{G_2}}\right) \tag{6.41}$$

To simulate the excitation and propagation pattern in the anisotropic smooth muscle syncytium we employ the Hodgkin-Huxley formalism described by

$$C_m\frac{\partial V_m}{\partial t} = -(I_{m1} + I_{m2} + I_{ion}),$$

where C_m is the membrane capacitance, I_{ion} is the total ion current through the membrane. Substituting expressions for I_{m1} and I_{m2} given by Eqs. (6.38, 6.41), we obtain

$$\begin{aligned} C_m\frac{\partial V_m}{\partial t} = &-\frac{\widetilde{\mu}_1 - \widetilde{\mu}_2}{2\pi G(1+\widetilde{\mu}_1)(1+\widetilde{\mu}_2)}\iint\left(\hat{g}_{o1}\frac{\partial^2 V_m}{\partial X^{'2}} + \hat{g}_{o2}\frac{\partial^2 V_m}{\partial Y^{'2}}\right)\times \\ &\times\left[\left(\frac{\left(\alpha_1 - \alpha_1^{'}\right)^2}{G_1} - \frac{\left(\alpha_2 - \alpha_2^{'}\right)^2}{G_2}\right)\Big/\left(\frac{\left(\alpha_1 - \alpha_1^{'}\right)^2}{G_1} + \frac{\left(\alpha_2 - \alpha_2^{'}\right)^2}{G_2}\right)^2\right]d\alpha_1^{'}d\alpha_2^{'} - \\ &-\left(\hat{g}_{o1}\frac{\partial^2 V_m}{\partial \alpha_1^{'2}} + \hat{g}_{o2}\frac{\partial^2 V_m}{\partial \alpha_2^{'2}}\right)\left(\frac{\hat{g}_{i2}}{G_2} + \frac{2(\widetilde{\mu}_1 - \widetilde{\mu}_2)}{\pi(1+\widetilde{\mu}_1)(1+\widetilde{\mu}_2)}\tan^{-1}\sqrt{\frac{G_1}{G_2}}\right) - I_{ion}, \end{aligned} \tag{6.42}$$

where I_{ion} is the function depending on the type and ion channel properties of the biological tissue.

In the case of electrical isotropy, $\widetilde{\mu}_1 = \widetilde{\mu}_2 = \widetilde{\mu}$, the integral in Eq. (6.42) vanishes and we get

$$C_m\frac{\partial V_m}{\partial t} = -\frac{1}{(1+\widetilde{\mu})}\left(\hat{g}_{o1}\frac{\partial^2 V_m}{\partial \alpha_1^2} + \hat{g}_{o2}\frac{\partial^2 V_m}{\partial \alpha_2^2}\right) - I_{ion}. \tag{6.43}$$

Finally, the constitutive relations of mechanochemically active electrogenic biological medium include Eqs. (6.6)–6.8), (6.29), (6.42) and/or (6.43). The system is closed by providing the free energy, ion currents, initial and boundary conditions, and the function $Z_{ij} = Z_{ij}\left(V_m, \mu_i, \hat{g}_{ij}, \hat{g}_{oj}\right)$. It is noteworthy that the closed system of

equations describes the development of stresses in absence of active strains and *vice versa*, a condition which is unique to all biological materials.

Models are generally evaluated for the degree of parameters and constants involved as well as for their accurate and meaningful experimental determination. While phenomenological constitutive models are able to fit the experimental data with a high degree of accuracy, they are limited in that they do not give the insight into the underlying cause to the particulars of mechanical behavior. Fine molecular and structure-based models help avoid such ambiguities and are able to reveal the intricacies of functions of tissues.

6.3 Constitutive Relations for the Human Gastric Tissue

6.3.1 Uniaxial Tensile Characteristics

The mechanical properties of the wall of the stomach are highly specific and depend on the topographical site, food, environmental factors and age. In vitro uniaxial tension tests conducted in the directions of three structurally anisotropic axis, i.e. along the orientation of the longitudinal, circumferential and oblique smooth muscle layers, on specimens collected from different regions of the organ of males aged 20–50 years, convincingly demonstrate that the tissue has nonlinear, viscoelastic properties (Miftakhov 1981, 1983a) (Fig. 6.3). Since the experiments were performed on segments removed from the host, it was assumed that the muscle fibers were fully relaxed and the mechanical contribution was attributed to mechanochemically inert components of smooth muscle cells along with elastin and collagen fibers. To describe it quantitatively, the total force in the tissue can be decoupled into the passive and active component

$$T = T^p(\lambda_1, \lambda_2, c_0, \ldots, c_6) + T^a\left(\lambda_1, \lambda_2, Z_{mn}^{(*)}, \left[Ca^{2+}\right], c_7, \ldots, c_{11}\right), \tag{6.44}$$

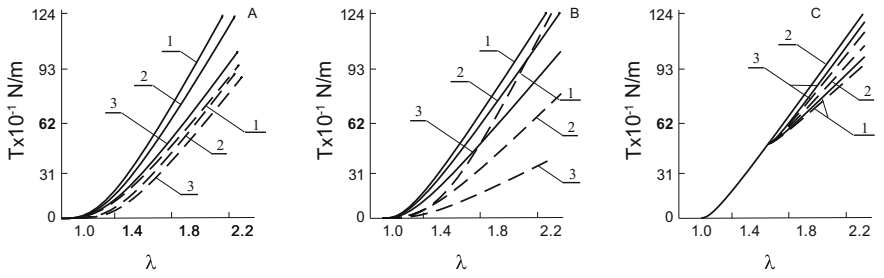

Fig. 6.3 Experimental force-stretch ratio curves of the human gastric tissue under uniaxial loading along the morphostructural axi of anisotropy. 1: longitudinal, $T_l(\lambda_l)$; 2: circumferential, $T_c(\lambda_c)$; 3: oblique, $T_o(\lambda_o)$. A: specimens from the age group of 20–29 years; B: 30–39 years; C: 40–49 years. *Solid lines* refer to the anterior and *dashed* to the posterior wall of the organ

where $c_0, \ldots, c_{11}$ are empirically estimated material constants of the tissue, $Z_{mn}^{(*)}$ is the "biofactor", $[Ca^{2+}]$ is the concentration of intracellular calcium.

Assuming the homogeneity of the stress-strain field and the incompressibility of the tissue, the force and stretch ratios were calculated. Analysis of the force-stretch ratio curves (T^p-λ) showed that the tissue was compliant at low levels of stretching, $1.0 < \lambda \leq 1.2$, with the force values varying $T^p \sim 0 \div 3.8{\cdot}10$ mN/cm, followed by a highly nonlinear transitory state, $1.2 < \lambda \leq 1.6$ and $T^p \sim 3.8 \cdot 10 \div 3.77 \cdot 10^2$ mN/cm. At greater levels of stretching $1.6 < \lambda \leq 2.4$ specimens demonstrated pure linear elastic behavior. The response remains characteristic for the tissue of the anterior and posterior walls of the stomach across all age groups. It should be noted that the posterior wall is the more compliant throughout the entire range of stretching. This is more prominent for $1.0 < \lambda \leq 1.2$ when the force T_{ant}^p exceeds the values of T_{post}^p by 40–50%.

Comparison of experimental curves obtained from different regions of the organ confirms the property of transverse curvilinear anisotropy. Age related changes of mechanical properties along the axis of anisotropy are uneven. Thus, the tissue is stiff longitudinally in the age group 20–39 years, while in the older group, 40–49 years, the wall becomes stiffer circumferentially. It is noteworthy that while insignificant differences between the loading and unloading curves are present due to "biological hysteresis", the force-stretch ration responses are independent of the stretching rate.

In general the wall of the stomach is stronger and more compliant longitudinally and obliquely rather than circumferentially. Thus, the maximum loads the tissue can withstand before rupture are: $\max T_l^p = 1.434 \cdot 10^3 \pm 5.34 \cdot 10^2$ mN/cm—the posterior wall (group II), $\max T_c^p = 1.176 \times 10^3 \pm 1.81 \times 10^2$ mN/cm—the anterior wall (group I), and $\max T_o^p = 1.29 \times 10^3 \pm 1.81 \times 10^2$ mN/cm—the anterior wall (group I). These values decrease by 29% with age, from group I through group III (Table 6.1). Interestingly, the posterior wall is weaker compared with the anterior wall. In both directions the ultimate stretch ratios are similar $\max\lambda \simeq 2.4 \pm 0.1$ (Miftakhov 1983b).[1]

The uniaxial force-stretch ratio approximation of experimental data in the preferred axes of structural anisotropy yields

$$T_{c,l}^p = \begin{cases} 0, & \lambda_{c,l} \leq 1.2 \\ c_0\left[c_1 + c_2\left(\lambda_{c,l}^{\alpha} - 1\right)\right], & \lambda_{c,l} > 1.2 \end{cases} \tag{6.45}$$

Here $c_0 = 15.1$ mN/cm and the values of other constants are given in Table 6.2.

[1]Recent experimental findings of investigations of the human cadaveric stomach under uniaxial quasistatic and volumetric dynamic loadings (Egorov et al. 2002; Saraf et al. 2007; Rosen et al. 2008; Lim et al. 2009) simply reaffirm the results first recorded by the author.

Table 6.1 Maximal forces and stretch ratios values for the human stomach

Age group	Axis	Anterior wall		Posterior wall	
		max$T$ (mN/cm)·10^2	maxλ	max$T$ (mN/cm)·10^2	maxλ
I	l	16.91 ± 4.48	2.4 ± 0.2	10.30 ± 3.04	2.4 ± 0.1
	c	11.76 ± 1.81	2.4 ± 0.2	9.68 ± 1.58	2.4 ± 0.2
	o	12.90 ± 1.81	2.4 ± 0.2	10.38 ± 1.61	2.4 ± 0.2
II	l	14.03 ± 2.69	2.4 ± 0.1	14.34 ± 5.34	2.4 ± 0.1
	c	10.61 ± 2.46	2.3 ± 0.1	11.68 ± 4.49	2.3 ± 0.2
	o	12.11 ± 3.61	2.3 ± 0.1	9.99 ± 2.19	2.4 ± 0.1
III	l	9.57 ± 2.81	2.3 ± 0.1	9.15 ± 2.99	2.2 ± 0.1
	c	8.99 ± 2.46	2.2 ± 0.1	8.81 ± 2.99	2.3 ± 0.1
	o	9.07 ± 1.27	2.3 ± 0.3	11.68 ± 2.46	2.2 ± 0.2

Here age group distribution—I: 20–29 years, II: 30–39 years, III: 40–49 years; and the corresponding directions of anisotropy: l—longitudinal, c—circumferential, o—oblique

Table 6.2 Empirical constants for uniaxial $T^p_{c,l}(\lambda_{c,l})$ function

Age group	Axis	Anterior wall			Posterior wall		
Constants		α	c_1	c_2	α	c_1	c_2
I	l	0.47	−4.27	57.05	0.7	−17.31	131.15
	c	0.68	−14.61	123.15	0.65	−10.71	95.2
	o	0.55	−5.46	74.26	0.6	−9.48	84.68
II	l	0.72	−13.52	164.82	0.3	0.86	24.92
	c	0.62	−7.13	84.53	0.93	−83.2	451.87
	o	0.97	−94.55	474.95	1.2	−141.91	564.34
III	l	1.16	−306.99	1205.64	0.39	3.08	29.69
	c	0.66	−5.45	112.55	1.1	−181.45	913.16
	o	0.66	−8.76	132.25	0.67	−11.68	131.26

Abbreviations and notations are as in Table 6.1

6.3.2 *Histomorphological Analysis of Changes in the Tissue During Uniaxial Loading*

Microscopic analysis of the dynamics of crack nucleation and crack growth within the wall of the stomach reveals that the first small randomly oriented cracks occur along the cell contacts in the mucosal and submucosal layers at $1.1 < \lambda_l \leq 1.3$ and $T^p_l \sim 20 \div 30$ mN/cm (Miftakhov 1981; Miftahof and Nam 2010). They align perpendicular to the axis of the applied force. Uncurling and reorientation of collagen and elastin fibers occur in the submucosal layer. SMCs behave passively.

Collagen and elastin fibers become fully straightened at $\lambda_l = 1.4 \div 1.5$ and $T^p_l = 120 \div 135$ mN/cm. There is a loosening in the dense packaging of the fibrillary matrix with the development of multiple small fractures of elastin fibers. Significant damage appears in mucosa at $\lambda_l = 1.4$ with development of a fracture growing

outside the thickness of the wall. The total rupture of the mucosal layer occurs at $\lambda_{l} = 1.5$, $T_l^p \sim 130$ mN/cm.

At $\lambda_{l} \sim 1.5$ and $T_l^p = 350 \div 435$ mN/cm the fully unfolded collagen fibers bear the main stretch load, while SMCs begin to slide against each other. Small pores, areas of nucleation, start to develop in the stressed muscle layer. These grow into multiple cracks that steadily increase in size, and at $\lambda_l \sim 1.8 \div 2$, $T_l^p = 650 \div 700$ mN/cm, finally, form a structural defect. Further extension to the levels of $\max\lambda_l \sim 2.2 \div 2.4$ leads to the fragmentation and multiple rupture of collagen fibers and the disintegration of smooth muscle elements.

6.3.3 Biaxial Tensile Characteristics

The biaxial tests conducted on square-shaped tissue specimens collected from different regions of the human stomach reveal the full in-plane mechanical properties of the wall of the organ (Miftakhov 1983c, 1985). The edges of the specimens are aligned parallel and perpendicular to the orientation of the longitudinal and circular smooth muscle fibers which define the principal axis of transverse anisotropy. The experimental protocol to obtain quasistatic force-stretch ratio curves use constant stretch ratios of $\lambda_l : \lambda_c$. The tissue under biaxial loading exhibits a complex response including nonlinear elasticity, transverse anisotropy, finite deformability, with no dependence on the stretch rate (Fig. 6.4). The curves $T^p_{c,l}(\lambda_{c,}\, \lambda_l)$ show that as the stretch ratio λ_c increases gradually from 1 to 1.4, the extensibility along λ_l decreases from 1.9 to 1.5. The biomaterial is stiffer longitudinally: for $1.0 < \lambda_l < 1.3$ the intensity of $T_l\,(\lambda_{l,}\, 1.4) > T_l\,(\lambda_{l,}\, 1.2)$ by 50–100%. For $\lambda_{c,l} > 1.4$ and $1 \leq \lambda_{l,c} \leq 1.6$ the force-stretch ratio curves display

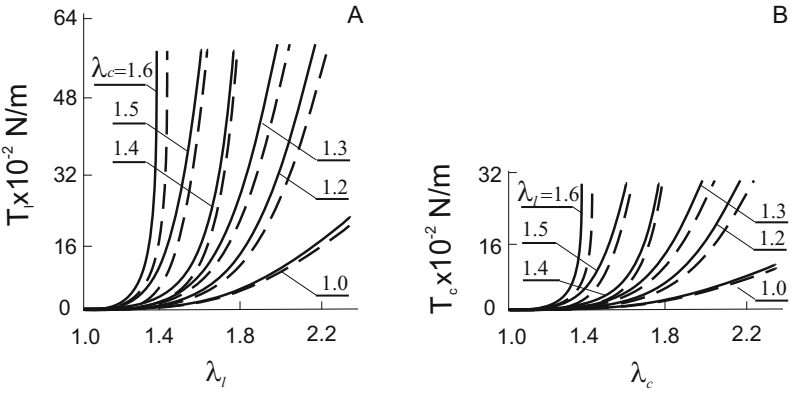

Fig. 6.4 Characteristic experimental biaxial force-stretch ratio curves $T_i(\lambda_l,\lambda_c)$ $(i = l, c)$ of the human gastric tissue for the age group 20–29 years. (**a**): $1.0 \leq \lambda_l \leq 1.6, \lambda_c = \text{const}$; (**b**): $1.0 \leq \lambda_c \leq 1.6, \lambda_l = \text{const}$. *Solid lines* refer to the anterior and *dashed* to the posterior wall of the organ

linear relationships. The maximum force the tissue bears during the biaxial tests is $\max T_{c,l}\ (\lambda_c,\ \lambda_l) = 2200 \pm 180$ mN/cm and $\max\lambda_{c,l} = 1.5 - 2.3$ which depends on the ratio $\lambda_l{:}\lambda_c$. The tissue of the posterior wall of the organ is more compliant and withstands lower maximal forces of rupture when compared with the anterior wall. Experiments show that the shear force applied to specimens is less than $(\max T^p_{c,l})\cdot 10^{-2}$ relative to the axial stretch force.

Results for different age groups (I-III) show an overall decrease in deformability and $\max T^p_{c,l}$ on average by 50%.

The in-plane passive T^p_i forces under biaxial loading are approximated by

$$T^p_{l(c)} = \lambda_l^{\alpha 1}\lambda_c^{\alpha 2}\tilde{c}_0 \exp\left(c_3 + c_4\lambda_l^2 + c_5\lambda_c^2 + c_6\lambda_l\lambda_c\right), \tag{6.46}$$

where $\tilde{c}_0 = 19.6$ mN/cm and the values of other constants are given in Table 6.3.

The ECM is an integral and dynamic component of a biological material. Macromolecular compositions and structural architectures of the matrix are tissue specific and are strongly influenced by the biomechanical forces under which they operate. The fibrillary collagen-elastin network provides the dominant response for applied forces. The human stomach wall under uniaxial and biaxial quasistatic stretching exhibits a characteristic nonlinear "triphasic" behavior with a transition between the low and high elastic states. The region of small λ $(1.0 \leq \lambda \leq 1.2)$

Table 6.3 Empirical constants for biaxial $T^p_{l(c)}(\lambda_l, \lambda_c)$ functions

		Anterior wall		Posterior wall	
Age group	Axis	$\lambda_c = \text{const}$	$\lambda_l = \text{const}$	$\lambda_c = \text{const}$	$\lambda_l = \text{const}$
I	$\alpha 1$	−2.71	4.49	−3.19	2.59
	$\alpha 2$	4.84	31.3	−13.53	−3.91
	c_3	−1.96	4.22	−5.74	−1.79
	c_4	−0.61	0.96	−0.22	0.49
	c_5	−1.9	−5.17	3.53	2.56
	c_6	6.22	−1.07	5.54	0.89
II	$\alpha 1$	1.88	1.79	0.62	2.98
	$\alpha 2$	25.47	14.57	22.39	30.18
	c_3	1.51	0.36	1.99	3.38
	c_4	1.24	1.28	0.16	1.52
	c_5	−4.24	−1.67	−5.73	−5.63
	c_6	0.8	0.49	4.25	0.03
III	$\alpha 1$	3.61	2.01	−4.66	4.26
	$\alpha 2$	23.96	9.29	−13.61	23.54
	c_3	3.65	−0.23	−5.24	1.98
	c_4	−0.59	1.96	−0.36	2.68
	c_5	−4.99	−0.08	2.81	−2.26
	c_6	2.45	0.66	6.47	−3.08

Here $\lambda_{c,l} = \text{const}$ applies that the fixed parameter attains constant values $1.2 \leq \lambda_{c,l} \leq 1.6$

structurally corresponds to the removal of a crimp in the collagen first at the fibrillar, and then at the molecular levels. The great compliance of the tissue at this stage could be ascribed to the presence of α–smooth muscle actin on SMC and calponin on collagen fibers (Nguyen et al. 2016). In the linear elastic region of deformation, $\lambda \geq 1.4$, the stiffness of the biocomposite increases considerably. This process is concomitant with the extension of the collagen triple helices and the cross-links between them. The deformation disrupts the repulsive forces on the negatively charged GAGs and destabilizes the matrix-fiber interaction. The densely packed network loosens, allowing macro-structural reorientation and alignment of the fibers—the change in the weaving angle at the interlocking nodes—along the applied stretch forces.

The observed age related differences in biomechanical properties of the human gastric tissue are endorsed by changes in pH, electrolyte concentration, free radicals, acetylation, etc. However, these questions are beyond the scope of this book.

6.3.4 Active Forces

Investigations into uniaxial and biaxial mechanical properties of actively contracting tissue remain a challenging area in biomechanics. At the time of writing, there is no experimental data available on in-plane active behavior of the wall of the human stomach. The main problem is to keep specimens physiologically viable and stable, i.e., for in vitro samples to reproduce myoelectrical patterns that are consistent with those observed in vivo. Thus, it is practically impossible to sustain and to control simultaneously slow wave spiking and contractile activity of smooth muscle syncytia.

Current theories of motility of the gastrointestinal tract suggest that there are reciprocal mechanical relationships between the longitudinal and circular muscle syncytia. Such coordination leads to generation of propagating peristaltic waves, in contrast to non-propagating spastic type of activity which is a result of simultaneous contraction of both muscle syncytia. This fact, together with the fine fibrillar structure of the smooth muscle, suggests that active forces are produced only in preferred directions, either longitudinal or circumferential, and as such can be characterized in full by uniaxial tests. Furthermore, constructive modeling requires formulation of the excitation-contraction coupling phenomenon that provides a link between electrical events and muscle mechanics. The contractile apparatus of myocytes consists of thin-actin and thick-myosin filaments, a family of special proteins and kinases, e.g., light chain myosin, tropomyosin, calmodulin, *h*–caldesmon, calponin, myosin light chain kinase and myosin phosphatase. Actin filaments are single helical coils of actin associated with tropomyosin and caldesmon. Myosin filaments are made out of two coil rod–like structure heavy chains with a globular head domain. The key player in the dynamics of the transformation of microscopic properties of electrical excitatory events into

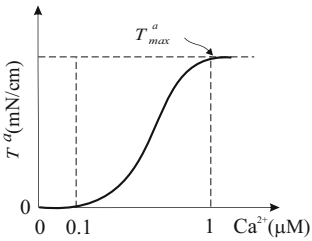

Fig. 6.5 A typical active force-intracellular calcium relation curve, $T^a_{l,c}\left[Ca_i^{2+}\right]$, for smooth muscle

macroscopic contractions is free intracellular Ca^{2+}. Although many details of this process have become established within the last decade, a convincing experimental correlation between ultrastructural changes and force development has not been clarified yet.

As an approximation of the excitation-contraction phenomenon we adopt the experimental active force—intracellular Ca^{2+} relationship given by (Fig. 6.5)

$$T^a_{c,l} = \begin{cases} 0, & \left[Ca_i{}^{2+}\right] \le 0.1\ \mu M \\ c_7 + c_8\left[Ca_i{}^{2+}\right]^4 + c_9\left[Ca_i{}^{2+}\right]^3 + c_{10}\left[Ca_i{}^{2+}\right]^2 + c_{11}\left[Ca_i{}^{2+}\right], & 0.1 < \left[Ca_i{}^{2+}\right] \le 1\mu M \\ \max T^a, & \left[Ca_i{}^{2+}\right] > 1\mu M \end{cases} \tag{6.47}$$

where $\left[Ca_i^{2+}\right]$ is the intracellular concentration of calcium ions.

References

Egorov VI, Schastlivtsev IV, Prut EV, Baranov AO, Turusov RA (2002) Mechanical properties of the human gastrointestinal tract. J Biomech 35(10):1417–1425. doi:10.1016/S0021-9290(02)00084-2

Lim Y-J, Deo D, Singh TP, Jones DB, De S (2009) In situ measurement and modeling of biomechanical response of human cadaveric soft tissues for physics-based surgical simulation. Surg Endosc 23(6):1298–1307

Miftakhov RN (1981) Micromechanics of tissue fracture in uniaxial elongation. In: Shells Interactions with Fluids. Academy of Sciences of the USSR, Moscow, pp 205–214

Miftakhov RN (1983a) Experimental and numerical investigations of soft shells. PhD thesis, Kazan State University, Kazan

Miftakhov RN (1983b) Investigation of the human stomach tissue in uniaxial loading. In: Hydroelasticity of shells. Academy of Sciences of the USSR, Moscow, pp 163–171

Miftakhov RN (1983c) Experimental investigations of the stomach under complex loading. In: Hydroelasticity of shells. Academy of Sciences of the USSR, Moscow, pp 172–181

Miftakhov RN (1985) Experimental investigation of the stomach tissue in biaxial loading. In: Invest on theory of plates and shells Kazan University Press, Kazan, pp 35–46

Miftahof RN, Nam HG (2010) Mathematical foundations and biomechanics of the digestive system. Cambridge University Press, Cambridge

Nguyen T-U, Bashur CA, Kishore V (2016) Impact of elastin incorporation into electrochemically aligned collagen fibers in mechanical properties and smooth muscle cell phenotype. Biomed Mater. doi:10.1088/1748-6041/11/2/025008

Nikitin NL (1980) A model of the muscle tissue with alternating number of contracting fibers. Mech Compos Mater 1:113–120

Plonsey RL, Barr RG (1984) Current flow patterns in two-dimensional anisotropic bisyncytia with normal and extreme conductivities. Biophys J 43:557–571

Rosen J, Brown JD, De S, Sinanan M, Hannaford B (2008) Biomechanical properties of abdominal organs in vivo and postmortem under compression loads. J Biomech Eng. doi:10.1115/1.2898712

Saraf H, Ramesh KT, Lennon AM, Merkle AC, Roberts JC (2007) Mechanical properties of soft human tissues under dynamic loading. J Biomech 40(9):1960–1967

Chapter 7
Signal Transduction Mechanisms

The enchanting charms of this sublime science reveal only to those who have courage to go deeply into it.
Carl Friedrich Gauss

7.1 Biological Preliminaries

"Little Brain"—the enteric nervous system (ENS)—of the human stomach is comprised of a large number of neurons, 46,260 ± 3.829 (neurons/cm^2) (Mandić et al. 2016). Formed by a population of vagal and truncal derived neural crest multipotent stem cells (NCSCs), neurons colonize the organ in a rostral-caudal progression. They group together to form morphofunctional units known as ganglia. These ganglia are diverse in terms of their number, morphology, size and the number of neurons they contain. The density of ganglia distribution is not constant, i.e. it is relatively sparse in the fundus of the stomach and denser in the antrum and pylorus. Quantitative analysis reveals that an average ganglion is formed of 3.4–5.4 neurons that are spread over a surface area of $(1.8 \pm 0.3) \times 10^2$ mm^2 (Knowles et al. 2011). Most of the cells possess two major morphological forms—Dogiel type I and II—uniaxonal and multiaxonal respectively, although bipolar, ovoid, polygonal or stellar shapes have also been described. The actual size of matured neurons ranges within $(29.6 \pm 2.25) \times 10$ μm^2 (Mandić et al. 2016).

Maturation and differentiation of distinct neurons is an asynchronous and heterogenous process. Three major groups of molecules have been suggested as regulating the NCSCs' proliferation and survival: transmembrane tyrosine kinase—glial cell line-derived neurotrophic factor, endothelin-3-G protein-coupled receptor complex, and transcription factors such as *Sox*10 and *Phox*2b. Throughout the dynamics of intricate processes which are poorly understood, it is believed that they control the neurogenesis of the ENS (Sasselli et al. 2012; Metzger 2010; Gariepy 2001).

Immunoreactivity for neurotransmitters and the expression of pan-neuronal markers changes throughout growth with the full spectrum of gastric chemical coding developing only after birth. The exact pathways involved still remain unclear. There is experimental evidence though to suggest that overexpression of

R.N. Miftahof, *Biomechanics of the Human Stomach*,
DOI 10.1007/978-3-319-59677-8_7

the glial cell line-derived neurotrophic factor in postmitotic cells, bone morphogenic proteins, Mash1, a basic helix-loop-helix transcription factor, along with other synthetic enzymes, e.g., tyrosine hydroxylase, catecholamine, dopamine-β-hydroxylase, choline acetyltransferase, gives rise to distinct cell lineage (Wang et al. 2010; Blaugrund et al. 1996; Chalazonitis et al. 2008).

Immunohistochemical studies have demonstrated that matured neuronal cells in the ENS can co-localize multiple neurotransmitters and/or modulators (Nusbaum et al. 2001; Merighi, 2002; Pimont et al. 2003; Burnstock, 2004; Trudeau and Gutiérrez, 2007; Teschemacher and Christopher 2008). A quantitative analysis of co-localization in the fundus of the human stomach shows that 8.3 ± 3.1% of all neurons are positive both for ACh and SP, 4.9 ± 12.6%—ACh/VIP, 3.1 ± 1.8%—ACh/NO, 3.1 ± 1.8%—ACh/NO/VIP, and 1.1 ± 0.7%—ACh/NO/VIP/SP (Pimont et al. 2003). Such coexistence suggests that cells may simultaneously release more than one substrate and that co-transmission may take place. The phenomenon is ubiquitous and is therefore considered the rule rather than the exception. Indeed, the co-release of neurotransmitters—ACh, 5-HT, NO, SP, galanin, enkephaline, glutamate, γ-amino butyric acid, dopamine—and peptides—vasoactive intestinal peptide (VIP), calcitonin gene-related peptide, adenosine triphosphate (ATP)—has been recorded in the human stomach (Miller et al. 2001; Belai and Burnstock 2000; Anlauf et al. 2003). The process is highly regulated in response to various physiological, chemical and pathological signals. However, the exact mechanisms and how these occur remains an open question that has not, so far, been addressed in detail.

A class of interstitial cells of Cajal (ICC) and platelet-derived growth factor receptor α cells (PDGFRα^+) that are distinct in their origin, phenotype, morphology and ultrastructure, are present within smooth muscle syncytia of the human stomach. Deriving embryologically from the mesencymal lineage, they possess typical features attributed either to primitive smooth muscle or the "fibroblast-like" interstitial cells (Young 1999; Sanders et al. 2014). The recent advance in antibody labeling has shown that only cells expressing the gene product of *c-Kit*, a proto-oncogene that encrypts a tyrosine kinase receptor (Kit), differentiate and mature into ICC. However, no specific markers for PDGFRα^+ precursor cells have been identified. The roles of location, stem cell factor and pathology, amongst others which may be responsible for the development of a Kit-positive precursor into a functional ICC or a SMC, remain to be discovered.

The appearance of precursor ICC follows strongly after colonization of the stomach by neurons from NCSCs. Functional immunochemical studies on matured ICC have confirmed: (i) the presence of soluble guanylate cyclase, the physiological receptor for NO, (ii) the translocation of PKC isozymes from the cytoplasm to the membrane in response to cholinergic stimulation and activation of μ_2 and μ_3, receptors, and anoctamin-1 (ANO1), Ca^{2+}-activated Cl^- channel, (iii) the internalization of NK_1 and NK_3 receptors after the application of exogenous SP; (iv) the presence of VIP receptors as well as non-selective cation channels TRP4 and TRP6 (Southwell et al. 1996; Vannucchi and Faussone-Pellegrini 1997; Huber et al. 1998; Lavin et al. 1998; Epperson et al. 2000; Kim et al. 2003; Wang et al. 2003; Iino et al.

2004; Kito 2011; Zhu et al. 2011; Zhang et al. 2011). Currently there is no strong functional evidence to support the hypothesis of the involvement of P2X, P2Y and $VPAC_{1/2}$ receptors in signal transduction on ICC (Lecci et al. 2002). Additionally, L-, and possibly T-type, Ca^{2+} as well as tetrodotoxin-insensitive Na^{+} transmembrane ion channels have been implemented in mechanosensitivity of ICC in response to applied axial/shear stretches and positive/negative pressures (Kraichely and Farrugi 2007). PDGFRα^{+} cells have P2Y1 receptors and SK3 channels, suggesting these cells are purinergic mediators of ATP, ADP and β-nicotinamide adenine dinucleotide.

7.2 System Compartmentalization

Neurohormonal modulation and electromechanical coupling in ganglia and smooth muscle syncytia involve a cascade of chemical processes including synthesis, storage, stimulation, release, diffusion and binding of various substrates to specific receptors with activation of intracellular second messenger systems and the generation of a variety of physiological responses. Qualitative analysis and quantitative evaluation of each and every step experimentally is very difficult, and sometimes practically impossible. Therefore, different classes of mathematical models of modulation and synaptic neurotransmission, ranging from the most comprehensive "integrated"—microphysiological—to "reductionist"—deterministic—have been proposed to study intricacies of the processes of neuroendocrine regulations. A microphysiological approach attempts to reproduce reality in great detail leading to mathematically challenging and computationally demanding tasks. By contrast, deterministic models aim to capture accurately phenomenological behavior of the system. They not only provide macroscopic explanation of complex biophysical processes, but are general enough to offer a coherent description of essential biochemical reactions within the unified framework. These models are inherently flexible and can accommodate spatiotemporal and structural interactions into a tractable representation.

Let a synapse (neuronal or neuromuscular) be an open three compartmental system. Compartment 1 comprises presynaptic elements where synthesis and storage of a neurotransmitter occurs. For example, in the case of cholinergic or adrenergic synapses it corresponds morphologically to a nerve terminal of the unmyelinated axon; for substance P, it is comprised of the endoplasmic reticulum, the Golgi apparatus and the membrane transport system for exocytotic release and large dense core vesicles for storage, and for serotonin)—enterochromaffin cells.

Ligands, i.e. acetylcholine, adrenalin, 5-HT, SP, etc, are released upon neural stimulation by exocytosis to the synaptic cleft and bloodstream. The common sequence of events involved in the dynamics of their transduction includes:

(i) depolarization of the nerve terminal or cell membrane;
(ii) influx of extracellular calcium through voltage-gated Ca^{2+} channels;

(iii) binding of free cytosolic Ca_i^{2+} to transmitter-containing vesicles;
(iv) release of vesicular/granular stored ligand, L_v, into the synaptic cleft.

Propagation of the wave of depolarization, V, in the nerve terminal is accurately described by the modified Hodgkin–Huxley system of equations (Miftahof et al. 2009)

$$C_m^f \frac{\partial V}{\partial t} = \frac{1}{2R_a^f} \frac{\partial}{\partial \alpha}\left(d_f^2(\alpha)\frac{\partial V}{\partial \alpha}\right) - \left(I_{Na}^f + I_K^f + I_{Cl}^f\right), \tag{7.1}$$

$$d_f(\alpha) = \begin{cases} d_f, & L^s < \alpha \le L^s - L^s{}_0 \\ 2d_f & \alpha > L^s - L^s{}_0, \ \ t > 0, \quad \alpha \in (0, L^s). \end{cases}$$

Here $L^s{}_0$ is the length of the synaptic terminal, and the meaning of other parameters and constants is as described above. The above ion currents are defined by

$$\begin{aligned} I_{Na}^f &= g_{Na}^f m_f^3 h_f (V - V_{Na}) \\ I_K^f &= g_K^f n_f^4 h_f (V - V_K) \\ I_{Cl}^f &= g_{Cl}^f (V - V_{Cl}), \end{aligned} \tag{7.2}$$

where $g_{Na}^f, g_K^f, g_{Cl}^f$ are the maximal conductances for Na^+, K^+ and Cl^- currents, respectively, V_{Na}, V_K, V_{Cl} are the equilibrium potentials for the respective ion currents, and m_f, n_f, h_f are the state variables that are calculated from

$$\mathrm{d}y/\mathrm{d}t = \alpha_y(1 - y) - \beta_y y \quad y = \left(m_f, n_f, h_f\right). \tag{7.3}$$

The activation, α_y, and deactivation, β_y, parameters satisfy the following empirical relations

$$\begin{aligned} \alpha_{m,f} &= \frac{0.1T(2.5 - V)}{\exp(2.5 - 0.1V)} \\ \beta_{m,f} &= 4T\exp(-V/18) \\ \alpha_{h,f} &= 0.07T\exp(-0.05V) \\ \beta_{h,f} &= T/(1 + \exp(3 - 0.1V)) \\ \alpha_{n,f} &= \frac{0.1T(10 - V)}{\exp(1 - 0.1V) - 1} \\ \beta_{n,f} &= 0.125T\exp(-0.125V). \end{aligned} \tag{7.4}$$

Here T is temperature.

The cytosolic calcium turnover is given by

$$\frac{d\left[Ca_i^{2+}\right]}{dt} = g_{syn}^{Ca} V(t)\left[Ca_0^{2+}\right] - k_b\left[Ca_i^{2+}\right], \tag{7.5}$$

where g_{syn}^{Ca} is the conductivity of the voltage-gated Ca^{2+}-channel at the synaptic end, k_b is the intracellular buffer system constant.

Finally, the release of a stored fraction of the ligand, L_v, is described by the state diagram

$$\frac{d[X_2]}{dt} = -k_0[X_1][X_2], \tag{7.6}$$

Here $X_1 := \left[Ca_i^{2+}\right], X_2 := [L_v]$ are concentrations of the cytosolic Ca^{2+} and vesicular stored ligand, respectively, k_0 is the rate constant of association of Ca_i^{2+} with calcium-dependent centers on the vesicles, k_1 is the diffusion constant.

At $t = 0$ the nerve axon and the synapse are assumed to be at the resting state and the concentrations of reacting components are known

$$m_f(0) = m_{f,0} \quad h_f(0) = h_{f,0}, \quad n_f(0) = n_{f,0}, \quad V(0,\alpha) = 0, \quad L_v(0) = L_{v,0}. \tag{7.7}$$

The synapse is excited at the free end ($\alpha = 0$) by the electric impulse of an amplitude $\overset{0}{V}{}^f$ and a duration t^d, and the presynaptic terminal end ($\alpha = L$) remains unexcited throughout.

$$V(0,t) = \begin{cases} \overset{0}{V}, & 0 < t < t^d \\ 0, & t \geq t^d \end{cases}, V(L,t) = 0. \tag{7.8}$$

Assume that the dynamics of release of SP satisfy

$$\frac{d[SP_i]}{dt} = \frac{B_{\text{tr}}([SP_i] - [SP_{\text{o}}])}{K_{\text{tr}} + [SP_i]}, \quad SP_i(0) = SP_{i0} \tag{7.9}$$

Here B_{tr}, K_{tr} are the parameters that are referred to the process of exocytosis $[SP]_{i,\text{o}}$ are the concentrations of SP inside (subscript i) and outside (o) the cell.

Upon their release, neurotransmitters and hormones passively diffuse through the synaptic cleft (compartment 2) towards the postsynaptic membrane. The synaptic cleft across many synaptic types has the width of ≈12–20 nm. It contains N-cadherin, adhesion molecules, microtubules organized in periodic transsynaptic complexes and roughly regular patches. Their function is only beginning to be understood (Yamagata et al. 2003).

Compartment 3—the postsynaptic membrane—contains a complex network of surface membrane proteins which modulate the transmission. It involves the following processes:

(v) binding of free ligand in the cleft, L_c, to the G-protein coupled receptor, R, and its conformational change, $L_c \cdot R$;
(vi) active configuration of the receptor, R^*, (the $L_c \cdot R^*$ reactive complex is able to produce a biological effect, i.e. the postsynaptic potential, V_{syn});

(vii) binding of $L_c \cdot R^*$ to G protein, the formation of the $L_c \cdot R^* \cdot G$—complex and the initiation of guanosine diphosphate/guanosine triphosphate (GDP/GTP) exchange;
(viii) the dissociation of G protein α and $\beta\gamma$ subunits with the subsequent release of G_{act} protein that interacts with downstream effector pathways;
(ix) enzymatic, E, clearance of the excess of L_c in the synaptic cleft through the formation of intermediate complexes, $L_c \cdot E$ and ES, and the final metabolite, S.

They are described by the following state diagram (Fig. 7.2).

Here $k_{\pm i}$ are the forward $(+i)$ and backward $(-i)$ rate constants of chemical reactions, $\mathrm{C}_j\left(j = \overline{1,4}\right)$ are the intermediate complexes, and the meaning of other parameters as described above.

Assuming that:

(i) the distribution of reactive substrates is uniform throughout and no chemical gradients exist;
(ii) the total enzyme concentration does not change over time, $E_0 = \text{constant}$;
(iii) the total ligand concentration is much larger than the total enzyme concentration;
(iv) no product is present at the beginning of the reaction, and
(v) the maximum rate of chemical reaction occurs when the enzyme is saturated, i.e. all enzyme molecules are tied up with a substrate,

then all reactions are of the first order and satisfy the Michaelis–Menten kinetics. Hence the system of equations for the ligand conversion is given by

$$d\mathbf{X}/\mathrm{d}t = \mathbf{A}\mathbf{X}(t), \tag{7.10}$$

where the vector $\mathbf{X}(t) = \left(X_j\right)^{\mathrm{T}}\left(j = \overline{1,20}\right)$ has the components

$$\begin{array}{llll} X_1 = \left[\mathrm{Ca}_i^{2+}\right], & X_2 = [L_v], & X_3 = \left[L_v \cdot \mathrm{Ca}_i^{2+}\right], & X_4 = [L_c], \\ X_5 = [R], & X_6 = \left[R^*\right], & X_7 = \left[L_c \cdot R^*\right], & X_8 = [L_c \cdot R], \\ X_9 = \left[L_c \cdot R^* \cdot G\right], & X_{10} = \left[R^* \cdot G\right], & X_{11} = [A_c \cdot E], & X_{12} = [G], \\ X_{13} = [C_1], & X_{14} = [C_2], & X_{15} = [C_3], & X_{16} = [C_4], \\ X_{17} = \left[G'\right], & X_{18} = [G_{act}], & X_{19} = [ES], & X_{20} = [S]. \end{array}$$

The matrix $\mathbf{A}\left(a_{ij}\right)\ \left(i,j = \overline{1,20}\right)$ has the non-zero elements

$$\begin{array}{ll} a_{11} = g_{syn}^{Ca} V^f(t)\left[\mathrm{Ca}_0^{2+}\right], & a_{12} = -k_0[X_1], \\ a_{13} = k_{-0} & a_{22} = -k_0[X_1], \\ a_{23} = k_{-0} & a_{32} = k_0[X_1], \\ a_{33} = -(k_{-0} + k_1), & a_{43} = k_1, \\ a_{44} = k_2([E_0] - [X_8]) + k_6[X_5] + k_{-8}[X_6] + k_{-11}[X_{10}], & \end{array}$$

$$a_{47} = k_8, \qquad a_{48} = k_{-6},$$
$$a_{49} = k_{11}, \qquad a_{4,11} = k_{-2},$$
$$a_{55} = -(k_{-5} + k_6)[X_4], \qquad a_{56} = k_5[X_{12}],$$
$$a_{58} = k_{-6}, \qquad a_{65} = k_{-5},$$
$$a_{66} = -k_{-8}[X_4] - (k_5 + k_{-10}k_{19}[X_{18}])[X_{12}],$$
$$a_{67} = k_8[X_{12}], \qquad a_{6,10} = k_{10},$$
$$a_{6,16} = k_{17}, \qquad a_{76} = k_{-8}[X_4],$$
$$a_{77} = -(k_{-7} + k_8 + k_9)k_{19}[X_{12}][X_{18}],$$
$$a_{78} = k_7, \qquad a_{79} = k_{-9}k_{12}[X_{40}],$$
$$a_{7,14} = k_{16}, \qquad a_{85} = k_6[X_4],$$
$$a_{87} = k_{-7}[X_{12}], \qquad a_{88} = -k_{-6} - k_7,$$
$$a_{97} = k_9k_{19}[X_{12}][X_{18}], \qquad a_{99} = -k_{-9} - k_{11} - k_{12}[X_{40}],$$
$$a_{9,10} = k_{-11}[X_4], \qquad a_{10,6} = k_{-10}[X_{12}],$$
$$a_{10,9} = k_{11}, \qquad a_{10,10} = -(k_{10} + k_{-11})[X_4] - k_{13}[X_{40}],$$
$$a_{11,4} = k_2([X_{41}] - [X_8]), \qquad a_{11,11} = -(k_{-2} + k_3),$$
$$a_{11,19} = k_3, \qquad a_{12,6} = k_{-5} + k_{-8}[X_4],$$
$$a_{12,8} = k_7 \qquad a_{12,9} = k_{-9},$$
$$a_{12,12} = -(k_5 + k_{-10}k_{19}[X_{18}])[X_6] - (k_{-7} + k_8 + k_9k_{19}[X_{18}])[X_7],$$
$$a_{12,10} = k_{10}, \qquad a_{13,9} = k_{12}[X_{40}],$$
$$a_{13,13} = -k_{14}[X_{39}], \qquad a_{13,14} = k_{-14},$$
$$a_{14,13} = k_{14}[X_{39}], \qquad a_{14,14} = -(k_{-14} + k_{16}),$$
$$a_{15,10} = k_{13}[X_{40}], \qquad a_{15,15} = -k_{15}[X_{39}],$$
$$a_{15,16} = k_{-15}, \qquad a_{16,15} = k_{15}[X_{39}],$$
$$a_{16,16} = -(k_{17} + k_{-15}), \qquad a_{17,14} = k_{16},$$
$$a_{17,16} = k_{17}, \qquad a_{17,17} = -k_{18},$$
$$a_{18,17} = k_{18}, \qquad a_{18,18} = -k_{19},$$
$$a_{19,11} = k_3, \qquad a_{19,19} = -(k_{-3} + k_4),$$
$$a_{19,20} = k_{-4}([X_{41}] - [X_8]), \qquad a_{20,19} = k_4,$$
$$a_{20,20} = -k_{-4}([X_{41}] - [X_8]).$$

Here $[X_{39}], [X_{40}], [X_{41}]$ are given concentrations of *GTP*, *GDP* and *E* enzymes, respectively. In case of SP its release is described by Eq. (7.9).

The generation of the excitatory/inhibitory postsynaptic potential, $V_{syn}^{(+,-)}$, is given by Miftahof et al. (2009)

$$C_p \frac{dV_{syn}^{(+,-)}}{dt} + V_{syn}\left(\mp\Omega[X_9] + R_v^{-1}\right) = \frac{V_{syn,0}}{R_v}, \tag{7.11}$$

where C_p is the capacitance of the postsynaptic membrane, R_v is the resistance of the synaptic structures, Ω is the empirical constant, $V_{syn,0}$ is the resting postsynaptic potential.

Given the concentrations of reacting components and the state of the synapse

$$\mathbf{X}(0) = \mathbf{X}_0, \quad V_{syn} = 0, \tag{7.12}$$

Equations (7.1)–(7.12) provide mathematical formulation of the dynamics of the common pathway of neurotransmission at the synaptic site.

The quantitative assessment of the velocities of reactions shows that the rates, k_{12}, k_{13}, of exchange of G protein for GDP at $L_c \cdot R^* \cdot G$ and $R^* \cdot G$ sites, respectively, are significantly smaller compared to the rates of other reactions. Hence, the system (Figs. 7.1 and 7.2) can be viewed as a combination of rapid equilibrium segments interconnected through slow, rate-limiting steps. The characteristic feature of such

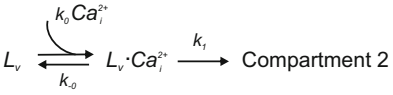

Fig. 7.1 The state diagram of a transmitter release from the presynaptic terminal

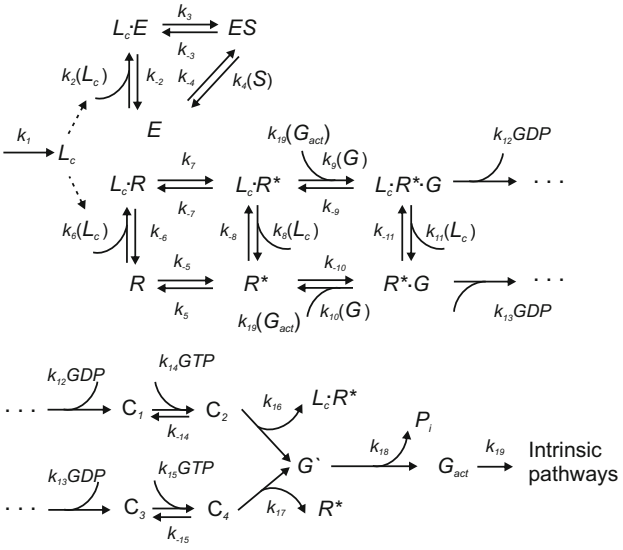

Fig. 7.2 The state diagram of a transmitter conversion at the postsynaptic membrane

system is that it attains the steady state when the rapid segment has already reached quasi-equilibrium. This fact allows us to simplify the system (Eq. 7.19) as follows.

Let $\tilde{f}_1$ and $\tilde{f}_2$ be the fractional concentration factors of the rapid segment "product"-substrates

$$\tilde{f}_1 = [X_9]/[Y], \quad \tilde{f}_2 = [X_{10}]/[Y], \tag{7.13}$$

where Y is

$$[Y] = [X_9] + [X_{10}] + [X_{12}].$$

Define the association constant as

$$K_1 = \frac{[X_6][X_{12}]}{[X_{10}]}, \quad K_2 = \frac{[X_4][X_{10}]}{[X_9]},$$
$$K_3 = \frac{[X_7][X_{10}]}{[X_9]}, \quad K_4 = \frac{[X_4][X_6]}{[X_9]},$$

after simple algebra, for $\tilde{f}_1$,we have

$$\tilde{f}_1 = \frac{\frac{[X_4][X_6]}{K_1K_2}}{1 + \frac{[X_4][X_6]}{K_1K_2} + \frac{[X_6]}{K_1}} = \frac{[X_4][X_6]}{K_1K_2 + [X_6]([X_4] + K_2)},$$

$$\tilde{f}_2 = \frac{\frac{[X_6]}{K_1}}{1 + \frac{[X_4][X_6]}{K_1K_2} + \frac{[X_6]}{K_1}} = \frac{K_2[X_6]}{K_{10}K_{11} + [X_6]([X_4] + K_2)}. \tag{7.14}$$

Then, concentration distribution equations for the main reactants can be obtained in the form (for details see King and Altman 1956; Cha 1968)

$$(D)\frac{[Y]}{[Y']} = k_{14}k_{15}k_{16}k_{17}k_{18}k_{19}[X_{39}]^2$$

$$(D)\frac{[X_{13}]}{[Y']} = k_{12}k_{15}k_{17}k_{18}k_{19}\tilde{f}_1[X_{39}](k_{-14} + k_{16})$$

$$(D)\frac{[X_{14}]}{[Y']} = k_{12}k_{14}k_{15}k_{17}k_{18}k_{19}\tilde{f}_1[X_{39}]^2$$

$$(D)\frac{[X_{15}]}{[Y']} = k_{11}k_{14}k_{16}k_{18}k_{19}\tilde{f}_2[X_{39}](k_{-15} + k_{17})$$

$$(D)\frac{[X_{16}]}{[Y]} = k_{11}k_{14}k_{15}k_{16}k_{18}k_{19}\tilde{f}_2[X_{39}]^2$$

$$(D)\frac{[X_{17}]}{[Y']} = k_{14}k_{15}k_{16}k_{17}\tilde{f}_2[X_{39}]^2\left(k_{12}\tilde{f}_1 + k_{11}\tilde{f}2\right) \tag{7.15}$$

where

$$\left[Y'\right] = [Y] + [X_{13}] + [X_{14}] + [X_{15}] + [X_{16}] + [X_{17}],$$

and D is the sum of all the values on the right side of Eqs. (7.15). Note that Eqs. (7.15) are algebraic equations. The initial velocity equation for Y complexes formation is given by

$$d[Y]/\mathrm{d}t = k_{18}k_{19}[X_{17}]. \tag{7.16}$$

Finally, substituting X_{17} from Eq. (7.15) and making use of Eqs. (7.14) we arrive at

$$\frac{1}{[Y']}\frac{d[Y]}{dt} = \frac{k_{14}k_{15}k_{16}k_{17}k_{18}k_{19}[X_{39}]^2\left[\frac{k_{12}\frac{[X_4][X_6]}{K_1K_2}+k_{11}\frac{[X_6]}{K_1}}{1+\frac{[X_4][X_6]}{K_1K_2}+\frac{[X_6]}{K_1}}\right]}{\left\{\begin{array}{l} k_{14}k_{15}k_{16}k_{17}k_{18}k_{19}[X_{39}]^2+ \\ k_{12}k_{15}k_{17}k_{18}k_{19}[X_{39}](k_{-14}+k_{16})\left[\frac{\frac{[X_4][X_6]}{K_1K_2}}{1+\frac{[X_4][X_6]}{K_1K_2}+\frac{[X_6]}{K_1}}\right]+ \\ +k_{12}k_{14}k_{15}k_{17}k_{18}k_{19}[X_{39}]^2\left[\frac{\frac{[X_4][X_6]}{K_1K_2}}{1+\frac{[X_4][X_6]}{K_1K_2}+\frac{[X_6]}{K_1}}\right]+ \\ +k_{14}k_{15}k_{16}k_{17}[X_{39}]^2\left[\frac{k_{12}\frac{[X_4][X_6]}{K_1K_2}+k_{11}\frac{[X_6]}{K_1}}{1+\frac{[X_4][X_6]}{K_1K_2}+\frac{[X_6]}{K_1}}\right]+ \\ +k_{11}k_{14}k_{15}k_{16}k_{18}k_{19}[X_{39}]^2\left[\frac{\frac{[X_6]}{K_1}}{1+\frac{[X_4][X_6]}{K_1K_2}+\frac{[X_6]}{K_1}}\right]+ \\ +k_{11}k_{14}k_{16}k_{18}k_{19}[X_{39}](k_{-15}+k_{17})\left[\frac{\frac{[X_6]}{K_1}}{1+\frac{[X_4][X_6]}{K_1K_2}+\frac{[X_6]}{K_1}}\right] \end{array}\right\}},$$

or, after some algebraic rearrangements, in the form

$$\frac{1}{[Y']}\frac{d[Y]}{dt} = \frac{k_{14}k_{15}k_{16}k_{17}k_{18}k_{19}[X_{39}][k_{12}[X_4]+k_{11}K_2]}{\left\{\begin{array}{l}[X_4][X_{39}]k_{14}k_{15}k_{17}[k_{16}k_{18}k_{19}+k_{12}k_{18}k_{19}+k_{12}k_{16}]+\\ +[X_{39}]k_{14}k_{15}k_{16}K_2\left[k_{17}k_{18}k_{19}\left(1+\frac{K_1}{[X_6]}\right)+k_{11}k_{17}+k_{11}k_{18}k_{19}\right]+\\ [X_4][k_{12}k_{15}k_{17}k_{18}k_{19}(k_{-14}+k_{16})]+k_{11}k_{14}k_{16}k_{18}k_{19}K_2(k_{-15}+k_{17})\end{array}\right\}}. \tag{7.17}$$

Both of the mathematical formulations, i.e. the system of differential equations (7.10) or a simplified model given by Eq. (7.17), supplemented with initial and boundary conditions, provide a detailed description of electrochemical coupling at a synapse. In practice, the preference for either of them depends on the intended application and is entirely the researcher's choice.

7.3 cAMP-Dependent Pathway

The activated $G\alpha_{q11/12/13}$ alpha subunit can bind to and activate the adenylyl cyclase (AC) enzymes. A diversity of ACs isoforms have been identified and their expression provides a mechanism for integrating the responses to various neurotransmitters both positively and negatively. Thus, the same stimulus may trigger different physiological responses in gastric smooth muscle depending not only on the type of receptors involved, but also on the type of adenylyl cyclase to which they are coupled.

The proposed structure of AC consists of a short amino terminal region and two cytoplasmic domains. The latter are separated by two extremely hydrophobic domains which take the form of six transmembrane helices. The catalytic core of the enzyme consists of a pseudosymmetric heterodimer composed of two highly conserved portions of the cytoplasmic domains. It binds one molecule of $G\alpha_{i-q}$ which, in turn, catalyzes the conversion of ATP into cyclic adenosine monophosphate. cAMP influences a wide range of physiological effects including: (i) the increase in Ca^{2+} channel conductance, (ii) the activation of protein kinase C (PKC) and protein kinase A (PKA) enzymes, (iii) the regulation of GDP-GTP exchange factor (Rho-GEF), RhoA and RhoK kinases.

Protein kinase C enzymes comprise a family of 11 isoenzymes that are divided into three subfamilies—conventional, novel, and atypical—based on their second messenger requirements for activation. Conventional PKCs ($\alpha,\beta_1,\beta_2,\gamma$) require free Ca_i^{2+}, 1,2-diacylglycerol (DAG), and a phospholipid; novel PKCs ($\delta,\varepsilon,\eta,\theta,\mu$) need only DAG, and atypical PKCs (ζ,ι,λ) require none of them for activation.

PKCs consist of a variable regulatory and a highly conserved catalytic domain, tethered together by a hinge region. The regulatory domain contains two subregions, namely C1 and C2. The C1 subregion has a binding site for DAG and phorbol esters and C2 subregion acts as a Ca^{2+} sensor and is functional only in

PKCs α, β_1, β_2 and γ. Upon their activation, kinases are translocated to the plasma membrane by RACK proteins where they remain active for a long period of time. The effect is attributed to the property of diacyglycerol per se. Binding of cAMP to the regulatory subunit causes the release of catalytic subunits and the transfer of ATP terminal phosphates to PKC-potentiated inhibitory protein (CPI-17) at T38 which, in turn, inhibits the catalytic subunit of myosin light chain phosphatase (MLCP). The result is an increase in the affinity of MLCK for the calcium-calmodulin complex and smooth muscle contraction.

Protein kinase A is a holoenzyme that consists of two regulatory and two catalytic subunits. Binding of cAMP to the two binding sites on the regulatory subunits causes the release of the catalytic subunits and the transfer of ATP terminal phosphates to myosin light chain kinase. The result is a decrease in the affinity of MLCK for the calcium-calmodulin complex and SM relaxation. Additionally, PKA may promote relaxation by inhibiting phospholipase C, intracellular Ca^{2+} entry, and by activating BK_{Ca} channels and calcium pumps. PKA activity is controlled entirely by cAMP. Under low levels of cAMP, it remains intact and catalytically inactive.

The level of cAMP is regulated both by the activity of adenylyl cyclase and by phosphodiesterases (PDEs) that degrade it to 5′-AMP. At least 11 families of PDE isoenzymes are identified. Their hydrolytic activity is determined by the catalytic domain and conserved areas of amino acids specific to each family. Thus, PDE3 and 4 hydrolyze cAMP in the stomach; PDE5 demonstrates dual specificity to cAMP and cGMP (Murthy et al. 2001; Cho et al. 2006; Cai et al. 2015). Another mechanism that reduces the production of cAMP is the activation of $G\alpha_{i-q/11}$ proteins which directly inhibits adenylyl cyclase through the MAPK signaling cascade.

The state diagram of the cAMP-dependent pathway as described above is shown in Fig. 7.3.

The system of equations for the cAMP-pathway activation is given by

$$d\mathbf{X}/\mathrm{d}t = \mathbf{B}\mathbf{X}(t), \tag{7.18}$$

where $\mathbf{X}(t) = \left(X_j\right)^{\mathrm{T}}\left(j = \overline{21,26}\right)$ has the components

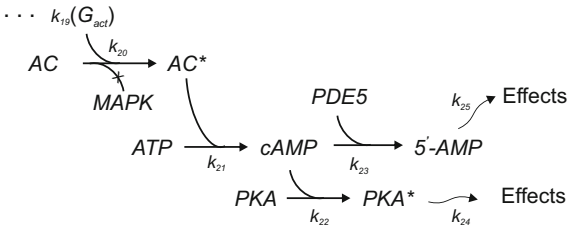

Fig. 7.3 The state diagram of activation of the cAMP-dependent intrinsic pathway

$$X_{21} = [AC], \quad X_{22} = [ATP], \quad X_{23} = [cAMP],$$
$$X_{24} = [PKC], \quad X_{25} = \left[PKC^{*}\right], \quad X_{26} = \left[5^{'} - AMP\right],$$

and the square matrix $\mathbf{B}\left(b_{ij}\right)$ $\left(i,j = \overline{6,6}\right)$ has the non-zero elements

$$b_{11} = -k_{19}k_{20}[X_{18}], \quad b_{22} = -k_{21}[X_{27}],$$
$$b_{32} = k_{21}[X_{27}], \quad b_{33} = -k_{23}[X_{28}]_0,$$
$$b_{44} = -k_{22}[X_{23}],$$
$$b_{54} = k_{22}[X_{23}], \quad b_{55} = -k_{24},$$
$$b_{63} = k_{23}[X_{28}]_0, \quad b_{66} = -k_{25}.$$

The active form of adenylyl cyclase, $X_{27} \coloneqq AC^{*}$, is obtained from

$$[X_{27}](t) = [X_{21}]_0 - [X_{21}](t), \tag{7.19}$$

where $[X_{21}]_0 = \text{const}$ is the initial concentration of the enzyme. We also assume that the level of phosphodiesterase enzyme, $[X_{28}]_0 \coloneqq PDE$, remains constant throughout.

The initial conditions provide concentrations of the reacting components

$$\mathbf{X}(0) = \mathbf{X}_0. \tag{7.20}$$

7.4 PLC Pathway

Activation of G-protein coupled receptors results in downstream stimulation of the intracellular phospholipase C-protein kinase C (PKC) pathway. Four β isoforms of the PLC enzyme have been isolated from the gastrointestinal tract. They are triggered by Ca^{2+}, but are differently regulated by G proteins. PLCβ1 and PLCβ4 are sensitive to $G\alpha_{q/11}$, whereas PLCβ2 and PLCβ3 can be activated by $G\alpha_{q/11}$ and $G_{\beta\gamma}$ subunits. Without exception, these lead to the breakdown of inositide-4,5-biphosphate (PIP_2) and the generation of second messenger molecules—inositol-1,4,5-triphosphate (IP_3) and DAG. IP_3 is a highly soluble structure. It diffuses quickly through the cytosol towards the sarcoplasmic reticulum. Here it binds to R_{IP3} surface receptors and triggers the mobilization of stored Ca^{2+}.

Diacylglycerol consists of two fatty acid chains covalently bonded to a glycerol molecule. Compared to IP_3, it is hydrophobic and therefore remains bound to the plasma membrane. DAG has a number of functions including the activation of PKC. Together with acyl-CoA it is converted to triacylglycerol by the addition of a

third fatty acid to its molecule. The reaction is catalyzed by two distinct isoforms of diglyceride acyltransferases.

The simplified state diagram of the PLC pathway is outlined in Fig. 7.4.

The corresponding system of equations is given by

$$d\mathbf{X}/\mathrm{d}t = \mathbf{C}\mathbf{X}(t) + \mathbf{C_0}, \tag{7.21}$$

where $\mathbf{X}(t) = \left(X_j\right)^{\mathrm{T}}\left(j = \overline{29,34}\right)$ has the components

$$\begin{array}{lll} X_{29} = [PIP_2], & X_{30} = [IP_3], & X_{31} = [DAG], \\ X_{32} = [DAGT], & X_{33} = [PKC], & X_{34} = [R_{\mathrm{IP3}}]. \end{array}$$

The matrix $\mathbf{C}\left(c_{ij}\right)\ \left(i,j = \overline{6,6}\right)$ has the non-zero elements

$$\begin{array}{ll} c_{11} = -k_{19}k_{26}[X_{18}], & c_{21} = -c_{11}, \\ c_{22} = -k_{27}, & c_{31} = c_{21}, \\ c_{33} = -k_{28}[X_{32}] - k_{29}k_{30}[X_1][X_{33}],, & \\ c_{44} = -k_{28}[X_{31}], & c_{55} = -k_{29}k_{30}[X_1][X_{31}], \\ c_{66} = -k_{27}[X_{30}] - k_{-27}, & \end{array}$$

and the vector-column is: $\mathbf{C_0} = (0, k_{-27}[X_{37}], 0, 0, 0, k_{-27}[X_{37}])^{\mathrm{T}}$.

Concentrations of the active form of protein kinase C, $X_{35} \coloneqq PKC^*$, and the activated IP_3-R_{IP3}—complex, $X_{36} \coloneqq IP_3 \cdot R_{\mathrm{IP3}}$, can be obtained from the algebraic relations

$$\begin{array}{l} [X_{35}](t) = [X_{38}]_0 - [X_{33}](t) \\ [X_{36}](t) = [X_{37}]_0 - [X_{34}](t). \end{array} \tag{7.22}$$

Here $[X_{37}]_0, [X_{38}]_0$ are the initial concentrations of the IP_3-receptor on the endoplasmic reticulum and PKC enzyme, respectively.

The dynamics of intracellular calcium release from the stores is described by Miftahof et al. (2009)

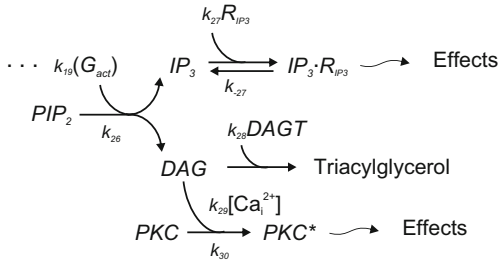

Fig. 7.4 The state diagram of activation of the PLC-pathway

$$\frac{d[X_1]}{dt} = \tilde{k}_0\left(\tilde{k}_1 - \tilde{k}_2[X_{36}]^3[X_1] - \left[\mathrm{Ca}^{2+}_{\mathrm{SR}}\right]\right) - \frac{\tilde{k}_3[X_1]}{[X_1]^2 - \tilde{k}_4}, \tag{7.23}$$

where $\tilde{k}_i$ $(i = 0, 4)$ are the kinetic parameters related to the release of sarcoplasmic $\mathrm{Ca}^{2+}_{\mathrm{SR}}$.

Provided that initial concentrations of reactive substrates are known, the system of Eqs. (7.21)–(7.23) models the PLC pathway dynamics.

7.5 Co-transmission by Multiple Neurotransmitters

Functional co-transmission implies that various postsynaptic receptors exist in the vicinity of the presynaptic terminal or an adjacent cell. In the context of such a configuration, one transmitter/modulator could affect the action of another. For example, it may shunt and modify the time course of excitation/inhibition signals, provide presynaptic neuromodulation and/or synapse-specific adaptation, control differentially modulation of neuroeffector circuits, activate synergistically multiple receptors of the same or different postjunctional cells. Multiple neurotransmission also adds a safety factor to the communication process and thus compensates for activity- or pathology-dependent alterations in postsynaptic receptor subunits. These mechanisms appear to be extremely useful because cell-to-cell signaling is not fully constrained by synaptic wiring and synapse independence.

The quantitative features of integrative physiological phenomena in the human stomach are defined by contributions from the myriad of interconnecting cross-talk intracellular signaling pathways. The combined state diagram of ligand-receptor binding, activation of second messenger systems and exertion of electromechanical effects is given in Fig. 7.5. It is apparent that elements of one pathway cross-regulate and share components of another pathway in the transduction process.

The corresponding governing system of equations is given by

$$d\mathbf{X}/\mathrm{d}t = \mathbf{D}\mathbf{X}(t) + \mathbf{C_0}, \tag{7.24}$$

where

$$\mathbf{D}(m \times n) = \begin{pmatrix} a_{ij} \\ (i,j = 1,20) & 0 & 0 \\ 0 & b_{kl} & 0 \\ 0 & (k,l = 1,6) & c_{kl} \\ 0 & 0 & \end{pmatrix}, \quad \mathbf{X} = \begin{pmatrix} X_1 \\ \vdots \\ X_{26} \\ X_{29} \\ \vdots \\ X_{34} \end{pmatrix}, \quad \mathbf{C_0} = \begin{pmatrix} 0 \\ \vdots \\ 0 \\ C_{30} \\ \vdots \\ C_{34} \end{pmatrix}.$$

The elements of **X, B** and **C** are defined by Eqs. (7.10, 7.18, 7.21). Algebraic relationships (7.19, 7.22) are used to calculate current concentrations of the

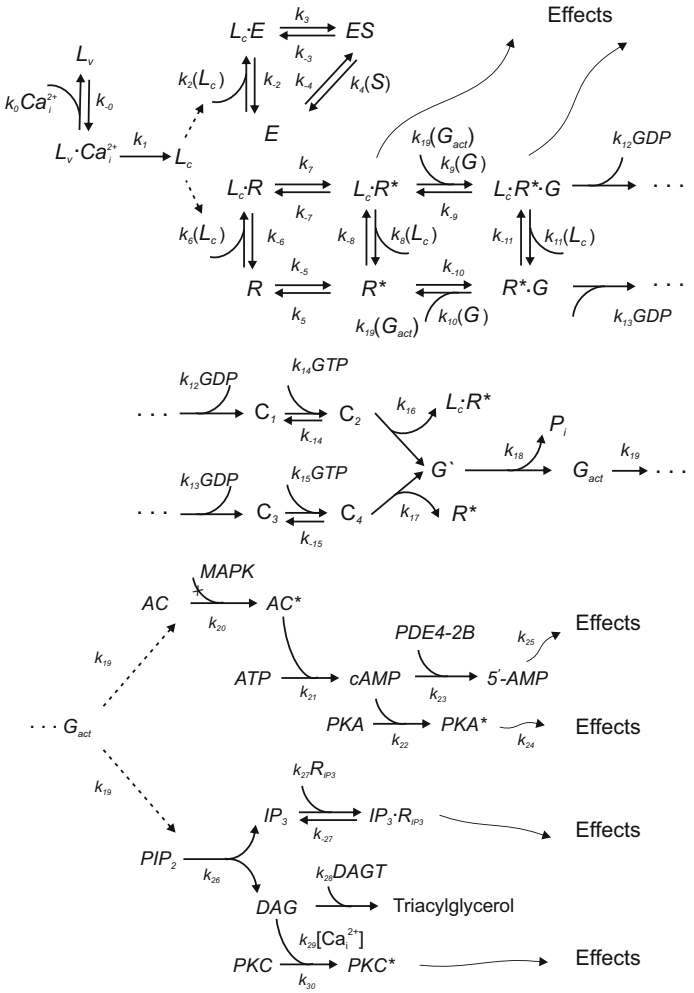

Fig. 7.5 A scheme of multiple pathway neurotransmission and regulation in the human stomach

reactants X_{27}, X_{35} and X_{36}, while the values of $X_{28,37-41}$ refer to initial concentrations of substrates and are defined a priori.

Assuming the level of separate or conjoint activation of final components, i.e. $L_c \cdot R^*, 5^{'}-AMP, PLC^*, PKC^*$ and $IP_3 \cdot R_{\mathrm{IP3}}$, is taken as a measure of pathway output, responses of gastric SMC to stimulatory signals may be:

(i) depolarization of the cell membrane, which is described by Eq. (7.11),
(ii) increase in permeability of ion channels

$$g_p(t) = g_p[X_q]/[X_q]_{\max}, \tag{7.25}$$

where the channel selectivity (p) depends on the transmitter and the receptor type (q) involved, e.g., $(p,q) \propto (BK_{Ca}, NO), (Ca_i^{2+}, SP), (L\text{-}Ca_i^{2+}, 5\text{-HT})$,

(iii) augmentation of contraction/relaxation, which in one-dimensional case, T^a, is given by Eq. (6.45), and in case of in-plane forces, $T^p_{l(c)}$, by Eq. (6.46).

References

Anlauf M, Schafer MK, Eiden L, Weihe E (2003) Chemical coding of the human gastrointestinal nervous system: cholinergic, VIPergic, and catecholaminergic phenotypes. J Compar Neurol 459:90–111

Belai A, Burnstock G (2000) Pattern of distribution and co-localization of NOS and ATP in the myenteric plexus of human fetal stomach and intestine. Neuroreport 11:5–8

Blaugrund E, Pham TD, Tennyson VM, Lo L, Sommer L, Anderson DJ, Gershon MD (1996) Distinct subpopulations of enteric neuronal progenitors defined by time of development, sympathoadrenal lineage markers and Mash-1-dependence. Development 122:309–320

Burnstock J (2004) Cotransmission. Curr Opin Pharmac 4:47–52

Cai Y-L, Zhang M-H, Huang X, Jiang J-Z, Piao L-H, Jin Z, W-X X (2015) CNP-pGC-cGMP-PDE3-cAMP signal pathway upregulated in gastric smooth muscle of diabetic rats. Gastroenter Res Prac 2015:1–9

Cha S (1968) A simple method for derivation of rate equations for enzyme-catalyzed reactions under the rapid equilibrium assumption or combined assumptions of equilibrium and steady state. J Biol Chem 25:820–825

Chalazonitis A, Pham TD, Li Z, Roman D, Guha U, Gomes W, Kan L, Kessler JA, Gershon MD (2008) Bone morphogenetic protein regulation of enteric neuronal phenotypic diversity: relationship to timing of cell cycle exit. J Compar Neurol 509:474–492

Cho SH, Park H, Kim JH, Ryu YH, Lee SI, Conklin JL (2006) Effect of sildenafil on gastric emptying in healthy adults. J Gastroenter Hepat 21(1 Pt 2):222–226

Epperson A, Halton WJ, Callaghan B, Doherty P, Walker RL, Sanders KM, Ward SM, Horowitz B (2000) Molecular markers expressed in cultured and freshly isolated interstitial cells of Cajal. Am J Physiol 279:C529–C539

Gariepy CE (2001) Intestinal motility disorders and development of the enteric nervous system. Ped Res 49(5):605–613

Huber A, Trudrung P, Storr M, Franck H, Schusdziarra V, Ruth P, Allescher HD (1998) Protein kinase G expression in the small intestine and functional importance for smooth muscle relaxation. Am J Physiol Gastroint Liver Physiol 275(4):G629–G637

Iino S, Ward SM, Sanders KM (2004) Interstitial cells of Cajal are functionally innervated by excitatory motor neurons in the murine intestine. J Physiol 556:521–530

Kim TW, Koh SD, Ordog T, Ward SM, Sanders KM (2003) Muscarinic regulation of pacemaker frequency in murine gastric interstitial cells of Cajal. J Physiol 546:415–425

King EL, Altman C (1956) A schematic method of deriving the rate laws for enzyme catalyzed reactions. J Phys Chem 60:1375–1378

Kito Y (2011) The functional role of intrasmuscular interstitial cells of Cajal in the stomach. J Sm Musc Res 47(2):47–53

Knowles CH, Veress B, Kapur RP, Wedel T, Farruga G, Vanderwinden JM, Geboes K, Smith VV, Martin JE, Lindberg G, Milla PJ, De Giorgio R (2011) Quantitation of cellular components of the enteric nervous system in the normal human gastrointestinal tract-report on behalf of the Gastro 2009 International Working Group. Neurogastroent Mot 23:115–124

Kraichely RE, Farrugi G (2007) Mechanosensitive ion channels in interstitial cells of Cajal and smooth muscle of the gastrointestinal tract. Neurogastroent Mot 19:245–252

Lavin ST, Southwell BR, Murphy R, Jenkinson KM, Furness JB (1998) Activation of neurokinin 1 receptors on interstitial cells of Cajal of the guinea-pig small intestine by substance P. Histochem Cell Biol 110:263–271

Lecci A, Santicioli P, Maggi CA (2002) Pharmacology of transmission to gastrointestinal muscle. Curr Opin Pharmacol 2:630–641

Mandić P, Filipović T, Gašić M, Djukić-Macut N, Filipović M, Bogosavljević I (2016) Quantitative morphometric analysis of the myenteric nervous plexus ganglion structures along the human digestive tract. Vojnosanitetski Pregled March:46–53

Merighi A (2002) Costorage and coexistence of neuropeptides in the mammalian CNS. Prog Neurobiol 66:161–190

Metzger M (2010) Neurogenesis of the enteric nervous system. Arch Ital Biol 148:73–83

Miftahof RN, Nam HG, Wingate DL (2009) Mathematical modeling and simulation in enteric neurobiology. World Scientific Publishing, Singapore

Miller SM, Reed D, Sarr MG, Farrugia G, Szurszewski JH (2001) Haem oxygenase in enteric nervous system of human stomach and jejunum and co-localization with nitric oxide synthase. Neurogastroent Mot 13:121–131

Murthy KS, Zhou H, Makhlouf G (2001) PKA-dependent activation of PDE3A and PDE4 and inhibition of adenylyl cyclase V/VI in smooth muscle. Am J Physiol 282:C508–C517

Nusbaum MP, Blitz DM, Swensen AM, Wood D, Marder E (2001) The roles of co-transmission in neural network modulation. Trends Neurosci 24(3):146–154

Pimont S, Bruley des Varannes S, Le Neel JC, Aubert P, Galmiche JP, Neunlist M (2003) Neurochemical coding of myenteric neurones in the human gastric fundus. Neurogastroent Mot 15:655–662

Sanders KM, Ward SM, Koh SD (2014) Interstitial cells: regulators of smooth muscle function. Physiol Rev 94:859–907

Sasselli V, Pachnis V, Burns A (2012) The enteric nervous system. Dev Biol 366:64–73

Southwell BR, Woodman HL, Murphy R, Royal SJ, Furness JB (1996) Characterisation of substance P-induced endocytosis of NK1 receptors on enteric neurons. Histochem Cell Biol 106:563–571

Teschemacher AG, Christopher DJ (2008) Cotransmission in the autonomic nervous system. Exp Physiol 94(1):18–19

Trudeau L-E, Gutiérrez R (2007) On cotransmission & neurotransmitter phenotype plasticity. Mol Inter 7:138–146

Vannucchi MGGR, Faussone-Pellegrini MS (1997) NK1 receptor expression in the interstitial cells of Cajal and neurons and tachykinins distribution in rat ileum during development. J Comp Neurol 383:153–162

Wang XY, Ward SM, Gerthoffer WT, Sanders KM (2003) PKC-epsilon translocation in enteric neurons and interstitial cells of Cajal in response to muscarinic stimulation. Am J Physiol Gastroint Liver Physiol 285:G593–G601

Wang H, Hughes I, Planer W, Parsadanian A, Grider JR, Vohra BP, Keller-Peck C, Heuckeroth RO (2010) The timing and location of glial cell line-derived neurotrophic factor expression determine enteric nervous system structure and function. J Neurosci 30:1523–1538

Yamagata M, Sanes JR, Weiner JA (2003) Synaptic adhesion molecules. Curr Opin Cell Biol 15:621–632

Young HM (1999) Embryological origin of interstitial cells of Cajal. Microsc Res Tech 47 (4):303–308

Zhang R-X, Wang XY, Chen D, Huizinga JD (2011) Role of interstitial cells of Cajal in the generation and modulation of motor activity induced by cholinergic neurotransmission in the stomach. Neurogastroent Mot 23:e356–e371

Zhu MH, Sung IK, Zheng H, Sung TS, Britton FC, O'Driscoll K, Koh SD, Sanders KM (2011) Muscarinic activation of Ca^{2+}-activated Cl^- current in interstitial cells of Cajal. J Physiol 589 (Pt18):4565–4582

Chapter 8
Intrinsic Regulatory and Effector Systems

The mathematics is not there till we put it there.
Arthur Eddington

8.1 Nervous and Interstitial Cell Plexi

After the colonization of the gastrointestinal tract by NCSCs is complete, a complex network of neuronal and glial cells arranged in interconnected ganglia is generated. Different subtypes of ganglionic cells, based on a combination of their morphology, neurochemical coding, electrophysiological responses, connections, projections and function are identified in the enteric nervous system. Morphofunctional and projectile classification reflects on intrinsic primary afferent, ascending (orally)/descending (aborally) inter-, motor, intestinofugal, secretomotor and vasomotor neurons. By contrast, electrophysiological taxonomy is based mainly on firing pattern characteristics. Thus S–type neurons exhibit brief action potentials and lack a prolonged slow after-hyperpolarization phase, whilst AH–type neurons show prominent long lasting (up to 20 s) hyperpolarization dynamics. The neuro-chemo-functional division into cholinergic, nitrergic, serotonergic, etc becomes superfluous because neurons co-localise and co-release multiple neurotransmitters and simultaneously exert excitatory and/or inhibitory effects.

The ENS is organized in a strict hierarchical manner. Its morphofunctional elements (ganglia) are assembled in three anatomically distinct spatially dispersed plexi (the myenteric—Auerbach's, the submucous—Meissner's, and the mucous nervous plexus) (Hansen 2003). These are unevenly represented throughout the gastrointestinal tract. Auerbach's plexus, distributed within defined planes between the longitudinal and circumferential SM layers, is prominent in the human stomach, while Meissner's plexus appears to be very sparse. Confocal microscopy studies show that the structure of the Auerbach's plexus resembles a rectangular network with an average spacing between ganglia ~200–500 μm. Numerous overlapping polysynaptic pathways ensure the effective and efficient transmission of information coded in the form of electrochemical signals within the plexus.

R.N. Miftahof, *Biomechanics of the Human Stomach*,
DOI 10.1007/978-3-319-59677-8_8

A set of interstitial cells of Cajal and "fibroblast-like" cells are widely dispersed intermuscularly within the gastric wall. In the fundus, the ICC appear as bipolar cells and in the body and antrum of the stomach they show the multipolar morphology with highly ramified processes. Connected through multiple electrical synapses, they form an extensive network of their own. Because of its location and close proximity to Auerbach's plexus, the network is termed ICC-MY. ICC cell bodies, processes and ramifications form intramuscular networks with elongated, thin meshes and sheaths around ganglia and nerve strands. It is noteworthy that the ICC-MY anastomosing network enfolds myenteric ganglia but is not intrinsic to them (Manneschi et al. 2004). Another set of ICC/PDGFRα^+ cells is present intramuscularly, predominantly in the circular smooth muscle layer, and is referred to as ICC/PDGFRα^+–IM. ICC, PDGFRα^+ form a sheath around smooth muscle and also send branches within muscle bundles thus giving rise to a three-dimensional network within the SM thickness (Manneschi et al. 2004). Firmly connected through gap junctions with SMCs they create a multicellular SM/ICC/PDGFRα^+ syncytium (SIP). Within a SIP, SMC and ICC: (i) associate closely with nerve bundles and varicosities of myenteric neurons, (ii) express receptors for various neurotransmitters, and (iii) receive an extensive input from vagal efferent tracts. The nature of ICC-myenteric nerve connections is either a close contact of 20–200 nm or a synapse-like contact of 20 nm. The latter comes from immunohistochemical staining studies for synaptic specific molecules, e.g. soluble N-ethylmaleimide-sensitive factor attachment protein receptor and synaptosomal-associated protein-25 (Kito 2011). These synapses involve multiple excitatory and inhibitory neurotransmission by ACh, NO, SP, VIP and ATP (Mitsui and Komuro 2002).

The functional integrity of SIP is maintained by electrical synapses and multiple ionic conductances among its structural elements. Although consensus on the nature of ion channels has not yet been reached, there is an experimental electrophysiological and pharmacological indication supporting the notion that voltage-dependent Ca^{2+} (presumably L- and/or T-type), Na^+, Ca^{2+}-activated K^+ and Cl^- channels play a leading role (Rich et al. 1998; Huizinga et al. 2004; Strege et al. 2003; Baker et al. 2013; Sanders et al. 2014).

The histoarchitecture of the ENS, as described above, allows the ad hoc formation of intrinsic neuronal circuits within, and guarantees the stability and high degree reliability of its function. Despite the fact that the human stomach is under the control of the central nervous system via the *vagus* nerve, the possibility of generating intrinsic reflexes independently from the CNS places Auerbach's plexus and ICC-MY in a unique position to operate autonomously (Aldrete et al. 1982; Stoddard et al. 1973, 1975).

8.2 Smooth Muscle

Electrical properties, i.e. rhythmic low amplitude depolarizations (slow waves) and the generation of action potentials (spikes) by smooth muscle cells of the gastrointestinal tract depend on the balanced function of transmembrane ion channels:

voltage-dependent L- and T-type Ca^{2+}, large conductance Ca^{2+}-activated K^+, voltage-gated K^+, and Cl^- channels. L-type Ca^{2+} channels in the human stomach are formed of five distinct subunits: α1, α2, β2/3, δ and γ. The α1C-subunit contains the channel pore, voltage sensor and drug binding sites, while α_2, β, δ and γ-subunits modulate the channel's permeability. These channels possess characteristics of long-lasting, high-voltage dependence and ensure the main influx of extracellular calcium ions during depolarization.

T-type Ca^{2+} channels differ from L-type channels in their α-subunits (Bielefeldt 1999; Perez-Reyes 2003). They are activated at low voltage and remain open for a short period of time (Hill-Eubanks et al. 2011). Experimental data suggests that they are responsible for the generation of spikes and pacemaker activity, as well as playing a key role in regulating the frequency of phasic contractions.

Potassium channels constitute a superfamily of four channels: the large conductance Ca^{2+}-activated K^+ (BK_{Ca}), small conductance (SK_{Ca}), voltage–gated (K_v), and ATP–sensitive (K_{ATP}) potassium channels. BK_{Ca} channel constitutes six transmembrane proteins. The channel's sensitivity to calcium and activity is regulated by phosphorylation of the pore-forming α-subunit. This offers a mechanism whereby cyclic nucleotides and protein kinase C modulate channel function (Tian et al. 2008). Two types of K_v channels are identified: delayed rectifying and rapidly inactivating. They are formed by a single unit of six transmembrane proteins and the pore-hairpin loop. The channels remain uncoupled at low $[Ca_i^{2+}]$ and switch to a calcium sensor mode with an increase in intracellular calcium. Together with SK_{Ca}, they determine the resting membrane potential, action potential repolarization, excitability and muscle contractility.

The role of Ca^{2+} activated Cl^- channels has been implicated in the origin of slow waves in gastrointestinal smooth muscle. They have distinctive biophysical properties and their activity is triggered by oscillations in cytosolic Ca_i^{2+}. However, until the structure and electrophysiology of these channels are identified, we can only speculate on their function.

8.3 Modeling of Electrical Activity of Cells

Electrical activity in ganglionic neurons and ICC is ubiquitous and is essential to maintain vital functions of the body. It is manifested by a variety of patterns of discharges and the specificity of transduction mechanisms that enable the system to integrate and to coordinate the overall behaviors in space and time.

At the level of mathematical modeling of neuronal activity two types of complexity must be dealt with: the interplay of ion channel dynamics that underlie the excitability, and the neuronal morphology that allows neurons to communicate signals among them. Despite significant advancements in simulation and a large number of proposed mathematical models of excitable media, the only biologically plausible and accurate model remains the Hodgkin–Huxley (H-H) model (1952). It contains a current balance equation that satisfies Kirchoff's law

$$C_m^f \frac{dV}{dt} = -\sum_{i=1}^{n} g_i x_i^p y_i^p (V - V_i) + I_{appl}(t), \tag{8.1}$$

and relaxation equations for ionic conductances

$$\begin{aligned} \frac{dx_i}{dt} &= \frac{x_{i\infty}(V) - x_i}{\tau_{x_i}(V)}, \qquad i = \overline{1,n}, \\ \frac{dy_i}{dt} &= \frac{y_{i\infty}(V) - y_i}{\tau_{y_i}(V)}, \qquad i = \overline{1,n}. \end{aligned} \tag{8.2}$$

Here C_m^f is the membrane capacitance, V is the membrane potential, V_i is the Nernst potential for the i^{th} ion, g_i is the maximal conductance of the channel for the different ion-selective channels, $x_i^p(x_{i\infty})$, y_i^p $(y_{i\infty})$ are the actual (steady) state activation and inactivation variables, respectively, τ_{x_i} and τ_{y_i} are the relaxation time constants, $I_{appl}(t)$ is the applied current. The nonlinear system (8.1, 8.2) accurately reproduces the rich dynamic behavior in various excitable tissues ranging from tonic bursting to chaos, and from stationary to traveling wave phenomena. Such versatility and reliability is a result of mathematical formulation that incorporates explicitly/implicitly intrinsic properties of the cell membrane. Dynamic systems analysis of (8.1, 8.2) has provided insights into how cell activity is shaped by individual parameters. Thus, it has been demonstrated that a qualitative change from large amplitude, stable periodic behavior to small amplitude and unstable periodic oscillations—a subcritical Hopf bifurcation—can be achieved by an increase in $\left[Ca_0^{2+}\right]$, a reduction in membrane maximal K^+ conductance, or by a shift of the Nernst potential for K^+ in the depolarizing direction (Holden and Yoda 1981).

Several other models, which are simplifications of the Hodgkin–Huxley model to mimic membrane potential and ion current dynamics (Fitzhugh 1955; Kepler and Marder 1993; Wilson 1999; Gerstner and Kistler 2002; Izhikevich 2003) have demonstrated their robustness in describing complex electrical events in large populations of neurons and neural fields. However, their applications in "electronic pharmacological" studies are severely limited because of constructive biological insufficiencies (Miura 2002).

At the time this book was written there was not enough experimental evidence on electrophysiological properties of neuronal and smooth muscle cells of the human stomach. The following considerations are based on the projections from the groundwork provided by in vivo and in vitro studies on various animal models.

8.4 Electrical Activity of Neurons and ICC

The primary afferent (sensory) neurons have not been definitely identified and there is still considerable controversy concerning their location and projections. They have smooth cell bodies, and could be adendritic, pseudo-uniaxonal or multiaxonal

(with two or more long processes). There is a tendency to primary and secondary branching of the neurites close to the soma, and there a few or no synaptic inputs. The receptive fields, mechanoreceptors, are free nerve endings and are located in the mucosa and the submucous layer.

Motor neurons cells are uniaxonal and multidendritic. Dendrites are of intermediate length, relatively little branched and project to SIP. The distinguishing characteristic of their electrical behavior is that they discharge long trains of spikes. These patterns resemble all-or-nothing events and are independent of the initial stimulus.

Mechanoreceptors convert mechanical stimuli (stretch deformation) to the receptor potential via activation of Na^+ selective ion channels. Then the dynamics of the dendritic receptor potential is given by

$$\begin{aligned} C_m^e \frac{dV^e}{dt} &= -\left(\tilde{I}_{Na} + \tilde{I}_K + \tilde{I}_{Cl}\right) - \left(V^d - V^e\right)/R_m \\ \gamma \frac{dV^d}{dt} &= -V^d + k\left(V^d - V^e\right)/R_m \end{aligned} \tag{8.3}$$

where V^d, V^e are the nerve dendritic and ending receptor potentials, respectively,

C_m^e is the dendritic membrane capacitance, R_m is the membrane resistance, γ, k are the membrane time and numerical constants. $\tilde{I}_{Na}, \tilde{I}_K, \tilde{I}_{Cl}$ are the sodium, potassium and chloride currents

$$\begin{aligned} \tilde{I}_{Na} &= \tilde{g}_{Na}\tilde{m}^3\tilde{h}\left(\tilde{V}^e - \tilde{V}_{Na}\right), \\ \tilde{I}_K &= \tilde{g}_K\tilde{n}^4\left(\tilde{V}^e - \tilde{V}_K\right), \\ \tilde{I}_{Cl} &= \tilde{g}_{Cl}\left(\tilde{V}^e - \tilde{V}_{Cl}\right). \end{aligned} \tag{8.4}$$

Here $\tilde{g}_{Na}, \tilde{g}_K, \tilde{g}_{Cl}$ are the maximal conductances for Na^+, K^+, Cl^- channels, $\tilde{m}, \tilde{h}, \tilde{n}$ are probabilities of opening these channels, $\tilde{V}_{Na}, \tilde{V}_K, \tilde{V}_{Cl}$ are the reversal potentials of Na^+, K^+, Cl^- currents. The activation and deactivation of ion channels is described by

$$\frac{dy^*}{dt} = \psi\left(\tilde{\alpha}_y(1 - y^*) - \tilde{\beta}_y y^*\right) \qquad \left(y^* = \tilde{m}, \tilde{h}, \tilde{n}\right), \tag{8.5}$$

where ψ is the temperature scale factor, $\tilde{\alpha}_y$ is the rate of switching channels from a closed to an open state, and $\tilde{\beta}_y$ is the rate of reverse. They are obtained from the approximation of experimental data

$$\begin{aligned} \tilde{\alpha}_m &= 0.221\exp(e(t) + 0.01V^e) \\ \tilde{\beta}_{m\infty} &= 4.5\exp(-V^e/18) \\ \tilde{\alpha}_h &= 0.048\exp(-V^e/36) \\ \tilde{\beta}_h &= 0.12/(1 + \exp(3.4 - 0.2V^e)) \\ \tilde{\alpha}_n &= 0.33\exp(1.1 - 0.1V^e) \\ \tilde{\beta}_n &= 0.185\exp(-V^e/80). \end{aligned} \tag{8.6}$$

Here $\varepsilon(t)$ is the applied deformation.

The dynamics of action potentials at the soma of neuronal and interstitial cells is given by

$$C_n^s \frac{dV_n^s}{dt} = -\sum_j I_j + I_{\text{ext}}, \tag{8.7}$$

where C_n^s is the membrane capacitance of the soma of a neuron, I_j ($j = \text{Ca}^{2+}$, Ca^{2+}-K^+, Na^+, K^+, Cl^-) are ion currents carried through specified ion channels (their choice and inclusion in the model depends on biological characteristics of the cell), $I_{\text{ext}} = V/R_{ICC}$ is the external membrane current, and R_{ICC} is the input cellular resistance and the ion currents are defined as

$$\begin{aligned} I_{Ca} &= g_{Ca(i)} z_{Ca} \left(V_n^s - V_{Ca(i)}\right) / \left(1 + \vartheta_{Ca}\left[\text{Ca}_i^{2+}\right]\right), \\ I_{Ca-K} &= g_{Ca-K(i)} \rho_\infty \left(V_n^s - V_{Ca-K(i)}\right) / \left(0.5 + \left[\text{Ca}_i^{2+}\right]\right), \\ I_{Na} &= g_{Na(i)} m_{Na}^3 h_{Na} \left(V_n^s - V_{Na(i)}\right), \\ I_K &= g_{K(i)} n_K^4 \left(V_n^s - V_{K(i)}\right), \\ I_{Cl} &= g_{Cl(i)} \left(V_n^s - V_{Cl(i)}\right). \end{aligned} \tag{8.8}$$

where $V_{Ca(i)}, V_{Ca-K(i)}, V_{Na(i)}, V_{K(i)}, V_{Cl(i)}$ are the reversal potentials and $g_{Ca(i)}$, $g_{Ca-K(i)}$, $g_{Na(i)}$, $g_{K(i)}$, $g_{Cl(i)}$ are the maximal conductances of channels, ϑ_{Ca} is the parameter of calcium inhibition of the Ca^{2+} channels, $\left[\text{Ca}_i^{2+}\right]$ is the intracellular concentration of free calcium. Here subscript i is referred to a respective neuron/cell. For example, for ICC and ENS neurons it yields, respectively,

$$\begin{aligned} \frac{d\left[\text{Ca}_i^{2+}\right]}{dt} &= 0.2 z_{Ca}(V_{Ca} - V_i) / \left(1 + \vartheta_{Ca}\left[\text{Ca}^{2+}\right]_i\right) - 0.3\left[\text{Ca}_i^{2+}\right], \\ \frac{d\left[\text{Ca}_i^{2+}\right]}{dt} &= 0.234 \cdot 10^{-4} z_{Ca}(V_{Ca} - V_i) / \left(1 + \vartheta_{Ca}\left[\text{Ca}^{2+}\right]_i\right) - 0.003\left[\text{Ca}_i^{2+}\right] \end{aligned} \tag{8.9}$$

Dynamic variables z_{Ca}, ρ_∞, m_{Na}, h_{Na} and n_K are

$$\begin{aligned} dz_{Ca}/dt &= (z_\infty - z_{Ca})/\tau_z, \\ dh_{Na}/dt &= \lambda_h (h_\infty - h_{Na})/\tau_h, \\ dn_K/dt &= \lambda_n (n_\infty - n_K)/\tau_n, \\ m_{Na} &= m_\infty(V_i), \\ \rho_\infty &= [1 + \exp 0.15(V_i + 47)]^{-1}. \end{aligned} \tag{8.10}$$

In the above $m_\infty, h_\infty, n_\infty, z_\infty$ are calculated as

$$
\begin{aligned}
&y_\infty = \alpha_{y\infty}/\left(\alpha_{y\infty} + \beta_{y\infty}\right), \quad (y = m, h, n)\\
&\tau_y = 1/\left(\alpha_y + \beta_y\right)\\
&z_\infty = \left[1 + \exp(-0.15(V_i + 42))\right]^{-1},
\end{aligned}
\tag{8.11}
$$

where

$$
\begin{aligned}
\alpha_{m\infty} &= \frac{0.12(V_i + 27)}{1 - \exp(-(V_i + 27)/8)}\\
\beta_{m\infty} &= 4\exp(-(V_i + 47)/15)\\
\alpha_{h\infty} &= 0.07\exp(-(V_i + 47)/17)\\
\beta_{h\infty} &= \left[1 + \exp(-(V_i + 22)/8)\right]^{-1}\\
\alpha_{n\infty} &= \frac{0.012(V_i + 12)}{1 - \exp(-(V_i + 12)/8)}\\
\beta_{n\infty} &= 0.125\exp(-(V_i + 20)/67).
\end{aligned}
$$

The relationship, as above, refer to neurons of the ENS. In case of ICC they become different, e.g. $\alpha_{h\infty} = 0.09\exp(-(V_i + 47)/25)$.

Initial conditions assume the physiological status of a cell at rest and the modeof their excitation/inhibition. Thus, assuming that ICC discharges electrical signals of given amplitude $\overset{0}{V}_i$ and duration t_i^d, and receives input signals, excitatory (EPSP) or inhibitory (IPSP) postsynaptic potentials, from the myenteric neurons; the concentration of intracellular calcium ions and the state of channel activity are known, we get

$$
\text{at } t = 0: \quad V_i = \begin{cases} \text{EPSP or IPSP}, & 0 < t < t_i^d \\ \overset{0}{V}_i, & t \geq t_i^d \end{cases},
\tag{8.12}
$$

$$
\left[\mathrm{Ca}_i^{2+}\right] = \left[\overset{0}{\mathrm{Ca}}_i^{2+}\right], \quad z = z_\infty, \quad h_{Na} = h_{Na\infty}, \quad n_{Na} = n_{Na\infty}.
$$

A distinctive feature of neurons is their morphology. Much of the research recently has been directed at understanding the impact of anatomical architecture on signal integration within a neuron and neuronal ensembles. Originally, a single, electrically equivalent cable model was used to simulate the generation and propagation of voltage waves and current changes in the axon and dendrites (Hodgkin and Huxley 1952; Schierwagen 2009)

$$
C_m^f \frac{dV}{dt} = \frac{d_\mathrm{f}}{2R_a^f} \frac{\partial^2 V}{\partial x^2} - \sum_{i=1}^{n} g_i x_i^p y_i^p (V - V_i) + I_{\mathrm{appl}}(t),
\tag{8.13}
$$

where R_a^f is the membrane resistance, d_f is the cross-sectional diameter of the nerve fiber, α is the Lagrange coordinate ($0 \leq \alpha \leq L^s$) of the axon, and the meaning of other parameters and constants is as described above. However, it could not answer

questions related to the synaptic transmission. As an extension, compartmental models have been developed (see Chap. 7) to explore the role of evolving dendritic morphology and to embrace biological mechanisms at molecular and cellular levels that support the temporal and spatial stability of signaling in diverse neuronal topologies (Graham and van Ooyen 2006).

8.5 Electrical Activity of SIP

Following the general principles of Hodgkin–Huxley formalism, the system of equations of the dynamics of the membrane potential $V_{c,l}$ generation in a SIP unit is described as

$$\lambda C_m \frac{dV_{c,l}}{dt} = -\sum_j \tilde{I}_j \tag{8.14}$$

where, λ is the numerical parameter, C_m is the SIP membrane capacitance, and $\tilde{I}_j$ are the fast and slow inward Ca^{2+}, BK_{Ca}, voltage dependent K^+ and leak Cl^- currents given by

$$\begin{aligned}
&\tilde{I}^f_{Ca} = \tilde{g}^f_{Ca}\tilde{m}_I^3\tilde{h}\left(V_{c,l} - \tilde{V}_{Ca}\right),\\
&\tilde{I}^s_{Ca} = \tilde{g}^s_{Ca}\tilde{x}_{Ca}\left(V_{c,l} - \tilde{V}_{Ca}\right),\\
&\tilde{I}_K = \tilde{g}_K\tilde{n}^4\left(V_{c,l} - \tilde{V}_{Ca}\right),\\
&\tilde{I}_{Ca-K} = \tilde{g}^f_{Ca-K}\left[Ca^{2+}\right]\left(V_{c,l} - \tilde{V}_{Ca}\right)/\left(0.5 + \left[Ca^{2+}\right]\right),\\
&\tilde{I}_{Cl} = \tilde{g}_{Cl}\left(V_{c,l} - \tilde{V}_{Ca}\right).
\end{aligned} \tag{8.15}$$

Here $\tilde{V}_{Ca}$, $\tilde{V}_K$, $\tilde{V}_{Cl}$ are the reversal potentials, and $\tilde{g}^f_{Ca}$, $\tilde{g}^s_{Ca}$, $\tilde{g}_K$, $\tilde{g}_{Ca-K}$, $\tilde{g}_{Cl}$ are the maximal conductances for the respective ion currents, $\tilde{m}, \tilde{h}, \tilde{n}$ and $\tilde{x}_{Ca}$ are dynamic variables described by

$$\begin{aligned}
&\tilde{m}_I = \tilde{\alpha}_m/\left(\tilde{\alpha}_m + \tilde{\beta}_m\right),\\
&\lambda\hbar\frac{d\tilde{h}}{dt} = \tilde{\alpha}_h\left(1 - \tilde{h}\right) - \tilde{\beta}_h\tilde{h},\\
&\lambda\hbar\frac{d\tilde{n}}{dt} = \tilde{\alpha}_n(1 - \tilde{n}) - \tilde{\beta}_n\tilde{n},\\
&\lambda\tau_{xCa}\frac{d\tilde{x}_{Ca}}{dt} = \frac{1}{\exp(-0.15(V_{c,l} + 50))} - \tilde{x}_{Ca},\\
&\lambda\frac{d\left[Ca^{2+}\right]}{dt} = \wp_{Ca}\tilde{x}_{Ca}\left(\tilde{V}_{Ca} - V_{c,l}\right) - \left[Ca^{2+}\right]
\end{aligned} \tag{8.16}$$

where the activation $\tilde{\alpha}_y$ and deactivation $\tilde{\beta}_y$ ($y = m, n, h$) parameters of ion channels satisfy the following empirical relations

$$\begin{aligned}
\tilde{\alpha}_m &= 0.1(50 - \tilde{V}_{c,l})/(\exp(5 - 0.1\tilde{V}_{c,l}) - 1),\\
\tilde{\beta}_m &= 4\exp((25 - \tilde{V}_{c,l})/18),\\
\tilde{\alpha}_h &= 0.07\exp((25 - 0.1\tilde{V}_{c,l})/20),\\
\tilde{\beta}_h &= [1 + \exp(5.5 - 0.1\tilde{V}_{c,l})]^{-1},\\
\tilde{\alpha}_n &= 0.01(55 - \tilde{V}_{c,l})/(\exp(5.5 - 0.1\tilde{V}_{c,l}) - 1),\\
\tilde{\beta}_n &= 0.125\exp((45 - \tilde{V}_{c,l})/80).
\end{aligned} \tag{8.17}$$

Here $\tilde{V}_{c,l} = (127V_{c,l} + 8265)/105$, τ_{xCa} is the time constant and $\wp_{Ca}$ is the parameter referring to the dynamics of calcium channels, $\hbar$ is the numerical constant.

The evolution of voltage-dependent Ca^{2+}-channels is defined by

$$\tilde{g}^s_{Ca} = \delta(V_{c,l})\tilde{g}^s_{Ca} \tag{8.18}$$

where

$$\delta(V_{c,l}) = \begin{cases} 1, & \text{for } V_{c,l} \geq V_{p(c,l)} \\ 0, & \text{otherwise} \end{cases} .$$

The discharge of the pacemaker, ICC-MY, initiates the electrical wave of depolarization V^s_l in the SIP syncytium. Electrophysiological extracellular recordings of the dynamics of the propagation of V^s_l revealed anisotropic electrical properties of the longitudinal SIP syncytium. The dynamics of V^s_l is described by Eq. (6.42)

$$C_m \frac{\partial V^s_l}{\partial t} = I_{m1}(\alpha_1, \alpha_2) + I_{m2}(\alpha_1 - \alpha'_1, \alpha_2 - \alpha'_2) + I_{ion}, \tag{8.19}$$

where I_{m1}, I_{m2} are the transmembrane currents described by Eqs. (6.38, 6.41). The intra- and extracellular conductivity $\hat{g}_{i(0)}$ of the syncytium is defined by

$$\hat{g}_{i(0)} := 1/R^m_{i(o)}, \tag{8.20}$$

where $R^m_{i(0)}$ is the intra- (subscript i) and extracellular (o) membrane resistance. According to Ohm's law

$$R^m_{i(0)} = \frac{R^{ms}_{i(0)}\lambda_{c,l}}{\tilde{S}_{s,l}}, \tag{8.21}$$

where $\lambda_{c,l}$ are the stretch ratios and $\tilde{S}_{c,l}$ are the cross-sectional areas of the SIP syncytium, $R^{ms}_{i(0)}$ is the specific resistance. Substituting Eq. (8.21) into (8.20) and assuming that $\tilde{S}_{c,l}$ is constant throughout deformation, we obtain

$$\hat{g}_{i(0)} = \frac{\tilde{S}_{c,l}}{R^m_{i(0)}\lambda_{c,l}} := \frac{\hat{g}^*_{i(0)}}{\lambda_{c,l}}, \tag{8.22}$$

where $\hat{g}^*_{i(0)}$ have the meaning of maximal intracellular and interstitial space conductivities. Substituting Eq. (8.22) into (6.38, 6.41), we find

$$I_{m1}(\alpha_1,\alpha_2) = M_{vs}\left\{\frac{2(\mu_{\alpha_2}-\mu_{\alpha_1})}{(1+\mu_{\alpha_1})(1+\mu_{\alpha_1})}\tan^{-1}\left(\frac{d\alpha_1}{d\alpha_2}\sqrt{\frac{G_{\alpha_2}}{G_{\alpha_1}}}\right)+ \right.$$
$$\left.+\frac{\hat{g}^*_{0,\alpha_2}}{G_{\alpha_1}}\right\}\left(\frac{\partial}{\partial\alpha_1}\left(\frac{\hat{g}^*_{0,\alpha_1}}{\lambda_c}\frac{\partial V^s_l}{\partial\alpha_1}\right)+\frac{\partial}{\partial\alpha_2}\left(\frac{\hat{g}^*_{0,\alpha_2}}{\lambda_l}\frac{\partial V^s_l}{\partial\alpha_2}\right)\right),$$

$$I_{m2}(\alpha_1,\alpha_2) = M_{vs}\iint_S \frac{(\mu_{\alpha_1}-\mu_{\alpha_2})}{2\pi(1+\mu_{\alpha_1})(1+\mu_{\alpha_1})}\frac{(\alpha_2-\alpha'_2)/G_{\tilde{s}_2}-(\alpha_1-\alpha'_1)/G_{\alpha_1}}{\left[(\alpha_1-\alpha'_1)/G_{\tilde{s}_1}-(\alpha_2-\alpha'_2)/G_{\alpha_2}\right]^2}$$
$$\times\left(\frac{\partial}{\partial\alpha_1}\left(\frac{\hat{g}^*_{0,\alpha_1}}{\lambda_c}\frac{\partial V^s_l}{\partial\alpha_1}\right)+\frac{\partial}{\partial\alpha_2}\left(\frac{\hat{g}^*_{0,\alpha s_2}}{\lambda_l}\frac{\partial V^s_l}{\partial\alpha_2}\right)\right)d\alpha'_1 d\alpha'_2,$$
$$\mu_{\alpha_1} = \hat{g}^*_{0,\alpha_1}/\hat{g}^*_{i,\alpha_1},\quad \mu_{\alpha_2} = \hat{g}^*_{0,\alpha_2}/\hat{g}^*_{i,\alpha_2},$$
$$G_{\alpha_1} = \frac{\hat{g}^*_{0,\alpha_1}+\hat{g}^*_{i,\alpha_1}}{\lambda_c},\ G_{\alpha_2} = \frac{\hat{g}^*_{0,\alpha_2}+\hat{g}^*_{i,\alpha_2}}{\lambda_l},\ G = \sqrt{G_{\alpha_1}G_{\alpha_2}}. \tag{8.23}$$

where α_1, α_2 are Lagrange coordinates of the longitudinal and circular SIP syncytia, respectively, and the meaning of other parameters as described above.

The total ion current I_{ion} is given by

$$I_{ion} = \tilde{g}_{Na}\hat{m}^3\hat{h}\left(V^s_l-\tilde{V}_{Na}\right)+\tilde{g}_K\hat{n}^4\left(V^s_l-\tilde{V}_K\right)+\tilde{g}_{Cl}\left(V^s_l-\tilde{V}_{Cl}\right), \tag{8.24}$$

where $\tilde{g}_{Na}, \tilde{g}_K, \tilde{g}_{Cl}$ represent maximal conductances, $\tilde{V}_{Na}, \tilde{V}_K, \tilde{V}_{Cl}$ reversal potentials of Na^+, K^+, and Cl^- currents. The dynamics of change in the probability variables $\hat{m}, \hat{h}, \hat{n}$ of opening of the ion gates are obtained from

$$\frac{d\hat{y}}{dt} = \hat{\alpha}_{\hat{y}}(1-\hat{y}) - \hat{\beta}_{\hat{y}}\hat{y} \quad \left(y = \hat{m}, \hat{h}, \hat{n}\right). \tag{8.25}$$

The activation $\hat{\alpha}_{\hat{y}}$ and deactivation $\hat{\beta}_{\hat{y}}$ parameters are given by

$$\begin{aligned}
\hat{\alpha}_m &= 0.005\left(V^s_l-\tilde{V}_m\right)/\left(\exp 0.1\left(V^s_l-\tilde{V}_m\right)-1\right)\\
\hat{\beta}_m &= 0.2\exp\left(\left(V^s_l+\tilde{V}_m\right)/38\right)\\
\hat{\alpha}_h &= 0.014\exp\left(-\left(\tilde{V}_h+V^s_l\right)/20\right)\\
\hat{\beta}_h &= 0.2/\left(1+\exp 0.2\left(\tilde{V}_h-V^s_l\right)\right)\\
\hat{\alpha}_n &= 0.006\left(V^s_l-\tilde{V}_n\right)/\left(\exp 0.1\left(V^s_l-\tilde{V}_n\right)-1\right)\\
\hat{\beta}_n &= 0.75\exp\left(\tilde{V}_n-V^s_l\right).
\end{aligned} \tag{8.26}$$

By contrast the circular SIP syncytium possesses properties of electrical isotropy. The dynamics of the propagation of the electrical wave V_c^s along it satisfies Eq. (6.43)

$$C_m \frac{\partial V_c^s}{\partial t} = \frac{M_{vs}}{1+\mu_{\alpha_1}} \left\{ \frac{\partial}{\partial \alpha_1} \left(\frac{\hat{g}_{0,\alpha_1}^*}{\lambda_c} \frac{\partial V_c^s}{\partial \alpha_1} \right) + \frac{\partial}{\partial \alpha_2} \left(\frac{\hat{g}_{0,\alpha_1}^*}{\lambda_l} \frac{\partial V_c^s}{\partial \alpha_2} \right) \right\} - I_{ion}, \tag{8.27}$$

where Eqs. (8.24)–(8.26) are used to calculate I_{ion}. In the above formulas V_l^s should be substituted by V_c^s.

The above system of equations, complemented by initial and boundary conditions constitute the mathematical model of coupled electromechanical syncytia of the human stomach and reproduces:

(i) generation of slow waves;
(ii) their propagation in the longitudinal and circumferential SIP syncytia;
(iii) production of action potentials.

The commonly used initial conditions assume that the electrical potentials of the circular and longitudinal SIP syncytia attain equilibrium values $V_{c,l}^r$; the concentrations of intracellular calcium ions in muscle cells are known

$$\text{at } t=0: \quad V_{c,l} = V_{c,l}^r,\ V_{c,l}^s = 0,\ \left[\text{Ca}_i^{2+}\right] = \left[\overset{0}{\text{Ca}_i^{2+}}\right], \tag{8.28}$$

and the dynamic variables of various ion channels are defined by

$$\hat{m} = \hat{m}_\infty,\ \hat{h} = \hat{h}_\infty,\ \hat{n} = \hat{n}_\infty,\ \tilde{h} = \tilde{h}_\infty,\ \tilde{n} = \tilde{n}_\infty,\ \tilde{x}_{Ca} = \tilde{x}_{Ca}^\infty \tag{8.29}$$

Boundary conditions should be specified depending on a particular problem.

8.6 Electromyogenic Circuits

The analysis of the regulatory mechanisms of gastric motility has, so far, involved the study of signal transduction mechanisms in a linear steady-state mode. Theories describing biological regulatory systems remain inadequate because the knowledge of their operational principles is frustratingly sketchy. A framework for investigating the informational and computational capabilities of neuronal networks is based on the general scheme: one-layer feedback or multi-layer feed-forward performance, with 'artificial' neurons linked by 'artificial' synapses. These models are a drastic simplification of a biological prototype. Although many clinical effects were predicted with some rate of success, such approaches do not encompass the existing complexity of nonlinear dynamic interactions among intertwined signaling polysynaptic pathways. Awareness of the nonlinear correlation of molecular

interactions becomes of paramount importance with a burgeoning understanding of cellular mechanisms of multiple neurotransmission.

A brief outline of existing and proposed neuronal circuits in the gastric wall and mathematical descriptions of their dynamics are given below. The reader can create their own cellular assemblies by linking different constructive elements to meet specific model requirements.

8.6.1 An Inhibitory Neuronal Circuit

The relative temporal and spatial integration of excitatory and inhibitory signals at any individual neuron depends on the synapse and properties of neuron per se. The adrenergic and nonadrenergic inhibitory nerves reduce the excitability and firing frequency in SIPs and ICC-MY, and suppress the intrinsic reflex pathways. The final result is the slowing down of gastric motility. The following nomenclature of synapses is adopted depending on their location on the neuron: axo-axonic, axo-somatic, axo-dendritic and dendro-denritic. The particular combination of neurotransmitters and receptors involved in the dynamics of transduction correlates with specific functional classes of nerves.

Consider a two neuronal circuit composed of an excitatory and inhibitory neuron which interact at the axo-axonal synapse as shown in Fig. 8.1. Assume that the action potential propagating along the axon and the IPSP sum up linearly

$$V_{sum} = V|_{s=s*} + V_{syn}^{(-)}, \tag{8.30}$$

where $s = s^*$ is the Lagrange coordinate of the synapse. The mathematical formulation of the problem includes the system of equations for: the action potential propagation along the axons (7.1)–(7.4); electrochemical signal transduction mechanisms at the synapse (7.5, 7.6, 7.8, 7.10); the inhibitory postsynaptic potential development (7.11); synaptic interaction at the axo-axonal synapse (8.30) with specified initial and boundary conditions (7.7, 7.8, 7.12).

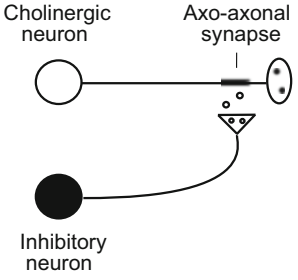

Fig. 8.1 A two neuronal assembly with an axo-axonal inhibitory synapse

8.6.2 SIP-Mechanosensory-Motor Neuron Circuit

Consider SIP linked to a ganglion represented by the afferent primary sensory and the effector motor neurons. The given arrangement acts as a motor-sensory unit in the stomach and can operate independently with a certain degree of automaticity. It generates: (i) non-propagating slow waves through ICC-MI and its myogenic component, (ii) spikes, (iii) contractions (deformations) of SMC, (iv) dendritic action potentials at the free nerve endings of the sensory neuron, (iv) the propagating wave of depolarization in axons, (v) action potentials at the somas of the sensory and motor neurons, (vi) EPSP at chemical, axo-somatic, and electrical synapses. It is noteworthy that the motor neuron makes direct synaptic-like contact with ICC-IM and SM of SIP (Fig. 8.2).

The mathematical formulation of the problem as stated above comprises of a system of equations: (7.1)–(7.6), (7.8), (7.10)–(7.11), (8.3)–(8.11), (8.14)–(8.18), initial and boundary conditions (7.7), (7.8), (7.12), (8.12), (8.28) and (8.29).

8.6.3 A Network of Excitable Cells

Currently little is known about histomorphological topology of interganglionic connectivity within Auerbach's plexus in the human stomach. Quantitative analysis of ICC distribution has demonstrated a significantly lower number of cells in the body and antrum of the organ compared to the fundus. On the other hand, the area covered by the ICC network is similar in each gastric region. This could be due to the difference in the morphology and the degree of ramification of ICC. Although it is difficult to provide a morphofunctional correlation between Auerbach's and

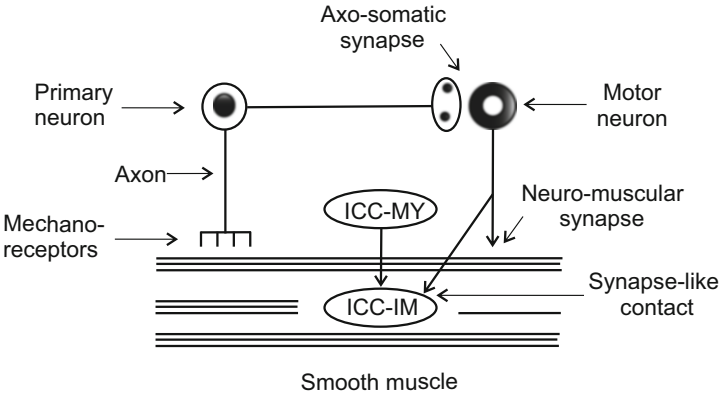

Fig. 8.2 Cellular arrangements in the SIP-motor neuron unit

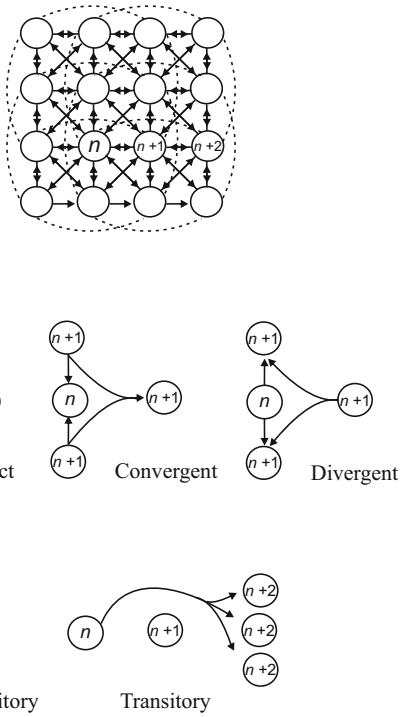

Fig. 8.3 The structure of a functional element of the MP-ICC/PDGFRα^{+}-MY (IM) network and exercised interneuronal arrangements

ICC-MY plexi connectivity, it is reasonable to assume the following neuronal correlates (Fig. 8.3)

(i) *direct*—connects n and the adjacent, oral or aboral, $(n + 1)$ neurons;
(ii) *transitory*—passes signals from n to $(n + 2)$ neuron;
(iii) *divergent*—communicates signals from n to $(n + i)$ $(i = 1, 2, ...)$ interneurons;
(iv) *convergent*—transmits signals from $(n + i)$ interneurons to n neuron;
(v) *local inhibitory*—provides self-inhibition within a ganglion.

Such a discrete network architecture of weakly connected oscillators, SIPs, enables a dynamical framework for universal (stability, phase-locked oscillatory activity) and intrinsic (action potentials, electrochemical coupling) patterns of physiological behavior. The spatio-temporal symmetry of connectivity guarantees the occurrence of rhythmic activities including slow waves of different frequencies and amplitude, and travelling waves. The spontaneous desynchronization of firing activity of cells and breaking of symmetry may enhance a network's ability to generate a variety of irregular myoelectrical rhythms, e.g. reverberating waves, gastric arrhythmias. However, the nonlinear delayed feedback control mechanisms counteract abnormal interactions and thus restore the natural frequencies of oscillation in the system.

References

Aldrete JS, Shepard RB, Halpern NB, Jimenez H, Piantodosi S (1982) Effects of various operations on the electrical activity of the human stomach recorded during the postoperative recovery period. Ann Surg 195(5):662–668

Baker SA, Hennig GW, Salter AK, Kurahashi M, Ward SM, Sanders KM (2013) Distribution and Ca^{2+} signaling of fibroblast-like (PDGFRα^{+}) cells in the murine gastric fundus. J Physiol 591:6193–6208

Bielefeldt K (1999) Molecular diversity of voltage-sensitive calcium channels in smooth muscle cells. J Lab Clin Med 133:469–477

Fitzhugh R (1955) Mathematical models of threshold phenomena in the nerve membrane. Bull Math Biophys 17:257–278

Gerstner W, Kistler WI (2002) Spiking neuron models. Single neurons, populations, plasticity. Cambridge University Press, Cambridge

Graham B, van Ooyen A (2006) Mathematical modelling and numerical simulation of the morphological development of neurons. BMC Neurosci 7(Suppl 1):S9. doi:10.1186/1471-2202-7-S1-S9

Hansen MB (2003) The enteric nervous system I: Organization and classification. Basic Clin Pharm Toxicol 92(3):105–113. doi:10.1034/j.1600-0773.2003.t01-1-920301.x

Hill-Eubanks DC, Werner ME, Heppner TJ, Nelson MT (2011) Calcium signaling in smooth muscle. Cold Spring Harb Perspect Biol 3:1–22

Hodgkin A, Huxley A (1952) A quantitative description of membrane current and its application to conduction and excitation in nerve. J Physiol (London) 117:500–544

Holden AV, Yoda M (1981) Ionic channel density of excitable membrane may act as a bifurcation parameter. Biol Cyber 42:29–38

Huizinga JD, Golden CM, Zhu Y, White EJ (2004) Ion channels in interstitial cells of Cajal as targets forneurotransmitter action. Neurogastroenterol Motil 16(Suppl 1):106–111

Izhikevich EM (2003) Simple model of spiking neurons. IEEE Trans Neur Netw 14:1569–1572

Kepler TB, Marder E (1993) Spike initiation and propagation on axons with slow inward currents. Biol Cyber 68:209–214

Kito Y (2011) The functional role of intrasmuscular interstitial cells of Cajal in the stomach. J Smooth Muscle Res 47(2):47–53

Manneschi LI, Pacini S, Corsani L, Bechi P, Faussone-Pellegrini MS (2004) Interstitial cells of Cajal in the human stomach: distribution and relationship with enteric innervation. Histol Histopathol 19:1153–1164

Mitsui R, Komuro T (2002) Direct and indirect innervation of smooth muscle cells of rat stomach, with special reference to the interstitial cells of Cajal. Cell Tissue Res 309(2):219–227

Miura RM (2002) Analysis of excitable cell models. J Comput Appl Math 144:29–47

Perez-Reyes E (2003) Molecular physiology of low-voltage-activated t-type calcium channels. Physiol Rev 83:117–161

Rich A, Farrugia G, Sarr MG, Szurszewski J (1998) Calcium currents in interstitial cells from human jejunum. Gastroenterology 114:A826

Sanders KM, Ward SM, Koh SD (2014) Interstitial cells: regulators of smooth muscle function. Physiol Rev 94:859–907

Schierwagen A (2009) Mathematical and computational modeling of neurons and neuronal ensembles. In: Moreno-Diaz R, Pichler F, Quesada-Arencibia A (eds) EUROCAST, LNS 5717. Springer, Berlin, pp 159–166

Stoddard CJ, Waterfall WE, Brown BH, Duthie HL (1973) The effects of varying the extent of the vagotomy on the myoelectrical and motor activity of the stomach. Gut 14:657–664

Stoddard CJ, Waterfall WE, Brown BH, Duthie HL (1975) The immediate and delayed effects of differernt types of vagotomy on human gastric myoelectrical activity. Gut 16:165–170

Strege PR, Ou Y, Sha L, Rich A, Gibbons SJ, Szurszewski JH, Sarr MG, Farrugia G (2003) Sodium current in human intestinal interstitial cells of Cajal. Am J Physiol Gastroint Liv Physiol 285:G1111–G1121

Tian L, McClafferty H, Chen L, Shipston MJ (2008) Reversible tyrosine protein phosphorylation regulates large conductance voltage- and calcium-activated potassium channels via cortactin. J Biol Chem 283:3076–3076

Wilson HR (1999) Spikes, decisions, and actions: the dynamical foundations of neuroscience. Oxford University Press, Oxford

Chapter 9
Pharmacology of Gastric Dysmotility

Mathematics takes us to the region of absolute necessity...
Bertrand Russell

9.1 Pharmacological Preliminaries

Successful drug discovery requires deep understanding of the mechanisms of diseases, the full biological context of the drug target and biochemical mechanisms of drug action. It should involve a multilevel conceptual framework which would allow the integration and variation of parameters and constants within the biological system with high precision. A systems computational biology approach as a thorough quantitative and qualitative interrogation of biological processes within the physiological milieu in which they function, provides a new paradigm to study the combined behavior of interacting components through the integration of experimental, mathematical and computational methods.

The development of drugs for clinical use calls for standard test models in which a large number of substances can be analyzed simultaneously to determine how and whether drugs contribute to the overall physiological response. Mathematical modeling and simulations in the form of virtual laboratories offer a uniform platform for bridging gaps in our understanding of intricate biological mechanisms and for generating new hypotheses that are not realizable within a conventional laboratory setting. Verified experimentally, they serve as predictors in the iterative process of identification, validation and evaluation of drug targets, assist in developing new drug treatment strategies, and supply a valuable insight into questions of drug design, efficacy and safety.

The majority of pharmacological agents used in clinical practice act to alter the processes responsible for transmission by facilitating or inhibiting: (i) release, (ii) enzymatic degradation of the neurotransmitter or modulator, (iii) function of specific postsynaptic receptors, (iv) second messenger system, or (v) intracellular regulatory pathways. For example, N-type calcium ion channel blockers—derivatives of ω-conopeptides—interfere with the dynamics of cytosolic Ca_i^{2+} in the presynaptic nerve terminal. The decreased intracellular calcium concentration

R.N. Miftahof, *Biomechanics of the Human Stomach*,
DOI 10.1007/978-3-319-59677-8_9

prevents activation of calmodulin protein and movement of vesicles containing neurotransmitters towards the presynaptic membrane. Chemical agents that facilitate cholinergic and adrenergic neurotransmission can inhibit true and pseudo-acetylcholinesterase, monoamine oxidase and catechol-O-methyltransferase enzymes in the synaptic cleft.

There are more than 20 families of receptors that are present in the plasma membrane altogether representing over 1000 proteins of the receptorome (Strachan et al. 2006). Transmembrane and intracellular receptors, having a wide array of potential ligands, are being used as drug targets. To date only a small percentage of the receptorome has been characterized. The abilities of a ligand to react with a receptor depend on its specificity, affinity, and efficacy. Selectivity is determined by chemical structure and is related to physicochemical association of the drug with a recognition (orthosteric) site on the receptor. The probability at which the ligand occupies the recognition site is referred to as affinity, and the degree at which the drug produces the physiological effect is defined as efficacy. Since different receptors are expressed in the human stomach, it is evident that disparate ligands acting alone or conjointly may elicit similar responses.

A given receptor may contain one or more binding sites for various ligands and can be linked to different second messenger systems. The interaction of a drug with the site that is topographically distinct from the orthosteric site is called allosteric (Monod et al. 1965). The essential features of an allosteric drug-receptor interaction are: (i) the binding sites do not overlap, (ii) interactions are reciprocal in nature, and (iii) the effect of an allosteric modulator could be either positive or negative with respect to association and/or function of the orthosteric ligand. Thus, the binding of a drug to the receptor changes its conformational state from the original tensed to the relaxed form thereby either facilitating or inhibiting the linking of the transmitter.

Drugs that act at receptors are broadly divided into agonists and antagonists. Ligands that interact with the orthosteric site of a receptor and trigger the maximum response are called full agonists. Related to them structurally are partial agonists but with lower biological efficacy. They are regarded as ligands with both agonistic and antagonistic effects, i.e. in the case of conjoint application of a full and partial agonist, the latter competes for receptor association and causes a net decrease in its activation (Kenakin 2004). In practice, partial agonists either induce or blunt a physiological effect, depending on whether an inadequate or excessive amount of endogenous transmitter is present, respectively.

Receptors that exhibit intrinsic basal activity and that may initiate biological effects in the absence of a bound ligand are called constitutively active. Their function is blocked by application of inverse agonists—drugs that not only inhibit the association of an agonist with the receptor but also interfere with its activity. This pharmacokinetic characteristic distinguishes them from true competitive antagonists. Many drugs that have been previously classified as antagonists are being reclassified as inverse agonists.

A class of drugs that have selectivity and affinity, but no efficacy for their cognate receptor are called antagonists. Antagonists that interact reversibly at the active site are known as competitive. Once bound, they block further association of

an agonist with the receptor and thus prevent the development of a biological response. Ligands that react allosterically are called non-competitive. They stop the conformational changes in the receptor necessary for its activation. A subtype of non-competitive ligands that require agonist-receptor binding prior to their association with a separate allosteric site is called uncompetitive. Their characteristic property is related to the effective blocking of higher, rather than lower, agonist concentrations.

Ligands that affect second messenger system function are classified according to the enzyme they act on. There are competitive selective and nonselective cAMP, PKA, PKC, PDE, DAG, Ca^{2+}-ATPase, etc activators and inhibitors. Since a single enzyme is often involved in multiple regulatory pathways, drugs of this category have a narrow therapeutic index and many side effects. Despite their pharmacokinetic and clinical limitations, they are widely used in laboratory research as a new approach in the management of gastrointestinal motility disorders.

All drugs, depending on the stability of the drug-acceptor complex that is being formed, show reversible or irreversible interaction. Reversible ligands have strong chemical affinity to a natural transmitter or modulator and normally form an unstable complex which quickly dissociates into a drug and a "receptor". By contrast, irreversible drugs are often chemically unrelated to the endogenous transmitter and covalently bind to the target creating a stable complex.

9.2 Model of Competitive Antagonist Action

Let L_{At} be the competitive reversible antagonist. A part of the state diagram of signal transmission that describes ligand action is shown in Fig. 9.1, while other reactions in the general cycle remain unchanged.

Assuming that the reactions of association/dissociation of the antagonists (L_{At}) with the receptor (R) and the drug-receptor complex ($L_{At} \cdot R$) formation satisfy the Michaelis-Menten kinetics, the governing system of equations (7.24) is

$$d\mathbf{X}_{At}/dt = \mathbf{D}_{At}\mathbf{X}_{At}(t) + \mathbf{C}_{0,At}. \tag{9.1}$$

The matrix $\mathbf{D}_{At}$ is the extension of the matrix $\mathbf{D}$ (Eq. 7.10)

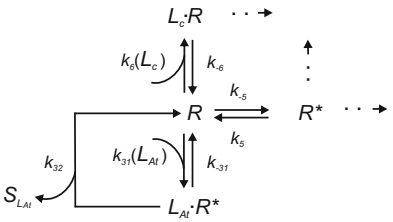

Fig. 9.1 The state diagram of signal transduction in the presence of a reversible antagonist

$$\mathbf{D}_{At} = \begin{pmatrix} a_{ij} & \cdots & & 0 & 0 \\ & & b_{kl} & 0 & 0 \\ 0 & \cdots & 0 & c_{kl} & 0 \\ & & & d_{35,35} & d_{35,36} \\ 0 & \cdots & & d_{36,35} & d_{36,36} \end{pmatrix}, \quad \mathbf{X}_{At}(t) = \begin{pmatrix} X_1 \\ \vdots \\ X \\ X_{29} \\ \vdots \\ X_{34} \\ X_{42} \\ X_{43} \end{pmatrix}, \quad \mathbf{C}_{0,At} = \begin{pmatrix} 0 \\ \vdots \\ 0 \\ C_{30} \\ \vdots \\ C_{34} \\ 0 \\ 0 \end{pmatrix},$$

where the modified elements and new elements are given by

$$\begin{aligned} a_{5,21} &= -k_{31}[X_5], \quad a_{5,22} = k_{-31} + k_{32}, \\ d_{35,35} &= -k_{31}[X_5], \quad d_{35,36} = k_{-31}, \\ d_{36,35} &= k_{31}[X_5], \quad d_{36,36} = -(k_{-31} + k_{32}). \end{aligned}$$

New components of the vector $\mathbf{X}_{At}$ are define: $X_{42} \coloneqq L_{At}$, $X_{43} \coloneqq L_{At} \cdot R$. To close the system, it should be complemented by initial values for L_{At} and $L_{At} \cdot R$.

In case of partial chemical equilibrium, which could be achieved after prolonged treatment with the antagonist, the dynamics of the receptor, drug and drug-receptor complex conversions can be described by,

$$\begin{aligned} \frac{d\left[X_{5(42)}\right]}{dt} &= -k_{31}[X_5][\bar{X}_{42}] + k_{-31}[\bar{X}_{43}] \\ \frac{d[X_{43}]}{dt} &= k_{31}[X_5][\bar{X}_{42}] - k_{-31}[\bar{X}_{43}]. \end{aligned} \tag{9.2}$$

Here $[\bar{X}_{42}], [\bar{X}_{43}]$ are equilibrium concentrations of the drug and the bounded complex, respectively. Summation of equations for $[X_5], [X_{43}]$ yields

$$\frac{d[X_5]}{dt} + \frac{d[X_{43}]}{dt} = 0 \quad \text{or} \quad [X_5](t) + [\bar{X}_{43}](t) = \text{const}, \tag{9.3}$$

from where letting the concentration of total available receptors $[X_5]_0 = \text{constant}$, we get

$$[X_5](t) = [X_5]_0 - [\bar{X}_{43}](t). \tag{9.4}$$

Since $d(L_{At} \cdot R)/\mathrm{d}t = 0$, substituting Eq. (9.4) into the second equation of (9.2) and after simple algebra, we obtain

$$[\bar{X}_{43}](t) = \frac{K^*[X_5]_0}{K^* + [\bar{X}_{42}]^{-1}}. \tag{9.5}$$

Here $K^* = k_{31}/k_{-31}$ is the Michaelis-Menten equilibrium constant.

Finally, the dynamics of receptors in presence of a competitive antagonist and a corresponding endogenous transmitter (L_c), e.g. ACh, adrenaline, is given by

$$[X_5](t) = [X_5]_0 - [\bar{X}_{43}](t) - [X_6](t) - [\bar{X}_8](t). \tag{9.6}$$

Here $[X_6](t)$ is the concentration of constitutively active receptors, and $[\bar{X}_8](t)$ is the equilibrium concentration of the $L_c \cdot R$-complex.

Substitution of Eq. (9.6) into (9.1) allows some simplifications in the governing system of equations.

9.3 Model of Allosteric Interaction

Two broad conceptual views underlie the majority of studies of allosterism. The first, developed initially in the field of enzymology, is based on the assumption that proteins possess more than one binding site that can react successively with more than one ligand. The second considers allosterism as the ability of receptors to undergo changes that eventually yield an alteration in affinity of the orthosteric sites for endogenous transmitters (Monod et al. 1965; Koshland et al. 1966).

Accordingly, two types of mathematical models, i.e. concerted and sequential, along with their various expansions and modifications, have been proposed to simulate cooperative binding. The concerted model assumes that:

(i) enzyme (receptor) subunits in equilibrium attain the identical—tensed or relaxed—conformation,
(ii) it is affected by an allosteric effector,
(iii) a conformational change in one subunit is conferred equally to all other subunits.

By contrast, the sequential model does not require the satisfaction of conditions (i) or (iii) but instead dictates an induced fit binding of the ligand with subsequent molding of the target instead.

Consider a modified part of the general state diagram of allosteric ligand-receptor interaction (Fig. 9.2). Positive non-competitive allosteric mechanism assumes binding of the ligand L_{All} to the receptor in the R^{T} conformation. The $L_{All} \cdot R^{\mathrm{R}}$-complex further associates with the endogenous transmitter L_c and produces the active complex—$L_c \cdot R^{\mathrm{R}} \cdot L_{All}$. In an instance of uncompetitive positive allosteric mechanism, the transmitter L_c binds to the R^{T}-receptor, changes its configuration to $L_c \cdot R^{\mathrm{R}}$ form, and only then the ligand L_{All} occupies the allosteric

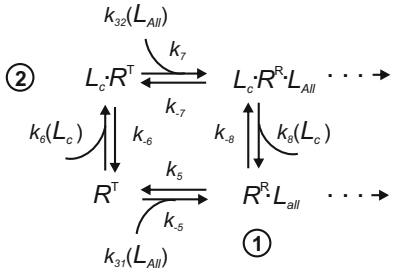

Fig. 9.2 The state diagram of allosteric ligand–receptor interaction

site. The $L_c \cdot R^R \cdot L_{All}$-complex reacts with the *G*-protein system and enters the cascade of chemical transformations as described above (Fig. 7.5).

Comparison of the unperturbed and current schemes gives: $X_5 \coloneqq R^T, X_6 \coloneqq L_{All} \cdot R^R$, $X_7 \coloneqq L_c \cdot R^R \cdot L_{All}$, $X_8 \coloneqq L_c \cdot R^T$. Assuming that all reactions satisfy the Michaelis-Menten kinetics, the system of equations for allosteric interaction is given by

$$d\mathbf{X}_{All}/dt = \mathbf{D}_{All}\mathbf{X}_{All}(t) + \mathbf{C}_{0,All}. \tag{9.7}$$

Here $\mathbf{X}_{All}(t) = (X_1, \ldots, X_{34}, X_{44})^T$, $\mathbf{C}_{0,At} = (0, \ldots C_{30}, 0, \ldots 0, C_{34}, 0)^T$, $X_{44} \coloneqq L_{All}$.

The matrix $\mathbf{D}_{All}$ contains the modified matrix $\mathbf{D}$ (Eq. 7.24) and the additional new elements

$$\begin{aligned}
a_{4,35} &= k_{-6}[X_8] + k_{31}[X_5],\\
a_{5,35} &= k_{-6}[X_8] - k_{31}[X_5],\\
a_{6,35} &= k_{31}[X_5],\\
a_{7,35} &= k_{32}[X_8],\\
a_{8,35} &= -(k_{-6} + k_{32})[X_8],\\
d_{35,4} &= k_5[X_6] + k_6[X_5],\\
d_{35,7} &= k_{-7},\\
d_{35,35} &= -k_{31}[X_5](k_{-6} + k_{32})[X_8].
\end{aligned}$$

By contrast to competitive antagonists which cause a theoretically limitless rightward shift of the dose-occupancy and dose-effect curves for endogenous transmitter, allosteric ligands attain a limit which is defined by the binding factor. Thus, allosteric agonists applied conjointly with agonists and endogenous transmitters, can enhance their spatial and temporal selectivity at the given receptor's site.

9.4 Allosteric Modulation of Competitive Agonist/Antagonist Action

One of the intriguing pharmacological properties of allosteric drugs is their potential ability to alter selectivity, affinity and efficacy of bound and non-bound competitive agonists/antagonists by enhancing or inhibiting their cooperativity at receptor sites. During the last decade, the effect of different allosteric compounds has been studied extensively in vivo and in vitro. For example, it was found that gallamine diminishes the affinity of bound acetylcholine and inhibits its negative ionotropic and chronotropic effects in the myocardium, while alcuronium exerts positive allosteric modulation on the affinity of ACh (Stockton et al. 1983; Tucek et al. 1990). Radioligand binding studies with the human adenosine A_1 receptor revealed the diverse regulatory effects of the allosteric modulator (PD81,723) on the affinity of a partial agonist (LUF5831), a full agonist (N^6-cyclopentyl-adenosine (CPA)), and an inverse agonist/antagonist (8-cyclopentyl-1,3-dipropylxanthine—DPCPX), for the receptor. Results demonstrated that it increased the affinity of CPA, slightly decreased the affinity of LUF5831 and significantly reduced the affinity of DPCPX (Heitman et al. 2006). Therefore, therapeutically, allosteric ligands are capable of modifying signals carried by the exogenous and/or endogenous ligands in the system.

Let the gastric wall under consideration be exposed simultaneously to a competitive agonist (antagonist), $L_{Ag(ant)}$, allosteric ligand, L_{All}, and the endogenous transmitter, L_c. The proposed state diagram of their interactions is shown in Fig. 9.3. It combines noncompetitive and uncompetitive allosteric mechanisms of action which involve binding of L_{All} to the receptor R^{T}, formation of the $L_{All} \cdot R^{\mathrm{R}}$-complex followed by binding of the agonist (antagonist) $L_{Ag(ant)}$ and the transmitter L_c to it, and an inverse sequence, i.e. binding of $L_{Ag(ant)}$ and L_c to the receptor R^{T} first with the subsequent addition of the ligand L_{All}. As a result of both processes, the $L_c \cdot L_{Ag(ant)} \cdot R^{\mathrm{R}} \cdot L_{All}$ active (inactive) complex is produced.

The governing system of equations for positive noncompetitive allosteric modulation of the agonist (antagonist) action is

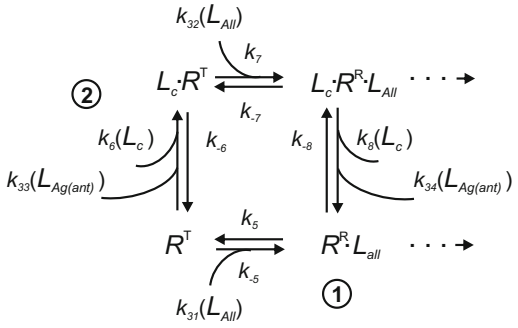

Fig. 9.3 The state diagram of the effects of a competitive agonist/antagonist and allosteric ligand on neurotransmission

$$d\mathbf{X}_{Am}/dt = \mathbf{D}_{Am}\mathbf{X}_{Am}(t) + \mathbf{C}_{0,Am}. \tag{9.8}$$

The vector of reacting components is $\mathbf{X}_{Am}(t) = (X_1, \ldots, X_{34}, X_{42}, \ldots, X_{46})^{\mathrm{T}}$, where $X_5 := R^{\mathrm{T}}$, $X_6 := L_{All} \cdot R^{\mathrm{R}}$, $X_7 := L_c \cdot R^{\mathrm{R}} \cdot L_{All} \cdot L_{Ag}$, $X_8 := L_c \cdot R^{\mathrm{T}} \cdot L_{Ag}$, $X_{42} := L_{Ag}$, $X_{43} := L_{Ag} \cdot R^{\mathrm{T}}$, $X_{44} := L_{All}$, $X_{45} := L_{All} \cdot R^{\mathrm{R}} \cdot L_{Ag}$, $X_{46} := L_{All} \cdot R^{\mathrm{R}} \cdot L_c$. The meaning of other components is as described in Eq. (7.24). The vector of constant concentrations of substrates is $\mathbf{C}_{0,Am} = (0, \ldots C_{30}, 0, \ldots 0, C_{34}, 0, \ldots 0)^{\mathrm{T}}$.

The matrix $\mathbf{D}_{Am}$ is obtained from the general matrix $\mathbf{D}$ where the following elements are adjusted and new elements are introduced

$$\begin{aligned}
a_{44} &= k_2([E_0] - [X_8]) + k_6[X_5] + (k_{-8} + k_5 + k_6)[X_6] + \\
&\quad + k_{-11}[X_{10}] + (k_{-8} + k_8)[X_{45}], \\
a_{4,42} &= k_{34}[X_6] + k_{-6}[X_{46}], \\
a_{4,44} &= k_{31}[X_5], \\
a_{5,42} &= k_5[X_6], \\
a_{5,44} &= -k_{31}[X_5], \\
a_{64} &= k_8[X_{45}] - k_6[X_6], \\
a_{65} &= k_{31}[X_{44}], \\
a_{66} &= -k_{-8}[X_4] - (k_5 + k_{-10}k_{19}[X_{18}])[X_{12}] - k_5([X_{42}] + [X_4]), \\
a_{6,42} &= k_{-6}[X_{45}] - k_{34}[X_6], \\
a_{7,45} &= k_{-8}[X_4] + k_3[X_{42}], \\
d_{42,4} &= (k_6 + k_8)[X_{45}], \\
d_{42,5} &= k_{31}[X_{44}], \\
d_{42,7} &= k_{-6}, \\
d_{42,42} &= (k_5 + k_{34})[X_6] + (k_{-6} + k_{34})[X_{46}], \\
d_{44,6} &= k_5[X_{42}], \\
d_{44,44} &= k_5[X_6] - k_{31}[X_5], \\
d_{45,6} &= k_{34}[X_{42}], \\
d_{45,7} &= k_8, \\
d_{45,45} &= -(k_{-8} + k_8)[X_4], \\
d_{46,6} &= k_6[X_4], \\
d_{46,7} &= k_8, \\
d_{46,46} &= -(k_{-6} + k_{34})[X_{42}].
\end{aligned}$$

In case of uncompetitive positive allosteric modulation the vector of reacting components is $\mathbf{X}_{Am}(t) = (X_1, \ldots, X_{34}, X_{42}, \ldots, X_{47})^{\mathrm{T}}$, where $X_{47} := L_c \cdot R^{\mathrm{T}}$ and the meaning of other components is as described above. The vector of constant concentrations of substrates remains unchanged. The matrix $\mathbf{D}_{Am}$ has new elements

$$
\begin{aligned}
a_{44} &= k_2([E_0] - [X_8]) + k_6[X_5] + (k_{-8} + k_5 + k_6)[X_6] + \\
&\quad + k_{-11}[X_{10}] - k_{-6}[X_{43}], \\
a_{4,42} &= k_{-6}[X_{47}], \\
a_{4,44} &= k_{-6}[X_8], \\
a_{54} &= k_{-6}[X_{43}], \\
a_{55} &= (k_{-5} + k_6)[X_4] - k_{33}[X_{42}], \\
a_{5,42} &= k_{-6}[X_{47}], \\
a_{7,44} &= k_{32}[X_8], \\
a_{88} &= -k_{-6} - k_{-7} - (k_{-6} + k_{32})[X_{44}], \\
a_{8,42} &= k_{33}[X_4], \\
a_{8,43} &= k_6[X_{44}], \\
d_{42,42} &= -k_{33}[X_5] + (k_{-6} + k_{33})[X_{47}], \\
d_{42,43} &= k_{-6}[X_4], \\
d_{42,44} &= k_{-6}[X_8], \\
d_{43,42} &= k_3[X_5], \\
d_{44,43} &= -(k_{-6} + k_6)[X_4], \\
d_{43,44} &= k_{-6}[X_8], \\
d_{44,7} &= k_{-7}, \\
d_{44,42} &= k_{33}[X_{47}], \\
d_{44,44} &= -(k_{-6} + k_{32})[X_8] + k_6[X_{43}].
\end{aligned}
$$

Initial concentrations of the reacting components close the system.

9.5 Model of a PDE-5 Inhibitor

Cyclic nucleotide phosphodiesterases are the enzymes catalyzing the hydrolysis and inactivation of the second messengers, cyclic adenosine monophosphate and cyclic guanosine monophosphate. PDE inhibitors potentially increase signaling by inhibiting the cAMP enzyme breakdown.

Let L_{PDE5} be the specific reversible PDE-5 inhibitor. The proposed state diagram of its association with the enzyme is given in Fig. 9.4.

The corresponding system of equations of chemical reactions is

$$d\mathbf{X}_{PDE}/dt = \mathbf{D}_{PDE}\mathbf{X}_{PDE}(t) + \mathbf{C}_{0,PDE}. \tag{9.9}$$

Here $\mathbf{X}_{Am}(t) = (X_1, \ldots, X_{26}, X_{28}, X_{29}, \ldots, X_{34}, X_{48})^{\mathrm{T}}$ where new components have been introduced: $X_{28} := PDE$, $X_{48} := L_{PDE4} \cdot PDE$, $X_{49} := L_{PDE5}$, and the vector $\mathbf{C}_{0,PDE} = (0, \ldots, C_{28}, C_{30}, 0, \ldots 0, C_{34}, C_{48})^{\mathrm{T}}$ where $C_{28} = C_{48} = k_{-35}[X_{49}]_0$.

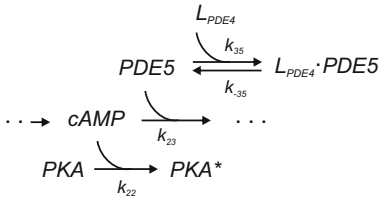

Fig. 9.4 The state diagram of signal transduction in the presence of a PDE-5 inhibitor

The matrix $\mathbf{D}_{PDE}$ can be obtained from $\mathbf{D}$ where the following elements have been changed and added

$$
\begin{aligned}
b_{33} &= -k_{23}[X_{48}],\\
b_{77} &= -k_{35}[X_{48}] - k_{23}[X_{23}],\\
b_{7,36} &= -k_{-35},\\
d_{36,36} &= -k_{-35} - k_{35}[X_{28}].
\end{aligned}
$$

In the above derivations we assumed that the drug is always available, i.e. $[L_{PDE5}] = [X_{49}]_0 = \text{constant}$. Hence, the dynamics of its conversion in the system can be calculated from an algebraic equation

$$[X_{49}](t) = [X_{49}]_0 - [X_{48}](t). \tag{9.10}$$

Initial concentrations of the reacting substrates should be provided to close the problem.

References

Heitman LH, Mulder-Krieger T, Spanjersberg RF, von Frijtag Drabbe Künzel JK, Dalpiaz A, Ijzerman AP (2006) Allosteric modulation, thermodynamics and binding to wild-type and mutant (T277A) adenosine A_1 receptors of LUF5831, a novel nonadenosine-like agonist. Br J Pharm 147(5):533–541

Kenakin T (2004) Principles: receptor theory in pharmacology. Trends Pharm Sci 25:186–192

Koshland DE Jr, Némethy G, Filmer D (1966) Comparison of experimental binding data and theoretical models in proteins containing subunits. Biochemistry 5(1):365-368

Monod J, Wyman J, Changeux JP (1965) On the nature of allosteric transitions: a plausible model. J Mol Biol 12:88–118

Stockton JM, Birdstall NJM, Burgen ASV, Hulme EC (1983) Modification of the binding-properties of muscarinic receptors by gallamine. Mol Pharm 23:551–557

Strachan RT, Ferrara G, Roth BL (2006) Screening the receptorome: an efficient approach for drug discovery and target validation. Drug Disc Today 11:708–716

Tucek S, Musilkova J, Nedoma J, Proska J, Shelkovnikov S, Vorlicek J (1990) Positive cooperativity in the binding of alcuronium and N-methylscopolamine to muscarinic acetyl-choline receptors. Mol Pharm 38:674–680

Chapter 10
A Model of the SIP/Ganglion Unit

Truth is ever to be found in simplicity, and not in the multiplicity and confusion of things.

Isaac Newton

10.1 Mathematical Formulation

The rest of this book will deal with various biomechanical applications of the theory of soft shells used to study the motility of the human stomach. To understand biological phenomena that underlie complex processes like peristalsis, gastroparesis, myenteric neuropathy, gastric arrhythmia, etc we begin with analysis of the basic myoelectrical phenomena.

Consider a one-dimensional biomechanical model of gastric smooth muscle connected to a myenteric ganglion—a SIP/ganglion unit. A distinction will not be made between the longitudinal and circular smooth muscle, therefore subscripts l and c can be omitted. The ganglion is represented by a chain of the primary sensory and motor neurons linked via the axo-somatic synapse. Free nerve endings of the sensory neuron are located on smooth muscle cell, the motor-neuron having the axo-SMC synapse on SIP. The reader should bear in mind that the motor neuron also forms a cholinergic synapse-like connection with ICC-IM.

Let the SIP unit have a length L. The governing equation of its motion is given by (see Eq. (6.85))

$$\rho \frac{\partial v}{\partial t} = \frac{\partial}{\partial \alpha} T, \qquad (0 \leq \alpha \leq L) \qquad (10.1)$$

where ρ represents density, v—velocity, T—force, and α—Lagrange coordinate of the unit, t is time. Assuming that the unit possesses viscoelastic mechanical properties, for the total force T

R.N. Miftahof, *Biomechanics of the Human Stomach*,
DOI 10.1007/978-3-319-59677-8_10

$$T = k_v \frac{\partial(\lambda - 1)}{\partial t} + T^a\left(\left[\mathrm{Ca}_i^{2+}\right]\right) + T^p(\lambda), \tag{10.2}$$

where T^a, T^p are the active and passive components that satisfy Eqs. (6.45, 6.47), λ is the stretch ratio, $[\mathrm{Ca}_i^{2+}]$ is the concentration of intracellular Ca^{2+} given by Eq. (8.17), and k_v is viscosity. Substituting Eq. (10.2) in (10.1) the following is obtained

$$\rho \frac{\partial v}{\partial t} = \frac{\partial}{\partial \alpha}\left(k_v \frac{\partial(\lambda - 1)}{\partial t} + T^a\left(\left[\mathrm{Ca}^{2+}\right]\right) + T^p(\lambda)T\right). \tag{10.3}$$

Myoelectrical cable properties of the unit are described by the modified Hodgkin-Huxley equations

$$C_m \frac{dV}{dt} = \frac{d_m}{R_s}\frac{\partial}{\partial \alpha}\left(\lambda(\alpha)\frac{\partial V}{\partial \alpha}\right) - \sum I_{ion}, \tag{10.4}$$

where the dynamics of ion currents, I_{ion}, satisfy Eqs. (8.25)–(8.27), d_m is the diameter and R_s is the specific resistance of the unit. The meaning of other parameters are as described above.

Myogenic electrical events are a result of activity of the autonomous oscillator. Its dynamics satisfies the system of Eqs. (8.15)–(8.19). Discharges of the cells of Cajal, V_i, are described by Eqs. (8.8)–(8.12). The dynamics of mechanoreceptor activity is given by Eqs. (8.4)–(8.7); the propagation of electrical signal along the axons of neurons is described by Eqs. (7.1)–(7.5); the processes of electrochemical coupling at the synapse with the generation of EPSP/IPSP are given by Eqs. (7.10)–(7.12); and the production of the primary sensory and motor neuron soma action potentials are given by Eqs. (8.8)–(8.12). In the case of the involvement of cAMP or PLC pathways in the cascade of intracellular reactions, additional systems of equations should be considered (see Chap. 8 for details).

The unit is initially in the resting state and concentrations of chemical compounds are known. The excitation is provided by discharges of ICC-MY/MI. The ends of the unit are clamped and remain unexcitable throughout.

10.2 Self-Oscillatory Dynamics of SIP

ICC-MY/IM in the body (corpus) of the human stomach discharge high amplitude spikes at their natural frequency of $\nu = 0.1$ Hz. These pass to the gastric smooth muscle syncytium where they excite multiple transmembrane ion channels. Upon stimulation, L-type Ca^{2+} channels show nonlinear dynamics with the current $\tilde{I}^s_{Ca}$ increasing at a rate of 4.6 nA/s to $\max \tilde{I}^s_{Ca} = -0.51$ nA. The channel remains

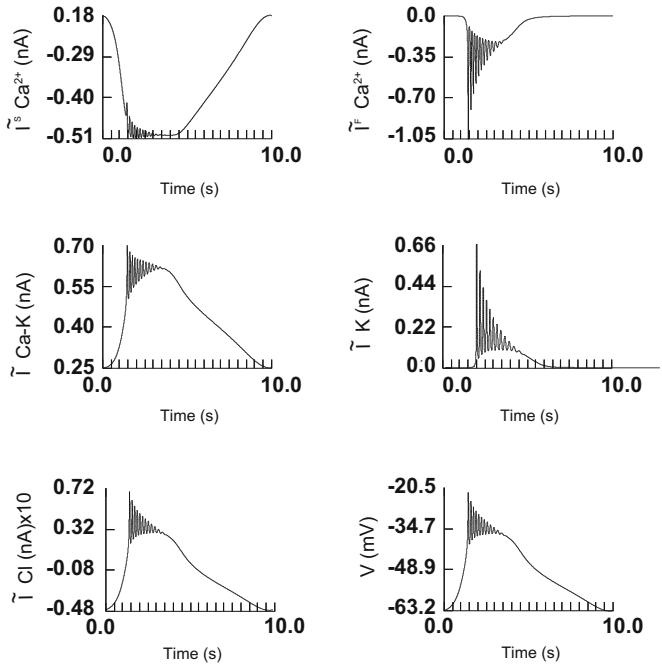

Fig. 10.1 The dynamics of transmembrane ion channels

fully open for the period of 3.2 s and returns to the unexcited state in the following 5.5 s (Fig. 10.1). There is a delay of 1.3 s after the excitation before T-type Ca^{2+} channels become active. The inward $\tilde{I}^f_{Ca}$ current almost instantly reaches its maximum, -1.05 nA. It oscillates for 2 s and attains the intensity of 0.35 nA. The channel stays active for 8.5 s. The outward K^+ ion current is detectable for approximately 5 s and follows the dynamics of $\tilde{I}^f_{Ca}$. It reaches $\max \tilde{I}_K = 0.66$ nA and decays at an average rate of 0.13 nA/s. The Ca^{2+}-activated K^+ current achieves ~0.65 nA in 1.5 s and remains at this level for 2.8 s. It then decreases over 6 s to the unexcitable state, $\tilde{I}_K = 0.25$ nA at $d\tilde{I}_K/dt = 0.07$ nA/s. The alternating chloride current changes direction from an inward $\tilde{I}_{Cl} = -0.48$ nA to an outward $\max \tilde{I}_{Cl} = 0.72$ nA. The Cl^- flux relates to the changes of the membrane potential V of the smooth muscle syncytium.

The ion channel activity triggers the production of slow waves of the amplitude $V = 39$ mV at the frequency 0.1 Hz. The wave rises exponentially from the resting value, $V^r = -69.8$ mV, to the maximum -28 mV. A few spikes of amplitude $V = 12$ mV are generated on the crest of slow waves. The characteristic feature of the gastric slow wave is the presence of the plateau phase of depolarization ~ -35.7 mV of a duration 3.8 s. It is followed by the slow decline of the membrane potential at a rate of 4.5 mV/s to the resting level (Fig. 10.2).

The concomitant intracellular processes are remarkable for fluctuations in free intracellular Ca^{2+} ion concentration. They are tightly linked to the dynamics of voltage-dependent and independent selective transmembrane ion channel and

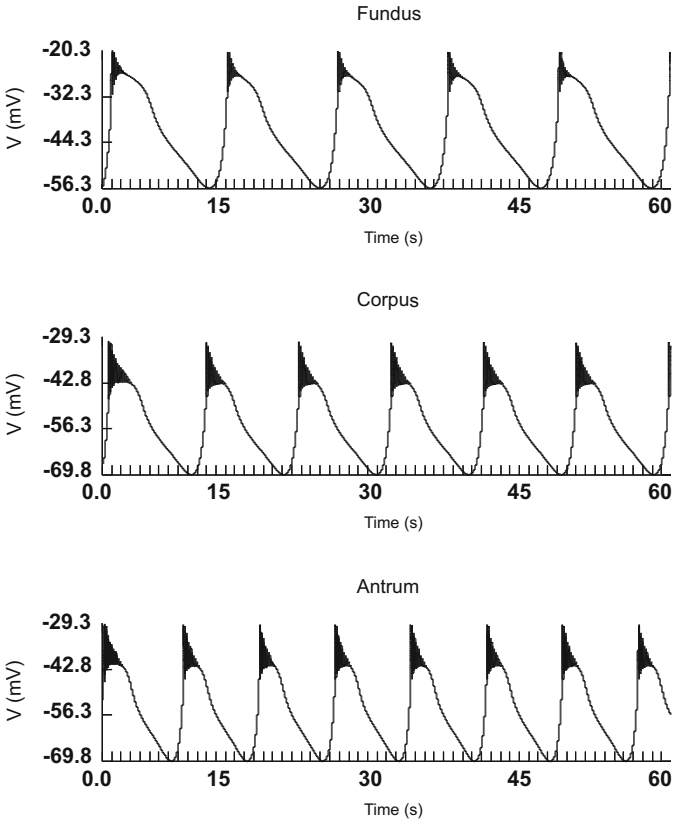

Fig. 10.2 Regional frequency and configuration variations of slow waves

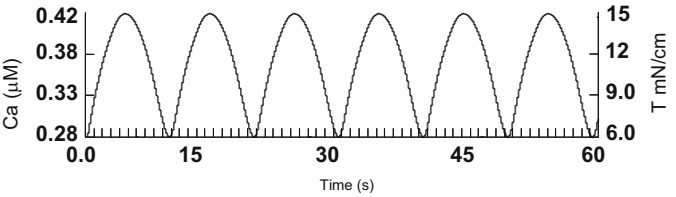

Fig. 10.3 Changes in intracellular calcium and force development in antral SIP

to the mechanisms of Ca^{2+} release from intracellular stores, i.e. the endoplasmic reticulum. The increase in calcium, max $[Ca_i^{2+}] = 0.42$ μM, leads to the activation of contractile proteins with the development of regular phasic contractions of amplitude $T^{\alpha} = 9$ mN/cm and a frequency of 0.1 Hz (Fig. 10.3). They are congruent with oscillations of Ca_i^{2+} and are preceded by slow waves. The degree of

deformation of SIP is relatively small and insufficient to stimulate mechanoreceptors of the primary sensory neuron. As a result the neurons of the ganglion remain idle.

The dynamics of intracellular calcium turnover in ICC and SMC plays a significant role in slow wave frequency. Thus, a reduction in: the activation of the IP_3—pathway, the release of Ca_i^{2+} from the IP_3—receptor operated cellular stores, and an influx of extracellular Ca^{2+} through transmembrane channels reduces the frequencies of ICC and slow waves to 0.084 Hz (Fig. 10.2). This type of myoelectrical activity is characteristic of the fundus of the human stomach. Conversely, a rise in the Ca_i^{2+} turnover, which could be the case of the antral region, has the opposite effect. The number of cycles and the frequency increases to 0.13 Hz.

10.3 Dynamics of the SIP/Ganglion Unit

Let the unit in the antrum of the human stomach of a length L be excited by discharges of: (i) the pacemaker cell at a frequency, $\nu = 0.12$ Hz, and (ii) by five consecutive mechanical stretches of intensity $0.8L$ applied at different frequencies: $\nu_{\mathrm{m}} = 0.132; 0.21; 0.62$ (Hz). Each deformation initiates a unitary action potential of amplitude $V^e = 85$ mV and a duration of 1.8 s at mechanoreceptors on SMCs. The spike propagates towards the soma of the sensory neuron where it triggers a rapid upstroke discharge of amplitude $V_p^s = 105.7$ mV. It subsides successively over 0.34 s to the stable level of -25 mV. These events produce a wave of depolarization of amplitude 75 mV which travels along the axon to the nerve terminal of the axo-somatic cholinergic synapse on the soma of the motor neuron (Fig. 10.4). There it evokes a short-term influx of calcium ions through Ca^{2+} voltage-dependent channels. The amount of free cytosolic calcium quickly rises to attain the maximum of 19.4 μM. Some of the ions are immediately absorbed by the intracellular buffer

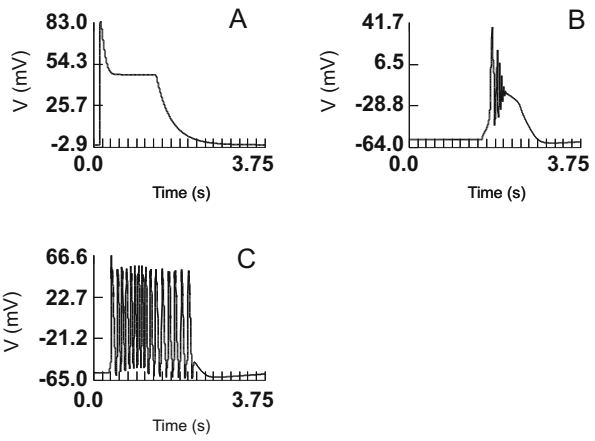

Fig. 10.4 Action potentials in the SIP/ganglion unit. Dendritic (**a**), somatic primary (**b**) and motor (**c**) neuron potentials

system whilst others diffuse towards the ACh containing vesicles. Calcium ions bind to the active centers on vesicles and elicit the release of stored acetylcholine, ACh_v. Initially, the increase of the free fraction of acetylcholine, ACh_f, is slow at an average rate of 0.5 μM/ms when the gush, ~10% of all ACh_v, is discharged at a max $d[ACh_v]/dt = 1.6$ μM/ms. Half of the amount, $ACh_f = 5.38$ μM, diffuses into the synaptic cleft where it occupies 99.2% of postsynaptic receptors. As a result the highly reactive (ACh_c-R)—complex, 0.11 μM, is formed. This leads to the generation of fEPSP of amplitude 87.1 mV. The complex is very unstable and quickly dissociates, releasing receptors.

The postsynaptic ACh undergoes further fission by acetylcholine esterase enzyme with the formation of (ACh_p - E)—complex. It rapidly breaks down into enzyme and choline which is reabsorbed by the nerve terminal and is then drawn into a new cycle of ACh synthesis.

The fast excitatory postsynaptic potential depolarizes the soma of the motor neuron (Fig. 10.4). This fires high amplitude spikes of amplitude $V_m^s = 96$ mV at a constant frequency 12.2 Hz over a period of 1.9 s. Again, a wave of depolarization of the amplitude 75 mV is generated which arrives at the presynaptic terminal of the nerve-ICC and nerve-SMC synapses. There the processes of electrochemical coupling with activation of muscarinic μ_2 and μ_3 type receptors on the smooth muscle cell and the generation of fEPSP, repeats the processes as described above at the axo-somatic synapse.

If the frequency of mechanical deformation equals the firing frequency of ICC, $\nu_m = \nu = 0.12$ Hz, the unit produces unaltered slow waves with action potentials of amplitude, $V = 35 \div 46.6$ (mV), at a constant frequency 7.8 Hz (Fig. 10.5). These appear regularly on the crest of each slow wave and last ~2.6 s. The smooth muscle

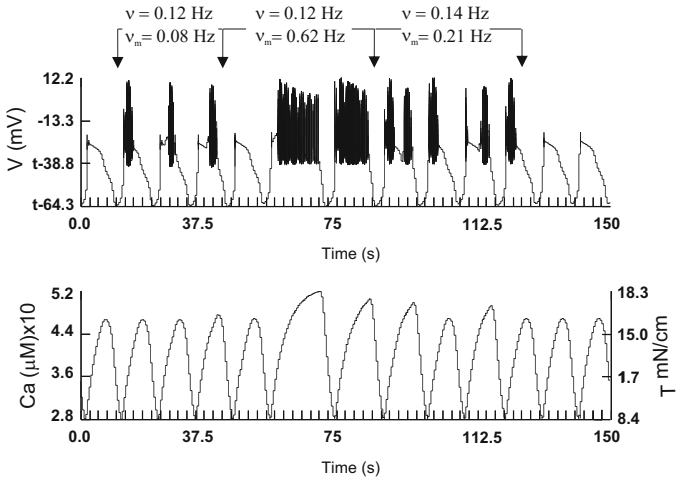

Fig. 10.5 The effects of the firing frequency of ICC and mechanical stimuli on the electromechanical activity of the antral SIP/ganglion unit

syncytium responds with phasic contractions of $\max T^a = 16.5$ mN/cm. The rate of contraction/relaxation is constant, $dT^a/dt = 0.98$ mN/cm·s.

An increase in ν_m to 0.62 Hz triggers a production of a continuous series of action potentials of an average amplitude $V = 38.8$ mV and a frequency 4.5 Hz. Each spike has a duration of 200 ms and shows an even upstroke and down stroke. The duration of slow waves increases to 34.1 s with their frequency decreasing to $\nu = 0.09$ Hz. The unit responds with strong intensive contractions reaching maximum, $T^a = 18.3$ mN/cm, at a rate of 0.37 mN/cm·s. The process of relaxation of the unit goes faster at $dT^a/dt = 1.11$ mN/cm·s.

The irregular spiking behavior by SIP is observed when $\nu_m = 0.21$ Hz, $\nu = 0.14$ Hz. Thus short duration, 5 s, high frequency, 9.8 Hz, and amplitude, 51.3 mV, action potentials are elicited in response to the ICC discharge, whilst spikes induced by mechanical stimuli have a lower frequency, 4.5 Hz, and amplitude, 45.8 mV. The frequency of slow waves also decreases to 0.11 Hz compared to the norm. The mechanical reaction of the unit becomes irregular. The duration and the rate of the rise and decline of the active force of contraction is variable: $t = 10 \div 12.5$ s, $dT^a/dt = 0.53 \div 0.67$ mN/cm·s and $0.92 \div 1.12$ mN/cm·s, respectively. The recorded maximum strength of T^a ranges between $16.1 \div 17.2$ mN.

The dynamics of intracellular calcium in SIP correspond to the dynamics of active force development with $\max [Ca_i^{2+}] = 0.52$ μM.

10.4 Co-transmission and Receptor Polymodality

10.4.1 Acetylcholine and Substance P

Cholinergic neurons are the most prominent in the ENS of the human stomach: only in the fundus of the organ do they constitute $(34.1 \pm 6.1)\%$ (Pimont et al. 2003). At the time of writing, no data was available on the density and spatial distribution of neurotransmitters in other parts of the organ such as the cardia, the body (corpus) and the antrum. Acetylcholine molecules are packed in vesicles at the presynaptic nerve terminals and are released upon stimulation by Ca^{2+}-dependent exocytosis. Postsynaptic metabotropic responses of ACh are mediated by muscarinic, μ_2 and μ_3—$G_{q/11}$, $G_{12/13}$—protein coupled receptors linked to the phospholipase C (PLC) intracellular signaling pathway. Ionotropic effect, on the other hand, is achieved through the activation of ligand gated voltage-dependent Ca^{2+}—channels. Normally, the electrophysiological outcome is characterized by the generation of fast excitatory postsynaptic potentials (fEPSP) of 0.1–0.3 ms duration.

Tachykinins are a family of structurally related neuropeptides: SP, neurokinin A and neurokinin B. A relatively small number of cells, $(2.3 \pm 1.1)\%$, in the fundus of the human stomach are immunoreactive to neuropeptide (Pimont et al. 2003).

Substance P exhibits a plethora of effects including the production of prolonged EPSP and contraction/relaxation of gastric smooth muscle by binding selectively to two distinct ionotropic, NK_1, and metabotropic, NK_3, receptors. Both receptors are members of the G-protein coupled receptor family and employ the IP_3 as well as adenylate cyclase—3′5′ adenosine cyclic monophosphate (cAMP) and protein kinase C (PKC) signaling pathways. They enhance the release of Ca^{2+} from the sarcoplasmic reticulum through ryanodine receptor channels and by opening L-type Ca^{2+} channels. Neurokinin A has a mainly neuronal action via NK_2 receptors.

Let ACh and SP be co-stored in the primary sensory and motor neurons. Assume that: (i) ACh release precedes SP, (ii) ACh and SP interact synergistically, rather than additively, (iii) in addition to muscranic type receptors distributed in the unit as described above, there are NK_1 and NK_2 type receptors on SMCs and NK_1, NK_3 receptors on the soma of the motor neuron and on ICC. These receptors are members of the G-protein coupled receptor family and employ the IP_3 signaling pathway in their signal transduction process.

The trigger in the release of SP is the rise of Ca_i^{2+}. This induces exocytosis of the neurotransmitter from the vesicular stores. The rate of SP release is not constant but rather depends on the $[Ca_i^{2+}]$ and the frequency of applied stimuli. As a response to a single excitation 0.2 μM, SP is released and increases 14.5 times after a high frequency, 0.5 Hz, stimulation. The free fraction of SP diffuses further into the synaptic cleft where max $[SP_c] = 0.056$ μM is recorded. There, a part of SP is utilized by neutral endopeptidase, aminopeptidase and angiotensin converting enzymes whilst another part reaches the postsynaptic membrane. A general tachykinin conformer of the NK receptor binds to SP to form a complex, max [SP-NK] = 0.042 μM. The latter activates guanine-nucleotide G protein, [SP-NK-DAG] = 50 nM, which initiates the PLC signaling pathway. This cleaves phosphatidyl IP_3 to release IP_3 and DAG. IP_3 stimulates the release of Ca^{2+} from the endoplasmic reticulum. Four molecules of Ca_i^{2+} bind to calmodulin which serves as a co-factor in the DAG—PKC pathway. The final step in the cascade is the phosphorylation/dephosphorylation of intracellular proteins by protein-phosphatase. The quantity of active proteins rises to 166 nM and remains at this level for the duration of stimulation. They alter the permeability of transmembrane ion channels and cause the generation of long lasting postsynaptic potentials of low amplitude, 20–40 mV.

SP acting alone has a profound effect on the firing rate of ICC and myoelectrical response of SIP. The frequency of pacemaker discharges increases nearly fourfold from the normal value. The smooth muscle syncytium becomes depolarized, $V = -40.5$ mV, and produces regular slow waves of average amplitude 26 mV at a $\nu = 4$ Hz. The amount of $[Ca_i^{2+}]$ quickly reaches 0.49 μM and stays at this level during the continued presence of reactive proteins. As a result, a long lasting, tonic-type contraction of intensity max $T^a = 25.4$ mN/cm develops (Fig. 10.6).

Consider the conjoint effect of ACh and SP on the dynamics of the SIP/ganglion unit. Let the unit be subjected to a complex electrical stimulation by ICC and mechanical distension at frequencies of $\nu = 0.1$ Hz and $\nu_m = 0.128$ Hz,

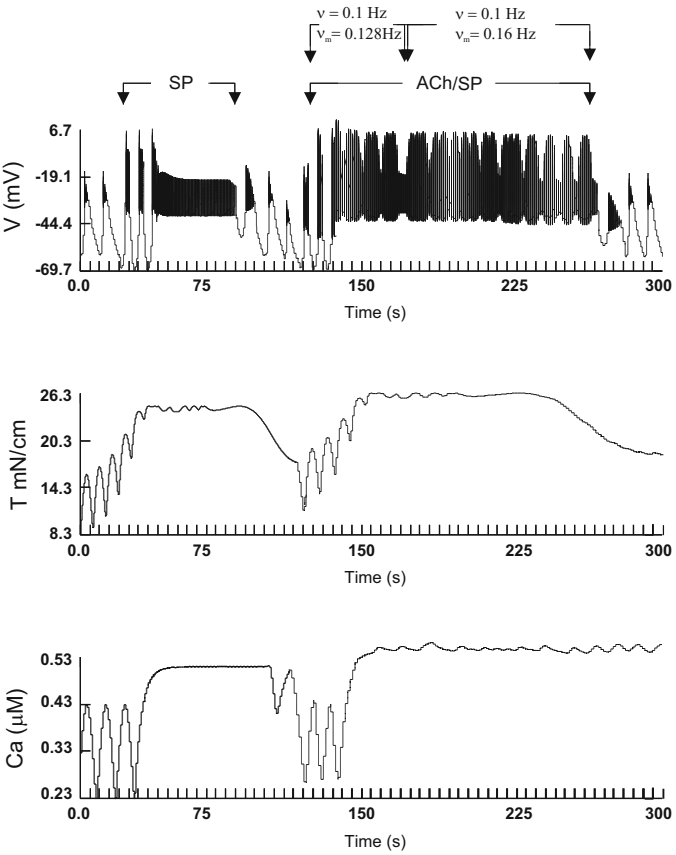

Fig. 10.6 The effect of neurotransmission by ACh, SP, firings of ICC and mechanical stimuli on the electromechanical activity of the antral SIP/ganglion unit

respectively. Fast excitatory postsynaptic action potentials triggered by ACh superimpose on the long-term potentiation curve elicited by SP. The maximum amplitude of depolarization reaches 55 mV (Fig. 10.7). A further increase in ν_{m} to 0.16 Hz does not change the already set pattern of electrical response. Maximum concentration of free calcium ions, 0.53 μM, is attained. As a result, SMCs produce a tonic-type contraction of max $T^a = 26.3$ mN/cm.

10.4.2 Nitric Oxide and Acetylcholine

The inhibitory neurotransmission in the human stomach is mediated by NO and VIP. There are (24.2 ± 4.4)% of neurons positive for NOS in the fundus of the human stomach (Tack et al. 2002; Pimont et al. 2003). NO is formed in the nerve

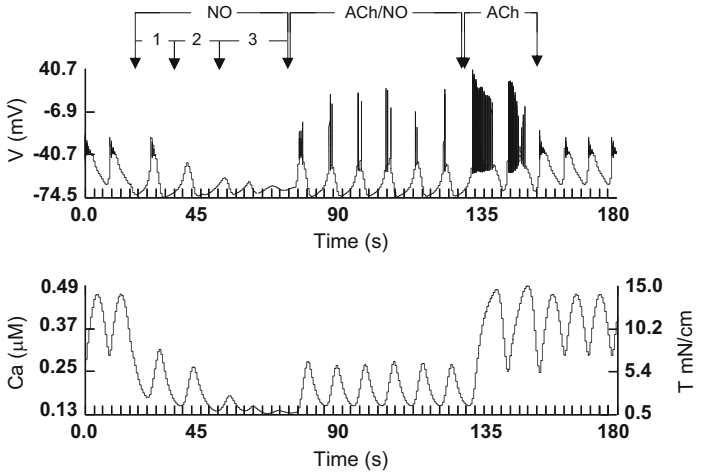

Fig. 10.7 The conjoint effect of ACh and NO released at increasing doses (1 through 3) on the electromechanical activity of the antral SIP/ganglion unit

terminals *de novo* on demand from the precursor, L-arginine, by the two classes of nitric oxide synthase (NOS) enzyme both constitutive and inductive (Thatte et al. 2009). The former is calcium-calmodulin dependent and responsible for rapid biosynthesis of the transmitter, while the latter is activated under protective or pathological states showing a slow rate of synthetic activity. NO elicits inhibitory pre- and postjunctional effects on ganglionic neurons and SMCs. Intracellularly, NO activates soluble guanylate cyclase with the production of 3′,5′-cyclic guanosine monophosphate (cGMP). This further upregulates protein kinase G which in turn phosphorylates phospholamban on the sarcoplasmic reticulum and increases the uptake of Ca_i^{2+}. The ionotropic effects of NO include the opening of large and small conductance K^+ channels, and the possible closure of Ca^{2+} dependent Cl^- and L-type Ca^{2+} channels (Tonini et al. 2000; Takahashi 2003; Koh and Rhee 2013).

Applied directly to gastric antral SIP at a low dose, NO hyperpolarizes the smooth muscle membrane by 6.5 mV, $V^r = -74.5$ mV. However, there are no changes in the dynamics of the upstroke potential of slow waves. An increase in the amount of NO reduces the frequency of ICC and the amplitude of slow waves, $\nu = 0.09$ Hz and $V = 14 \div 30$ mV, respectively (Fig. 10.7). These are linked to a decrease in Ca_i^{2+} to 0.13 μM. Subsequently, the smooth muscle relaxes to $\min T^a = 0.5$ mN/cm. It is noteworthy that NO does not affect the rates of contraction/relaxation, indicating that it does not impact the contractile apparatus of smooth muscle.

When SIP is exposed to ACh and NO conjointly it responds with a production of triplets of action potentials at a frequency of 3 Hz and the amplitude $V = 53 \div 60$ mV. The smooth muscle produces transient rhythmic contractions

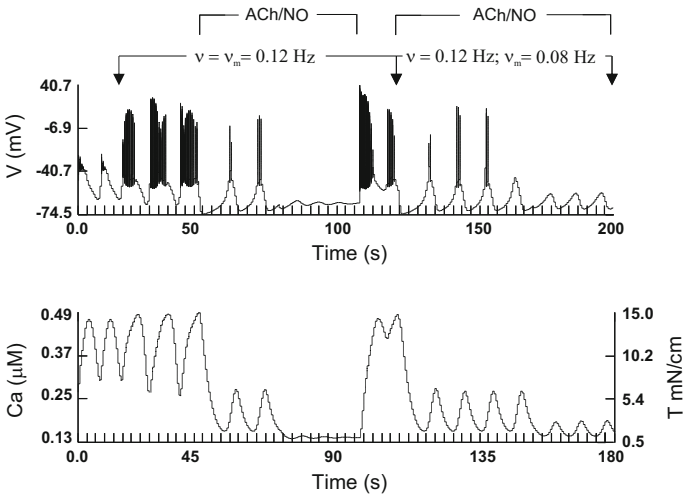

Fig. 10.8 The effect of NO, ACh, firing of ICC and mechanical stimuli on the electromechanical activity of the antral SIP/ganglion unit

of low intensity, $T^a = 4.9$ mN/cm. After NO is washed out, ICC recuperate their natural firing frequency and SMCs regain completely their basal muscle tone, 8.3 mN/cm. The addition of ACh elicits spikes of 65 mV on the crests of slow waves accompanied by strong phasic contractions of $\max T^a = 15$ mN/cm.

Let the SIP/ganglion unit under consideration be influenced by nitroxidergic and cholinergic neurotransmitters. Assume that: (i) ACh and NO are released concurrently and are short acting, (ii) muscarinic μ_2 and μ_3-type receptors are located on the somas of the sensory and motor neurons, SMCs and ICC, and (iii) NO is accessible to all ganglionic neurons. ICC discharge pacemaker potentials at a constant frequency of 0.12 Hz throughout, and mechanical stretches are applied intermittently at variable frequencies: $\nu_{\mathrm{m}} = 0.12$; 0.08 Hz. Results of simulations show that under experimental conditions, NO does not affect the electrical activity of the sensory motor neurons which continue to fire action potentials of unaltered amplitudes and durations. Mechanical stimuli also do not alter the pattern of electromechanical responses observed earlier (Fig. 10.8).

10.4.3 Vasoactive Intestinal Peptide, Substance P, Acetylcholine and Nitric Oxide

Vasoactive intestinal peptide (VIP) is widely distributed in the gastrointestinal tract and the human stomach (Currò et al. 2008). VIP is synthesized as a precursor

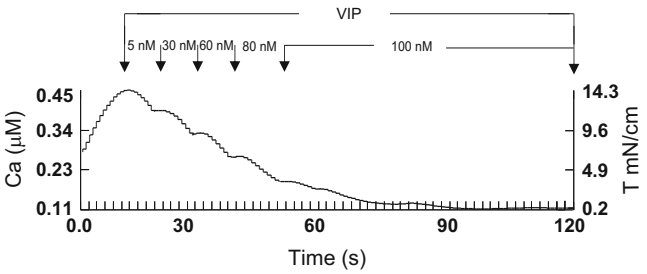

Fig. 10.9 The dose dependent effect of VIP on the mechanical activity of antral smooth muscle

molecule and cleaved further to the active peptide. It is stored in a vesicular form in presynaptic nerve terminals of myenteric neurons. Either brief high, $\geq$ 10 Hz, or sustained low frequency, 0.3–3 Hz, electrical stimuli trigger neuropeptide release into the synaptic cleft. Here it binds to $VPAC_2$ receptors and activates the cAMP/protein kinase A (PKA) transduction pathway (Lefebvre et al. 1995; Currò and Preziosi 1998; Igarashi et al. 2011). It is suggested that being a co-transmitter with NO (7.2 $\pm$ 6% of neurons in the fundus show NO/VIP co-localization), VIP stimulates intracellularly inducible NOS-NO-cGMP pathways and protein kinase G (Tonini et al. 2000; Ergün and Öğülener 2001; Dick et al. 2000). This subsequently leads to: (i) the transient release of Ca^{2+} ions from the sarcoplasmic reticulum via ryanodine receptor channels, (ii) the opening of BK_{Ca} and SK_{Ca} channels, and (iii) the inhibition of L-type Ca^{2+} channels (Sanders 2000). NO in turn facilitates VIP release at the presynaptic nerve terminal (Van Geldre and Lefebvre 2004).

Endogenously applied, VIP relaxes gastric antral SIP in a dose-dependent manner (Fig. 10.9). Thus, the rise in VIP from 3 nM to 100 nM decreases the resting muscle tone and the active force of contractions from 8.3 mN/cm to 0.2 mN/cm and 7.9 mN/cm to zero, respectively.

At frequencies $\geq$ 10 Hz, relaxations of gastric SIP are mostly mediated by conjointly released NO and VIP. Consider the effect of a subsequent release of SP, NO, VIP and ACh on the dynamics of the unit. SP evokes a long-lasting depolarization of SM with the development of a tonic-type contraction of $\max T^a = 26.3$ mN/cm. An incremental increase in the added amount of NO and VIP from 30 $\div$ 100 nM, hyperpolarizes the smooth muscle membrane, $V = -70.8$ mV, and eliminates the production of slow waves. There is a concomitant reduction in free intracellular calcium and the intensity of contractions. Maximum active force $T^a = 15$ mN/cm recorded at VIP 30 nM, reduces to $T^a = 3.7$ mN/cm at VIP 100 nM (Fig. 10.10). Interestingly, the smooth muscle still maintains its basal tone due to the presence of SP. Since the effect of NO is short-lasting, it is masked by the longer-lasting and more potent action of VIP. ACh and extensive mechanical stimulation of the unit cannot reverse the inhibitory effects induced by NO and VIP.

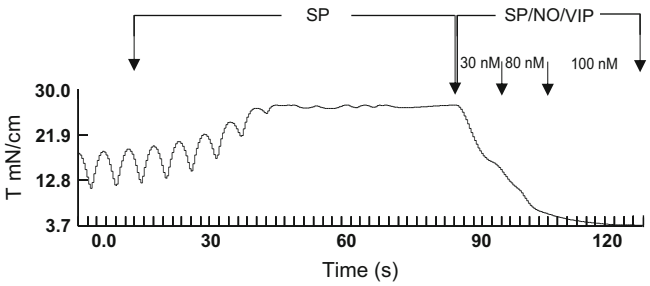

Fig. 10.10 The effect of neurotransmission by SP, NO and VIP, released at increasing doses, on the contractility of gastric smooth muscle

10.4.4 Acetylcholine, Serotonin and Nitric Oxide

The biogenic amine, serotonin (5-HT), is produced and stored in granules in the enterochromaffin cells and neurons of the myenteric plexus of the gut. The main factors leading to its exocytosis are mechanical or chemical stimuli. Serotonin acts as a neurotransmitter and a paracrine messenger with a wide range of physiological reactions. These are mediated through seven classes of 5-HT receptors (Gershon and Tack 2007; Gershon 2013). Their topographical distribution in the human stomach has not yet been precisely described and is based entirely on estimates obtained from animal and pharmacological studies. Thus, the presence of 5-HT_1 receptors in the organ is suggested from the experiments with sumatriptan and buspiron on fundal accommodation and gastric emptying of liquids (Tack et al. 1998a, b, 2007; Tack 2000). A gene cloning and physical mapping study has shown a low expression of 5-$HT_{3A/B}$ and a total lack of 5-$HT_{3D/E}$ receptor subunits in the human stomach (Niesler et al. 2003; Schemann and Neunlist 2004). The confirmation of these findings comes from the inability of 5-HT_3 receptor antagonists to improve symptoms of gastroparesis in patients (Broad et al. 2014). Although in vitro, auto-radiographic, quantitative reverse transcription-polymerase chain reaction, and in vivo clinical investigations infer the existence of 5-HT_4 receptors on the nerve terminals and somas of motor neurons of Auerbach's plexus, their immunoreactivity has not yet been demonstrated (Sakurai-Yamashita et al. 1999; Leclere and Lefebvre 2002; Mader et al. 2006; Broad et al. 2014). At the time of writing, the physiological role of other classes of receptors in the human stomach remains obscure.

Fully appreciating the importance of 5-HT in the regulation of gastric motility and taking into account the uncertainties regarding the details of its mechanisms of action, consider the effects of serotonin and 5-HT_4 receptors on myoelectrical activity of the gastric SIP/ganglion unit. In addition to morphostructural arrangements in the unit, assume there are 5-HT_4 receptors on the soma of the motor neuron. These are positively linked to Gα_s proteins and the adenyl cyclase second messenger—cAMP—signaling system. Their stimulation increases the

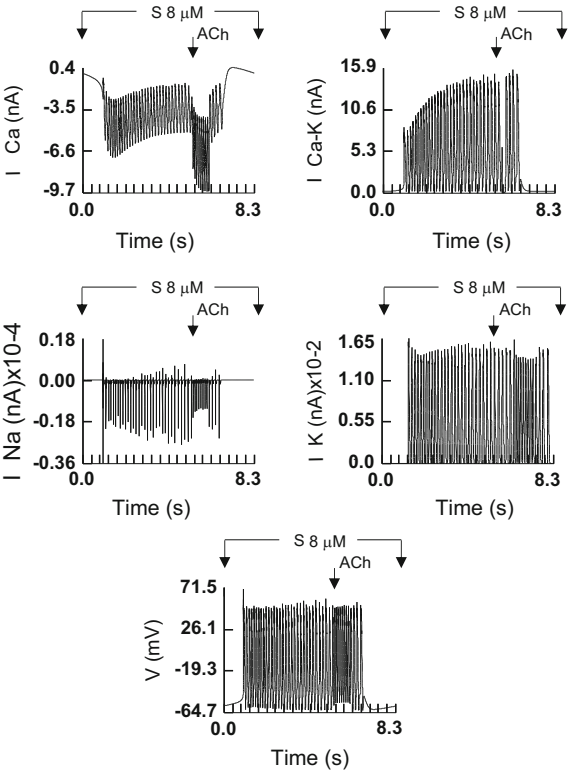

Fig. 10.11 The dynamics of transmembrane ion channels and somatic action potential development on the soma of the motor neuron in response to endogenous release of 5-HT and ACh

conductivity of Na^+ and, possibly, Ca^{2+} channels with a concurrent decrease in the permeability of BK_{Ca} and voltage-gated K^+ channels.

Let applied mechanical stretches be of intensity $0.8L$ and a frequency of $\nu_m = 0.137$ Hz. The conjoint release of ACh and 5-HT causes dose-dependent changes in the dynamics and the strength of ion channels on the soma of the motor neuron (Fig. 10.11). All channels reveal a beating oscillatory mode. Serotonin acting alone at 8 μM generates the inward Na^+ and Ca^{2+} currents of average amplitudes 1.8×10^3 nA and 3 nA, and the outward Ca^{2+}-activated K^+ and K^+ currents of 11.2 nA and 1.5×10^2 nA. An addition of ACh intensifies I_{Ca}, ($\max I_{Ca} = -9.7$ nA), and reduces twofold the strength of Na^+ influx, $\max I_{Na} = -0.9$ nA. In the presence of serotonin, ACh does not affect the outward currents. However, it has a significant effect on the frequency of fluctuations of ion channels which rises to 9.9 Hz. As a result, the motor neuron produces spikes of high frequency and amplitude $V_m^s = 110$ mV over a period of 6.3 s.

A number of generated action potentials propagate along the axon to the nerve-SMC synapse. Here they cause the cascade of events including cholinergic transduction, the production of multiple fEPSPs and spikes on slow waves and, finally, contractions of SIP. Serotonin alone triggers a rhythmic mechanical reaction with $\max T^a = 13.8$ mN/cm. Acting conjointly ACh and 5-HT do not affect the

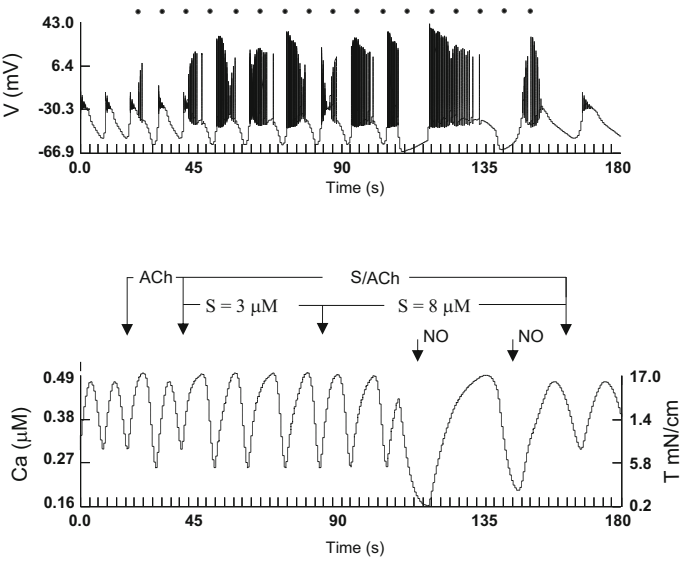

Fig. 10.12 The electromechanical response of the antral SIP/ganglion unit to a complex stimulation: ICC fire at their natural regional frequency, $\nu = 0.13$ Hz throughout; mechanical stimuli applied at a regular frequency of $\nu_m = 0.137$ Hz (*black dots*); neurotransmitters including ACh, 5-HT and NO released at the times indicated

phasic pattern of contractility. However, there is a dose-dependent increase in the strength and duration of generated active forces. Thus, $\max T^{\alpha} = 15.6$ mN/cm and 17 mN/cm are observed after addition of serotonin 3 μM and 8 μM, respectively (Fig. 10.12). Intermittent releases of NO at different quantities induce short-term relaxations and the decline in the resting smooth muscle tone to 0.2 mN/cm.

10.4.5 Motilin, Acetylcholine and Nitric Oxide

Motilin is a 22-amino-acid polypeptide produced primarily by endocrine "M" mucosal cells of the duodenum and jejunum, with a smaller quantity in the gastric antrum. It is stored mainly in cells found from base to neck of the oxyntic glands of the fundus and corpus with only a few in the antrum of the stomach (Wierup et al. 2007). Motilin is released regularly every 90–120 min during fasting. The dynamics of intracellular Ca^{2+} tightly regulates the process. The peptide is unique in its ability to accelerate gastric emptying in the interdigestive rather than in the postprandial state. It is believed that mechanical distension along with chemical changes in the microenvironment plays a part in this (Ohno et al. 2010; Sakata and Sakai 2011; Sanger et al. 2013; Sanger and Furness 2016). Pharmacological, immunohistochemical and transcription-polymerase chain reaction studies have provided compelling evidence about the distribution of motilin receptors—heterotrimeric guanosine triphosphate

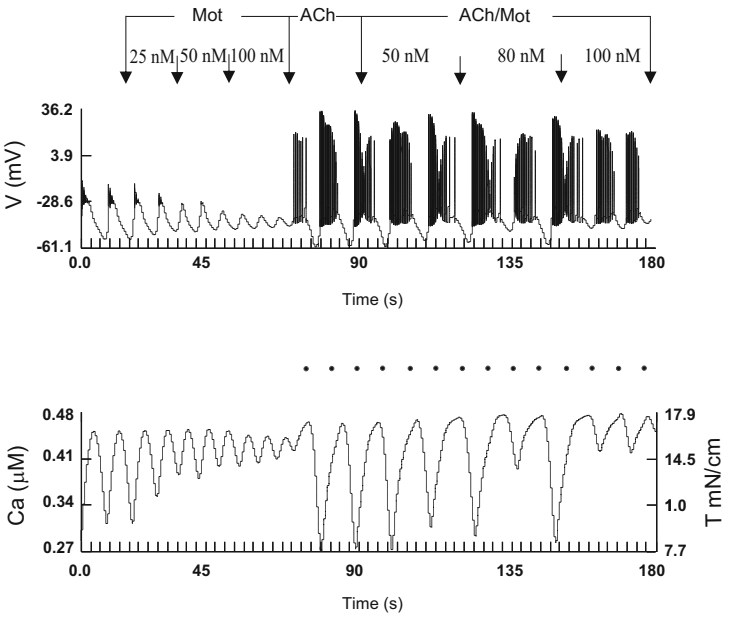

Fig. 10.13 The effect of ACh, motilin, firings of ICC and mechanical stimuli (*black dots*) on the electromechanical activity of the antral SIP/ganglion unit

G-protein coupled receptor 38 (GPR38)—on smooth muscle cells and neurons of Auerbach's plexus right across the human stomach (Lüdtke et al. 1989; Feighner et al. 1999; Miller et al. 2000; Takeshita et al. 2006; Sanger et al. 2013; Broad et al. 2014). However, there remain imponderables surrounding the complex transduction mechanisms by motilin. The in vivo and in vitro experimental results point to an intracellular G_q-mediated outflow of Ca^{2+} from the endoplasmic reticulum and an associated activation of transmembrane L-type Ca^{2+} channels (Shim et al. 2002). The effects of motilin on gastric contractile activity is dose-dependent. Thus, at low concentrations, 0.03–10 (nM), it affects myenteric cholinergic transduction by enhancing the prejunctional release of ACh, whilst at higher concentrations, 10–100 (nM), it directly evokes the mechanical reaction of smooth muscle (Coulie et al. 1998; Shim et al. 2002; Broad et al. 2012, 2016; Langworthy et al. 2016).

Consider the effects of the conjoint action of ACh, NO and high concentrations of motilin on myoelectrical activity of the antral SIP/ganglion unit. The case of low dose peptide resembles the results discussed in the previous paragraph of cholinergic signaling amplification at the motor neuron level with the production of prolonged contractions. In addition to the modeling assumptions formulated above, motilin GPR38 receptors are present on the smooth muscle syncytium. The unit is excited by discharges of pacemaker cells and external mechanical stretches.

Let ICC fire continuously at their natural frequency, $\nu = 0.13$ Hz. Acting alone at increasing doses, motilin steadily depolarizes the SMC membrane, $V = -54 \div -42$ mV, reduces the amplitude and shortens the duration of slow waves (Fig. 10.13). These changes correspond to a significant rise in the basal

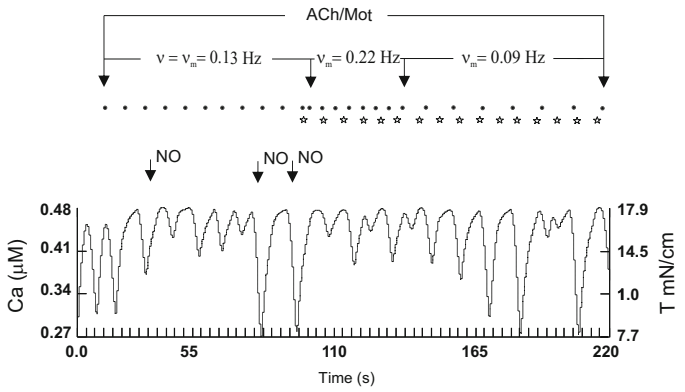

Fig. 10.14 The effect of ACh, motilin, an intermittent release of NO and irregular mechanical stimulation on the mechanical activity of the antral SIP/ganglion unit. ICC fire continuously at their natural regional frequency of $\nu = 0.13$ Hz (*open stars*)

muscle tone, 12–15 mN/cm, and a slight increase in the active force of contraction, $\max T^a = 16.1$ mN/cm. The activation of ganglion elements by applied deformations of intensity $0.8L$ at a frequency of $\nu_{\mathrm{m}} = 0.13$ Hz with the subsequent release of ACh at the motor neuron–SM syncytium synapse, results in the production of regular spikes on the crests of slow waves. The response of smooth muscle is strong phasic contractions of a magnitude, $T^a = 8.3$ mN/cm. The concomitant application of motilin at 50–100 nM does not affect the cholinergically mediated myoelectrical activity of the syncytium. However, the peptide evokes contractions of inconsistent amplitudes ranging from 2.9 mN/cm to 8.3 mN/cm. The dynamics of intracellular calcium oscillations is closely related to that of smooth muscle.

Interestingly, the release of a "puff" of NO to the unit which has been exposed to the action of ACh and motilin, fails to exert any inhibitory effect on smooth muscle (Fig. 10.14). Only when the addition of NO precedes ACh and motilin, are acute short-lasting relaxations with $\min T^a = 7.7$ mN/cm achieved.

The asynchrony between the firing rate of ICC and cholinergic reactions mediated by the ganglion in the presence of a high level of motilin, 85 nM, causes the production of active forces of wavering strength. Thus, at $\nu_{\mathrm{m}} = 0.22$ Hz and $\nu = 0.13$ Hz, short-lasting contractions of a duration 6.8 s and $\max T^a = 17.9$ mN/cm are generated. The muscle fails to relax completely. A minimum tension of $13.4 \div 16$ mN/cm is recorded. A lower frequency of ganglionic activity, $\nu_{\mathrm{m}} = 0.09$ Hz, allows a greater degree of relaxation, $\min T^a = 8$ mN/cm, and contractions of larger amplitude, 9.9 mN/cm. The observed inconsistency in the dynamics of $T^a(t)$ is due to the chronotropic allosteric interaction between the neurotransmitter, polypeptide and ICC.

References

Broad J, Mukherjee S, Samadi M, Martin JE, Dukes GE, Sanger GJ (2012) Regional- and agonist-dependent facilitation of human neurogastrointestinal functions by motilin receptor agonists. Br J Pharmacol 167:763–774

Broad J, Hughes F, Aleong C, Sifrim D, Sanger GJ (2014) Regionally dependent neuromuscular functions of motilin and 5-HT4 receptors in human isolated esophageal body and gastric fundus. Neurogastroent Mot 26:1311–1322

Broad J, Takahashi N, Tajimi M, Sudo M, Góralczyk A, Parampalli U, Mannur K, Yamamoto T, Sanger GJ (2016) RQ-00201894: a motilin receptor agonist causing long-lasting facilitation of human gastric cholinergically-mediated contractions. J Pharm Sci 130:60–65

Coulie B, Tack J, Peeters T, Janssens J (1998) Involvement of two different pathways in the motor effects of erythromycin on the gastric antrum in humans. Gut 43:395–400

Currò D, Preziosi P (1998) Non-adrenergic non-cholinergic relaxation of the rat stomach. Gen Pharm 447:119–131

Currò D, Ipavec V, Preziosi P (2008) Neurotransmitters of the non-adrenergic non-cholinergic relaxation of proximal stomach. Eur Rev Med Pharm Sci 12(Suppl 1):53–62

Dick JMC, Van Geldre JP, Timmermans JP, Lefebvre RA (2000) Investigation of the interaction between nitric oxide and vasoactive intestinal polypeptide in the guinea pig gastric antrum. Br J Pharm 129:751–763

Ergün Y, Öğülener N (2001) Evidence for the interaction between nitric oxide and vasoactive intestinal polypeptide in the mouse gastric fundus. J Pharm Exp Ther 299(3):945–950

Feighner SD, Tan CP, McKee KK, Palyha OC, Hreniuk DL, Pong SS, Austin CP, Figueroa D, MacNeil D, Cascieri MA, Nargund R, Bakshi R, Abramovitz M, Stocco R, Kargman S, O'Neill G, Van Der LHT, Ploeg Evans J, Patchett AA, Smith RG, Howard AD (1999) Receptor for motilin identified in the human gastrointestinal system. Science 284:2184–2188

Gershon MD (2013) 5-Hydrohytryptamine (serotonin) in the gastrointestinal tract. Curr Opin Endoc Diab Obes 20(1):14–21

Gershon MD, Tack J (2007) The serotonin signaling system: from basic understanding to drug development for functional GI disorders. Gastroenterology 132:397–414

Igarashi H, Fujimori N, Ito T, Nakamura T, Oono T, Nakamura K, Suzuki K, Jensen RT, Takayanagi R (2011) Vasoactive intestinal peptide (VIP) and VIP receptors – elucidation of structure and function for therapeutic applications. Int J Clin Med 2:500–508

Koh SD, Rhee P-L (2013) Ionic conductance(s) in response to post-junctional potentials. J Neurogastroent 19(4):426–432

Langworthy J, Parkman HP, Schey R (2016) Emerging strategies for the treatment of gastroparesis. Expert Rev Gastroent Hep 10(7):817–825

Leclere PG, Lefebvre RA (2002) Presynaptic modulation of cholinergic neurotransmission in the human proximal stomach. Br J Pharm 135:135–142

Lefebvre RA, Smits GJM, Timmermans J-P (1995) Study of NO and VIP as non-cholinrgic neurotrsansmitters in the pig gastric fundus. Br J Pharm 116:2017–2026

Lüdtke FE, Miller H, Golenhofen K (1989) Direct effects of motilin on isolated smooth muscle from various regions of the human stomach. Pflügers Archiv 414:558–563

Mader R, Kocher T, Hasier J, Wieczorek G, Pfannkuche H-J, Ito M (2006) Investigation of serotonin type 4 expression in human and non-human primate gastrointestinal samples. Eur J Gastroent Hep 18:945–950

Miller P, Roy A, St-Pierre S, Dagenais M, Lapointe R, Poitras P (2000) Motilin receptors in the human antrum. Am J Physiol Gastroint Liv Physiol 278:G18–G23

Niesler B, Frank B, Kepller J, Rappold GA (2003) Cloning, physical mapping and expression analysis of the human 5-HT3 serotonin receptor-like genes HTR3C, HTR3D and HTR3E. Gene 310:101–111

Ohno T, Mochiki E, Kuwano H (2010) The roles of motilin and ghrelin in gastrointestinal motility. Int J Pept. doi:10.1155/2010/820794

Pimont S, Bruley des Varannes S, Le Neel JC, Aubert P, Galmiche JP, Neunlist M (2003) Neurochemical coding of myenteric neurons in the human gastric fundus. Neurogastroent Mot 15:655–662

Sakata I, Sakai T (2011) The gut peptide hormone family, motilin and ghrelin. In: Aimaretti G (ed) Update on mechanisms of hormone action—Focus on metabolism, growth and reproduction. InTech, China

Sakurai-Yamashita Y, Takada K, Takemura K, Yamashita K, Enjoji A, Kanematsu T, Taniyama K (1999) Ability of mosapride to bind to 5-HT4 receptor in the human stomach. Jpn J Pharmacol 79(4):493–496

Sanders KM (2000) Postjunctional electrical mechanisms of enteric neurotransmission. Gut 47: iv23–iv25

Sanger GJ, Furness JB (2016) Ghrelin and motilin receptors as drug targets for gastrointestinal disorders. Nat Rev Gastroent Hep 13:38–48

Sanger GJ, Wang Y, Hobson A, Broad J (2013) Motilin: towards a new understanding of the gastrointestinal neuropharmacology and therapeutic use of motilin receptor agonists. Br J Pharm 170:1323–1332

Schemann M, Neunlist M (2004) The human enteric nervous system. Neurogastroent Mot 16:55–59

Shim SG, Rhee JC, Rhee PL, Choi KW, Jeon SK, Kang TM, Uhm DY, Lee JS, Sung IK, Kim HS (2002) Mechanisms of motilin action on smooth muscle of the human stomach. Korean J Gastroent 39(1):4–12

Tack J (2000) The physiology and pathophysiology of the gastric accommo-dation reflex in man. Verhandelingen – Koninklijke Academie Voor Geneeskunde van Belgie LXII(3):183–210

Tack J, Coulie B, Wilmer A, Andrioli A, Janssens J (1998a) Influence of sumatriptan on gastric fundus tone and on the reception of gastric distension in man. Gut 46:468–473

Tack J, Coulie B, Wilmer A, Peeters T, Janssens J (1998b) Action of the 5-hydroxytryptammine-1 receptor against sumatriptan on interdigestive gastro-intestinal motility in human. Gut 42:36–41

Tack J, Demedts I, Meulemans A, Schuurkes J, Janssens J (2002) Role of nitric oxide in the gastric accommodation reflex and in meal induced satiety in humans. Gut 51(2):219–224

Tack J, Berghe PV, Coulie B, Janssens J (2007) Sumatriptan is an agonist at 5-HT_{1P} receptors on myenteric neurones in the guinea-pig gastric antrum. Neurogastroent Mot 19:39–46

Takahashi T (2003) Pathophysiological significance of neuronal nitric oxide synthase in the gastrointestinal tract. J Gastroent 38:421–430

Takeshita E, Matsuura B, Dong M, Miller LJ, Matsui H (2006) Molecular characterization and distribution of motilin family receptors in the human gastrointestinal tract. J Gastroent 41:223–230

Thatte HS, He XD, Goyal RK (2009) Imaging of nitric oxide in nitrergic neuromuscular neurotransmission in the gut. doi:10.1371/journal.pone. 00004990

Tonini M, De GR, De Ponti F, Sternini C, Spelta V, Dionigi P, Barbara G, Stanghellini V, Corinaldesi R (2000) Role of nitric oxide- and vasoactive intestinal peptide-containing neurones in human gastric fundus strip relaxations. Br J Pharm 129:12–20

Van Geldre LA, Lefebrve RA (2004) Interaction of NO and VIP in gastro-intestinal smooth muscle relaxation. Curr Pharm Des 10(20):2483–2497

Wierup N, Björkquist M, Weström B, Pierzynowski S, Sundler F, Sjölund K (2007) Ghrelin and motilin are cosecreted from a prominent endocrine cell population in the small intestine. J Clin Endoc Met. doi:10.1210/jc.2006-2756

Chapter 11
Biomechanics of the Human Stomach

We all agree that your theory is crazy, but is it crazy enough?
Niels Bohr

11.1 Modeling of the Stomach as a Soft Biological Shell

Biological and mechanical data on the human stomach discussed and studied in detail in preceding chapters can be summarized briefly by the following biological postulates which are used in further evolution of the model:

(i) the organ is a thin soft biological shell; its wall is composed chiefly of two smooth muscle layers embedded in the ECM; smooth muscle fibers in the outer layer are orientated longitudinally and in the inner layer, circumferentially with respect to the cardia-pyloric axis of the stomach
(ii) smooth muscle fibers form two-dimensional electromechanical bisyncytia (layers) through gap junctions; SM layers have nonlinear viscoelastic mechanical properties which are non-uniform along the stomach, being compliant in the fundus and stiff in the antrum; the longitudinal layer also has anisotropic electrical characteristics whilst those of the circular layer are isotropic
(iii) contained within smooth muscle bisyncytia are clusters of widely dispersed interstitial cells of Cajal and platelet-derived growth factor receptor α cells; the firm links via electrical synapses and ionic conductances including L- and T-type Ca^{2+}, BK_{Ca} and Na^{+} channels ensure the electrogenic self-oscillatory activity of SIP; SIP are divided into pools according to their firing frequencies
(iv) the intrinsic regulatory system is comprised of Auerbach's (myenteric nervous) and ICC/PDGFRα^{+}–MY(IM) plexi; intramural Auerbach's nervous plexus is a regular two-dimensional network of spatially distributed interconnected ganglia, each ganglion being formed of primary sensory, motor and interneurons; the neurons may co-localize and co-release neurotransmitters on demand

R.N. Miftahof, *Biomechanics of the Human Stomach*,
DOI 10.1007/978-3-319-59677-8_11

(v) the separate networks of ICC/PDGFRα^+–MY(IM) serve the role of pacemakers, discharging action potentials continuously at their natural frequencies; the oscillators are arranged in pools according to their natural frequencies; two oscillators communicate weakly, if they have nearly equal frequency, such that the phase of one is sensitive to the phase of the other; two oscillators are strongly connected if they have equal frequencies, and two oscillators are disconnected if they have essentially different frequencies

(vi) Auerbach's and ICC/PDGFRα^+–MY(IM) plexi are connected via chemical synapses; there are low resistance electrical synapses and gap junctions between ICC-IM and SMCs; mechanoreceptors on the primary sensory neurons and ICC serve as a feedback signal to the plexi

(vii) electromechanical coupling and mechanical responses by SMCs are a result of the evolution of slow waves and spikes; the slow wave and spiking activity represents the integrated function of: voltage-dependent L- and T-type Ca^{2+}, voltage-dependent K^+, Ca^{2+}-activated K^+ and leak Cl^- ion channels on smooth muscle membrane, ICC/PDGFRα^+–MY(IM), and the myentyeric nervous plexus

(viii) the generation of active forces involves a multicascade process with the activation of intracellular contractile proteins; passive forces are explained by the mechanics of viscoelastic ECM.

Mathematical formulation of the electromechanical dynamics of the human stomach under complex loading makes up a system of equations: the dynamics of the soft bioshell—Eq. (4.97); myoelectrical activity in SIP—Eqs. (8.15)–(8.19); the dynamics of signal transduction within Auerbach's nervous plexus including the primary sensory, motor and interneurons and ICC—Eqs. (8.4)–(8.12), (8.14); the propagation of the wave of excitation within electrically anisotropic longitudinal and electrically isotropic circular smooth muscle syncytia—Eqs. (8.20)–(8.28); electrochemical coupling at synapses—Eqs. (7.10)–(7.11); cAMP dependent pathway—Eqs. (7.18)–(7.19); PLC pathway—Eqs. (7.21)–(7.22); co-transmission by multiple neurotransmitters—Eq. (7.24); constitutive relations for the tissue—Eqs. (6.45)–(6.47).

The characteristic feature of the bioshell is the possibility of the simultaneous coexistence of smooth—biaxial stressed, wrinkled—uniaxially stressed and unstressed zones. Thus, from corollaries 2, 4–6 (Chap. 4) it follows that if both λ_c and $\lambda_l > 1.0$, ($T_{l,c} > 0$) then Eqs. (6.46, 6.47) are used to calculate forces in the wall. If wrinkles develop, then either $\lambda_l \leq 1.0$, $\lambda_c > 1.0$, ($T_l = 0$, $T_c > 0$), or $\lambda_c \leq 1.0$, $\lambda_l > 1.0$, ($T_l > 0$, $T_c = 0$). The wrinkled zone is substituted by an ironed out zone made of a set of unbound muscle and connective tissue fibers aligned in the direction of the applied positive tension. Forces are calculated using Eqs. (6.45, 6.46). This is necessary for the conservation of surface smoothness and the preservation of the continuity of in-plane membrane forces.

In the following simulations it is assumed, otherwise specified, that the cardiac and pyloric ends of the stomach are clamped and remain unexcitable throughout. At

the initial moment of time the organ is in a state of electromechanical equilibrium. It is excited by electrical discharges of ICC and/or mechanical deformations.

11.2 Gastric Accommodation

The postprandial active expansion, the adjustment of the human stomach to the volume of the ingested meal, depends on: (i) the anatomical shape of the organ, (ii) the biomechanical properties of the wall and (iii) the physiological response—the accommodation reflex. The latter constitutes two separate chronotropically related, although clinically indistinguishable, receptive and adaptive relaxation phases. The first is of short duration and induced by swallowing and acute gastric distension, whilst the second is a prolonged neuro-hormonally mediated reaction to food. The reflex is associated with dilation of the organ, a non-rise in intraluminal pressure and an isotonic decrease in smooth muscle tone. These are modulated externally and intramurally by the vago-vagal and the myenteric plexus reflexes. Impaired gastric accommodation contributes to the pathogenesis of functional dyspepsia and is associated with diabetic vagal neuropathy, gastro-esophageal reflux disease, achalasia, vagotomy, distal gastrectomy and post-fundoplication among others (Jahnberg et al. 1975; Mearin et al. 1995; Undeland et al. 1998; Newton et al. 1999; Tack 2000; Di Stefano et al. 2005; Kindt and Tack 2006; Talley and Ford 2015; Talley 2016).

11.2.1 Gastric Tone in Organs of Variable Anatomical Shapes

An average minimal intragastric distending pressure in a healthy subject is ~8 kPa, equivalent to $\breve{V} \geq 30$ ml of content (de Zwart et al. 2002). To evaluate the gastric tone and the dynamics of stress-strain distribution in four radiologically distinct anatomical shapes (steer-horn, cascade, J-shape and fish-hook) of the human stomach during fasting, consider the inflation of the bioshell by intraluminal pressure $p(\breve{V})$. Assume that Auerbach's plexus is inactive throughout.

The strain distribution in the steer-horn and fish-hook stomachs at $p = 8$ kPa in the state of dynamic equilibrium is shown in Fig. 11.1. The cascade and J-shapes show similar patterns of deformation but are not given here. Maximal longitudinal elongation, $\lambda_l = 1.28$ (1.36), is recorded in the cardio-fundal regions. Values in parentheses refer to the fish-hook shape. By contrast, the fundus and corpus along the greater and lesser curvatures, along with the antrum-pylorus, experience extensive stretching circumferentially, $\lambda_c = 1.4$ (1.62). Most notably, the entire organ undergoes biaxial distension.

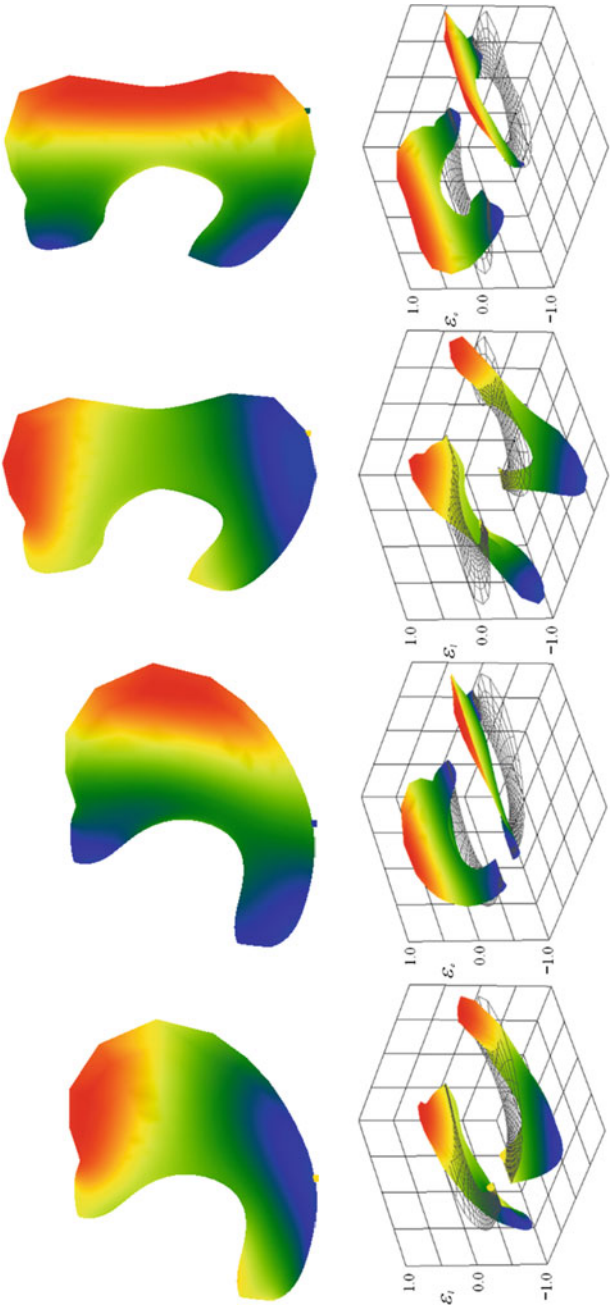

Fig. 11.1 The circumferential, λ_c, and longitudinal, λ_l, rates of elongation in the steer-horn and fish-hook shaped human stomachs at $p = 8$ kPa

Stress distribution analysis reveals disparities among different anatomical configurations of the bioshell. In the fundus there is a deviation in the magnitude of maximal longitudinal membrane forces, $\max T_l = 90.1$ (steer-horn); 78.2 (cascade), 89.0 (J-shape) and 93.7 (mN/cm) (fish-hook), with no significant variations in the circumferential direction, $\max T_c = 15.7$; 15.3; 15.8 and 17.3 (mN/cm) (Fig. 11.2). The body of the J- and fish-hook stomachs is uniformly stressed along the axi of structural anisotropy with the average $T_l = 68.4$ mN/cm, $T_c = 25.2$ mN/cm, and $T_l = 52.3$ mN/cm, $T_c = 18.5$ mN/cm, respectively. The bulk of the body of the steer-horn and cascade stomachs encounter biaxial tension, $T_l = 62.3$ mN/cm, $T_c = 15.3$ mN/cm, with the exception of small areas at the greater curvature and at the anatomical flexure of cascade formation. Here, maxima of $T_l = 70$ mN/cm, $T_c = 30.7$ mN/cm, and $T_l = 83.6$ mN/cm, $T_c = 61.8$ mN/cm, are observed. In the antrum and pylorus, total forces of intensity $T_l \simeq 30$ mN/cm, $T_c \simeq 14$ mN/cm are recorded. The circumferential tension of 15 mN/cm is registered across the antrum and pylorus of the J- and fish-hook stomachs. While these regions in the J-shape bioshell are evenly stressed longitudinally, $T_l \simeq 73$ mN/cm, in the fish-hook

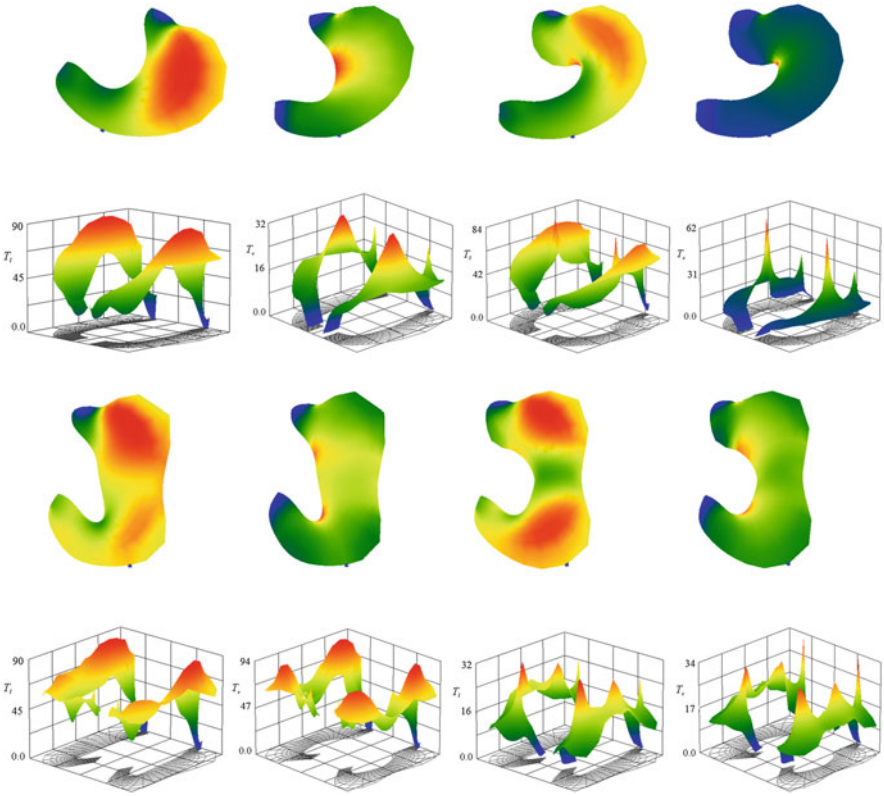

Fig. 11.2 Comparative total force T_c and T_l distribution in various anatomical shapes of the human stomach at $p = 8$ kPa

stomach the magnitude of T_l in the antrum, $T_l \simeq 86$ mN/cm, appears greater compared with the pylorus, $T_l \simeq 65$ mN/cm.

It is noteworthy that intraluminal pressure equivalent to mechanical stimulation does not trigger peristaltic activity in the bioshell. Despite the fact that SIPs continue generating action potentials and slow waves at their regular natural frequencies, there are no strong connections or synchronization in the firing of ICC-MY(IM). This is provided by intramural Auerbach's plexus. Contractions produced across different regions of the organ are indiscriminate and jumbled causing irregular changes in the shape.

Stiffening of the gastric wall commonly seen in patients with diabetis, systemic sclerosis, linitis plastica, chronic gastritis and normal aging, results in a decrease in deformability of the organ. For example, in the steer-horn stomach stretch ratios $\lambda_l = 1.2$, $\lambda_c = 1.12$ are recorded in the cardio-fundal region and the fundus, while in the body of the stomach at the greater curvature the distension attains $\lambda_l = 1.26$, $\lambda_c = 1.3$. There is a significant loss in deformability of the antrum-pylorus. As a result, intragastric volume reduces to 18.5 ml. Maxima $T_l = 120.3$ mN/cm, $T_c = 22.5$ mN/cm are registered in the fundus and body of the organ. In the antrum and pylorus total forces of average intensity $T_l \simeq 52.8$ mN/cm, $T_c \simeq 28.7$ mN/cm are recorded. Analogous changes are also attributed to the cascade, J- and fish-hook stomachs.

11.2.2 Dynamic Response of the Stomach to "Feeding"

A gradual increase in intragastric volume to 700 ml through drinking a viscous and/or nutrient saline solution (20 mPa·s) or tap water (1.002 mPa·s) raises intraluminal pressure to 21.3 and 30.1 kPa, respectively (Janssen et al. 2011). The process of "feeding" initiates the accommodation reflex. Although the details of the morphofunctional mechanisms remain elusive, it is conceivable, based on experimental evidence, that there is a decrease in chilonergic and an increase in nitrergic signaling at the SIP/ganglion unit (Lefebvre 2002; Kuiken et al. 2002; Janssen et al. 2011). The former is due to noradrenaline (NA) acting via α_2-adrenoceptors at neurons of the myenteric plexus and α_1-adrenoceptors at SMCs. The latter is a direct postjunctional effect of NO on smooth muscle (Thumshirn et al. 1999). Despite the extensive co-localization of VIP and NO, currently no affirmative physiological and pharmacological data exist to suggest the role of VIP as a cotransmitter (Tonini et al. 2000).

Consider the intraganglionic circuit comprised of cholinergic and adrenergic neurons linked via the adrenergic axo-axonal synapse as shown in Fig. 8.1. Let α_2- and α_1-adrenoceptors be on the axon and the nerve terminal of the adrenergic neuron, respectively. For mathematical formulation of the problem see Chap. 8.

Electrical stimuli of a given strength and intensity applied at the somas of neurons induce action potentials of amplitude $V_1 = V_2 = 75$ mV which propagate

along the unmyelinated axons. Upon arrival at the synapse, V_2 triggers the influx of Ca^{2+} and the exocytosis of NA from the 'releasable' store. The rate of release, although slow in the beginning, 0.66 μM/ms, accelerates towards the end, 2.87 μM/ms, of the process. Free noradrenaline, $[NA_f] = 97$ μM, diffuses into the synaptic cleft where $\max[NA_c] = 86.3$ μM, is registered. A major part of NA_c is rapidly inactivated by the uptake-1 and the catechol-*O*-methyltransferase dependent uptake-2 mechanisms. The rest of NA, 35.2 μM, binds to postsynaptic α_2-adrenoceptors. As a result 8.53 μM of the reactive (NA_p–Rα_2) complex is produced. This activates the intracellular second messenger system with the generation of an inhibitory postsynaptic potential of amplitude −76.2 mV and duration 2–3 ms.

To achieve inhibition of signal transduction along the axon, the amplitude, frequency and duration of the excitatory potential V_1 and the locally generated IPSP have to be subtly synchronized. The time delay, Δt, of interaction between the two signals plays an important role in the dynamics of V_{sum}. Thus, for $\Delta t \geq 1.68$ ms the amplitude and the velocity of V_1 remain unaffected. It reaches successfully the cholinergic synapse and initiates nerve-pulse transmission (Fig. 11.3). With the shortening of Δt, the inhibitory effect becomes more prominent. For a delay of 0.6 ms and 0.39 ms, the amplitude of V_1 is reduced to 44.2 mV and 9.5 mV, respectively. Further decrease in Δt or earlier development of IPSP results in a complete block of V_1. Similar dynamics are observed at the axo-somatic synapses but are not given here.

Assume that under normal conditions the stomach attains an anatomical and electrophysiological organization, and fine-tuning between the sympathetic and parasympathetic systems for the accommodation of a meal is required. Consider gastric response to feeding, i.e., an incremental increase in intragastric volume. The comparative analysis of electromechanical events during the dynamic process is carried out at representative points chosen in three areas of interest: the fundus, the corpus and the antrum of the steer-horn, cascade and fish-hook shape bioshells. Qualitatively and quantitatively results for the J-shape organ closely resemble those obtained for the fish-hook and, therefore, are not shown.

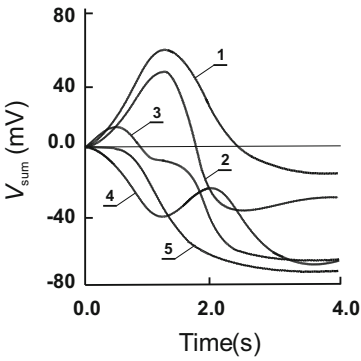

Fig. 11.3 Resulting potentials at the axo-axonal synapse of the inhibitory circuit. 1: $\Delta t = 1.68$ ms; 2: $\Delta t = 0.6$ ms; 3: $\Delta t = 0.39$ ms; 4: $\Delta t = 0$ ms; 5: $\Delta t = -1.5$ ms

In the presence of ACh the distension of the bioshell causes an increase in total forces from the baseline. There are configuration and region-dependent disparities in the stress-strain distribution. Thus, the fundus of the fish-hook shape stomach experiences maximal longitudinal tension, $T_l = 94$ mN/cm, whereas in the steer-horn organ, $\max T_l = 62$ mN/cm is developed (Fig. 11.4). This pattern reverses in the body of the bioshells where $\max T_l = 115$ and 95 (mN/cm) are recorded respectively. In the case of the cascade stomach the intensity of T_l in the above regions attains intermediate values.

The strongest membrane forces are produced in the distal part of the stomach. The antrum of the steer-horn shape bioshell is maximally stressed, $T_l = 155$ mN/cm and in the case of the cascade configuration, the lowest level, $T_l = 124$ mN/cm, is recorded. By contrast, the fish-hook stomach appears equally stressed circumferentially in the fundus and the corpus, $T_c = 203.5$; 215 (mN/cm),

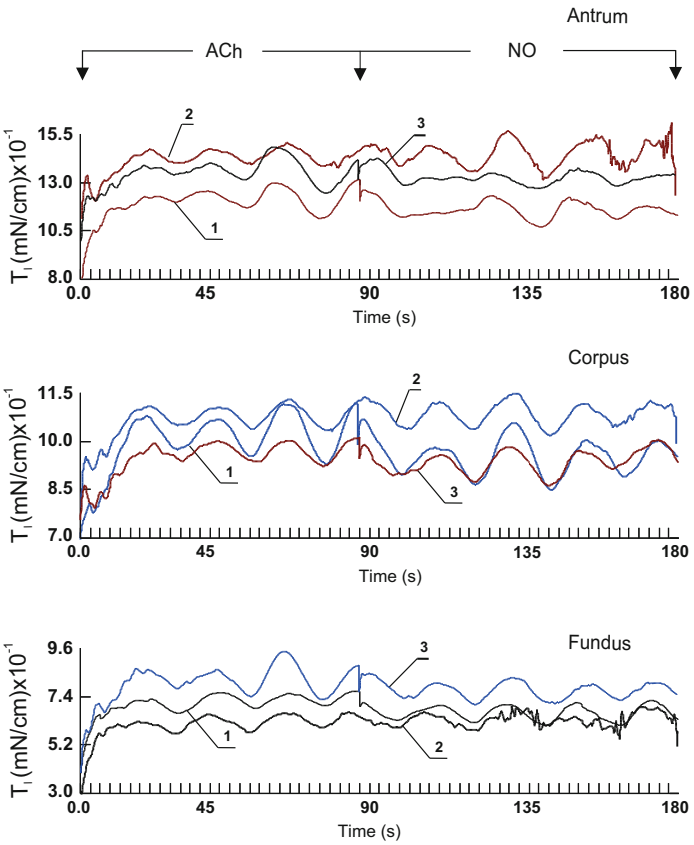

Fig. 11.4 Changes in the total force T_l in steer-horn (1), cascade (2), and fish-hook (3) shaped human stomachs during "feeding"

respectively, with max $T_c = 255$ mN/cm observed in the antrum. A similar pattern of force distribution is observed in the steer-horn shape: $T_c = 143$ mN/cm in the fundus; 186 mN/cm in the body, and 219 mN/cm in the antral region (Fig. 11.5).

The firing of ICC–IM at their natural regional frequencies, the increase in gastric volume, the activation of mechanoreceptors and the intraganglionic cholinergic signal transduction within the SIP/ganglion units initiate the contractile response in the bioshell. Maxima active membrane forces are generated in the body and antrum of the steer-horn and fish-hook stomachs, $T_l^a = 82.9$ mN/cm and $T_c^a = 106.5$ mN/cm but are significantly less in the fundus, $T_l^a = 41.5$ mN/cm and $T_c^a = 52.8$ mN/cm. The amplitude of contractions also varies across the organ from the smallest being recorded in the fundus, 8.5 ÷ 11.8 mN/cm to the greatest in the antrum, 19.6 ÷ 35.3 mN/cm.

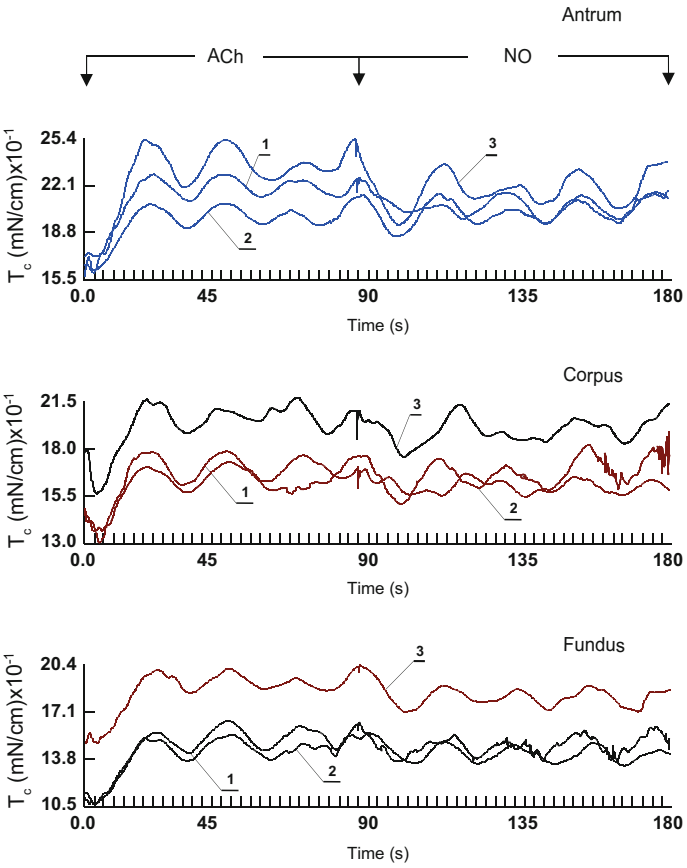

Fig. 11.5 Changes in the total force T_c in steer-horn (1), cascade (2), and fish-hook (3) shaped human stomachs during "feeding"

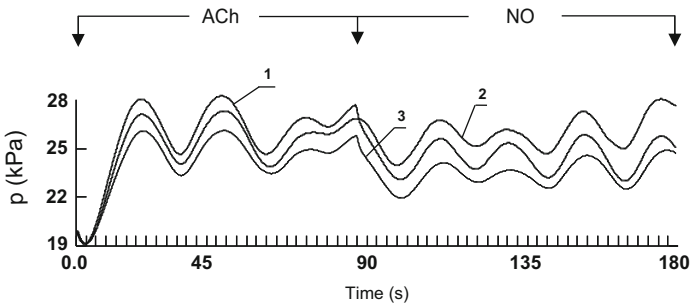

Fig. 11.6 Variations in intragastric pressure, $p(\breve{V})$, during "feeding". Notations are as in Fig. 11.4

The dynamics of intragastric pressure reflects the combined effect of passive viscoelastic and active forces in the bioshell during an increase in $\breve{V}$. The baseline distending pressure for $\breve{V} = 650$ ml varies between 25.8 kPa in the fish-hook, to 27.3 kPa in the cascade stomach. It undulates at an average amplitude of 7.3 kPa and frequencies which correspond to the oscillatory activity of SIPs (Fig. 11.6).

The elimination of the release of ACh at SIP/ganglia units and the application of NO directly to longitudinal and circumferential smooth muscle syncytia have a marked effect on gastric accommodation. There is a considerable reduction in the intensity of circumferential forces across all regions of the stomach, $T_c = 192$ mN/cm (fundus); 200 mN/cm (corpus), and 240 mN/cm (antrum) of the fish-hook and $T_c = 137$ mN/cm (fundus); 170 mN/cm (corpus), and 210 mN/cm (antrum) of the cascade shape organ (Fig. 11.5). The gastric wall produces low amplitude weak contractions ranging from $7 \div 10$ (mN/cm) in the distal, and $20 \div 26$ (mN/cm) in the proximal parts. Notably, there are no discernable changes in the magnitude and dynamics of T_l (Fig. 11.4). The circumferential smooth muscle layer is more responsive to relaxation by endogenous NO when compared to the longitudinal layer. This allows the organ to expand circumferentially rather than longitudinally as one might expect. As a result there is a concomitant fall in intraluminal p against the initial distending pressure.

11.3 Dynamics of the ICC/PDGFRα$^+$–MY(IM) Network

The pacemaker activity and the subsequent production of slow waves in the human stomach can be offered by both ICC/PDGFRα$^+$–MY and IM plexi. These are non-homogenous and demonstrate subtle region-dependent morphofunctional differences including shape, distribution and electrophysiological characteristics of ICC. The greatest number of cells are present in the fundus, 31.7 ± 1.8 (per area of 0.12 mm^2), with a lesser amount found in the corpus, 19.6 ± 1.8 and the antrum (the exact quantitative data is not available) (Manneschi et al. 2004; Yun et al. 2010).

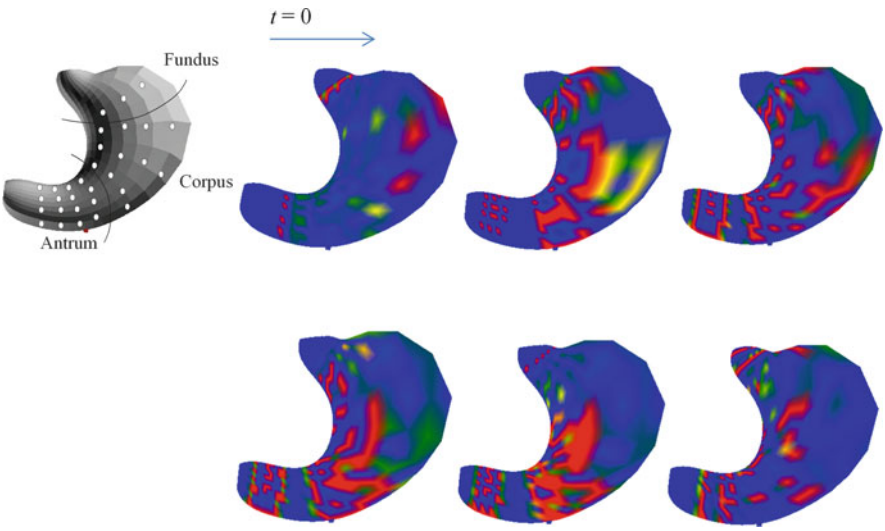

Fig. 11.7 Self-synchronization of myoelectrical activity in the ICC/PDGFRα^{+}–MY(IM) (*open circles*) network

Their density across the gastric wall is also uneven with the largest number of ICC located: (i) in the submucous layer of the fundus, 8 ± 0.7, and the corpus, 4.1 ± 0.7, and (ii) along the myenteric border, 6.3 ± 0.5 (fundus) and 4.3 ± 0.6 (corpus). The cell distribution in the circular and longitudinal smooth muscles in the proximal part of the organ is relatively homogenous and varies from 3.4 to 6.1 per 0.12 mm^2. Cytological analyses reveal small fusiform bodies of ICC with two long slender processes and a few ramifications in the fundus. Larger cells with three or more processes and multiple thin ramifications rich in protrusions are found in the corpus and antrum. Interconnected via gap junctions (electrical synapses), they form a polygonal multi-dimensional network (Fig. 11.7). The ICC of different regions have ascribed well-defined electrical properties, i.e., the amplitude of generated spikes is ~90–100 mV, their natural frequencies being: $0.08 \div 0.09$ Hz (fundus), $0.09 \div 0.1$ Hz (corpus), and $0.12 \div 0.13$ Hz (antrum).

The nature of gap junctions along with structural symmetry of connections are essential for reciprocal synchronization as well as a feed-forward propagation of excitation in the network. Discharging sporadically at random regions, weakly connected ICC generate nuclei of transient depolarizations of maximum amplitude 80 mV and duration ~0.5 s (Fig. 11.7). These make the signal transmission incoherent. The time and cluster firing locking helps establish some degree of organization among cells, i.e., even weakly coupled neurons firing at their own frequencies when depolarized simultaneously start firing nearly in synchrony. They confluence to create spatio-temporal patterns of electrical activity of various intensities in the fundus, corpus and antrum. Despite the synaptic symmetry, the excitation in the proximal and central part of the stomach propagates more efficiently

longitudinally, while in the antrum, circumferentially. In the body close to the lesser curvature, signals evolve into a target pattern which is, however, short-lived and thus cannot sustain signal transmission. The network becomes desynchronized with firing occurring at random locations.

The effect of synchronization and stabilization of firing activity in the network can be attributed to the presence of a dominant pacemaker (DP) which establishes and sustains the required strong connectivity among cells. In the human stomach, it is considered conventionally to be a group of specialized ICC found along the greater curvature in the corpus. Recent clinical evidence indicates the possible existence and occurrence of multiple pacemakers in different parts of the organ. At the time of writing, information on the origin and defining oscillatory properties of DPs was not available. Proposed mechanisms including group-cluster, voltage-dependent and intracellular Ca^{2+} transients are speculative and do not support the essentials of observable dynamics.

Let the dominant pacemaker be in the corpus along the greater curvature of the stomach. This spontaneously produces signals of high amplitude, 100 mV, and frequency, 0.12 Hz, which precede the time-scale of discharges of neighbouring cells. Assume that a time- and frequency-lock condition is imposed on ICC of the fundus, corpus and antrum, i.e., they oscillate harmoniously at their natural region-specific frequencies. The DP offers the pacing and coordinated spread of excitation across the network even when action potentials produced by a cell are of subthreshold levels. Simultaneous activity of ICC in the vicinity can result in an amplified potential that is above the required threshold. There is less nucleation within the fundus, whereas most of the body and the proximal part of the antrum form target patterns of electrical activity (Fig. 11.8). These sweep the entire organ during the

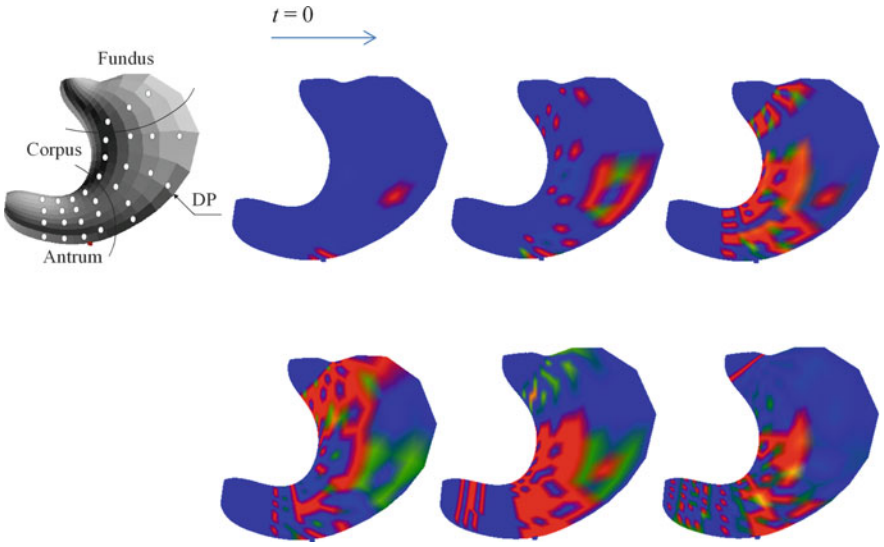

Fig. 11.8 Synchronization of myoelectrical activity in the ICC/PDGFRα^{+}–MY(IM) network by the dominant pacemaker (DP)

following 0.7 s. With the cessation of the DP, the network regains its original state with ICC discharging incoherently.

11.4 MP–ICC/PDGFRα$^+$–MY(IM) Interactions

Immunolabeling, ultrastructural, *c-Kit* mutation, gene modulation, mechanical and electrophysiological studies provide compelling evidence that the ICC/PDGFRα$^+$–MY(IM) plexus functions cooperatively with, and serves as, an intermediary for signal transduction between the myenteric nervous plexus and SIP syncytia in the stomach (Zhang et al. 2011; Sanders et al. 2012; Blair et al. 2014). The dynamics of the SIP/ganglion unit has been extensively studied in the previous chapter. Here the main focus is on analyzing synchronization of electrical activity between the two networks, the MP and ICC/PDGFRα$^+$–MY(IM). Despite similarities in architecture, they differ in: (i) morphology (a homogenous pool of identical cells vs. various neurons), (ii) density (3583 ± 500 cells/cm^2 vs. $46{,}260 \pm 3289$ neurons/cm^2), (iii) functional unit (a single cell vs. interconnected ganglia of 3–5 neurons), (iv) synapses (homotypic electrical, excitatory only vs. chemical, both excitatory and inhibitory, with multiple neurotransmitters and polymodal receptors), (v) dynamic pattern (continuous self-oscillatory type vs. organization of electromechanical processes into coherent physiological responses), (vi) propagation (spatio-temporal synchronization of sporadically occurring nuclei of excitation vs. quiescent, or wave of depolarization and/or hyperpolarization formation).

The myenteric plexus is non-uniformly distributed in a space between the longitudinal and circumferential smooth muscle layers of the stomach. It is sparse in the proximal and dense in the distal part of the organ. Neuronal ganglia are entwined through direct, bypass, divergent, convergent and backward inhibitory dendro-somatic and axo-somatic synaptic connections in a rectangular two-dimensional neuronal network (see Chap. 7). Its cytoarchitectural mesh measures ~200–500 μm.

The MP and ICC/PDGFRα$^+$–MY(IM) plexi coupled together via synapse-like structures, form a large-scale dynamic system. Their exact nature, density and distribution are not known. Two biologically feasible but mutually exclusive theories can be offered at this stage: a homogenous even distribution vs. a cluster-type arrangement. The former supports the notion of random occurrence whilst the latter favors the presence of morphofunctionally distinct areas of pacemaker activity. The duplicity is overcome due to excessive plasticity and adaptability, the synapse-like structures ensuring the leading role of the MP in producing requisite signaling patterns as well as a high degree of flexibility. The release of a balanced combination of neurotransmitters adds a large number of tuneable parameters to the system, e.g. the concentration of chemical substances and receptors, association and dissociation rates of chemical reactions etc. This enables the desired modulations of intensity, shape, phase lags and frequency of discharges of ICC.

Assume there are two neurotransmitters, ACh and NA, involved in signal transduction dynamics within the MP. This rather restricted assumption is used as proof of concept only and can be expanded to include other transmitters if and when required. Suppose that the generated fast excitatory and inhibitory postsynaptic potentials summate linearly on somas of neurons, with the resultant potential triggering spikes if a defined threshold value is exceeded. Otherwise, the neuron remains unexcited.

At rest, the MP remains quiescent while ICC demonstrate sporadic oscillatory activity. Multiple scattered nuclei of discharges are produced over the entire gastric surface. In the fundus and the distal part of the corpus, cell clusters firing at nearly equal frequencies undergo self-synchronization.

Let mechanical stretch stimuli, $n = 5$, of intensity $\varepsilon\,(t) = 0.6L$, and a frequency of $\nu_{\mathrm{m}} = 0.114$ Hz be applied at a single ganglion in the proximal part of the corpus along the greater curvature of the stomach. These generate regular action potentials at the free nerve endings that travel towards the sensory neuron and further to the inter- and motor neurons. Dispersed interneuron axonal projections support the spread of excitation among myenteric ganglia (Fig. 11.9). The frequency of discharges by interneurons is irregular and depends on the intensity of synaptic activity, the release of neurotransmitters and binding to postsynaptic receptors. The detailed quantitative analysis of electrical and chemical processes involved is given in Chap. 10. Bursts of action potentials of amplitude 76.4 mV are produced. These form a wave of depolarization which propagates at a velocity of ~3.3 mm/s in the longitudinal and ~2.95 mm/s in a circumferential direction. Experimental measurements conducted on healthy volunteers using a novel noninvasive high resolution electrogastrogram give similar results (Gharibans et al. 2017).

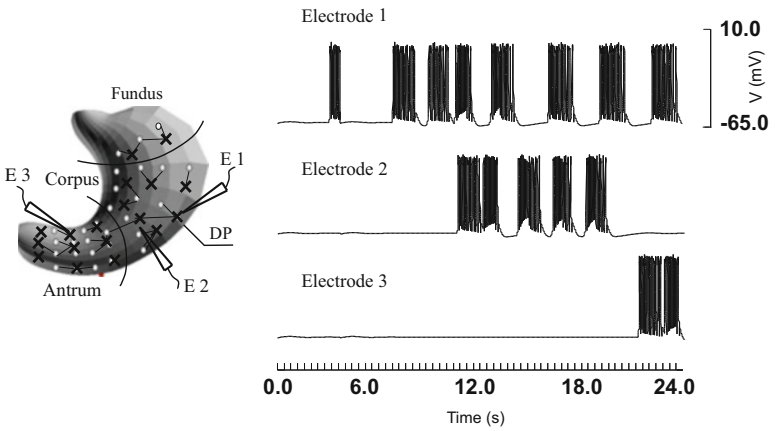

Fig. 11.9 Myoelectrical activity in the MP–ICC/PDGFRα^{+}–MY(IM) network. DP is the dominant pacemaker; *crosses* refer to the myenteric nervous plexus ganglia; *open circles* represent ICC/PDGFRα^{+}–MY(IM)

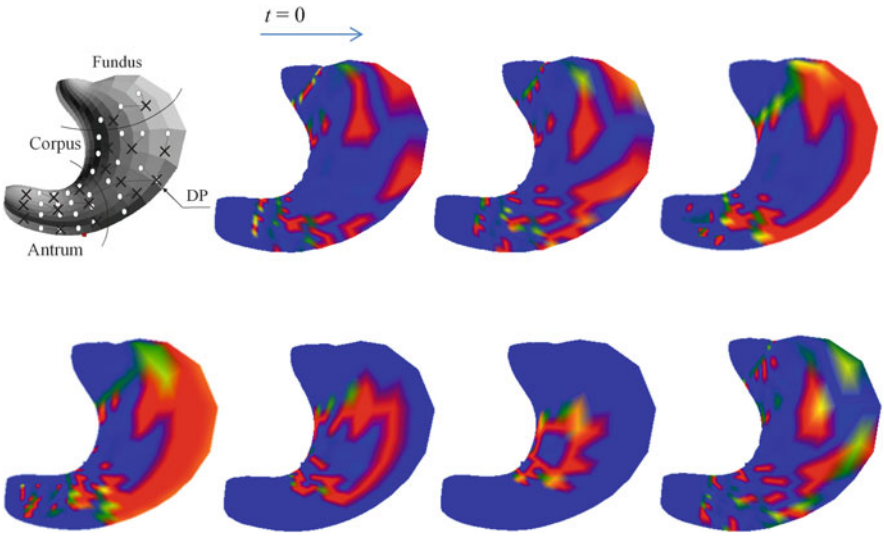

Fig. 11.10 The spatiotemporal organization and propagation of myoelectrical patterns in the MP–ICC/PDGFRα$^+$–MY(IM) network. Notations are as in Fig. 11.9

The wave of excitation reorganizes and enhances the motor-neuron—synapse-like associations between the two networks at each ganglionic site. These provide an essential signaling input to realize time, space and frequency-dependent firing synchronization of ICC. Strong connections are achieved in the cellular ensemble and a coherent traveling wave is successfully formed (Fig. 11.10). Over a period of subsequent neuronal stimulations, the global intercellular and oscillatory coupling in the ICC/PDGFRα$^+$–MY(IM) network is attained. With the cessation of neuronal activity in the MP, ICC/PDGFRα$^+$–MY(IM) become desynchronized and resume random oscillations.

11.5 Slow Wave and Electromechanical Activity in the Human Stomach

Fundamental motor functions of the human stomach are closely related to electrical wave processes (Muraki et al. 1991; Ou et al. 2003; Lyford et al. 2002; Lyford and Farrugia, 2003). A large repertoire of movements is a result of intricately regulated signal exchanges between the MP–ICC/PDGFRα$^+$–MY(IM) plexi (control system) and electromyogenic gastric smooth muscle syncytia. Intercellular structural arrangements and the transduction mechanisms responsible remain controversial. There is compelling experimental evidence for and against the existence of gap junctions between ICC-MY and SMCs. By contrast, there is strong consensus supported by ultrastructural studies, that there is low resistance electrical connectivity

between intramuscular ICC and SMCs. Based on close morphological associations to motor neurons and the expression of multiple receptors for neurotransmitters, it is speculated that ICC–IM, along with myenteric motor neurons, function as mediators of neural inputs to smooth muscle (Faussone-Pellegrini et al. 1977; Zhang et al. 2011; Klein et al. 2013; Blair et al. 2014; Sanders 2000; Sanders et al. 2014).

Pacemaker signals from neuro-interstitial plexi are reflected as prolonged, low amplitude (slow wave) and short, high amplitude (spike) membrane potential changes of SMCs. Using flexible printed circuit board arrays from the serosa of the anterior wall of the body (corpus) of the intact human organ, the highest frequency of pacemaker signals recorded during surgeries is 0.06 Hz. The lowest, in the antropyloric region, is 0.04 Hz (Koch 2011). A more recent thorough investigation of slow wave dynamics in excised longitudinal and circular smooth muscle strips using intracellular microelectrodes, has revealed the highest frequency in the antrum region, 0.12–0.13 Hz, the intermediate in the corpus, 0.087–0.1 Hz, and the lowest in the fundus, 0.08–0.09 Hz (El-Sharkawy et al. 1978; Rhee et al. 2011). Although slow waves are ubiquitous across the stomach, it is noteworthy that spikes are predominantly generated in the distal corpus, antrum and pylorus.

Despite smooth muscle possessing well developed cell-to-cell connections through gap junctions, its passive membrane properties—the corresponding values of internal resistance, time and length constants $125 \div 300\ \Omega\cdot$cm, 100–250 ms, and 1.34 ± 0.21 mm respectively—do not favor the propagation of slow waves. The process is orchestrated by the control system which guarantees stabilization and sustainability of slow wave dynamics.

Assume that at the initial moment of time SM syncytia are in a stable state. The excitation from the MP–ICC/PDGFRα^{+}–MY(IM) plexi is conveyed to SMCs at the sites of their direct contacts defined by the topography of chemical and electrical synapses. These trigger the generation of slow waves ($0 < t < 37$ s) which undulate at characteristic frequencies of corresponding ICC–MY(IM). Simulated electromyogenic traces recorded from the circular smooth muscle layer in the fundus, proximal body and antrum of the human stomach are shown in Fig. 11.11a. For $50 < t < 60$ s, the propagating wave of electrical activity in the control system (Fig. 11.10) synchronizes in space and time SM membrane potential oscillations. The three areas under consideration become time-, phase- and frequency-interlocked and produce the front of, what appears to be, a spreading slow wave (Fig. 11.12). Spikes occurring on the crests of slow waves are a result of cholinergic inputs from the myenteric motor neurons (Fig. 11.11b). The independent concurrent effect of the latter is through activation of muscarinic receptors on SMCs. In the absence of coordinative signaling, syncytia continues to be desynchronized for 22 s. With the next wave of excitation, $80 < t < 90$ s, strong connectivity is re-established and a new slow wave front is formed.

Slow waves, per se, induce mechanical responses in the fundus but not in the distal regions of the stomach where high amplitude action potentials are required. These activate voltage-dependent calcium channels on the smooth muscle membrane and cause a rapid influx of extracellular calcium. A rise in the free cytosolic calcium ion concentration triggers the cascade of intracellular reactions

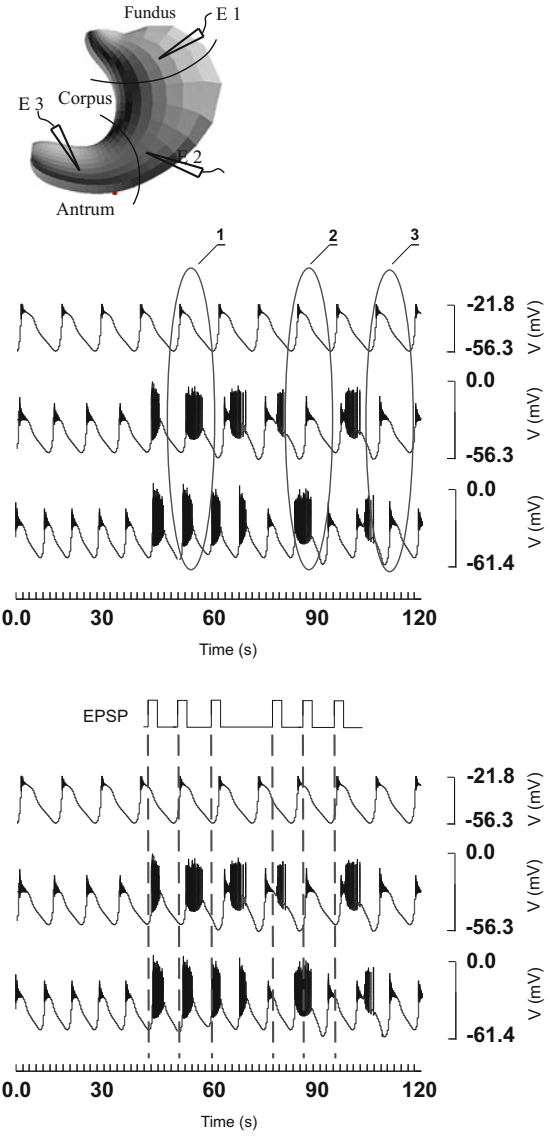

Fig. 11.11 The proposed mechanism of slow wave organization. EPSPs represent cholinergic inputs from motor neurons

with the generation of active forces of contraction. These are concomitant in phase and time with Ca^{2+} oscillations. The active forces in the fundus and body of the steer-horn type stomach are: $T^a{}_l = 61.4$ mN/cm and $T^a{}_c = 74.3$ mN/cm. The cardia and antrum-pylorus experience lower stresses: $T^a{}_l = 3.0$–3.6 mN/cm and $T^a{}_c = 3.7$–4.4 mN/cm. The most intense contractions are produced by the longitudinal syncytium in the corpus, $\max T^a{}_l = 79.2$ mN/cm. There is a small zone at the lesser curvature where $\max T^a{}_c = 105.3$ mN/cm. The fundus

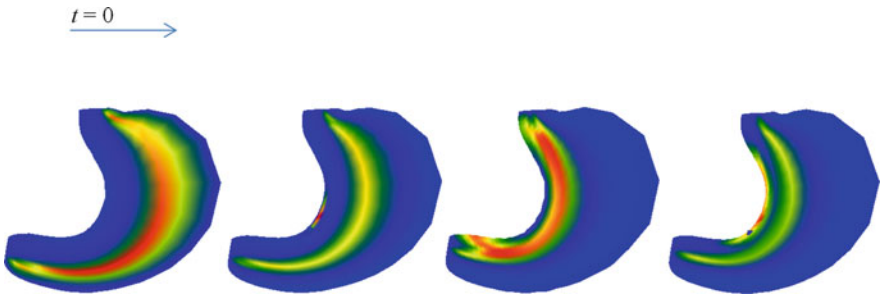

Fig. 11.12 The spatial propagation of an organized slow wave

undergoes uniform contractions in both smooth muscle layers: $T^a{}_l = 69.1$ mN/cm, $T^a{}_c = 84.7$ mN/cm.

Wrinkles that originate in the antrum-pylorus extend along the greater curvature to the distal part of the body of the organ. Uniaxial longitudinal stretching persists also in the cardia. Additionally, there are wrinkles along the longitudinal axis at the lesser curvature of the bioshell.

The pattern of total force distribution is similar to that reported earlier. Greater tension is consistent with the generation of active forces by muscle syncytia. Maxima $T_l = 151$ mN/cm, $T_c = 224$ mN/cm are recorded in the body, and $\max T_l = 27$ mN/cm, $\max T_c = 53$ mN/cm—in the cardia and pylorus of the stomach.

Stretching of ICC–IM and activation of mechanoreceptors of the primary sensory neurons produce signals that are transferred to the control system to generate an inhibitory response. The effect is attained through the nitrergic and "vipergic" neuro-modulatory mechanisms according to the dynamics discussed in previous paragraphs.

Before closing this chapter, the reader is reminded that considerations above rely on data obtained mainly from animal investigations. This information, if correct and applicable to the human stomach, could help in answering fundamental questions regarding: the normal physiology of the pacemaker, the diversity of its behavior, its variability in frequencies, space-cyclic meandering, MP–ICC/PDGFRα^+–MY synchronization, slow wave formation and propagation.

References

Blair PJ, Rhee P-L, Sanders KM, Ward SM (2014) The significance of interstitial cells in neurogastroenterology. J Neurogastroenterol Motil 20(3):294–317

De Zwart IM, Mearadji B, Lamb HJ, Eilers PH, AAM M, de Roos A, Kunz P (2002) Gastric motility: comparison of assessment with real time MP imaging or barostat measurement – initial experience. Radiology 224(2):592–597

Di Stefano M, Miceli E, Mazzocchi S, Tana P, Corazza GR (2005) The role of gastric accommodation in the pathophysiology of functional dyspepsia. Eur Rev Med Pharm Sci 9(1):23–28
El-Sharkawy TY, Morgan KG, Szurszewski JH (1978) Intracellular electrical activity of canine and human gastric smooth muscle. J Physiol 279:291–307
Faussone-Pellegrini MS, Cortesini C, Romagnoli P (1977) Sull'ultrastruttura della tunica muscolare della porzione cardiale dell'esofago e dello stomaco umano con particolare riferimento alle cosiddette cellule interstiziali del Cajal. Arch Ital Anat Embriol 82:157–177
Gharibans AA, Kim S, Kunkel DC, Coleman TP (2017) High-resolution electrogastrogram: a novel, noninvasive method for determining gastric slow-wave direction and speed. IEEE Trans Biomed Eng 64(4):807–815
Jahnberg T, Martinson J, Hultén L, Fasth S (1975) Dynamic gastric response to expansion before and after vagotomy. Scan J Gastroent 10:593–598
Janssen P, Verschueren S, Ly HG, Vos R, Van Oudenhove L, Tack J (2011) Intragastric pressure during food intake: a physiological and minimally invasive method to assess gastric accommodation. Neurogastroenterol Motil 23:e153–e154
Kindt S, Tack J (2006) Impaired gastric accommodation and its role in dyspepsia. Gut 55 (12):1685–1691
Klein S, Seidler B, Kettenberger A, Sibaev A, Rohn M, Feil R, Allescher H-D, Vanderwinden J-M, Hormann F, Schemann M, Rad R, Storr MA, Schmid RM, Schneider G, Saur D (2013) Interstitial cells of Cajal integrate excitatory and inhibitory neurotransmission with intestinal slow-wave activity. Nat Comm 4:1630. doi:10.1038/ncomms2626
Koch KL (2011) The electrifying stomach. Neurogastroenterol Motil 23:815–818
Kuiken SD, Vergeer M, Heisterkamp SH, Tytgat GNJ, Boeckxstaens GEE (2002) Role of nitric oxide in gastric motor and sensory functions in healthy subjects. Gut 51(2):212–218
Lefebvre RA (2002) Pharmacological characterization of the nitrergic innervation of the stomach. Verhandelingen – Koninklijke Academie Voor Geneeskunde van Belgie 64(3):151–166
Lyford GL, Farrugia G (2003) Ion channels in gastrointestinal smooth muscle and interstitial cells of Cajal. Curr Opin Pharm 3:583–587
Lyford GL, Strege PR, Shepard A, Ou Y, Ermilov L, Miller SM, Gibbons SJ, Rae JL, Szurszewski JH, Farrugia G (2002) Alpha 1C (Cav1.2) L-type calcium channel mediates mechanosensitive calcium regulation. Am J Physiol Cell Physiol 283:C1001–C1008
Manneschi LI, Pacini S, Corsani L, Bechi P, Faussone-Pellegrini MS (2004) Interstitial cells of Cajal in the human stomach: distribution and relationship with enteric innervation. Histol Histopathol 19:1153–1164
Mearin F, Papo M, Malagelada J (1995) Impaired gastric relaxation in patients with achalasia. Gut 36:363–368
Muraki K, Imaizumi Y, Watanabe M (1991) Sodium currents in smooth muscle cells freshly isolated from stomach fundus of the rat and ureter of the guinea-pig. J Physiol 442:351–375
Newton M, Kamm M, Burnham W, Roy A, Roeloffs JMM, Akkermans LMA (1999) Gastric compliance, sensation, and the relaxation response to a nitric oxide donor in health and reflux oesophagitis. Digestion 60:572–578
Ou Y, Strege P, Miller SM, Makielski J, Ackerman M, Gibbons SJ, Farrugia G (2003) Syntrophin gamma 2 regulates SCN5A gating by a PDZ domain-mediated interaction. J Biol Chem 278:1915–1923
Rhee P-L Lee JY, Son HJ, Kim JJ, Rhee JC, Kim S, Koh SD, Hwang SJ, Sanders KM, Ward SM (2011) Analysis of pacemaker activity in the human stomach. J Physiol 589(24):6105–6118
Sanders KM (2000) Postjunctional electrical mechanisms of enteric neurotransmission. Gut 47: iv23–iv25
Sanders KM, Koh SD, Ro S, Ward SM (2012) Regulation of gastrointestinal motility-insights from smooth muscle biology. Nat Rev Gastroent Hep 9(11):633–645
Sanders KM, Ward SM, Koh SD (2014) Interstitial cells: regulators of smooth muscle function. Physiol Rev 94:859–907

Tack J (2000) The physiology and pathophysiology of the gastric accommodation reflex in man. Verhandelingen – Koninklijke Academie Voor Geneeskunde van Belgie LXII(3):183–210
Talley N (2016) Functional dyspepsia: new insights into pathogenesis and therapy. Korean J Med 31(3):444–456
Talley NJ, Ford AC (2015) Functional dyspepsia. New Eng J Med 373:1853–1863
Thumshirn M, Camilleri M, Choi MG, Zinsmeister AR (1999) Modulation of gastric sensory and motor functions by nitrergic and alpha2-adrenergic agents in humans. Gastroenterology 116:573–585
Tonini M, De Giorgio R, De Ponti F, Sternini C, Spelta V, Dionigi P, Barbara G, Stanghellini V, Corinaldesi R (2000) Role of nitric oxide- and vasoactive intestinal peptide-containing neurones in human gastric fundus strip relaxations. Br J Pharm 129:12–20
Undeland KA, Hausken T, Gilja O, Aanderud S, Berstad A (1998) Gastric meal accommodation studied by ultrasound in diabetes. Relation to vagal tone. Scan J Gastroent 38:236–241
Yun H-Y, Sung R, Kim YC, Choi W, Kim HS, Kim H, Lee GJ, You RY, Park S-M, Yun SJ, Kim M-J, Kim WS, Song Y-J, Xu W-X, Lee SJ (2010) Regional differences of interstitial cells of Cajal (ICC) in human stomach. Korean J Physiol Pharm 14:317–324
Zhang R-X, Wang XY, Chen D, Huizinga JD (2011) Role of interstitial cells of Cajal in the generation and modulation of motor activity induced by cholinergic neurotransmission in the stomach. Neurogastroenterol Motil 23:e356–e371

Chapter 12
Biomechanics of the Postsurgical Stomach

Nature is relentless and unchangeable, and it is indifferent as to whether its hidden reasons and actions are understandable to man or not.

Galileo Galilei

The normal physiology of the human stomach has been studied in Chaps. 10 and 11. The following chapters are concerned primarily with modeling and computer simulations of pathological processes in the organ. In the discussion of results, attention is given to findings which are specific to the phenomenon under investigation only. The reader is advised to consult previous parts of the book for comparison.

12.1 Gastrectomy

Gastrectomy is a surgical procedure whereby a part of the stomach is removed. Depending on the percentage of the organ resected, it is differentiated into: antrectomy (30%), hemigastrectomy (50%) and subtotal gastrectomy (80%). The three major types of reconstruction that reestablish gastrointestinal continuity are Billroth I (end-to-end gastroduodenostomy), Billroth II (end-to-side gastrojejunostomy), and Roux-en-Y (gastrojejunostomy) (Fig. 12.1). Gastrectomy is reserved for patients suffering from: (i) gastric cancer, (ii) peptic ulcers which are refractory to medical therapy and complicated by perforation, bleeding, pyloric obstruction, and intractable *Helicobacter pylori* infection, and (iii) gastrointestinal stromal tumors. The prevalence of these diseases, morbidity and health care costs worldwide is enormous. In the case of peptic ulcer disease expenditure related to work loss, hospitalization, and outpatient care (excluding medication costs) in the US in 2016 alone was US$5.65 billion.

Morphostructural damages, a decrease in intragastric volume, $\breve{V}$, and a reduction in the myenteric and ICC/PDGFRα^{+}-MY(IM) plexi incurred after gastrectomy

R.N. Miftahof, *Biomechanics of the Human Stomach*,
DOI 10.1007/978-3-319-59677-8_12

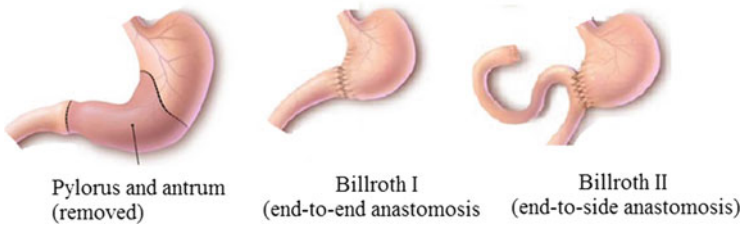

Fig. 12.1 Types of gastrectomies with Billroth I and II reconstructions

lead to impaired functionality, a loss of reservoir capacity, adaptive relaxation, mixing, and propulsion in the gastric remnant. These changes are manifested clinically as dumping syndrome, gastric stasis, reflux esophagitis, afferent loop syndrome etc. and are attributed to rapid, delayed or retrograde emptying of an ingested meal (Woodfield and Levine 2005; Obradović et al. 2006; Mochiki et al. 2007; Nomura et al. 2012; Chong et al. 2015; Weledji 2016; García-Díaz et al. 2016). The gravity of the postgastric surgery disturbances could range from self-limiting and spontaneously resolving to severely debilitating. In the case of the latter, instigated therapy is required, usually with limited success or re-operation. Understanding of the pathogenesis and biomechanics of postoperative changes may help improve surgical technique and alleviate possible complications.

Let the initial shape of the human stomach be the fish-hook type. Consider the effects of antrectomy and hemigastrectomy on motility and stress-strain distribution in the resected organ accomplished according to Billroth I and Billroth II procedures. To analyze the dynamics of $T_{l,c}$ (λ_l, λ_c) during fasting, accommodation relaxation and fed states, let intraluminal pressure $p(\breve{V})$ in the bioshell increase incrementally from 2 to 10 kPa. Suppose that the dominant pacemaker exists and is located close to the greater curvature in the gastric body and additional pacemaker cells are positioned in the duodenum.

In the postantrectomy stomach during fasting: $\breve{V} \approx 15$ ml $\propto p(\breve{V}) \sim 6$ kPa, the maximum stress in the longitudinal direction is attained in the fundus and corpus, $\max T_l = 19.8$ mN/cm, after Billroth I reconstruction procedure. There is an even total force distribution circumferentially, $T_c = 25.4$ mN/cm, in the majority of the gastric remnant with a small area along the lesser curvature where $\max T_c = 50.9$ mN/cm is recorded. The duodenum, a biocylinder, experiences uniform tension in both directions with $\max T_l = 4.8$ mN/cm and $\max T_c = 9.9$ mN/cm, respectively (Fig. 12.2).

The network of ICC displays random oscillatory activity. Its firing pattern, scattered nuclei of high amplitude potentials, is similar to that observed under normal physiological conditions. The DP provides limited synchronization of ICC but fails to organize coordinated propagation of slow waves and mechanical responses in SM syncytia.

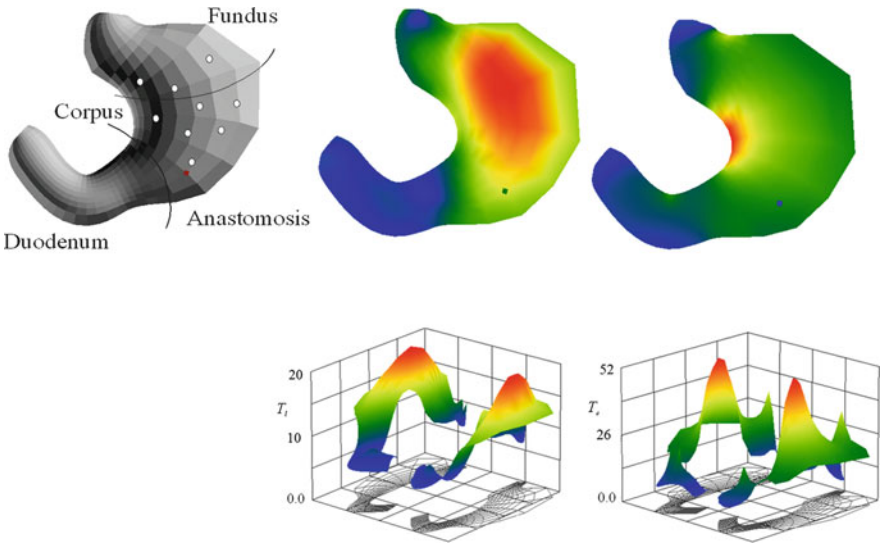

Fig. 12.2 The distribution of total forces T_c and T_l in the human stomach and duodenum after antrectomy with Billroth I reconstruction. Open circles represent ICC/PDGFRα$^+$-MY(IM)

After the "ingestion" of a meal, $\breve{V} \approx 100$ ml $\propto p(\breve{V}) \simeq 10$ kPa, the cardia and fundus stretch mainly longitudinally, $\lambda_l = 1.23$, whereas the fundus and corpus along the greater and lesser curvatures, deform circumferentially with $\lambda_c = 1.44$. The gastric remnant retains the ability of accommodation in response to intraluminal distension. It reacts to an increase in $\breve{V}$ with a decrease in the basal distending pressure (19.2 kPa) by 3.8 kPa. The variations in amplitude of p quickly decline to 0.5 kPa before reaching a stable value of 17.5 kPa. The subsequent release of NO has a minimal effect on relaxation, min$p = 16.8$ kPa. The reader needs to remember that the accommodation reflex involves multiple neurotransmission and regulatory mechanisms which have been studied in full in previous chapters.

Despite anatomical diminution in size of the MP-ICC/PDGFRα$^+$-MY (IM) network, its neuromodulatory and oscillatory properties remain intact. There are sustained synchronized waves of excitation (Fig. 12.3). Their amplitude, rhythm or velocity of propagation are not altered by the postsurgical procedure. However, surgical disruption of the integrity of plexi prevents their spread to the duodenum at the site of the anastomosis.

Close intercellular contacts provided during surgery via the close opposition of anastomotic ends and reparative processes in smooth muscle and connective tissue, re-establish electromechanical continuity in a postsurgical stomach. Slow wave activity originating in the corpus and the duodenum prompt mechanical reactions in SM. In the absence of synchronization the stomach and duodenum contract

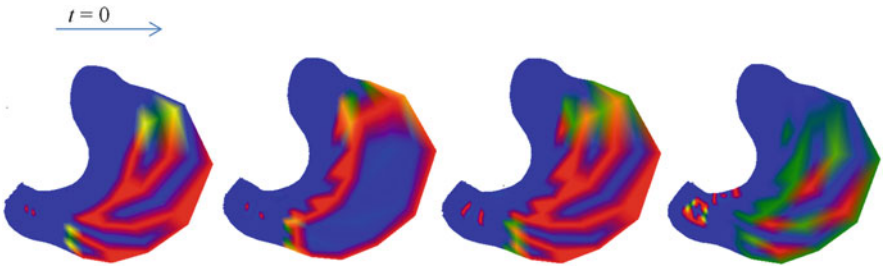

Fig. 12.3 Gastric myoeletrical activity after postantrectomy with Billroth I reconstruction

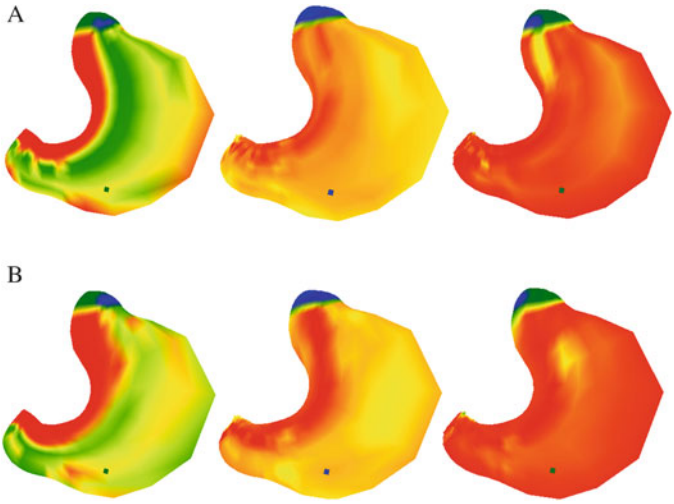

Fig. 12.4 The dynamics of total forces T_l (**a**) and T_c (**b**) after postantrectomy and Billroth I reconstruction

discordantly. Only after attaining the time, phase and frequency-interlock between the two parts is the propagating wave of active force generated. Contractions in the longitudinal and circular smooth muscle layers occur with a short time delay and show similar dynamics. Stronger forces are recorded from the circular SM layer: $T_l^a = 17.6 - 66.2$ mN/cm, $T_c^a = 25.96 - 85.9$ mN/cm (Fig. 12.4). In the case of persistent synchronized signaling, tonic type contractions in the entire gastric remnant and the duodenum are produced: $\max T_l^a = 64.7$ mN/cm, $\max T_c^a = 84.5$ mN/cm. Maxima total membrane forces induced in the bioshell are: $\max T_l = 216.4$ mN/cm, $\max T_c = 350.9$ mN/cm in the fundus and midcorpus.

The consecutive changes in configuration indicate the independent disjoint mechanical activity in the stomach and duodenum (Fig. 12.5). Peristaltic

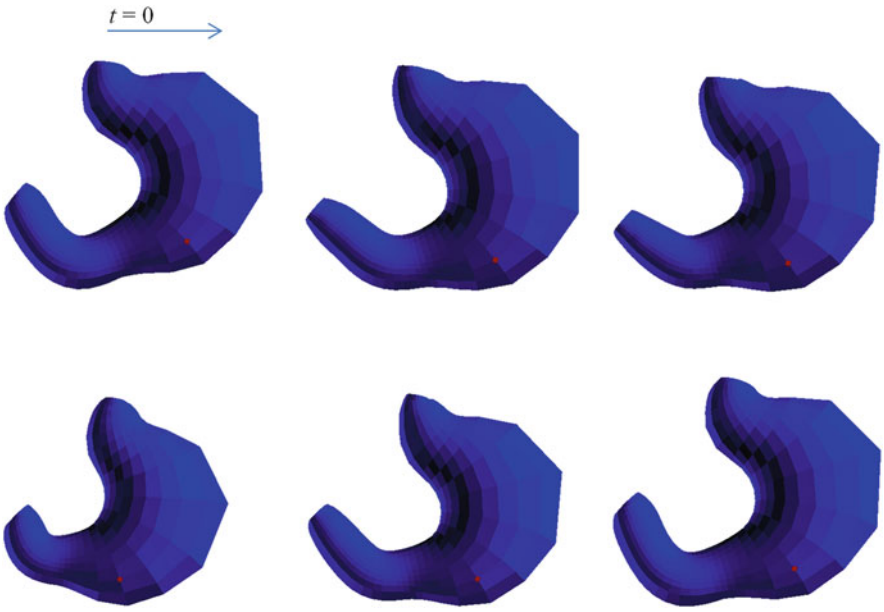

Fig. 12.5 Contractions of the human stomach remnant after Billroth I reconstruction

contractions are poorly coordinated and fail to organize in aborally propagating waves, although they appear efficient enough to squeeze the gastric content to the duodenum.

During fasting, the gastric remnant of the cascade-shape stomach after hemigastrectomy according to Billroth II reconstruction experiences biaxial stress-strain state with maxima $T_l = 9.3$ mN/cm, $T_c = 13.8$ mN/cm with a focus of concentration of tension, $\max T_c = 53.6$ along the lesser curvature at the site of the anastomosis (Fig. 12.6). There is a uniform total membrane force distribution along the afferent and stump of the efferent intestinal loops: $T_l = 4.6$ mN/cm, $T_c = 9.4$ mN/cm.

Spontaneous random discharges of ICC at their natural regional frequency are found in the fundus and proximal part of the corpus of the resected stomach. Sporadic confluences of scattered nuclei of electrical activity develop across the remnant (Fig. 12.7). When strong connectivity and synchronization within the MP-ICC/PDGFRα^+-MY(IM) network is achieved, a propagating wave of excitation is formed which triggers slow wave activity in the longitudinal and circular smooth muscle syncytia (Fig. 12.8). As a result a coordinated mechanical wave of contraction-relaxation develops. In fed state, stress-strain distribution resembles qualitatively that observed in fasting, although the quantitative analysis shows slight fluctuations in the magnitude of the total membrane forces with each contraction.

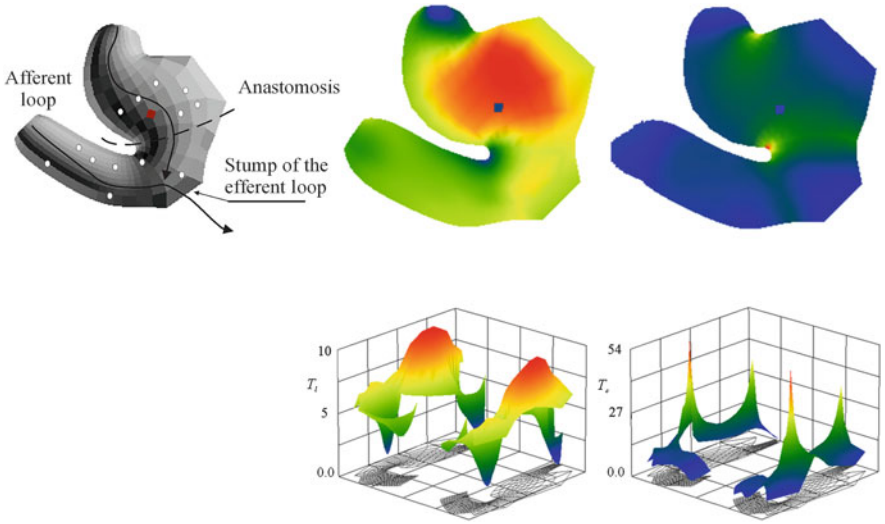

Fig. 12.6 Total force T_c and T_l distribution in the human stomach after hemigastrectomy with Billroth II reconstruction. Open circles represent ICC/PDGFRα^+-MY(IM)

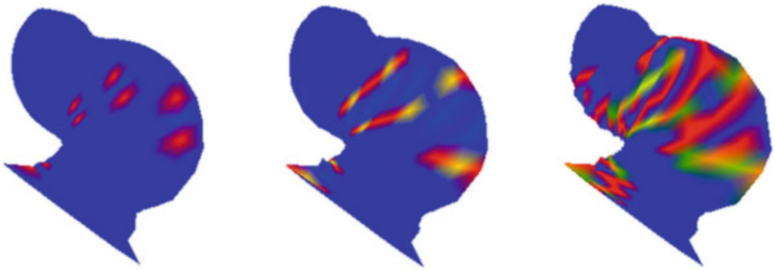

Fig. 12.7 Myoelectrical activity in the ICC/PDGFRα^+-MY(IM) network in the human stomach after hemigastrectomy

The pacemakers in the afferent intestinal loop, firing independently, produce the migrating myoelectrical complex with SM contractions that spread freely towards the efferent loop.

12.2 Vagotomy

The vagus nerve provides a conduit for bidirectional communication between the CNS and the stomach (Travalgi and Anselmi 2016). Upon entering the abdominal cavity through the diaphragmatic hiatus, the left (anterior) and right (posterior)

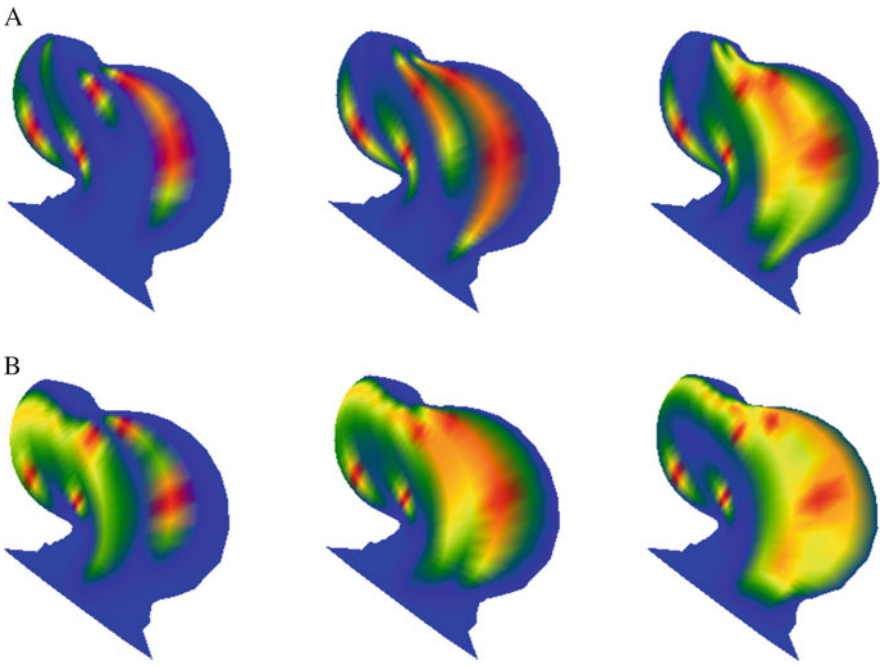

Fig. 12.8 Slow wave dynamics in longitudinal (**a**) and circumferential (**b**) gastric smooth muscle syncytia after hemigastrectomy

vagal trunks distribute gastric, coeliac and hepatic branches. The gastric branch gives rise to: (i) criminal nerve of Grassi which innervates the cardia and fundus, and (ii) the posterior and anterior nerves of Latarjet which supply the corpus, antrum, and pylorus.

The coordination of electromechanical processes in the stomach is determined by interplay between the intramural (MP-ICC/PDGFRα^{+}-MY(IM) network) and the extramural (extrinsic) vagal input, known as the vagovagal (sensory-motor) reflex. The details underlying the neurocircuitry of the reflex are obscure. Morphofunctional elements implicated in the reflex comprise the nucleus tractus solitarius (NTS), the dorsal motor nucleus of the vagus (DMV) and the nucleus ambiguus. All are located within the caudal brainstem. NTS serves as a centre for processing information of both a mechanical and chemical nature. Histomorphological animal studies have proposed two possible mechanoreceptor candidates for the vagus nerve: intraganglionic laminar endings (IGLEs) and intramuscular arrays (IMAs). The former are aggregates of terminal puncta found in close anatomical proximity or within myenteric ganglia, whereas the latter consist of arrays of neurite terminals running parallel to muscle bundles in the longitudinal and/or circular SM layers. Interestingly, IGLEs and IMAs can intimately associate with ICC-IM(MY) (Fox et al. 2000; Murphy and Fox 2010). Their distribution within the organ is uneven with IGLEs dense throughout the stomach,

and IMAs predominantly traced in the fundus and pylorus. Although it has been confirmed by electrophysiological investigations that IGLEs act as low threshold tension and stretch receptors, the functionality of IMAs is not clear. It has been hypothesized that they are stretch-sensitive receptors. (Berthoud et al. 2004; Zagorodnyuk et al. 2001; Song et al. 2009; Stakenborg et al. 2013; Hepworth et al. 2015).

NTS neurons do not fire action potentials spontaneously, but are activated by vagal afferent inputs which convey information on the stress-strain status of the stomach. From the NTS, integrated signals relay to the DMV which, along with the nucleus ambiguus, encompass efferent motor fibers. These interact directly with virtually all myenteric ganglia—a fact which has been proven immunohistochemically with the detection of c–Fos and phosphorylated c-AMP response element binding protein, i.e., markers for neuronal activity (Berthoud et al. 2001; Zheng and Berthoud 2000). In addition, DMV neurons per se demonstrate slow spontaneous intrinsic discharges suggesting that it could be the origin of pacing for the gastric pacemaker (Travagli et al. 1991)!

Operations on the vagus nerves of the stomach (vagotomy) were once commonly performed to treat and prevent peptic ulcer disease. With the development of acid-suppressive medications, mainly proton pump inhibitors and histamine receptor type 2 antagonists, the need for surgical intervention has greatly decreased. However, in the treatment of refractory and complicated ulcers, vagotomy still remains the procedure of choice, either per se or in conjunction with gastrectomy. The three basic types of vagotomy are: (i) truncal—denervation of the anterior and posterior vagal trunks at the level of the gastroesophageal junction, (ii) selective—the division of the gastric nerves of Latarjet only after it branches into the coeliac and hepatic nerves, and (iii) highly selective—interruption of nerve supply to the proximal two thirds of the organ (mainly the fundus and corpus), whilst the innervation of the antrum and pylorus remains unaltered (Fig. 12.9).

Postoperative recordings of the gastric myoelectrical and motor activity in patients who have undergone different extents of vagotomy have clearly demonstrated: (i) no significant variations in the frequency but a reduction in the amplitude and the irregular pattern of slow waves, (ii) a decrease in number of spike bursts, and (iii) diminished or absent mechanical waves of contraction. These findings correlate strongly with the degree of vagal denervation and are more conspicuous

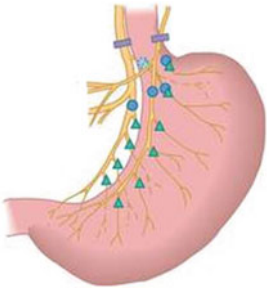

Fig. 12.9 Types of vagotomies: truncal (*bar*), selective (total gastric) (*circles*), proximal (highly selective) (*triangles*)

after truncal and selective vagotomy compared to the highly selective procedure (Stoddard et al. 1973, 1975; Hinder and Kelly 1997; Aldrete et al. 1982).

The unique characteristic of the MP is its ability to integrate heterogeneous sensory and motor signals into local reflexes independent from the external vagal inputs. It is noteworthy that the adeptness of ICC/PDGFRα$^+$-MY(IM) to perform this task per se is limited. Although the vagus nerve and associated CNS nuclei are not included in the current mathematical model of the human stomach, their effects can be simulated implicitly. Assume that vagotomy impairs coupling within the MP-ICC/PDGFRα$^+$-MY(IM) network. None of the types of vagotomy affect spontaneous oscillatory activity of SIPs. These continue discharging high amplitude action potentials at natural regional defined frequencies.

The concomitant distension of the stomach with the "ingested" meal and the subsequent stimulation of mechanoreceptors induce the generation and propagation of waves of depolarization in the sensory-motor neuronal chain. These organize local electromechanical reflexes within discrete myenteric ganglia—SIP units—and can be traced as far as the axonal projections of motor neurons. Myogenic responses appear sporadic and temporal (spatially discordant), i.e., the occurrence of slow waves is indiscriminate and associated contractions are disorganized.

The distant spread of excitation within the MP relies on interneuronal arrangements and direct stimulatory signals from the vagus. In the absence of the latter, the plexus cannot generate the propagation of excitation or sustain interconnectivity among ganglia. No areas of dominant firing pacing emerge and no strong connectivity among MP, ICC/PDGFRα$^+$ and SM across the stomach develop. As a result, no coordinated peristaltic waves are formed in the organ.

Highly selective vagotomy salvages the far proximal branches ("crow's foot") of the nerve of Latarjet, thus preserving the innervation of the distal part of the human stomach. The desired coordination and synchronization of electrical oscillations and motility is observed in the antrum and pylorus only. In the rest of the stomach, however, electromechanical processes occur haphazardly.

12.3 Bariatric Surgery

Worldwide the population is getting "heavier" day by day. Currently in the US 1 in 3 are considered overweight and nearly 1 in 9, obese. If this trend continues, it is predicted that by 2018 nearly 43% of all Americans will suffer obesity. The signs are more alarming if one considers that associated medical conditions such as cardiovascular diseases, diabetes mellitus, dyslipidemia and cancer, to name a few, affect lifestyle and lead to premature death. Furthermore, the treatment, either medical or surgical, carries a high cost—approximately US$147 billion in the USA in 2016.

Whereas a medical approach is used to address mild and moderate obesity problems, bariatric surgery remains the most effective treatment for morbid obesity. The most universally performed procedures are: Roux-en-Y gastric bypass

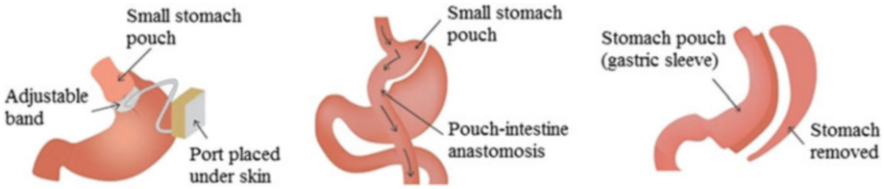

Fig. 12.10 Types of bariatric surgeries

(RYGB), sleeve gastrectomy (SG), adjustable gastric banding (AGB), and biliary pancreatic diversion (BPD) (Weledji 2016; García-Díaz et al. 2016; Angrisani et al. 2015; Quercia et al. 2014) (Fig. 12.10). The common element in all operations is the creation of small size gastric pouches of different shapes by irreversibly cutting part of the stomach and reconnecting it with the small intestine through various types of anastomoses. The shapes of newly formed pouches vary from golf ball (RYGB, AGB) to banana-like (SG, BPD). In the case of AGB, though, a silicone band about 1 cm in width lined by an inflatable cuff is placed around the fundus to produce a pouch. The adjustment of cuff pressure through the external abdominal port allows a patient to regulate the pouch opening and thus outflow of its content.

The main complication associated with altered motility following bariatric surgery is dumping syndrome. While the condition typically resolves over time, ~12% of all patients experience it for more than 2 years after surgery.

Consider stress-strain distribution and motility patterns in the gastric remnant following SG and BPD. These are equivalent to partial gastrectomy. However, in both cases the lesser curvature and pylorus remain intact while the anatomical shape of the stomach (steer-horn, cascade, J-type or fish-hook) becomes cylindrical. The surgery is categorized as restrictive (SG) and restrictive-malabsorptive (BPD), i.e., as a result the functional volume of the stomach decreases while endocrine and metabolic processes are either unaltered (SG) or minimally affected (BPD). The operation procedure per se does not influence the dynamics of interplay within the remaining MP-ICC/PDGFRα^{+}-MY(IM)-SM system or the occurrence of dominant pace-makers. In the simulations that follow, assume that the DP is located in the region corresponding to the distal part of the stomach.

Sporadic discharges of intact ICC-MY confluence randomly and form nuclei of oscillatory activity. These are scattered over the surface of the gastric remnant. The DP and signaling inputs from the MP establish strong links within the ICC network. There is a prevalent connectivity along the circumferential axis which is dimension related. The synchronization of ICC firing leads to the generation of waves of excitation. Their anterior fronts encircle the remnant and spread orally and aborally over the surface of the organ (Fig. 12.11).

The depolarization of smooth muscle at points of direct contact with motor neurons and ICC-IM, triggers the production of slow waves with a maximum amplitude 44 mV. Although initially dispersed, waves spread over SM syncytia and merge to form a continuous front. The velocity of their propagation

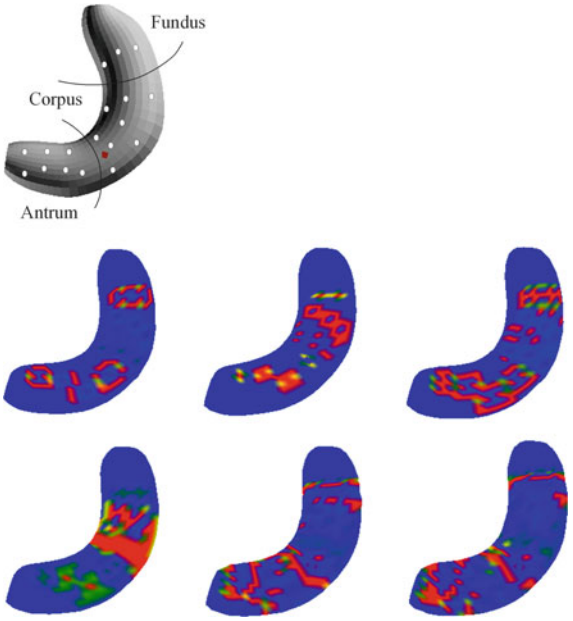

Fig. 12.11 Myoelectrical activity in the ICC/PDGFRα^{+}-MY (IM) (*open circles*) network after sleeve gastrectomy

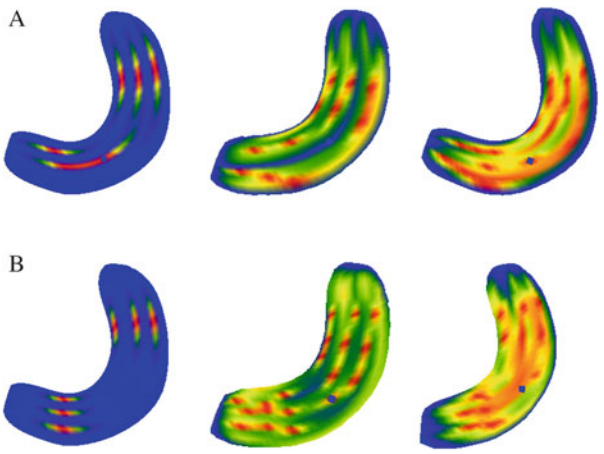

Fig. 12.12 Slow wave dynamics after sleeve gastrectomy

depends on the strength of connectivity within the system. When it happens, the collision of waves undulating at the same phase and frequency cause the amplification and prolongation of myoelectrical activity over an extended area (Fig. 12.12).

Owing to its cylindrical shape and a significant decrease in intragastric volume, the remnant's ability to distend and accommodate even a small amount of "ingested" meal, $\breve{V} \approx 50$ ml $\propto p(\breve{V}) \simeq 5$ kPa, is severely hampered. The stress-strain analysis shows that the "biocylinder" undergoes biaxial tension with a maximum longitudinal total membrane force along the "greater" and "lesser" curvature, $T_l = 36.1$ mN/cm, $T_l = 28.9$ mN/cm, respectively, and circumferential—$T_c = 125.4$ mN/cm (Fig. 12.13).

Slow waves organize the mechanical reaction in the bioshell. Earlier synchronization and coordination of contractions is achieved in the circumferential SM layer. The remnant experiences even tension across regions, $T_c = 152.1$ mN/cm, except in a local area along the "lesser" curvature where $\max T_c = 183.5$ mN/cm is generated. By contrast, full synchronization in the longitudinal SM layer needs time to develop. First seen as uncoordinated contractions in the corpus, $T_l = 83.6$ mN/cm, these evolve into a strong force, $T_l = 73.9$ mN/cm, in the distal

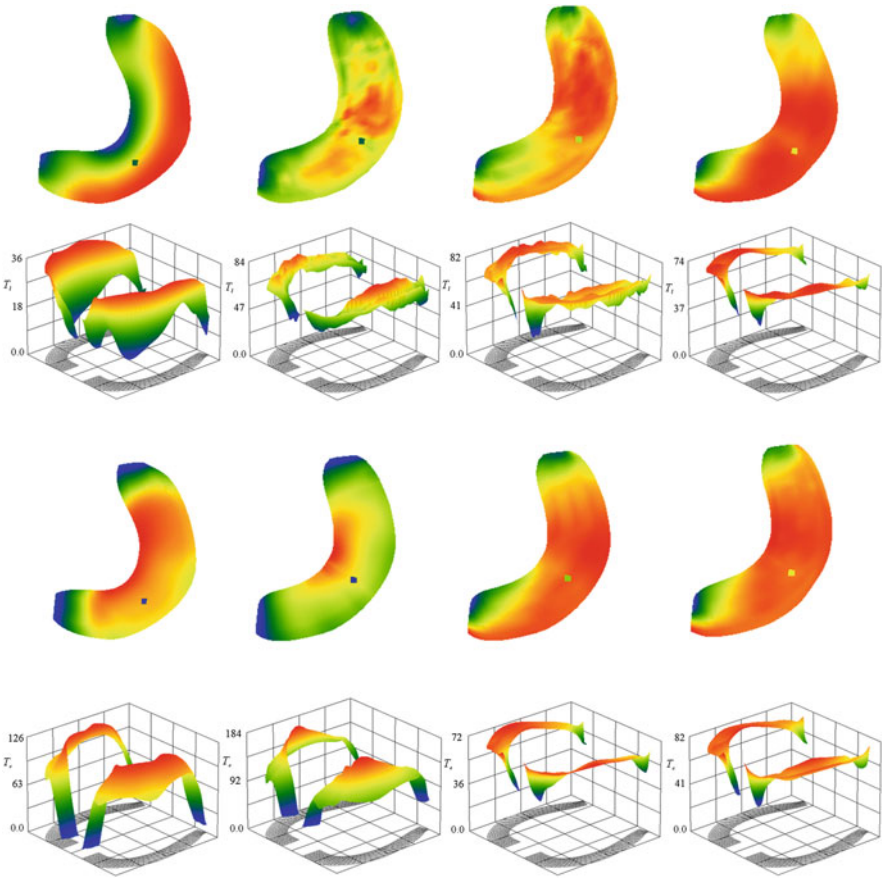

Fig. 12.13 Total force T_l and T_c distribution after sleeve gastrectomy

fundus, entire corpus and antrum. The reciprocally organized contractility of smooth muscle layers ensures the effective propulsion of the gastric content.

AGB is a predominantly restrictive procedure whereby a small round-shaped pouch is formed in the cardia-fundal region. Being minimally invasive, the operation does not inflict any morphostructural damage to the organ. The location of the dominant pacemaker remains unchanged—the area close to the greater curvature in the distal corpus—as well as the MP-ICC/PDGFRα^{+}-MY(IM)-SM complex. The electrodynamics including the oscillatory behavior of ICC-MY(IM), the spread of

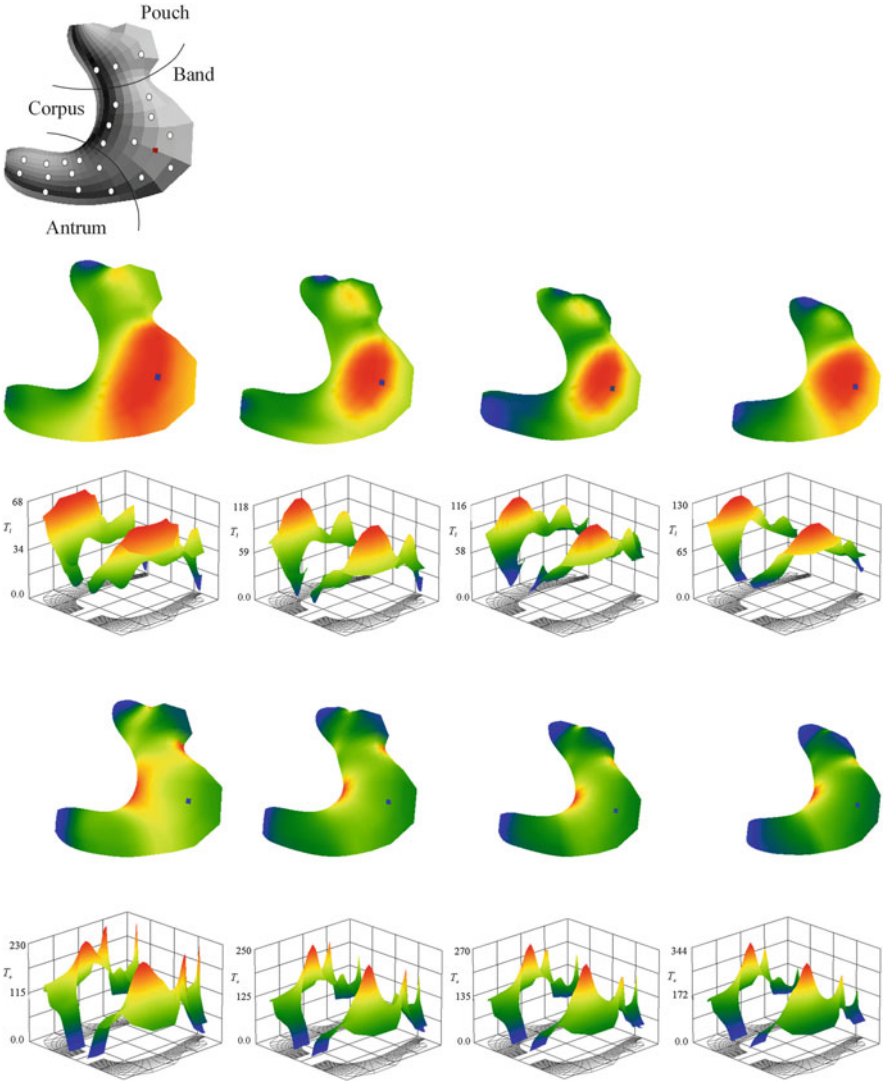

Fig. 12.14 Total force T_l and T_c distribution after adjustable gastric banding (AGB)

Fig. 12.15 Shapes of the post AGB human stomach during different stages of contractile activity

excitation within the myenteric plexus, the interplay and synchronization within the MP-ICC network, and the generation of slow waves and mechanical responses are similar to that recorded under normal physiological conditions.

The presence of a pouch in the proximal part of the stomach affects the stress-strain distribution in the organ. During fasting two zones of high level tension are detected in the bioshell: at the angle of His, where maxima $T_c = 187.1$ mN/cm, $T_l = 45.8$ mN/cm develop, and along the greater curvature at the site of the band placement, $\max T_c = 202.3$ mN/cm, $\max T_l = 45.8$ mN/cm. The pouch itself is unevenly stressed circumferentially with $\max T_c = 112.3$ mN/cm along the lesser curvature, and $T_c = 67.4$ mN/cm along the greater curvature whilst longitudinally, the membrane force distribution is uniform, $T_l = 32.5$ mN/cm. The area around the band is wrinkled with $\lambda_l = 1.1$–1.3 and $\lambda_c < 1$. The major part of the body of the stomach is evenly stressed, $T_l = T_c = 67.4$ mN/cm. There is a rise in intensity of circumferential total membrane forces in the region of the lesser curvature, $\max T_c = 232.2$ mN/cm, with a concomitant decrease in tension longitudinally, $\max T_l = 47.1$ mN/cm. The forces in the antrum-pylorus are: $T_l = 45.8$ mN/cm and $\max T_c = 112$ mN/cm (Fig. 12.14).

The ingestion of a meal and the development of active forces, $\max T_l^a = 87.5$ mN/cm, $T_c^a = 107.4$ mN/cm, initiate propagating peristaltic contractions in the organ. There is an increase in the strength of membrane forces in both circumferential and longitudinal smooth muscle layers across the pouch and the corpus, $T_l = 130.1$ mN/cm, $T_c = 195$ mN/cm, and the antrum-pylorus, $T_l = 64$ mN/cm and $\max T_c = 175$ mN/cm. These are accompanied by changes in the configuration and size of the stomach. It is important that the pouch contracts actively assuring the physiological propulsion of gastric content (Fig. 12.15).

References

Aldrete JS, Shepard RB, Halpern NB, Jimenez H, Piantodosi S (1982) Effects of various operations on the electrical activity of the human stomach recorded during the postoperative recovery period. Ann Surg 195(5):662–668

Angrisani L, Santonicola A, Iovino P, Formisano G, Buchwald H, Scopiano N (2015) Bariatric surgery worldwide 2013. Obes Surg 25:1822–1832

Berthoud HR, Paterson LM, Zeng H (2001) Vagal-enteric interface: vagal activation-induced expression of c-Fos and p-CREB in neurons of the upper gastrointestinal tract and pancreas. Anat Rec 262(1):29–40

Berthoud HR, Blackshaw LA, Brookes JH, Grundy D (2004) Neuroanatomy of extrinsic afferents supplying the gastrointestinal tract. Neurogastroenterol Motil 16(Suppl 1):28–33

Chong A, Ha J-M, Kim S (2015) Gastric emptying scan after distal subtotal gastrectomy: differences between Billroth I and II and predicting the presence of food residue at endoscopy. Int J Clin Exp Med 8(11):20769–20777

Fox EA, Phillips RJ, Martinson FA, Baronowsky EA, Powley TL (2000) Vagal afferent innervation of smooth muscle in the stomach and duodenum of the mouse: morphology and topography. J Comp Neurol 428:558–576

García-Díaz JJ, Ferrer-Márquez M, Moreno-Serranoa A, Barreto-Rios R, Alarcón-Rodríguezc R, Ferrer-Ayzaa M (2016) Outcomes, controversies and gastric volume after laparoscopic sleeve gastrectomy in the treatment of obesity. Cir Cir 84(5):369–375

Hepworth KL, Wang X-Y, Huizinga JD, Ratcliffe EM (2015) Anat Rec 298:1780–1785

Hinder RA, Kelly KA (1997) Human gastric pacesetter potential. Sit of origin, spread, and response to gastric transection and proximal gastric vagotomy. Am J Surg 133:29–33

Mochiki E, Asao T, Kuwano H (2007) Gastrointestinal motility after digestive surgery. Surg Today 37:1023–1032

Murphy MC, Fox EA (2010) Mice deficient in brain-derived neurotrophic factor have altered development of gastric vagal sensory innervation. J Comp Neurol 518:2934–2951

Nomura E, Lee SW, Tokuhara T, Kawai M, Uchiyama K (2012) Functional outcomes according to the size of the gastric remnant and type of reconstruction following open and laparoscopic proximal gastrectomy for gastric cancer. Hepatogastroenterology 59(118):677–1681

Obradović VB, Artiko V, Stefanović BM, Petrović MN, Petrović NS (2006) Simultaneous dynamic study of gastric emptying and changes of serum levels of gut hormones in patients after peptic ulcer surgery. Nucl Med Rev 9(1):51–55

Quercia I, Dutia R, Kotler DP, Belsley S, Laferrére B (2014) Gastrointestinal changes after bariatric surgery. Diabetes Metab 40(2):87–94

Song X, Chen BN, Zagorodnyuk VP, Lynn PA, Blackshaw LA, Grundy D, Brunsden AM, Costa M, Brookes SJ (2009) Identification of medium/high-threshold extrinsic mechanosensitive afferent nerves to the gastrointestinal tract. Gastroentererology 137 (1):274–284

Stakenborg N, Di Giovangiulio M, Boeckxstaens GE, Matteoli G (2013) The versatile role of the vagus nerve in the gastrointestinal tract. Eur Med J 1:106–114

Stoddard CJ, Waterfall WE, Brown BH, Duthie HL (1973) The effects of varying the extent of the vagotomy on the myoelectrical and motor activity of the stomach. Gut 14:657–664

Stoddard CJ, Waterfall WE, Brown BH, Duthie HL (1975) The immediate and delayed effects of different types of vagotomy on human gastric myoelectrical activity. Gut 16:165–170

Travagli RA, Gillis RA, Rossiter CD, Vicini S (1991) Glutamate and GABA-mediated synaptic currents in neurons of the rat dorsal motor nucleus of the vagus. Am J Physiol 260(1):G531–G536

Travalgi RA, Anselmi L (2016) Vagal neurocircuitry and its influence on gastric motility. Nat Rev Gastroenterol Hepatol 13:389–401

Weledji EP (2016) Overview of gastric bypass surgery. Int J Surg 5:11–19

Woodfield CA, Levine MS (2005) The postoperative stomach. Eur J Radiol 53(3):341–352

Zagorodnyuk VP, Chen BN, Brookes SJ (2001) Intraganglionic laminar endings are mechanotransduction sites of vagal tension receptors in the guinea-pig stomach. J Physiol 534(Pt 1):255–268

Zheng H, Berthoud HR (2000) Functional vagal input to gastric myenteric plexus as assessed by vagal stimulation-induced Fos expression. Am J Physiol Gastrointest Liver Physiol 279(1): G73–G81

Chapter 13
Dysmotility of the Human Stomach

To know what you know and what you do not know, that is the knowledge.

Confucius

Dysmotility is an ill-defined term that encompasses a wide spectrum of gastrointestinal disorders based on either/or radiologically, scintigraphically and manometrically confirmed abnormal motility and pathologically documented neuromusclular disease. Nosologically these range from loco-regional: achalasia, gastro-esophageal reflux disease, gastroparesis, colonic pseudo-obstruction and Hirschprung's disease, to panenteric conditions such as functional dyspepsia, chronic intestinal pseudo-obstruction, irritable bowel syndrome and slow transit constipation. The aetiology of dysmotility in approximately 80% of cases is uncertain, and hence these are considered to be primary/idiopathic. The remaining 20% are secondary to systemic diseases: diabetes, scleroderma and systemic lupus erythematosus among others. The onset and severity of a disease correlates with the nature and level of morphofunctional changes: gastric dysrhythmias, cytopathies, immune reactions with the production of autoantibodies, myopathies, uncoordinated contractility, delayed emptying etc. Owing to considerable complexity and an overlap between the histomorphological variants and clinical entities, it is instructive to analyze their pathophysiological effects separately.

13.1 Gastric Arrhythmias

Normal gastric myoelectrical activity in man is characterized by a stable rhythm at frequencies: 0.08–0.09 Hz in the fundus, 0.087–0.1 Hz in the corpus, and 0.12–0.13 Hz in the antrum. Any deviation from these is described as gastric arrhythmia. Slow waves of increased (decreased) frequency and of regular, fixed-shape and amplitude are classified as tachygastria (bradygastria). By contrast, those of irregular periods, configurations and fluctuating amplitude are known as tachy-arrhythmia (bradyarrhythmia), respectively.

R.N. Miftahof, *Biomechanics of the Human Stomach*,
DOI 10.1007/978-3-319-59677-8_13

The clinical significance of gastric arrhythmia per se and its association with gastrointestinal dysmotility is not well established. However, it can be noted that gastroparesis, chronic unexplained nausea and vomiting, functional dyspepsia, truncal and highly selective vagotomy infrequently present with different types of gastric arrhythmia (Stoddard et al. 1981; Qi et al. 2002; Yarandi and Srinivasan 2014; O'Grady and Abell 2015). In addition, neurohormonal disbalance caused by the administration of insulin, cholecystokinin, glucagon and glucagon-like peptides, oxytocin, prostaglandin E_2, vasopressin, a gonadotropin releasing hormone, an excessive production of progesteron or estrogen, and certain drugs, e.g. atropine, scopolamine, ephedrine, opioids, domperidone and ondansetron can induce or ameliorate the condition (Stoddard et al. 1981; Hasler et al. 1995; Owyang and Hasler 2002; Ohlsson and Janciauskiene 2007; Coleski and Hasler 2009).

The precise morphofunctional genesis of gastric arrhythmia remains unclear, although the disruption in the vagal control, myenteric neuropathy, interstitial cell of Cajal pathology (Cajalopathy) and destruction, neuromyopathy, channelopathies and, possibly, genetic defects have been suggested as underlying mechanisms.

Consider the effect of deficiency and variations in the frequency and duration of firing of ICC on myoelectrical responses of the antral SIP/ganglion unit. If the frequency of ICC discharges is increased from its natural frequency to 0.14 Hz, the SIP/motor neuron unit starts spontaneously producing action potentials of varying amplitude, $V = 35 \div 46.6$ (mV), at a constant frequency of 4.6 Hz (Fig. 13.1). These appear regularly on the crest of each slow wave and last ~5.4 s. The smooth muscle syncytium responds with phasic contractions of $T^a = 13.7$ mN/cm.

A reduction in firing frequencies to 0.102 and 0.06 Hz, with a concomitant increase both two- and threefold in the duration of spike production by ICC does not affect the rhythmicity and the electrical pattern of slow waves. However, there is a skip in spiking response, i.e., action potentials are generated on every third and fourth slow wave. No changes are observed though in the mechanical reaction of SIP.

An increase or decrease in ν to 0.19 and 0.107 Hz while sustaining the natural duration of pacemaker discharges, leads to myoelectrical arrhythmia (Fig. 13.2). Slow waves become distorted with an alteration in their duration and frequency and the pattern of spiking becomes irregular. The amplitude, frequency and the duration of action potentials are highly variable: $V = 33 \div 50$ (mV), $\nu = 3.2 \div 8.9$ (Hz) and $t = 1.17 \div 5.3$ (s). When $\nu = 0.19$ Hz, there is a loss in regularity in contractions. A prolonged contraction of ~20 s and strength $T^a \simeq 13.4$ mN/cm develops. Interestingly, if $\nu = 0.107$ Hz, the electrical activity changes to regular irregular, i.e., the irregular pattern of slow wave and spiking observed during the first 1.5 min of the response is repeated. Despite these changes, SMCs maintain regular phasic contractions of $T^a \simeq 16.5 \div 18$ mN/cm.

The range of impaired function of ICC/PDGFRα^+-MY(IM), resulting from aging, apoptosis and transdifferentiation attenuates the excitation dynamics in the network (Farrugia 2008; Gibbons et al. 2009; Huizinga et al. 2009; Manetti et al. 2010; Gomez-Pinilla et al. 2011). A depletion in the number of cells in the

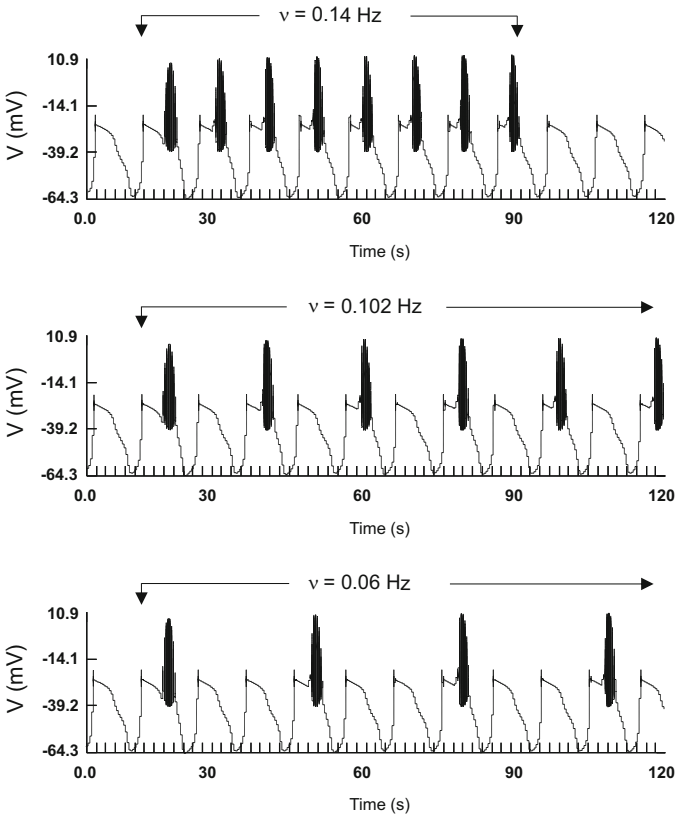

Fig. 13.1 The effect of the firing frequency of ICC/PDGFRα^{+}-MY(IM) on the rhythmicity of the antral SIP/ganglion unit

corpus and antrum of the stomach changes the pattern of signal transmission. The synchronized activity is detectable only in the fundus where depolarization spreads evenly throughout the network (Fig. 13.3). Sporadic discharges with nuclei of self-organized electrical activity are seen in a chain of remaining ICC in the corpus along the lesser curvature and antrum. Interestingly firing at a lower natural frequency after several periods, cells of the fundus entrain cells in the damaged areas and ensure the distal spread of excitation.

Under these conditions, the functional integrity of the MP becomes essential to sustain normal gastric motility. Assume that processes of production, storage and release of key neurotransmitters, ACh, SP, NO, VIP, 5-HT, NA, motilin and their receptor fields within Auerbach's plexus are unaffected. The wave of depolarization coordinates the development and formation of a peristaltic wave. Areas of active forces of an amplitude $T_l^a = 76.8$ mN/cm expand across the surface of the bioshell and form a continuous propagating wave of contraction of max $T_l^a = 73.9$ mN/cm and wavelength ~6 cm. The lack of ICC in the antrum delays the mechanical

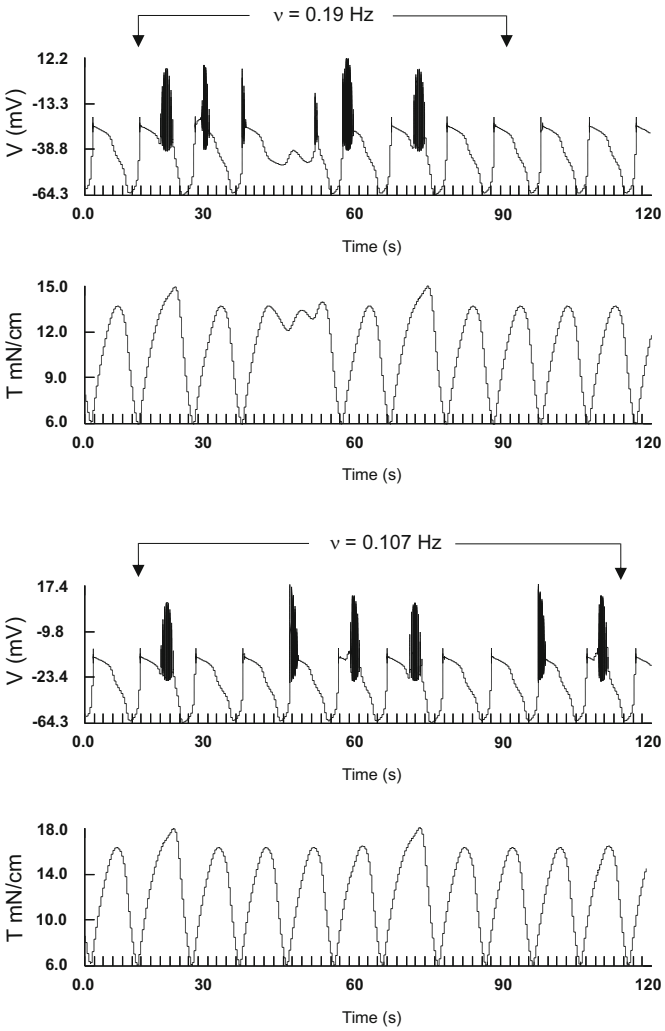

Fig. 13.2 The effect of duration and firing frequency of ICC/PDGFRα^{+}-MY(IM) on the myoelectrical activity of the antral SIP/ganglion unit

reaction in the region which never attains the tension usually observed. There are qualitative similarities in the dynamics of contractility in the circumferential SM layer although quantitatively, forces of greater average intensity, $T_c^a = 96.8$ mN/cm are produced. It could be concluded at this stage that gastric arrhythmias induced specifically by the impairment of ICC are not necessarily associated with abnormal gastric motility.

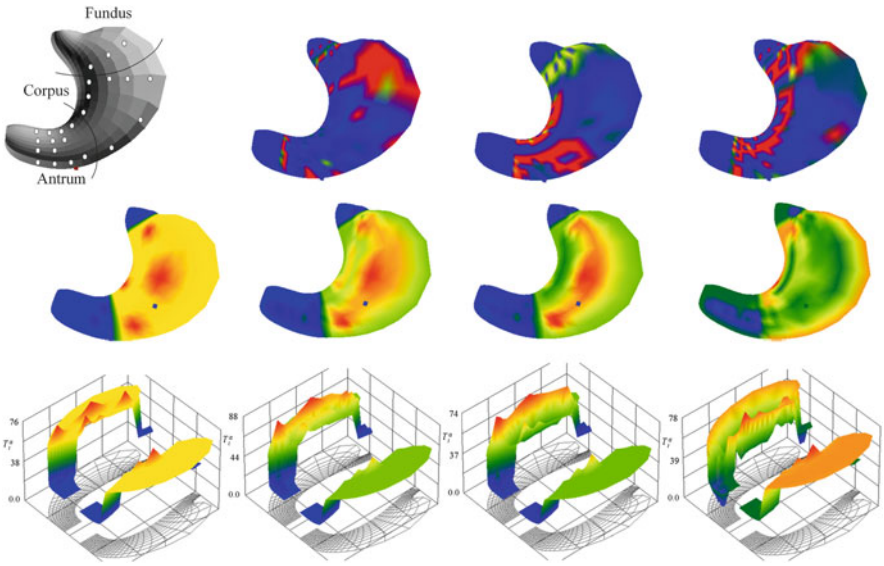

Fig. 13.3 The effect of a depletion of ICC/PDGFRα^{+}-MY(IM) on the myoelectrical (*top row*) and contractile activity (*middle and bottom rows*) of the stomach

13.2 Myenteric Neuropathy

Myenteric neuropathy is the term reserved only for disease that is histopathologically evident as damage or loss of enteric neurons. Depending on whether or not there are inflammatory/immune changes, myoneuropathies are distinguished as inflammatory or degenerative. Morphologically, for example, these may present with lymphocytic and plasma cell infiltrates, type 1 antineuronal nuclear antibodies (ANNA-1), free radicals, intracellular fibrosis, mitochodrialopathy, chaotic disarrangement of axonal neurofilaments, dense residual and lamellar inclusion bodies, changes in glial cells ensheathing axons, the sequestration of synaptic vesicles in membranous envelops, the widening of intracellular spaces, hypo-, aganglionosis, neuronal aplasia, dysplasia and degeneration (De Giorgio et al. 2004; Di Nardo et al. 2008; Manetti et al. 2010; Kashyap and Farrugia 2010; Knowles et al. 2013). Concomitant pathophysiological hallmarks of the structural abnormalities include altered voltage-gated calcium, $Ca_v2.1$ (P/Q), $Ca_v2.2$ (N), and potassium channel signaling, disrupted inhibitory and excitatory synaptic neurotransmission, impaired nerve-pulse transduction and electrochemical connectivity among others (Talamonti et al. 2006; Lefebvre 2002; Paine et al. 2013).

Myenteric neuropathies can be detected in patients with gastroparesis, paraneoplastic (e.g. small cell lung cancer, thymoma), infectious (Chaga's disease), neurological (encepholomyeloneuropathy), and connective tissue (scleroderma) disorders. Some of these patients have clinical symptoms of gastrointestinal

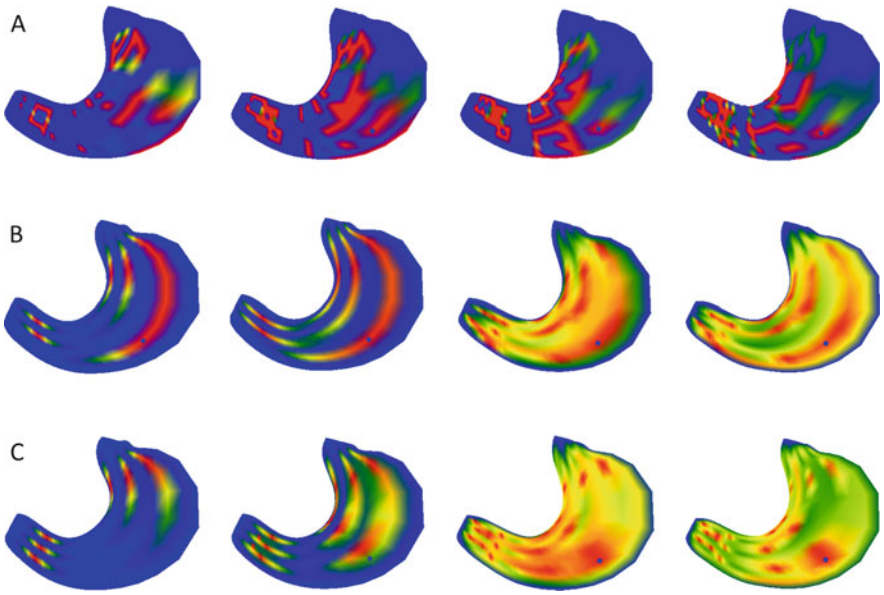

Fig. 13.4 Myoelectrical activity in the MP-ICC/PDGFRα^{+}-MY(IM) network (**a**) and slow wave formation and propagation in longitudinal (**b**) and circumferential (**c**) gastric smooth muscle syncytia: a case of hypoganglionitis and deficient nitrergic neurotransmission

dysmotility. It should be noted though, that nerves and ICC develop independently and that impairment of one does not automatically lead to loss of the other (Huizinga et al. 2001).

Aganglionosis with normal ICC in the human stomach has not been documented in medical literature. There is a single report of neuronal aplasia with unaltered development of ICC in the small intestine of a full-term infant (Huizinga et al. 2001). From a simulation perspective, the absence of Auerbach's plexus with intact/absent ICC-MY(IM) is a trivial setting. In the former case, SIPs display patterns of electromechanical activity defined by the natural dynamics of dispersed ICC, as described earlier (Chap. 11). There are uncoordinated, non-propagating localized contractions of normal strength and duration. Propagating peristaltic waves can only be seen when synchronization in oscillations within the ICC network is achieved. Hypothetically combined neuronal and ICC aplasia is not "compatible" with life. The stomach resembles a soft inert "sac".

The electromechanical activity of the SIP syncytium in the event of uniform myenteric hypoganglionitis with deficient nitrergic neurotransmission and unaffected ICC-MY(IM) is similar to that studied previously (Chap. 10). The sparsely distributed neurons of the MP plexus cannot entrain the ICC-MY(IM) network. The latter displays patchy zones of synchronized oscillations scattered across the surface of the stomach (Fig. 13.4). Non-propagating standing low waves of a maximal amplitude 76 mV and wavelength ~3 cm are formed. Within 2 s these subside in intensity to $V = 48$ mV and eventually disappear.

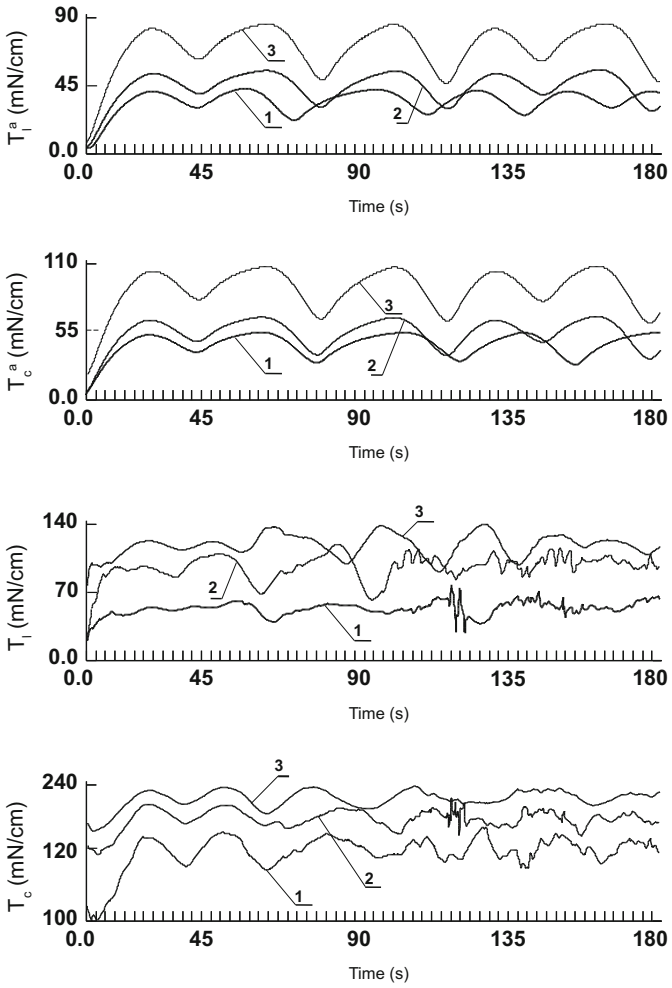

Fig. 13.5 The dynamics of active and total forces $T_l^{(a)}$ in the fundus (1), corpus (2), and antrum (3) of the stomach: a case of myenteric neuropathy

The loss of inhibitory signaling in the SIP/ganglion units and the unopposed conjoint action of ACh and SP result in an increase in the intensity and duration of active forces generated by longitudinal and circumferential smooth muscle (Fig. 13.5). Maxima active forces developed in the fundus, corpus and antrum are: max $T_l^a = 43; 46$ and $88\ (\mathrm{mN/cm})$, and max $T_c^a = 54; 57$ and $109\ (\mathrm{mN/cm})$, respectively. The amplitude of contraction is greatest in the gastric antrum, $\delta T_l^a \simeq \delta T_c^a \simeq 35 \div 40\ \mathrm{mN/cm}$. There is a frequency gradient in contractions highest in the proximal, 0.033 Hz, and lowest, 0.027 Hz, in the distal part of the stomach. The lasting excitatory stimulation leads to the development of tonic

contractions throughout the entire organ. Thus, the dynamics of total force show a sustained tonicity of the longitudinal SM layer and undulations in the circumferential layer in the fundus of the organ where an average $T_l^a = 63$ mN/cm and $T_c^a = 80 \div 100$ mN/cm, is recorded. The intensity of forces increases steadily. For $60 < t < 135$ s it reaches the maximum $T_l = 110$ (140) mN/cm and $T_c = 180$ (240) mN/cm in the body (antrum), corresponding to the time of co-release and action of SP.

At the time of writing, no information was available regarding nicotinic acetylcholine receptors (nAChRs) in Auerbach's plexus in the human stomach. Immunohistochemical, pharmacological and electrophysiological data obtained from animal experiments reveals the receptor localization to somas, dendrites, pre- and postsynaptic terminals of inter- and motor neurons of enteric (intestinal) ganglia (Kirchgessner and Liu 1998; Schneider and Galligan 2000). Functional and clinical evidence strongly suggests that nicotinic receptors mediate the signal transduction, facilatate the release of neurotransmitters and elicit the generation of fEPSPs in the gastrointestinal tract (Pardi et al. 2002; Mandl and Kiss 2007).

Let nAChRs be present mainly on inter- and motor neurons of the MP of the human stomach. Consider the effect of antibodies against nAChRs on motility. The system is stimulated by mechanical (ingestion of food) and external electrical signals (vagal inputs). Under current model assumptions, the neurotransmission by 5-HT, ACh (acting at muscarinic μ2 and μ3 type receptors), SP, NO, VIP, smooth muscle and ICC remain intact.

There is normal sporadic oscillatory and myogenic activity at SIP syncytia and SIP/ganglion units. The block of nicotinic ACh transmission has a profound detrimental effect on the spread of excitation and the sustainability of local reflexes in the myenteric plexus. This becomes inert. As a result, there is weak connectivity and a lack of synchronization in slow wave dynamics and mechanical reactions. Irregular local contractions across the organ are seen with no coordinated peristalsis.

Note: defective nAChRs in the enteric plexus are associated with the megacystic-megacolon-intestinal hypoperistalsis syndrome. This lethal disease is manifested with a largely dilated urinary bladder and functional intestinal obstruction in newborns. Despite the morphological integrity of the MP, no peristaltic movements are detected although there is normal spontaneous myogenic activity (Kubota et al. 1989; De Biasi 2002; Melek et al. 2009).

13.3 Gastroparesis

Gastroparesis is a syndrome of objectively delayed gastric emptying of a liquid or solid meal in the absence of any organic or structural obstruction. In nearly 40% of cases (idiopathic), the predisposing factors for the condition are unknown while the rest are secondary to: long-standing diabetes type 1 or 2 (29%); postsurgical

complications following vagotomy, distal gastrectomy, fundoplication, Roux-en-Y-procedure (13%); neoplastic diseases such as small cell lung cancer, pancreatic cancer, untreated breast cancer; iatrogenic, induced by opiate analgetics (morphine, oxycodone), anticholinergic agents, diabetic (exenatide) and immunosuppressant (cyclosporine), medications (Kashyap and Farrugia 2008; Paine et al. 2013; Camillieri et al. 2013; Tack 2015).

No consensus has yet been reached regarding the pathophysiology of gastroparesis. However, invariable ultrastructural changes in most cell types—neuronal, interstitial, smooth muscle and connective—are found in full thickness biopsies from patients irrespective of idiopathic or secondary gastroparesis. There is a significant reduction in the number of nerve ganglia, calculated as a percentage of the total area, in the corpus (4.76 ± 1.52)% (control) vs. (1.37 ± 0.7)% (deceased) and the antrum (4.86 ± 1.71)% vs. (1.63 ± 0.98)% (Zaráte et al. 2003); a decline in density of neuronal nitric oxide synthase (nNOS)-positive (2.06 ± 0.33% vs. 0.41 ± 0.18% per 2.5 mm^2 of the visual field), SP-positive (0.52 ± 0.06% vs. 0.07 ± 0.01%), and VIP-positive cells (Iwasaki et al. 2006); morphological alterations in nerve structures consistent with myenteric degenerative/inflammatory neuropathy (Badyánszki and Bódi 2012). There is a substantial depletion of both intramuscular and myenteric ICC (147.4 ± 11.4 vs. 66.1 ± 23.3 per 2.5 mm^2 area), with clear indications of cellular dysmorphism, apoptotic changes, mitochodrialopathy, and the complete disruption of gap, desmosome- and synapse-like junctions between ICC, nerves and smooth muscle (Ördög et al. 2009; Faussone-Pellegrini et al. 2011; Bashashati and McCallum 2015). The majority of SMCs show no discernible lesions and gap junctions are intact. However, there are cells which demonstrate morphofunctional changes: swollen mitochondria; disordered arrangement of myofilaments; fibrosis with thin collagen fibrils encasing SMCs; atrophy; an increase in distance between cells; patchy or continuous tenfold thickening of the basal lamina (0.6 vs. 0.06 μm); change in phosphorylation of myosin light chain; a reduction in calmodulin and PKC levels etc (Pasricha et al. 2008; Faussone-Pellegrini et al. 2011). The connective stroma always present with excessive fibrosis and haphazardly dispersed collagen fibrils. In the case of paraneoplastic gastroparesis, there is production of ANNA-1 and anti-nAChR antibodies etc (Pardi et al. 2002; Kashyap and Farrugia 2008).

Combined together, these morphostructural alterations are responsible for the signs and symptoms of dysmotility observed clinically. For instance: the lack of peptodergic and nitrergic neurons along with the deficiency of both ICC-MY and ICC-IM in the antropyloric region in patients with congenital hypertrophic pyloric stenosis, result in a sustained tonic contractility and delayed emptying of the stomach; the production of ANNA-1 and antibodies against nAChRs linked to both idiopathic and paraneoplastic forms of gastroparesis; hypoganglionosis with a significant decrease in ganglion size and the expression of nNOS, along with the total loss of ICC in the corpus and antrum commonly seen in diabetic gastroparesis (Vanderwinden and Rumessen 1999; Vernino et al. 2000; Pardi et al. 2002; Zaráte et al. 2003; Forster et al. 2005; Ördög, 2008; Lin et al. 2010; Badyánszki and Bódi 2012; Breuer 2012; Yarandi and Srinivasan 2014).

Unfortunately, until now no direct reliable electrical or mechanical experimental investigations have been conducted on the gastroparetic tissue. To simulate the gastroparetic stomach, the following properties of the model of the physiological human stomach have been adjusted to fit the experimental data obtained merely from morphological evaluations of biopsy specimens from affected organs, using light and transmission electron microscopy and immunohistochemical staining:

(i) the number of myenteric ganglia and ICC-MY(IM) decreases uniformly across the bioshell by 80%; ICC is a set of randomly dispersed individual cells; the firing rate of ICC is lower than their natural frequencies because of the altered dynamics of the activation/inactivation of transmembrane ion channels, a result of mitochondrialopathy; the MP and ICC-MY(IM) are disengaged; there are some synaptic contacts between SMCs and motor neurons
(ii) the neurotransmission depends entirely on unaltered ACh mechanisms; no non-adrenergic or non-cholinergic inhibitory nerves are present
(iii) the electrical conductivity in longitudinal and circumferential SM syncytia is reduced; the membrane capacitance, geometrical characteristics and specific resistance of somas, axons, dendrites, nerve-terminals, synaptic structures, and SMCs are altered
(iv) $T^p(\lambda_l, \lambda_c)$ change reflecting the stiffening of tissue; the ability to generate active forces by SMCs, $T^a_{l,c}$, is markedly decreased.

Under the conditions specified which relate to a severe case of gastroparesis, the fasting stomach displays sporadic discharges of ICC in different regions. Nuclei of high amplitude oscillatory potentials of an amplitude 78 mV remain continuosly disconnected. The pattern of electrical activity is consistent with gastric bradyarrhythmia. No synchronization of electrical firing activity in the morphologically disrupted MP- ICC-MY(IM)-SIP is ever achieved. The intrinsic control system of the stomach stays inoperable.

There is a weak accommodation response of the bioshell to the rise in intraluminal pressure, $p(\breve{V}) = 8$ kPa, ("fed" state). The organ retains the configuration homeomorphic to the initial shape. The stomach experiences biaxial strain states in all anatomical zones with average strain ratios: $\lambda_l \sim 1.06$, $\lambda_c \sim 1.1$. The level of stretching in the circumferential direction is sufficient to trigger unitary action potentials, $V^e = 65$ mV, at mechanoreceptors of the sensory neurons. These propagate towards the soma of the motor neuron where upon induction of cholinergic transduction mechanisms and the production of fEPSP of amplitude 87.1 mV, spikes, $V^s_m = 90$ mV and $\nu = 12.2$ Hz, are generated. The process of electrochemical coupling at the motor neuron-SMC synapse involving muscarinic receptors is as described above. Non-propagating localized slow waves of low amplitude, $V = 15$–18 mV and of frequency defined by the natural firing rate of ICC, are generated in the SIP syncytium. No spikes can be seen on the crests of slow waves.

There are high intensity total membrane forces, $T_l \simeq 121$ (210) mN/cm, $T_c \simeq 196$ (264) mN/cm in the body (antrum) compared to the norm, mainly due to

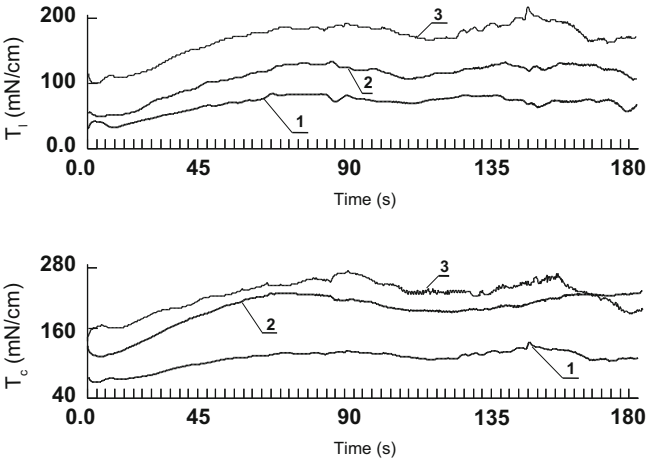

Fig. 13.6 The dynamics of total forces T_l and T_c in the fundus (1), corpus (2), and antrum (3) of the stomach: a case of gastroparesis

the passive component, $T^p_{l,c}$ (Fig. 13.6). Smooth muscle layers generate tonic-type contractions. The strength of active forces is small, reaching the maximum of $T^a_l = 33.7\ (67)$ mN/cm, $T^a_c = 43.1\ (95.3)$ mN/cm in the body (antrum). No coordinated peristaltic activity can be seen in the gastroparetic stomach.

The characteristic feature of paraneoplastic gastroparesis, in addition to those described above, is the production of ANNA-1 and anti-nAChRs antibodies. To reproduce the condition requires a modification in the model assumption (ii): the neurotransmission becomes dependent entirely on ACh and muscarinic μ_2, μ_3—type receptors located primarily on SM. This results in a complete failure by myenteric ganglia to form local sensory-motor reflexes and to communicate excitation within the hypoganglionic plexus. The stomach exhibits dysrhythmic ICC activity, an absence of slow waves and the loss of tone with indiscriminate SM twitches.

13.4 Functional Dyspepsia

Functional dyspepsia (FD) is a heterogenous, ill defined medical condition that encompasses two syndromes: epigastric pain and postprandial distress with no obvious organic explanations (Talley and Ford 2015; Talley 2016). The global prevalence of FD varies between 5 and 11% and, because of its negative affect on life style and productivity in the workplace, it bears considerable financial implications, approximately US$20 billion annually in the US alone.

The aetiology of FD is non-conclusive and is derived from the results of cohort studies since no reliable models or diagnostic modalities exist to evaluate

accurately conceivable causes. Most commonly implicated hypothesized factors are: infection (*Helicobacter pylori*), changes in the intestinal microbiome, inflammation, genetic predisposition, disturbances in gut hormone balance, psychosocial stress, iatrogenic.

The pathophysiology of the condition is also obscure. Experimental data obtained mainly from animal studies, indicate: a possible down-regulation of miRNA-1 and miRNA-133 that silence genes involved in SMC proliferation, apoptosis and differentiation; the myenteric nerves and SMCs infringement with eosinophils, macrophages, mast cells, and intraepithelial lymphocytes, an enhanced number of T—cells, and the increase in cytokine levels (cachexin, interleukin-10 and -1β); gene modifications—Gnb3, serotonin transporter protein, T-allele of nNOS, and TRPV1 related to acid sensitivity and tetrodotoxin-resistant sodium channel; overproduction of cholecystokinin and ghrelin (Holtmann et al. 2004; Tahara et al. 2010; Saito et al. 2011; Futagami et al. 2011; Sarnelli et al. 2013; Park et al. 2014); abnormal food distribution and hypersensitivity to distension (Tack et al. 2004; Di Stefano et al. 2005; Bisschops and Tack 2007). Taken together, these findings can be condensed into the following pathogenic categories: inflammatory myenteric neuropathy with possible Cajalopathy, (although at the time of writing no experimental or clinical evidence is available to prove or reject the notion), myopathy, affected nerve signal transduction, and channelopathy. Additionally, since there is a frequent overlap in symptoms and clinical presentations of FD with other maladies such as gastroparesis, gastric dysrhythmias, gastroesophageal reflux disease and irritable bowel syndrome among others, it has been suggested that these may share the same pathophysiological mechanisms.

The palette of motility abnormalities observed in patients with FD include solitary or combined signs of delayed, normal or rapid gastric emptying of solids; antral hypomotility; fundic disaccommodation: hypersensitivity to distension. However, some patients have none of these abnormalities!

The biomechanics of FD cannot be analyzed with precision at this stage due to the lack of required information concerning the degree of morphostructural tissue damage and altered electromechanical properties. However, extrapolations can be made based on the results of modeling investigations of the human stomach with affected gastric rhythms, myenteric neuropathy and gastroparesis. These are left to the diligent reader as an exercise.

References

Badyánszki M, Bódi N (2012) Diabetes-related alterations in the enteric nervous system and its microenvironment. World J Diabetes 3(5):80–93

Bashashati M, McCallum RW (2015) Is interstitial cells of Cajalopathy present in gastroparesis? J Neurogastroenterol Motil 21(4):486–493

Bisschops R, Tack J (2007) Dysaccommodation of the stomach: therapeutic nirvana? Neurogastroenterol Motil 19:85–93

Breuer C (2012) The role of interstitial cells of Cajal in gastrointestinal motility disorders – What the gastroenterologist has to know. In: Smith AC (ed) Constipation: causes, diagnosis and treatment. InTech, China

Camillieri M, Parkman HP, Shafi MA, Abell T, Gerson L (2013) Clinical guideline: management of gastroparesis. Am J Gastroenterol 108:18–37

Coleski R, Hasler WL (2009) Coupling and propagation of normal and dysrhythmic gastric slow waves during acute hyperglycaemia in healthy human. Neurogastroenterol Motil 21:492–4e2

De Biasi M (2002) Nicotinic mechanisms in the autonomic control of organ systems. J Neurobiol 53(4):568–579

De Giorgio R, Guerrini S, Barbara G, Stanghellini V, De Ponti F, Corinaldesi R, Moses PL, Sharkey K, Mawe GM (2004) Inflammatory neuropathies of the enteric nervous system. Gastroenterology 126(7):1872–1883

Di Nardo G, Blandizzi C, Volta U, Colucci R, Stanghellini V, Barbara G, Del Tacca M, Tonini M, Corinaldesi R, De Giorgio R (2008) Review article: molecular, pathological and therapeutic features of human enteric neuropathies. Aliment Pharmacol Ther 28:25–42

Di Stefano M, Miceli E, Mazzocchi S, Tana P, Corazza GR (2005) The role of gastric accommodation in the pathophysiology of functional dyspepsia. Eur Rev Med Pharmacol Sci 9(1):23–28

Farrugia G (2008) Interstitial cells of Cajal in health and disease. Neurogastroenterol Motil 20 (Suppl. 1):54–63

Faussone-Pellegrini GM, Pasricha PJ, Bernard CE, Lurken MS, Smyrk TC, Parkman HP, Abell TL, Snape WJ, Hasler WL, Ünalp-Arida A, Nguyen L, Koch KL, Calles J, Lee L, Tonascia J, Hamilton FA, Farrugia G (2011) Ultrastructural differences between diabetic and idiopathic gastroparesis. J Cell Mol Med 16(7):1573–1581

Forster J, Damjanov I, Lin Z, Sarosiek I, Wetzel P, McCallum RW (2005) Absence of the interstitial cells of Cajal in patients with gastroparesis and correlation with clinical findings. J Gastrointest Surg 9:102–108

Futagami S, Shimpuku M, Yin Y, Shindo T, Kodaka Y, Nagoya H, Nakazawa S, Fujimoto M, Izumi N, Ohishi N, Kawagoe T, Horie A, Iwakiri K, Sakamoto C (2011) Pathophysiology of functional dyspepsia. J Nip Med Sch 78(5):280–285

Gibbons SJ, De Giorgio R, Pellegrini MSF, Garrity-Park MM, Miller SM, Schmalz PF, Young-Fadok TM, Larson DW, Dozois EJ, Camillieri M, Stanghellini V, Szurszewski JH, Farrugia G (2009) Apoptotic cell death of human interstitial cells of Cajal. Neurogastroenterol Motil 21 (1):85–93

Gomez-Pinilla PJ, Gibbons SJ, Sarr MG, Kendrick ML, Shen KR, Cima RR, Dozois EJ, Larson DW, Ordog T, Pozo MJ, Farrugia G (2011) Changes in interstitial cells of Cajal with age in human stomach and colon. Neurogastroenterol Motil 23(1):36–44

Hasler WL, Soudah HC, Dulai G, Owyang C (1995) Mediation of hyperglycaemia-evoked gastric slow wave dysrhythmias by endogenous prostaglandins. Gastroenterology 108:727–736

Holtmann G, Siffert W, Haag S, Mueller N, Langkafel M, Senf W, Zotz R, Talley NJ (2004) G-protein beta 3 subunit 825 CC genotype is associated with unexplained (functional) dyspepsia. Gastroenterology 126:971–979

Huizinga JD, Berezin I, Sircar K, Hewlett B, Donnelly G, Bercik P, Ross C, Algoufi T, Fitzgerald P, Der T, Riddell RH, Collins SM, Jacobson K (2001) Development of interstitial cells of Cajal in a full-term infant without an enteric nervous system. Gastroenterology 120 (2):561–567

Huizinga JD, Zarate N, Farrugia G (2009) Physiology, injury and recovery of interstitial cells of Cajal: basic and clinical science. Gastroenterology 137(5):1548–1556

Iwasaki H, Kajimura M, Osawa S, Kanaoka S, Furuta T, Ikuma M, Hishida A (2006) A deficiency of gastric interstitial cells of Cajal accompanied by decreased expression of neuronal nitric oxide synthase and substance P in patients with type 2 diabetes mellitus. J Gastroenterol 41:1076–1087

Kashyap P, Farrugia G (2008) Enteric autoantibodies and gut motility. Gastroenterol Clin North Am 37(2):397–410

Kirchgessner AL, Liu MT (1998) Immunohistochemical localization of nicotinic acetylcholine receptors in the guinea pig bowel and pancreas. J Comp Neurol 390:497–514
Knowles CH, Lindberg G, Panza E, De Giorgio R (2013) New perspectives in the diagnosis and management of enteric neuropathies. Nat Rev Gastroenterol Hepatol 10:206–218
Kubota M, Ikeda K, Ito Y (1989) Autonomic innervation of the intestine from a baby with megacystic mictocolon intestinal hypoperistalsis syndrome: II. Electrophysiological study. J Pediatr Surg 24:1267–1270
Lefebvre RA (2002) Pharmacological characterization of the nitrergic innervation of the stomach. Verh K Acad Geneeskd Belg 64(3):151–166
Lin Z, Sarosiek I, Forster J, Damjanov I, Hou Q, McCallum RW (2010) Association of the status of interstitial cells of Cajal and electrogastrogram parameters, gastric emptying and symptoms in patients with gastroparesis. Neurogastroenterol Motil 22:56–e10
Mandl P, Kiss JP (2007) Role of presynaptic nicotinic acetylcholine receptors in the regulation of gastrointestinal motility. Brain Res Bull 72:194–200
Manetti M, Milia AF, Benelli G, Messerini L, Matucci-Cerenic M, Ibba-Manneschi L (2010) The gastric wall in systemic sclerosis patients: a morphological study. Ital J Anat Embryol 115 (1/2):115–121
Melek M, Edirne Y, Beger B, Cetin M (2009) Megacystis-micro-colon-intestinal hypoperistalsis syndrome: a case report. Gastroenterol Res Pract. doi:10.1155/2009/282753
O'Grady G, Abell T (2015) Gastric arrhythmias in gastroparesis: low and high resolution mapping of gastric electrical activity. Gastroenterol Clin North Am 44(1):169–184
Ohlsson B, Janciauskiene S (2007) New insights into the understanding of gastrointestinal dysmotility. Drug Target Insights 2:229–237
Ördög T (2008) Interstitial cells of Cajal in diabetic gastroenteropathy. Neurogastroenterol Motil 20:8–18
Ördög T, Hayashi Y, Gibbons SJ (2009) Cellular pathogenesis of diabetic gastroenteropathy. Minerva Gastroenterol Dietol 55(3):315–343
Owyang C, Hasler W (2002) Physiology and pathophysiology of interstitial cells of Cajal: from bench to bedside VI. Pathogenesis and therapeutic approaches to human gastric dysrhythmias. Am J Physiol Gastrointest Liver Physiol 283:G8–G15
Paine P, McLaughlin J, Lal S (2013) Review article: the assessment and management of chronic severe gastrointestinal dysmotility in adults. Aliment Pharmacol Ther 38:1209–1229
Pardi DS, Miller SM, Miller DL, Lawrence JB, Szurszewski JH, Lennon V, Farrugia G (2002) Paraneoplastic dysmotility: loss of interstitial cells of Cajal. Am J Gastroenterol 97 (7):1828–1833
Park JM, Baeg MK, Lim CH, Cho YK, Choi MG (2014) Nitric oxide synthase gene polymorphisms in functional dyspepsia. Dig Dis Sci 59:72–77
Pasricha P, Pehlivanov ND, Gomez G, Vittal H, Lurken MS, Farrugia G (2008) Changes in the gastric enteric nervous system and muscle: a case report on two patients with diabetic gastroparesis. BMC Gastroenterol 8:21–29
Qi H-B, Luo J-Y, Zhu Y-L, Wang X-Q (2002) Gastric myoelectrical activity and gastric emptying in diabetic patients with dyspeptic symptoms. World J Gatroenterol 8(1):180–182
Saito Y, Suzuki H, Tsugawa H, Suzuki S, Matsuzaki J, Hirata K, Hibi T (2011) Dysfunctional gastric emptying with down-regulation of muscle specific MicroRNAs in helicobacter pylori-infected mice. Gastroenterology 129(1):189–198
Sarnelli G, D'Alessandro A, Pesce M, Palumbo I, Cuomo R (2013) Genetic contribution to motility disorders of the upper gastrointestinal tract. World J Gastrointest Pathophys 4:65–73
Schneider DA, Galligan JJ (2000) Presynaptic nicotinic acetylcholine receptors in the myenteric plexus of guinea pig intestine. Am J Physiol Gastrointest Liver Physiol 279:G528–G535
Stoddard CJ, Smallwood RH, Duthie HL (1981) Electrical arrhythmias in the human stomach. Gut 22:705–712
Tack J (2015) Gastroparesis. Curr Opin Gastroenterol 31(6):499–505

Tack J, Bisschops R, Sarnelli G (2004) Pathophysiology and treatment of functional dyspepsia. Gastroenterology 127:1239–1255

Tahara T, Shibata T, Nakamura M, Yamashita H, Yoshioka D, Hirata I, Arisawa T (2010) Homozygous TRPV1 315C influences the susceptibility to functional dyspepsia. J Clin Gastroenterol 44:e1–e7

Talamonti L, Li Q, Beyak M (2006) Sensory motor abnormalities in severe gut dysmotility: role of anti-HuD neuronal antibodies. Neurogastroenterol Motil 18:669–715

Talley N (2016) Functional dyspepsia: new insights into pathogenesis and therapy. Korean J Med 31(3):444–456

Talley NJ, Ford AC (2015) Functional dyspepsia. N Engl J Med 373:1853–1863

Vanderwinden JM, Rumessen JJ (1999) Interstitial cells of Cajal in human gut and gastrointestinal disease. Microsc Res Tech 47:344–360

Vernino S, Low PA, Fealey RD, Steward JD, Farrugia G, Lennon VA (2000) Autoantibodies to ganglionic acetylcholine receptors in autoimmune neuropathies. N Engl J Med 343 (12):847–855

Yarandi SS, Srinivasan S (2014) Diabetic gastrointestinal motility disorders and the role of enteric nervous system: Current status and future directions. Neurogastroenterol Motil 26(5):611–624

Zaráte N, Mearin F, Wang X-Y, Hewlett B, Huizinga JD, Malagelada J-R (2003) Severe idiopathic gastroparesis due to neuronal and interstitial cells of Cajal degeneration: pathological findings and management. Gut 52:966–970

Chapter 14
Prokinetics in Treatment of Gastric Motility Disorders

Each problem that I solved became a rule which served afterwards to solve other problems.

Rene Descartes

14.1 Current Principles

Congenital abnormalities, postsurgical and medical conditions such as gastroparesis, gastric arrhythmias, myenteric neuropathies, functional dyspepsia and Parkinson's disease to name a few, have the common manifestation of altered gastric movements in the form of either atony, hypo- or hypermotility. These are a result of pathological changes in the anatomical structure of the organ, the central and myenteric nervous system, interstitial cells of Cajal and the coordinated interplay between them. For example, the enhanced apoptosis of the enteric neurons and ICC, the decrease in NO synthase protein expression, the damage to the vagus nerve, and marked stromal fibrosis have been identified in the pathogenesis of gastroparesis (Grover et al. 2011; Ördög et al. 2009; Zaráte et al. 2003; Chen et al. 2003; Gibbons et al. 2009; Lin et al. 2010; Badyánszki and Bódi 2012; Harberson et al. 2010; Kim et al. 2012; Stevens et al. 2013); truncal and/or selective vagotomy, antrectomy, pyloroplasty and Roux-en-Y reconstruction, as well as partial gastrectomy (Bilroth I and II procedures) have been attributed to the development of postsurgical dysmotility and dumping syndrome (Dong et al. 2006); degenerative dysplasia and paraneoplastic syndromes associated with inflammatory neuropathic abnormalities have been shown to play a role in hypomotility (Di Nardo et al. 2008; De Giorgio et al. 2000; Yarandi and Srinivasan 2014); cholinergic downregulation of ICC-IM and irregular initiation, aberrant conduction, and low amplitude electrical activity in SIP could contribute to gastric arrhythmogenesis (O'Grady and Abell 2015); peptic ulcer and indomethacin may lead to hypermotility (Liebermann-Meffert et al. 1982; Takeuchi et al. 1990).

The current mainstay prokinetic therapy of gastrointestinal motility disorders relies on the use of metoclopramide, domperidone, erythromycin, azithromycin and clarithromycin. Symptomatic treatment for associated hyperacidity, nausea, vomiting and pain is provided by proton pump inhibitors (omeprazole,

R.N. Miftahof, *Biomechanics of the Human Stomach*,
DOI 10.1007/978-3-319-59677-8_14

lansoprazole), phenothiazines (thiethyperazine, prochlorperazine), antihistamines (promethazine), tricyclic antidepressants (amitriptyline, nortriptiline), opioids and their derivatives (tramadol, methadone, gabapentin). Endoscopic intrapyloric injections of botulinum toxin, an acetylcholine secretion interrupter, and administration of sildenafil, a phosphodiesterase 5 inhibitor, have demonstrated some effectiveness in the treatment of pylorospasm and impaired gastric accommodation (Sarnelli et al. 2004; Patil et al. 2005; Kindt and Tack 2006; Cho et al. 2006). The implantation of electrical gastric stimulation devices has shown a limited success clinically.

Although the existing drugs offer some improvement in the management of symptoms, their overall efficacy, tolerability and toxicity are still less than optimal. Several non-selective serotonin and dopamine receptor agonists/antagonists such as cisapride, tegaserod, renzapride, itopride, clebopride and mosapride have been developed, and are currently available on the market to treat abnormal gastrointestinal movements. They have been approved for use in a number of European and Asian countries, but not in the US because of cardiac safety and other potential life threatening clinical outcomes (Tack et al. 2012). Potential novel formulations such as selective non-macrolide motilin receptor agonists, (camicinal, raqualia and cempra, 5-HT_4 agonists), velusetrag, ghrelin agonist—relamorelin, and non-selective motilin/ghrelin receptor agonist—RQ-00201894, are currently under different stages of development and investigation (Chapman et al. 2016; Broad et al. 2016; Camilleri 2016). Therefore, these drugs and other "promising" experimental compounds are not given full attention in this book.

14.2 Bensamides

Despite serious adverse side effects including akathisia, acute dystonia, tardive dyskinesia and supraventricular tachycardia, metoclopramide is the only US Federal Drug Administration-approved medication for patients with gastroparesis (Acosta and Camilleri 2015; Camilleri 2016). It is classified as a dopamine (D_2), serotonin 5-HT_3 receptor antagonist and 5HT_4 receptor agonist. Transmembrane heptahelical 5-HT_4 receptors are a part of the G-protein coupled receptor family. These are positively linked to the stimulatory G_s protein and cAMP-PKA-dependent pathway. The receptors are expressed in SMCs (Streutker et al. 2006). The resultant effects of their activation are: an increase in Na^+, BK_{Ca}, Ca^{2+} and a decrease in K^+ ion channel permeability; enhanced neuronal ACh release; strengthened contractility. Multiple splice variants: 5-$HT_{4(a)}$, 5-$HT_{4(b)}$, h5-$HT_{4(c)}$, h5-$HT_{4(d)}$, h5-$HT_{4(g)}$, h5-$HT_{4(i)}$ and 5$HT_{4(n)}$ have been identified in the central nervous system in humans. Observations have suggested their cell, tissue and disease specific expression in the gastroparetic human stomach and duodenum (van Lelyveld et al. 2008).

5-HT_3 receptors are a transmembrane assembly of homo- and heteropentameric (A-E) subunits surrounding a water-filled cation selective channel (Lummis 2012).

Located pre- and postsynaptically on myenteric inter- and motor neurons, these modulate neurotransmission and thus contribute to signal transduction and motility. It is mainly the homomeric, 5-HT_{3A}, and heteromeric, 5-HT_{3AB} receptors mediate rapidly activating and desensitizing inward Na^+, K^+ and Ca^{2+} ion currents in the human stomach (Wouters et al. 2007). The role of other subunits is still unknown.

In vitro investigations of metoclopramide on isolated longitudinal and circumferential specimens from the human stomach have shown convincingly that the concurrent ability of the drug to block D_2 and 5-HT_3 receptors does not facilitate cholinergic neurotransmission induced by subtle stimulation of 5-HT_4 receptors (Broad et al. 2014). Furthermore, domperidone acts mainly within the brainstem area postrema and does not support antagonism of endogenous dopamine in neuronally-mediated contractions in the human stomach (Sanger and Andrews 2006; De Maeyer et al. 2008; Sanger 2009). Following this argument in order to analyze the effect of metoclopramide on motility of the human stomach per se in gastroparesis, functional dyspepsia and myenteric neuropathy, the action of the drug is assumed predominantly through the 5-HT_4 receptors.

Let the model conditions of gastroparesis be satisfied as stated previously (Chap. 13). It is noteworthy that structural damages are incurred in the myenteric nervous plexus. Although motor neurons are capable of producing and releasing ACh, their response to excitation of somatic and presynaptic axonal 5-HT_4 receptors is sluggish due to alterations in expression of the latter. By contrast, although entangled in the network of excessive collagen fibers, SMCs sustain their functionality and react to direct 5-HT_4 receptor stimulation. Viable ICC-MY(IM) and motor neurons discharge at the same frequencies, $\nu = \nu_{\mathrm{m}} = 0.12$ Hz, with a phase shift (time-disintegrated).

Despite morphological disruptions, the antral SIP/ganglion unit shows low amplitude slow waves, $V = 23.2$ mV, and spike, $V = 5.6$ mV, electrical activity. Desynchronized discharges of ICC–IM and motor neurons, and the activation of cholinergic neurotransmission (wherein 78.2 mM of neurotransmitter is released from the vesicular stores) are observed. Only 5.38 mM reaches the SM postsynaptic membrane and 0.11 mM of ACh binds to muscarinic μ_2 and μ_3 receptors. The ACh-receptor complex is formed, and induces an intracellulalr second messenger system with activation of SM transmembrane ion channels and contractile proteins. L-type Ca^{2+} channels display irregular patterns of activity (Fig. 14.1). The intensity of $\tilde{I}^{s}_{Ca}$ is unstable and varies from -0.6 to -0.08 nA. The dynamics of T-type Ca^{2+} channel is brisk with rapid opening and closure. The inward $\tilde{I}^{f}_{Ca}$ has the maximum strength of $-0.06 \div -0.15$ nA. The outward Ca^{2+}—activated K^+ and voltage dependent K^+ ion current are of intensities: $\tilde{I}_{Ca-K} = 0.45 \div 1.33$ nA and $\tilde{I}_K = 0 \div 0.77$ nA. The alternating chloride current relates to the variations of the membrane potential V, changing its direction from an inward $\tilde{I}_{Cl} = -0.66$ nA to an outward max $\tilde{I}_{Cl} = 0.21$ nA. These trigger action potentials on the crests of slow waves of variable amplitude, $V = 23.2 \div 27.1$ mV, and duration. Such behavior is consistent with tachyarrhythmia. As a result, uneven contractions of the strength, $T^a = 5.5$ mN/cm are generated. The significant increase in the total force,

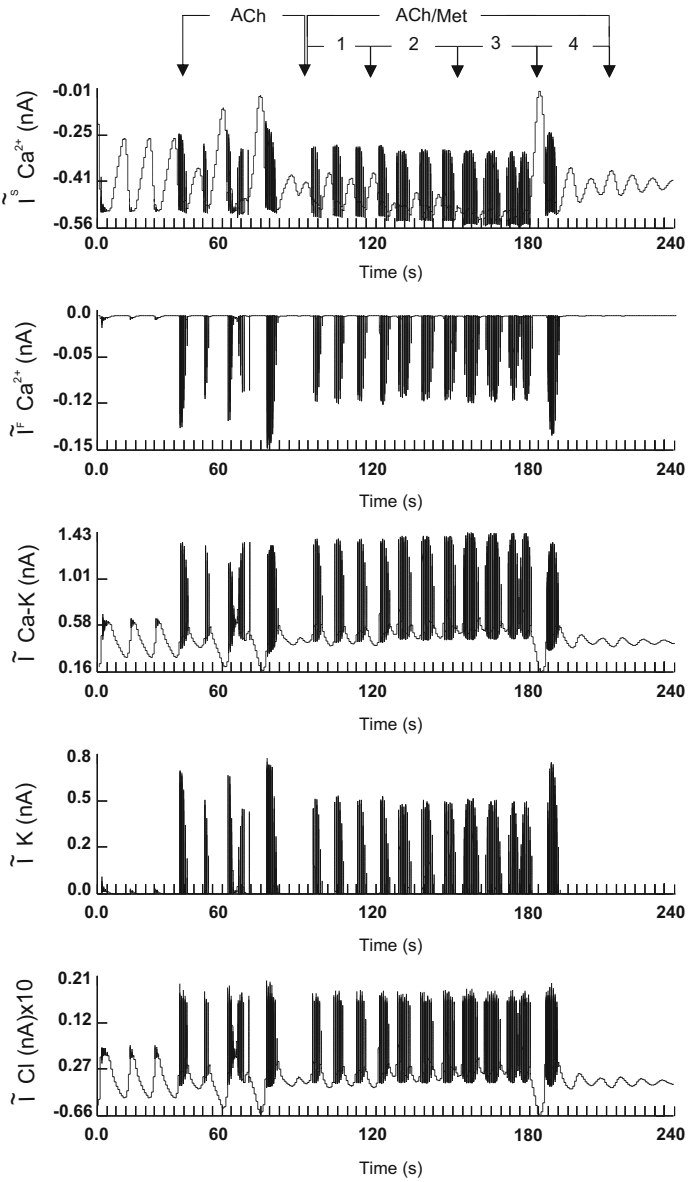

Fig. 14.1 The dynamics of transmembrane ion channels and the total force in antral gastroparetic SIP after treatment with metoclopramide at increasing doses (1 through 4)

$\max T = 26$ mN/cm is mainly due to the presence of collagen fibres which stiffen the biomaterial.

The effect of metoclopramide on the myoelectrical activity of the SIP/ganglion unit is dose-dependent. Acting conjointly with endogenous ACh, the drug: reduces the amplitude of $\tilde{I}^{s}_{Ca}$ and $\tilde{I}^{f}_{Ca}$; intensifies $\tilde{I}_{Ca-K}$ and decreases $\tilde{I}_{K}, \tilde{I}_{Cl}$; depolarizes the

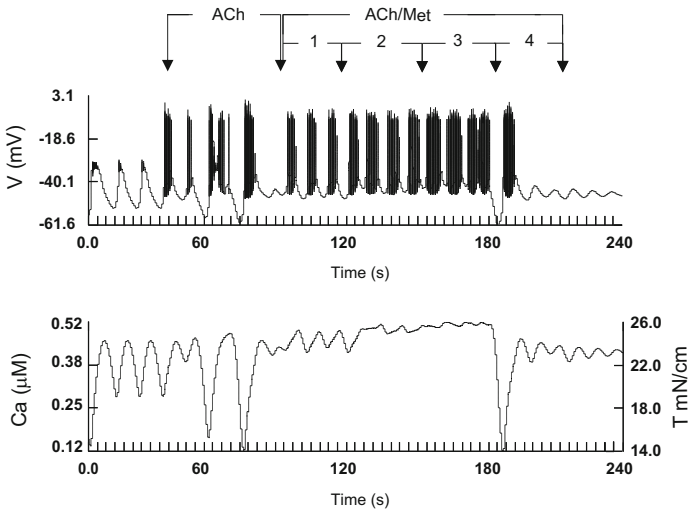

Fig. 14.1 (continued)

resting membrane potential of SMCs, $V^r = 50.2$ mV; decreases the amplitude, $V \sim 10 \div 15$ mV, restores and stabilizes the rhythmicity of slow waves; induces phasic bursting of spikes, $V = 25$ mV, at a constant frequency of 2.5 Hz. At low concentrations metoclopramide initiates phasic contractions, at moderate concentrations tonic-type contractions are produced and at high concentrations it ceases myoelectrical and phasic contractile activity.

The reaction of the SIP/ganglion unit to the drug changes if its morphofunctional integrity is preserved, along with the ability of the motor neuron to respond directly to the stimulation of somatic and presynaptic nerve-terminal 5-HT_4 receptors. Assume that ICC-MY(IM) and the motor neuron are frequency and phase disengaged, i.e., these fire at a frequency of $\nu = 0.096$ Hz (normal value of ν for the antrum: 0.12–0.13 Hz) and $\nu_m = 0.12$ Hz, respectively.

Metoclopramide, acting specifically at neuronal 5-HT_4 receptors, increases twofold the frequency of discharges by the motor neuron, $\nu_{mn} = 0.2$ Hz. This produces action potentials of $V_m^s = 96$ mV at a frequency 12.2 Hz. The motor neuron entrains ICC and synchronizes the oscillatory myoelectrical activity of the unit (Fig. 14.2). Compared with the previous case, a larger amount of free acetylcholine is released, $ACh_f = 83.3$ mM, and (ACh-R) = 0.16 mM is formed. As a result, regular rhythmic slow waves of amplitude $V = 20$ mV and spikes, $V \sim 54$ mV, at a frequency of 2.8 Hz are generated. Smooth muscle produces strong regular phasic contractions. The recorded amplitude of total force is 12.27 mN/cm with $\max T \simeq 20$ mN/cm.

The following concomitant stimulation of 5-HT_4 receptors on SM at a low dose sustains phasic contractility with a positive effect on the strength, $\max T = 22$ mN/cm. The qualitative and quantitative effects of metoclopramide on myoelectrical activity of SIP are similar to those described above. At high concentrations the drug changes

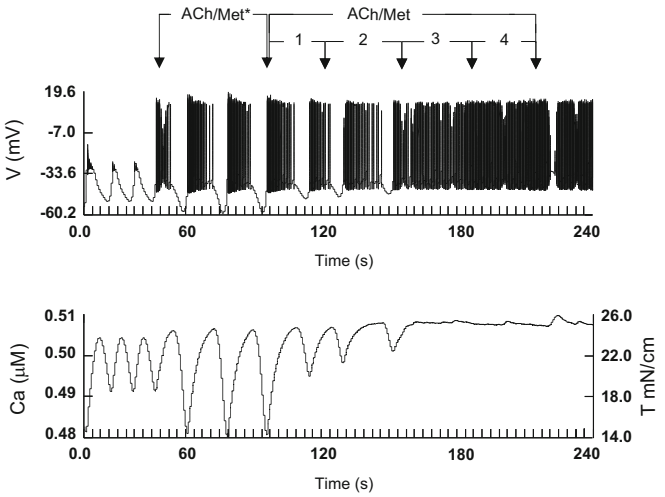

Fig. 14.2 Electromechanical activity of the antral SIP/ganglion unit after the addition of of metoclopramide. Notations are as in Fig. 14.1

the pattern of spiking from phasic bursting to beating with $V = 46.5$ mV, $\nu = 3.58$ Hz, and ceases regular phasic contractions. SM develops a long-lasting contraction of $\max T = 26$ mN/cm.

The results of numerical simulations demonstrate that, in the case of structural disarrangement within and between the MP and ICC network, metoclopramide can reinstate focally normal patterns of myoelectrical and mechanical activity at discrete SIP/ganglia units. The distribution of multiple foci along a "chain" of disconnected ganglia indicates that, despite close proximity, the foci do not form a continuous front (Fig. 14.3). Metoclopramide does not organize and sustain a coordinated propagation of electromechanical waves in the organ. The integrity and functionality of the myenteric nervous plexus is essential in achieving the desirable pharmacological effect. Only then does the drug synchronize discharges of inter- and motor neurons, entrain firing of detached ICC, and restores the rhythmicity of occurrence and propagation of slow waves and phasic (propulsive) contractions (Fig. 14.4).

14.3 Dihydroquinoline

Velusetrag, a selective 5-HT_4 receptor agonist initially designed for treatment of chronic idiopathic constipation, has demonstrated a potential to accelerate gastric motility in patients with both idiopathic and diabetic gastroparesis. At the time of writing, the drug, still being an investigational medicine, has been given fast track designation by FDA. Based on the results of the numerical simulations of

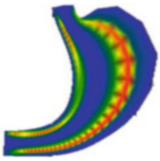

Fig. 14.3 A 'chain' of disconnected loci of myoelectrical activity in the gastroparetic stomach after treatment with metoclopramide

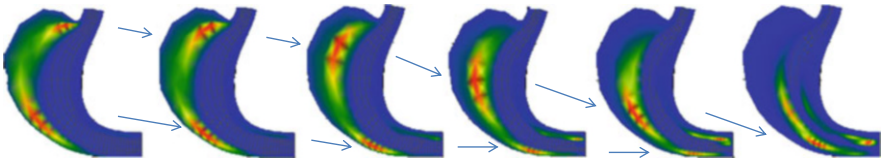

Fig. 14.4 The restoration of slow wave rhythmicity by metoclopramide in the gastroparetic stomach: a case of intact myenteric nervous plexus

metoclopramide, it could be projected that velusetrag may improve symptoms of gastroparesis by regulating its myoelectrical and contractile activity at the organ level in a selective group of patients only with pathological morphofunctional changes at the MP, ICC and SM as discussed above. It should be noted though, that in spite of qualitative similarities there are quantitative differences in biomechanical responses to velusetrag and metoclopramide because of their pharmacokinetic properties.

14.4 Acetylcholinesterase Inhibitors

Itopride hydrochloride is prescribed to treat nausea, diabetic gastroparesis and functional dyspepsia in Japan and Asia, but is not licensed in the USA. Despite a good safety profile, the drug has failed in phase III clinical studies. The pharmacological mechanism of itopride is attributed to the combined ability to block D_2 receptors and to inhibit the anticholinesterase enzyme. Assuming the dopaminergic paradigm, (pharmacological effect achieved through D_2 receptor antagonism at the brainstem area), itopride's action at the level of the stomach can be viewed as an AChE inhibitor along with other drugs such as neostigmine, pyridostigmine and acotiamide. These have been satisfactory in the treatment of gastroparesis associated with N-type Ca^{2+} channel and nAChR antibodies, and postprandial distress syndrome (Pasha et al. 2006; Talley and Ford 2015; Talley 2016).

Let's define the spectrum of medical conditions and analyze the potential efficacy of AChE inhibitors to treat them. Randomized, placebo-controlled studies of itopride have demonstrated no significant acceleration or modification of gastric emptying and motor patterns in healthy volunteers (Choung et al. 2007). These outcomes, when no abnormalities in the MP– ICC–MY(IM)–SM system

are present, seem obvious. The addition of AChE inhibitors leads to an expected rise in the amount of available ACh in the cleft and postsynaptically, $ACh_c = 5.42$ mM, (ACh-R) = 0.124 mM, regardless of a slight increase in amplitude of fEPSPs ($V^{+}_{syn} = 89.1$ mV). There is no change in the neuronal firing pattern and most importantly, the dynamics of the spread of the wave of excitation within the intact MP is not altered (Miftahof et al. 2009). The response of the SIP/ganglion unit to itopride with normal multiple neurotransmission involving ACh, SP, NO, VIP, and 5-HT is as described above (Chap. 10).

The failure of itopride to improve symptoms of gastroparesis in patients with longstanding diabetes mellitus is due to the severity of pathological damages in morphostructural elements of the organ (Stevens et al. 2008). It can be envisioned, retrospectively, that random scattered foci of discoordinated electromechanical activity and low strength non-propagating contractions are produced. However, these recordings have never been taken at the time of investigations.

It could be proposed that AChE inhibitors should be reserved to treat gastroparesis with preserved functional integrity, signal transduction and unaltered nervous inhibitory mechanisms in the MP–ICC–MY(IM)–SM complex, which correspond to an early light to mild stage of the disease and functional dyspepsia. However, even in this case only a selected group of patients could benefit from treatment, in particular, those who meet the strict criteria stated above. Thus, patients with the increased production of ghrelin as a pathophysiological basis of functional dyspepsia, commonly present with a tonically contracted stomach, wherein the application of AChE inhibitors will only worsen the condition (Venkova and Greenwood-van Meerveld 2008; Miftahof et al. 2009). It should be stressed at this point that these speculations are based entirely on the analysis of the effects of drugs on the "isolated" organ where no extrinsic vagal control is included. This may change the perspective of the approach.

14.5 Botulinum Toxin

Botulinum toxin (BTx) blocks the sites for Ca^{2+} ion binding on presynaptic vesicles and as such prevents the release of ACh into the synaptic cleft. From previous discussions it becomes obvious that a local intragastric injection of BTx will have a detrimental effect on motility of the organ in patients with severe gastroparesis. However, it may have a positive effect only in cases when at least one or, preferably, two excitatory signal transduction mechanisms involving SP and/or 5-HT are sustained. Relaxation and opening of the pyloric sphincter plays a pivotal role in the biomechanics of gastric emptying. Even disorganized, randomly occurring contractions of sufficient strength may initiate and support movements of the content to the duodenum. The accurate evaluation of propulsive activity requires a significant modification in the model with the addition of the second phase (gastric content) and modeling of wall-content interactions. This is beyond the scope of the present book.

14.6 Motilides

There is considerable interest in developing promotility drugs known as 'motilides'. Currently, these comprise a small group of macrolide antibiotics (erythromycin, azithromycin and clarithromycin) and investigative nonmacrolide agents (camicinal, raqualia and cempra). The former are non-selective and the latter are selective GPR38 motilin receptor agonists. The pharmacological effects of 'motilides' on the gastrointestinal tract are strictly dose-dependent and mediated: at low doses, through neuronal, and at high doses, through smooth muscle motilin receptors (Chap. 10). Their clinical use remains limited despite the fact that they facilitate intrinsic cholinergic signal transduction, trigger the interdigestive (phase III) myoelectrical complexes, increase the amplitude and enhance antral contractility, accelerate gastric emptying of both solids and liquids in healthy, critically ill (feed intolerant) and diabetic patients, (Sanger and Furness 2016). Macrolides and erythromycin in particular, are reserved for treatment of acute gastroparesis only because of their potential to: build up tolerance rapidly (responsiveness to the drug drops within 2 weeks of the onset of therapy); inhibit purinergic neurotransmission; prolong the cardiac QT interval; interact with medications metabolized by cytochrome P450 CYP 3A4; cause tachyphylaxis; exacerbate bacterial resistance. Camicinal, a compound with a relatively good safety record, is still undergoing experimental phase II clinical trials (Moshiree et al. 2010; Lee and Kim 2012; Camilleri 2013; Sanger et al. 2013; Broad and Sanger 2013; Dukes et al. 2010; Hobson et al. 2015; Quigley 2015; Camilleri 2016; Chapman et al. 2016; Hellström et al. 2016). At the time of writing, information on pharmacokinetics and pharmacodynamics of raqualia and cemptra were not available in the public domain.

The prokinetic effects of 'motilides' on the healthy human stomach is evident and similar to those observed under physiological multiple neurotransmission involving motilin and an increased release of ACh (Chap. 10). Separate SIP/ganglion units, the MP–ICC–MY(IM)–SM complex operating synchronously, generate spatially coordinated rhythmic slow waves and propagate electromechanical waves of contraction. The biomechanics of stress-strain development and distribution in the organ resemble qualitatively those described under normal conditions (Chaps. 10 and 11). However, the quantitative comparison indicates an increase in the intensity of total forces by 8–12%, and the frequency of ICC and neuronal activity on average by 17% and slow waves by 5%.

Consider the model specified as above to study the pharmacological effectiveness of 'motilides' on biomechanics of mild and severe gastroparesis. At the antral SIP, the administration of erythromycin at a low dose stimulates the production of irregular slow waves with spikes on their crests (Fig. 14.5). The most prominent effects, though, are the increase in free cytosolic Ca^{2+}, $\max[Ca^{2+}] = 0.61$ μM, and the strength of regular phasic contractions. Higher doses of the drug synchronize the generation of slow waves of amplitude, $V = 9$ mV, and at a frequency, $\nu = 0.05$ Hz, inducing strong SM contractions of $\max T = 30.5$ mN/cm. As the dose of erythromycin increases, the smooth muscle membrane becomes steadily depolarized at $V = -39.8$ mV. Smooth muscle contracts tonically.

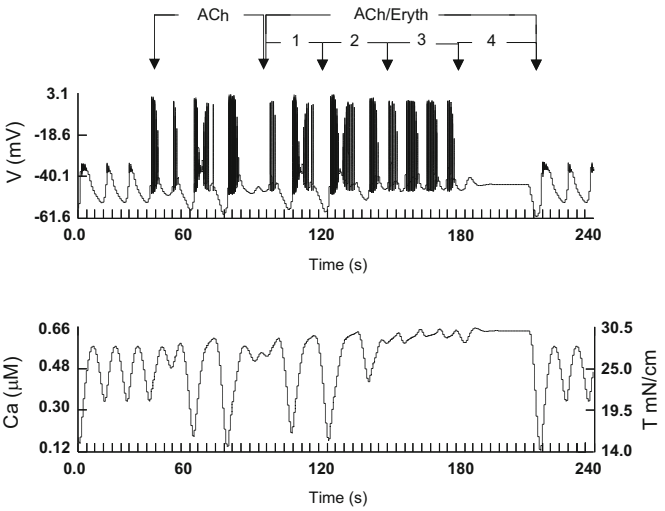

Fig. 14.5 The effect of erythromycin added at increasing doses (1 through 4) on electromechanical activity of the antral SIP/ganglion unit

The dynamics of peristaltic activity in the stomach does not differ from that observed with metoclopramide (Figs. 14.3, and 14.4). Erythromycin itself has neither reparative or integrative abilities to reconnect pathologically separated morphostructrural elements including ICC, neurons of the MP, SMCs, or to re-establish their functionality. With the existing modeling approach, it is not feasible to reproduce and explain in full the clinical improvements in gastric motility caused by erythromycin in the case of gastroparesis.

14.7 PDE-5 Inhibitor

Sildenafil, a type 5 specific phosphodiesterase inhibitor, is commonly used to treat erectile dysfunction in men. Acting independently, the drug alters intragastric distribution of content without affecting total gastric emptying or gastric clearance. On the other hand, a combination therapy of sildenafil and BTx demonstrates a synergistic relaxing effect on the spastic pylorus (Cho et al. 2006).

Consider the interplay between SP, NO, VIP and sildenafil on the biomechanics of the antral SIP/ganglion unit pretreated with BTx. The elimination of ACh from the system does not affect the dynamics of slow wave production. These are generated at their regional frequency of $\nu = 0.12$ Hz and amplitude of $V = 27.9$ mV (Fig. 14.6). However, action potentials are of low amplitude and short duration, $V = 5.3$ mV, $\Delta t = 0.1$ s. The release of SP and the activation of $NK_{1,3}$ and NK_2 receptors on SM and myenteric neurons respectively, converts the phasic bursting pattern of electrical activity to beating: $\nu \sim 6$ Hz, $V = 32$ mV. The

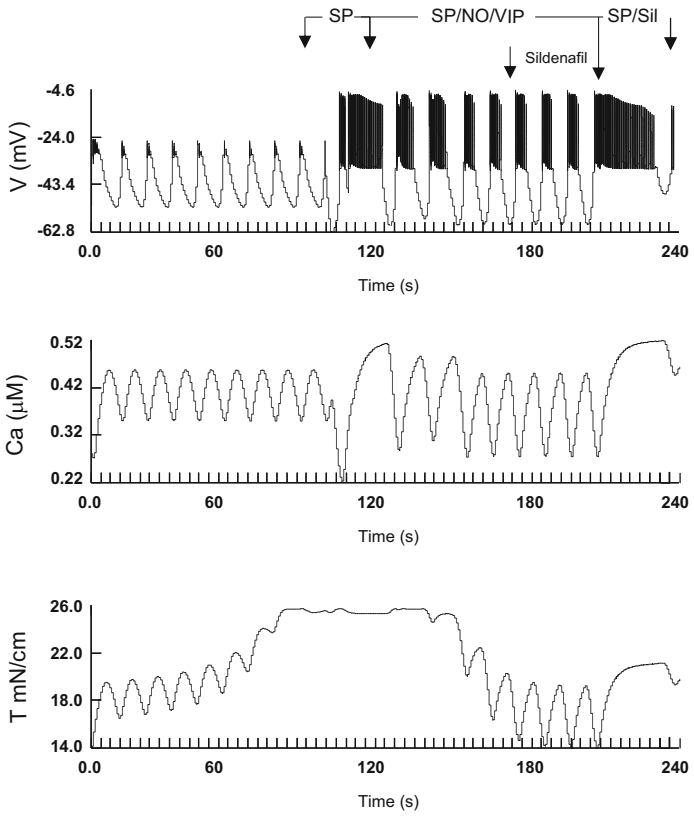

Fig. 14.6 The effect of SP, NO, VIP and sildenafil (Sil) on the electromechanical activity of the antral SIP/ganglion unit pretreated with botulinum toxin

total force steadily rises to a maximum: $T = 26.2$ mN/cm. The co-relase of NO and VIP restores rhythmicity of slow waves, spiking and phasicity of contractions. The intensity of T reduces to 20 mN/cm. The subsequent addition of sildenafil does not alter the myoelectrical activity and relaxes SM further to $T = 17$ mN/cm.

Assume that the MP–ICC–MY(IM)–SM complex is intact as may occur in the case of functional dyspepsia. Under the experimental conditions stated above, the stomach generates coordinated peristaltic movements qualitatively similar to those in the "healthy" organ. However, due to a decrease in strength of total forces, the intragastric volume and its capacitance increases compared to the normal stomach.

Let the nitrergic and vipergic neurotransmission be damaged as seen in patients with spastic pyloric stenosis. Substance P and sildenafil acting conjointly cause tonic-type contractions of antral SM of decreased intensity, $T = 19.1$ mN/cm.

The reader should remember that many biological parameters and constants employed in the model are not known because of their inaccessibility in intact human tissue. There is also a lack of adequate "tools" to evaluate them. Such

parameters have been adjusted during numerical simulations to reproduce the data that has been inferred from in vivo and in vitro experiments. Therefore, the theoretical results of the virtual simulations described above should be viewed as conjecture, accepted until proven otherwise, to explain the intricacy of intertwined multi-hierarchical coupled electrical, chemical and mechanical processes in the human stomach, rather than as a proof to often contradictory experimental observations.

References

Acosta A, Camilleri M (2015) Prokinetics in gastroparesis. Gastroenterol Clin North Am 44:97–111

Badyánszki M, Bódi N (2012) Diabetes-related alterations in the enteric nervous system and its microenvironment. World J Diabetes 3(5):80–93

Broad J, Sanger GJ (2013) The antibiotic azithromycin is a motilin receptor agonist in human stomach: comparison with erythromycin. Br J Pharmacol 168:1859–1867

Broad J, Góralczyk A, Mannur K, Dukes GE, Sanger GJ (2014) Drugs acting at 5-HT4, D2, motilin, and ghrelin receptors differ markedly in how they affect neuromuscular functions in human isolated stomach. Neurogastroenterol Motil 26(6):851–861

Broad J, Takahashi N, Tajimi M, Sudo M, Góralczyk A, Parampalli U, Mannur K, Yamamoto T, Sanger GJ (2016) RQ-00201894: a motilin receptor agonist causing long-lasting facilitation of human gastric cholinergically-mediated contractions. J Pharmacol Sci 130:60–65

Camilleri M (2013) Pharmacological agents currently in clinical trials for disorders in neurogastroenterology. J Clin Invest 123(10):4111–4120. doi:10.1172/JCI70837

Camilleri M (2016) Novel diet, drugs, and gastric interventions for gastroparesis. Clin Gastroenterol Hepatol 14(8):1072–1080

Chapman MJ, Deane AM, O'Connor SL, Nguyen NQ, Fraser RJL, Richards DB, Hacquoil KE, Johnson LSV, Barton M, Dukes GE (2016) The effect of camicinal (GSK962040), a motilin agonist, on gastric emptying and glucose absorption in feed-intolerant critically ill patients: a randomized, blinded, placebo-controlled, clinical trial. Crit Care 20:232–234

Chen S, Khan ZA, Cukiernik M, Chakrabarti S (2003) Differential activation of NF-kB and Ap-1 in increased fibronectin synthesis in target organs of diabetic complications. Am J Physiol Endocrinol Metab 284:1089–E1097

Cho SH, Park H, Kim JH, Ryu YH, Lee SI, Conklin JL (2006) Effect of sildenafil on gastric emptying in healthy adults. J Gastroenterol Hepatol 21(1 Pt 2):222–226

Choung RS, Talley NJ, Peterson J, Camilleri M, Burton D, Harmsen WS, Zinsmeister AR (2007) A double-blind, randomized, placebo-controlled trial of itopride (100 and 200 mg three times daily) on gastric motor and sensory function in healthy volunteers. Neurogastroenterol Motil 19(3):180–187

De Giorgio R, Barbara G, Stanghellini V, Cogliandro RF, Arrigoni A, Santini D, Ceccarelli C, Salvioli B, Rossini FP, Corinaldesi R (2000) Idiopathic myenteric ganglionitis underlying intractable vomiting in a young adult. Eur J Gastroenterol Hepatol 12:613–616

De Maeyer JH, Lefebvre RA, Schuurkers JAJ (2008) 5-HT_4 receptor agonists: similar but not the same. Neurogastroenterol Motil 20:99–112

Di Nardo G, Blandizzi C, Volta U, Colucci R, Stanghellini V, Barbara G, Del Tacca M, Tonini M, Corinaldesi R, De Giorgio R (2008) Review article: molecular, pathological and therapeutic features of human enteric neuropathies. Aliment Pharmacol Ther 28:25–42

Dong K, Yu XJ, Li B, Wen EC, Xiong W, Guan QL (2006) Advances in mechanisms of postsurgical gastroparesis syndrome and its diagnosis and treatment. Chin J Dig Dis 7:76–82

Dukes GE, Barton M, Dewit O, Stephens K, Vasist L, Young M, Richards D, Alpers D, Williams P (2010) Safety/tolerability, pharmacokinetics (PK), and effect on gastric emptying (GE) with 14-days repeat oral dosing of the motilin receptor agonist, GSK962040, in healthy male and female volunteers. Neurogastroenterol Motil 22(S1):14–15

Gibbons SJ, De Giorgio R, Pellegrini MSF, Garrity-Park MM, Miller SM, Schmalz PF, Young-Fadok TM, Larson DW, Dozois EJ, Camillieri M, Stanghellini V, Szurszewski JH, Farrugia G (2009) Apoptotic cell death of human interstitial cells of Cajal. Neurogastroenterol Motil 21 (1):85–93

Grover M, Farrugia G, Lurken MS, Bernard CE, Faussone-Pellegrini MS, Smyrk TC, Parkman HP, Abell TL, Snape WJ, Hasler WL, Ünalp-Arida A, Nguyen L, Koch KL, Calles J, Lee L, Tonascia J, Hamilton FA, Pasricha PJ (2011) Cellular changes in diabetic and idiopathic gastroparesis. Gastroenterology 140:1575.e8–1585.e8

Harberson J, Thomas RM, Harbison SP, Parknan HP (2010) Gastric neuromuscular pathology in gastroparesis: analysis of full-thickness antral biopsies. Dig Dis Sci 55(2):359–370

Hellström PM, Tack J, Johnson LV, Hacquoil K, Barton ME, Richards DB, Alpers DH, Sanger GJ, Dukes GE (2016) The pharmacodynamics, safety, and pharmacokinetics of single doses of the motilin agonist, camicinal, in type 1 diabetes mellitus with slow gastric emptying. Br J Pharmacol 173(11):1768–1777

Hobson R, Farmer AD, Dewit OE, O'Donnell M, Hacquoil K, Robertson D, Barton ME, Dukes GE (2015) The effects of camicinal, a novel motilin agonist, on gastro-esophageal function in healthy humans-a randomized placebo controlled trial. Neurogastroenterol Motil 27 (11):1629–1637

Kim ER, Kim KM, Lee JY, Joo M, Kim S, Noh JH, Ward SM, Koh SD, Rhee PL (2012) The clue of interstitial cell of Cajalopathy (ICCpathy) in human diabetic gastropathy: the ultrastructural and electrical clues of ICCpathy in human diabetic gastropathy. Exp Toxicol Pathol 64:521–526

Kindt S, Tack J (2006) Impaired gastric accommodation and its role in dyspepsia. Gut 55 (12):1685–1691

Lee A-L, Kim C-B (2012) The effect of erythromycin on gastrointestinal motility in subtotal gastroectomized patients. J Korean Surg Soc 82:149–155

Liebermann-Meffert D, Müller C, Allgöwer M (1982) Gastric hypermotility and antropyloric dysfunction in gastric ulcer patients. Br J Surg 69(1):11–13

Lin Z, Sarosiek I, Forster J, Damjanov I, Hou Q, McCallum RW (2010) Association of the status of interstitial cells of Cajal and electrogastrogram parameters, gastric emptying and symptoms in patients with gastroparesis. Neurogastroenterol Motil 22:56–e10

Lummis SCR (2012) 5-HT_3 receptors. J Biol Chem 287(48):40239–40245

Miftahof RN, Nam HG, Wingate DL (2009) Mathematical modeling and simulation in enteric neurobiology. World Scientific Publishing, Singapore

Moshiree B, McDonald R, Hou W, Toskes PP (2010) Comparison of the effect of azithromycin versus erythromycin on antroduodenal pressure profiles of patients with chronic functional gastrointestinal pain and gastroparesis. Dig Dis Sci 55:675–683

O'Grady G, Abell T (2015) Gastric arrhythmias in gastroparesis: low and high resolution mapping of gastric electrical activity. Gastroenterol Clin North Am 44(1):169–184

Ördög T, Hayashi Y, Gibbons SJ (2009) Cellular pathogenesis of diabetic gastroenteropathy. Minerva Gastroenterol Dietol 55(3):315–343

Pasha SF, Lunsford TN, Lennon VA (2006) Autoimmune gastrointestinal dysmotility treated successfully with pyridostigmine. Gastroenterology 131(5):1592–1596

Patil CS, Singh VP, Jain NK, Kulkarni SK (2005) Inhibitory effect of sildenafil on gastrointestinal smooth muscle: role of NO-CGMP transduction pathway. Indian J Exp Biol 43:167–171

Quigley EMM (2015) Prokinetics in the management of functional gastrointestinal disorders. J Neurogastroenterol Motil 21(3):330–336

Sanger GJ (2009) Translating 5-HT_4 receptor pharmacology. Neurogastroenterol Motil 21:1235–1238

Sanger GJ, Andrews PLR (2006) Treatment of nausea and vomiting: gaps in our knowledge. Auton Neurosci 129:3–16

Sanger GJ, Furness JB (2016) Ghrelin and motilin receptors as drug targets for gastrointestinal disorders. Nat Rev Gastroenterol Hepatol 13:38–48

Sanger GJ, Wang Y, Hobson A, Broad J (2013) Motilin: towards a new understanding of the gastrointestinal neuropharmacology and therapeutic use of motilin receptor agonists. Br J Pharmacol 170:1323–1332

Sarnelli G, Sifrim D, Janssens J, Tack J (2004) Influence of sildenafil on gastric sensorimotor function in humans. Am J Physiol Gastrointest Liver Physiol 287:G988–G992

Stevens JE, Russo A, Maddox AF, Rayner CK, Phillips L, Talley NJ, Giguère M, Horowitz M, Jones KL (2008) Effect of itopride on gastric emptying in longstanding diabetes mellitus. Neurogastroenterol Motil 20(5):456–463

Stevens JE, Jones KL, Rayner CK, Horowitz M (2013) Pathophysiology and pharmacotherapy of gastroparesis: current and future perspectives. Expert Opin Pharmacother 14(9):1171–1186

Streutker C, Colley EC, Hillsley K, Hicks GA, Kelly SM, Stead RH (2006) 5-HT4 receptor immunoreactivtiy (5-HT4-IR) is expressed in non-neuronal cells of the human gastrointestinal (GI) tract. Neurogastroenterol Motil 18:672

Tack J, Camilleri M, Chang L, Chey WD, Galligan JJ, Lacy BE, Müller-Lissner E, Quigley MM, Schuurkes J, De Maeyer JH, Stanghellini V (2012) Systematic review: cardiovascular safety profile of 5-HT4 agonists developed for gastrointestinal disorders. Aliment Pharmacol 35 (7):745–767

Takeuchi K, Okada M, Niida H, Okabe S (1990) Possible mechanisms involved in gastric hypermotility caused by indomethacin in the rat. Role of glycoprivic response. Dig Dis Sci 35(8):984–992

Talley N (2016) Functional dyspepsia: new insights into pathogenesis and therapy. Korean J Med 31(3):444–456

Talley NJ, Ford AC (2015) Functional dyspepsia. N Engl J Med 373:1853–1863

Van Lelyveld N, Ter Linde J, Schipper M, Samsom M (2008) Serotonergic signaling in the stomach and duodenum of patients with gastroparesis. Neurogastroenterol Motil 20:448–455

Venkova K, Greenwood-van Meerveld B (2008) Application of ghrelin to gastrointestinal diseases. Curr Opin Investig Drugs 9:1103–1107

Wouters MM, Farrugia G, Schemann M (2007) 5-HT receptors ion interstitial cells of Cajal, smooth muscle and enteric nerves. Neurogastroenterol Motil 19(2):5–12

Yarandi SS, Srinivasan S (2014) Diabetic gastrointestinal motility disorders and the role of enteric nervous system: Current status and future directions. Neurogastroenterol Motil 26(5):611–624

Zaráte N, Mearin F, Wang X-Y, Hewlett B, Huizinga JD, Malagelada J-R (2003) Severe idiopathic gastroparesis due to neuronal and interstitial cells of Cajal degeneration: pathological findings and management. Gut 52:966–970

Chapter 15
So, Could It All Be True?

How is error possible in mathematics?
Henry Poincare

15.1 The Existence of Solution to the One-Dimensional Dynamics Problem of Soft Shells

The complexity of the proposed biomechanical model of the human stomach should not be underestimated. The governing system of nonlinear partial and ordinary differential equations has been solved numerically using *ABS Technologies*® platform. This employs hybrid finite difference and finite element methods of second order accuracy, with respect to spatial and time variables. Although the results reproduce qualitatively, and sometimes quantitavely, in vivo and in vitro experiments, the fundamental question is whether or not these reflect the exact phenomena. This is essential in a modern day research environment with much simulation software supported by astounding graphical tools available in the public domain. Given to a fervent investigator where little or no experience or understanding of how to apply it correctly, deceptive results can easily follow. This is common not only in a community of computational biologists, where opinions and decisions are dominated and dictated by biologists but among engineers as well. Thus, a comparison of ten reputable analysis codes has shown an enormous discrepancy and variability of solutions to the very same mathematical problem. Possible explanations are: (i) "strong sensitivities of both a physical and computational nature", and (ii) abuse, driven by a desire to obtain a result at any cost, pushing the software beyond the range of its validity (Cook et al. 2001).

In this chapter the proof of the existence of solutions to one- and two-dimensional nonlinear dynamic problems of soft shells is provided (Shagidullin 2001).

Consider a soft "thread" of length L^s under the mass, $p(s)$, and local $[f(s,t)]$ forces. The boundary value one-dimensional dynamics problem is given by [see Eqs. (4.86), (4.60)]

R.N. Miftahof, *Biomechanics of the Human Stomach*,
DOI 10.1007/978-3-319-59677-8_15

$$\rho\frac{\partial^2 u_1}{\partial t^2}=\frac{\partial}{\partial s}\left(\frac{T(\lambda)}{\lambda}\frac{\partial u_1}{\partial s}\right)+p(s)\frac{\partial u_2}{\partial s}+f_1(s,t)+\varepsilon\frac{\partial^2\dot{u}_1}{\partial s^2},$$

$$\rho\frac{\partial^2 u_2}{\partial t^2}=\frac{\partial}{\partial s}\left(\frac{T(\lambda)}{\lambda}\frac{\partial u_2}{\partial s}\right)-p(s)\frac{\partial u_1}{\partial s}+f_2(s,t)+\varepsilon\frac{\partial^2\dot{u}_2}{\partial s^2}, \tag{15.1}$$

$$u_i(0,t)=u_i(l,t)=0, \tag{15.2}$$

$$u_i(s,0)=h_i(s),\ \partial u_i/\partial t(s,0)=v_i(s),\quad i=1,2 \tag{15.3}$$

where $\bar{u}(u_1(s,t),u_2(s,t))$ is the displacement vector, $\dot{u}=\partial u/\partial t$, and the meaning of other parameters is as described in Chaps. 1–4. Here the terms $\varepsilon\left(\partial^2\dot{u}_i/\partial s^2\right)$—"artificial viscosity"—have been added. These are commonly used in numerical algorithms to guarantee computational stability.

Introducing the notations

$$u=(u_1,u_2),\ f=(f_1,f_2),\ u'=\left(\frac{\partial u_1}{\partial s},\frac{\partial u_2}{\partial s}\right),\ \dot{u}=\left(\frac{\partial u_1}{\partial t},\frac{\partial u_2}{\partial t}\right),$$

$$|u|=\sqrt{u_1^2+u_2^2},\quad h=(h_1,h_2),\quad v=(v_1,v_2),\quad \sigma=(\sigma_1,\sigma_2),$$

$$\sigma_i=\frac{T(\lambda)}{\lambda}\frac{\partial u_i}{\partial s},\qquad P=\begin{bmatrix}0 & p\\ -p & 0\end{bmatrix},$$

Eqs. (15.1, 15.2, and 15.3) can be rewritten

$$\rho\ddot{u}-\varepsilon\dot{u}'-\sigma'-Pu'=f,$$

$$u(0,t)=u(L,t)=0, \tag{15.4}$$

$$u(s,0)=h(s),\quad \dot{u}(s,0)=v(s).$$

Let: (i) $\Omega=(0,L^s)$ and $L_2(0,T;X)$ denote a set of square integrable functions defined on the Banach space X: $\|v\|^2_{L_2(0,T;X)}=\int_0^T\|v\|^2_X dt$; (ii) H be the space of vector-functions $u=(u_1,u_2):\forall u_i(i=1,2)\in L_2(\Omega)$; (iii) V be the space of vector-functions with components from the Sobolev space $\overset{0}{W}{}_2^1$, and $V^*:=\mathrm{adj}V$ which contains dyads (v_1^*,v_2^*):$v_i^*\in W_2^{(-1)}$; (iv) operators A and B, $A(B)$: $V\to V^*$ be defined by

$$<Az,w>=\varepsilon\int_\Omega z'\cdot w'ds, \tag{15.5}$$

$$<Bz,w>=\int_\Omega\sigma(z)\cdot w'ds-\int_\Omega Pz'\cdot wds, \tag{15.6}$$

where $\langle\cdot,\cdot\rangle$ is the duality condition between the spaces V and V^*; $z\cdot w=z_1w_1+z_2w_2$.

Definition. The vector function $u=(u_1,u_2)$ is called a general solution to the problem (15.1), (15.2), and (15.3) if

$$u,\dot{u}\in L_2(0,T;V),\quad \ddot{u}\in L_2\left(0,T;V^*\right), \tag{15.7}$$

$$u(s,0)=h(s)\ \text{ in } V,\quad \dot{u}(s,0)=v(s)\ \text{ in } H, \tag{15.8}$$

and the equation

$$\rho\ddot{u}+A\dot{u}+Bu=f, \tag{15.9}$$

holds. The latter suggests the equality of elements in the space $L_2(0,T;V^*)$ and is equivalent to the statement that for $\forall w\in L_2(0,T;V)$ the identity

$$\int_0^T <\rho\ddot{u}+A\dot{u}+Bu,w>dt=\int_0^T <f,w>dt$$

is valid.

From Eqs. (15.7) it is apparent that $u\in C(0,T;V)$, $\dot{u}\in C(0,T;H)$, and therefore Eqs. (15.8) hold. It follows from Eqs. (15.5)–(15.7): $A\dot{u},B\dot{u}\in L_2\left(0,T;V^*\right)$. Furthermore, since $\ddot{u}\in L_2\left(0,T;V^*\right):\rho\ddot{u}\in L_2\left(0,T;V^*\right)$ if $\|\rho(s)\|_{L_\infty(\Omega)}\le$ const.

Our proof of the existence and uniqueness of solution will be based on

Theorem 1. Let: (i) V be a separable Hilbert space densely embedded into another Hilbert space H, $X=L_2(0,T;V)$; (ii) for a given μ, $A+\mu I:X\to X^*$ be a radial-continuous strongly monotone Volterra operator, (I is the embedding operator of X into X^*); (iii) $B:X\to X^*$ be the Lipschitz continuous Volterra operator. Then for $\forall a_0\in V, a_1\in H, f\in X^*$

$$\ddot{u}+A\dot{u}+Bu=f, \tag{15.10}$$

$$u(0)=a_0,\quad \dot{u}(0)=a_1,\quad u\in C(0,T;V),\quad u'\in X,$$

has a unique solution $u\in X$and $\dot{u}\in X$, $\ddot{u}\in X^*$.

To prove that the operators A and B satisfy the conditions of the theorem 1 consider

Lemma 1. The operator A, defined by Eq. (15.5), is continuous and strongly monotone.

Proof. The statement is evident. Thus for $\forall\mu\ge 0$ the operator $(A+\mu I)$ satisfies the conditions of the theorem 1.

Lemma 2. The operator B, defined by Eq. (15.6), is Lipschitz continuous and

$$\left|\int_0^T <Bz-Bv,w>dt\right|\le M\|z-v\|_X\|w\|_X. \tag{15.11}$$

Proof. Suppose $B=B_1+B_2$, where the operators B_1 and B_2 are defined by

$$\left|\int_0^T < B_1 z, w > dt\right| = \int_0^T \int_\Omega \sigma(z) w' ds dt = \int_0^T \int_\Omega \left(\left(\sigma_1(z) w' + \sigma_2(z) w'\right) ds dt,$$

$$\left|\int_0^T < B_2 z, w > dt\right| = \int_0^T \int_\Omega P z' \cdot w ds dt = \int_0^T \int_\Omega \left(\left(p z'_2 w_1 - p z'_1 w_2\right) ds dt.\right.$$

Then

$$\left|\int_0^T < B_2 z - B_2 v, w > dt\right| = \left|\int_0^T \int_\Omega \left(p\left(z'_2 - v'_2\right) w_1 - p\left(z'_1 - v'_1\right) w_2\right) ds dt\right| \leq$$

$$\leq \|p\|_{L_\infty(\Omega)} \int_0^T \|z - v\|_V \|w\|_H dt.$$

This guarantees the continuity of the operator B_2 with the Lipschitz constant depending on $\|p\|_{L_\infty(\Omega)}$. Moreover,

$$\int_0^T < B_1 z - B_1 v, w > dt = \int_0^T \int_\Omega \sum_{i=1}^2 \left(\frac{T(\lambda(z))}{\lambda(z)} \frac{\partial z_i}{\partial s} - \frac{T(\lambda(v))}{\lambda(v)} \frac{\partial v_i}{\partial s}\right) \frac{\partial w_i}{\partial s} ds dt. \tag{15.12}$$

Let

$$f^*(\lambda(z)) = \frac{T\lambda(z)}{\lambda(z)}.$$

Consider the expression

$$f^*(\lambda(z)) \frac{\partial z_i}{\partial s} - f^*(\lambda(v)) \frac{\partial v_i}{\partial s} =$$

$$= \int_0^1 \frac{\partial}{\partial \theta} \left[f^*(\lambda(v + \theta(z - v))) \frac{\partial(v_i + \theta(z_i - v_i))}{\partial s}\right] d\theta =$$

$$= \int_0^1 \left\{ f^*(\lambda(v + \theta(z - v))) \frac{\partial(z_i - v_i)}{\partial s} + \frac{f_\lambda{}'^*(\lambda(v + \theta(z - v)))}{\lambda(v + \theta(z - v))} \frac{\partial(z_i - v_i)}{\partial s} \times \right.$$

$$\left. \times \sum_{j=1}^2 \left[\frac{\partial\left(z_j - v_j\right)}{\partial s} \frac{\partial\left(v_j + \theta\left(z_j - v_j\right)\right)}{\partial s}\right] \frac{\partial\left(v_j + \theta\left(z_j - v_j\right)\right)}{\partial s} \right\} d\theta$$

On substituting the above in Eq. (15.12), we obtain

$$\left|\int_0^T < B_1 z - B_1 \upsilon, w > dt\right| = \left|\int_0^T \int_\Omega \int_0^1 f^*(\lambda(\upsilon + \theta(z-\upsilon))) \times\right.$$

$$\times \sum_{i=1}^{2} \left(\frac{\partial (z_i - w_i)}{\partial s}\right) \frac{\partial w_i}{\partial s} d\theta ds dt. + \int_0^T \int_\Omega \int_0^1 \frac{f_\lambda'^*(\lambda(\upsilon + \theta(z-\upsilon)))}{\lambda(\upsilon + \theta(z-\upsilon))} \sum_{j=1}^{2} \frac{\partial \left(z_j - \upsilon_j\right)}{\partial s} \times$$

$$+ \int_0^T \int_\Omega \int_0^1 f_\lambda'^*(\lambda(\upsilon + \theta(z-\upsilon)))\lambda(z-\upsilon)\lambda(\upsilon + \theta(z-\upsilon))\lambda(w) \times d\theta ds dt$$

$$\leq M \|z - \upsilon\|_X \|w\|_X,$$

where $M = \text{const}$ such that

$$\left|f^*(\xi)\right| \leq \frac{M}{2}, \quad \left|f_\xi'^*(\xi)\xi\right| \leq \frac{M}{2} \quad \forall \xi \geq 1.$$

This proves the lemma.

Theorem 2. Let $\rho(s) = \text{const}, |\rho(s)| \leq C$ for $\forall s \in \Omega$. Then for $\forall f \in L_2(0, T; V^*)$, $h \in V, \upsilon \in H$ there exists a unique general solution to the problem (15.1), (15.2) and (15.3).

The proof follows directly from lemmas 1, 2 and the theorem 1. It is noteworthy that the theorem is also valid for the first nonhomogeneous boundary-value problem.

15.2 The Existence of Solution for the Two-Dimensional Dynamics Problem of Soft Shells

Let the undeformed surface S of a soft shell, referred to an orthogonal Cartesian coordinate system, be parameterized by curvilinear coordinates $x_j(\alpha_1, \alpha_2)$, $(j = 1, 2, 3)$ (Chap. 4). Let a point $M(\alpha_1, \alpha_2) \in S$ be described by the position vectors $\bar{r}(\alpha_1, \alpha_2)$. The equations of the equilibrium of the soft shell under the influence of forces $f(x)$ is given by

$$\begin{gathered} -\text{div}(\beta_0(\lambda)\nabla\varphi \cdot \nabla\varphi^T \cdot \nabla\varphi(x) + \beta_1(\lambda)\nabla\varphi(x)) = f(x), \quad x \in S \\ \varphi(x) = \varphi_0(x), \quad x \in \partial S. \end{gathered} \tag{15.13a}$$

The matrix $\nabla\varphi(x) = (\partial x_j/\partial\alpha_i)(j = 1, 2, 3; i = 1, 2)$ of the gradient of deformation $\nabla \overset{*}{\bar{r}}$ allows decomposition: $\nabla\varphi(x) = V(x) \cdot O(x)$, where $V(x)$ is the rate of elongations and $O(x)$ is the orthogonal tensor. Scalar functions $\beta_0(\lambda_1, \lambda_2)$, $\beta_1(\lambda_1, \lambda_2)$ given by

$$\beta_0 = -\frac{\theta(\lambda_1,\lambda_2)\lambda_2^2 - \theta(\lambda_2,\lambda_1)\lambda_1^2}{\lambda_2^2-\lambda_1^2}\cdot\frac{1}{\lambda_1\lambda_2},$$
$$\beta_1 = \frac{\theta(\lambda_1,\lambda_2)\lambda_2^2 - \theta(\lambda_2,\lambda_1)\lambda_1^2}{\lambda_2^2-\lambda_1^2}\cdot\frac{\lambda_1^2+\lambda_2^2}{\lambda_1\lambda_2} + \lambda_1\lambda_2\frac{\theta(\lambda_1,\lambda_2)-\theta(\lambda_2,\lambda_1)}{\lambda_1^2-\lambda_2^2}, \tag{15.14}$$

are the invariants $i_1(x) = \lambda_1^2(x) + \lambda_2^2(x), \quad i_2(x) = \lambda_1^2(x) + \lambda_2^2(x)$ of the matrix $G = \nabla\varphi\nabla\varphi^T(x)$ and belong to class C^3 outside a neighborhood of $(i_1, i_2) = (0, 0)$. Here $\lambda = (\lambda_1, \lambda_2)$ are the eigenvalues of $V(x)$. The principal membrane forces $\theta(\lambda_1,\lambda_2), \theta(\lambda_2,\lambda_1) \propto T_1, T_2$ of the shell define a domain D of permissible (λ_1, λ_2) for a given positive θ.

Using the Piola tensor notation

$$P = \beta_0(\lambda)\nabla\varphi\cdot\nabla\varphi^T\cdot\nabla\varphi(x) + \beta_1(\lambda)\nabla\varphi(x),$$

Equation (15.13a) can be written in the compact form

$$\begin{aligned} -\mathrm{div}P(\varphi) &= f(x), \quad x\in S \\ \varphi(x) &= \varphi_0(x), \quad x\in\partial S. \end{aligned} \tag{15.13b}$$

Consider the deformed shell in the static state. The deformation $\varphi_H(x) = \lambda_0 x$ is the solution to Eq. (15.13a) for $\varphi_0(x) = \lambda_0 x$, $x \in \partial S$, and $f(x) = 0$, $x \in S$. The solution to the above problem also exists if $f(x)$ is chosen from a neighborhood of zero in the space $[L_p(S)]^3$.

Let the functional space of $\varphi(x)$ be the Sobolev space $\mathbf{W} \equiv \left[W_p^{(2)}(S)\right]^3, p \geq 3$. Since the spaces $W_p^k(\Omega)$ are algebras for $kp > n$, where n is the dimension of the domain Ω, and since

$$i_1(x) = \sum_{\alpha=1}^{2}\sum_{i}^{3}\left(\frac{\partial\varphi_i}{\partial x_\alpha}\right)^2, i_2(x) = \sum_{i}^{3}\left(\frac{\partial\varphi_i}{\partial x_1}\right)^2\sum_{i}^{3}\left(\frac{\partial\varphi_i}{\partial x_2}\right)^2 - \left(\sum_{i}^{3}\frac{\partial\varphi_i}{\partial x_1}\frac{\partial\varphi_i}{\partial x_1}\right)^2, \tag{15.15}$$

then the invariants $i_1(x), i_2(x) \in W_p^{(1)}(S)$ and owing to the embedded theorems these depend continuously on x in the close domain $\overline{S}$. It is apparent from the above that the $\beta_0, \beta_1 \in W_p^{(1)}(S)$ if $\inf\limits_{S_0}[\lambda_1\varphi(x), \lambda_2\varphi(x)] > 0$.

Denote the neighborhood of $\varphi_H(x)$ as $B(\varphi_H)$ defined by $\|\varphi - \varphi_H\|_W < C$. The choice of C is dictated by the requirement: for $\forall\varphi \in B|\lambda_1\varphi(x), \lambda_2\varphi(x) \geq \delta > 0$, where δ is a positive number.

To compute the Fréchet derivative of the Piola tensor P at a point φ_H, let $\Psi(x) \in \mathbf{W}$ be such that $\varphi = \varphi_H + \psi$, $\varphi \in B$. First, calculate the variations δi_1 and δi_2 of the matrix G. We have

$$\begin{aligned} i_1(\varphi) = \mathrm{tr}G = \mathrm{tr}[(\nabla\varphi_H + \nabla\psi)\cdot(\nabla\varphi^T{}_H + \nabla\psi^T)] = 2\lambda_0^2 + \\ +\mathrm{tr}(\nabla\varphi_H\cdot\nabla\psi^T + \nabla\psi\cdot\nabla\varphi^T{}_H) + \mathrm{tr}(\nabla\psi\cdot\nabla\psi^T) = \\ = 2\lambda_0^2 + 2\lambda_0\mathrm{tr}\mathbf{e}(x) + \|\nabla\psi\|_2^2. \end{aligned} \tag{15.16}$$

Here $\|\nabla\psi\|_2$ is the Euclidean norm of the matrix $\nabla\psi$; $\mathbf{e}$(x) is a linear operator generated by the deformation $\psi(x)$ in $S(x_1, x_2)$

$$\mathbf{e}(x) = \begin{pmatrix} \dfrac{\partial\psi_1(x)}{\partial\alpha_1} & \dfrac{1}{2}\left(\dfrac{\partial\psi_2}{\partial\alpha_1} + \dfrac{\partial\psi_1}{\partial\alpha_2}\right) \\ \dfrac{1}{2}\left(\dfrac{\partial\psi_2}{\partial\alpha_1} + \dfrac{\partial\psi_1}{\partial\alpha_2}\right) & \dfrac{\partial\psi_2}{\partial\alpha_2} \end{pmatrix}.$$

Note that

$$\nabla\varphi_H\cdot\nabla\psi^T + \nabla\psi\cdot\nabla\varphi^T{}_H = 2\lambda_0^2\mathbf{e}(x), \quad \nabla\varphi_H\cdot\nabla\psi^T = \lambda_0^2 I_2. \tag{15.17}$$

Since $G^2 - i_1G + i_2I_2 = 0$ (the Hamilton-Cayley theorem), therefore

$$2i_2 = i_1^2 - \mathrm{tr}\left(G^2\right). \tag{15.18}$$

Using Eqs. (15.17), the trace of the matrix $G^2$and $(\mathrm{tr}G(\varphi))^2$yield

$$\begin{aligned} &\mathrm{tr}\left(G^2(\varphi)\right) = \mathrm{tr}\left[\nabla\varphi_H\cdot\nabla\varphi_H^T + \nabla\varphi_H\cdot\nabla\psi^T + \nabla\psi\cdot\nabla\varphi_H^T + \nabla\psi\cdot\nabla\psi^T\right]^2 = \\ &= \mathrm{tr}\left[\nabla\varphi_H\cdot\nabla\varphi_H^T\right)^2 + \nabla\varphi_H\cdot\nabla\varphi_H^T\cdot\nabla\varphi_H\cdot\nabla\psi^T + \nabla\varphi_H\cdot\nabla\varphi_H^T\cdot\nabla\psi\cdot\nabla\varphi_H^T + \\ &\quad +\nabla\varphi_H\cdot\nabla\psi^T\cdot\nabla\varphi_H\cdot\nabla\varphi_H^T + \nabla\psi\cdot\nabla\varphi_H^T\cdot\nabla\varphi_H\cdot\nabla\varphi_H^T\right] + O\left(\|\nabla\psi\|_2^2\right) = \\ &= \mathrm{tr}\left[G^2(\varphi_H) + 2\left(\nabla\varphi_H\cdot\nabla\varphi_H^T\right)\left(\nabla\varphi_H\cdot\nabla\psi^T + \nabla\psi\cdot\nabla\varphi_H^T\right) + O\left(\|\nabla\psi\|_2^2\right)\right. = \\ &\qquad = 2\lambda_0^4 + 4\lambda_0^3\mathrm{tr}\mathbf{e}(x) + O\left(\|\nabla\psi\|_2^2\right); \\ &(\mathrm{tr}G(\varphi))^2 = \left(2\lambda_0^2 + 2\lambda_0\mathrm{tr}\mathbf{e}(x) + \|\nabla\psi\|_2^2\right)^2 = 4\lambda_0^4 + 8\lambda_0^3\mathrm{tr}\mathbf{e}(x) + O\left(\|\nabla\psi\|_2^2\right). \end{aligned}$$

As a result of derivations, we get finally,

$$\delta i_1 = i_1(\varphi) - i_1(\varphi_H) = 2\lambda_0\mathrm{tr}\mathbf{e}(x) + O\left(\|\nabla\psi\|_2^2\right), \tag{15.19a}$$

$$\delta i_2 = i_2(\varphi) - i_2(\varphi_H) = 2\lambda_0^3\mathrm{tr}\mathbf{e}(x) + O\left(\|\nabla\psi\|_2^2\right). \tag{15.19b}$$

The variation of the product $\nabla\varphi\cdot\nabla\varphi^T\cdot\nabla\varphi$ is given by

$$\begin{aligned} \delta\Pi = \nabla\varphi\cdot\nabla\varphi^T\cdot\nabla\varphi - \nabla\varphi_H\cdot\nabla\varphi_H^T\cdot\nabla\varphi_H = \\ = \nabla\psi\cdot\nabla\varphi_H^T\cdot\nabla\varphi_H + \nabla\varphi_H\cdot\nabla\psi^T\cdot\nabla\varphi_H + \\ +\nabla\varphi_H\cdot\nabla\varphi_H^T\cdot\nabla\psi + O\left(\|\nabla\psi\|_2^2\right), \end{aligned}$$

where $O\left(\|\nabla\psi\|_2^2\right)$ indicates that the module of each entry of the matrix is less than $C\|\nabla\psi\|_2^2$, $C = \text{const}$. Making use of the equalities

$$\nabla\varphi_H = \lambda_0\begin{pmatrix}1&0&0\\0&1&0\end{pmatrix},\ \ \nabla\varphi_H\cdot\nabla\varphi_H^T = \lambda_0^2\begin{pmatrix}1&0\\0&1\end{pmatrix} = \lambda_0^2 I_2,\ \ \nabla\varphi_H^T\cdot\nabla\varphi_H = \lambda_0^2\begin{pmatrix}1&0&0\\0&1&0\\0&0&0\end{pmatrix},$$

we obtain

$$\nabla\psi\cdot\nabla\varphi_H^T\cdot\nabla\varphi_H = \lambda_0^2\begin{pmatrix}\dfrac{\partial\psi_1}{\partial\alpha_1} & \dfrac{\partial\psi_2}{\partial\alpha_1} & 0\\ \dfrac{\partial\psi_1}{\partial\alpha_2} & \dfrac{\partial\psi_2}{\partial\alpha_2} & 0\end{pmatrix},\quad \nabla\varphi_H\cdot\nabla\varphi_H^T\cdot\nabla\psi = \lambda_0^2\nabla\psi,$$
$$\nabla\varphi_H\cdot\nabla\psi^T\cdot\nabla\varphi_H = \lambda_0^2\begin{pmatrix}\dfrac{\partial\psi_1}{\partial\alpha_1} & \dfrac{\partial\psi_1}{\partial\alpha_2} & 0\\ \dfrac{\partial\psi_2}{\partial\alpha_1} & \dfrac{\partial\psi_2}{\partial\alpha_2} & 0\end{pmatrix}.$$

Subsequently, $\delta\Pi$ takes the final matrix form

$$\delta\Pi = 2\lambda_0^2\begin{pmatrix}\dfrac{\partial\psi_1}{\partial\alpha_1} & \dfrac{1}{2}\left(\dfrac{\partial\psi_2}{\partial\alpha_1}+\dfrac{\partial\psi_1}{\partial\alpha_2}\right) & 0\\ \dfrac{1}{2}\left(\dfrac{\partial\psi_2}{\partial\alpha_1}+\dfrac{\partial\psi_1}{\partial\alpha_2}\right) & \dfrac{\partial\psi_2}{\partial\alpha_2} & 0\end{pmatrix}. \tag{15.20}$$

Hence the variation of the Piola tensor is found to be

$$\begin{aligned}P(\varphi)-P(\varphi_H) &= \beta_0(\varphi)\Pi(\varphi)+\beta_1(\varphi)\nabla\varphi-\beta_0(\varphi_H)\Pi(\varphi_H)-\beta_1(\varphi_H)\nabla\varphi_H = \\ &= (\beta_0(\varphi)-\beta_0(\varphi_H))\Pi(\varphi)+\beta_0(\varphi_H)\delta\Pi+ \\ &+ (\beta_1(\varphi)-\beta_1(\varphi_H))\nabla\varphi+\beta_1(\varphi_H)\nabla\psi = \\ &= \delta\beta_0\Pi(\varphi_H)+\beta_0(\varphi_H)\delta\Pi+\delta\beta_0\delta\Pi+\delta\beta_1\nabla\varphi_H+\beta_1(\varphi_H)\nabla\psi+\delta\beta_1\nabla\psi.\end{aligned} \tag{15.21}$$

The variations of $\beta_0(i_1,i_2)$, $\beta_1(i_1,i_2)$ are given by

$$\begin{aligned}\delta\beta_k &= \beta_k(i_1(\varphi),i_2(\varphi))-\beta_k(i_1(\varphi_H),i_2(\varphi_H)) = \\ &= \frac{\partial\beta_k}{\partial i_1}\big(i_1^0,i_2^0\big)\delta i_1+\frac{\partial\beta_k}{\partial i_2}\big(i_1^0,i_2^0\big)\delta i_2+R_k; \qquad k=0,1; \\ R_k &= \int_0^1(1-t)\big(D^2\beta_k\big(i_1^0+th_1,i_2^0+th_2\big)h,h\big)dt,\end{aligned} \tag{15.22}$$

where we adopt the following notations: $\beta_k^0 = \beta_k(\varphi_H), i_k^0 = i_k(\varphi_H),\ h = \left(\delta i_1^0, \delta i_2^0\right)$, $D^2\beta_k = \left(\frac{\partial^2\beta_k}{\partial i_\alpha \partial i\beta}\right)_{\alpha,\beta=1}^2$. On substituting Eqs. (15.19a, 15.19b), (15.20), (15.22) in (15.21), we obtain finally,

$$P(\varphi) - P(\varphi_H) = 2\lambda_0^2\beta_0(\varphi_H)\begin{pmatrix} \frac{\partial\psi_1}{\partial\alpha_1} & \frac{1}{2}\left(\frac{\partial\psi_2}{\partial\alpha_1} + \frac{\partial\psi_1}{\partial\alpha_2}\right) & 0 \\ \frac{1}{2}\left(\frac{\partial\psi_2}{\partial\alpha_1} + \frac{\partial\psi_1}{\partial\alpha_2}\right) & \frac{\partial\psi_2}{\partial\alpha_2} & 0 \end{pmatrix} + \\ + \left(\lambda_0^2\beta_0(\varphi_H) + \beta_1(\varphi_H)\right)\nabla\psi + \\ + 2\left[\left(\lambda_0^3\frac{\partial\beta_0}{\partial i_1} + \lambda_0^5\frac{\partial\beta_0}{\partial i_2}\right) + \left(\lambda_0\frac{\partial\beta_1}{\partial i_1} + \lambda_0^3\frac{\partial\beta_1}{\partial i_2}\right)\right]\nabla\varphi_0\mathbf{tre} + R.$$

The derivatives $(\partial\beta_k/\partial\alpha_j)$ are calculated at a point $\left(i_1^0, i_2^0\right)$. The matrix R has entries $CR_k\Phi(x)$ where $C = \text{const}$ defined by λ_0. $\Phi(x)$ is the product of a finite (or empty) number of derivatives $\partial_\alpha\psi_i$.

The bilinear form under the integral sign in Eq. (15.22) is a function from the space $W_p^{(1)}(S)$ because: the functions $i_1(x), i_2(x)$ are continuous; $\beta_0(i_1, i_2), \beta_1(i_1, i_2) \in C^3$ with respect to i_1, i_2 and sufficiently small $\delta i_1, \delta i_2$ [Eqs. (19a), (19b)]; and $\psi \in \left[W_p^{(2)}\right]^3$. According to the general theorems of the Lebesgue integral the interchange of a derivative and an integral is permissible in Eq. (15.22). Moreover, since $W_p^{(1)}(S)$ is the algebra, the analysis of R shows that $R \in \left[W_p^1\right]^3$ and

$$R = O\left(\|\nabla\psi\|^2\right), \quad \|\text{div}R\|_{L_2(S)} = O\left(\|\nabla\psi\|_W^2\right). \tag{15.23}$$

As a consequence of Eqs. (15.22), (15.23), the Fréchet derivative of the operator $\text{div}P(\varphi(x))|_{\varphi_H(x)}\left(\text{div}P(\varphi(x)) : \mathbf{W} \to \mathbf{L}, \left(\mathbf{L} = [L_2(S)]^3\right)\right)$, is found to be

$$D\{\text{div}P(\varphi(x))\}\psi = \text{div}\left\{2\lambda_0^2\beta_0(\varphi_H)\begin{pmatrix} \frac{\partial\psi_1}{\partial\alpha_1} & \frac{1}{2}\left(\frac{\partial\psi_2}{\partial\alpha_1} + \frac{\partial\psi_1}{\partial\alpha_2}\right) & 0 \\ \frac{1}{2}\left(\frac{\partial\psi_2}{\partial\alpha_1} + \frac{\partial\psi_1}{\partial\alpha_2}\right) & \frac{\partial\psi_2}{\partial\alpha_2} & 0 \end{pmatrix} + \right. \\ + \left[\lambda_0^2\beta_0(\varphi_H) + \beta_1(\varphi_H)\right]\nabla\psi + 2\left[\left(\lambda_0^3\frac{\partial\beta_0}{\partial i_1} + \lambda_0^5\frac{\partial\beta_0}{\partial i_2}\right) + \right. \\ \left. \left. + \left(\lambda_0\frac{\partial\beta_1}{\partial i_1} + \lambda_0^3\frac{\partial\beta_1}{\partial i_2}\right)\right]\cdot\lambda_0\left(\frac{\partial\psi_1}{\partial\alpha_1} + \frac{\partial\psi_2}{\partial\alpha_2}\right)\begin{pmatrix} 1\,0\,0 \\ 0\,1\,0 \end{pmatrix}\right\} \equiv \text{div}\mathrm{L}(\psi). \tag{15.24}$$

Thus we have proven

Lemma 3. There exists the Fréchet derivative [Eq. (15.24)] of the operator function

$$\mathrm{div}P(\varphi(x)) : \mathbf{W} \to \mathbf{L}$$

corresponding to a linearized problem

$$-\mathrm{div}\Big\{\big[\lambda_0^2\beta_0(\varphi_H)+\beta_1(\varphi_H)\big]\mathrm{grad}\overline{\psi}+2\lambda_0^2\beta_0(\varphi_H)\mathbf{e}(\overline{\psi})+2\big(\lambda_0^4\frac{\partial\beta_0}{\partial i_1}+ \\ +\lambda_0^6\frac{\partial\beta_0}{\partial i_2}+\lambda_0^2\frac{\partial\beta_1}{\partial i_1}+\lambda_0^4\frac{\partial\beta_1}{\partial i_2}\big)\mathrm{tre}(\overline{\psi})I_2\Big\}=\bar{f}(x), \tag{15.25}$$

$$-\big(\lambda_0^2\beta_0(\varphi_H)+\beta_1(\varphi_H)\big)\Delta\psi_3=f_3(x),\qquad x\in S. \tag{15.26}$$

Here

$$\psi(x)=(\psi_1,\psi_2,\psi_3),\quad \overline{\psi}(x)=(\psi_1,\psi_2),\quad \mathbf{e}(\overline{\psi})=\big(\big(\partial_i\psi_j+\partial_j\psi_i\big)/2\big)_{i,j=1,2},$$
$$\bar{f}=(f_1,f_2),f_i\in L_2(S),\psi(x)=0,\qquad x\in\partial S.$$

On substituting Eqs. (15.14), (15.25) in (15.26), after some algebra, we get

$$-\mathrm{div}\left\{\left[-2\theta_0+\lambda_0\left(\frac{\partial\theta_0}{\partial\lambda_1}-\frac{\partial\theta_0}{\partial\lambda_2}\right)\right]\mathbf{e}(\psi)+\theta_0\nabla\psi+\left[\theta_0+\lambda_0\frac{\partial\theta_0}{\partial\lambda_2}\right]\mathrm{tre}(\psi)I_2=\overline{f},\right. \tag{15.27}$$

$$-\theta_0\Delta\psi_3=f_3, \tag{15.28}$$

$$\psi|_{\partial S}=0, \tag{15.29}$$

where $\theta_0=\theta(\lambda_0,\lambda_0)$.

The coordinate ψ_3 is found by solving Eq. (15.28) directly. To find ψ_1,ψ_2 consider the boundary-value problem, Eq. (15.27), in weak formulation, i.e. find $u=(\psi_1,\psi_2)$ in $\mathbf{V}=\left[\overset{0}{W}{}_2^1\right]^3$ such that for $\forall v(x)\in\mathbf{V}$, u satisfies the variational inequality

$$\int_S\left[\left(-2\theta_0+\lambda_0\frac{\partial\theta_0}{\partial\lambda_1}-\lambda_0\frac{\partial\theta_0}{\partial\lambda_2}\right)\mathbf{e}(u)\cdot\cdot\,\mathbf{e}(v)+\theta_0\nabla u\cdot\cdot\nabla v+\right. \\ \left.+\left(\theta_0+\lambda_0\frac{\partial\theta_0}{\partial\lambda_2}\right)\mathrm{tre}(u)\cdot\mathrm{tre}(v)\right]dx=\int_S(f_1v_1+f_2v_2)dx. \tag{15.30}$$

Lemma 4. The symmetrical bilinear form $B(u,v)$ [Eq. (15.30)] on $\mathbf{V}$is strictly positive if one of the following conditions holds

$$\frac{\partial\theta_0}{\partial\lambda_1}>\max\left\{\frac{\partial\theta_0}{\partial\lambda_2},\left|\frac{\partial\theta_0}{\partial\lambda_2}+\frac{1}{\lambda_0}\frac{\partial\theta_0}{\partial\lambda_1}\right|\right\}; \tag{15.31}$$

or

$$-3\frac{\partial\theta_0}{\partial\lambda_1}<\frac{\partial\theta_0}{\partial\lambda_2}<\frac{\partial\theta_0}{\partial\lambda_1},\qquad \frac{\partial\theta_0}{\partial\lambda_1}>0; \tag{15.32}$$

or

$$-5\frac{\partial\theta_0}{\partial\lambda_1}<\frac{\partial\theta_0}{\partial\lambda_2}<\frac{1}{3}\frac{\partial\theta_0}{\partial\lambda_1},\qquad \frac{\partial\theta_0}{\partial\lambda_1}>0. \tag{15.33}$$

Proof. After simple algebra of the right-hand side of (15.30), we get

$$\begin{aligned}B(u,v)=\lambda_0\frac{\partial\theta_0}{\partial\lambda_1}\left(\left\langle\frac{\partial u_1}{\partial\lambda_1},\frac{\partial v_1}{\partial\lambda_1}\right\rangle+\left\langle\frac{\partial u_2}{\partial\lambda_2},\frac{\partial v_2}{\partial\lambda_2}\right\rangle\right)+\left(-2\theta_0+\lambda_0\frac{\partial\theta_0}{\partial\lambda_1}-\lambda_0\frac{\partial\theta_0}{\partial\lambda_2}\right)\times\\ \frac{1}{2}\left\langle\frac{\partial u_2}{\partial\lambda_1}+\frac{\partial u_1}{\partial\lambda_2},\frac{\partial v_2}{\partial\lambda_1}+\frac{\partial v_1}{\partial\lambda_2}\right\rangle+\theta_0\left(\left\langle\frac{\partial u_1}{\partial\lambda_2},\frac{\partial v_1}{\partial\lambda_2}\right\rangle+\left\langle\frac{\partial u_2}{\partial\lambda_1},\frac{\partial v_2}{\partial\lambda_1}\right\rangle\right)+\\ +\left(\theta_0+\lambda_0\frac{\partial\theta_0}{\partial\lambda_2}\right)\left(\left\langle\frac{\partial u_1}{\partial\lambda_1},\frac{\partial v_2}{\partial\lambda_2}\right\rangle+\left\langle\frac{\partial u_2}{\partial\lambda_2},\frac{\partial v_1}{\partial\lambda_1}\right\rangle\right)=\\ \lambda_0\frac{\partial\theta_0}{\partial\lambda_1}\left(\left\langle\frac{\partial u_1}{\partial\lambda_1},\frac{\partial v_1}{\partial\lambda_1}\right\rangle+\left\langle\frac{\partial u_2}{\partial\lambda_2},\frac{\partial v_2}{\partial\lambda_2}\right\rangle\right)+\frac{\lambda_0}{2}\left(\frac{\partial\theta_0}{\partial\lambda_1}-\frac{\partial\theta_0}{\partial\lambda_2}\right)\left(\left\langle\frac{\partial u_2}{\partial\lambda_1},\frac{\partial v_2}{\partial\lambda_1}\right\rangle+\right.\\ \left.\left\langle\frac{\partial u_1}{\partial\lambda_2},\frac{\partial v_1}{\partial\lambda_2}\right\rangle\right)+\frac{\lambda_0}{2}\left(\frac{\partial\theta_0}{\partial\lambda_1}+\frac{\partial\theta_0}{\partial\lambda_2}\right)\left(\left\langle\frac{\partial u_1}{\partial\lambda_1},\frac{\partial v_2}{\partial\lambda_2}\right\rangle+\left\langle\frac{\partial u_2}{\partial\lambda_2},\frac{\partial v_1}{\partial\lambda_1}\right\rangle\right).\end{aligned}$$

Using the integral relation for $u_2,v_1\in\overset{0}{W}{}^1_p(S)$

$$\int_S\frac{\partial u_2}{\partial\lambda_1}\cdot\frac{\partial v_1}{\partial\lambda_2}dx=\int_S\frac{\partial u_2}{\partial\lambda_2}\cdot\frac{\partial v_1}{\partial\lambda_1}dx,$$

the previous equality becomes

$$\begin{aligned}B(u,v)=\lambda_0\frac{\partial\theta_0}{\partial\lambda_1}\left(\left\langle\frac{\partial u_1}{\partial\lambda_1},\frac{\partial v_1}{\partial\lambda_1}\right\rangle+\left\langle\frac{\partial u_2}{\partial\lambda_2},\frac{\partial v_2}{\partial\lambda_2}\right\rangle\right)+\frac{\lambda_0}{2}\left(\frac{\partial\theta_0}{\partial\lambda_1}-\frac{\partial\theta_0}{\partial\lambda_2}\right)\times\\ \times\left(\left\langle\frac{\partial u_2}{\partial\lambda_1},\frac{\partial v_2}{\partial\lambda_1}\right\rangle+\left\langle\frac{\partial u_1}{\partial\lambda_2},\frac{\partial v_1}{\partial\lambda_2}\right\rangle\right)+\frac{\lambda_0}{4}\left(\frac{\partial\theta_0}{\partial\lambda_1}+\frac{\partial\theta_0}{\partial\lambda_2}\right)\times\\ \times\left(\left\langle\frac{\partial u_1}{\partial\lambda_1},\frac{\partial v_2}{\partial\lambda_2}\right\rangle+\left\langle\frac{\partial u_1}{\partial\lambda_2},\frac{\partial v_2}{\partial\lambda_1}\right\rangle+\left\langle\frac{\partial u_2}{\partial\lambda_2},\frac{\partial v_1}{\partial\lambda_1}\right\rangle+\left\langle\frac{\partial u_1}{\partial\lambda_1},\frac{\partial v_1}{\partial\lambda_2}\right\rangle\right).\end{aligned}$$

The scalar product $\langle\varphi,\psi\rangle$ in $L^2(S)$is given by

$$<\varphi,\psi>=\int_S\varphi(x)\psi(x)dx.$$

Denoting $\xi_1=\partial v_1/\partial\lambda_1,\xi_2=\partial v_2/\partial\lambda_1,\xi_3=\partial v_1/\partial\lambda_2,\xi_4=\partial v_2/\partial\lambda_2$ and using the expressions obtained for $B(u,v)$, the term under the integral sign ensues the quadratic form $\sum_{i,j=1}^{4}a_{ij}\xi_i\xi_j=\Phi(\xi)$. The matrix $A=(a_{ij})$ has one of the forms

$$A = \begin{bmatrix} \lambda_0 \dfrac{\partial \theta_0}{\partial \lambda_1} & 0 & 0 & \theta_0 + \lambda_0 \dfrac{\partial \theta_0}{\partial \lambda_2} \\ 0 & \dfrac{\lambda_0}{2}\left(\dfrac{\partial \theta_0}{\partial \lambda_1} - \dfrac{\partial \theta_0}{\partial \lambda_2}\right) & -\theta_0 + \dfrac{\lambda_0}{2}\left(\dfrac{\partial \theta_0}{\partial \lambda_1} - \dfrac{\partial \theta_0}{\partial \lambda_2}\right) & 0 \\ 0 & -\theta_0 + \dfrac{\lambda_0}{2}\left(\dfrac{\partial \theta_0}{\partial \lambda_1} - \dfrac{\partial \theta_0}{\partial \lambda_2}\right) & \dfrac{\lambda_0}{2}\left(\dfrac{\partial \theta_0}{\partial \lambda_1} - \dfrac{\partial \theta_0}{\partial \lambda_2}\right) & 0 \\ \theta_0 + \lambda_0 \dfrac{\partial \theta_0}{\partial \lambda_2} & 0 & 0 & \lambda_0 \dfrac{\partial \theta_0}{\partial \lambda_1} \end{bmatrix}, \tag{15.34}$$

or

$$A = \begin{bmatrix} \lambda_0 \dfrac{\partial \theta_0}{\partial \lambda_1} & 0 & 0 & \dfrac{\lambda_0}{2}\left(\dfrac{\partial \theta_0}{\partial \lambda_1} + \dfrac{\partial \theta_0}{\partial \lambda_2}\right) \\ 0 & \dfrac{\lambda_0}{2}\left(\dfrac{\partial \theta_0}{\partial \lambda_1} - \dfrac{\partial \theta_0}{\partial \lambda_2}\right) & 0 & 0 \\ 0 & 0 & \dfrac{\lambda_0}{2}\left(\dfrac{\partial \theta_0}{\partial \lambda_1} - \dfrac{\partial \theta_0}{\partial \lambda_2}\right) & 0 \\ \dfrac{\lambda_0}{2}\left(\dfrac{\partial \theta_0}{\partial \lambda_1} + \dfrac{\partial \theta_0}{\partial \lambda_2}\right) & 0 & 0 & \lambda_0 \dfrac{\partial \theta_0}{\partial \lambda_1} \end{bmatrix}, \tag{15.35}$$

or

$$A = \begin{bmatrix} \lambda_0 \dfrac{\partial \theta_0}{\partial \lambda_1} & 0 & 0 & \dfrac{\lambda_0}{4}\left(\dfrac{\partial \theta_0}{\partial \lambda_1} + \dfrac{\partial \theta_0}{\partial \lambda_2}\right) \\ 0 & \dfrac{\lambda_0}{2}\left(\dfrac{\partial \theta_0}{\partial \lambda_1} - \dfrac{\partial \theta_0}{\partial \lambda_2}\right) & \dfrac{\lambda_0}{4}\left(\dfrac{\partial \theta_0}{\partial \lambda_1} + \dfrac{\partial \theta_0}{\partial \lambda_2}\right) & 0 \\ 0 & \dfrac{\lambda_0}{4}\left(\dfrac{\partial \theta_0}{\partial \lambda_1} + \dfrac{\partial \theta_0}{\partial \lambda_2}\right) & \dfrac{\lambda_0}{2}\left(\dfrac{\partial \theta_0}{\partial \lambda_1} - \dfrac{\partial \theta_0}{\partial \lambda_2}\right) & 0 \\ \dfrac{\lambda_0}{4}\left(\dfrac{\partial \theta_0}{\partial \lambda_1} + \dfrac{\partial \theta_0}{\partial \lambda_2}\right) & 0 & 0 & \lambda_0 \dfrac{\partial \theta_0}{\partial \lambda_1} \end{bmatrix}. \tag{15.36}$$

Since all principal minors of the matrices A (15.34), (15.35), and (15.36) are strictly positive, the forms $\Phi(\xi)$ and $B(u, \upsilon)$ are strictly positive, and the conditions (15.31), (15.32), and (15.33) are satisfied. This proves the lemma.

Lemma 5. Let $S(x_1, x_2)$ be a domain with the Lipschitz boundary ∂S. Assume that the conditions of lemma 2 and one of the conditions (15.31, 15.32, and 15.33) hold. Then if $\bar{f}(x) \in \left(L^2(S)\right)^2$ there exists a unique solution to the problem (15.30) in $\mathbf{V}$.

Proof. Let us show that $B(\upsilon, \upsilon)$ defines a norm equivalent to $\|\upsilon\|_{\mathbf{V}}$. This requires the $\mathbf{V}$-ellipticity of B: $\exists\, \gamma > 0 : B(u, \upsilon) \geq \gamma \|\upsilon\|^2$, $\forall\, \upsilon \in \mathbf{V}$. The last inequality will be

satisfied if all principal minors of the matrix $M(\gamma) = A - \gamma I$ are strictly positive. The principal minors of $M(\gamma)$ are polynomials of γ. Their constants are independent of x, and for $\gamma = 0$ are strictly positive (lemma 4). Therefore, the required $\gamma > 0$ exists.

Since $B(u, v)$ is symmetric, $\mathbf{V}$-elliptic and bounded in $\mathbf{V}$, the existence of solution to the variational problem (15.30) is ensured by the Lax-Milgram lemma.

The proof of the existence of solution to the nonlinear problem (15.13a) is based on the proof of regularity of the weak solution to the linear problem [Eqs. (15.27–15.28)].

Lemma 6. Let: (i) $S(x_1, x_2)$ be a domain with the boundary $\partial S \in C^2$; (ii) $f(x) \in [(L^p(S))]^2$, $p > 2$; (iii) the condition (15.33) holds. Then the weak solution $u(x) \in \mathbf{V}$ to Eq. (15.30) belongs to the space $\mathbf{W}_p^2(S)$ and satisfies Eqs. (15.27) in $L^p(S)$. $\left(\mathbf{W}_p^k(S)\right.$is the Cartesian product of Sobolev spaces $\mathbf{W}_p^k(S) = \left[W_p^k(S)\right]^2\Big)$.

Proof. On denoting $D_j\psi_l$ as $p_j^{(l)}$, the system (15.27) can be rewritten

$$-D_1 a_1(p) - D_2 a_2(p) = \bar{f},$$

where

$$a_1 = \left(a_1^{(1)}, a_1^{(2)}\right), a_2 = \left(a_2^{(1)}, a_2^{(2)}\right),$$

$$a_1^{(1)} = \lambda_0\left(\frac{\partial\theta_0}{\partial\lambda_1}p_1^{(1)} + \frac{1}{4}\left(\frac{\partial\theta_0}{\partial\lambda_1} + \frac{\partial\theta_0}{\partial\lambda_2}\right)p_2^{(2)}\right),$$

$$a_1^{(2)} = \lambda_0\left(\frac{1}{2}\left(\frac{\partial\theta_0}{\partial\lambda_1} - \frac{\partial\theta_0}{\partial\lambda_2}\right)p_1^{(2)} + \frac{1}{4}\left(\frac{\partial\theta_0}{\partial\lambda_1} + \frac{\partial\theta_0}{\partial\lambda_2}\right)p_2^{(1)}\right),$$

$$a_2^{(1)} = \lambda_0\left(\left(\frac{\partial\theta_0}{\partial\lambda_1} + \frac{\partial\theta_0}{\partial\lambda_2}\right)p_1^{(2)} + \left(\frac{\partial\theta_0}{\partial\lambda_1} - \frac{\partial\theta_0}{\partial\lambda_2}\right)p_2^{(1)}\right),$$

$$a_2^{(2)} = \lambda_0\left(\left(\frac{\partial\theta_0}{\partial\lambda_1} + \frac{\partial\theta_0}{\partial\lambda_2}\right)p_1^{(1)} + \frac{\partial\theta_0}{\partial\lambda_1}p_2^{(2)}\right).$$

The matrix $\left(\partial a_i^{(k)}/\partial p_j^{(l)}\right)_{i,j,k,l=1}^2$ coincides with the matrix A (15.36). The estimate (15.33) guarantees strong ellipticity to the system Eqs. (15.27). If the boundary $\partial S \in C^2$ and $\bar{f} \in \mathbf{L}^2(S)$, then the weak solution $u(x) \in \mathbf{W}_2^2(S) \cap \mathbf{W}_2^{1^0}(S)$ (Syarle 1992). The regularity of $u(x)$ can also be proven with the help of the theorem concerning the regularity of solutions of strong elliptic systems with limited nonlinearity (if $f(x) \in \mathbf{L}^\infty(S) \to u(x) \in \mathbf{W}_q^2(S)$ for $\forall q$) (Koshelev 1986). The remaining proof of the lemma is easily obtained by using routine differentiation by parts of the variational equality (15.30) in Sobolev spaces.

(*Note*: As a corollary of lemmas 3, 4, the mapping A

$$v(x) \in \mathbf{W}_2^2(S) \cap \overset{0}{\mathbf{W}}{}_2^1(S) \rightarrow -\mathrm{div}\left[\theta_0 \nabla v + \left(-2\theta_0 + \lambda_0\left(\frac{\partial \theta_0}{\partial \lambda_1} - \frac{\partial \theta_0}{\partial \lambda_2}\right)\right)\mathbf{e}(v) + \right.$$
$$\left. + \left(\theta_0 + \lambda_0 \frac{\partial \theta_0}{\partial \lambda_2}\right)\mathrm{tre}(v) I_2 \in \mathbf{L}^p(S),\right.$$

is an injection (a weak solution is unique) and surjection (a solution to $A(v) = f$ exists for $\forall f \in \mathbf{L}^2$) for $p = 2$, and it has the index, ind $A = 0$. However, in the case of a uniformly elliptic linear problem, the index A does not depend on p and thus, ind $A = 0$ for $\forall p \geq 2$).

Going back to the main problem given by Eq. (15.13a) for $\varphi_H(x) = \lambda_0 x$, $x \in \partial S$. The proof of existence and continuity of the Fréchet derivative of div$P(\varphi)$ in $B(\varphi_H)$ are obtained easily using the embedding theorems and the fact that $W_p^k(\Omega_n)$ $(kp > n)$ are the algebras. It is noteworthy that the trilinear mapping $\nabla\varphi\nabla\varphi^T\nabla\varphi$ has derivatives of all orders and $\beta_1(i_1, i_2)$, $\beta_2(i_1, i_2)$ are continuously differentiable with respect to i_1, i_2 $(\beta_1, \beta_2 \in C^4)$ for $\varphi \in B(\varphi_H)$. From the note above, the Fréchet derivative fulfills the isomorphism of spaces $\mathbf{W}_p^2(S) \cap \overset{0}{\mathbf{W}}{}_1^2(S)$ and $\mathbf{L}_p$, and thus, the implicit function theorem (Syarle 1992) can be applied. Therefore, we state

Theorem 3. Let $S(x_1, x_2)$ be a domain with the boundary $\partial S \in C^2$. Assume that the condition (15.33) for $\theta(\lambda_1, \lambda_2)$ and the constant λ_0 are satisfied. Then a zero neighborhood of U in the space $[L_p(S)]^3$ and a zero neighborhood of Φ in the space $\left\{\varphi : \varphi \in \left[W_p^2(S)\right]^3; \varphi = 0 \text{ on} \partial S\right\}$ exist such that for $\forall f \in U$ the system (15.13a) has a unique solution in a set: $\varphi_H + \Phi \subseteq B(\varphi_H)$.

All of this proves the mathematical validity of our model of the human stomach as a soft biological shell and the numerical results presented in this book. However, questions related to their accuracy and reliability, i.e., the analysis of computational algorithms used to run these simulations are described elsewhere.

15.3 What Is Next?

The reader should have realized that this book provides a framework for the collaborative research of physiologists, pharmacologists, mathematicians, computational biologists and medical doctors. A holistic approach to problems of the biomechanics of the human stomach, supported by examples of everyday clinical scenarios, has been emphasized as a required and rewarding way to proceed. It is to a research team and its members to identify the most important and significant questions to be asked and answered, and to unravel the mysteries of the maladies that affect the motility of the stomach. Such a quest will lead eventually to the discovery of their rational and effective treatment. As one man said:

Somewhere, something incredible to be known.
Carl Sagan

References

Chelkak SI (1986) On differentiation of solutions to quasi-elliptic systems of the second order. Mathematics 4:56–62

Cook RD, Malkus DS, Plesha ME, Witt RJ (2001) Concepts and applications of finite element analysis. Wiley, Chichester

Koshelev AI (1986) Regular solutions of elliptic equations and systems. Nauka, Moscow

Shagidullin RR (2001) Problems of mathematical modeling of soft shells. Kazan Mathematical Society, Kazan

Syarle F (1992) Mathematical theory of elasticity. Mir, Moscow

Index

R.N. Miftahof, *Biomechanics of the Human Stomach*,
DOI 10.1007/978-3-319-59677-8